A Consistent Approach to the Buckling Design Analysis of Rigid Jointed Steel-frames subject to Sidesway.

DEPARTMENT OF CIVIL AND ENVIRONMENTAL ENGINEERING
UNIVERSITY COLLEGE LONDON
UNIVERSITY OF LONDON

A CONSISTENT APPROACH TO THE BUCKLING DESIGN ANALYSIS OF RIGID JOINTED STEEL-FRAMES SUBJECT TO SIDESWAY

By

Philotheos G. LOKKAS

Thesis submitted for the degree of Doctor of Philosophy

March 1996

To

my family

Abstract

Many buckling design procedures for framed structures, having the possibility of sidesway, implicitly encourage engineers to attain a state, where for any column, considered as part of the frame, two buckling modes, sway and non-sway, occur simultaneously.

This research aims to develop a design methodology which takes into account the stiffness and strength interactions between a beam-column and its surrounding frame for both non-sway and sway modes. It extends past treatment of the elastic-plastic buckling in a single mode to circumstances where more than one mode contributes to the non-linear elastic behaviour and consequently elastic-plastic failure. To capture the multi-mode buckling behaviour it is shown that more than one imperfection must be considered. Two interrelated approaches have been developed.

Theoretical developments aim to provide:

• general expressions for calculating the rotational and translational stiffnesses of an idealised sub-frame to be employed in the general analysis procedures;

• complete Eigenvalue analysis for the column, where the stiffness of its surrounding frame is taken into account;

• generalisation of the Ayrton - Perry analysis for elastic-plastic buckling to the case where two active elastic buckling modes, controlled by two independent imperfection parameters, are involved. This requires development of a new simplified design procedure;

• computer software suitable for providing a simple, convenient, but accurate

design for single or multi-mode buckling.

An experimental programme has been designed to:

• provide a force controlled test rig which allows independent control of vertical and horizontal load levels required to cover a wide parametric range;

• allow an extensive test programme on different frame geometries to assess the validity of the theoretical model developed for both sway and non sway buckling modes.

An assessment of the provisions in existing design procedures for multi-mode buckling shows that even where this is treated, it provides an inadequate prediction of buckling capacity. The alternative model developed is suggested to provide a practical and realistic method for multi-mode buckling phenomena.

Acknowledgements

I am deeply indebted to my supervisor, Professor J. G. A. Croll, for his enduring and constructive guidance, apt remarks, advice and encouragement throughout the course of this research. Without his generous support and help this research would have been very difficult.

I would also like to extend my appreciation and thanks to:

1. The technical staff for their assistance in the preparation of the experimental results. In particular I am especially grateful to Messrs J. Jackson and M. Saytch for their thoroughness, care, expertise and friendship throughout.

2. My friend and colleague R. Abdelgadir for his co-operation and substantial support.

3. My fellow students for providing a friendly atmosphere.

I would also like to express my sincere gratitude to the Greek Ministry of Education, which, through the Technical Educational Institute (T.E.I.) of Larissa, where I work, approved my leave of absence and financed me during my studies.

A special word of thanks is finally due to my family; my wife, Jasmin, for her patience, care, understanding and love, despite the efforts for doing her MA courses; my daughters Kelly and Minnie, who have always been a source of constant inspiration and encouragement.

List of Contents

Notation

A summary of the more important symbols used in the text is presented here. All symbols, however, are also defined as they first appear in the text.

A	Cross-sectional area.
A_i	Arbitrary constant of the solution of the differential equation.
A_{il}	Ratio between an arbitrary constant A_i and A_1 .
C	Rotational spring constant.
c	Distance of the extreme fibres from the centroidal axis.
E	Elastic modulus.
e	Eccentricity of the applied load.
E_r	Reduced modulus.
E_s	Slope of the stress-strain diagram in the strain hardening portion.
E_t	Tangent modulus.
H	Horizontal load.
I	Moment of Inertia.
K	Translational spring constant.
k, k_{ci}	$\sqrt{P/EI}$, $\sqrt{P_{ci}/EI}$.
L	Length of column.
L_e	Effective length ($=\gamma L$).
M	Total bending moment.

M^l	Linear bending moment.
M_{eq}	Equivalent moment.
M_{eql}	Equivalent moment due to end moments in the absence of transverse forces.
M_o	Maximum end moment.
M_{ol}	Largest bending moment in the column due to transverse loadings.
M_p	Plastic moment of capacity (= $S\sigma_y$).
M_{pc}	Plastic moment capacity in the presence of axial load.
M_u	Strength of the member under bending moment alone.
M_y	Yield moment (= $Z\sigma_y$).
m_A, m_B	End-resistant moments.
m_A^l, m_B^l	End moments in a general mixed system of loading obtained from a linear analysis.
P	Axial load.
P_b	Buckling load.
P_c	The lowest elastic critical load.
p_c	Dimensionless ratio of the first two coinciding critical-loads $\left(= \frac{P_c}{P_y}\right)$.
P_{ci}	Elastic critical load of the i^{th} critical mode.
P_{cn}	Elastic critical load of the column as a part of a frame without sway (braced).
P_{cs}	Elastic critical load of the column as a part of a frame with sway (unbraced).

P_E Euler load.

P_{fh} First hinge load.

P_{fy} First yield load.

P_t Tangent modulus load.

P_u Axial compression capacity of an axially loaded column proposed by design codes.

P_y Squash load in the absence of bending moment ($= \sigma_y A$).

p_1, p_2 Non-dimensional load at first yield and full plasticity $\left(= \frac{P_{fy}}{P_y}, \frac{P_{fh}}{P_y} \right)$.

p_{cs}, p_{cn} The first two non-dimensional critical loads $\left(= \frac{P_{cs}}{P_y}, \frac{P_{cn}}{P_y} \right)$

$q^n(x)$ Transverse load in a non-proportional loading system.

$q^p(x)$ Transverse load in a proportional loading system.

r Radius of gyration; dimensionless constant ($= \frac{C}{EI/L}$).

S Plastic section modulus.

T Tangent modulus $(=d\sigma/d\varepsilon)$.

t Dimensionless constant ($= \frac{K}{EI/L^3}$).

u, w Beam-column displacement components.

w Total deflection.

w^o Equivalent initial deflection.

w_i Amplitude factor of the i^{th} critical mode.

w_i^n	Modal non-proportional loading imperfection.
w_i^o	Modal geometric imperfection.
w_i^p	Modal proportional loading imperfections.
$\overline{w}_i^p$	i^{th} amplitude of proportional loading imperfections for a unit axial load.
X, W	Local rectangular Cartesian coordinates.
x, w	Global rectangular Cartesian coordinates.
Z, Z_P	Elastic, plastic section modulus.
α	Numerical coefficient characterizing each one of the SSRC column design curves; Robertson's constant; curvature parameter associated with the sway critical mode.
α_1, α_2, α_3	Parameters relating the axial load and bending moment in the ultimate strength method for non-rectangular cross sectional shapes.
γ	Effective length factor.
β	Curvature parameter associated with the non-sway critical mode.
δ	Measured deflection obtained from experimental results ($= w - w^o$).
ϵ	Axial strain.
ζ_i	Modal equivalent imperfection factor ($= w_i^o + w_i^p + w_i^n$).
η	Factor involved in the stiffness of the theoretical model ($= EI_2/L_2$).
θ, θ_A, θ_B	Angular rotations.
λ	Slenderness ratio.
λ_1	Limiting slenderness ratio when $\sigma_E = \sigma_y$ ($= \pi\sqrt{E/\sigma_y}$).

$\bar{\lambda}$	Dimensionless slenderness ratio (= λ / λ_1).
λ_{cr}	Elastic critical load factor.
λ_f	Failure load factor of an elastic-plastic structure.
λ_o	Limiting slenderness ratio (= $\pi\sqrt{E_s/\sigma_y}$).
λ_p	Idealized rigid-plastic failure load factor.
ξ_i	Total modal equivalent imperfection.
ρ	Imperfection parameter.
ρ_s, ρ_n	Elastic dimensionless imperfection parameters corresponding to the sway and non-sway critical modes.
ρ_s^*, ρ_n^*	Elastic-plastic dimensionless imperfection parameters corresponding to the sway and non-sway critical modes.
σ	Average compression stress (= P/A).
σ_E	Average Euler stress(= P_E/A).
σ_u	Axial compression stress capacity of an axially loaded column proposed by design codes.
σ_p	Proportional limit stress.
σ_y	Yield stress.
$\phi_i(x)$	Characteristic function of the ith critical mode.
$\bar{\phi}_i(x)$	Normalized characteristic function of the ith critical mode.
$\phi_i''(x)$	Curvature.

Chapter 1

Multi-mode Buckling Phenomena

1.1 Historic Highlights of Buckling

The behaviour and design of steel members and frames has long been the subject of research for a number of researchers.

Regarding the strength of struts, the first paper was published in 1729 by Van Musschenbroek[1]. He recognised that the strength of a long column relates inversely to the square of the column length. His work was empirical, based only on experiments.

Euler, in 1759, published his famous paper where he investigated the elastic stability of a centrally loaded isolated strut using a mathematical approach which is known as the Bifurcation or Eigenvalue approach. Under the assumptions that the member is perfectly straight, the material is fully elastic and the deflection is small, a linear differential equation can be written based on the slightly deformed geometry of the member.

The eigenvalue solution which emerges from the characteristic differential equation gives the critical load of the strut. This load appears when bifurcation of equilibrium takes place. At this level of load, the originally straight member ceases to be stable. At and above this load a small lateral displacement will no longer disappear when the disturbance is removed. This load, is referred to as the *critical load* or *Euler load*, and is given by

$$P_E = \frac{\pi^2 EI}{(KL)^2} \tag{1.1}$$

where :

I : is the second moment of area of the cross section

L : is the unbraced length of the member

K : is an effective length factor to account for the end conditions of the member.

This formula gives a good prediction for the behaviour of slender columns provided the axial stresses in the member do not exceed the proportional limit, and the member remains fully elastic.

Although the most recent developments have been based on Euler's formula, there was considerable debate following its establishment. The experimental work at that time showed that columns not only bent from the onset of loading but also failed under loads much less than Euler's limiting load. Investigators following Euler soon abandoned his formula concentrating instead on stocky columns for which the onset of plasticity was the controlling influence on buckling. However, little additional progress was made for the next five decades.

It was Young[2] in 1807 who realised that if the column was originally bent, any axial load, however small, would increase the curvature. He attributed all kinds of irregularities observed in experiments to unavoidable initial strut curvature, material non-homogeneity and eccentricity of loading. He pointed out that under Euler's assumed conditions the column should remain straight even if the load should exceed the critical one.

Furthermore, he established formulae giving the total deformation of the axially loaded strut in terms of either the initial deflection or eccentricity. In conclusion he derived a load limit at which struts would crush rather than buckle.

In 1845, A. H. E. Lamarle[3] pointed out that Euler's formula should be used only for slenderness ratio beyond a certain limit and that experimental data should be relied upon for smaller ratios.

The most important and essential development in buckling was actually done in 1886 by Ayrton and Perry[4]. They found that the effect of eccentricity is the same as that of the initial curvature, and any probable want of homogeneity in specimens

might also be accounted for by a term of the same kind. So they suggested an **equivalent initial deflection,** w^o, to be taken into account. Under the assumption that w^o has a sine form in a column, they found the total deflection to be

$$w = \frac{1}{1 - \frac{P}{P_E}} w^o \tag{1.2}$$

where P is the axial force and P_E is the Euler load. They rearranged Eq. (1.2) as

$$\frac{1}{\delta} = \frac{P_E}{w^o} \cdot \frac{1}{P} - \frac{1}{w^o} \tag{1.3}$$

where $\delta = w - w^o$ is the measured deflection at the mid-point of the strut obtained from experimental results, and they noted that Eq. (1.3) represents a linear relationship between $1/\delta$ and $1/P$, allowing experimental evidence to be interigated to determine the controlling critical load P_E and equivalent imperfection w^o. This approach later recast by Southwell (1926), was used by Ayrton and Perry to reinterpret and explain many of the earlier experiments on strut buckling, such as those of Hodkinson[5] (1840, 1857, 1860). As an index of buckling they limited the total stress on the extreme fibre of the cross section (sum of stresses due to axial load and bending moment), to that of the yield stress of the material. The buckling strength, P_{fy}, of the strut calculated by this procedure, was found to be a function of the elastic critical load, P_E, (Euler load), the squash load, P_y, (axial load required to produce a plastic section in the absence of bending moment) and the equivalent initial imperfection, ρ. This strength is given by the equation

$$(P_E - P_{fy})(P_y - P_{fy}) = \rho P_{fy} P_E \tag{1.4}$$

Adaptations of this expression now form the basis of most modern codes of practice on column design.

In 1889, the French engineer A. Considère[6] performed a series of 32 tests on columns. He observed that the stresses on the concave side of the column, (according to explanations given in Appendix A, section A.1), increased with the tangent modulus, E_t, while the stresses on the convex side decreased with E. He showed, therefore, why the Euler formula was not applicable to inelastic buckling, and he stated that the effective modulus, E_r, was between E and E_t. Although he made no attempt to evaluate the effective modulus, he is responsible for beginning the reduced-modulus theory.

In the same year, quite independently, the German Engineer F. Engesser[7] suggested the tangent-modulus theory (see Appendix A, section A.1). He denoted the tangent modulus by $T\ (=d\sigma/d\varepsilon)$ and proposed that for the critical load, T be substituted by E in Euler's formula. Later, in March 1895, Engesser again presented the tangent modulus theory[8], without knowing of Considère's work.

Three months later the Polish-born F. Jasinski, then a Professor in St. Petersburg, pointed out that Engesser's tangent-modulus theory was incorrect, called attention to Considère's work, and presented the reduced-modulus theory[9]. He also stated that the reduced modulus, E_r, could not be calculated theoretically. In response, and only one month later, Engesser acknowledged the error in the tangent modulus approach and showed how to obtain the reduced modulus for any cross section[10].

The reduced-modulus theory was also presented by Theodore von Karman in 1908[11] and 1910[12]. In the latter paper he derived formulas for E_r for rectangular and idealized wide-flange sections (i.e. sections without a web). He extended the theory to include the effects of eccentricities on the buckling load, and he showed that the maximum load decreases rapidly as the eccentricity increases.

The English elastician R.V. Southwell also presented the reduced modulus theory. In his paper in 1912[13] he derived the theory using a modified length for the column instead of a reduced modulus for the material. His work was independent of the others although the basic concepts were similar. In 1932 he made a correct

evaluation of the initial deflection w^o used initially by Ayrton and Perry. Rearranging eq. (1.3), yields

$$\delta = P_E \cdot \frac{\delta}{P} - w^o \tag{1.5}$$

which shows that if values of δ are plotted against δ/P, they should fall in a straight line, with an intercept of δ axis equal to w^o and a slope P_E. In experiments reported by von Karman for slender columns, the best fitting line for each set of data was drawn and the slope of this line was compared with the Euler theoretical load, where, a very close agreement was observed. This clever method, apart from verifying the validity of what was found by Young and Ayrton and Perry, is a convenient way of experimentally deducing the equivalent imperfection of a column.

Having obtained the correct value of geometric imperfections, the strength of a column can be calculated from the Ayrton-Perry formula, Eq. (1.4). A comparison between this strength and the failure load obtained experimentally would then be the only consistent approach of verifying the above formula.

The reduced-modulus theory was the accepted theory of inelastic buckling until 1946, when the American engineer F. R. Shanley pointed out the logical paradoxes in both theories. In a remarkable one-page paper[14], he explained what was not correct with the generally accepted theories and proposed his own theory that resolved the paradoxes. Five months later, in a second paper[15] he gave further analyses to support his earlier theory and gave results from tests on columns.

1.2 Scene Setter

Buckling design analysis has been approached many years ago with the aim to mainly assess the load carrying capacity of a given column on the basis of its geometric and material data.

In a brief description, the process, which can generally be followed on this approach, for columns where there is just a single buckling mode actively controlling their behaviour, could comprise as basic steps

a) In the theoretical field, based on the boundary conditions of an imperfect column

1) The determination of elastic critical load for each mode. This load can be obtained as the Eigenvalue of the characteristic equation which comes from the governing differential equation, written with respect to the deformed configuration of the structure.

2) Tracing the curves which express

i) the total deformation of the column in terms of its total initial equivalent imperfection (geometric, loading), critical load and current axial load,

ii) the deformation corresponding to a full section plasticity of the column in terms of its squash and current axial load,

a close upper bound estimation of the buckling load at full plasticity can be obtained as an intersection point of the above two curves.

b) Experimentally

1) In the elastic region, by recording the axial load along with the lateral displacement, the elastic critical load and the effective imperfection can be obtained through the Southwell Plot technique.

2) In the elasto-plastic region up to collapse, the maximum load carrying capacity appears at the moment that comparatively large deformations have been developed without any increase of the corresponding axial load.

However, in the design procedure of a structure, it is usual to design *separate components* with a consistent factor of safety. This factor might be less than expected if spread of plasticity along the member length is disregarded; nevertheless this reduction is usually very low and reasonable because the structure is modelled

in a manner that all the beams remain elastic, while in all columns the first plastic hinges occur *simultaneously.*

This mechanism is considered to be a collapse one, although might still be able to carry more load up to the actual collapse state.

While this approach is widely acceptable, there might be some cases, where, under certain conditions, a situation can be developed, in which *the separate buckling modes actively interact with each other.* This happens in the case of biaxial buckling or in a column considered as a part of a frame having the possibility of side sway.

These circumstances are not adequately covered by the present design practice, where the whole mechanism by which failure takes place is not clear enough. A lot of emphasis is put on slenderness of columns, where only linear analysis is considered, whilst less attention has been paid to imperfections without any reference in structures with more than one degrees of freedom.

1.3 Structures with one or more degrees of freedom

A structure that presents one or more degrees of freedom has by definition a configuration which at any instant of time can be completely defined by one or more independent co-ordinates, where one or more measurements are required, such as a displacement or an angle.

In practice, virtually all structures usually require many degrees of freedom to define their response. However, with some simplifying assumptions, many such structures can be regarded as having fewer, or even only one, degree-of-freedom.

In the portal frame for example in Fig. 1-1(a), the swaying motion of the rigid horizontal member is defined by the displacement Δ_1, and the frame can be regarded as having only one degree of freedom. Similarly in the n-storey frame of the same figure with horizontal rigid members, the structure is assumed to sway only in its plane without rotation of joints. For a complete definition of the configuration

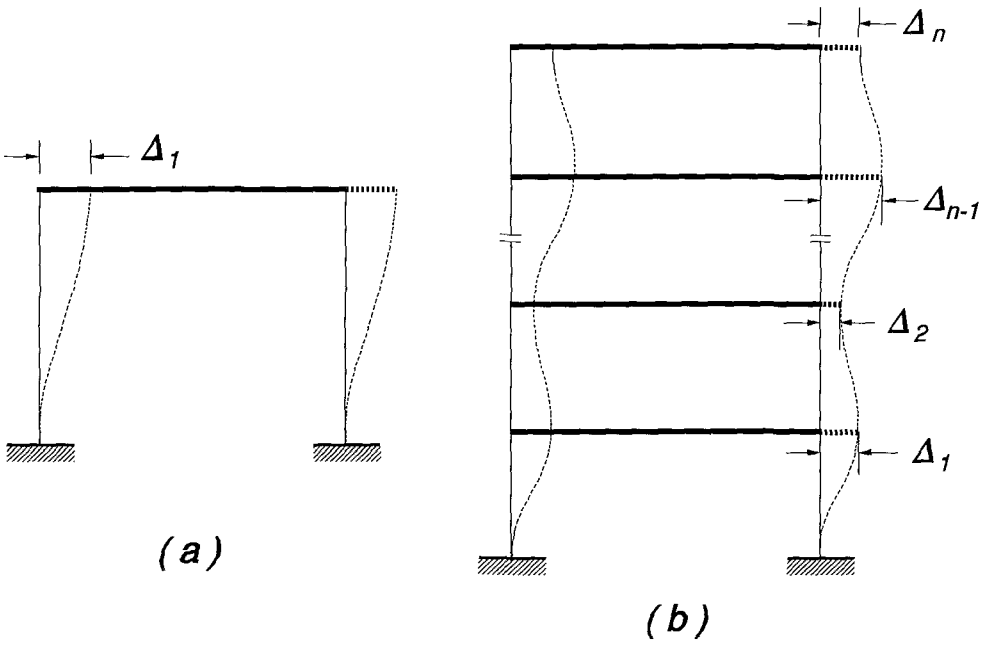

Figure 1-1

of the structure, n independent coordinates, (Δ_1 to Δ_n inclusively) are required; thus it has n degrees of freedom. Examples of one or two degrees of freedom could also be the buckling phenomenon of isolated columns, regarded in one or two directions (uniaxial or biaxial buckling), where the final configuration can be defined by one or two coordinates respectively.

When buckling is considered in a structure possessing many degrees of freedom, the resulting phenomenon may involve a multi-mode buckling. Multi-mode buckling phenomena may in turn involve a number of different forms of buckling modal interactions.

1.4 Modal Interactions

As a phenomenon, buckling appears generally in beam-columns, where a large number of modes takes place. The level of critical load is one of the main

characteristics for each mode. The mode corresponding to the minimum critical load is the most crucial from the point of view that it may substantially affect the overall response of the beam-column. This response might also be partially affected by the subsequent critical load, in particular when this subsequent value appears to be close to the previous one.

To take an example, beam-columns always present a possibility of buckling in two directions, coinciding with the two axes (major and minor) of their cross section. These two directions are identical with the column's so called 'two degrees of freedom' in the sense that the column may buckle in planes containing these directions. Depending on the geometry of the beam-column and specially of its cross section, the levels of the first critical loads, corresponding to each one of these directions, might be different or close to each other. For identical boundary column's conditions and significant difference of critical loads, the critical buckling mode is the one about the minor axis; the overall design, based on the characteristics of the column with respect to this axis only, leads to the buckling strength of the column, while a large amount of the buckling resistance about the major axis remains unutilized. However, in the case where the critical loads of the two directions are close to each other, (and this is a point that structural engineers normally pay considerable attention), a simultaneity of buckling might occur about both axes.

An *interaction* of both buckling modes which takes place here, results in a possible reduction in the load carrying capacity of the beam column. Depending on the surrounding the beam-column frame and its boundary conditions, this modal interaction might be **weak** or **strong** and take place as an **elastic** or **plastic** buckling phenomenon. The following examples illustrate these cases, which are classified in the subsequent subsections.

1.4.1 Elastic Buckling

The interaction here is taking place before the initiation of yielding in the beam-column and might be either weak or strong.

a) Weak Interaction

Consider an axially loaded column as a part of a frame having the possibility of sway, or equally a beam-column subjected to biaxial buckling. Let us assume that the first two critical loads in both cases are reasonably close to each other.

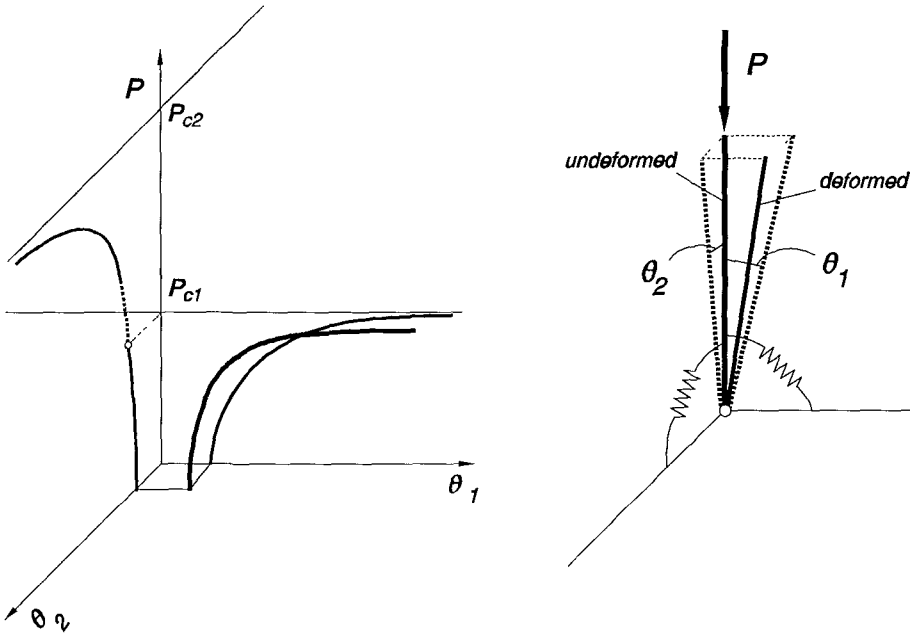

Figure 1-2

Under a monotonically increased loading system, **development of one buckling mode does not affect the buckling of the second mode.** Consequently this case may well be considered in terms of the superposition of the contributing modes. Fig. 1-2 shows the modelling for this case and the characteristic deformations of the column for both degrees of freedom versus the applied axial load.

The heavy curve, represents the resultant of the two curves made up of the two deformations θ_1 and θ_2 separately. It has a projection on the P-θ_1 plane, which is very close to the θ_1 (say) mode, due to the weak interaction of the other (θ_2

mode).

b) Strong Interaction

As a representative example of a strong interaction in the elastic buckling, can be considered a radio mast built in the form of a space-truss. Here, the two modes of buckling, expressed by the corresponding degrees of freedom, may be represented as the **overall** mode, referring to the beam-column as a whole structure, and the **local** mode, corresponding to each member of the structure separately, with critical load values which are reasonably close to each other. Fig. 1-3 shows schematically how these two modes relate to each other, while Fig. 1-4 provides the basic modelling for obtaining each one separately and the characteristic deformation of a local member participating to both local (θ_L) and overall (θ_o) distortions.

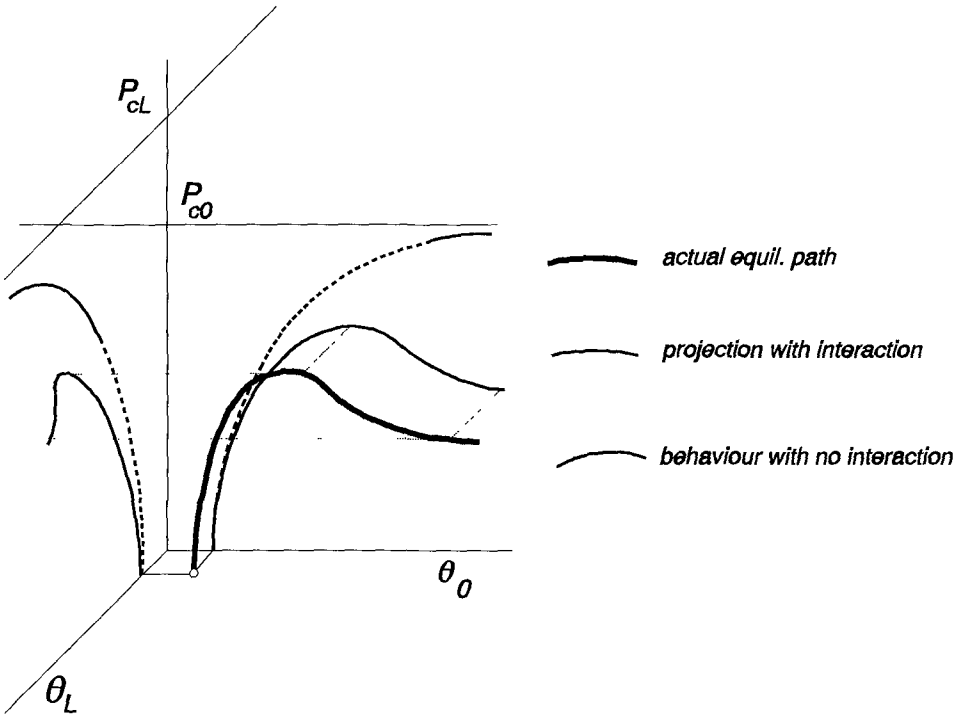

Figure 1-3

Once again the heavy-line represents the resultant of the interaction between the two deformation modes (overall and local); it has projections onto either the P-θ_o

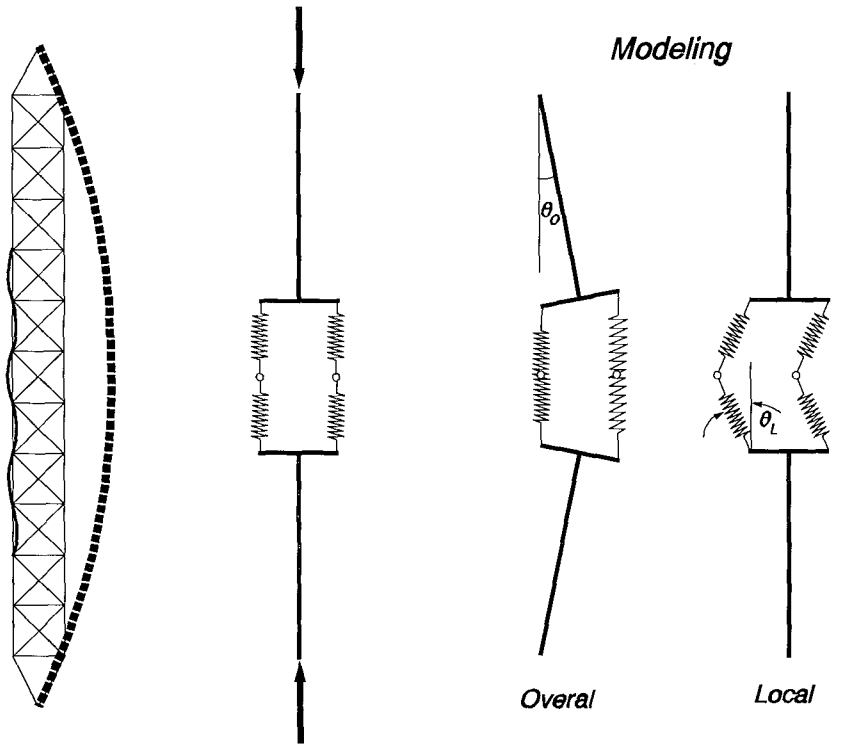

Figure 1-4

or the P-θ_L plane, that are very different from those that would occur (shown dotted) if either one of these modes were acting alone. This is in contrast with the behaviour exhibited in the example of Fig. 1-2.

This is an example in which the **development of one mode** (the overall mode) generates additional axial compression force which **exacerbates the development of buckling in the second mode** (local mode). Alternatively, this form of strong interaction could be interpreted as a situation in which the **development of the second mode** (the local mode) reduces the axial stiffness of the flange and hence **weakens the resistance to the buckling into the first mode** (the overall mode). Either way the modes interact strongly, with the effect that a highly unstable form of imperfection sensitive buckling can ensue.

An important example of strong interaction between the overall and local buckling modes, is believed to have occurred in the collapse of Quebec Bridge (1907). The main frame of this bridge, having the form of a doubly braced truss

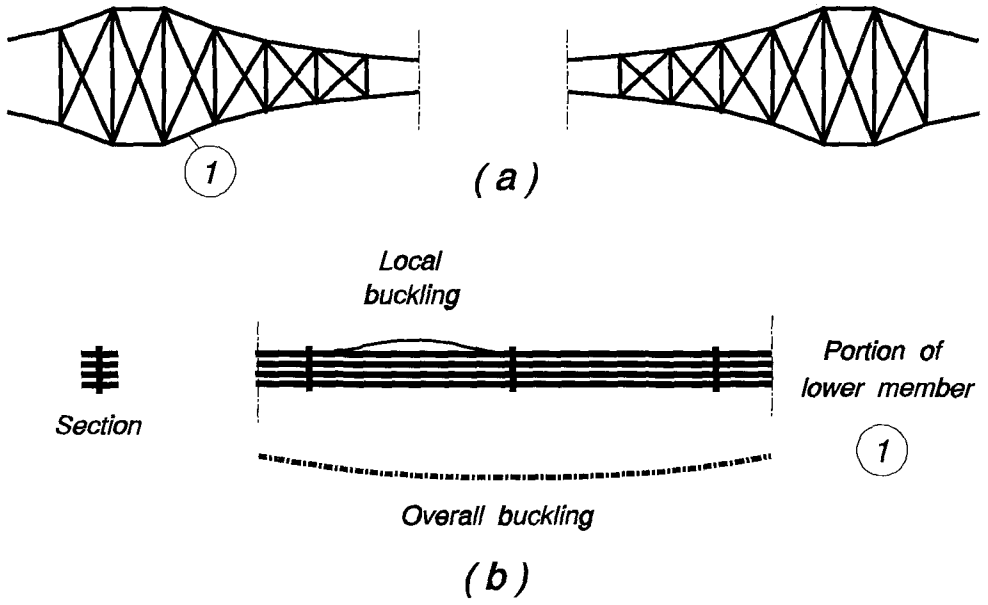

Figure 1-5

shown in Fig. 1-5a, had at the supports, as lower compression members, beam-columns built from flat strips laminated and tied together at discrete locations along the length as shown in Fig. 1-5b. Due to the strong elastic interaction between the overall and local buckling that took place on these single and composite members, there was a reduction in the ultimate load carrying capacity with the result that entire cantilevered span collapsed just prior to the completion of erection.

1.4.2 Plastic Buckling

The interaction here takes place after the initiation of yielding while the beam-column shows an elasto-plastic behaviour and again might be either weak or strong.

a) Weak Interaction

Let us again consider a beam-column as part of a frame which has the

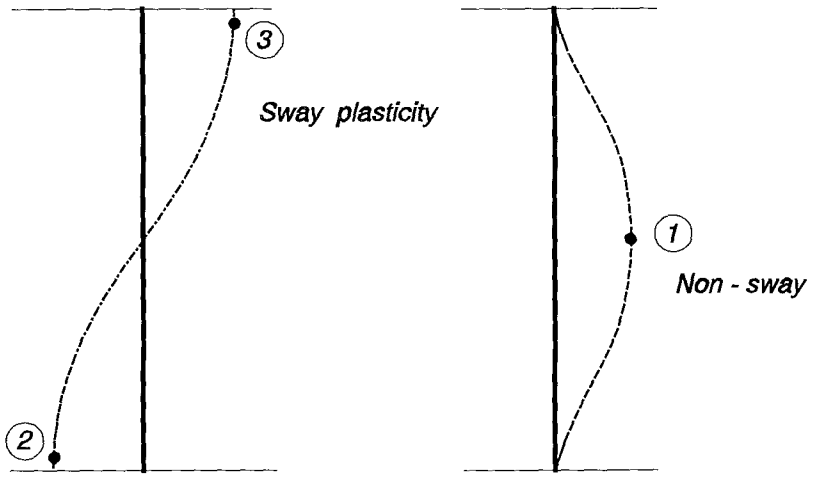

Figure 1-6

possibility of sidesway. For a certain stiffness of the surrounding frame, where the first two critical loads are close to each other, if the column presents only non-sway (out of straightness) imperfections, its plastic failure, as a result of the buckling development in this mode, will not affect the plastic failure in the other (sway) mode. This is because the plastic hinge (1), formed due to the maximum bending moment, responsible for this failure, occurs at or near the middle of the column, where the corresponding moment for the other mode is almost zero.

Similar thoughts can be applied for the case where the column presents only sway imperfections, except that the maximum moments and consequently the first hinge(s) (2), (3) occur at the end(s) of the column.

Fig. 1-6 shows the location of plastic hinge formation due to a separate buckling development in each mode.

Therefore for a gradually increasing loading system, **the plastic failure in mode 1 has little effect on the plastic failure in mode 2.**

b) Strong Interaction

The previous case, in the presence of both imperfections has a different

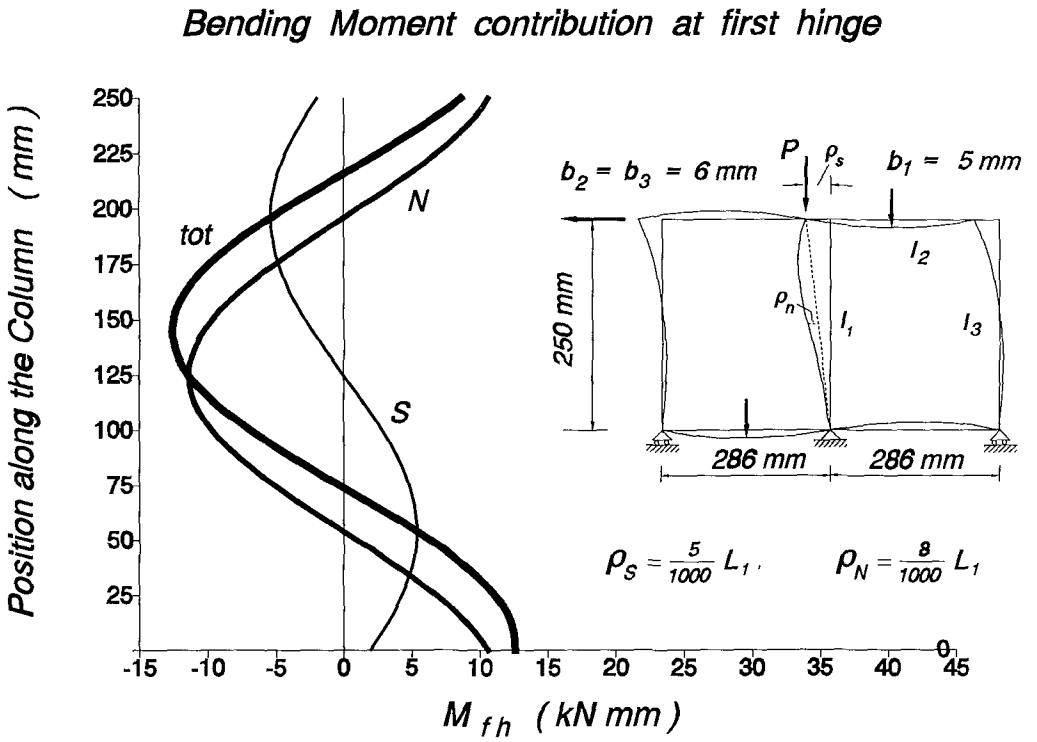

Figure 1-7

response. The maximum bending moment, as shown in Fig. 1-7, is affected differently by each mode according to its associated imperfections; failure could be initiated somewhere near the middle or at the ends of the column. In this case therefore **plastic failure in mode 1 could interact strongly with the plastic failure in mode 2.**

1.5 The Scope of this Project

The modal interactions discussed in the preceding section coupled with the buckling developments by Ayrton and Perry lead to the conclusion that the main parameter affecting the load carrying capacity of a given beam-column is its initial imperfections and the ratio of elastic / squash load. The term imperfections involves any physical shortcomings appeared at random in the beam-column, along with deflections coming from any lateral loads and/or bending moments applied prior to

the application of axial loading. Unless these imperfections are properly taken into consideration, there is no consistent approach for calculating the strength of the column. In the absence of the above imperfections an axially loaded column is merely a perfect column which fails due to either elastic stability or material failure.

Following this line of thought, in the case where a beam-column exhibits two buckling modes, sway and non-sway, a *total equivalent imperfection parameter* (TEI), that embraces both geometric and loading imperfections is introduced for each mode. Based on this parameter, the design of the beam-column becomes consistent, allowing interaction between elastic stability and plastic collapse.

The magnitude of geometrical imperfection is random, depending on the manufacturing process and the quality of workmanship; the loading imperfections can be evaluated through a linear analysis neglecting the effects of axial load.

The main objective of the present work is to provide a framework for the evaluation of each TEI and its use in an extended form of the Ayrton-Perry formula; this allows a more generalised form for beam-columns with two or more active buckling modes. To this end special consideration is given to the development of analyses that are sufficiently simple and might be used in design offices.

The historical developments on beam-columns and the shortcomings of the current design methods are discussed in Chapter 2.

The concept of elastic buckling in idealized rigidly jointed frame models is presented in Chapter 3. This involves the definition of several idealized models for frame analysis, which may or may not include sway. The idealized model used for obtaining a design formula in the sway case is also presented along with the case of a braced idealized model.

In Chapter 4 the non-linear elastic response is related to that of the simplified linearised model. This leads to the definition and use of each TEI which allows complete specification of the non-linear elastic response of the column. A theoretical background on imperfect columns is also added in this Chapter.

The interaction between elastic nonlinearities and plastic collapse in the presence of imperfections is outlined in Chapter 5. Presented in this Chapter is also the generalized Ayrton-Perry formula.

Chapter 6 outlines the experimental procedure adopted for tests on a properly justified frame model. It shows the possibility of predicting the collapse load through a known imperfection parameter for each mode.

The experimental verification of this parameter through the Southwell Plot, together with comparisons of test results with theory are presented in Chapter 7. The theoretical results are obtained through an extended computer program made for this purpose.

In Chapter 8 some existing design methods are outlined and a new simplified procedure is proposed.

Final conclusions and recommendations for further studies are incorporated in Chapter 9.

Chapter 2

Beam-Column & Frame Buckling

2.1 Beam-Columns under General loading

A member is termed a beam-column when it is subjected to both axial compression and bending moment. The latter may arise from transverse loads acting on the member, from couples applied at any section, and/or from end moments resulting from eccentricity of the applied axial loads at one or both of its ends. In a rigid jointed frame, this moment may be generated as a result of frame action in resisting the applied loads. Before any discussion of columns as components of rigid-jointed frames, a brief description on the strength of isolated beam-columns will be developed. These columns are assumed to be under a known system of loading, where the plane of loading is identical to the plane of actual buckling.

When a beam-column is subjected to a gradually increasing system of loading, it initially resists the applied loads in a purely elastic way. However, when the load reaches a certain level, called first yield load, the extreme fibres at some location will start to yield. From this point onwards the section behaves inelastically causing deformations at an ever-increasing rate. The maximum load carrying capacity is reached when the member, having formed the first plastic hinge(s), continues to deform at no increase of the applied loading.

Analytical solutions to the estimation of strength of such members have followed one of the two methods:

a) The elastic method (working stress criterion) and

b) The elastic-plastic method (ultimate strength criterion).

The first method is based on the idea that a lower bound to the actual collapse load can be realised by using the elastic limit value, whereas the second method requires the determination of the actual load-deformation response of the member in the elastic-plastic regime of behaviour under increasing applied loads.

Aiming to clarify the difference the two kinds of analytical solutions, both methods are discussed in the next sections along with some interaction formulae.

2.2 Working Stress Criterion

The problem of eccentrically loaded columns was tackled as a stress problem, where, the axial failure load was considered to be that which caused at the extreme fibres initiation of yielding. On the assumption that the material remains linearly elastic up to the yield point, the deflection of the member can be determined in terms of the applied load and its eccentricity. The action of axial load on the deflection, however, causes additional bending moment. In the cross section where the maximum bending moment of the member occurs, the maximum compression stress in the extreme fibres is expressed by the sum of the stress due to axial load and due to bending moment. In the case where the end axial loads P are applied with equal eccentricities e this approach yields the so called Secant formula

$$\sigma_{max} = \frac{P}{A}\left[1+\left(\frac{ec}{r^2}\right)\sec\frac{L}{2r}\sqrt{\frac{P}{AE}}\right] \tag{2.1}$$

where c is the distance of the extreme fibres from the centroidal axis. Since the formula in the absence of eccentricity is reduced to a pure compression formula, an equivalent eccentricity e_o is introduced so that the effect of any initial imperfection can be taken into account. The secant formula takes thus the form

$$\sigma_{max} = \frac{P}{A}\left[1+\left(\frac{(e+e_o)c}{r^2}\right)\sec\frac{L}{2r}\sqrt{\frac{P}{AE}}\right] \tag{2.2}$$

For the purpose of design, the average stress P/A is taken by limiting the maximum compression strength to the yield stress. By the same procedure, for the case of unequal end eccentricities, a more comprehensive solution can be carried out.

This was given by Young[16] and is fully presented by Timoshenko[17].

The accuracy of the above approach for a practical estimation of the strength of beam-columns has been checked by Austin[18] for cases of equal eccentricities. He assumed that the effect of initial imperfection for these tests would be negligible and concluded that the first yield criterion may considerably underestimate the ultimate strength of short beam-columns with solid cross sections bent in the weak direction.

2.3 Ultimate Strength Criterion

In order to determine the ultimate load capacity of a beam-column the real deformed shape has to be traced during the loading. This can only be done when the relation between the internal bending moment and the curvature of the member has been established. This relationship is linear for elastic behaviour of the column otherwise it becomes non-linear. The internal bending moment, being the sum of moments due to applied loads and due to the interaction between axial load and lateral deflection, is a linear function of displacement. If this function is replaced into the moment-curvature relation, a linear or non-linear differential equation can be obtained, depending on whether an elastic or inelastic behaviour is assumed. A direct integration of this equation yields the deformed shape of the column. While this integration is straightforward for the elastic range, it becomes very complicated when the column exceeds the elastic limit.

A considerable amount of research has been dedicated to the problem of inelastic behaviour of beam-columns. Among the researchers who contributed to that problem were Kármán[12] in 1910, who was the first to investigate numerically the inelastic behaviour of rectangular cross sections loaded with small eccentricities. His work was continued by Chwalla[19] on columns with different loading conditions and shapes of cross sections.

Jezek[20] in 1936, was the first to develop an analytical method on

eccentrically loaded columns of rectangular cross section beyond the elastic limit. Assuming elastic perfectly plastic material response, he established the moment-curvature relationship along the column's length.

Horne[21] in 1956, following the same procedure, gives the moment-curvature relationships of a rectangular cross section made of an elastic perfectly plastic material, with a finite drop of stress at yield. Making use of these results he showed the determination of the collapse load without having to resort to numerical procedures.

Galambos and Ketter[22] in 1959, studied the ultimate carrying capacity of pin-ended wide flange beam-columns. Following numerical procedures they considered two loading conditions, where, a bending moment is applied only at one end as well as equal end moments are applied to both ends. In their calculations a symmetric residual stress pattern was assumed, but no use of initial imperfection was made.

An alternative long-standing numerical method for the study of elasto-plastic behaviour of beam-columns failing due to bending was given by the column deflection curves (CDCs). In each family of these curves each one corresponds to the equilibrium of a simply supported column with different length, deflected under a constant axial load. If a suitable portion of the CDCs is considered, the different deflected shapes of a given beam-column for the different stages of bending moments can be obtained, provided the column's axial load is the same as that of CDCs. The concept of CDCs was first used by Kármán and developed further by Horne and many other investigators.

The differential equation of equilibrium is usually expressed in terms of lateral deflection of the column. For a direct integration of this equation beyond the elastic limit, Chen and Santathantaporn[23] remarked that the curvature of an elastic-perfectly-plastic column loaded eccentrically plays exactly the same role as the deflection. This consideration allows simpler solutions for the maximum loading capacity which may be obtained with fewer necessary steps. Theoretically obtained

results of these curves were compared with existing solutions and a good agreement was observed. Chen continued this work and later derived interaction curves relating the axial thrust, lateral load and slenderness ratio with various values of end eccentricities. Again this work was extended with expressions for the moment expressed explicitly in terms of curvature for different cross sections including the influence of residual stresses.

To solve the problem of elastic-plastic behaviour of beams-columns Chen and Atsuta[24] used column curvature curves (CCCs) obtained analytically in a similar way to the CDCs. They also gave interaction relationships between thrust and end moment for their ultimate strength.

2.4 Interaction Formulae

In the previous section several methods for obtaining the load carrying capacity of a beam-column were described. Even for simple cases the solutions required time consuming and intensive computational work. For this reason over the past five decades different researchers have tried and developed other methods which are considerably simpler and give solutions close to the exact ones.

The building codes, based on this line of thinking, make use of one or two design procedures to determine the strength of beam-columns. To provide safe combinations of the applied loads they use either charts (or tables) or interaction formulae. These formulae relate the ratios P/P_u and M/M_u where P and M are the axial load and bending moment at failure respectively, whereas P_u and M_u are appropriate measures of the strength of the member under respectively axial load or bending moment alone.

If the design aims to attaining the first yield, then P_u and M_u should be taken as the first yield conditions. For an ultimate load design, P_u is taken as the ultimate axial strength of the column, $P_p = \sigma_y A$ the corresponding axial strength suggested

by codes, and M_u is taken as the full plastic moment M_p.

In a slender beam-column under a loading system where P is the axial load and M^l is the maximum primary bending moment (obtaining from a linear analysis without the effect of axial load), the theoretical upper limit of thrust P will be the elastic critical load P_E. An axially loaded column, failing at load level P_u, will lead to a design criterion $P/P_u \leq 1$. On the other hand, in the absence of axial load, the strength of the beam-column will be influenced only by the primary bending moment, thus yielding the design criterion $M^l/M_u \leq 1$. In a combined action of axial load and bending moment on the beam-column, an interaction formula of the form

$$f\left(\frac{P}{P_u}, \frac{M^l}{M_u}\right) \leq 1 \tag{2.3}$$

will govern the strength of the beam-column at failure. Formulae based on Eq. (2.3) seem to provide exact results when the extreme cases are considered, i.e. either axial load or bending moment acting alone. For combined loading cases they lose some of their accuracy due to certain simplifying approximations. These approximations have been made on the basis of curve fitting either from available test results or exact numerical solutions. For predicting the strength of a beam-column under general loading a linear interaction of P/P_u and M^l/M_u was primitively introduced in the form

$$\frac{P}{P_u} + \frac{M^l}{M_u} \leq 1 \tag{2.4}$$

This equation was proved to be inadequate for the design of steel or aluminium beam-columns due to the effects of axial load in producing additional bending moments. Better results would therefore be obtained if M^l were replaced by M, i.e.

$$\frac{P}{P_u} + \frac{M}{M_u} \leq 1 \tag{2.5}$$

where M is the value of bending moment, which, due to the combined effect of axial load and further deformation of the member is difficult to determine. The attention was therefore directed to simplify the procedure to obtaining M for some particular loading patterns.

The maximum bending moment occurring at mid-height of a beam-column under axial load P and equal opposite end moments M_o is approximated as

$$M = M_o\left(\frac{P_E}{P_E - P}\right) \tag{2.6}$$

In this equation the term in parentheses may be considered as an amplification factor since it amplifies the primary moment M_o to give the final one (primary + secondary). The equation also applies to eccentrically loaded columns under same eccentricities e, where the term M_o is replaced by Pe. Although the maximum bending moment in Eq. (2.6) is less than the exact one[25] this equation is currently being used by most codes of practice as the basis for the interaction formula for the strength of beam-columns. Substitution of M from Eq. (2.6) into (2.5) results in

$$\frac{P}{P_u} + \frac{M_o}{M_u\left(1 - \frac{P}{P_E}\right)} \leq 1 \tag{2.7}$$

In the case of non equal end moments M_o and βM_o, where $-1 \leq \beta \leq 1$, the greater end moment M_o is recommended to be used, although it may lead to over-conservative results, particularly in the case of double curvature.

An extensive, approximate mathematical study of this problem started in 1947 by Massonnet, who, in cooperation with Campus[26] suggested that Eq. (2.7) should take the form

$$\frac{P}{P_u} + \frac{C_m M_o}{M_u\left(1 - \frac{P}{P_E}\right)} \leq 1 \tag{2.8}$$

where $C_m = \sqrt{0.3(1+\beta^2)+0.4\beta}$. Later on, having realized the non-conservative nature of Eq. (2.8), he proposed the relationship

$$\frac{P}{P_y} + \frac{M_o}{1.18M_p} \leq 1 \qquad M_o \leq M_p \tag{2.9}$$

based on a mechanism consideration at the end of the member. A lot of work has been undertaken by many other investigators to provide a proper moment factor, C_m, to provide better results.

When a simply supported beam-column is under a transverse loading pattern, the use of C_m factor becomes meaningless. The total moment along the beam-column is

$$M = M^l + Pw \tag{2.10}$$

where M^l is the primary moment due to transverse loading before the axial load is applied and w is the total lateral deflection. In order to ensure a safe design, it is necessary to find the maximum moment by solving the differential equation of the beam-column with the proper boundary conditions at the ends. However, for design purposes it is more convenient to use a simplified approach. On the assumption that the maximum moment occurs at or near the mid-span, use of Eq. (1.1) in Eq. (2.10) yields for bending moment

$$M = M^l + P\left(\frac{P_E}{P_E - P}\right)w^l \tag{2.11}$$

where w^l is the primary deflection produced by the primary moment alone. Since w^l is a linear function of M^l, this can be written

$$M = M^{l}\left(\frac{1+\psi\dfrac{P}{P_E}}{1-\dfrac{P}{P_E}}\right) \tag{2.12}$$

where $\psi = \dfrac{w^{l}P_E}{M^{l}} - 1$. This allows a more generalised interaction formula to be written

$$\frac{P}{P_u} + \frac{C_m M^{l}}{M_u\left(1-\dfrac{P}{P_E}\right)} \leq 1 \tag{2.13}$$

in which

$$C_m = 1 + \psi\frac{P}{P_E} = 1 + \frac{P}{P_E}\left(\frac{w^{l}P_E}{M^{l}} - 1\right). \tag{2.14}$$

Several investigators compared the interaction formula of Eq. (2.8) with available experimental and numerical results for both eccentrically and laterally loaded beam-columns and generally they observed a good agreement.

Ballio and Campanini[27] in 1981, used a computer program to examine 1000 cases simulated the behaviour of beam-columns hinged at their ends, with different slenderness ratios, section properties or loading patterns. For all cases a sinusoidal geometric imperfection of ***L/1000*** was considered. The results were checked against the interaction formula, which, was found to be conservative in some cases and non-conservative in some others.

2.5 Design Formula for Ultimate Capacity

For the analysis and design of beam-columns most of the design codes make use of interaction formulae. In the case where equal end moments are applied on a

beam-column, the ECCS[28] recommendations introduce the equation

$$\frac{P}{P_y} + \frac{M_o + Pe^*}{M_p(1 - P/P_E)} \leq 1 \qquad \textbf{(2.15)}$$

where e^* is a notional eccentricity which accounts for all imperfections and M_o is a linear bending moment.

The value of e^* is obtained from Eq. (2.15) in the absence of bending moment M_o where P is the axial compression capacity of the column obtained from appropriate **ECCS** column design curves. The expression for e^* is

$$e^* = \frac{M_p}{P_y}\left(\frac{P_y}{P_p} - 1\right)\left(1 - \frac{P_p}{P_E}\right) \quad . \qquad \textbf{(2.16)}$$

Nethercot and Taylor[29] in 1977, simplified Eq. (2.15), which was then included in the revised BS 449. The new interactive formula, having the form

$$\frac{P}{P_p} + 0.5 \cdot \frac{P}{P_p} \cdot \frac{M_o}{M_p} + \frac{M_o}{M_p} \leq 1 \qquad \textbf{(2.17)}$$

is today being used in BS 5950[30].

In the case of unequal end moments, the codes use the concept of the equivalent uniform moment factor, where, M_o in Eqs. (2.7), (2.15) and (2.17) is replaced by $M_{eq} = C_m M_o$, in which M_o is the maximum end moment. In BS 5950 the expression for C_m is

$$C_m = 0.57 + 0.33\beta + 0.10\beta^2 \geq 0.43 \qquad \textbf{(2.18)}$$

The concept of equivalent uniform moment factor is also employed for the cases of laterally loaded beam-columns.

The European recommendations assume

$$M_{eq} = | M_{eq1} + M_{o1} | \tag{2.19}$$

where M_{eq1} is the equivalent moment due to end moments in the absence of transverse forces whereas M_{o1} is the largest bending moment due to transverse loading only. M_{o1} can be determined if the column is considered as simply supported without end moments. If M_{o1} has an opposite sign of the maximum end moment, or the absolute value of M_{o1} is less than twice the absolute value of this end moment, the ECCS assumes $M_{o1} = 0$.

Comparisons between the interaction formulae show some minor discrepancies between them. This might be due to the fact that, depending on the geometry of the member and its loading conditions, there is always a minor degree of inaccuracy, ascribed to various reasons, some of which are described below.

(a) Case of equal end moments : For very small slenderness ratios, λ, where there is no problem of elastic stability, the ECCS interaction formula becomes

$$\frac{P}{P_y} + \frac{M_o}{M_p} = 1 \tag{2.20}$$

whereas the corresponding from BS 5950 is

$$\frac{P}{P_y} + 0.5 \cdot \frac{P}{P_y} \cdot \frac{M_o}{M_p} + \frac{M_o}{M_p} \leq 1 \tag{2.21}$$

In a non-dimensional plot of P/P_y versus M/M_y Eq. (2.20) represents a straight line, and Eq. (2.21) a concave curve; however, a numerical solution provides a convex curve. This means that both formulae underestimate the ultimate load as the slenderness decreases. The degree of conservatism depends on the cross section shape and can be more than 60%. Fig. 2-1 shows the solution obtained from Eq.

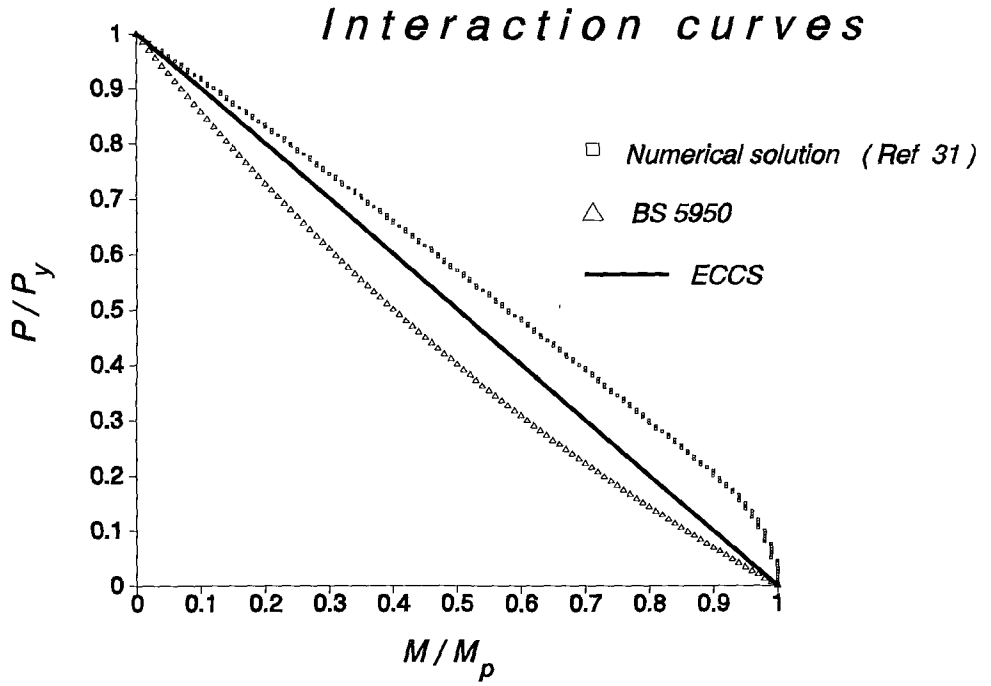

Figure 2-1

(2.20) and (2.21) in comparison with a numerical solution[31] obtained for the case of H section buckling about its weak axis.

As the slenderness ratio λ increases, the elastic instability effects start to appear. Curves obtained numerically tend to gradually change form, from the concave (low λ) into convex (high λ), whereas Eqs. (2.7), (2.15) and (2.17) predict a concave behaviour. The degree of this change depends on the amplification factor $P_E/(P_E-P)$, which converts the primary moments into total moments. Fig. 2-2 shows the change of this factor in comparison with its theoretical form[32], where, as the load increases, approaching the Euler load, its value becomes less conservative. Hence the degree of conservatism decreases when the slenderness increases. Even though the overall design may still be safe (except for high slenderness ratios), there is not a uniform degree of safety in every case of slenderness.

(b) Case of unequal end moments : In this case the resulting equivalent

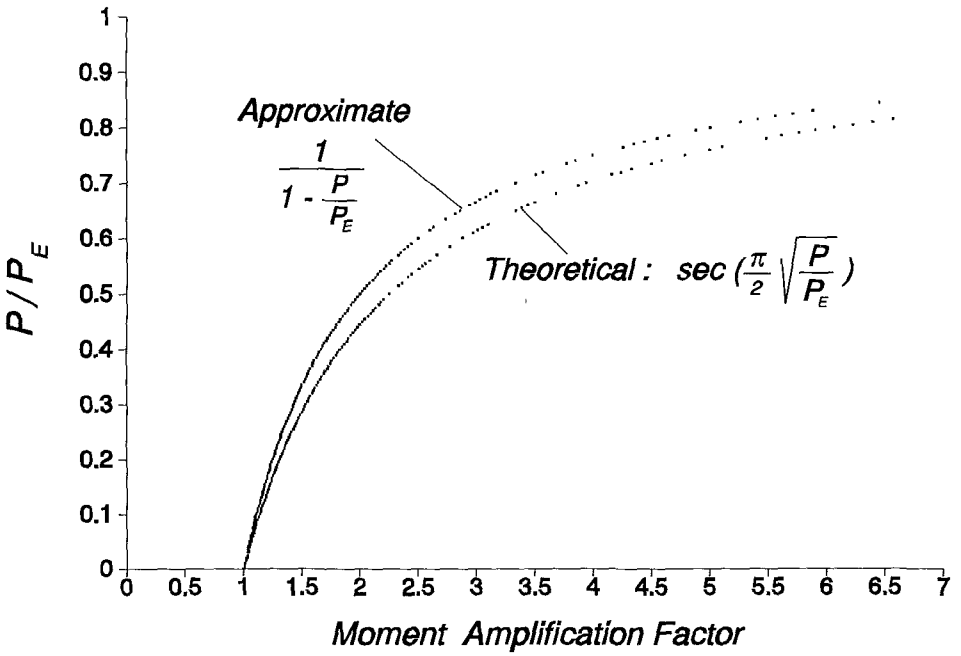

Figure 2-2

uniform moment $M_{eq} = C_m M_o$ is independent of the applied axial load and consequently the interaction given by equations (2.7), (2.15) and (2.17), if M_o is replaced by M_{eq}, does not relate to that defined by equations (2.20) an (2.21). This event combined with the fact that C_m is always less than unity, implies that the use of interaction formulae for low axial load, even for high slenderness ratios, may not lead to safe results.

A second limiting interaction relationship can be found on the basis that the plastic hinge will form at the end of the column with the highest bending moment. Therefore the following inequality must be satisfied,

$$M_o \leq M_{pc} \tag{2.22}$$

where M_{pc} is the plastic moment capacity of the column in the presence of axial load. The relation between M_{pc} and axial load can be found by statics.

Where the first interaction formula is used to predict the strength of a beam-column, C_m often underestimates the bending moments. This, coupled with the non-conservative nature of C_m, despite the conservative nature of Eqs. (2.20) and (2.21), may result in an unsafe design.

(c) Case of transverse loading : In this case, with or without end moments BS 5950 assumes that in the relation $M_{eq} = C_m M_o$, M_o is the maximum value of the primary moments. No allowance is made for the shape of the primary moments diagram and C_m has been taken as unity. In the case of combined end moments, when the lateral load is relatively small the value of C_m should be approximated to the value obtained when the end moments act alone. But this is not usually the case.

In the European recommendations this shortcoming is partially overcome by the use of Eq. (2.19). Again no reference is made for the shape of the primary moment diagram caused by transverse loading.

2.5.1 Conclusion

Several interaction formulae have been introduced in this section with the aim of achieving a fit for numerical results. The lack of crucial information on each set of numerical or test results, caused inaccurate results to be obtained when the formula is applied to an extended range of variables and parameters, having an influence on the load carrying capacity of beam-columns.

The interaction Eq. (2.7) for example, formulated for an **I**-section column with two equal end moments bending about its major axis, was found to give overly conservative results for other loading patterns. It was also found that for a similar column bent about its minor axis, both overly conservative and in some cases non-conservative results might be obtained[33]. Introducing C_m, a factor to cover the influence that the shape of bending moment has on the load capacity for columns

under unequal end moments, was found to give unsatisfactorily results.

The approaches which rely on C_m, do not cover the problem of other situations, like those arising from a different type of loading pattern. One of the main parameters which influences the load carrying capacity of beams-columns is the loading pattern of the member. Different loading patterns generate different deformed shapes of the member. If on these shapes an initial unintentional geometric imperfection, either as out of plumbness or out of straightness is added, the action of an axial load causes higher values on the induced bending moments. The influence of this parameter can be adequately taken into account if the column is considered as having imperfections. This idea will be developed in this thesis.

2.6 Historical Developments of Frame Buckling

The discussion developed in the preceding sections concerned the behaviour of pinned columns which are under a general system of loading. In reality, however, columns rarely exist alone. They are usually components of frames connected with beams to build a monolithic construction. Due to the nature of connections an interaction is always developed between beams and columns. The simplest way to take account of the interaction between a column and the remainder of the rigid jointed multistorey frame where it is connected to is to consider the column as a beam-column which is restrained at both ends. The main differences which distinguish a pinned beam-column from a restrained one are the following:

a) If a perfect elastic pinned beam-column can carry the Euler load, a similar restrained one is able to carry a higher load when sway is prevented and a higher or lower load if sway exists. In the sway case the load is a function of the stiffness of the surrounding frame.

b) In a pinned beam-column any known end-moments and/or eccentricities remain the same while the axial load is increased. This is not the case, however in a similar restrained beam-column, where, these magnitudes change due to interaction

between the column and the remainder of the frame.

A review of the past work in the area of frame buckling has been provided by Massonet[34] and Johnston[35]. In designing of frames various procedures have been employed. Some of these procedures, where the frames have already been designed, involve a check for the instability limit load, whereas others are approaches where the design of the frame is modified to take into account any instability effects. More historical developments for these procedures can be found in the reference[36]. Here four of the main procedures which are now being used are summarized.

2.6.1 The Effective-Length Design Procedure

This procedure may be classified as a design method. When a frame is under a monotonically increasing loading at its joints, like in axially loaded struts, there will be no flexural deformation until the load level reaches a particular value, called the elastic critical load. For a perfect pinned column this is the Euler load

$$P_E = \frac{\pi^2 EI}{L^2} \tag{2.23}$$

In an effective-length design procedure the elastic critical load of a frame's column is compared with the Euler load of a similar pinned column. For this comparison the frame is modelled as a set of columns which are elastically restraint at their ends. On the assumption they remain elastic, their maximum load capacity is the elastic critical load. Eq. (2.23) may therefore be used to determine the critical load of the column in the frame by substituting the value of γL for L, where γ is defined as the effective length factor. The value of γ is a function of the stiffness of the frame surrounding the column. When sway of the frame is completely prevented, this value varies between 0.5 (both ends fixed) and 1 (pinned ends). For sway frames the value of γ may extend from 1 to infinity. Many attempts have been made in the past to

evaluate γ by means of alignment charts. BS 5950 makes use of the effective length charts suggested by Wood[37] in 1974.

If the effective length factor γ has been calculated, the critical load of any restrained column can be obtained as the Euler load of a similar pinned column of length γL.

In real structures columns are usually subjected to both axial loads and bending moments. The procedure in the effective length design requires the structure to be analysed under various combinations of loading using a linear analysis. Then the calculated axial load and end moments of each column are applied on a nominal pin-ended column of length γL. The interaction formulae given in Sections 2.4 and 2.5 are used to derive a suitable column section. A shortcoming arising from this procedure (apart from what has already been mentioned), is that the effect of reduction of the column's stiffness has been neglected.

In ECCS and BS 5950 this method is suggested for design of members under compression in non-sway frames. For sway frames BS 5950 suggests the same method, under the condition that the frame is taken to be under vertical loading and has been designed as a non-sway frame, so that the member stability should be checked. The ECCS accepts this method provided all the forces have been determined using a second order analysis.

2.6.2 The Amplified Sway Method

This method is a design method utilizing the isolated beam column approach. The forces and bending moments are calculated through a linear elastic analysis. In order to account for frame instability, the moments due to horizontal forces, which cause sway, are amplified by a factor. In BS 5950 this factor is given by $\lambda_{cr}/(\lambda_{cr}-1)$, where λ_{cr} is the elastic critical load factor, i.e. the ratio of the sway critical load to the axial load, and can be obtained by an approximate formula given

by Horne[38]. After the calculation of the increased forces and moments for each column, the member can be designed through the same procedure as that of isolated columns. Since the effect of frame instability has been incorporated in the amplification factor, the effective length of the column is taken as the one which results through the effective length factor. Additionally this standard requires that the frame is also checked as a non-sway frame under the actual vertical loadings, according to a procedure described later in section 8.4.

In AISC/LRFD[39] the amplified sway factor is recommended as

$$\frac{1}{1-\left(\frac{\Sigma P}{\Sigma H}\right)\frac{\Delta}{L}} \tag{2.24}$$

or alternatively

$$\frac{1}{1-\frac{\Sigma P}{\Sigma P_c}} \tag{2.25}$$

where ΣP and ΣH is respectively the sum of axial loads and shear forces acting on the storey, Δ is the translational deflection of the storey due to horizontal forces taken from linear analysis, L is the storey height and ΣP_c is the sum of $\pi^2 EI/(\gamma L)^2$, in which γ is the effective length factor of each column. The maximum moment in a member, as a result of sway, may be calculated from the primary moment using either of the above amplified factors, where the effect of member instability is also incorporated. Moments due to a linear elastic analysis for a non-sway frame are amplified through a factor $C_m/(1-P/P_c)$, where C_m is given from Eq. (2.14) and P_c as defined above. The two magnified moments are then summed together to give the total moment, M, which is used in an interaction formula. The ultimate strength interaction formulae are

$$\begin{aligned} &\frac{P}{P_p} + \frac{8M}{9M_p} \le 1 , \qquad \frac{P}{P_p} \ge 0.2 \\ &\frac{P}{2P_p} + \frac{M}{M_p} \le 1 , \qquad \frac{P}{P_p} < 0.2 \end{aligned} \tag{2.26}$$

where P_p is the compressive axial strength of the column proposed by design code with length γL obtained from effective length chart.

2.6.3 The Merchant-Rankine-Wood Formula

Fig. 2-3 shows the limiting stress for a pin-ended steel strut of mild steel having a nominal yield stress 250 N/mm^2. The heavy line of this figure implies that slender struts buckle elastically at stresses defined by BC whereas stocky struts collapse by yielding. Tests on real struts have shown that the ultimate stress lies somehow below the composite curve DBC in the region of B. A rough estimate of the ultimate stress may be obtained from the interaction formula

$$\frac{1}{\sigma} = \frac{1}{\sigma_E} + \frac{1}{\sigma_y} \tag{2.27}$$

This equation provides a transition curve between the two extreme cases. In stocky struts σ_E is large and σ approaches σ_y. In slender struts σ_E is small and $1/\sigma_y$ can be neglected in comparison with $1/\sigma_E$, leaving $\sigma = \sigma_E$.

Eq. (2.27) is known as the Rankine[40] formula and is represented in Fig. 2-3 by the broken line DC.

Merchant[41] in 1954, argued that instead of its component parts, the whole structure could be designed in a similar way to that of isolated columns. He suggested that the Euler load in Rankine's formula could be replaced by the elastic critical load of the structure and respectively the squash load by the rigid-plastic collapse load. The resulting modified formula for the design of a multi-story frame

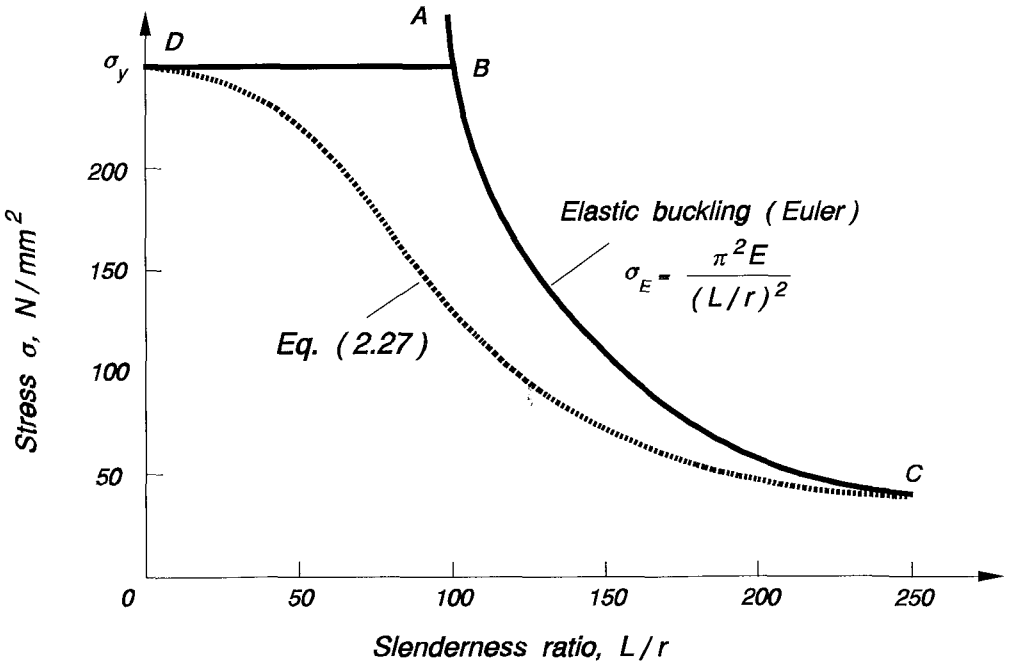

Figure 2-3

becomes

$$\frac{1}{\lambda_f} = \frac{1}{\lambda_p} + \frac{1}{\lambda_{cr}} \tag{2.28}$$

where λ_f is the failure load factor of an elastic-plastic structure, λ_p is the idealized rigid-plastic collapse load factor and λ_c is the elastic critical load factor. Horne[42] compared the Merchant-Rankine load with the results obtained from a series of tests on single bay model frames of 3, 5 and 7 stories, where he found that the formula provides a lower bound to the test results. For the purpose of avoiding too conservative results, Wood[37] modified the formula so that

$$\lambda_f = \frac{\lambda_p}{0.9 + \frac{\lambda_p}{\lambda_{cr}}} \qquad for \qquad 4 \le \frac{\lambda_{cr}}{\lambda_p} \le 10 \tag{2.29}$$

He suggested that for $\lambda_{cr}/\lambda_p \geq 10$, failure should be given by $\lambda_f = \lambda_p$ and also for $\lambda_{cr}/\lambda_p < 4$ an elastic-plastic second order analysis should be used.

The Merchant-Rankine-Wood formula is an empirical approach in which the effects of imperfections and different type of loading patterns are inadequately taken into account. Although this approach provides lower bound solutions for certain structures with particular imperfections, the experimental results depicted in Fig. 11 in reference 36 are quite scattered and considerably different from their theoretical prediction.

2.6.4 Second Order Elasto-Plastic Analysis

Unlike a first-order analysis in which the equilibrium relationships are written with respect to the original (undeformed) geometry, in a second order elasto-plastic analysis the equilibrium equations are written on the basis of the deformed geometry of the structure. This often entails an iterative type of procedure to obtain solutions. This is due to the fact that, during the formulation of the equilibrium relationships, the deformed geometry of the structure is not known. The analysis, thus, proceeds in a step-by-step incremental manner. This can be a highly non-linear situation and a fairly sophisticated computer program needs to be used to tackle the problem. Various approaches have been developed by many investigators described in reference 22.

This procedure might be useful for those structures whose member sizes are known in advance, and the objective is to check the load carrying capacity of the structure. In most cases, however, designers need to analyse and design structures whose member sizes are yet to be determined. In these cases, the method requires a number of trial steps to be implemented, where, the member sizes are revised after each step before the most appropriate set of sizes can be selected. This often requires a substantial amount of computational effort.

2.6.5 Conclusions

In this section various methods have been described for the analysis and design of rigid-jointed frames. Two of them, the Merchant-Rankine-Wood formula and the second order elasto-plastic analysis are considered as analysis approaches and can be used for frames whose member sizes are known in advance. Use of these methods for structures with unknown member sizes is a very difficult trial and error problem, and therefore time consuming. More appropriate methods in these cases are those which are classified as a design procedure.

In the effective-length method the structural members are inaccurately modelled with pin-ended beam-columns, where any end moments are calculated from a linear analysis in the whole structure. Therefore the loading conditions of a real structure are usually violated and consequently this modelling cannot effectively represent its behaviour. Apart from this shortcoming both the effective-length method and the amplified sway method use for design purposes the interaction formulae discussed in sections 2.4 and 2.5, the deficiencies of which have been discussed in Subsection 2.5.1. A brief summary of these deficiencies may be

a) For isolated beam-columns:

- vagueness in relating loading imperfections to the particular load, i.e. use of effective moment for unequal end moments;
- similar problems for lateral loading, i.e. the use of equivalent end moments;
- possible inadequacy of yield/failure criterion.

b) For columns in frames with no sidesway:

- all of the above, but in addition
- lack of clear definition of buckling mode and hence appropriate modal imperfections (both loading and geometric).

Chapter 3

Idealized Frame Models

3.1 The Concept of Buckling in Idealized Frame Models

In Chapter 2 a number of historical developments on beam-columns and frame buckling was discussed and various interaction formulae were presented. In this Chapter the buckling response on several possible idealized models, restricted or not against sidesway, will be examined. Consider the two structures in Fig. 3-1; structure (a) is a braced frame whereas in frame (b) there is a possibility of sidesway. Both structures have initially geometrically perfect members, which are

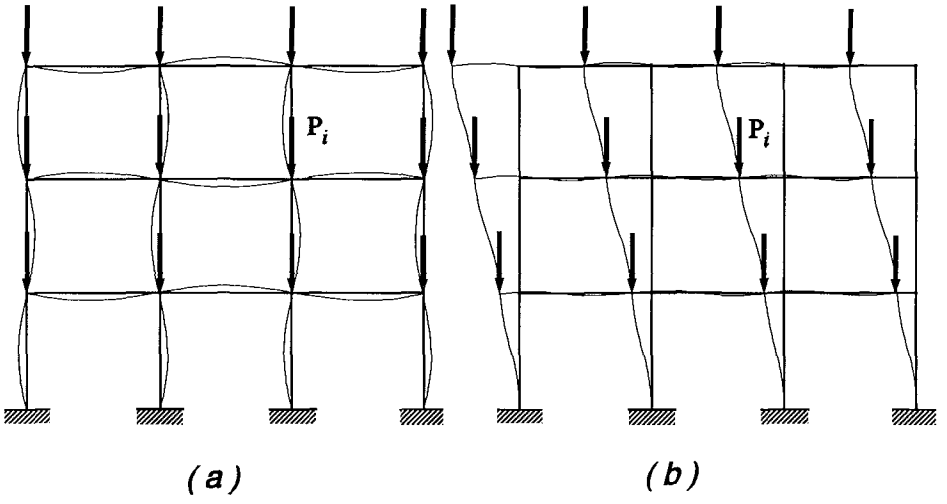

Figure 3-1

subjected to a set of point loads P_i at their joints. If the members remain elastic as loads are increased, there will be no flexural deformation until a particular level of loading is achieved. This load level is the so called 'elastic critical load', under which a bifurcation of equilibrium is possible. The buckling shape of the frames is shown by a thin line in figure 3-1.

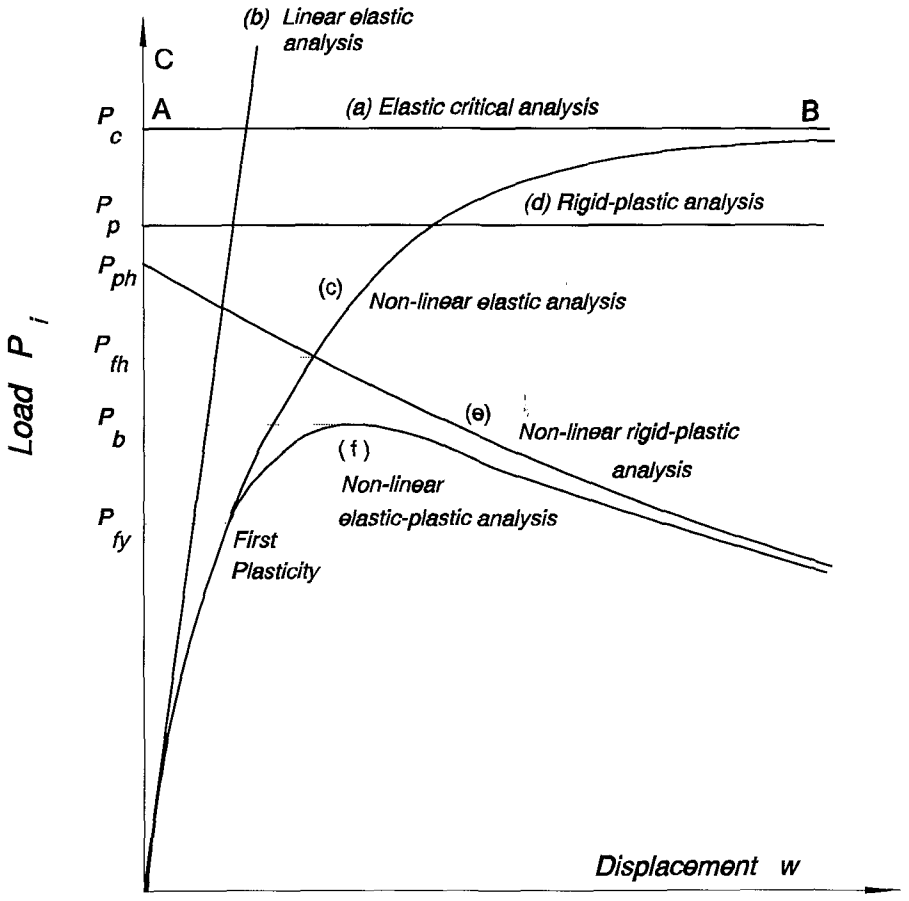

Figure 3-2

Fig. 3-2 demonstrates the lateral displacements w caused by the monotonically increased loads P_i. The mathematical solution of this model gives zero displacement up to the critical load P_{i_c} (point A). At this level the displacement becomes indeterminate following the path AB.

If the displacement at the bifurcation point A is prevented, the frame may sustain theoretically higher loads causing the curve following path AC. This results in another bifurcation of equilibrium at a higher load. Mathematically an infinite number of bifurcation points (elastic critical loads) may exist, giving each time a different buckled shape of the structure, called 'elastic critical mode' shape.

Depending on the bracing or not of the structure these shapes may be

different; in the first case they do not present any sway (horizontal displacement between the top and the bottom of the column) whilst in the second case, depending on the frame geometry, they present a sway mode at every pair of consecutive buckling modes.

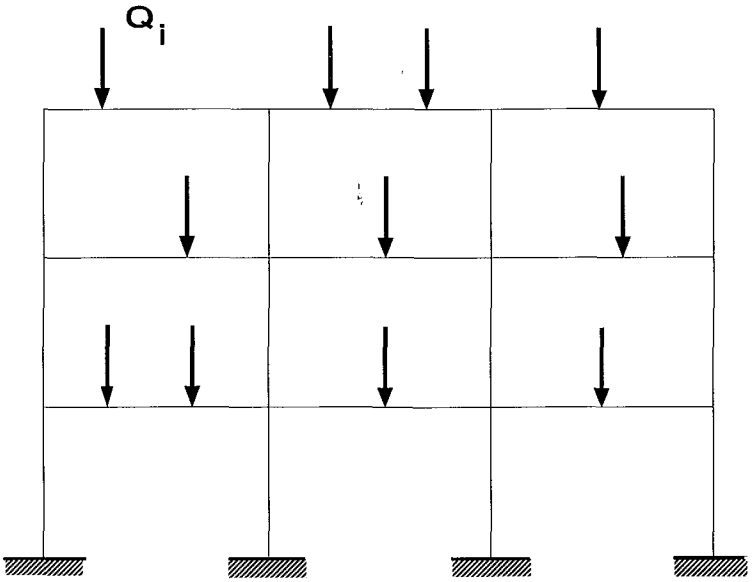

Figure 3-3

Consider now the structure of fig. 3-3 subjected to loads Q_i, monotonically increased and proportional to loads P_i. This causes the internal axial loads of columns to be also proportional to P_i. Such assumption is assumed to be valid in multistorey frames, where the important frame instability effects are due to the axial loads in the columns.

The load displacement curve for this structure would be as shown by curve (c) of Fig. 3-2 provided the material remained elastic at all locations. Here no bifurcation occurs and the frame will start to deform from the onset of loading. Curve (c) becomes asymptotic to curve (a) corresponding to the elastic critical load. The analysis followed to obtain curve (c) is a non-linear elastic analysis.

The actual state of loading of Fig. 3-3 may be thought of as the superposition of two loading cases. The one in Fig. 3-4a, consists of only the internal axial loads in the columns, which, from the elastic critical analysis point of view, reduces to that

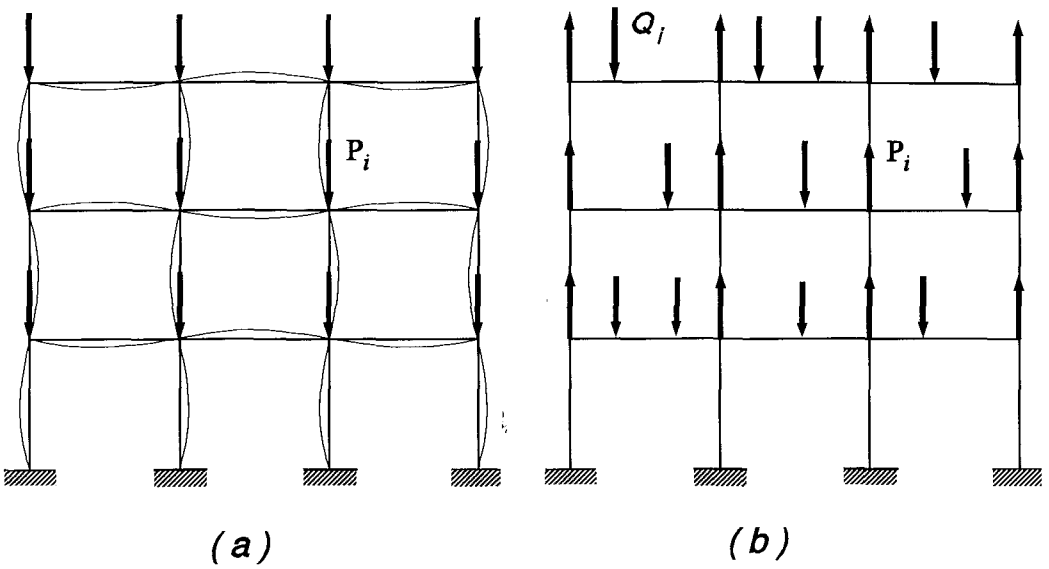

Figure 3-4

of Fig. 3-1; the other in Fig. 3-4b, consists of the actual state of loading, plus a locally self-equilibrating form of loading condition, such that no internal axial load is imposed on the columns. Superposition of the loads of Fig. 3-4(b) onto those of Fig. 3-4(a) will result in the actual case of Fig. 3-3.

For the load of Fig. 3-4(b) there will be no elastic critical load and the load-displacement relationship will be linear, shown by line (b) in Fig. 3-2. The analysis employed for this case is a linear elastic analysis.

Between curves (b) and (c) there is a difference in displacements at a given load level, which becomes larger as the load increases. This is due to the instability effects. In fact, in the case of fig. 3-4b, a state of pure bending is induced in the columns, which causes lateral deflections. These deflections are linear, and are intimately related to the linear bending moments in the absence of axial load. If the loading type of fig. 3-4a is acting in conjunction with the initial linear deflection of type 3-4b, it produces extra bending moment and, as a result, additional displacements. The situation is similar to that of a simply supported column which is originally bent.

The loading conditions which produce bending moments in the columns of

a frame can thus be thought of as an other kind of imperfections.

The above structures have been considered as perfectly elastic, without any effect of plasticity on their failure load. Taking plasticity into account, let us first assume that the structure of fig. 3-4b has a rigid plastic material. In this case a bifurcation of equilibrium takes place when the loads reach a certain value which may be less or greater than the elastic critical load. At this level of load enough plastic hinges form simultaneously and the structure becomes a mechanism, where no further increase of loading is possible. In the absence of axial load in the columns the load-displacement relation of fig. 3-2 is the horizontal line (d).

If the same rigid plastic material is considered for the structure as loaded in Fig. 3-3, the load-deflection curve will through a non-linear rigid-plastic analysis, be given by curve (e).

An idealized condition which is closer to the real behaviour of the structure is taken by considering that its material, under the type loading of Fig. 3-3, is elastic-plastic. The first part of the load-deflection curve is actually the first part of curve (c) until at a load level P_{fy} the structure will at some location have a stress that reaches the yield, initiating the increasing importance of plasticity. Further increase of load causes progressive plastic hinge formation and a resulting deflection which is greater than that occurring if the structure had behaved elastically. This load level is considered to be a close estimate to the buckling collapse load P_b, and the material has reached the last stage of its elastic-plastic behaviour which has already started since the initiation of yielding. After the buckling collapse load the curve (f) approaches asymptotically the non-linear rigid plastic curve (c). The aim of the non-linear elastic-plastic analysis is to estimate the buckling load, P_b, corresponding to the peak point of curve (f) in the load deformation curve of Fig. 3-2.

3.2 Idealized Non-sway Buckling Model

The design procedure outlined in chapter 2 assumes the structure to remain effectively elastic up to the point of failure. If the design criterion is the achievement of first yield in a structure (permissible stress design), it will be considered that all members of the structure have been design to reach first yield at the same load level; even if this criterion is the achievement of collapse (limit state design), it is still assumed that the structure has been designed to remain elastic up to this load, when plastic hinges will be formed in all columns simultaneously, whereas the beams still remain elastic. The first yield condition provides a lower bound solution whereas the latter criterion furnishes an upper bound solution for predicting the ultimate load of the structure.

The simplest way to isolate a column from the remainder of a non-sway structure such as Fig. 3-3, but take into account the interaction between them, is to consider a column as elastically restrained by rotational springs at both ends.

In Fig. 3-5 the free body diagram of the column is shown. The axial load P and the bending moments m_A^l and m_B^l are due to the action of the frame sustaining the applied loads and are obtained through a linear analysis (where the secondary effects of axial load are neglected). Local loads q^p and q^n which are proportional and non-proportional to the axial load might also act laterally to the column. In order to take into account the instability effects as well as the additional moment due to interaction of axial load and initial linear displacement, two rotational springs at the ends of the column are considered to have stiffnesses C_A and C_B; m_A and m_B are additional end moments which are produced when the axial load is applied and the member begins to deform.

Two other idealized models are shown in Fig. 3-6. The member in Fig. 3-6a is under axial load only, while there is no axial load in the member of Fig. 3-6b. In this way information about elastic critical loads and mode shapes can be obtained from case (a) while the loading imperfections may be determined from the loading condition of the case (b).

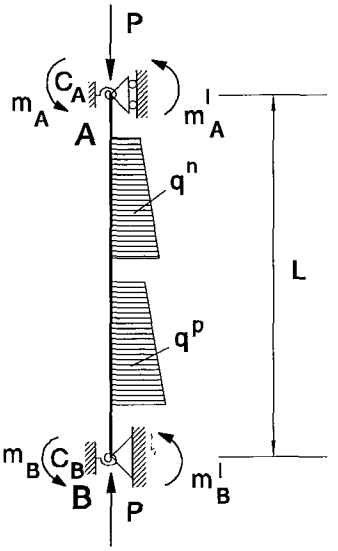

Figure 3-5

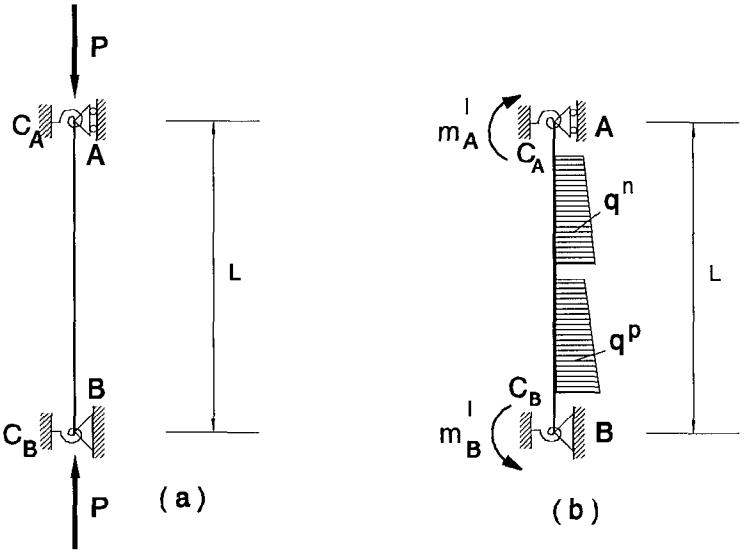

Figure 3-6

The load-displacement curves for these three models would be similar in form to those that have been drawn for the whole structure in Fig. 3-2. In this Figure, P is the axial load of the single column of each model, while P_b is the buckling load of the appropriate beam-column. The intersection between curves (c) and (e), denoted by a load level corresponding to P_{fh}, is obtained under the assumption that

the column remains elastic until the first plastic hinge occurs. This provides an upper bound solution for P_b; a lower bound solution for P_b is the level P_{fy}, at which the column starts to yield.

It is the estimation of these upper and lower bounds to the collapse load that will form the basis of design analysis developed in this thesis. For this, it is evident that the non-linear elastic response of curve (c) plays the vital role.

In order to obtain the non-linear elastic response of curve (c) in Fig. 3-2, the linear elastic response, given by curve (b) in Fig. 3-2, is a necessary first step along with the prediction of the elastic critical loads and the corresponding critical mode shapes, indicated by curve (a) in Fig. 3-2.

3.3 Linear Bending Analysis

When a structure is under a known system of loadings and the members are required to be determined, an estimate of member sizes has to be made in order to find the internal forces in each section. The size of each member may then be revised before the most appropriate set of member section sizes can be selected. So a number of trials may be made until the structure is designed. This procedure applying to both linear and non-linear elastic analysis, demands a substantial time of computer. Specially for the non-linear elastic analysis, it is not easy to perform a desk method, since the Eulerian differential equation, based on the deformed structure, has to be up-to-dated for each incremental displacement.

In the linear bending analysis, independently of the effects of axial loads on the rigidity of the members, the relationship between moment and curvature for each member is linear.

A most effective method of a linear analysis was the moment distribution method, introduced by Hardy Cross, in which the end moments in each member of a structure can be calculated by hand. The development of matrix methods in structural engineering combined with the availability of fast computers, allows today

an exact linear analysis to be performed in a fairly routine way. The procedure is based on the fact that the relationship between loads and its displacements of a structure is linear and can be written in a general matrix form as

$$[K_E]\{w\} = \{F\} \tag{3.1}$$

where $[K_E]$ is the flexural stiffness matrix, $\{w\}$ is a column matrix of displacements and $\{F\}$ is a column matrix of forces. Solving this equation for the unknown displacements enable moments and internal forces to be obtained.

The real values, however, for the internal forces of a beam-column may be very different from those predicted by a linear analysis. This is because in the calculation of bending moments, the additional deflections and hence the additional bending moments due to interaction between axial load and displacements, are neglected. However, a safe and economical design has always to take these moments into account because they provide the basis for the initial imperfections.

3.4 Elastic Critical Analysis of Columns without Sway

Consider the elastic perfect column of length L having rotational springs at both ends and subject to an axial load P as shown in Fig. 3-6a. Being a member of a rigid-jointed frame with no imperfection, column AB will not have any lateral deformation before the load reaches the elastic critical load P_c. At this stage a bifurcation of equilibrium takes place and a small lateral load will produce a bent shape that does not disappear when the lateral load is removed. The deformation of the column will be resisted by the two rotational springs, which produce the moments m_A and m_B at the ends, as indicated in Fig. 3-7.

Since the column does not sustain any lateral loads along its length, the differential equation for its deflected form is

$$EIw^{iv}(x) + Pw''(x) = 0 \tag{3.2}$$

where $w^{iv}(x)$ and w'' are the fourth and second derivatives of the displacement $w(x)$. This equation is a homogeneous linear differential equation of the fourth order and is valid for any type of end condition. Its general solution involving four arbitrary constants takes the form

$$w(x) = A_1\sin(kx) + A_2\cos(kx) + A_3\frac{x}{L} + A_4 \tag{3.3}$$

where constants A_1, A_2, A_3 and A_4 are determined from the end boundary conditions, and k is given by

$$k = \sqrt{\frac{P}{EI}} \, . \tag{3.4}$$

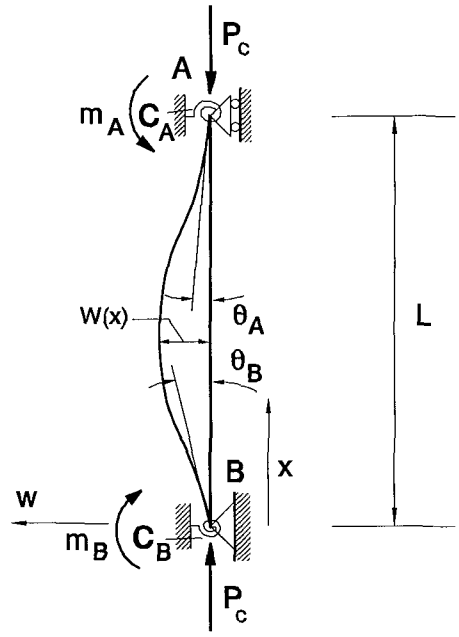

Figure 3-7

For the determination of constants the conditions of restraints at both ends of the member will be considered. At both ends the displacement is zero at the supports, so that

$$w(0) = w(L) = 0 \, . \tag{3.5}$$

Two further conditions relating the resistant moment from the spring stiffnesses (C_A, C_B) to the rotations (θ_A, θ_B) are given as

$$\begin{aligned} m_A &= C_A\theta_A \qquad & EIw''(L) &= C_A w'(L) \\ & \quad or & & \\ m_B &= C_B\theta_B & EIw''(0) &= -C_B w'(0) \end{aligned} \tag{3.6}$$

where

$$\left[\frac{dw}{dx}\right]_{x=L} = \theta_A \;, \quad \left[\frac{dw}{dx}\right]_{x=0} = -\theta_B \tag{3.7}$$

Combining equation (3.3) with the relevant four end conditions, a set of four linear, homogeneous equations in the constants A_1, A_2, A_3, and A_4 are obtained. For arbitrary values of k, and hence P, these equations are satisfied only when A_1 to A_4 are zero, showing that the displacement w is zero and the column remains straight. In order to have a deflecting configuration of equilibrium, that is non-trivial solutions of this set of equations, the determinant $\Delta(k)$ of the coefficient matrix has to be equal to zero. The condition $\Delta(k) = 0$ furnishes an equation for the parameter k, which is the only unknown in this equation. Actually, this equation, being transcendental in k, gives an infinite number of roots k_{ci} $(i = 1,2,..)$ referred to as the characteristic values of the parameter k, which define, through Eq. (3.4), an infinite number of critical loads $P_{ci} = EIk_{ci}^2$. The four constants A_{1i}, A_{2i}, A_{3i} and A_{4i} associated with the characteristic value k_{ci} of the i^{th} critical load can be obtained by introducing the value k_{ci} into the four boundary condition equations. Since the determinant of the coefficients of these equations is zero, this leaves only three independent equations for four unknowns. Taking one of the unknowns, A_{1i}, as an arbitrary constant value and calculating the other in terms of this value, a set of ratios

$$\bar{A}_{2i} = \frac{A_{2i}}{A_{1i}}, \quad \bar{A}_{3i} = \frac{A_{3i}}{A_{1i}}, \quad \bar{A}_{4i} = \frac{A_{4i}}{A_{1i}} \tag{3.8}$$

allows the critical mode shape to be determined. Substituting these values into Eq. (3.3), the deflection function of the buckled column associated with k_{ci} is obtained as

$$w_i(x) = A_{1i}\left[\sin(k_{ci}x) + \bar{A}_{2i}\cos(k_{ci}x) + \bar{A}_{3i}\frac{x}{L} + \bar{A}_{4i}\right]. \tag{3.9}$$

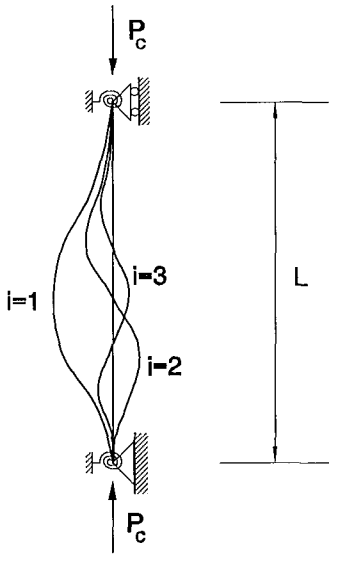

Figure 3-8

This deflection function is indeterminate as to magnitude, (A_{1i} remains an arbitrary constant), but is definite as to shape, since the function in brackets, the so called characteristic function of the i^{th} critical mode, $\phi_i(x)$, is known. The elastic critical loads P_{ci} are thus defined in terms of characteristic values of k_{ci} of an eigenvalue problem whose characteristic functions are the critical modes $\phi_i(x)$. The critical mode shapes of a beam-column with rotational restraints at its ends is shown in Fig. 3-8.

The calculation of the elastic critical load of the column given in Fig. 3-7 is based on the condition $\Delta(k) = 0$. Assuming the rotational springs have linear characteristics, the former condition results in

$$\left[\frac{k_cL}{\tan(k_cL)} - \frac{(k_cL)^2}{r_A} - 1\right]\cdot\left[\frac{k_cL}{\tan(k_cL)} - \frac{(k_cL)^2}{r_B} - 1\right] = \left[1 - \frac{k_cL}{\sin(k_cL)}\right]^2 \tag{3.10}$$

where $$r_A = \frac{C_A L}{EI}, \qquad r_B = \frac{C_B L}{EI} \quad .$$

If the values of C_A and C_B are known, the roots of Eq. (3.10) in terms of k_{ci} will provide for this column, the elastic critical loads $P_{ci} = EIk_{ci}^2$.

The solution of this non-linear equation is usually realised through charts relating k_c to r_A and r_B. For simplicity reasons, in most codes of practice, the stability of the restrained column is compared with the stability of a simply supported column of effective length $L_e=\gamma L$, in which γ is the so called effective length factor and can be calculated under the assumption that the elastic critical load of the restrained column, P_c, is equal to the Euler load, P_E, of this simply supported column, so that

$$P_E = \frac{\pi^2 EI}{(\gamma L)^2} = EIk_c^2 = P_c \qquad \textbf{(3.11)}$$

yielding

$$k_c L = \frac{\pi}{\gamma} \quad . \qquad \textbf{(3.12)}$$

Substituting (3.12) into (3.10) allows the effective length factor of a column with both ends rotationally restrained to be found in terms of r_A and r_B. In most codes of practice a set of effective length charts are often employed to give the effective lengths of columns with ends rotationally restrained.

In the case of equal rotational restraint at both ends of the column, so that $C_A = C_B = C$, Eq. (3.10) is reduced to

$$\frac{k_c L}{\tan(k_c L)} - \frac{EI}{LC}(k_c L)^2 - 1 = \pm\left[\frac{k_c L}{\sin(k_c L)} - 1\right], \qquad \textbf{(3.13)}$$

from which two forms of buckling configuration may occur:

a) The **symmetric** shape, coming from the positive right-hand-side, may easily be shown to yield

$$\frac{\tan\left(\frac{k_c L}{2}\right)}{\frac{k_c L}{2}} = -\frac{2EI}{LC}, \tag{3.14}$$

which is a result already familiar from the 'Elastic Buckling of Columns and Frames', [Eq. (2-10) of Appendix C] and

b) The **antisymmetric** shape from the negative right-hand-side, which,

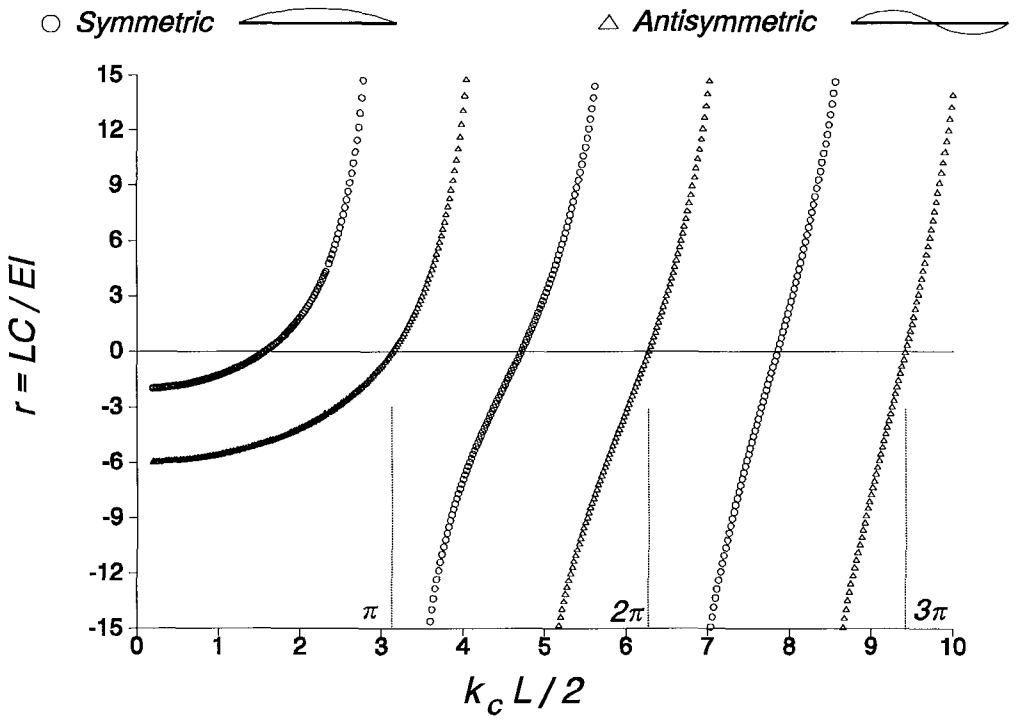

Figure 3-9

similarly gives the equation

$$\frac{1}{\tan\left(\frac{k_c L}{2}\right)} = \frac{2EI\left(\frac{k_c L}{2}\right)}{LC} + \frac{1}{\frac{k_c L}{2}}, \tag{3.15}$$

again familiar, from the same theory [Eq. (2-11) in Appendix C].

Introducing the notation $r = \frac{LC}{EI}$, the solutions for the first three critical modes $(0 - 3\pi)$ of $\frac{k_c L}{2}$, coming from equations (3.14) and (3.15) can be given for both shapes (symmetric and antisymmetric) in a graphical form for varying r, as shown in Fig. 3-9.

3.5 Critical Mode Shapes of Non-sway Columns

Harmann[43] was the first to realise that the elastic buckled shape of an axially loaded, originally straight bar having any end conditions is a sine wave. Ayrton and Perry[4] in their analysis had already assumed that the configuration of the geometric imperfection is a half sine wave, which is exactly the shape of the first critical mode of a simply supported column.

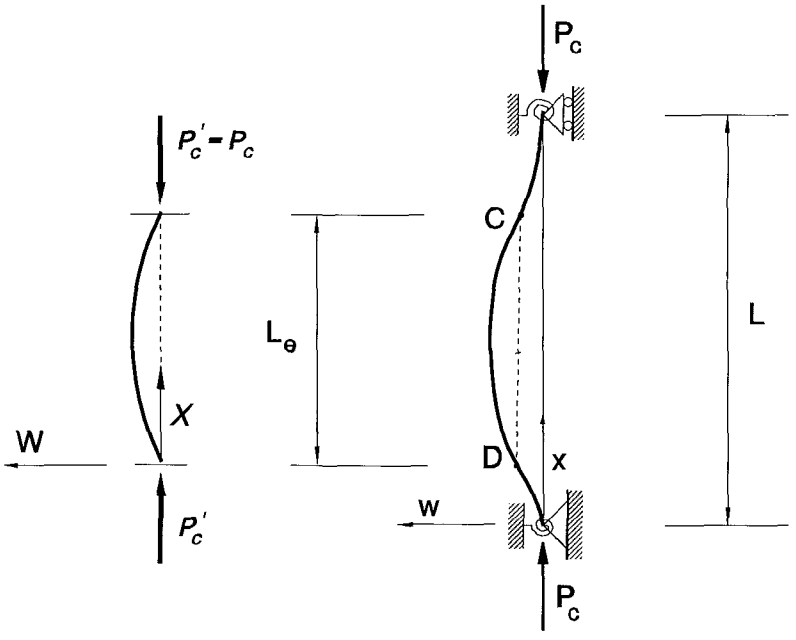

Figure 3-10

In the buckled shape of the restrained column in Fig. 3-10 there are two

points of contraflexure, C and D. At these points there is no resistant against rotation, and the resultant forces and moments at each end of the column should pass through them. The free body diagram of the part CD holds two axial loads, P_c', at the ends and its behaviour is similar to that of a simply supported axially loaded column. The elastic critical load is thus the Euler load of a column with length L_e, i.e.

$$P_c' = \frac{\pi^2 EI}{L_e^2} . \tag{3.16}$$

The angle of CD with the vertical is infinitesimally small, so P_c' is assumed to be equal to P_c In the above formula L_e is the effective length of the column, which therefore has the meaning of the portion of the column that lies between two adjacent points of contraflexure in the column's deflected shape.

If P_E is the Euler load for the pinned column of length L, the elastic critical load P_c can be written in the form

$$P_c = \frac{\pi^2 EI}{(\gamma L)^2} = \frac{P_E}{\gamma^2} \tag{3.17}$$

in terms of the effective length factor γ, whose mathematical value, is thus,

$$\gamma = \sqrt{\frac{P_E}{P_c}} \tag{3.18}$$

The deflected shape of the column with respect to the (X,W) axes is

$$W(X) = A\sin\left(\frac{\pi X}{L_e}\right) . \tag{3.19}$$

This equation is valid not only for the portion CD of the column but also for its

entire length.

3.6 Elastic Critical Analysis of Columns with Sway

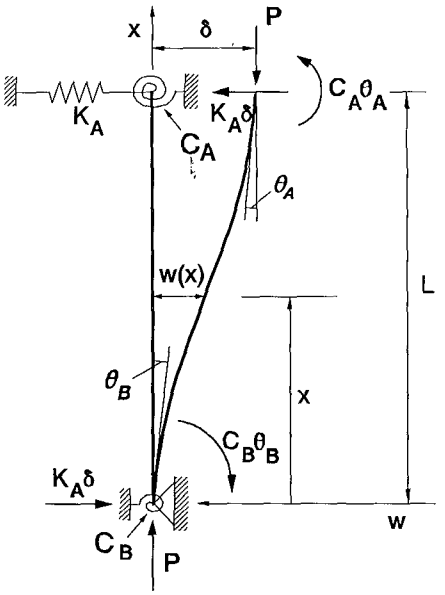

Figure 3-11

A more general case for a perfectly straight column elastically restrained against rotation at both ends and against translation at the top is considered in Fig. 3-11. In this case, the rotational end restraints are again achieved by rotational springs with spring constants C_A and C_B while the top restraint against translation is accomplished by a translational spring with spring constant K_A. From the buckling configuration, shown in the same figure, the differential equation for the deflection curve is

$$EI\frac{d^2w}{dx^2} = -M \tag{3.20}$$

where

$$-M = P(\delta - w) - K_A\delta(L - x) - C_A\theta_A \ . \tag{3.21}$$

Substitution for M in (3.20) yields the governing differential equation

$$EI\frac{d^2w}{dx^2} + Pw = K_A\delta x + \delta(P - K_AL) - C_A\theta_A \ , \tag{3.22}$$

which, for $k = \sqrt{\frac{P}{EI}}$, has the general solution

$$w = C_1 \sin kx + C_2 \cos kx + \frac{K_A\delta}{P}x + \delta\left(1 - \frac{K_AL}{P}\right) - \frac{C_A\theta_A}{P} \ . \tag{3.23}$$

The boundary conditions require

$$\begin{aligned} w(0) &= 0 \ , \qquad w(L) = \delta \\ \left.\frac{dw}{dx}\right|_{x=0} &= \theta_B \ , \qquad \left.\frac{dw}{dx}\right|_{x=L} = \theta_A \end{aligned} \tag{3.24}$$

where

$$\theta_B = \frac{P\delta - K_A\delta L - C_A\theta_A}{C_B} \ . \tag{3.25}$$

Applying the preceding conditions in (3.23) yields

$$\begin{bmatrix} 0 & 1 & 1 - \frac{K_AL}{P} & -\frac{C_A}{P} \\ \sin kL & \cos kL & 0 & -\frac{C_A}{P} \\ k & 0 & \frac{K_A}{P} - \frac{P}{C_B} + \frac{K_AL}{C_B} & \frac{C_A}{C_B} \\ k\cos kL & -k\sin kL & \frac{K_A}{P} & -1 \end{bmatrix} \begin{bmatrix} C_1 \\ C_2 \\ \delta \\ \theta_A \end{bmatrix} = \begin{bmatrix} 0 \\ 0 \\ 0 \\ 0 \end{bmatrix} \tag{3.26}$$

In order to have a non-trivial deflected shape of equilibrium, the determinant of the

coefficients of the system must be equal to zero. Introducing the non-dimensional notation

$$t = \frac{K_A}{EI/L^3} \quad and \quad r_i = \frac{C_i}{EI/L} \qquad (i = A, B) \tag{3.27}$$

the characteristic equation may be rewritten

$$\begin{vmatrix} 0 & 1 & 1-\dfrac{t}{(kL)^2} & -\dfrac{r_A}{(kL)^2} \\ \sin kL & \cos kL & 0 & -\dfrac{r_A}{(kL)^2} \\ kL & 0 & \dfrac{t}{(kL)^2}-\dfrac{(kL)^2}{r_B}+\dfrac{t}{r_B} & \dfrac{r_A}{r_B} \\ kL\cos kL & -kL\sin kL & \dfrac{t}{(kL)^2} & -1 \end{vmatrix} = 0 , \tag{3.28}$$

which, after developing and rearranging, leads to the general solution for the case shown in Fig. 3-11, i.e.

$$\frac{1}{(kL)^3}\left\{\left[(kL)^4-(kL)^2(r_A r_B+t)+r_B t(r_A-1)-r_A t\right]\frac{kL}{r_B}\sin kL - \right.$$
$$\left. -\left[(kL)^4(r_A+r_B)-(kL)^2 t(r_A+r_B)-2r_A r_B t\right]\frac{\cos kL}{r_B}-2r_A t\right\} = 0 . \tag{3.29}$$

In this equation, by putting t = 0, we obtain the simplified condition

$$\tan kL = \frac{kL(r_A+r_B)}{(kL)^2-r_A r_B} \tag{3.30}$$

which is the case of a column subjected to rotational restraints at both ends with uninhibited lateral sway. By setting $r_A = 0$ in Eq. (3.29) we obtain the condition

$$t = \frac{(kL)^2\left(1 - \frac{kL}{r_B}\tan kL\right)}{1 - \left(\frac{kL}{r_B} + \frac{1}{kL}\right)\tan kL}\ , \qquad \textbf{(3.31)}$$

which is the case of a column subjected to a rotational restraint at one end and a translational restraint at the other.

Gurfinkel and Robinson[44] were the first to consider the analysis of the above case. In their theoretical approach, where the buckling behaviour of elastically restrained columns was taken into account, they reached up to Eq. (3.28). In the absence of substantial recommendations for an overall solution, a magnitude for the first critical load was provided through graphs, where, the value of kL could be obtained relating two of the given values r_A, r_B and t; this is because in their solution they considered a column subjected to one the following cases of restraints:

1) a rotational at both ends with uninhibited lateral sway and

2) a rotational at one end and a translational at the other end.

Considering the general case where all three restraints are present, for known values of r_A, r_B and t, the transcendental Eq. (3.29) yields an infinite number of values of kL. The critical loads can then be determined by the equation

$$P_{c_i} = (k_{c_i}L)^2\frac{EI}{L^2}\ . \qquad \textbf{(3.32)}$$

A computer program in FORTRAN, the basic steps of which are given in the Appendix G, has been developed to calculate the roots (values $\boldsymbol{k_{ci}L}$) of equation (3.29), leading thus in the calculation of the critical loads through Eq. (3.32).

Also two separate programs in BASIC, based on the Newton-Raphson approximation, have been made to verify the values of kL derived from section 3.4, for both the symmetric and antisymmetric shape, as well as the values of kL for the special case of Eq. (3.29), when the translational stiffness is infinity. The excellent agreement shows that the braced case of section 3.4 can well be considered as a

special case of section 3.6.

3.7 The Orthogonality Relations of Critical Modes

Consider a column with pinned, fixed or free ends. These end conditions, which are the most frequent in a structure, result obviously in two boundary condition equations, as follows

$$\begin{array}{llll} \textit{Pinned end} & w = 0 & \textit{and} & w'' = 0 \\ \textit{Fixed end} & w = 0 & \textit{and} & w' = 0 \\ \textit{Free end} & w'' = 0 & \textit{and} & EIw''' + Pw' = 0 \end{array} \qquad (3.33)$$

The characteristic functions which arise from the governing differential equation of a single member having any combination of the above boundary conditions have fundamental properties of outstanding importance known as *orthogonality relations*. For the critical modes these relations are given by Bleich[45] as

$$\int_0^L \phi_i'(x)\,\phi_j'(x)\,dx = 0 \qquad (3.34)$$

and

$$\int_0^L EI\,\phi_i''(x)\,\phi_j''(x) = 0 \qquad (3.35)$$

where x is the distance along the member and $\phi_i(x)$, $\phi_j(x)$ are two different characteristic functions associated respectively with the i^{th} and j^{th} critical modes. The primes indicate differentiation with respect to x while *EI* is the flexural rigidity - not necessarily uniform - along the member.

For each critical mode a normalizing relation between the characteristic function $\phi_i(x)$ and the corresponding elastic critical load P_{ci} can be written as

$$\int_0^L EI\phi_i''^2(x)dx = P_{ci}\int_0^L \phi_i'^2(x)dx \quad . \tag{3.36}$$

The validity of the orthogonal relations for the characteristic functions of a plane elastic frame were verified by Ariaratnam[46] and completed by Horne[47] for more general cases. For a plane elastic frame the orthogonality relations are similarly

$$\sum_M P\int_0^L \phi_i'(x)\phi_j'(x)dx = 0 \tag{3.37}$$

$$\sum_M \int_0^L EI\phi_i''(x)\phi_j''(x)dx = 0 \tag{3.38}$$

while the normalizing relation is

$$\sum_M \int_0^L EI\phi_i''^2(x)dx = \sum_M P_{ci}\int_0^L \phi_i'^2(x)dx \tag{3.39}$$

where $\sum_M$ denotes summation for all members, while P and P_{ci} are the axial and the corresponding critical load of each member of the frame. The first relation (3.33) was found to be valid for any structure having a linear elastic behaviour at its supports whilst the second one (3.34) was found to be valid only for those structures that are pinned, fixed or free ended.

It can be shown that the critical mode shapes $\phi_i(x)$ corresponding to all critical loads P_{ci} (i=1,2,...) form a complete set of orthogonal functions. We may therefore expand any arbitrary deflected configuration w, satisfying the same geometric boundary conditions like the functions $\phi_i(x)$, as an absolutely and uniformly convergent series of the form

$$w = \sum_{i=1}^{\infty} w_i\phi_i(x) \tag{3.40}$$

where w_i is an amplitude factor associated with the i^{th} critical mode.

Chapter 4

The Non-linear Elastic Response

Theoretical background

4.1 Introduction

In the preceding chapter an elastic critical analysis of idealised buckling models with and without sway has been discussed. This chapter will be focused on the general concept of imperfections, as the primary reason for a non-linear elastic response of a beam-column.

When a structure is subjected to a system of forces, its members will in reality start to bend from the onset of loading. This is due to the inevitable imperfections which originate from either the initially out-of-straight form of members or the material and loading conditions of the structure. These imperfections are generally classified as geometric or loading imperfections. Structural imperfections due to cooling process of hot-rolled steel members or welding usually cause stresses to be locked into the structural members and are often a cause of geometric imperfections when the member is cut and locked in stresses are released.

The loading imperfections may be divided into two categories; these are the proportional loading imperfections and the non-proportional loading imperfections, with the distinction depending on whether the loads producing the imperfection are proportional to or independent to the axial loads.

When the effect of axial load on the stiffness of the structure is ignored, the load - displacement relationship in the structure is linear. The existence of imperfections, however, along with the axial loads, results in a non-linear relationship between load and displacement. The objective of this chapter is to relate the non-linear elastic response of the structure to its linear one through a simple and

general formula.

4.2 Geometric Imperfections

Consider the column in Fig. 4-1 as a component of a rigid frame with an initial deflection $w^o(x)$. Under the axial loads P the column deflects even more. Let $w(x)$ be the incremental displacement caused by the application of the axial load shown in the same figure.

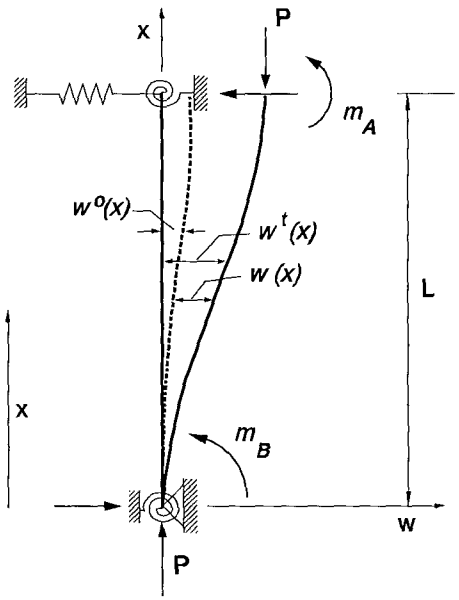

Figure 4-1

If $\phi_i(x)$ (i=1,2,3,...) are the characteristic functions of the critical modes, the initial deflection can be expressed, in terms of the set of orthogonal deflections, in the form

$$w^o(x) = \sum_{i=1}^{\infty} w_i^o \phi_i(x) \quad , \tag{4.1}$$

where w_i^o is an unknown amplitude factor, termed as modal geometric imperfection.

The total deflection of the column, $w^t(x)$, produced when the axial load is applied, is given by the equation

$$w^t(x) = \sum_{i=1}^{\infty} w_i^t \phi_i(x) \quad , \tag{4.2}$$

where w_i^t is the amplitude factor of the modal **total** displacement. The differential equation of equilibrium in this case takes the form

$$EI\left[w^{t\,iv}(x) - w^{o\,iv}(x)\right] + P w^{t\,//}(x) = 0 \quad , \tag{4.3}$$

where *iv* denotes the fourth differentiation of displacements with respect to x, measured from one end of the member. Substituting Eqs. 4.1 and 4.2 into 4.3 we obtain

$$EI\sum_{i=1}^{\infty} w_i^t \phi_i^{iv}(x) - EI\sum_{i=1}^{\infty} w_i^o \phi_i^{iv}(x) + P\sum_{i=1}^{\infty} w_i^t \phi_i^{//}(x) = 0 \quad . \tag{4.4}$$

The critical mode shape $\phi_i(x)$ corresponding to the critical load P_{ci} will obviously satisfy the Eulerian differential equation

$$EI\phi_i^{iv}(x) + P_{ci}\phi_i^{//}(x) = 0 \quad . \tag{4.5}$$

Substitution of $\phi_i^{iv}(x)$ from Eq. (4.5) into (4.4) gives

$$\sum_{i=1}^{\infty} P_{ci} w_i^o \phi_i^{//}(x) - \sum_{i=1}^{\infty} P_{ci} w_i^t \phi_i^{//}(x) + P\sum_{i=1}^{\infty} w_i^t \phi_i^{//}(x) = 0 \quad . \tag{4.6}$$

If Eq. (4.5) is multiplied by $\phi_j(x)$ and integrated over the whole length, through the orthogonality relations $\int \phi_i' \phi_j' dx = 0 \quad i \neq j$ between the critical modes,

it can be proved, that equation (4.6) is satisfied for each separate mode, i.e. for the i^{th} term,

$$w_i^t = \frac{P_{ci}}{P_{ci}-P} w_i^o \qquad (i = 1, 2, 3, ...) \quad . \tag{4.7}$$

In a similar way, the amplitude factor associated with the non-linear **incremental** deflection due to the axial load only, is given by

$$w_i = \frac{P}{P_{ci}-P} w_i^o \quad . \tag{4.8}$$

Substituting w_i^t from Eq. (4.7) into (4.2) we obtain the total displacement with respect to the undeformed state of a geometrically imperfect beam-column

$$w^t(x) = \sum_{i=1}^{\infty} \frac{P_{ci}}{P_{ci}-P} w_i^o \phi_i(x) \quad . \tag{4.9}$$

4.3 Loading Imperfections - Proportional Loading

Fig. 4-2 shows a beam-column which is under a lateral load q^p that is proportional to the axial load P. The column, is considered to be a member of a rigid-jointed frame which is also loaded proportionally. The frame, in resisting the applied load on the column, may result in two end moments m_A^p and m_B^p that are proportional to the axial load P. They can be obtained through a linear analysis (where the effect of axial load is neglected).

Application of axial load on the column results in additional moments and displacements. These additional moments, shown in the same figure as m_A and m_B, are due to the interaction between the axial load and the linear initial displacement.

The differential equation of equilibrium for the linear idealization case shown in Fig. 4-2a prior to the application of axial load is

$$EI(w^{p}(x))^{iv} = q^{p}(x) \quad , \tag{4.10}$$

where $w^{p}(x)$ is the linear displacement of the column in a proportional loading system. This linear deflection, in terms of characteristic functions of critical modes, can be expressed as

$$w^{p}(x) = \sum_{i=1}^{\infty} w_i^{p} \phi_i(x) \quad , \tag{4.11}$$

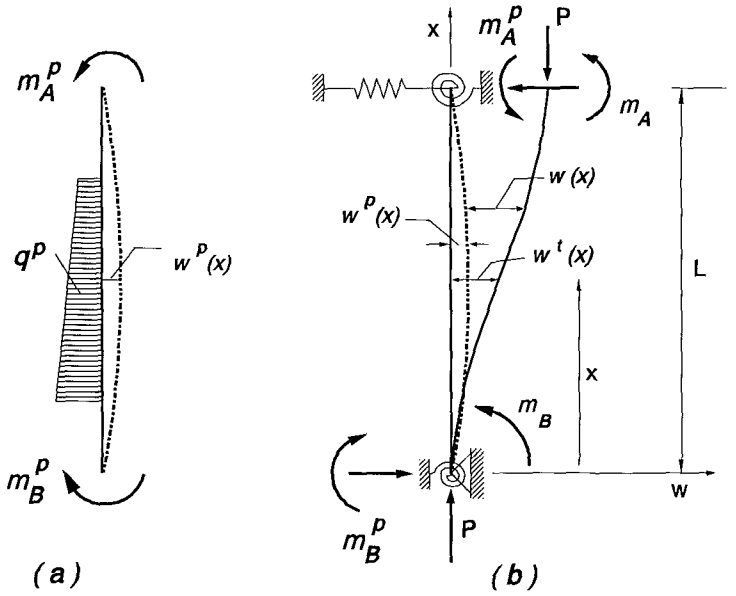

Figure 4-2

where w_i^{p} is the amplitude of the i^{th} critical mode in the linear displacement due to the same system of loading, termed as modal proportionate load imperfection. The differential equation for the case of complete loading, shown in Fig. 4-2b, becomes

$$EIw^{t^{iv}}(x) + Pw^{t''}(x) = q^{p}(x) \quad . \tag{4.12}$$

Putting $q^p(x)$ from Eq. (4.10) into (4.12) yields the equation

$$EI\left[w^{t\,iv}(x) - w^{p\,iv}(x)\right] + Pw^{t\,''}(x) = 0 \quad , \tag{4.13}$$

which is similar to Eq. (4.3), with $w^p(x)$ substituted for $w^o(x)$. Following the same procedure as that of section 4.2 and recalling the orthogonality relations, the i^{th} modal amplitude factors, w_i^t and w_i, for a proportional loading system are

$$w_i^t = \frac{P_{ci}}{P_{ci}-P} w_i^p \quad \text{and} \quad w_i = \frac{P}{P_{ci}-P} w_i^p \quad (i = 1, 2, 3, ...) \tag{4.14}$$

Making use of Eq. (3.40), with w_i expressed through (4.14), the total displacement of a perfect column, under a proportional-loading imperfection system, in terms of its linear displacement, is

$$w^t(x) = \sum_{i=1}^{\infty} \frac{P_{ci}}{P_{ci}-P} w_i^p \phi_i(x) \quad . \tag{4.15}$$

4.4 Loading Imperfections - Non-proportional Loading

The beam-column in this case is considered as a straight member of a rigid jointed frame but subjected to a lateral load which is not proportional to the axial load. The local beams connected to the column, may also have lateral loads that are independent from the axial load of the column. As a result, non-proportional end moments are induced on the column. During the loading procedure, it is assumed that the lateral loads on the local beams, together with any lateral load on the column, are applied prior to the application of the axial load.

In Fig. 4-3a the linearly deflected shape of such a beam-column is shown, where end moments and displacements $w^n(x)$ are produced. The differential

equation of equilibrium for this linear case may be written as

$$EI(w^n(x))^{iv} = q^n(x) \quad . \tag{4.16}$$

When the axial load is applied, additional displacements along with extra end moments m_A and m_B are produced to give the deflected shape of total loading shown in Fig. 4-3b. Since the linear deflection $w^n(x)$ satisfies the same geometric boundary conditions as the characteristic functions $\phi_i(x)$, it can be considered as an absolute and uniformly convergent series of the form

$$w^n(x) = \sum_{i=1}^{\infty} w_i^n \phi_i(x) \quad , \tag{4.17}$$

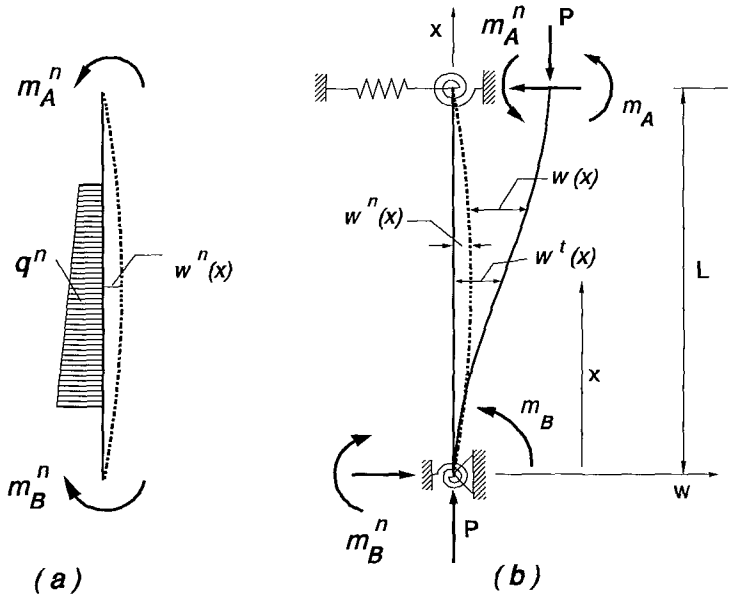

Figure 4-3

where w_i^n is the amplitude of the i^{th} critical mode representation of the linear displacement of the non-proportionally loaded system; this could be termed the modal non-proportionate load imperfection. The differential equation of equilibrium

for the complete loading case of Fig. 4-3b takes the form

$$EIw^{t\,iv}(x) + Pw^{t\,//}(x) = q^n(x) \quad . \tag{4.18}$$

Substituting $q^n(x)$ from Eq. (4.16) into (4.18) yields

$$EI\left[w^{t\,iv}(x) - w^{n\,iv}(x)\right] + Pw^{//}(x) = 0 \quad . \tag{4.19}$$

A procedure similar to that described in section 4.2 will give the modal displacements w_i^t and w_i for the i^{th} term of the non-proportional loading system

$$w_i^t = \frac{P_{ci}}{P_{ci}-P} w_i^n \quad \textit{and} \quad w_i = \frac{P}{P_{ci}-P} w_i^n \quad (i = 1, 2, 3, ...) \tag{4.20}$$

and the relationship between the total non-linear deflection $w^t(x)$ and the linear displacement $w^n(x)$

$$w^t(x) = \sum_{i=1}^{\infty} \frac{P_{ci}}{P_{ci}-P} w_i^n \phi_i^n(x) \tag{4.21}$$

4.5 General Case of Imperfections

The distinct cases of a certain kind of imperfection which so far have been examined, may be combined with each other, to give a general case of all possible kinds of imperfections. Consider a beam-column which is not originally straight but possesses an initial deflection $w^o(x)$. The column is subjected to a loading system q^p that is proportional to the axial load, along with another, non-proportional system of loading q^n. The load q^n, acting first alone, produces on the column a deflection $w^n(x)$, accompanied by moments $m^n(x)$. Similarly the load q^p, when applied, produces the corresponding amounts of moment $m^p(x)$ and deflection $w^p(x)$.

Retrieving the final forms for deflections of the preceding sections, we can express the above general case. Equations (4.7), (4.14) and (4.20) show that for a given axial load, the i^{th} modal amplitude factor of the total deflection of the member, w_i^t, is proportional to the i^{th} modal amplitude factor of the corresponding displacement, obtained from the fundamental (linear) state, where the effect of axial load is ignored. Moreover the relation between w_i and the axial force is not linear.

The linearity of w_i^t with respect to w_i^o, w_i^p and w_i^n, indicates that the principle of superposition, widely used when lateral loads act on a beam, can also be applied to the case of a beam-column which combines all the kinds of imperfections but in a somehow modified form. Any increase Δw_i coming from a corresponding increase of the lateral load q^n will be superimposed provided the **same** axial load acts on the member. The modal amplitude factor, w_i^t, therefore, for the general case where there is a combination of imperfections on a beam-column, can be expressed by the form

$$w_i^t = \frac{P_{ci}}{P_{ci}-P}\left(w_i^o + w_i^n\right) + \frac{P}{P_{ci}-P}w_i^p \quad , \tag{4.22}$$

where

$$\zeta_i = w_i^o + w_i^p + w_i^n \tag{4.23}$$

is an amplitude factor of the **total equivalent imperfection** termed as modal equivalent imperfection.

The corresponding total deflection, measured from the initially straight position of the column, is

$$w^{t}(x) = \sum_{i=1}^{\infty} \frac{P_{ci}}{P_{ci}-P} \zeta_i \phi_i(x) \quad , \tag{4.24}$$

while the non-linear incremental deflection due to the application of axial load is

$$w(x) = w^{t}(x) - w^{o}(x) - w^{n}(x) = \sum_{i=1}^{\infty} \frac{P}{P_{ci}-P} \zeta_i \phi_i(x) \quad . \tag{4.25}$$

The derivation of equations used in this chapter is independent of the geometry of the cross section of the members. This is what makes the Ayrton-Perry equation, initially discussed in section 1.1, have a general character.

When the non-linear deflection function has been established, the other non-linear components, such as rotation and bending moment can readily be obtained. The rotation, for instance, of the beam-column measured from the straight position of the member at each point, can be obtained by the first derivative of Eq. (4.24) with respect to x

$$\theta(x) = \sum_{i=1}^{\infty} \frac{P_{ci}}{P_{ci}-P} \zeta_i \phi_i'(x) \quad . \tag{4.26}$$

The total bending moment at each section of the beam-column may be derived from the moment-curvature relation as

$$M(x) = -EI\left[w^{t''}(x) - w^{o''}(x)\right] \quad , \tag{4.27}$$

where $M(x)$ is the function of the total bending moment. It must be noted that any geometric distortions are supposed to be stress free. Substitution of $w(x)$ from Eq. (4.25) into (4.27) and rearranging yields

$$M(x) = -EI \sum_{i=1}^{\infty} \frac{P}{P_{ci}-P} \zeta_i \phi_i''(x) + m^{p}(x) + m^{n}(x) \quad , \tag{4.28}$$

where

$$m^{p}(x) = -EIw^{p''}(x)$$
$$m^{n}(x) = -EIw^{n''}(x) \qquad (4.29)$$

are bending moments obtained from a linear analysis in a proportionate and non-proportionate loading system respectively and $\phi_i''(x)$ is the curvature of the i^{th} critical mode function. The first of the three terms on the right hand side of Eq. (4.28) comprises the additional bending moment caused by the imperfections while the other two terms are linearly obtained moments, i.e. before the axial load is applied.

The modal equivalent imperfection, ζ_i, is the only unknown in Eqs. (4.24), (4.25) and (4.28). The geometric imperfection, depending on the manufacturing procedure of the structural members and erection of the structure, is a random imperfection and therefore, has to be determined statistically. On the contrary, the loading imperfections of a structure, either proportionate to the axial load or non-proportionate, may be calculated mathematically.

4.6 Characteristic Function of Non-sway Critical Modes

Consider a column as a component of an intermediate floor in a multi-storey and multi-span framed structure. If the end conditions of the member are similar, the critical mode shapes of the column will be symmetrical or asymmetrical with respect to an axis perpendicular to the mid-length of the column. This assumption of symmetry is not far from reality for internal members of rigid-jointed frames and controlled experimental testing, where identical end conditions are provided.

Fig. 4-4 shows the first three critical mode shapes of a column with these characteristics. From the Harmann method, introduced in section 3.5, the buckling shape of each critical mode is a portion of a sine curve which exists between a

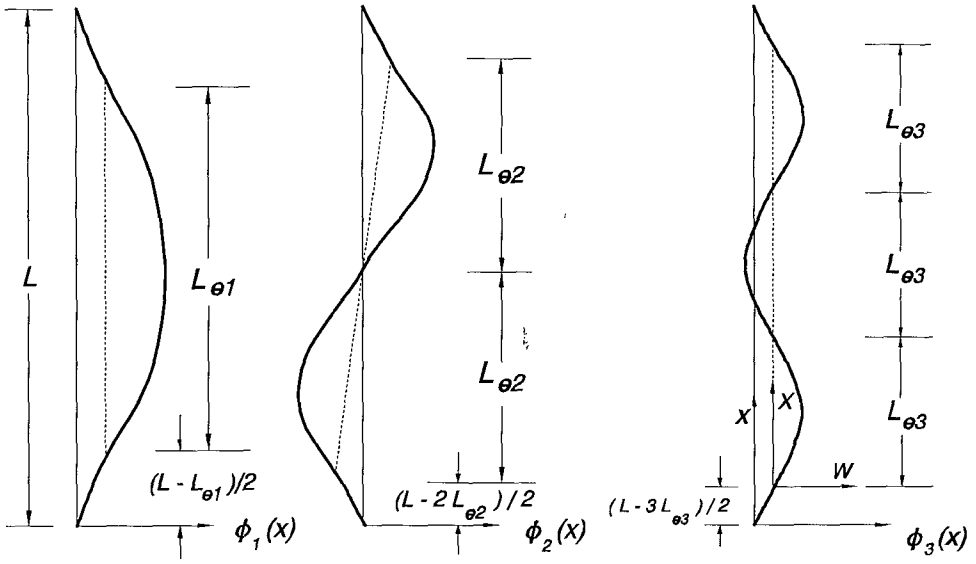

Figure 4-4

certain number of points of contraflexures. This curve, in terms of a local co-ordinate system, is given by the Eq. (3.19)

$$W(X) = A\sin(kX) = A\sin\left(\frac{\pi}{L_e}X\right) \tag{4.30}$$

where L_e is the effective length of the column.

Using Eq. (3.9), the deflection function of the buckled column, being the general solution associated with the characteristic value $k_{ci} = \pi/L_{ei}$ of the i^{th} critical mode in the same **local** coordinate system, is

$$W_i(X) = A\left[\sin(k_{ci}X) + B\cos(k_{ci}X) + CX + D\right]. \tag{4.31}$$

Noting that $X = x - \dfrac{L - iL_{ei}}{2}$, Eq. (4.31) can be written in terms of the global system, (x,w), as

$$w_i(x) = A\left\{\sin\left[\frac{\pi}{L_{ei}}\left(x-\frac{L-iL_{ei}}{2}\right)\right]+B\cos\left[\frac{\pi}{L_{ei}}\left(x-\frac{L-iL_{ei}}{2}\right)\right]+Cx+\bar{D}\right\}, \quad (4.32)$$

where

$$\bar{D} = D - C\frac{L-iL_{ei}}{2} \quad (4.33)$$

The terms in curly brackets of Eq. (4.32), according to what was referred in section 3.4, constitute the characteristic function $\Phi_i(x)$ of the i^{th} critical mode

$$\Phi_i(x) = \sin\left(\frac{\pi x}{L_{ei}}+\frac{i\pi}{2}-\frac{\pi L}{2L_{ei}}\right)+B\cos\left(\frac{\pi x}{L_{ei}}+\frac{i\pi}{2}-\frac{\pi L}{2L_{ei}}\right)+Cx+\bar{D}\ . \quad (4.34)$$

The constants B, C and $\bar{D}$ can be calculated from the conditions

$$\begin{aligned}&\Phi_i(x) = 0 \quad at \quad x = 0 \quad and \quad x = L\ ,\\ &\Phi_i''(x) = 0 \quad at \quad x = \frac{L-iL_{ei}}{2}\ .\end{aligned} \quad (4.35)$$

Application of the latter condition gives

$$0 = -\left(\frac{\pi}{L_{ei}}\right)^2\sin(0)-B\left(\frac{\pi}{L_{ei}}\right)^2\cos(0) \qquad or \qquad B = 0\ . \quad (4.36)$$

The first condition now yields

$$\bar{D} = -\sin\left(\frac{i\pi}{2}-\frac{\pi L}{2L_{ei}}\right), \quad (4.37)$$

while from the second condition, after some trigonometric manipulations we obtain

$$C = -\frac{2}{L}\sin\left(\frac{\pi L}{2L_{ei}}\right)\cos\left(\frac{i\pi}{L_{ei}}\right). \tag{4.38}$$

The final form, therefore, of the characteristic function of the i^{th} critical mode, may be written as

$$\Phi_i(x) = \sin\left(\frac{\pi x}{L_{ei}} + \frac{i\pi}{2} - \frac{\pi L}{2L_{ei}}\right) - \frac{2x}{L}\sin\left(\frac{\pi L}{2L_{ei}}\right)\cos\left(\frac{i\pi}{2}\right) - \sin\left(\frac{i\pi}{2} - \frac{\pi L}{2L_{ei}}\right). \tag{4.39}$$

If we differentiate Eq. (4.39) twice with respect to x, we obtain the curvature of the critical modes

$$\Phi_i''(x) = -\frac{P_{ci}}{EI}\sin\left(\frac{\pi x}{L_{ei}} + \frac{i\pi}{2} - \frac{\pi L}{2L_{ei}}\right). \tag{4.40}$$

Making use of Eq. (4.28), Eq. (4.40) enables the bending moment at any section to be calculated while the column has buckled in its i^{th} mode.

4.7 Elastic-plastic Path of Imperfect columns

The analysis developed in section 4.5 for the general case of imperfections allows a complete determination of the behaviour of imperfect columns with any arbitrary boundary conditions, if the total equivalent imperfection is given.

An imperfect column starts to deflect from the onset of axial loading. This deflection, given through Eqs. (4.24) and (4.25), gives rise to bending moments, which in turn increase the curvature. The result is that, while the column might still be in the elastic region, its response to the applied load is non-linear.

The maximum stress appears at the extreme fibres of the concave side of the cross section where the maximum bending moment occurs and is given by

$$\sigma_m = \frac{P}{A} + \frac{M}{Z} \quad . \tag{4.41}$$

Substituting for M from Eq. (4.28), the maximum stress becomes

$$\sigma_m = \frac{P}{A} + \frac{EI}{Z}\left[\sum_{i=1}^{\infty} \frac{P}{P_{ci}-P}\zeta_i \phi_i''(x)\right] + \frac{m^p(x)}{Z} + \frac{m^n(x)}{Z} \tag{4.42}$$

If the end conditions of the member are similar, the critical mode shapes will be symmetric or antisymmetric with respect to an axis perpendicular to its mid-length. In this case, the displacement

$$w_i(x) = \zeta_i \cdot \phi_i(x) \tag{4.43}$$

of the i^{th} mode is convenient to be expressed in terms of the corresponding normalized characteristic function

$$\bar{\phi}_i(x) = \frac{\phi_i(x)}{\phi_{i_{max}}} \quad , \tag{4.44}$$

because then, in the expression of displacement,

$$w_i(x) = \zeta_i \phi_{i_{max}} \cdot \bar{\phi}_i(x) = \xi_i \cdot \bar{\phi}_i(x) \quad , \tag{4.45}$$

the amplitude factor, ξ_i, of the i^{th} mode, is the maximum deflection in that mode. If we further assume that the contribution of the first symmetric critical mode to the deflection and bending moment is very much greater than the contribution of subsequent modes (in an example of section B.4 in Appendix B the corresponding contribution of the first sway mode is highlighted), then, in the absence of linear end-moments m^p and m^n, the expression for the bending moment occurring at any cross-section along the column, can be written as

$$M(x) = \frac{P_{cl} \cdot P}{P_{cl} - P} \xi_1 \alpha_1(x) \tag{4.46}$$

and hence stress as

$$\sigma(x) = \frac{P}{A} + \frac{1}{Z} \cdot \frac{P_{cl} \cdot P}{P_{cl} - P} \xi_1 \alpha_1(x) \tag{4.47}$$

where

$$\alpha_1(x) = \frac{\cos\left[\frac{\pi L}{2L_{el}}\left(1 - \frac{2x}{L}\right)\right]}{1 - \cos\left(\frac{\pi L}{2L_{el}}\right)} = -\frac{\bar{\phi}_1''(x)}{k_{cl}^2} \quad . \tag{4.48}$$

Eqs. (4.46 to (4.48) are obtained by combining relations (4.39), (4.40) and (4.43).

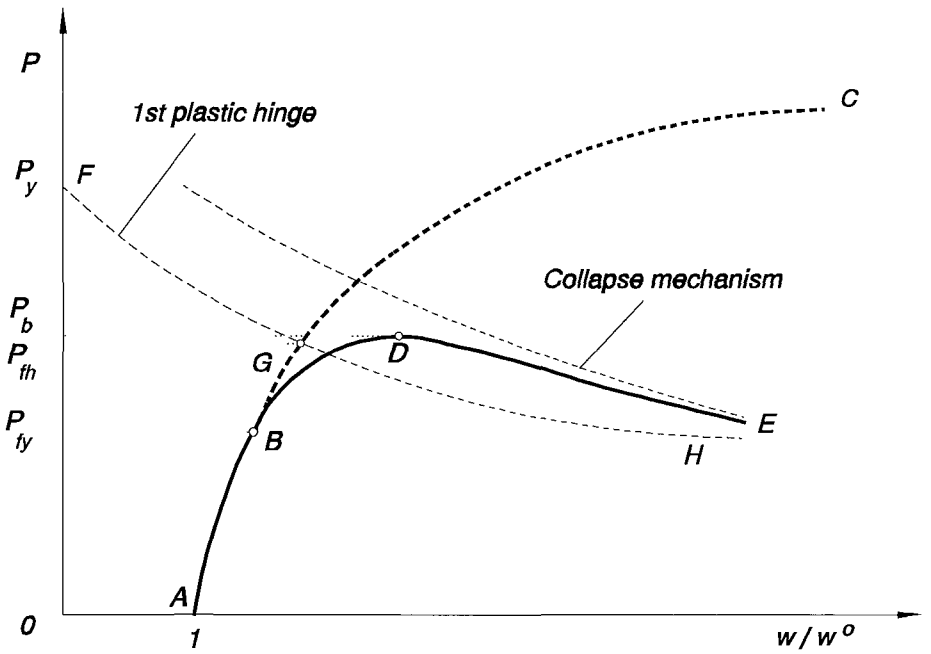

Figure 4-5

As the load is increased, the stress in the extreme fibres of the cross section will eventually reach the yield level. The load which causes the initiation of yielding is termed as first yield load, P_{fy} and is shown as point ***B*** in Fig. 4-5. The first yield load is a lower bound to the collapse load and constitutes a failure criterion chosen by Ayrton and Perry.

As the axial load is increased further, plastic yielding spreads over the section area and the column deviates from its elastic non-linear path, following a new path BDE. This is due to the higher rate of increase of column's local curvature after the inception of first yielding. The elastic-plastic portion BD of the curve is very difficult to define. To overcome this difficulty the column is assumed to follow its elastic path. The point of intersection, G, with the plastic collapse curve, is then taken as a close estimate of the upper bound to the collapse load. The real buckling load P_b corresponds to point D and lies somewhere close to the level of point G.

4.8 Amplitude Factors

The non-linear elastic response of a structure, as discussed in the present Chapter, was found to be related to its linear one. This relationship, concerning displacements and bending moments for a general case of loading, is expressed by Eqs. (4.24) and (4.28). From the above equations it can be seen that both total displacement, $w(x)$ and moment, $M(x)$, embrace two parts. The first one is a non-linear function of the axial load and expresses the load-displacement interaction; the second one is obtained from a linear idealization and is independent of or proportionate to the axial load. The linear displacements, usually called primary deflections, may be the result of geometric and/or proportional and/or non-proportional loading imperfections.

The primary deflections are generally termed as imperfections and they compose the main reason for the existence of the non-linear part in both previous equations. The objective of this section is to calculate and simplify the non-linear

part of both the displacements and the bending moments. For this purpose, the characteristic function of critical modes $\phi_i(x)$ was calculated in Section 4.6.

The primary deflections can be expressed in terms of the characteristic functions of critical modes as

$$\begin{aligned} w^o(x) &= \sum_{i=1}^{\infty} w_i^o \phi_i(x) \\ w^p(x) &= \sum_{i=1}^{\infty} w_i^p \phi_i(x) \\ w^n(x) &= \sum_{i=1}^{\infty} w_i^n \phi_i(x) \end{aligned} \qquad \textbf{(4.49)}$$

where $w^o(x)$ is the initial deflection, $w^p(x)$ is the linear displacement as a result of proportional loading and $w^n(x)$ is the linear deflection due to the non-proportional loading. Relevant to these displacements are the amplitude factors w_i^o, w_i^p, w_i^n for each critical mode.

Each term of Eqs. (4.49) is a part of the related primary deflection associated with the specified critical mode. If this specific part is multiplied by an amplification factor of $P/(P_{ci}-P)$, then the non-linear portion of this part is generated. For each kind of displacement, the summation of these linear parts along with their non-linear portions for each mode, form, according to Eq. (4.24), the total displacement of the member.

Since the elastic critical loads of lower modes are considerably lower than those of higher modes, the amplification factors for the lower modes are much greater than those of higher modes. Consequently, the contribution of lower critical modes to the non-linear part of the displacement is most important, even if only the first symmetric and antisymmetric critical modes are taken into account.

Apart from displacements, these arguments can be applied to the bending

moments. The non-linear part of bending moment in Eq. (4.28) is considered to be generated if each linear-bending-moment-term, is multiplied by the amplification factor, $P/(P_{ci}-P)$ associated with the i^{th} critical mode. Thus it can be concluded that the most vital portion of bending moments is associated with the first symmetric and antisymmetric critical modes. Consequently, little accuracy will be lost if we take the contribution of only the first two critical modes, to the development of the non-linear moments.

To determinate the non-linear contributions to deflections or bending moments due to the first symmetric and antisymmetric critical modes, the corresponding amplitude factors, need to be determined. Among the three amplitude factors of Eq. (4.49), w_i^o is associated with geometric imperfection, which is random. Therefore it cannot be evaluated theoretically. Since the other two amplitude factors are dependent on the loading condition of the member they can be calculated mathematically.

The procedure that follows in determining the amplitude factors of the loading imperfections is unified for both loading systems, proportional and non-proportional. This is because the amplitude factors are dependent on the pattern of loading and not on the system of loading (proportional or non-proportional). As a matter of fact, each system of loading has exactly the same contribution in forming the total deflection or bending moment, according to Eqs. (4.24) and (4.28). So we can interchange the two systems by replacing the superscripts p and n between each other.

Every pattern of loading can be considered as the result of superimposing a symmetrical and antisymmetrical loading pattern. In sections where the magnitude of deflection associated with symmetric critical modes becomes crucial, the contribution of antisymmetric critical modes becomes lower and vice versa. Therefore, the calculation of amplitude factors comprises only two cases of loading patterns, symmetric and antisymmetric.

4.9 Amplitude Factors of Loading Imperfections

The orthogonality conditions for critical modes of elastic members with any kind of boundary conditions were discussed in Chapter 3. The solutions from the eigenvalue analysis, which were also discussed there, lead to a set of linear homogeneous equations where a non-trivial result at each critical load P_{ci} requires

$$EI\phi_i^{iv}(x) + P_{ci}\phi_i''(x) = 0 \qquad i = 1,2,... \tag{4.50}$$

In order to determine the amplitude factors of a non-proportionate loading imperfection, Eq. (4.50) is multiplied by the linear displacement $w^n(x)$ and is integrated over the entire length L of the member

$$\int_0^L EI\phi_i^{iv}(x)w^n(x)dx + P_{ci}\int_0^L \phi_i''(x)w^n(x)dx = 0 \quad . \tag{4.51}$$

Integrating the left hand side of Eq. (4.51) by parts and equating to zero transforms this equation into

$$\begin{aligned} &\int_0^L EI\phi_i''(x)w^{n''}(x)dx - P_{ci}\int_0^L \phi_i'(x)w^{n'}(x)dx \\ &= -\left\{w^n(x)\left[EI\phi_i'''(x) + P_{ci}\phi_i'(x)\right]\right\}_0^L + \left[w^{n'}(x)EI\phi_i''(x)\right]_0^L \quad . \end{aligned} \tag{4.52}$$

Eq. (4.52) holds for a member of the structure; by summing this equation for the entire frame we obtain

$$\begin{aligned} &\sum_M \int_0^L EI\phi_i''(x)w^{n''}(x)dx - P_{ci}\int_0^L \phi_i'(x)w^{n'}(x)dx \\ &= -\sum_M \left\{w^n(x)\left[EI\phi_i'''(x) + P_{ci}\phi_i'(x)\right]\right\}_0^L + \sum_M \left[w^{n'}(x)EI\phi_i''(x)\right]_0^L \quad . \end{aligned} \tag{4.53}$$

The two terms of the right hand side of this equation represent the work done by shear forces and bending moments at the ends of the members. Hence due to equilibrium considerations at the joints of the structure, these terms vanish except where they refer to the ends of the members at points of support. If it is assumed

that the frame is supported so that the reactions at the external supports do not work when the structure deforms, (i.e. a pinned, free, or fixed end support), the terms on the right hand side entirely vanish, and equation (4.53) becomes

$$\sum_M \int_0^L EI\phi_i''(x)w^{n''}(x)dx - \sum_M P_{ci}\int_0^L \phi_i'(x)w^{n'}(x)dx = 0 \quad . \tag{4.54}$$

Expressing $w^n(x)$ in terms of critical mode functions and substituting into the second term of Eq. (4.55), using the orthogonal relation (3.37) yields

$$\sum_M \int_0^L EI\phi_i''(x)w^{n''}(x)dx - w_i^n \sum_M P_{ci}\int_0^L \phi_i'^2(x)dx = 0 \quad . \tag{4.55}$$

Using the normalising relation (3.39) in Eq. (4.55), the i^{th} amplitude factor of the non-proportional loading imperfection can be obtained

$$w_i^n = \frac{\sum_M \int_0^L EI\phi_i''(x)w^{n''}(x)dx}{\sum_M \int_0^L EI\phi_i''^2(x)dx} \quad . \tag{4.56}$$

Conversely the expression for $w^n(x)$ can be substituted into the first term of Eq. (4.54), where, following the same procedure as above, yields

$$w_i^n = \frac{\sum_M \int_0^L P_{ci}\phi_i'(x)w^{n'}(x)dx}{\sum_M \int_0^L P_{ci}\phi_i'^2(x)dx} \quad . \tag{4.57}$$

The same procedure may be used for the case of proportional loading. Here the same formula as Eq. (4.56) is obtained, except that the superscript n is replaced by the corresponding p.

An example of using the amplitude factor, as expressed in Eq. (4.56), for calculating the sway loading imperfection when both ends are fixed rollers, is given in section B.4 of Appendix B.

Chapter 5

Interaction of Elastic Stability - Material Failure

5.1 Elastic-Plastic Behaviour

Before analysing or designing a structure it is necessary to establish a mental image of the general behaviour of the material to be used. Then a theory can be developed to formulate and analyse a mathematical model of the structure. In steel structures a pure elastic material never exists in reality. The term 'inelastic' may be used for a structure to show that its material does not follow Hooke's law. The simplest case of inelastic response is a plastic behaviour which occurs when the material is elastic-plastic. A realistic material behaviour of Fig. 5-1 may be thus idealised to a form shown in Fig. 5-2. In this idealisation the region of linear elasticity is considered to finish when the yield stress is reached, after which follows the region of perfect plasticity. For this reason the term perfect plastic material is often applied to an elastic-plastic material.

Structural steels may be idealised as elastic-plastic materials because they have sharply defined yield points and undergo large strains during yielding. The assumption of perfect plasticity after the yield point, means that the effects of strain hardening are disregarded. However, since strain hardening provides an increase in the strength of the steel, it is generally safe to disregard it. The upper yield point of rolled steel sections, for instance in a stress-strain diagram, is not often exhibited; normally it is ignored and the lower yield point is taken as index of the yield stress. The same applies for the strain ε_{sh} at the beginning of strain-hardening which is usually considerably greater than that at yield point ε_y.

Current research on structures and strength of materials is generally

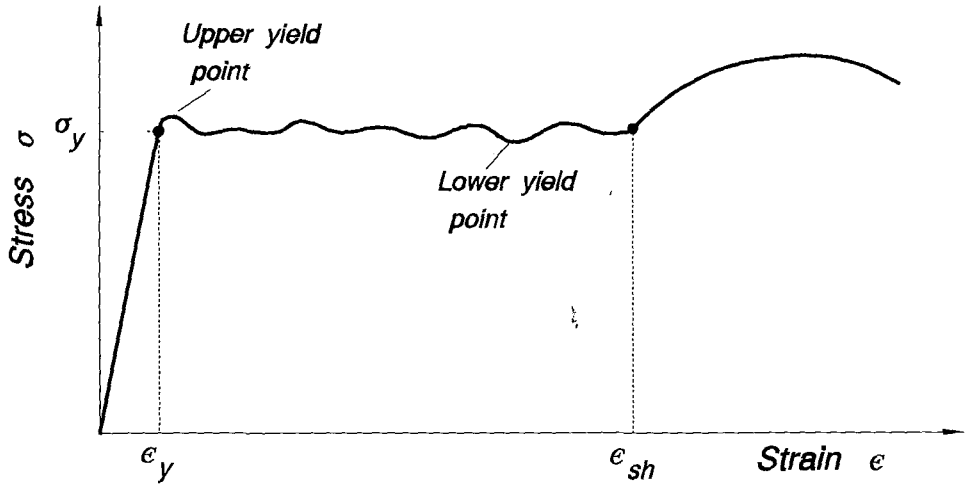

Figure 5-1

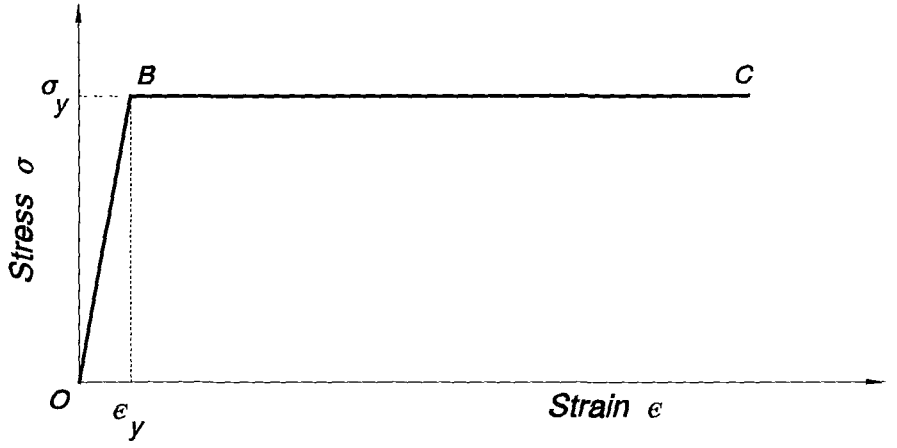

Figure 5-2

concentrated on both their elastic and plastic behaviour. In an attempt to model this behaviour in ductile materials such as mild steels, the yield characteristics were first specified before the elastic-plastic theory is developed.

In Fig. 5-2 line OBC is considered as representative of the stress-strain relationship of the steel structure and constitutes the basis of the elastic-plastic theory, where elastic strains are taken into account. Therefore, in the design of a

steel structure, this theory allows consideration of both the elastic stability and material failure.

5.2 Design Model

The term 'design' in structural engineering may have a multiple use, usually referring to the determination of either the cross section of one or more structural members or their maximum loading capacity, so that a structure, as a whole, having been made with economy and elegance, can safely resist the forces to which it may be subjected.

Depending on the use of the structure, the definition for the safe design varies. If the structure is made so that no permanent distortion is created when it is under the applied loads, the elastic theory will be employed. In this case, the design criterion -called working stress design - will be based on the fact that the maximum stresses which develop on the elements must remain lower than the yield stress.

On the other hand in determining the ultimate load capacity of a structure, the size of its members are chosen in such a way that a simultaneous collapse should be possible to occur. In this case the elastic-plastic theory is used, where it is assumed that the members remain elastic up to collapse load, when a plastic hinge is produced somewhere in the member. This design criterion is called the ultimate strength design.

In the design of steel structures on the basis of their ultimate load capacity, referred to as plastic design, the service loads for the structure are multiplied by the load factor to obtain the ultimate loads. The structure is designed for ultimate-load conditions, using the concepts of plastic analysis. This approach contrasts with the more familiar elastic design, in which a safety factor is applied to the yield stress to give an allowable stress after which the structure is designed through concepts of elastic analysis, so that the allowable stress is not exceeded.

The essential difference between the two methods is that plastic design leads to a structure having a more or less uniform factor of safety against failure of all its parts, whereas an elastically designed structure has a uniform factor of safety against yielding. Due to redistribution of bending moments during the inelastic action, it is obvious that structures designed by these two methods will have different relative proportions of their parts.

5.3 Strength Model

Consider the beam-column in Fig. 5-3 as a component of a rigid-jointed frame subjected to a general loading system (proportional and non proportional). During

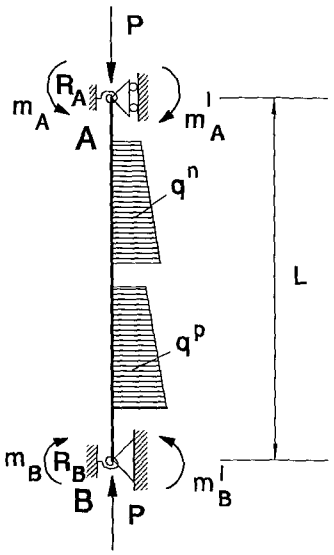

Figure 5-3

loading, each cross section is under the combined action of an axial force P and a bending moment M, as shown in Fig. 5-4a. For an elastic-plastic material in the elastic range, the stress distribution across the depth of the cross section varies linearly from one extreme fibre to another.

If the design criterion is to achieve first yield in structural members, the maximum stress, occurring at the extreme fibres of the cross section, where the

maximum bending moment is located, has to remain below or equal to the yield

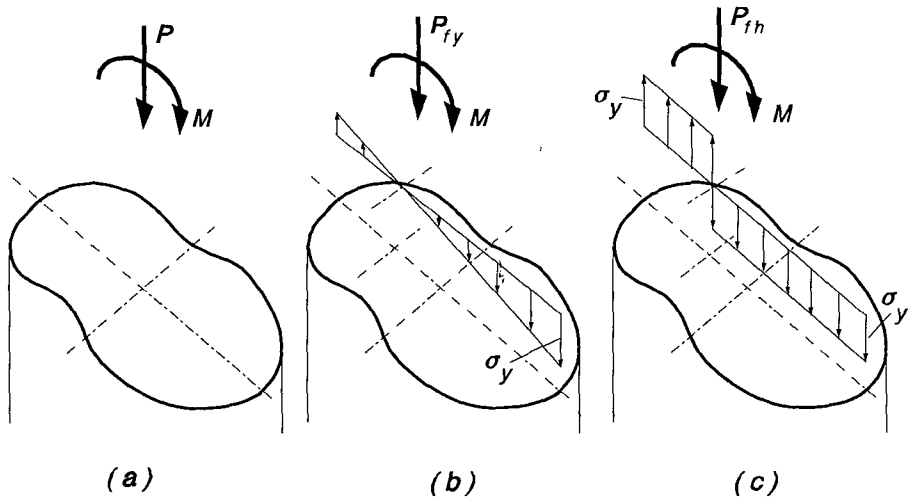

Figure 5-4

stress, as shown in Fig. 5-4b. Denoting with P_{fy} the axial load required to produce the yield stress σ_y at one of the extreme fibres, regardless of the geometry of the cross section, the relationship between the axial load and the bending moment is governed by the equation

$$\frac{P}{A} + \frac{M}{Z} \leq \sigma_y \quad or \quad \frac{P}{P_y} + \frac{M}{M_y} \leq 1, \tag{5.1}$$

where A is the area and Z the elastic modulus of the cross section.

In Fig. 5-5, Eq. (5.1) is represented from line AB, showing the strength limits as long as the material remains elastic. In this graph, $P_y = A\sigma_y$ is the axial load of the column at full yield condition in the absence of bending moment, and $M_y = Z\sigma_y$ is the elastic moment capacity of the member in the absence of axial load.

If the design criterion is to achieve the ultimate load capacity of the member, once one of the extreme fibres yields, the stress in this fibre should remain constant

until the stresses in all the fibres of the cross section reach the yield point, as shown in Fig. 5-4c. Let P_{fh} be the axial load required to produce this situation. Unlike the working stress method, the relation between axial load and bending moment in the ultimate strength method depends on the geometry of the cross-section and generally can be written as

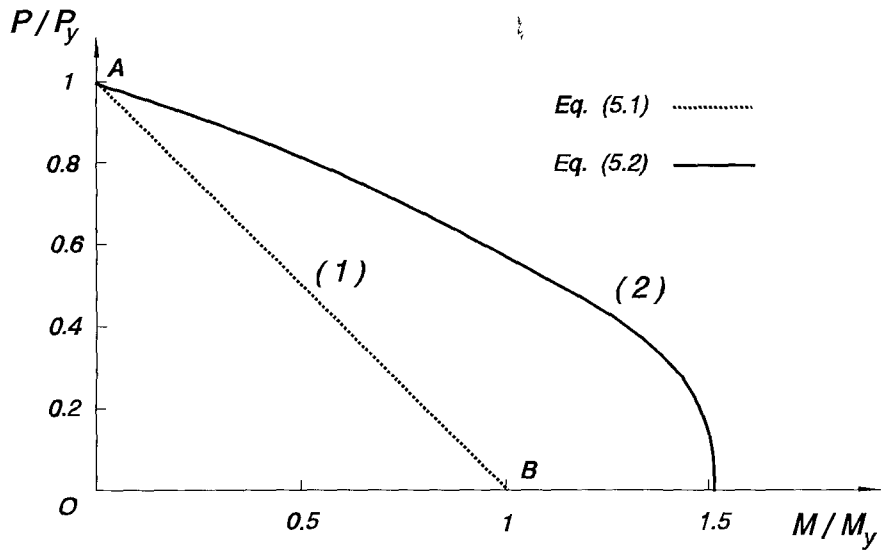

Figure 5-5

$$\frac{M}{M_p} + \alpha_1\left(\frac{P_{fh}}{P_y}\right) + \alpha_2\left(\frac{P_{fh}}{P_y}\right)^2 = \alpha_3 \ , \tag{5.2}$$

where $M_p = S\sigma_y$ is the plastic moment capacity of the cross-section in the absence of axial load and S is the plastic section modulus. The parameters α_1, α_2 and α_3 vary for different cross-sectional shapes. For a rectangular cross-section, Eq. (5.2) becomes

$$\frac{M}{M_p} + \left(\frac{P_{fh}}{P_y}\right)^2 = 1 \ . \tag{5.3}$$

It was found by Chen[48] and Nethercot[49] that for the same shape of cross-section the parameters α_1, α_2 and α_3 do not vary significantly when the size of the section changes. As an approximation for the sections of the same shape, these parameters from both investigators are given in table 5.1. Chen's parameters refer to a wide flange section bending about its major and minor axis, while Nethercot's refer to rolled **I** and **H** sections.

Table 5.1 Function parameters of Eq. (5.2)

For .. $\leq \frac{P_{fh}}{P_y} \leq$		α_1		α_2		α_3	
Chen	Nethercot	Che	Net	Che	Net	Che	Net
Bending about **s t r o n g** axis							
0 .. 0.225	0 .. 0.200	0	0	2.378	2.5	1	1
0.225 .. 1	0.200 .. 1	1.03	1.125	0.085	0	1.115	1.125
Bending about **w e a k** axis							
0 .. 0.252	0 .. 0.447	0	0	0.185	0.5	1	1
0.252 .. 1	0.447 .. 1	-0.82	0	1.709	1.125	0.888	1.125

Fig. 5-5 shows the expression given by Nethercot for the weak axis. The ratio M_p / M_y is taken to be 1.51, which is almost correct for **I** and **H** sections bending about their minor axis.

5.4 Linear Failure - Squash Load

In the preceding section it has been assumed that the internal forces of each cross-section were known. In reality, however, these forces not only are unknown but they have to be analysed and calculated as accurately as possible. The linear analysis is the first and simplest stage for this calculation, based on the elastic theory, where the equations of equilibrium are derived assuming that the structure remains undeformed.

Although the stress-strain relationship includes both the elastic and plastic responses of a structure, the stiffnesses of its members are assumed to be constant during the increase of load. As a result, a linear relationship between load and displacement may exist. In this case a line which represents the change between the load and the moment in an ever-increasing system of loading (Fig. 5-6), will intersect the plastic failure curves 1 and 2 at different points, providing thus a limit of failure in this analysis.

This type of failure is often called *linear failure.* Since this analysis disregards the effect of instability, the only criterion considered in determination of the member sizes and/or the loading capacity is material failure. Therefore, axial loads, corresponding to the intersection points of the load-moment line with plastic curves 1 and 2, are loads of material failure.

The axial loads which correspond to the intersection points with curves 1 and 2 are termed material failure loads occurring at the first yield, P_{fy}, and the first hinge, P_{fh}, respectively. Referring back to Fig. 5-3 where a beam-column is under an increasing axial load, three different cases of linear failure are considered.

a) Without loading imperfections

In the absence of loading imperfections, during the increase of axial load, no bending moment will be developed along the member length, even if the member

is not perfectly straight. This is because the effect of instability is ignored in linear analysis. In Fig. 5-6 this analysis is shown by the line OA. This line intersects both plastic failure curves 1 and 2 at the same point A, where $P/P_y = 1$.

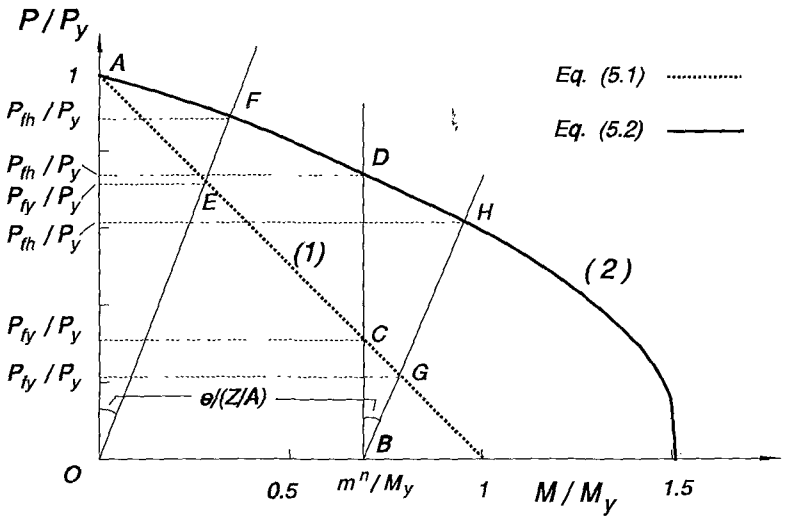

Figure 5-6

In the absence of bending moment, the load corresponding to this point is called the squash load. Here the material failure loads corresponding to the first yield and first hinge are equal, i.e.

$$\frac{P_{fy}}{P_y} = 1 \qquad \textbf{(5.4)}$$

$$\frac{P_{fh}}{P_y} = 1 \,. \qquad \textbf{(5.5)}$$

b) Non-proportional loading system

The presence of a non-proportional loading system here results in the existence of a bending moment, which is independent of the axial load. The

magnitude of this moment is obtained for each cross-section through a linear analysis. If m^n is the maximum bending moment on the member, during the increasing axial load, line BCD, with B at m^n/M_y in Fig. 5-6, will represent the result of this analysis. This line intersects the plastic failure curves 1 and 2 at points C and D, corresponding to linear failure of the member through the working stress method and ultimate strength method respectively. The corresponding material failure loads, occurring here at two levels, can be obtained by replacing P and M with P_{fy} and m^n in Eq. (5.1) and also M with m^n in Eq. (5.2), i.e.

$$\frac{P_{fy}}{P_y} = 1 - \frac{m^n}{M_y} \tag{5.6}$$

$$\alpha_1\left(\frac{P_{fh}}{P_y}\right) + \alpha_2\left(\frac{P_{fh}}{P_y}\right)^2 = \alpha_3 - \frac{m^n}{M_p} \; . \tag{5.7}$$

c) Proportional loading system

Here all the non-proportionate load components of the member are zero and the linear analysis provides a linear relationship between axial load and bending moment. If m^p is the linear bending moment in a typical cross section, the term $e=m^p/P$ may express an initial eccentricity of loading, which remains constant throughout the load increase. In this case the straight line OEF, representing the load-moment relation, has a slope, $e/(Z/A)$, with the vertical axis.

The material failure loads, obtained from the intersection points of OEF with the plastic failure curves 1 and 2, occur at different levels, as in case (b). They can be calculated by substituting P and M for P_{fy} and $P_{fy}e$ in Eq. (5.1) and also M for $P_{fh}e$ in Eq. (5.2), i.e.

$$\frac{P_{fy}}{P_y} = \frac{1}{1 + e/(Z/A)} \tag{5.8}$$

$$\left(\frac{e}{S/A} + \alpha_1\right)\frac{P_{fh}}{P_y} + \alpha_2\left(\frac{P_{fh}}{P_y}\right)^2 = \alpha_3 \; . \tag{5.9}$$

d) General mixed loading system

As a final case, the member is considered to be under both a proportional and non-proportional loading system, as shown in Fig. 5-3. If m^n and m^p are the corresponding magnitudes of bending moments, since m^p depends on the axial force, it can be written as $m^P = P \cdot e$, where e is the initial eccentricity. In this case, line BGH, with B at m^n/M_y and at a slope $e/(Z/A)$ as in the previous case shows the result of this linear analysis. This line intersects the plastic failure curves 1 and 2 at points G and H, providing thus the corresponding squash loads for the two methods. Substituting P and M for P_{fy} and $m^n+P_{fy}e$ in Eq. (5.1), P_{fy} is obtained, while putting $m^n+P_{fh}e$ in place of M in Eq. (5.2) the corresponding expression for P_{fh} can be derived.

$$\frac{P_{fy}}{P_y} = \frac{1 - \dfrac{m^n}{M_y}}{1 + \dfrac{e}{Z/A}} \tag{5.10}$$

$$\left(\frac{e}{S/A} + \alpha_1\right)\frac{P_{fh}}{P_y} + \alpha_2\left(\frac{P_{fh}}{P_y}\right)^2 = \alpha_3 - \frac{m^n}{M_y} \,. \tag{5.11}$$

5.5 Elastic Critical Load

The material failure load as discussed in the preceding section is a limit load for a beam-column, when the material failure is considered. Similarly the elastic critical load is another limit when we refer to elastic stability of the member. The analytical calculation of the elastic critical load was discussed in chapter 3. The instability problem in a rigid jointed frame may be generally classified as either member or frame instability.

When a frame is completely braced against side-sway, the only instability problem is member instability. The lowest elastic critical load can be obtained either by an eigenvalue analysis or by effective length charts. In a frame where side sway

is not prevented, both member instability and frame instability have to be considered.

Regarding both member and frame instability in chapter 3, the Eigenvalue analysis showed that a perfect column might bifurcate at several load levels. Each one of them is the elastic critical load corresponding to a different mode (shape) of the unstable member. In determining the buckled shape of this column two kinds of critical modes may be classified:

i) Symmetric, associated with non-sway and

ii) Antisymmetric, associated with sway.

The term symmetry is used here when the buckled shape is symmetric with respect to an axis perpendicular to the mid-length of the column, whereas antisymmetry is used when the buckled shape is symmetric with respect to the mid-point of the column. For a member, considered as part of a rigid-jointed frame, the ratio of the loads for the first symmetric critical mode to the first antisymmetric one can vary, depending on the boundary conditions (end restrains) and the stiffness of the surrounding frame.

The main theme of this thesis is to highlight those situations where the first two critical loads, as a result of the frame geometry, may be close together and consequently both critical modes contribute to the elastic-plastic imperfection sensitivity. In design and analysis the first critical load is of supreme importance because it provides an upper bound solution for an elastic-plastic beam-column when the effect of material failure is not involved in the corresponding procedure.

5.6 Design Criteria

In the discussion developed in previous Chapters, it was established that the imperfection approach is the only rational way to predict the strength of a column presenting one degree of freedom. According to this analysis, the column strength for this degree of freedom was found to be a function of the Euler's critical load,

P_c, and the total equivalent imperfection.

For a given column, presenting more than one degrees of freedom (biaxial buckling, sidesway frame-buckling), an efficient design would therefore meet the following requirements:

a) maximization of Euler's critical load

b) minimization of total equivalent imperfection and

c) close buckling strength for each of the available degrees of freedom of the column.

The first requirement can be covered through any standard structural mechanics text book while the second can be accomplished by improvements in the manufacturing process, the quality of workmanship and the loading pattern of the structure. The third requirement, concerning the simultaneity of buckling in all the degrees of freedom, is a subject of the coming theoretical investigation and does not appear to have been addressed in the available design codes. The term simultaneity of buckling has here a relative meaning, indicating that the difference between the buckling strengths should be as small as possible; if the buckling strength of one degree of freedom is significantly higher than that to initiate instability or failure to the other degree(s), then a situation arises at failure, in which much of the buckling resistance with respect to the other degree(s) remains unutilized. This simultaneity may be accomplished as a result of optimisation of the column's geometry in combination with an optimisation of its surrounding frame, i.e. by a proper choice of cross section sizes and lengths of the frame. Such optimisation is shown in Fig. 6-1 for the sway and non-sway critical loads versus the ratio of the beam's over the column's second moment of area.

Equivalent argument could be applied for biaxial buckling; Fig. 5-7 shows in sketch that for a column with constant I section, its critical loads, corresponding to each of the two axes, being dependant on the cross sectional and effective length characteristics, may be represented by different curves, the intersection of which gives the optimum geometry with a simultaneity in buckling loads.

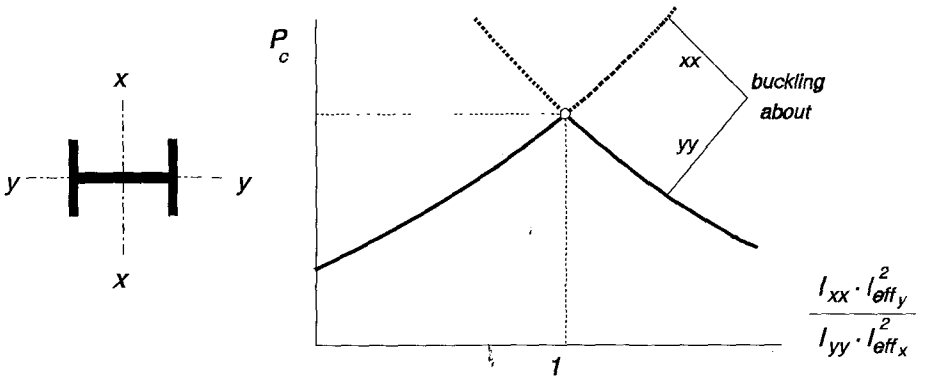

Figure 5-7

Columns with comparable strength with respect to all degrees of freedom will experience an interaction between various buckling parameters of these degrees. Possible reduction in the load carrying capacity, resulting from this interaction is not explicitly covered by current design codes, including those in BS 449 and BS 5950.

The criteria which are going to be used in the determination of the buckling strength, as described in the present Chapter, are:

1. **The First Yield Condition,** where the column is considered to have failed if the stress at some point on the cross section, at which the maximum bending moment occurs, reaches the yield level. The axial load causing the initiation of yielding in the column, according to this criterion, is a lower bound to the collapse load, and

2) **The First Plastic Hinge Formation,** where the column is considered to have failed when the stresses have reached yield at every point on the cross section at where maximum bending moment occurs. This consideration is not far from reality even for a restricted column which composes a part of a frame. This is because the second and third plastic hinges, necessary to convert the structure (after redistribution of bending moments) into a mechanism, are formed almost simultaneously without a significant increase of axial load. Therefore the load necessary to cause a plastic hinge formation may be considered as a close upper bound to the collapse load.

5.7 First Yield Analysis

The initial out-of-straightness, usually referred as the geometric imperfection, can be expressed in terms of a converging series as

$$w^o(x) = \sum_{i=1}^{\infty} w_i^o \phi_i(x) \tag{5.12}$$

where, for the i^{th} mode, $\phi_i(x)$ is the characteristic function and w_i^o is the amplitude factor termed as modal geometric imperfection.

If an axial load P is applied, a non-linear increase of deflection will be given by

$$w(x) = \sum_{i=1}^{\infty} \frac{P}{P_{ci}-P} w_i^o \phi_i(x) \tag{5.13}$$

which when added to the initial imperfection gives a total displacement

$$w^t(x) = \sum_{i=1}^{\infty} \frac{P_{ci}}{P_{ci}-P} w_i^o \phi_i(x) \quad . \tag{5.14}$$

The amplitude factor

$$w_i = \frac{P}{P_{ci}-P} w_i^o \tag{5.15}$$

which corresponds to the non-linear increase, can be similarly derived for proportional, w^p and non-proportional, w^n, loading imperfections because the corresponding equations are identical. So we can write

$$w_i = \frac{P}{P_{ci}-P} \zeta_i \tag{5.16}$$

where $\zeta_i = w_i^o + w_i^p + w_i^n$ is the amplitude factor of the total equivalent

imperfections.

The non-linear deflection due to the axial load, being therefore

$$w(x) = \sum_{i=1}^{\infty} \frac{P}{P_{ci} - P} \zeta_i \phi_i(x) \tag{5.17}$$

gives rise to the calculation of bending moment at any section, which thus is

$$M = -EIw''(x) = -EI \sum_{i=1}^{\infty} \frac{P}{P_{ci} - P} \zeta_i \phi_i''(x) + m^P + m^n \tag{5.18}$$

where $m^P(x) = -EIw^{P''}(x)$ and $m^n(x) = -EIw^{n''}(x)$ are linearly obtained bending moments.

The maximum stress of the column, occurring at the extreme fibres of the concave side of the cross section that bears the maximum bending moment, is given by the equation

$$\sigma_m = \frac{P}{A} + \frac{M}{Z} \tag{5.19}$$

which, after substitution for M from (5.18) yields

$$\sigma_m = \frac{P}{A} + \frac{EI}{Z} \left[\sum_{i=1}^{\infty} \frac{P}{P_{ci} - P} \zeta_i \phi_i''(x) \right] + \frac{m^P(x)}{Z} + \frac{m^n(x)}{Z} \tag{5.20}$$

If we consider that only two of the first critical modes contribute to the maximum bending moment, i.e. the sway mode, associated with antisymmetric configuration, and the non-sway, associated with symmetric, we can write

$$\sigma_m = \frac{P}{A} + \frac{EI}{Z} \left[\frac{P}{P_{cs} - P} \zeta_s \phi_s''(x) + \frac{P}{P_{cn} - P} \zeta_n \phi_n''(x) \right] + \frac{m^P(x)}{Z} + \frac{m^n(x)}{Z} \tag{5.21}$$

Assuming the column to have failed when $\sigma_m = \sigma_y$, in the absence of linear

moments, a lower bound to the collapse load, P_b, is given by the solution of the equation

$$\frac{P_y}{A} = \frac{P_b}{A} + \frac{P_{cs}P_b}{P_{cs}-P_b}\cdot\frac{\xi_s\alpha}{Z} + \frac{P_{cn}P_b}{P_{cn}-P_b}\cdot\frac{\xi_n\beta}{Z} \qquad (5.22)$$

where : P_{cs}, P_{cn} are respectively the 1st and 2nd critical loads,

ξ_s, ξ_n are the corresponding amplitudes of the total equivalent imperfections as defined from Eq. (4.45) and

α, β are curvature parameters which are numerically calculated and can be theoretically derived, as in Eq. (4.48), as follows:

The first derivative of the corresponding characteristic function (function-index s for α and n for β), is equated to zero, yielding the location of maximum deflection, which can then be calculated. If $\phi_{i_{max}}$ is the maximum value of the i^{th} characteristic function, the ratio $\frac{\phi_i(x)}{\phi_{i_{max}}}$ is the normalized characteristic function. The second derivative of this ratio divided by $-k_{ci}^2$ gives the corresponding value for α (i=s) and β (i=n).

A theoretical handling to solving this equation is not easy because the location of maximum bending moment for each mode-case is different. The maximum sum of bending moments for the first two modes, therefore, can only be calculated through computer based iteration techniques.

Rewriting Eq. (5.22) in a non-dimensional form and rearranging yields

$$p_1^3 - p_1^2(p_{cs}\rho_s\alpha + p_{cn}\rho_n\beta + p_{cs} + p_{cn} + 1) + p_1[p_{cs}p_{cn}(\rho_s\alpha + \rho_n\beta + 1) + p_{cs} + p_{cn}] - p_{cs}p_{cn} = 0 \qquad (5.23)$$

where: $p_1 = \frac{P_{fy}}{P_y}$ is the unknown non-dimensional load at first yield

$p_{cs} = \frac{P_{cs}}{P_y}$, $p_{cn} = \frac{P_{cn}}{P_y}$ are the first two non-dimensional critical loads and

$\rho_s = \xi_s \frac{A}{Z}$, $\rho_n = \xi_n \frac{A}{Z}$ are dimensionless imperfection parameters, in which Z is the elastic section modulus.

As $\rho_n \to 0$, Eq. (5.23) can be reduced to equation

$$p_1^3 - p_1^2(p_{cs}\rho_s\alpha + p_{cs} + p_{cn} + 1) + p_1[p_{cs}p_{cn}(\rho_s\alpha + 1) + p_{cs} + p_{cn}] - p_{cs}p_{cn} = 0 \quad (5.24)$$

which is the Ayrton-Perry expression for the sway buckling. Similarly, as $\rho_s \to 0$ Eq. (5.23) provides the Ayrton-Perry equation for the non-sway buckling

$$p_1^3 - p_1^2(p_{cn}\rho_n\beta + p_{cs} + p_{cn} + 1) + p_1[p_{cs}p_{cn}(\rho_n\beta + 1) + p_{cs} + p_{cn}] - p_{cs}p_{cn} = 0 \quad (5.25)$$

The above single-mode cases represent respectively the intersections of the (p, ρ_s) and (p, ρ_n) planes with the imperfection sensitivity surface at first yield shown in Fig. 5-8. Furthermore, they can be considered to be originated or derived from the original Ayrton-Perry equation (1.4), which is thus validated. Indeed, using the above notation, Eq. (1.4), for the non-sway case can be written as

$$(p_{cn} - p_1)(1 - p_1) - \rho p_1 p_{cn} = 0 , \quad (5.26)$$

which, after factorisation by $(p_1 - p_{cs}) \neq 0$ and rewriting, takes the form

$$p_1^3 - p_1^2(1 + p_{cs} + p_{cn} + \rho p_{cn}) + p_1(p_{cs} + p_{cn} + p_{cs}p_{cn} + \rho p_{cs}p_{cn}) - p_{cs}p_{cn} = 0 \quad (5.27)$$

that is exactly the same with the corresponding given in Eq. (5.25), where the parameter β is used to compensate for the buckling shape in this mode. Similarly Eq. (1.4) for the sway case can be written as

$$(p_{cs}-p_1)(1-p_1)-\rho p_1 p_{cs}=0\ , \tag{5.28}$$

which, after factorisation by $(p_1-p_{cn})\neq 0$ and rewriting, takes the form

$$p_1^3-p_1^2(1+p_{cs}+p_{cn}+\rho p_{cs})+p_1(p_{cs}+p_{cn}+p_{cs}p_{cn}+\rho p_{cs}p_{cn})-p_{cs}p_{cn}=0 \tag{5.29}$$

that is exactly the same with the corresponding given in Eq. (5.24), where the parameter α is used to compensate for the buckling shape in that mode.

In the case of loading imperfections, where a non-proportional linearly obtained bending moment m^n is present at the cross section of maximum moment coming from both modes, the total bending moment

$$m=\frac{PP_{cS}}{P_{cS}-P}\xi_s\alpha+\frac{PP_{cN}}{P_{cN}-P}\xi_N\beta+m^n\ , \tag{5.30}$$

arising from Eq. (5.21) must be simultaneously satisfied with

$$\frac{m}{m_p}=1-\left(\frac{P}{P_y}\right)^2\ , \tag{5.31}$$

holding for rectangular cross section where $P_y=\sigma_y bd$ and $m_p=\sigma_y bd^2/4$.

Eq. (5.30) can be non-dimensionalised with respect to *a plastic squash load*, P_p, defined from (5.31) as

$$\left(\frac{P_p}{P_y}\right)^2=1-\frac{m^n}{m_p}\ , \tag{5.32}$$

and therefore it becomes

$$\frac{m}{m_p}=\frac{PP_{cS}}{P_{cS}-P}\cdot\frac{\xi_s\alpha}{m_p}+\frac{PP_{cN}}{P_{cN}-P}\cdot\frac{\xi_N\beta}{m_p}+\frac{m^n}{m_p}=1-\left(\frac{P}{P_y}\right)^2\ ,\quad or \tag{5.33}$$

$$\frac{PP_{cS}}{P_{cS}-P}\cdot\frac{\xi_s\alpha}{m_p}+\frac{PP_{cN}}{P_{cN}-P}\cdot\frac{\xi_N\beta}{m_p}+\left(\frac{P}{P_y}\right)^2=\left(\frac{P_p}{P_y}\right)^2 . \tag{5.34}$$

Multiplication by $(P_y/P_p)^2$ gives

$$\frac{PP_{cS}}{P_{cS}-P}\cdot\frac{\xi_s\alpha}{m_p}\left(\frac{P_y}{P_p}\right)^2+\frac{PP_{cN}}{P_{cN}-P}\cdot\frac{\xi_N\beta}{m_p}\left(\frac{P_y}{P_p}\right)^2+\left(\frac{P}{P_p}\right)^2=1 , \tag{5.35}$$

which upon use of

$$p\equiv\frac{P}{P_p} , \quad p_{cS}\equiv\frac{P_{cS}}{P_p} , \quad p_{cN}\equiv\frac{P_{cN}}{P_p} \quad and \quad p_y\equiv\frac{P_y}{P_p} \tag{5.36}$$

results in

$$\frac{pp_{cS}}{p_{cS}-p}\cdot\frac{\xi_s\alpha}{m_p}P_yp_y+\frac{pp_{cN}}{p_{cN}-p}\cdot\frac{\xi_N\beta}{m_p}P_yp_y=1-p^2 , \quad or \tag{5.37}$$

$$pp_{cS}(p_{cN}-p)\rho_S^*p_y\alpha+pp_{cN}(p_{cS}-p)\rho_S^*\beta=(1-p^2)(p_{cN}-p)(p_{cS}-p) \tag{5.38}$$

where $\rho_S^*=\dfrac{\xi_S A\sigma_y}{\sigma_y Z_p}=\dfrac{\xi_S A}{Z_p}$ and $\rho_N^*=\dfrac{\xi_N A}{Z_p}$.

Solution of Eq. (5.38) for p yields p_{fp}, where from, eventually, the first yield over the squash load (in the absence of m^n) ratio can be obtained from

$$\frac{P_{fy}}{P_y}=p_{fp}\sqrt{1-\frac{m^n}{m_p}} \tag{5.39}$$

From this point of view, when loading imperfections arise from linearly applied bending moments, the final result of P_{fy}/P_y ratio has to be obtained through Eq. (5.39).

Given the geometry of the column, its first two critical loads and loading imperfection parameters are either known or can be calculated. Therefore, Eq. (5.23), which is independent of the shape of the cross section, can be solved by iterative techniques for the non dimensional buckling load.

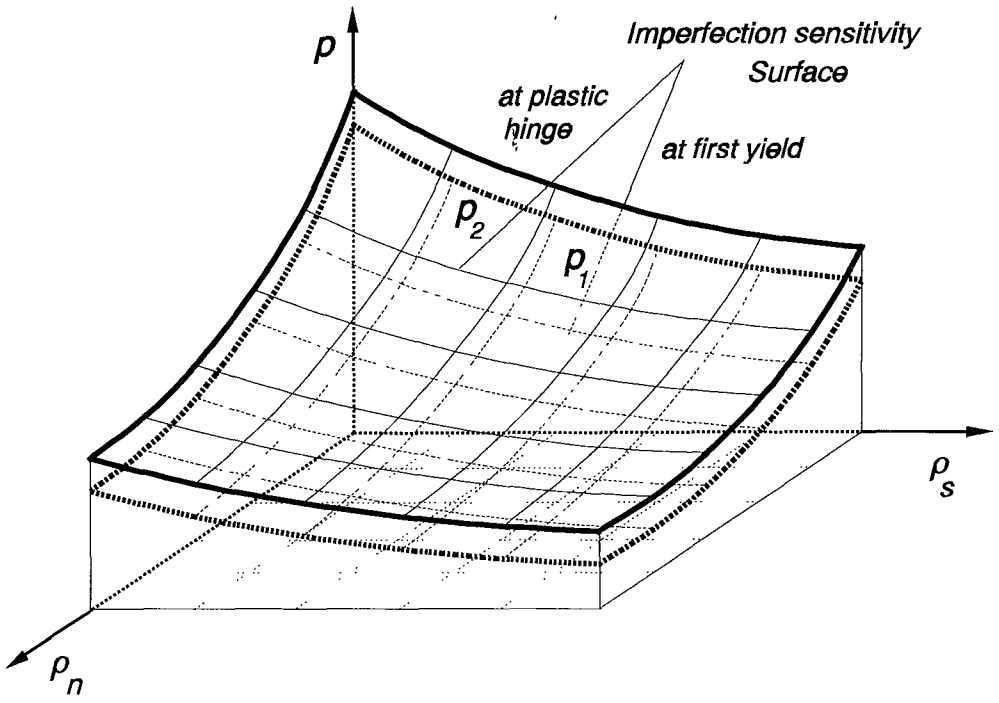

Figure 5-8

The solution of the above equation has been realised and verified through two independent iterative computational techniques, one of which is the Newton-Raphson approximation. This approximation has been incorporated in the main program for a cross-checking of the results. The algorithm of the subroutine which belongs to the main program is described in the end of section 5.8.

The objective here was to establish the extent of interaction between the imperfection parameters on the buckling strength of the column. This strength can be varying as shown in Fig. 5-8 for the p_1 surface.

For an illustrative frame geometry, the reduction of the buckling strength of the column at first yield, presenting sway and non-sway imperfections and obtained

through the above subroutine of the program, is given in Fig. 5-9.

The result highlights the effect that the sway and non-sway imperfections have on the quantative reduction of the yield load of the column. This reduction is increased as the difference between P_{cs} and P_{cn} decreases. The maximum reduction corresponds to $P_{cs} = P_{cn}$.

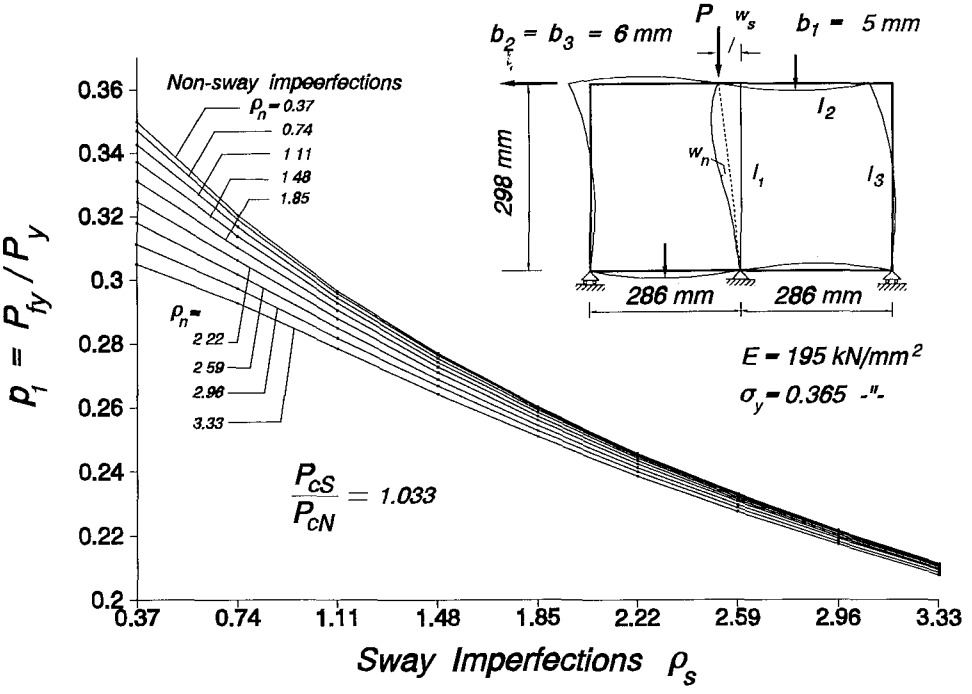

Figure 5-9

5.8 Plastic Collapse Analysis

In this section as a subsequent step of the first yield analysis, a mechanism by which a plastic failure occurs, is to be examined.

The Generalized Ayrton-Perry **(G.A.P.)** imperfection approach, as discussed in Section 4.5, has fully identified the non-linear response of imperfect columns. In Section 5.7 this approach has been extended to cover the case of two-mode-buckling, where it was found that for columns containing imperfections with respect to two different modes (degrees of freedom) occurring in the same plane, there will be two

modes contributing to the bending moments about the minor axis, both of which are non-linearly related to the axial load. This means that the bending moment at each cross section will have components contributed from both the sway and the non-sway modes.

For a given geometry of the column with corresponding boundary conditions arising from the stiffness of its surrounding frame and imperfections from both the sway and the non-sway modes, there always exists a plastic collapse surface, similar to the imperfection sensitivity surface of Fig. 5-8, which depicts all possible combinations between axial load and imperfections of both modes, that can exist in equilibrium with a fully plastic section.

In this coordinate system there is always a space-line, referred to as the Elastic Non Linear Path, which the above column follows as its axial load increases. This path is a function of the axial load, the first two critical loads, and the imperfection parameters corresponding to the first two modes.

The point where the elastic non-linear path intersects the plastic collapse surface is considered to be a close estimate of the upper bound solution to the collapse load.

The relationship between axial load and bending moment in an imperfect column has been given by Eq. (5.18). This equation, taking stresses for first yielding into account, has been eventually transformed into Eq. (5.22). Referring to this equation and following the same line of thought but in the case of full plasticity, we can end up in the equation

$$p_2^3 - p_2^2\left(p_{cs}\rho_s^*\alpha + p_{cn}\rho_n^*\beta + p_{cs} + p_{cn} + 1\right) + p_2\left[p_{cs}p_{cn}\left(\rho_s^*\alpha + \rho_n^*\beta + 1\right) + p_{cs} + p_{cn}\right] - p_{cs}p_{cn} = 0 \quad \textbf{(5.40)}$$

which is similar to Eq. (5.23), but, while p_{cs}, p_{cn} keep the same values,

$p_2 = \dfrac{P_{fh}}{P_y}$ is the unknown non-dimensional load at first hinge and

$\rho_s^* = \xi_s \dfrac{A}{Z_P}$, $\rho_n^* = \xi_n \dfrac{A}{Z_P}$ are dimensionless imperfection parameters, in which

Z_P is the **plastic** section modulus of the cross section.

For comparison reasons Fig. 5-10 illustrates the reduction of buckling strength of the column at first hinge, obtained for a frame geometry which is the same with that used for the first yield.

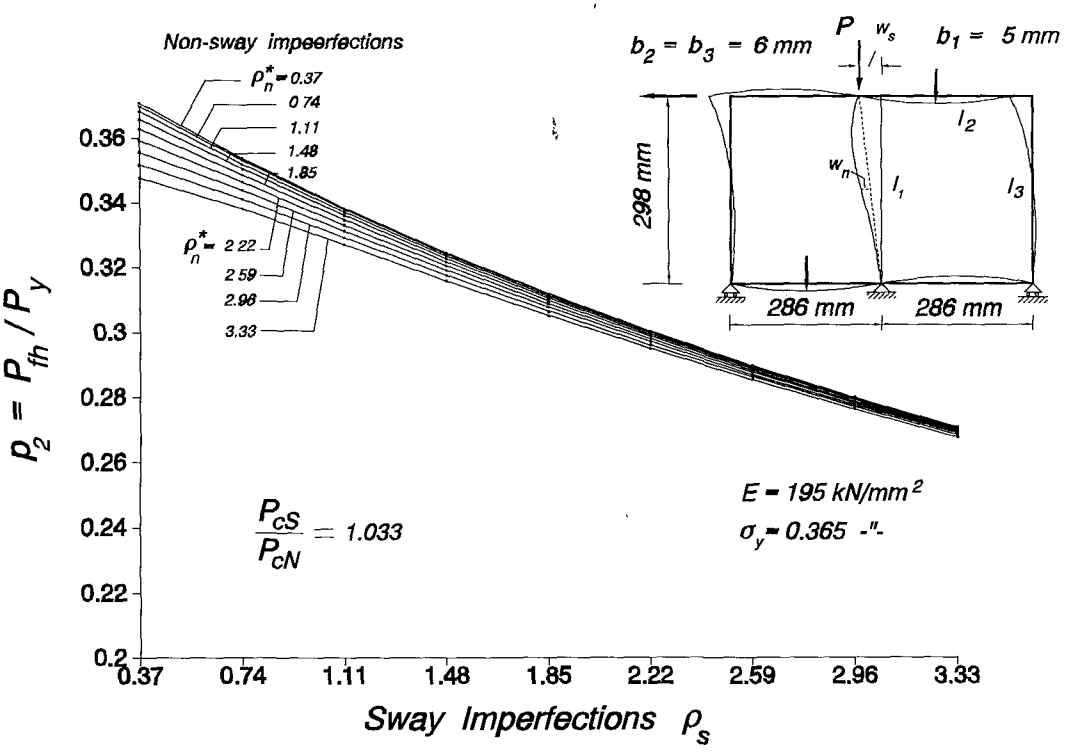

Figure 5-10

To cover not only the two-mode-contribution but a more general case, where a larger number of critical modes is demanded, an extension of the subroutine used in the main computer program for the first yield load, was developed according to the following algorithm:

a) Initially a zero axial load, P, is given. This load, which is increased at each step by small increments, dP, is then compared with the first critical load, P_{c1} and the squash load, P_y.

b) If $P < P_{c1}$ and $P < P_y$, then the following c, d and e steps are executed,

otherwise the first critical load or the squash load are respectively announced as failure load.

c) The contribution that each one of the demanded critical modes has,

i) in the deflection of the column (buckling shape)

ii) in the moment due to first yield, M_{fy} and plastic hinge, M_{ph} and

iii) in the elastic non-linear bending moment, M_{nl}, is calculated.

d) M_{nl} is compared with M_{fy}. If $M_{nl} < M_{fy}$, then the values of P, M_{nl}, M_{fy} and M_{ph} are recorded in a file to be further used as data for the elasto-plastic path graph and a new increment of load is added to the previous value. This procedure is repeated until either $M_{nl} = M_{fy}$, or $M_{nl} > M_{fy}$, when a negative half increment, -dP/2 is added, so that the load level for initiation of yielding should be exactly located, when after it is announced.

e) Provided that $P < P_{cr}$, the load-level for plastic hinge formation is similarly located and announced, when further calculations stop.

An output of the software results obtained for both first yield and first hinge failures is given at the end of this chapter.

5.9 The Effect of Buckling-mode-interaction

The phenomenon of interaction between the sway and the non-sway buckling modes, as discussed in Chapter 1, has different effects on the failure at different locations of the column.

For a column without imperfections belonging to a certain frame geometry, the first yield over the squash load ratio, p_1, has a definite value. Application of different combinations of imperfections (ρ_s, ρ_n) on this column, results of course in a reduction of p_1. The different values of p_1, corresponding to each pair of

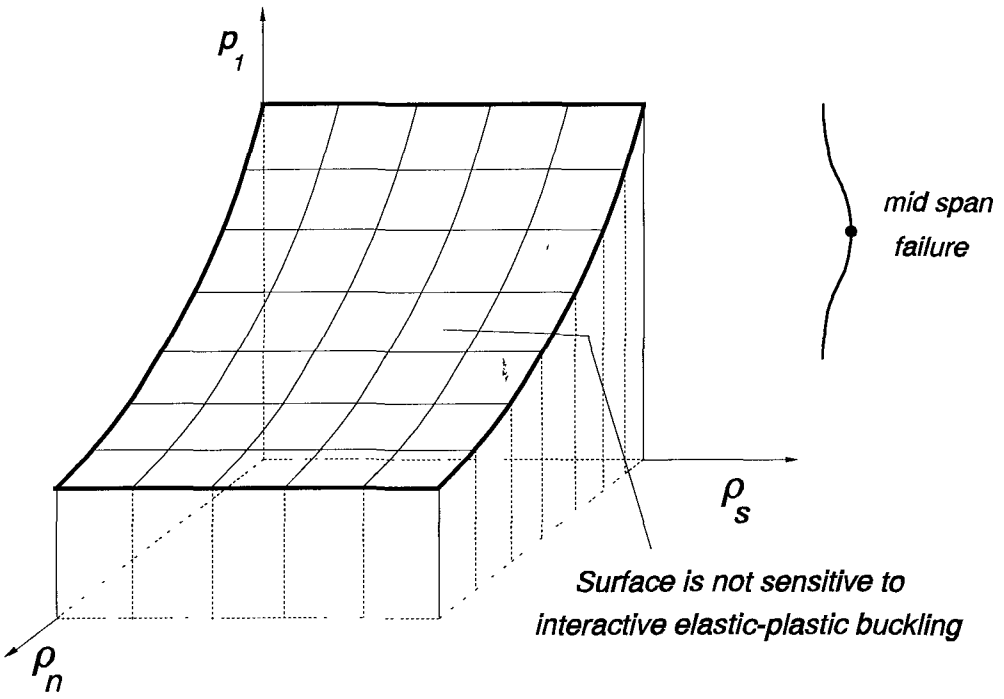

Figure 5-11

ρ_s, ρ_n may be depicted, as discussed in Section 5.7, in the first yield imperfection sensitivity failure surface p_1; for each failure point of the surface, the location of yielding along the column's length may be anywhere (end, mid span or somewhere in between). However, if we are interested in having yielding failure at a certain localized column area (mid span or ends), then the resulting points should compose a surface which may or may not be sensitive to interactive elastic-plastic buckling. This is because the failure effect of the sway imperfections is mainly limited at the ends of the column and secondarily at the middle. The same does not apply with the non-sway imperfections, which influence the yielding failure mainly at the mid span and secondarily at the ends.

Fig. 5-11 illustrates the effect of interaction between the two buckling modes in the presence of both imperfections when the yielding failure occurs at **mid span**, while Fig. 5-12 depicts a corresponding quantitative interaction effect for **end**

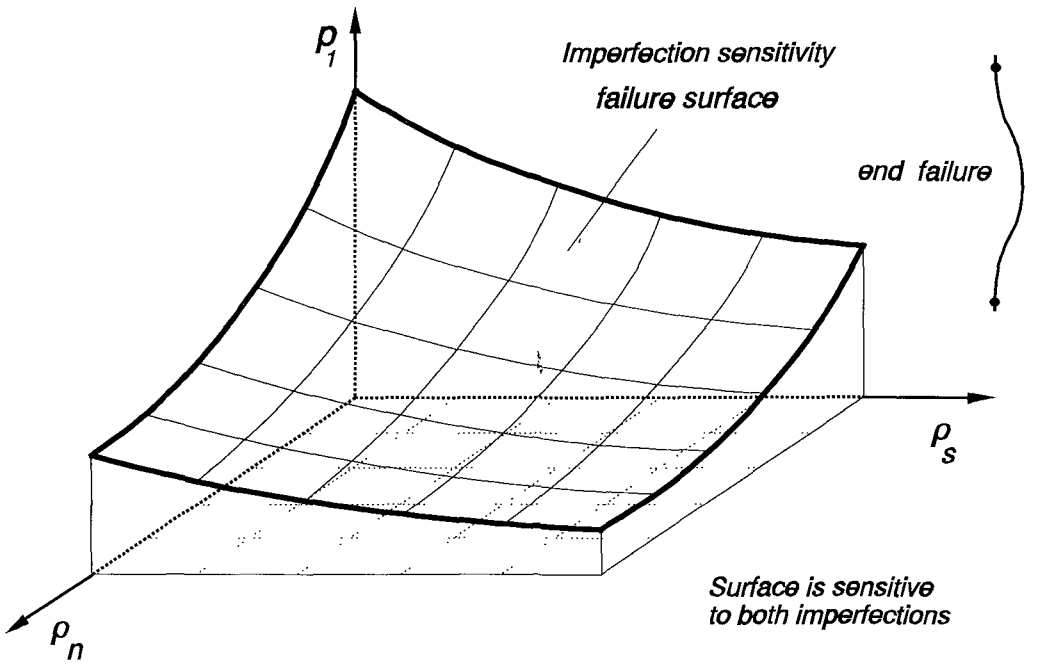

Figure 5-12

yielding failure. Both surfaces correspond to the same frame geometry where the same incremental amount of both imperfections was applied.

In Fig. 5-11, where only mid span failure is considered, p_1 does not seem to reduce in the presence of only ρ_s. This does not necessarily mean that p_1 is constant; it reduces according to Fig. 5-12 due to an end failure. However, if first yielding was prevented at the ends of the column, say by gradual local increase of cross section sizes, then p_1 would actually keep a constant value as shown in Fig. 5-11.

5.10 Output of Failure software Results

In this section a full set of data and results concerning the frame geometry and the graphs shown in Fig. 5-10 (first yield) and 5-11 (first plasticity) is presented

for a range of sway and non-sway imperfections.

M E M B E R P R O P E R T I E S

No	L	b	d	A	I	Zel	Zpl	Y.str
1	298.00	5.00	13.00	62.44	125.70	50.28	81.45	0.360
2	286.00	6.00	13.00	73.44	209.00	69.67	117.71	0.360
3	298.00	6.00	13.00	73.44	209.00	69.67	117.71	0.360

Rotational SYMMETRIC (Non-sway) Stiffness of frame = 1398.21 kN*mm/rad
Rotational ANTISYMMETRIC (Sway) Stiffness of frame = 1706.41 kN*mm/rad
Translational (Sway) Stiffness of frame = 27.93 N/mm

E I G E N V A L U E S & E I G E N V E C T O R S

Sol	kL	Pc	C1	C2	delta	theta_A	Mode-Case
1	5.642	8.7871	1.00	-0.332	0.000	0.006	Non-Sway
2	5.736	9.0802	1.00	3.560	-24.006	-0.005	* Sway

SQUASH Load = 22.477 kN

P O I N T 1 o f C U R V E 1
Run 1) For RHO_sway = 0.37, RHO_non-sway = 0.37, are:
First YIELD Load = 7.865 kN, Pfy/Py = 0.350 at x = 158.93 mm
First HINGE Load = 8.336 kN, Pfh/Py = 0.371 at X = 158.93 mm

P O I N T 1 o f C U R V E 2
Run 2) For RHO_sway = 0.37, RHO_non-sway = 0.74, are:
First YIELD Load = 7.801 kN, Pfy/Py = 0.347 at x = 173.83 mm
First HINGE Load = 8.314 kN, Pfh/Py = 0.370 at X = 168.87 mm

P O I N T 1 o f C U R V E 3
Run 3) For RHO_sway = 0.37, RHO_non-sway = 1.11, are:
First YIELD Load = 7.704 kN, Pfy/Py = 0.343 at x = 183.77 mm
First HINGE Load = 8.276 kN, Pfh/Py = 0.368 at X = 178.80 mm

P O I N T 1 o f C U R V E 4
Run 4) For RHO_sway = 0.37, RHO_non-sway = 1.48, are:
First YIELD Load = 7.580 kN, Pfy/Py = 0.337 at x = 188.73 mm
First HINGE Load = 8.223 kN, Pfh/Py = 0.366 at X = 183.77 mm

P O I N T 1 o f C U R V E 5
Run 5) For RHO_sway = 0.37, RHO_non-sway = 1.85, are:
First YIELD Load = 7.441 kN, Pfy/Py = 0.331 at x = 198.67 mm
First HINGE Load = 8.156 kN, Pfh/Py = 0.363 at X = 193.70 mm

P O I N T 1 o f C U R V E 6
Run 6) For RHO_sway = 0.37, RHO_non-sway = 2.22, are:

First YIELD Load = 7.295 kN, Pfy/Py = 0.325 at x = 203.63 mm
First HINGE Load = 8.079 kN, Pfh/Py = 0.359 at X = 198.67 mm
P O I N T 1 o f C U R V E 7
Run 7) For RHO_sway = 0.37, RHO_non-sway = 2.59, are:
First YIELD Load = 7.146 kN, Pfy/Py = 0.318 at x = 203.63 mm
First HINGE Load = 7.996 kN, Pfh/Py = 0.356 at X = 203.63 mm
P O I N T 1 o f C U R V E 8
Run 8) For RHO_sway = 0.37, RHO_non-sway = 2.96, are:
First YIELD Load = 6.998 kN, Pfy/Py = 0.311 at x = 208.60 mm
First HINGE Load = 7.907 kN, Pfh/Py = 0.352 at X = 203.63 mm
P O I N T 1 o f C U R V E 9
Run 9) For RHO_sway = 0.37, RHO_non-sway = 3.33, are:
First YIELD Load = 6.856 kN, Pfy/Py = 0.305 at x = 208.60 mm
First HINGE Load = 7.816 kN, Pfh/Py = 0.348 at X = 208.60 mm
P O I N T 2 o f C U R V E 1
Run 10) For RHO_sway = 0.74, RHO_non-sway = 0.37, are:
First YIELD Load = 7.201 kN, Pfy/Py = 0.320 at x = 153.97 mm
First HINGE Load = 7.949 kN, Pfh/Py = 0.354 at X = 153.97 mm
P O I N T 2 o f C U R V E 2
Run 11) For RHO_sway = 0.74, RHO_non-sway = 0.74, are:
First YIELD Load = 7.170 kN, Pfy/Py = 0.319 at x = 163.90 mm
First HINGE Load = 7.935 kN, Pfh/Py = 0.353 at X = 158.93 mm
P O I N T 2 o f C U R V E 3
Run 12) For RHO_sway = 0.74, RHO_non-sway = 1.11, are:
First YIELD Load = 7.120 kN, Pfy/Py = 0.317 at x = 168.87 mm
First HINGE Load = 7.910 kN, Pfh/Py = 0.352 at X = 168.87 mm
P O I N T 2 o f C U R V E 4
Run 13) For RHO_sway = 0.74, RHO_non-sway = 1.48, are:
First YIELD Load = 7.054 kN, Pfy/Py = 0.314 at x = 173.83 mm
First HINGE Load = 7.876 kN, Pfh/Py = 0.350 at X = 173.83 mm
P O I N T 2 o f C U R V E 5
Run 14) For RHO_sway = 0.74, RHO_non-sway = 1.85, are:
First YIELD Load = 6.975 kN, Pfy/Py = 0.310 at x = 178.80 mm
First HINGE Load = 7.834 kN, Pfh/Py = 0.349 at X = 178.80 mm
P O I N T 2 o f C U R V E 6
Run 15) For RHO_sway = 0.74, RHO_non-sway = 2.22, are:
First YIELD Load = 6.885 kN, Pfy/Py = 0.306 at x = 183.77 mm
First HINGE Load = 7.784 kN, Pfh/Py = 0.346 at X = 183.77 mm
P O I N T 2 o f C U R V E 7
Run 16) For RHO_sway = 0.74, RHO_non-sway = 2.59, are:
First YIELD Load = 6.787 kN, Pfy/Py = 0.302 at x = 188.73 mm
First HINGE Load = 7.728 kN, Pfh/Py = 0.344 at X = 188.73 mm
P O I N T 2 o f C U R V E 8
Run 17) For RHO_sway = 0.74, RHO_non-sway = 2.96, are:

First YIELD Load = 6.685 kN, Pfy/Py = 0.297 at x = 193.70 mm
First HINGE Load = 7.665 kN, Pfh/Py = 0.341 at X = 188.73 mm
P O I N T 2 o f C U R V E 9
Run 18) For RHO_sway = 0.74, RHO_non-sway = 3.33, are:
First YIELD Load = 6.581 kN, Pfy/Py = 0.293 at x = 193.70 mm
First HINGE Load = 7.599 kN, Pfh/Py = 0.338 at X = 193.70 mm
P O I N T 3 o f C U R V E 1
Run 19) For RHO_sway = 1.11, RHO_non-sway = 0.37, are:
First YIELD Load = 6.667 kN, Pfy/Py = 0.297 at x = 153.97 mm
First HINGE Load = 7.603 kN, Pfh/Py = 0.338 at X = 153.97 mm
P O I N T 3 o f C U R V E 2
Run 20) For RHO_sway = 1.11, RHO_non-sway = 0.74, are:
First YIELD Load = 6.649 kN, Pfy/Py = 0.296 at x = 158.93 mm
First HINGE Load = 7.593 kN, Pfh/Py = 0.338 at X = 158.93 mm
P O I N T 3 o f C U R V E 3
Run 21) For RHO_sway = 1.11, RHO_non-sway = 1.11, are:
First YIELD Load = 6.619 kN, Pfy/Py = 0.294 at x = 163.90 mm
First HINGE Load = 7.576 kN, Pfh/Py = 0.337 at X = 163.90 mm
P O I N T 3 o f C U R V E 4
Run 22) For RHO_sway = 1.11, RHO_non-sway = 1.48, are:
First YIELD Load = 6.579 kN, Pfy/Py = 0.293 at x = 168.87 mm
First HINGE Load = 7.552 kN, Pfh/Py = 0.336 at X = 163.90 mm
P O I N T 3 o f C U R V E 5
Run 23) For RHO_sway = 1.11, RHO_non-sway = 1.85, are:
First YIELD Load = 6.529 kN, Pfy/Py = 0.290 at x = 173.83 mm
First HINGE Load = 7.522 kN, Pfh/Py = 0.335 at X = 168.87 mm
P O I N T 3 o f C U R V E 6
Run 24) For RHO_sway = 1.11, RHO_non-sway = 2.22, are:
First YIELD Load = 6.471 kN, Pfy/Py = 0.288 at x = 173.83 mm
First HINGE Load = 7.486 kN, Pfh/Py = 0.333 at X = 173.83 mm
P O I N T 3 o f C U R V E 7
Run 25) For RHO_sway = 1.11, RHO_non-sway = 2.59, are:
First YIELD Load = 6.404 kN, Pfy/Py = 0.285 at x = 178.80 mm
First HINGE Load = 7.445 kN, Pfh/Py = 0.331 at X = 178.80 mm
P O I N T 3 o f C U R V E 8
Run 26) For RHO_sway = 1.11, RHO_non-sway = 2.96, are:
First YIELD Load = 6.334 kN, Pfy/Py = 0.282 at x = 183.77 mm
First HINGE Load = 7.400 kN, Pfh/Py = 0.329 at X = 178.80 mm
P O I N T 3 o f C U R V E 9
Run 27) For RHO_sway = 1.11, RHO_non-sway = 3.33, are:
First YIELD Load = 6.260 kN, Pfy/Py = 0.278 at x = 183.77 mm
First HINGE Load = 7.350 kN, Pfh/Py = 0.327 at X = 183.77 mm
P O I N T 4 o f C U R V E 1
Run 28) For RHO_sway = 1.48, RHO_non-sway = 0.37, are:

First YIELD Load = 6.225 kN, Pfy/Py = 0.277 at x = 153.97 mm
First HINGE Load = 7.291 kN, Pfh/Py = 0.324 at X = 153.97 mm
P O I N T 4 o f C U R V E 2
Run 29) For RHO_sway = 1.48, RHO_non-sway = 0.74, are:
First YIELD Load = 6.214 kN, Pfy/Py = 0.276 at x = 153.97 mm
First HINGE Load = 7.284 kN, Pfh/Py = 0.324 at X = 153.97 mm
P O I N T 4 o f C U R V E 3
Run 30) For RHO_sway = 1.48, RHO_non-sway = 1.11, are:
First YIELD Load = 6.193 kN, Pfy/Py = 0.276 at x = 158.93 mm
First HINGE Load = 7.270 kN, Pfh/Py = 0.323 at X = 158.93 mm
P O I N T 4 o f C U R V E 4
Run 31) For RHO_sway = 1.48, RHO_non-sway = 1.48, are:
First YIELD Load = 6.165 kN, Pfy/Py = 0.274 at x = 163.90 mm
First HINGE Load = 7.253 kN, Pfh/Py = 0.323 at X = 163.90 mm
P O I N T 4 o f C U R V E 5
Run 32) For RHO_sway = 1.48, RHO_non-sway = 1.85, are:
First YIELD Load = 6.132 kN, Pfy/Py = 0.273 at x = 168.87 mm
First HINGE Load = 7.231 kN, Pfh/Py = 0.322 at X = 163.90 mm
P O I N T 4 o f C U R V E 6
Run 33) For RHO_sway = 1.48, RHO_non-sway = 2.22, are:
First YIELD Load = 6.091 kN, Pfy/Py = 0.271 at x = 168.87 mm
First HINGE Load = 7.203 kN, Pfh/Py = 0.320 at X = 168.87 mm
P O I N T 4 o f C U R V E 7
Run 34) For RHO_sway = 1.48, RHO_non-sway = 2.59, are:
First YIELD Load = 6.045 kN, Pfy/Py = 0.269 at x = 173.83 mm
First HINGE Load = 7.173 kN, Pfh/Py = 0.319 at X = 173.83 mm
P O I N T 4 o f C U R V E 8
Run 35) For RHO_sway = 1.48, RHO_non-sway = 2.96, are:
First YIELD Load = 5.996 kN, Pfy/Py = 0.267 at x = 173.83 mm
First HINGE Load = 7.138 kN, Pfh/Py = 0.318 at X = 173.83 mm
P O I N T 4 o f C U R V E 9
Run 36) For RHO_sway = 1.48, RHO_non-sway = 3.33, are:
First YIELD Load = 5.939 kN, Pfy/Py = 0.264 at x = 178.80 mm
First HINGE Load = 7.099 kN, Pfh/Py = 0.316 at X = 178.80 mm
P O I N T 5 o f C U R V E 1
Run 37) For RHO_sway = 1.85, RHO_non-sway = 0.37, are:
First YIELD Load = 5.850 kN, Pfy/Py = 0.260 at x = 153.97 mm
First HINGE Load = 7.008 kN, Pfh/Py = 0.312 at X = 153.97 mm
P O I N T 5 o f C U R V E 2
Run 38) For RHO_sway = 1.85, RHO_non-sway = 0.74, are:
First YIELD Load = 5.840 kN, Pfy/Py = 0.260 at x = 153.97 mm
First HINGE Load = 7.001 kN, Pfh/Py = 0.311 at X = 153.97 mm
P O I N T 5 o f C U R V E 3
Run 39) For RHO_sway = 1.85, RHO_non-sway = 1.11, are:

First YIELD Load = 5.826 kN, Pfy/Py = 0.259 at x = 158.93 mm
First HINGE Load = 6.991 kN, Pfh/Py = 0.311 at X = 158.93 mm
P O I N T 5 o f C U R V E 4
Run 40) For RHO_sway = 1.85, RHO_non-sway = 1.48, are:
First YIELD Load = 5.808 kN, Pfy/Py = 0.258 at x = 158.93 mm
First HINGE Load = 6.978 kN, Pfh/Py = 0.310 at X = 158.93 mm
P O I N T 5 o f C U R V E 5
Run 41) For RHO_sway = 1.85, RHO_non-sway = 1.85, are:
First YIELD Load = 5.782 kN, Pfy/Py = 0.257 at x = 163.90 mm
First HINGE Load = 6.960 kN, Pfh/Py = 0.310 at X = 163.90 mm
P O I N T 5 o f C U R V E 6
Run 42) For RHO_sway = 1.85, RHO_non-sway = 2.22, are:
First YIELD Load = 5.754 kN, Pfy/Py = 0.256 at x = 168.87 mm
First HINGE Load = 6.940 kN, Pfh/Py = 0.309 at X = 163.90 mm
P O I N T 5 o f C U R V E 7
Run 43) For RHO_sway = 1.85, RHO_non-sway = 2.59, are:
First YIELD Load = 5.719 kN, Pfy/Py = 0.254 at x = 168.87 mm
First HINGE Load = 6.915 kN, Pfh/Py = 0.308 at X = 168.87 mm
P O I N T 5 o f C U R V E 8
Run 44) For RHO_sway = 1.85, RHO_non-sway = 2.96, are:
First YIELD Load = 5.682 kN, Pfy/Py = 0.253 at x = 173.83 mm
First HINGE Load = 6.888 kN, Pfh/Py = 0.306 at X = 168.87 mm
P O I N T 5 o f C U R V E 9
Run 45) For RHO_sway = 1.85, RHO_non-sway = 3.33, are:
First YIELD Load = 5.640 kN, Pfy/Py = 0.251 at x = 173.83 mm
First HINGE Load = 6.857 kN, Pfh/Py = 0.305 at X = 173.83 mm
P O I N T 6 o f C U R V E 1
Run 46) For RHO_sway = 2.22, RHO_non-sway = 0.37, are:
First YIELD Load = 5.525 kN, Pfy/Py = 0.246 at x = 153.97 mm
First HINGE Load = 6.748 kN, Pfh/Py = 0.300 at X = 149.00 mm
P O I N T 6 o f C U R V E 2
Run 47) For RHO_sway = 2.22, RHO_non-sway = 0.74, are:
First YIELD Load = 5.516 kN, Pfy/Py = 0.245 at x = 153.97 mm
First HINGE Load = 6.742 kN, Pfh/Py = 0.300 at X = 153.97 mm
P O I N T 6 o f C U R V E 3
Run 48) For RHO_sway = 2.22, RHO_non-sway = 1.11, are:
First YIELD Load = 5.508 kN, Pfy/Py = 0.245 at x = 158.93 mm
First HINGE Load = 6.735 kN, Pfh/Py = 0.300 at X = 153.97 mm
P O I N T 6 o f C U R V E 4
Run 49) For RHO_sway = 2.22, RHO_non-sway = 1.48, are:
First YIELD Load = 5.491 kN, Pfy/Py = 0.244 at x = 158.93 mm
First HINGE Load = 6.723 kN, Pfh/Py = 0.299 at X = 158.93 mm
P O I N T 6 o f C U R V E 5
Run 50) For RHO_sway = 2.22, RHO_non-sway = 1.85, are:

First YIELD Load = 5.475 kN, Pfy/Py = 0.244 at x = 163.90 mm
First HINGE Load = 6.710 kN, Pfh/Py = 0.299 at X = 158.93 mm
P O I N T 6 o f C U R V E 6
Run 51) For RHO_sway = 2.22, RHO_non-sway = 2.22, are:
First YIELD Load = 5.451 kN, Pfy/Py = 0.243 at x = 163.90 mm
First HINGE Load = 6.693 kN, Pfh/Py = 0.298 at X = 163.90 mm
P O I N T 6 o f C U R V E 7
Run 52) For RHO_sway = 2.22, RHO_non-sway = 2.59, are:
First YIELD Load = 5.427 kN, Pfy/Py = 0.241 at x = 163.90 mm
First HINGE Load = 6.674 kN, Pfh/Py = 0.297 at X = 163.90 mm
P O I N T 6 o f C U R V E 8
Run 53) For RHO_sway = 2.22, RHO_non-sway = 2.96, are:
First YIELD Load = 5.396 kN, Pfy/Py = 0.240 at x = 168.87 mm
First HINGE Load = 6.651 kN, Pfh/Py = 0.296 at X = 168.87 mm
P O I N T 6 o f C U R V E 9
Run 54) For RHO_sway = 2.22, RHO_non-sway = 3.33, are:
First YIELD Load = 5.366 kN, Pfy/Py = 0.239 at x = 168.87 mm
First HINGE Load = 6.627 kN, Pfh/Py = 0.295 at X = 168.87 mm
P O I N T 7 o f C U R V E 1
Run 55) For RHO_sway = 2.59, RHO_non-sway = 0.37, are:
First YIELD Load = 5.238 kN, Pfy/Py = 0.233 at x = 149.00 mm
First HINGE Load = 6.509 kN, Pfh/Py = 0.290 at X = 149.00 mm
P O I N T 7 o f C U R V E 2
Run 56) For RHO_sway = 2.59, RHO_non-sway = 0.74, are:
First YIELD Load = 5.232 kN, Pfy/Py = 0.233 at x = 153.97 mm
First HINGE Load = 6.504 kN, Pfh/Py = 0.289 at X = 153.97 mm
P O I N T 7 o f C U R V E 3
Run 57) For RHO_sway = 2.59, RHO_non-sway = 1.11, are:
First YIELD Load = 5.225 kN, Pfy/Py = 0.232 at x = 153.97 mm
First HINGE Load = 6.498 kN, Pfh/Py = 0.289 at X = 153.97 mm
P O I N T 7 o f C U R V E 4
Run 58) For RHO_sway = 2.59, RHO_non-sway = 1.48, are:
First YIELD Load = 5.213 kN, Pfy/Py = 0.232 at x = 158.93 mm
First HINGE Load = 6.489 kN, Pfh/Py = 0.289 at X = 158.93 mm
P O I N T 7 o f C U R V E 5
Run 59) For RHO_sway = 2.59, RHO_non-sway = 1.85, are:
First YIELD Load = 5.199 kN, Pfy/Py = 0.231 at x = 158.93 mm
First HINGE Load = 6.477 kN, Pfh/Py = 0.288 at X = 158.93 mm
P O I N T 7 o f C U R V E 6
Run 60) For RHO_sway = 2.59, RHO_non-sway = 2.22, are:
First YIELD Load = 5.183 kN, Pfy/Py = 0.231 at x = 163.90 mm
First HINGE Load = 6.465 kN, Pfh/Py = 0.288 at X = 163.90 mm
P O I N T 7 o f C U R V E 7
Run 61) For RHO_sway = 2.59, RHO_non-sway = 2.59, are:

First YIELD Load = 5.161 kN, Pfy/Py = 0.230 at x = 163.90 mm
First HINGE Load = 6.447 kN, Pfh/Py = 0.287 at X = 163.90 mm
P O I N T 7 o f C U R V E 8
Run 62) For RHO_sway = 2.59, RHO_non-sway = 2.96, are:
First YIELD Load = 5.140 kN, Pfy/Py = 0.229 at x = 163.90 mm
First HINGE Load = 6.430 kN, Pfh/Py = 0.286 at X = 163.90 mm
P O I N T 7 o f C U R V E 9
Run 63) For RHO_sway = 2.59, RHO_non-sway = 3.33, are:
First YIELD Load = 5.114 kN, Pfy/Py = 0.228 at x = 168.87 mm
First HINGE Load = 6.409 kN, Pfh/Py = 0.285 at X = 168.87 mm
P O I N T 8 o f C U R V E 1
Run 64) For RHO_sway = 2.96, RHO_non-sway = 0.37, are:
First YIELD Load = 4.984 kN, Pfy/Py = 0.222 at x = 149.00 mm
First HINGE Load = 6.287 kN, Pfh/Py = 0.280 at X = 149.00 mm
P O I N T 8 o f C U R V E 2
Run 65) For RHO_sway = 2.96, RHO_non-sway = 0.74, are:
First YIELD Load = 4.980 kN, Pfy/Py = 0.222 at x = 153.97 mm
First HINGE Load = 6.283 kN, Pfh/Py = 0.280 at X = 153.97 mm
P O I N T 8 o f C U R V E 3
Run 66) For RHO_sway = 2.96, RHO_non-sway = 1.11, are:
First YIELD Load = 4.973 kN, Pfy/Py = 0.221 at x = 153.97 mm
First HINGE Load = 6.278 kN, Pfh/Py = 0.279 at X = 153.97 mm
P O I N T 8 o f C U R V E 4
Run 67) For RHO_sway = 2.96, RHO_non-sway = 1.48, are:
First YIELD Load = 4.966 kN, Pfy/Py = 0.221 at x = 158.93 mm
First HINGE Load = 6.272 kN, Pfh/Py = 0.279 at X = 153.97 mm
P O I N T 8 o f C U R V E 5
Run 68) For RHO_sway = 2.96, RHO_non-sway = 1.85, are:
First YIELD Load = 4.953 kN, Pfy/Py = 0.220 at x = 158.93 mm
First HINGE Load = 6.261 kN, Pfh/Py = 0.279 at X = 158.93 mm
P O I N T 8 o f C U R V E 6
Run 69) For RHO_sway = 2.96, RHO_non-sway = 2.22, are:
First YIELD Load = 4.940 kN, Pfy/Py = 0.220 at x = 158.93 mm
First HINGE Load = 6.250 kN, Pfh/Py = 0.278 at X = 158.93 mm
P O I N T 8 o f C U R V E 7
Run 70) For RHO_sway = 2.96, RHO_non-sway = 2.59, are:
First YIELD Load = 4.924 kN, Pfy/Py = 0.219 at x = 163.90 mm
First HINGE Load = 6.237 kN, Pfh/Py = 0.277 at X = 163.90 mm
P O I N T 8 o f C U R V E 8
Run 71) For RHO_sway = 2.96, RHO_non-sway = 2.96, are:
First YIELD Load = 4.905 kN, Pfy/Py = 0.218 at x = 163.90 mm
First HINGE Load = 6.221 kN, Pfh/Py = 0.277 at X = 163.90 mm
P O I N T 8 o f C U R V E 9
Run 72) For RHO_sway = 2.96, RHO_non-sway = 3.33, are:

First YIELD Load = 4.886 kN, Pfy/Py = 0.217 at x = 163.90 mm
First HINGE Load = 6.204 kN, Pfh/Py = 0.276 at X = 163.90 mm
P O I N T 9 o f C U R V E 1
Run 73) For RHO_sway = 3.33, RHO_non-sway = 0.37, are:
First YIELD Load = 4.757 kN, Pfy/Py = 0.212 at x = 149.00 mm
First HINGE Load = 6.081 kN, Pfh/Py = 0.271 at X = 149.00 mm
P O I N T 9 o f C U R V E 2
Run 74) For RHO_sway = 3.33, RHO_non-sway = 0.74, are:
First YIELD Load = 4.753 kN, Pfy/Py = 0.211 at x = 153.97 mm
First HINGE Load = 6.079 kN, Pfh/Py = 0.270 at X = 153.97 mm
P O I N T 9 o f C U R V E 3
Run 75) For RHO_sway = 3.33, RHO_non-sway = 1.11, are:
First YIELD Load = 4.747 kN, Pfy/Py = 0.211 at x = 153.97 mm
First HINGE Load = 6.073 kN, Pfh/Py = 0.270 at X = 153.97 mm
P O I N T 9 o f C U R V E 4
Run 76) For RHO_sway = 3.33, RHO_non-sway = 1.48, are:
First YIELD Load = 4.742 kN, Pfy/Py = 0.211 at x = 153.97 mm
First HINGE Load = 6.068 kN, Pfh/Py = 0.270 at X = 153.97 mm
P O I N T 9 o f C U R V E 5
Run 77) For RHO_sway = 3.33, RHO_non-sway = 1.85, are:
First YIELD Load = 4.732 kN, Pfy/Py = 0.211 at x = 158.93 mm
First HINGE Load = 6.060 kN, Pfh/Py = 0.270 at X = 158.93 mm
P O I N T 9 o f C U R V E 6
Run 78) For RHO_sway = 3.33, RHO_non-sway = 2.22, are:
First YIELD Load = 4.720 kN, Pfy/Py = 0.210 at x = 158.93 mm
First HINGE Load = 6.050 kN, Pfh/Py = 0.269 at X = 158.93 mm
P O I N T 9 o f C U R V E 7
Run 79) For RHO_sway = 3.33, RHO_non-sway = 2.59, are:
First YIELD Load = 4.708 kN, Pfy/Py = 0.209 at x = 158.93 mm
First HINGE Load = 6.039 kN, Pfh/Py = 0.269 at X = 158.93 mm
P O I N T 9 o f C U R V E 8
Run 80) For RHO_sway = 3.33, RHO_non-sway = 2.96, are:
First YIELD Load = 4.693 kN, Pfy/Py = 0.209 at x = 163.90 mm
First HINGE Load = 6.027 kN, Pfh/Py = 0.268 at X = 163.90 mm
P O I N T 9 o f C U R V E 9
Run 81) For RHO_sway = 3.33, RHO_non-sway = 3.33, are:
First YIELD Load = 4.676 kN, Pfy/Py = 0.208 at x = 163.90 mm
First HINGE Load = 6.011 kN, Pfh/Py = 0.267 at X = 163.90 mm

Chapter 6

Experimental Developments

6.1 Review of Previous Experimental Work

Experimental work into buckling of simply supported columns started more than three hundred years ago. The first experiments were carried out in 1729 by Van Musschenbroeck, where he concluded that the strength of a long strut relates inversely to the square of its length. In 1759, Euler's Theory was developed; the experimental work that followed indicated that there were discrepancies between experimental results and his theory resulting in the abandonment of his theoretical developments for a period of time. These discrepancies prompted the creation of many empirical formulae, derived to provide lower limits to the scatter band of available experimental results. As described in chapter 2, it was Young, in 1807, who established a theoretical limit at which struts would crush rather than buckle. The contribution of the subsequent experimental work of Navier and Lamarle confirmed the application of Euler's theory to slender columns. Many other investigators presented empirical formulae in order to justify their own or other researchers' experimental work. In 1921, Salmon[50], wrote a very good review of the experimental work on column buckling.

However, the method of assessing the failure load of a column in a consistent way, that enjoys full respect even today, was introduced by Ayrton and Perry in 1886. They examined the validity of their analysis by comparing their theoretical predictions with results obtained from experiments conducted by Hodginson[5] a few decades before. It was the first time that a theory had been independently verified by experimental work done before.

In 1912, the elastician Southwell introduced a new method for interpreting the experimental results. His technique was developed on a similar but more general

basis than the one used by Ayrton and Perry. The work done by Southwell is still considered, as establishing the only convenient and consistent method for assessing the probable magnitude of imperfections present in the column. Unfortunately, his contribution seems to have been ignored by the vast majority of investigators undertaking experimental work on column buckling. As a result, the majority of past test results have failed to investigate the level of geometric and loading imperfections present in the test models with the consequence that much design is still based on empirical fits. Even in BS 5950, the inference of the imperfection level to ensure that the Ayrton and Perry formula provides the best fit curve for the scatter band of experimental results, was obtained empirically.

A recent experimental programme investigating the dependence of buckling upon the level of imperfections in columns was carried out at UCL[51] in 1992. In this programme, the column, from the instability point of view, was idealised as a member presenting only one degree-of-freedom, i.e. the column was examined either alone, or as a part of a **braced** frame. This situation, however, is not close to reality, where the majority of the axially loaded members (columns), considered either alone or as part of a frame, exhibit more than one - usually two - modes of buckling. The second mode of buckling may arise from the member showing an instability in another direction, or is a part of a frame which is not prevented from sidesway.

To extend the previous experimental programme to the case where buckling may involve more than one active buckling modes, a new series of experiments has been undertaken on the limited frame introduced in Chapter 3. The following sections describe the numerical experiments undertaken to choose a range of frame geometries to test the robustness of the theoretical model of Chapter 5.

6.2 The Objective of the Experiments

The present experimental work aims to examine the buckling behaviour of a beam-column, considered as a part of a frame which has the possibility of

sidesway. There are, therefore, two potentially critical modes of instability that have to be considered in the assessment of buckling for this system: the instability of the column as an independent member, and the instability arising from the sway possibility of the frame.

The main purpose of the present experimental work is to measure the **total imperfections** associated with the lowest sway and non-sway **buckling modes**. Of special interest is the case when the lowest two critical loads are close to each other. In these circumstances an interaction of the two modes is expected to take place, accompanied with a possible reduction of the ultimate capacity of the beam-column.

The Southwell Plot will be used as a tool, through which, the total imperfection, and a check on the critical load for each mode will be provided. These critical loads will then be compared with the corresponding loads obtained through theory (Eigenvalue problem). Having obtained the total imperfection for each mode, the theoretical load required to produce first yield and first hinge are calculated and compared with the buckling load obtained from the experiment. This part of work will assess the proposition that, provided the total imperfection is precisely known, the Generalized Ayrton and Perry formula can accurately predict the maximum load carrying capacity of the column. Another objective of the present experimental work is to illustrate how misleading the theoretical results can be if the imperfection effects are not taken into account.

Since the column is under a combination of axial load and bending moment, both the geometric and loading imperfections influence the load carrying capacity of the structure. The geometric imperfection is a random imperfection and its magnitude varies with different specimens. The loading imperfections, as developed in Chapter 4, depend on the loading pattern and the applied loads, and can be controlled to provide a wide variety of total imperfections. Based on the measured total imperfection obtained through the Southwell Plot, the theoretically calculated failure loads may then be compared with the experimentally observed collapse loads.

6.3 Numerical Experiments

The above procedure comprised initially a theoretical analysis as developed in chapter 3. Then, before starting any experimental work, a computer program was written in FORTRAN-77 which could carry out a critical load (Eigenvalue) analysis of a column considered as part of a frame which had the possibility of side-sway. This program also carried out a non-linear elastic and elasto-plastic analysis. Its use enabled various parametric studies to be undertaken, i.e. on the changes in P_{CN}, P_{CS}, for corresponding changes in the stiffness of the beams and columns of the frame, allowing for the final design of the test rig. Typical graphs of this study are shown in Appendix D.

Fig. 6-1 depicts the changes on the first sway and non-sway critical loads against the beam to central column second moment of area ratio, for a certain frame geometry. In all cases of geometries, an increase of the beam-stiffness only, had generally an incremental effect on the critical loads of the central column, which loads might be significantly different. When, however, this increase was combined with an increase of the stiffness of the side-columns, the difference between the first two (larger) values of critical loads was decreased, until at some stage it was negligible.

It is curious that if the geometry of the frame is kept constant, retaining $I_3/I_1>1.5$, for low stiffness of the beams, the first critical load, associated with the sway mode, is always less than the lowest critical load, associated with the non-sway. As the stiffness of the beams is increased, a point can be reached, where the first critical loads associated with sway and non-sway are equal. Further increase of the stiffness of the beams results in the sway critical load becoming greater than that of the non-sway mode. Apart from this pattern, expressed in Fig. 6-1, analogous patterns can be seen in the figures of the Appendix D, where the beams' stiffness, I_2/I_1, is kept constant but that of the outer columns, I_3/I_1, changes.

In conclusion:

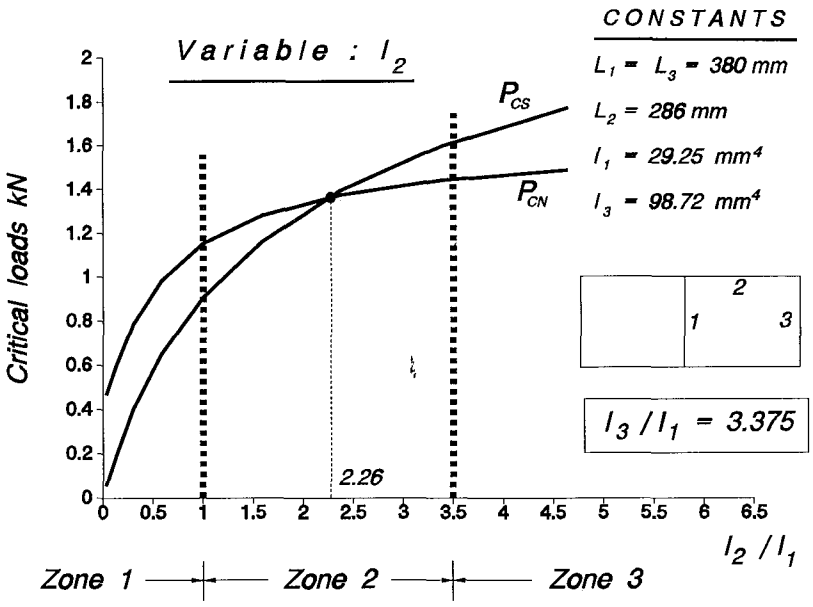

Figure 6-1

1) For low values of beam stiffness (I_2/I_1 < about 1), changes in outer column stiffness do not result in an intersection of the P_{CS} and P_{CN} curves.

2) For higher values of beam stiffness (I_2/I_1 > say 2.26), a cross-over of the curves occurs.

The above parametric studies show that an experimental programme, with $1 \leq I_2/I_1 \simeq I_3/I_1 \leq 3.5$, would provide a means of testing the range of behaviours, when the buckling case is:

i) Uncoupled sway (zone 1), where $P_{CS}/P_{CN} \ll 1$,

ii) Coupled sway and non-sway (zone 2), where $P_{CS}/P_{CN} \cong 1$, and

iii) Uncoupled non-sway (zone 3), where $P_{CS}/P_{CN} \gg 1$.

All the above zones are to be investigated through a variety of frame geometries, coming from different lengths and cross section sizes for beams and columns. The variety of cross sections, once they have a standard breadth of 13 mm,

will be dictated from the available in the market three different thicknesses, i.e. 3, 5 and 6 mm.

6.4 The Southwell Plot

The relationship between the total deflection, obtained in the elastic region from the original, absolutely straight position of the column, in terms of the geometric and loading imperfections in a general loading system, is given as

$$w^t(x) = \sum_{i=1}^{\infty} \frac{P_{ci}}{P_{ci}-P}\left(w_i^o + w_i^n\right)\phi_i(x) + \sum_{i=1}^{\infty} \frac{P}{P_{ci}-P} w_i^p \phi_i(x)$$

where w_i^o, w_i^n and w_i^p are respectively the i^{th} amplitudes of the geometric, non-proportional and proportional loading imperfections. If δ is a deflection, obtained as a difference between:

i) the above total deflection $w^t(x)$, and

ii) the initial imperfection, i.e.

a) geometric, $w^o(x)$, and/or

b) loading, $w^n(x)$, (non-proportional)

which is independent from the axial load, then δ becomes

$$\delta(x) = \sum_{i=1}^{\infty} \frac{P}{P_{ci}-P} \xi_i \phi_i(x) \qquad (6.1)$$

where $$\xi_i = w_i^o + w_i^p + w_i^n$$

is the amplitude of the **total equivalent imperfection** termed as modal equivalent imperfection.

This equation is applied to a beam-column having any kind of imperfections. In the experiments that have been carried out, the beams were always loaded non-proportionally; therefore $w_i^p = 0$, and Eq. (6.1) becomes

$$\delta(x) = \sum_{i=1}^{\infty} \frac{P}{P_{ci} - P}\left(w_i^o + w_i^n\right)\phi_i(x) \ . \tag{6.2}$$

At the top of the column, all the imperfections are associated with the lowest sway mode (symmetric about the column centre), whilst, at the middle of the column they are dominated by the lowest non-sway mode (symmetric with respect to an axis perpendicular to the mid column). Due to the fact that the contributions of higher order modes (sway or non-sway) to the deflected shape of the beam-column are negligible, Eq. (6.2), for the first sway and non-sway modes, becomes respectively

$$\delta_t = \frac{P}{P_{c_S} - P}\xi_s \tag{6.3}$$

$$\delta_m = \frac{\delta_t}{2} + \frac{P}{P_{c_N} - P}\xi_n \tag{6.4}$$

where ξ_s and ξ_n are respectively the total equivalent imperfections associated with the first sway and non-sway modes.

If Eqs. (6.3) and (6.4) are plotted in a form of δ/P versus δ, the resulting graph will be a straight line. This is the type of graph known as a Southwell Plot. The gradient of this line is the elastic critical load, whereas its intercept with the abscissa is the total equivalent imperfection that corresponds to the buckling mode under consideration.

Therefore, in order to experimentally assess the imperfections associated with the first sway and non-sway modes, the axial load, along with the corresponding deflections at both the top and the middle of the column, are the only necessary and

sufficient elements of data.

6.5 First-stage Experimental Equipment and Instrumentation

At the first stage of the above procedure the geometry of the members of the frame along with their material properties was determined. A solid rectangular cross-section of mild steel was used for all members. This type of cross-section, compared with other sections had a high shape-factor of $S/Z=1.5$ and therefore an extended elastic-plastic behaviour was expected. All the members had nominal dimensions of breadth b = 0.5 inch and depth d = 1 inch. The beam lengths were 500 *mm*. The length of the columns L could be varied from 302 *mm* to 702 *mm* with an approximate increment of 100 *mm* giving five different column lengths. Figs. A.1.1 to A.1.3 in Appendix A, show the geometry and a bending test made to determine the material properties at this stage.

The rig used to test this limited frame, shown in Photo 1 of Appendix F, is available in the Departmental laboratories at University College London. It was designed to test both isolated columns and limited frames up to a maximum load of 100 *kN*, through a jack incorporated at the bottom of the beam. A manufactured N.C.B./M.R.E. load cell, shown in Photo 2 on the top of the jack, is connected to a digital strain gauge monitor, to measure the axial load. Before starting the tests the load cell was calibrated to make sure there is a linear response in the loading range.

A trolley, shown in Photo 3, was designed to accommodate the top joint of the central column along with its horizontal beams of the frame, which were clamped to the column. The trolley had to move freely horizontally, through four special ball-bearings as shown in Photo 4. Four end-blocks, shown in Photo 7, were also specially designed to clamp the ends of the four beams with the corresponding ends of the side columns; the left and right bottom of them had a special base with a ball-bearing to enable rotation at the support point the frame. Two other blocks (top and bottom centre) were each used to connect the two beams together with the

central column. The six end-blocks resulted in the whole frame to behave as a monolithic construction. Finally a pulley mechanism, shown in Photo 7, was used for the application of horizontal load, through weights.

6.5.1 First stage Experimental Results

When the frame was under loading without axial load, its horizontal displacement was in excellent agreement with what was earlier calculated.

However, when an axial load P (either proportional to or independent of the horizontal load) was applied, as shown in Photo 8, the horizontal displacement of the frame ceased to follow the theoretical values. The greater the axial load that was applied, the larger was the discrepancy from the calculated values. Sometimes, at an interim stage of the experiment, while the proportional increment of P and H was normal, some unexplained jumps of displacement (see graph A.2.9 in Appendix A) were observed.

This phenomenon, being repeated for a series of experiments, led to the conclusion that:

(i) During the application of the axial load, an excessive rolling friction was developed in the ball-bearings.

(ii) Due to the high levels of axial load applied in earlier experiments taken up to failure, the tangent points of the circular surface of the rollers (cylinders) of the trolley created surface irregularities (ridges) on the flat bearing surface producing discontinuous performance of the roller bearings (see typical Photo 4).

An attempt was made to smooth these ridges and improve the conditions of the roller-bearings. However, although a substantial improvement had been effected on both the friction and the ridges, the problem still existed. A new series of tests followed where some minor jumps of deflection appeared. The friction, being always present, continued to constrain the deflections. Again, some minor ridges were

observed on the flat bars (rails).

This time the old surface of the bars was replaced with specially hardened pieces of steel. This, it was believed, would eliminate all the former imperfections of the trolley. Unfortunately it only needed a small number of tests to realise that even this, the best and probably last of all possible improvements, was not able to eliminate friction, despite the minimization of the ridging effect.

The idea of substituting the displacement controlled trolley for a force control using weights seemed eventually to be a reasonable method for eliminating the friction, although the applied axial load could not be as high as that obtained through the hydraulic jack.

To allow failure conditions to be produced, a smaller cross section of 13x3 *mm* was adopted. With this cross section the second moment of area is at least 100 times smaller than the second moment of area of the previous section (25x12 *mm*) with corresponding reductions in buckling loads. A new rig to accommodate a frame of these small-section-members was then carefully designed and constructed.

6.6 Geometry of the new Frame-model

In the experiments, for all the members of the idealized limited frame, a solid 'rounded' rectangular cross section was used. Compared with other cross-sections, this type has a higher shape-factor (S/Z = 1.62), therefore an extended elasto-plastic behaviour is expected. The members, taken from what was available in the market, had three nominal dimensions, i.e. a standard breadth of 13 mm, coupled with thicknesses of 3, 5 and 6 mm. Due to the non-pure-rectangular type of cross section, a special subroutine was incorporated in the main computer program to calculate cross-section properties (area, second moment of area, section modulus), required in the procedure of theoretical analysis.

The lengths of beams and columns were generally different for each test. As

a result of this, different slenderness ratios and various relative rigidities at the end-blocks of the column had to be taken into account. For each test, the frame geometry and the pattern of loading were selected to cover a certain range of the failure to squash load ratio as well as a certain range of P_{cS}/P_{cN} ratio, according to what was discussed in Section 6.3. This geometry was usually shown in a sub-figure which was incorporated in the main graph, were a certain information was given.

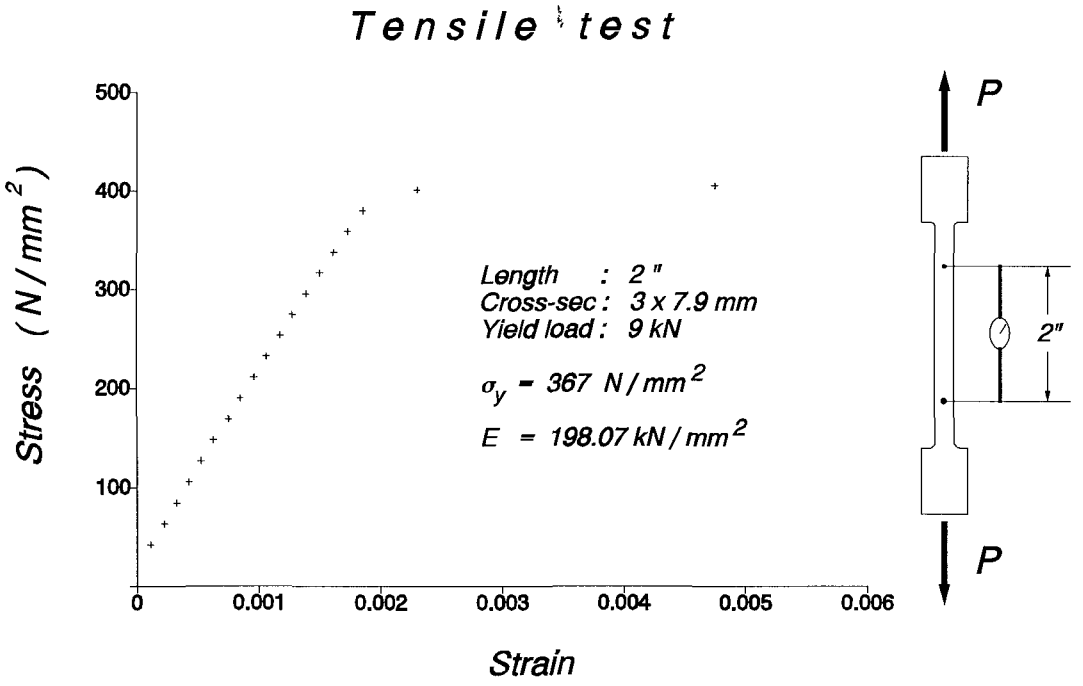

Figure 6-2

6.7 Material Properties

All the material used for the frame model in this experimental work was commercially available mild steel. Although it comprised three different cross sections which might have been chosen from different batches, each one of the test specimens was assumed to have effectively the same material properties.

The mean Young's modulus was calculated from three specimens, where three different types of experiments (tension, bending and cantilever) were carried

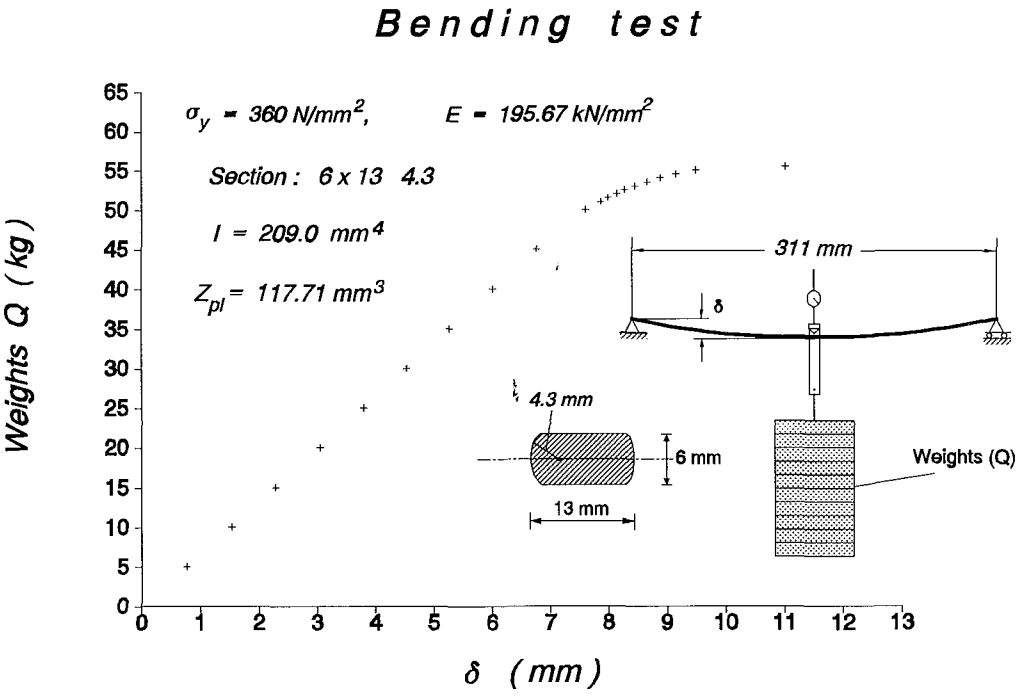

Figure 6-3

out, and was found to be 195 kN/mm^2, with a variation from the mean ±1.9%; the corresponding mean yield stress was 360 N/mm^2 with a variation from the mean ±1.7%. Figs. 6-2 to 6-4 show the corresponding graphs obtained from the results of the experiments conducted to define the material properties.

6.8 Experimental Environment for the new Frame

The main test-rig used for the new frame remained the same. However, in the new architecture, where the jack had to be removed, a stiff horizontal beam, the central part of which was supported and consequently would produce negligible deflection, had to accommodate the central, pinned support of the frame. A general arrangement of the test-rig is shown in Fig. 6-5.

Fig. 6-6 depicts a more detailed configuration of the overall frame, where a proper set of end-blocks was used to connect beams and columns. Details of these

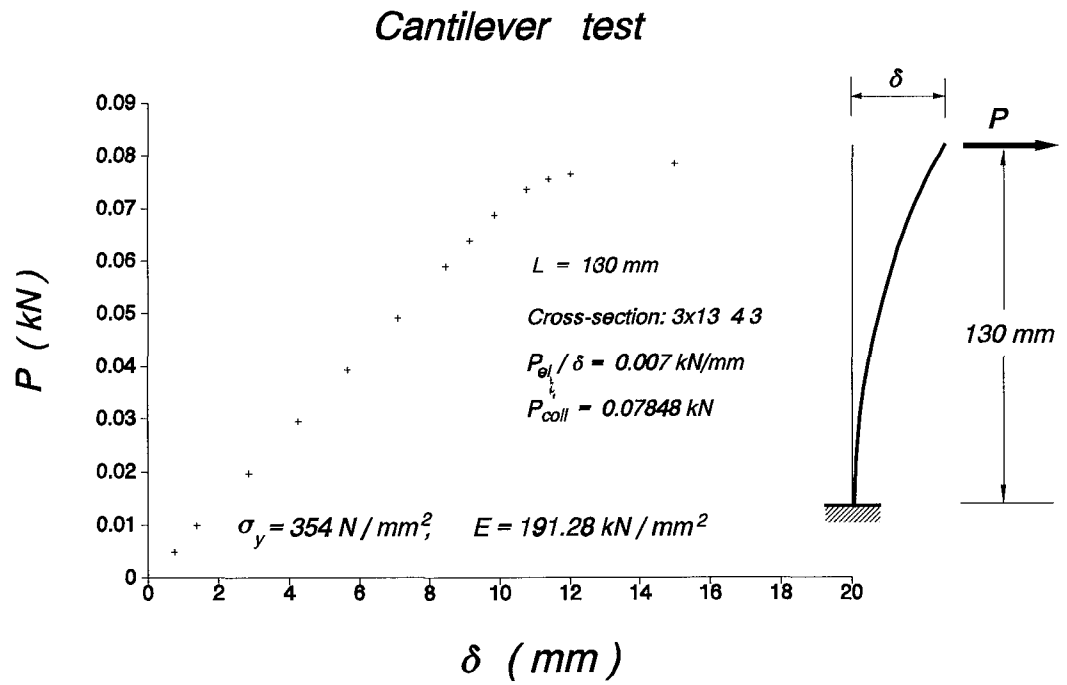

Figure 6-4

end-blocks are given in the next section.

Initially the test rig was designed to accommodate the rounded 3x13 mm section. For relatively slender columns of this section a failure could be possible, for axial load less than 120 kg, which was the maximum applicable weight load. Later on, however, it was ascertained that a larger amount of axial load needed to be applied on the column, so that a state of failure, even for less slender or almost perfect columns, should always be feasible. For this reason the load application system was changed. As shown in Fig. 6-8 and discussed in the next paragraph, the axial load was applied by a wheel nut through a gantry and a load-cell was specially designed and constructed, to accommodate and accurately measure axial loads up to 8 kN. It was machined from mild steel in a U-shape, as shown in Fig. 6-7. Foil strain gauges[52] were placed inside and outside its arms, which were connected in series on a measuring circuit. This circuit, consisting of a power supply and a bridge balance, provided, through a voltameter, a digital reading of the current axial load. A calibration of this load cell gave a sufficiently linear response, with a sensitivity

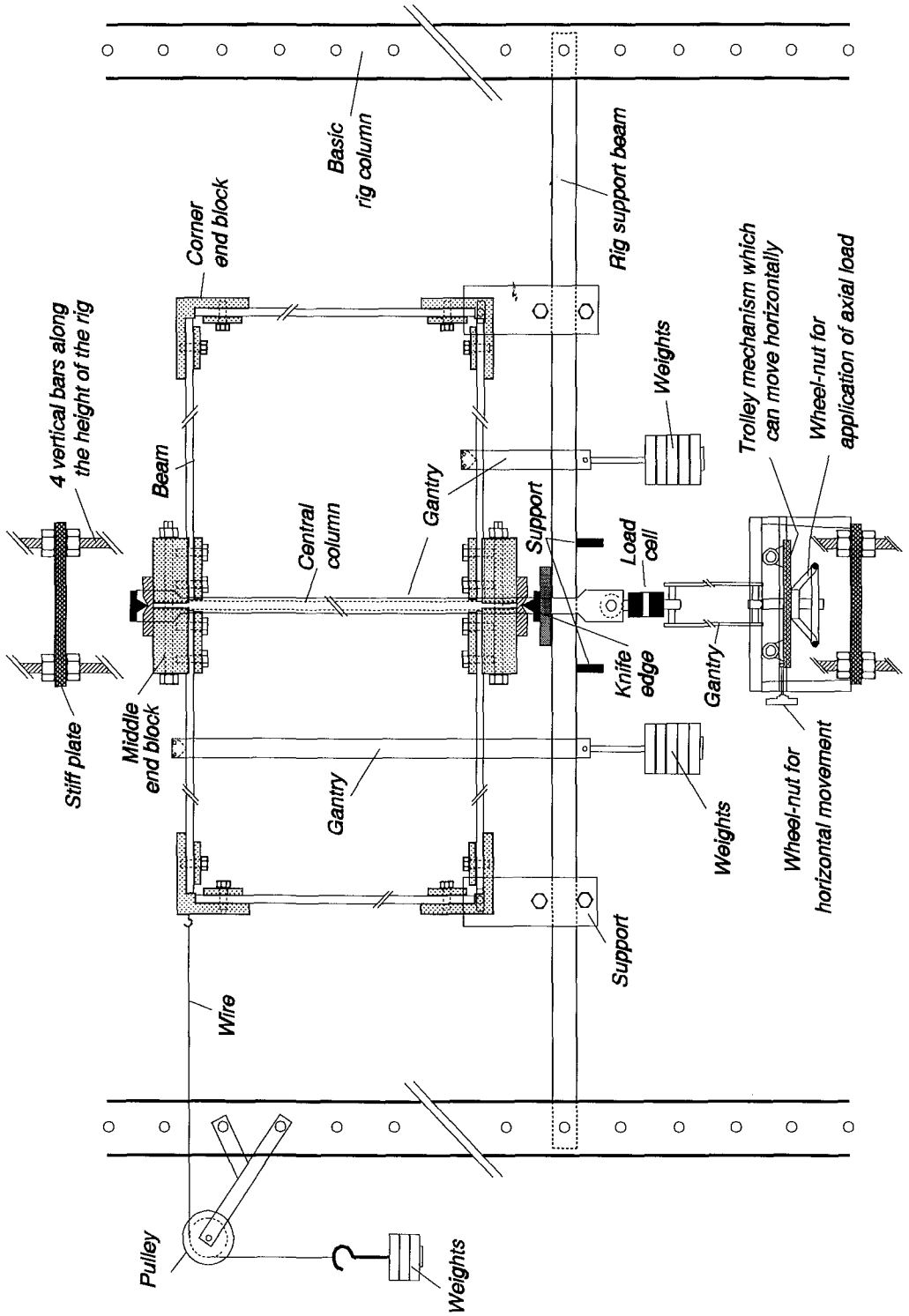

Figure 6-5 Overal view of the test-rig

of ± 0.01 *kN* over the range 0-8 kN.

The application of axial load was the next problem to be solved. The load

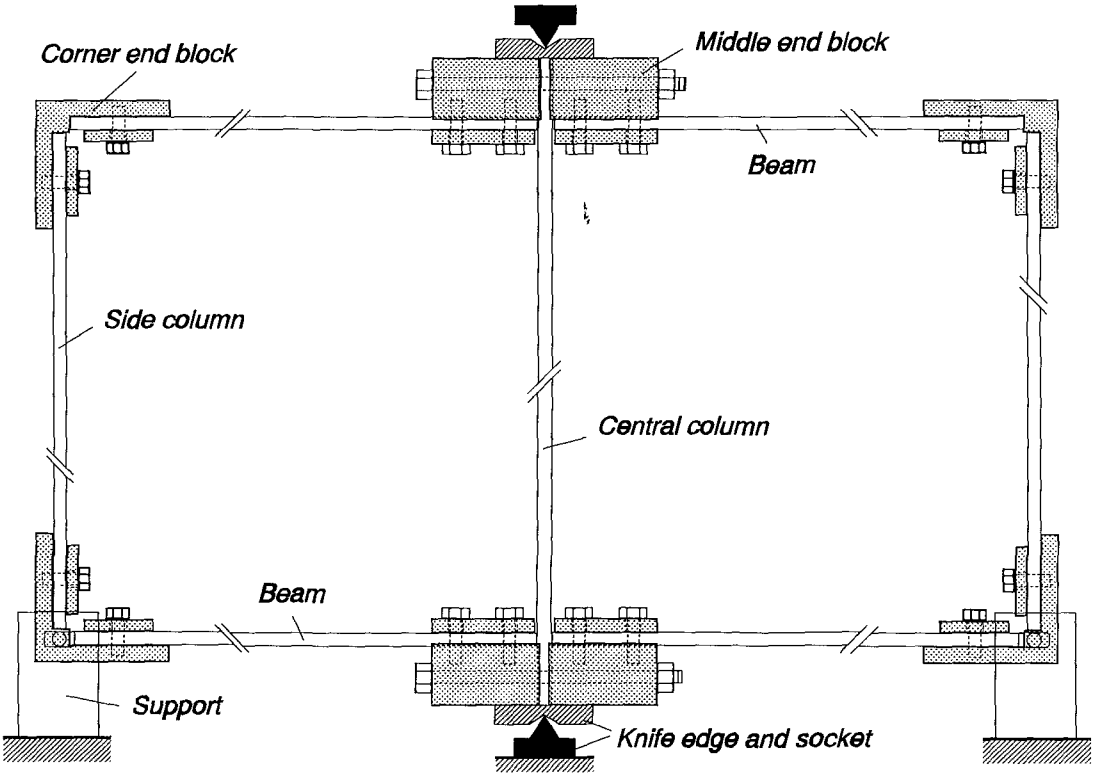

Figure 6-6

should be applied through a gantry, the upper end of which had a knife-edge resting on the upper end of the column. After discarding weights, a way had to be found, so that the gantry could always be kept vertical. This implied that the original point of application of axial load (lower end of gantry), which replaced the weights, had to always follow any possible horizontal movement of the top-knife-edge of the column.

Here, it has to be noted that the slightest horizontal movement of the original point of application of the axial load with respect to the top-knife-edge resulted in the development of a small horizontal component, which in turn affected both the horizontal deflections of the column (at top and mid-height). This would have the

effect of producing uncertain experimental conditions.

For this reason, the trolley mechanism, previously used at the first experimental stage, was modified, to allow the bottom of loading gantry to be adjusted to keep the gantry in the vertical position.

Fig. 6-8 shows the trolley mechanism. On this mechanism a special wheel-nut is fixed (left side of figure), so that at each experimental stage it can always accurately follow the horizontal movement of the column-top.

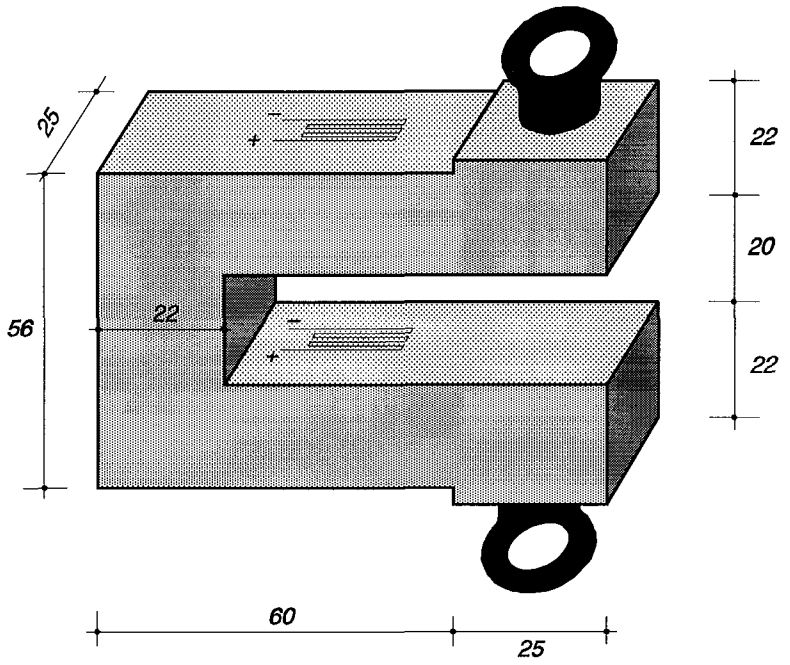

Figure 6-7

To enable the presence of sway loading imperfections at the top of the column, a pulley system, shown in Fig. 6-5, was used. This system could be put at either side of the rig, so that the horizontal deflection at the top of the column could be directed either to the right or to the left. For non-sway loading imperfections, two hangers were attached through gantries on the mid-span of the upper-left and lower-right beam. In all the experiments the weights used for non-sway imperfections were

the same for each beam, so that the maximum deflection would always occur at the mid-height of the column.

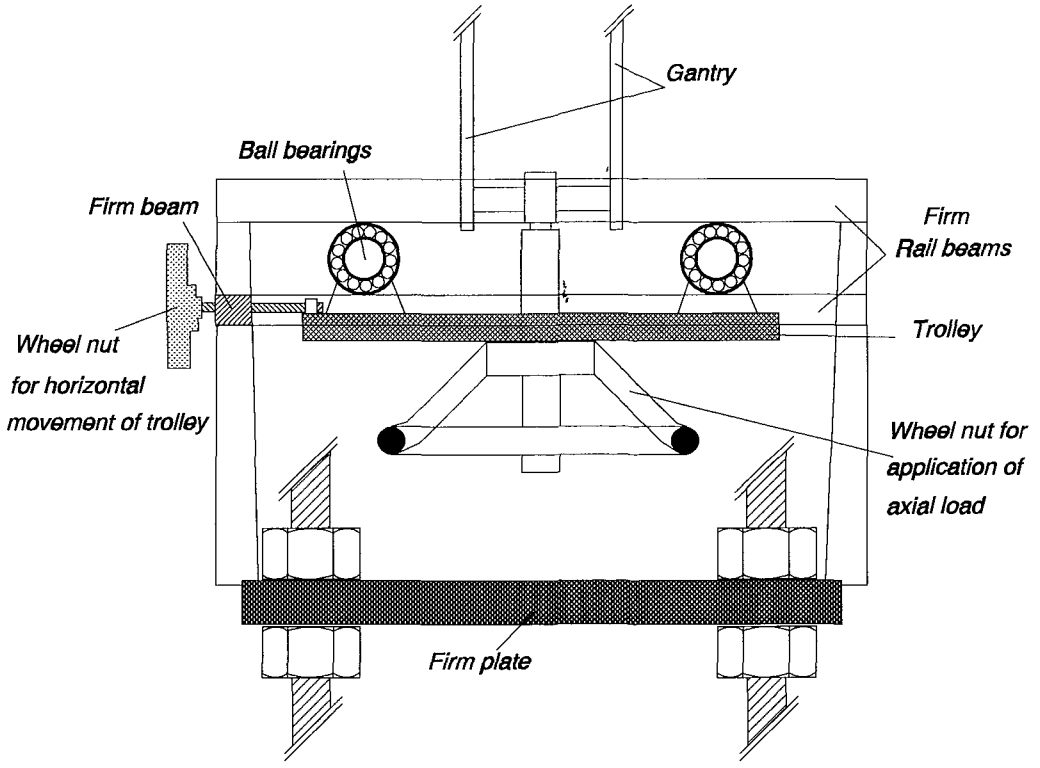

Figure 6-8

The lateral deflections of the column (at top and mid-height) were always measured through dial gauges. Their magnetic bases were attached to the fixed, stiff plate, of the rig.

6.9 The Set-up of Limited-frames

One of the major problems in performing the experiments was to enable easy replacement of the failed column members and yet ensure a rigid joint connection between beams and columns, so that the whole frame could have a monolithic response.

Figs. 6-9 and 6-10 show in detail two kinds of end-blocks (connectors) used to carry out the above task. Basically, each connection was designed to meet the

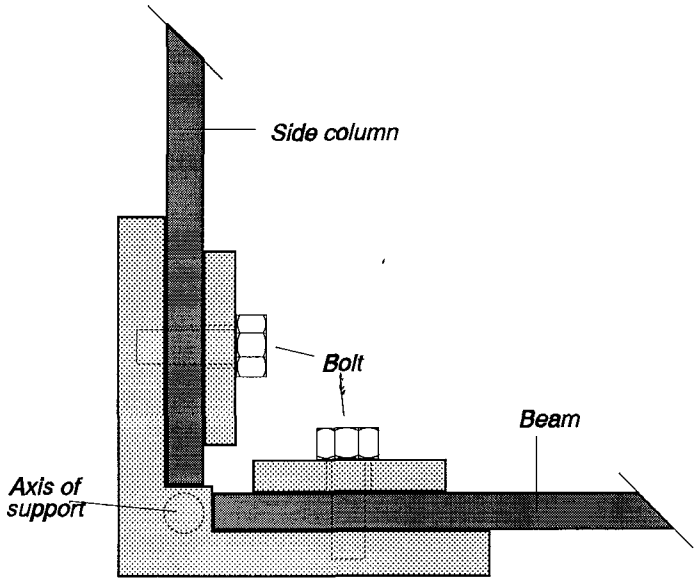

Figure 6-9

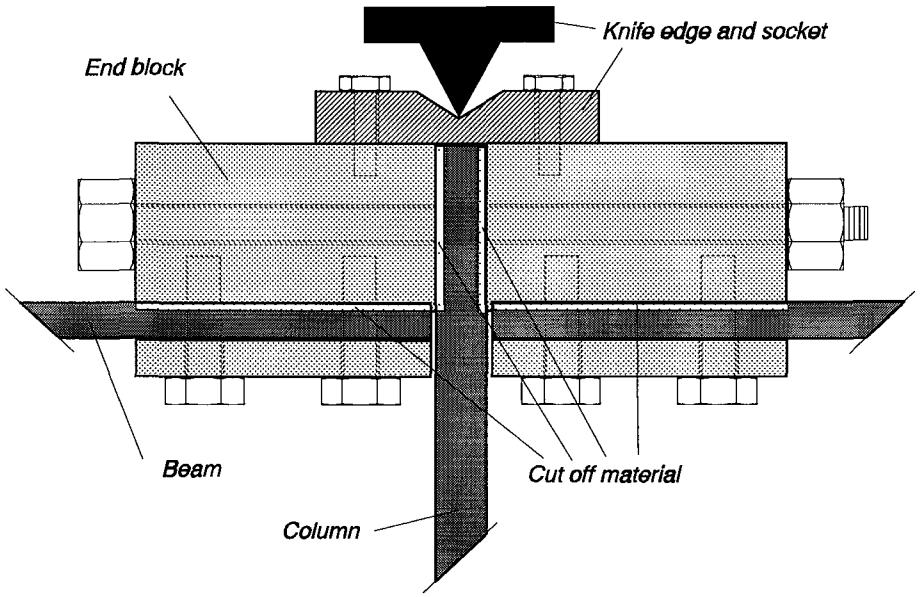

Figure 6-10

following requirements: firstly it should not have any weak point in it, nor should it create any similar point in the column or beam(s); secondly it should be rigid

enough to transfer without significant distortion any cross section force arising from statics; thirdly it should be easily assembled.

The corner end-block, shown in Fig. 6-9, provided a connection between a beam and a side column. All three pieces were of high strength steel, using bolts of similar material. To enable a rolling support for the two lower corners of the frame, a special cylindrical axis was turned at both sides, perpendicular to the frame plane. This axis is then accommodated in the holes of a corresponding pair of plates, strongly connected to the horizontal rig support beam.

Fig. 6-10 shows an end-block connecting two beams to the central column. It consists of two pairs of high-strength steel-plates which grip the two ends of the beams. Then, the upper plates, which are thicker, grip the end of the column, through two large bolts. Finally, on the top of these two thick plates, was placed a top plate with a V-notch. This was in contact with the knife-edge, and thus provided a free rotation of the joint in the plane of the frame. The dimensions of plates and bolts were designed to sustain the forces arising from the loading of the frame and the pre-tension of the bolts.

To ensure adequate clamping and alignment of both the beams and the column, the upper (thick) plates were manufactured so that a strip of material, of 1x13 mm cross-section, was removed across the middle of their two perpendicular sides. This 'cut off' material is shown in Fig. 6-10 as a less shaded area.

A spatial view of this end-block is also shown in Fig. 6-11, where some of the above details can be more easily understood.

6.10 The Test Procedure

Before starting the test procedure, a preliminary numerical experiment was always performed through the computer program. In this procedure a properly chosen combination of data on cross-section sizes and lengths of beams and columns

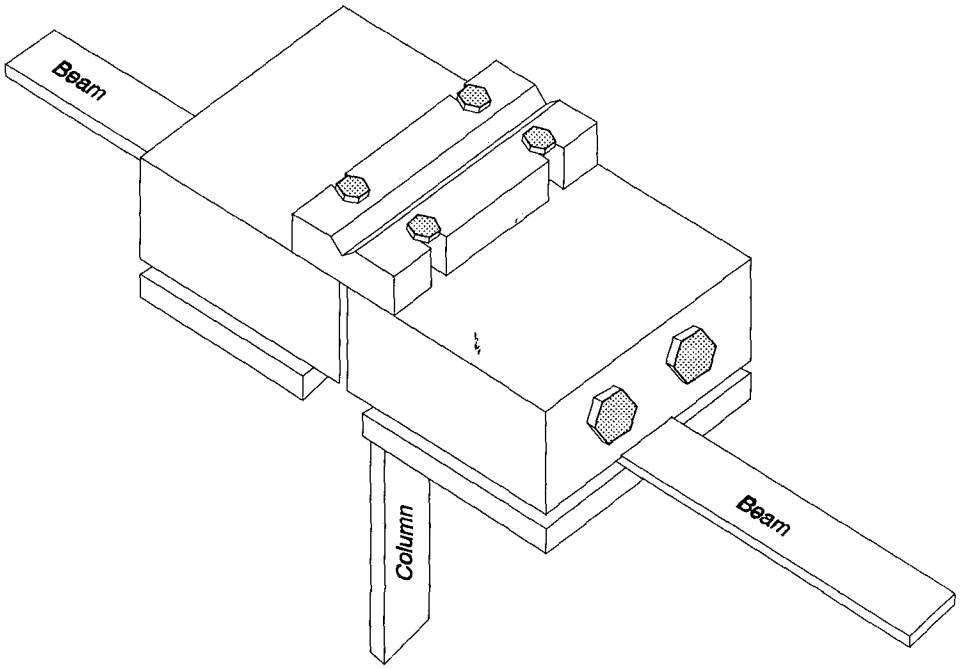

Figure 6-11

was given, so that, taking into account a known amount of imperfection(s) for one only or both buckling modes, the resulting behaviour should be at expected levels. These levels might be the restrictions arising from section 6.3, ensuring that the first two critical loads should be close to each other, while the buckling load, or the load necessary to form the first plastic hinge, or at least the first yield load, should not be more than 8 kN, which was the maximum tension capacity for the load cell measuring the axial load.

Having a whole picture of the experimental data along with the expected results from theory, the appropriate cross sections and lengths for beams and columns were first accurately cut and then carefully assembled. The stage of assembling was very important because all the members of the frame had to be correctly aligned before the bolts were tightened. This means the frame had to keep all its members in plane and have them straight with right angles between them; otherwise, apart from any frame-imperfections, there could be initial stresses locked

in the members which could affect the final results.

The whole frame was then put on the rig having 1) its bottom V-shaped plate rested on the knife-edge which was fixed on the horizontal beam and 2) its lower side end-blocks coupled into the corresponding holes of the supporting plates. The main task at this stage was to ensure a vertical position of the frame with its lower side end-blocks free to rotate and move horizontally, but not vertically.

The knife-edge of the upper gantry, used for application of the axial load, was next placed on the upper V-shaped plate of the column. Then the gantry was connected, through the load cell, with the corresponding gantry starting from the wheel-nut on the trolley mechanism. At this stage, the verticality of the upper gantry was checked with scrupulous care, through a plumb-line, to ensure absence of any horizontal component of axial load.

In order to get a first, rough idea of any initial geometric imperfection of the central column the following measurements were processed:

1) For the non-sway mode, the maximum deformation, existing in the middle of the length, was measured through a device with a dial gauge, made for this purpose and shown in Fig. 6-12.

2) For the sway mode, the horizontal distance between the gantry's knife-edge and the plumb-line was also taken through a dial gage.

To enable the measuring of horizontal deflections on both the top and mid-height of the central column, two dial gauges were placed on the stiff plate of the test rig. One more dial gauge was placed down on the trolley mechanism to measure its required horizontal movement, to follow the corresponding top deflection.

In order to produce loading imperfections on the central column:

1) For the non-sway mode, two gantries were suspended, with their knife-edge on the middle of the upper-left and lower-right beam respectively. The same weight was placed on each hanger, so that the rotations, produced on the ends of the

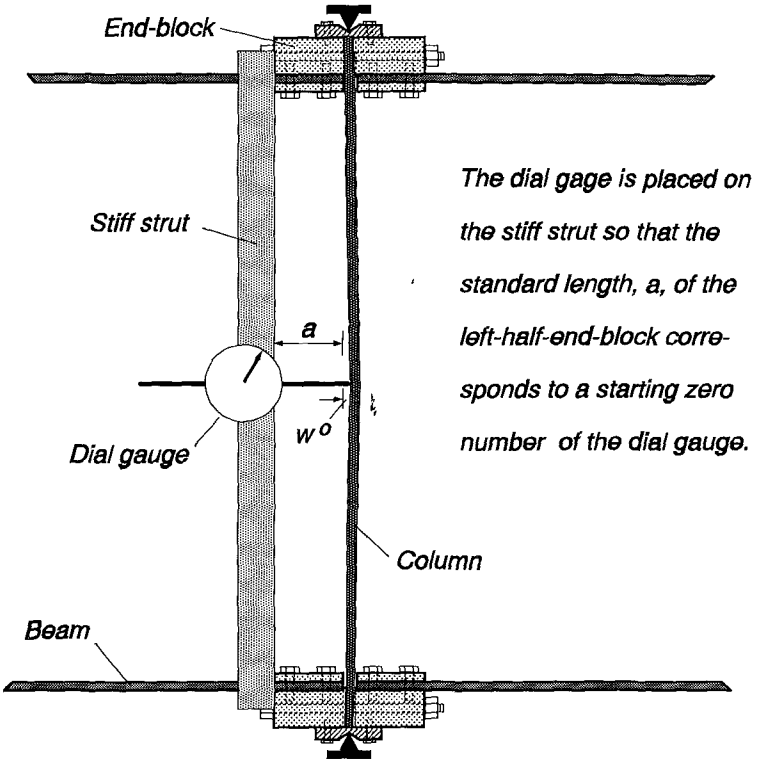

Figure 6-12

column, were equal, thus giving the column a symmetric deformed shape with the maximum deflection at the middle. This deflection was then measured and added to the corresponding geometric imperfection, to give the **total non-sway loading imperfection.**

2) For the sway mode, the pulley mechanism was placed at an appropriate height on the required side of the test rig. Through a wire connecting the top of the frame with the hanger, an appropriate level of weights could produce a horizontal deflection on the top. This deflection was added to the corresponding geometric (out of plumb-line) to give the **total sway loading imperfection.**

Setting up the test rig, was the most important part of the experiment and took much more time than that required for testing.

Having applied and measured the total loading imperfections, the axial load was applied through the wheel-nut on the lower trolley mechanism. The value of

axial load could be directly read on the screen of the strain-gauge-bridge-box, to which the load cell was connected. When the load level reached the intended value, readings were taken of the dial gauges for both the top and mid-height deflections of the column. At the same time, any horizontal deflection at the top of the column was compensated by adjusting the position of the trolley mechanism.

This loading procedure was continued until collapse. Collapse was confirmed when an attempt to increase load would lead to a drop in axial load, accompanied by large increases of deformations. These experimental results, consisting of the axial load and the corresponding deflections on the top and mid-height of column, were then properly processed to give the Southwell Plot for both modes.

On each specimen at least three tests were carried out. After each test the frame was unloaded, and then loaded again, so that a new set of experimental results was obtained. The purpose of re-testing was to allow the effects of different total equivalent imperfections on the buckling collapse load to be assessed. In these re-tests, a great part of total imperfections was attributed to geometric imperfections created by the permanent distortions from the previous tests.

6.11 Theoretical and Experimental Errors

The possible errors involved in both the theoretical calculations and experimental observations are discussed in this section.

6.11.1 Theoretical Errors

The main errors involved in the theoretical analysis are due to the assumption that the contribution of the higher sway and/or non-sway critical modes to the imperfections as well as to their subsequent effects on the non-linear part of the deflection are negligible.

For the loading imperfections it was shown theoretically in Section 4.8 that

the amplitude factors of the higher modes can be negligible compared with the corresponding associated with the first two modes. These higher modes have even smaller contribution to the non-linear part of either the deflection or bending moment.

Although the main theoretical errors are due to the elimination of the higher mode contributions, they are still negligible.

6.11.2 Experimental Errors

There are various factors that can affect the experimental results. The main errors encountered in the experimental procedure may be due to the:

1) experimental assessment of the material properties,

2) measurement of both sides of the specimen's cross section along with the overall frame geometry and the effective length of the column,

3) support and joint conditions,

4) set-up procedure and

5) reading accuracy.

Many of the effects of the above errors have been discussed in Chapter 6. Here a summary will be presented, highlighting the factors that influence the Southwell Plot.

Although the material properties were obtained through a carefully set up experimentation, there might be a minor reasonable deviation from their real values.

The dimensions and every cross sectional detail (radii of their curved angles) et.c. of the members were measured with an accuracy of $\pm 0.05\ mm$ whereas their lengths were measured up to $\pm 1\ mm$ accuracy. The above two types of errors do not actually affect the shape of the Southwell Plot but they might cause a discrepancy between the elastic critical loads obtained theoretically and experimentally. This

discrepancy may be significant if the length of the column between the two joints is not properly measured.

The theoretical model of the limited frame, as far as the boundary and joint conditions are concerned, seemed to give a good agreement between the theoretically calculated elastic critical loads and those obtained experimentally. The observed discrepancy was less than 5%. In two only cases on the sway mode this discrepancy was found to be 12% and 13%. This may be ascribed either to the inadequate horizontal movement of the trolley mechanism during the loading stages or to the lack of verticality of the applied axial load, causing development of a small horizontal component, which in turn affects the horizontal deflections of the column. Consequently the sway mode of the Southwell Plot, taking into account these deflections, might give points which deviate from the straight line. The regression line which in turn is obtained from these points, has a different slope from what it ought to have.

The set-up procedure has a different influence on the experimental points in the Southwell Plot. It is not easy to assess the likely effects of a misalignment when setting-up the frame model in the test rig. As discussed in Chapter 6 an incorrect setting of the model creates wrong values of displacement and load. This type of error significantly influences the experimental points in the Southwell Plot, especially at the earlier stages of loading.

Finally the reading accuracy of the applied load and the corresponding deflections play an important role on the location of the Southwell Plot points in particular at the early stages where the deflections are very small and therefore very sensitive in errors.

Chapter 7

Test Procedure and Comparisons between Experiments and Theory

7.1 Processing the Experimental Results

In this section typical experimental results are presented. Table 7_1 depicts the experimental data obtained from a certain test along with the results that are necessary to make the Southwell Plot for both modes.

The first three columns show the axial load levels and the corresponding dial gauge readings for deflections at both the top and mid-height of the column; these are the results obtained during the test. These data are enough to give the load versus deflections graph, shown in Fig. 7-1.

The fourth and fifth columns provide the derived results required for the Southwell Plot of the sway-mode shown in Fig. 7-2. Similarly, the sixth and seventh columns provide the necessary information for making the non-sway-mode Southwell Plot shown in Fig. 7-3. The sixth column shows the horizontal deflection in mm, at mid-height of the column, that **exclusively** corresponds to the non-sway-mode. Here it has to be noted, that the deflection, **measured** at mid-height of the column, is the algebraic sum of the following two deflections:

1) The whole non-sway deflection, attributed to the symmetric buckling-mode, and

2) Half the sway deflection, attributed to the antisymmetric buckling-mode. This deflection is to be added or subtracted, according to the given sway direction.

The seventh column, like the fifth, gives the ratio of the non-sway deflection divided by the corresponding axial load and allows the Southwell Plot of Fig. 7-3

Table 7_1 Test: 16M1

Experimental Data			Southwell Plot			
			Sway Mode		Non-Sway Mode	
Load P kN	Top-defl dial gauge readings	Mid-defl dial gauge readings	$\frac{\delta_t}{100}$ mm	$\frac{\delta_t}{100P}$ mm/kN	$\frac{\delta_m - \delta_t/2}{100}$ mm	$\frac{\delta_m - \delta_t/2}{100P}$ mm/kN
0	1621	1263	0.000	0.000	0.000	0.000
0.5	1630	1264	0.090	0.180	0.055	0.110
1	1636.5	1266	0.155	0.155	0.108	0.108
1.2	1643	1266	0.220	0.183	0.140	0.117
1.4	1649	1266	0.280	0.200	0.170	0.121
1.6	1656	1266	0.350	0.219	0.205	0.128
1.8	1661	1266	0.400	0.222	0.230	0.128
2	1667	1266	0.460	0.230	0.260	0.130
2.2	1673	1266	0.520	0.236	0.290	0.132
2.4	1680	1266	0.590	0.246	0.325	0.135
2.6	1686	1266	0.650	0.250	0.355	0.137
2.8	1695	1266	0.740	0.264	0.400	0.143
3	1703	1266	0.820	0.273	0.440	0.147
3.2	1714	1266	0.930	0.291	0.495	0.155
3.4	1726	1264	1.050	0.309	0.535	0.157
3.6	1736	1264	1.150	0.319	0.585	0.163
3.8	1750	1264	1.290	0.339	0.655	0.172
4	1766	1261.5	1.450	0.363	0.710	0.178
4.22	1782.5	1261	1.615	0.383	0.788	0.187
4.4	1794	1261	1.730	0.393	0.845	0.192
4.6	1818	1257	1.970	0.428	0.925	0.201
4.8	1844	1254	2.230	0.465	1.025	0.214
5	1870	1252	2.490	0.498	1.135	0.227
5.2	1899	1249	2.780	0.535	1.250	0.240
5.4	1934	1246	3.130	0.580	1.395	0.258
5.6	1968	1242	3.470	0.620	1.525	0.272
5.8	2022	1234	4.010	0.691	1.715	0.296
6	2077	1227	4.560	0.760	1.920	0.320
6.2	2164	1212	5.430	0.876	2.205	0.356
6.4	2243	1205	6.220	0.972	2.530	0.395
6.6	2370	1185	7.490	1.135	2.965	0.449

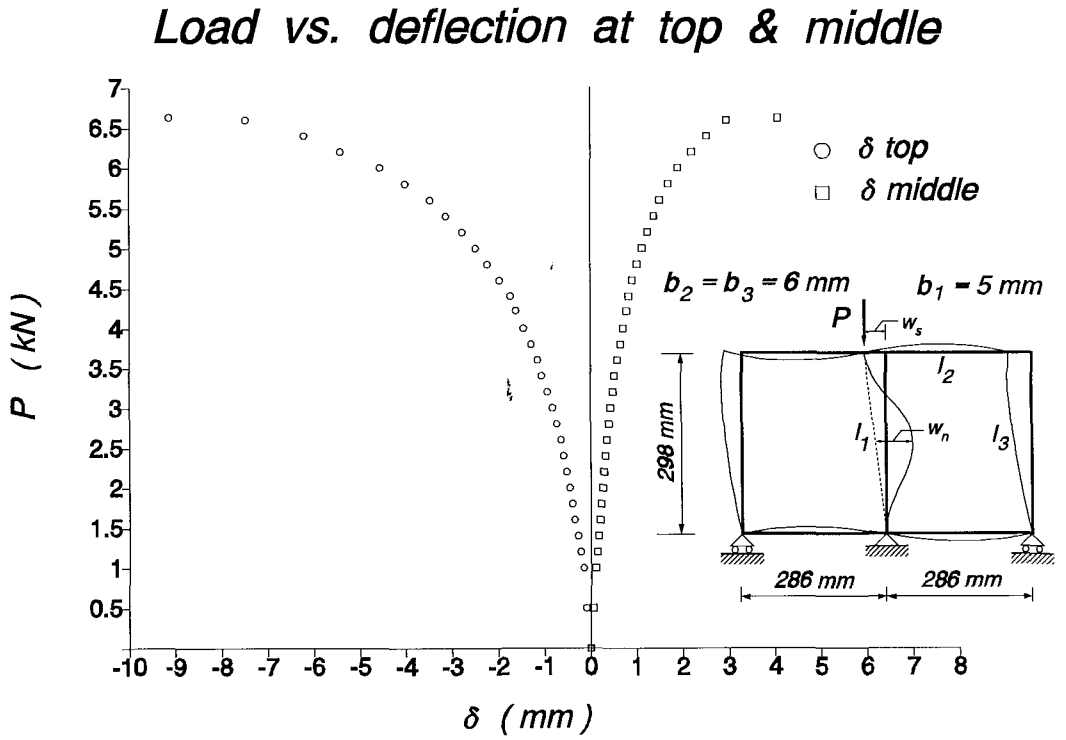

Figure 7-1

to be produced.

As discussed at the beginning of section 6.4, Southwell Plot is applicable over the elastic region. Therefore, when the best-fit line is to be drawn, any points of the graph corresponding to the elastic-plastic behaviour of the column need to be excluded. The same usually applies for a small number of points recorded at the early stage of loading, since these points are very sensitive to experimental error.

The procedure developed for the processing of the experimental results is continued in Figs. 7-4 and 7-5 which show the buckling shape and the bending moment contribution along the column for the first four critical modes (two sway and two non-sway) at the first yield. In the graph of Fig. 7-6 the change in the non-linear maximum bending moment, (occurring at any cross section along the column), against the applied axial load is again shown for the contributions from the first four buckling modes.

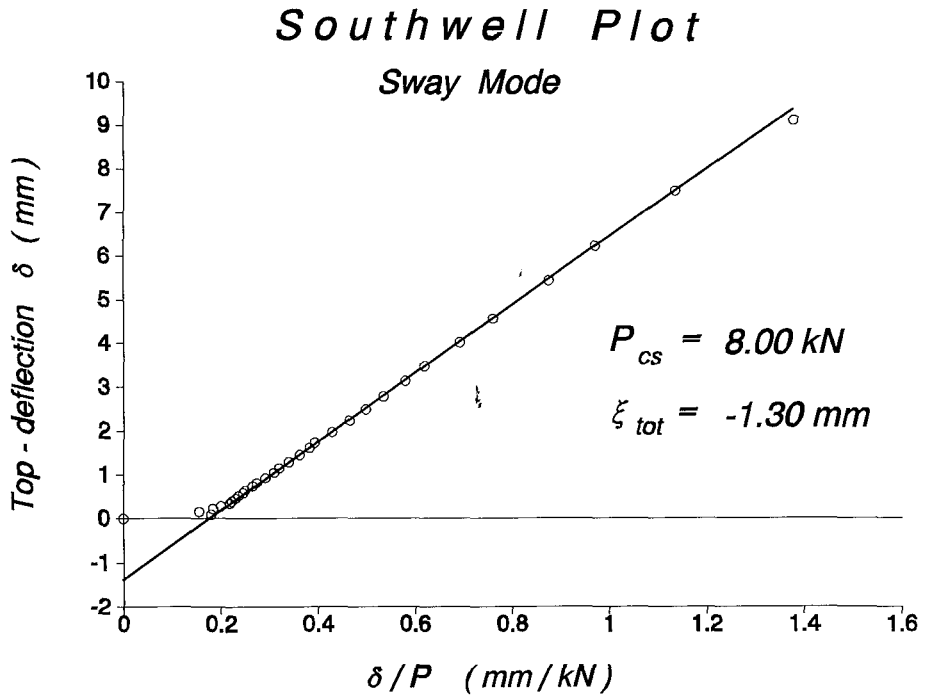

Figure 7-2

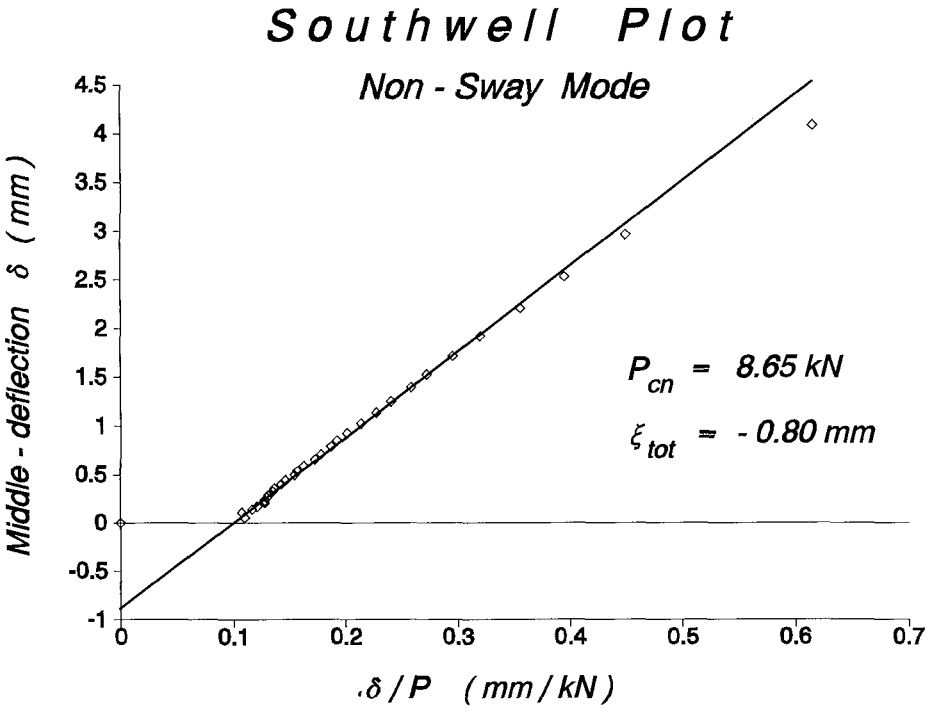

Figure 7-3

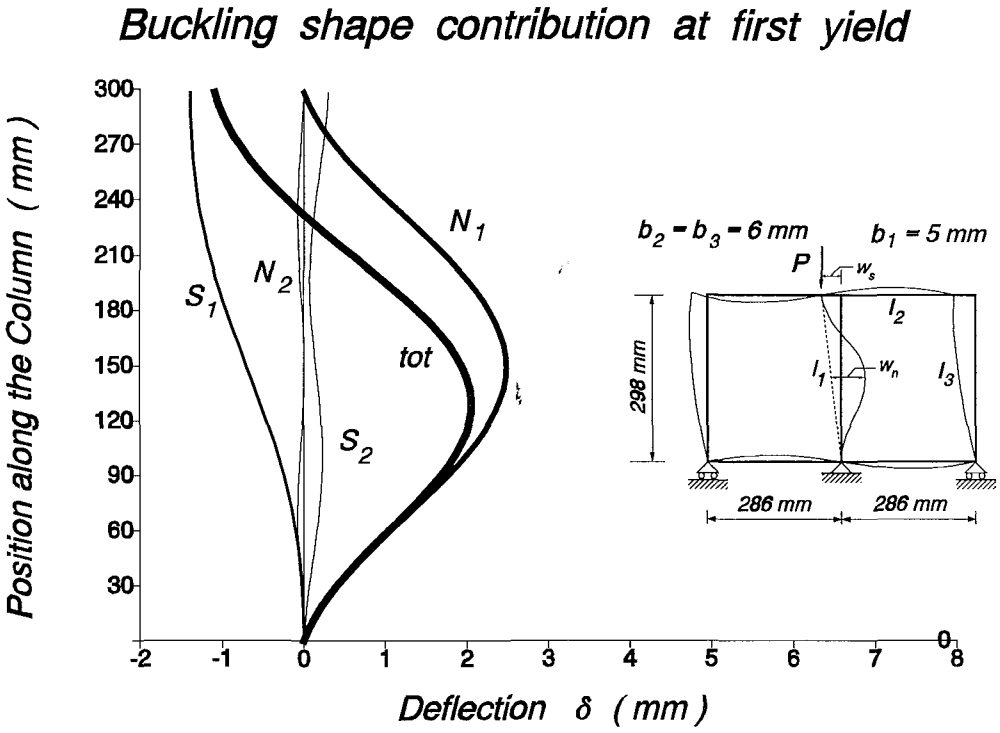

Figure 7-4

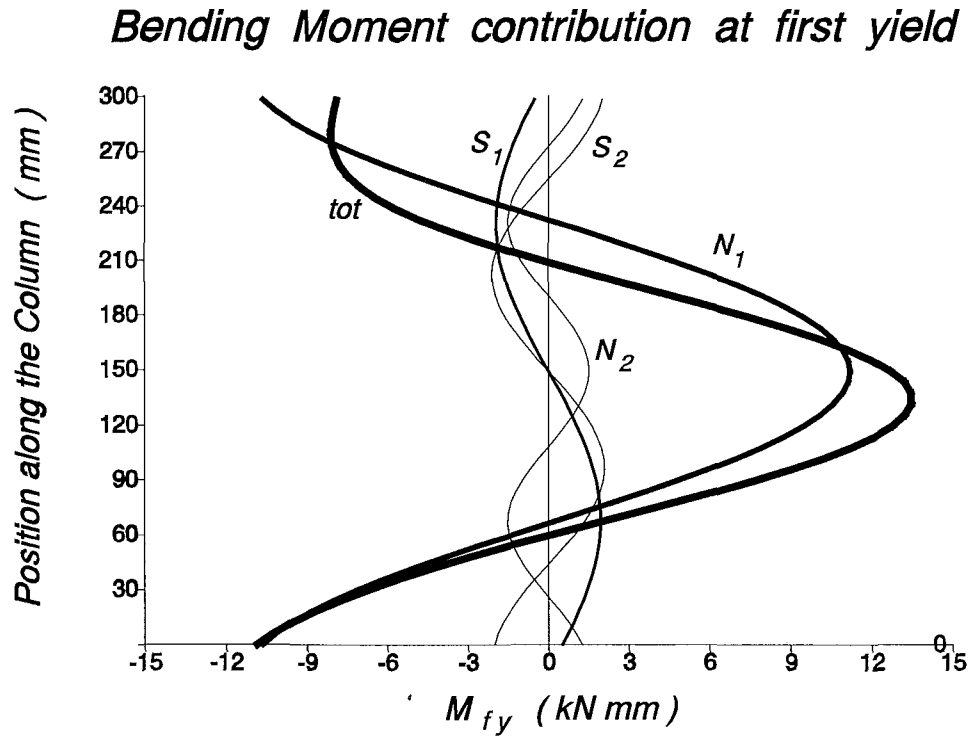

Figure 7-5

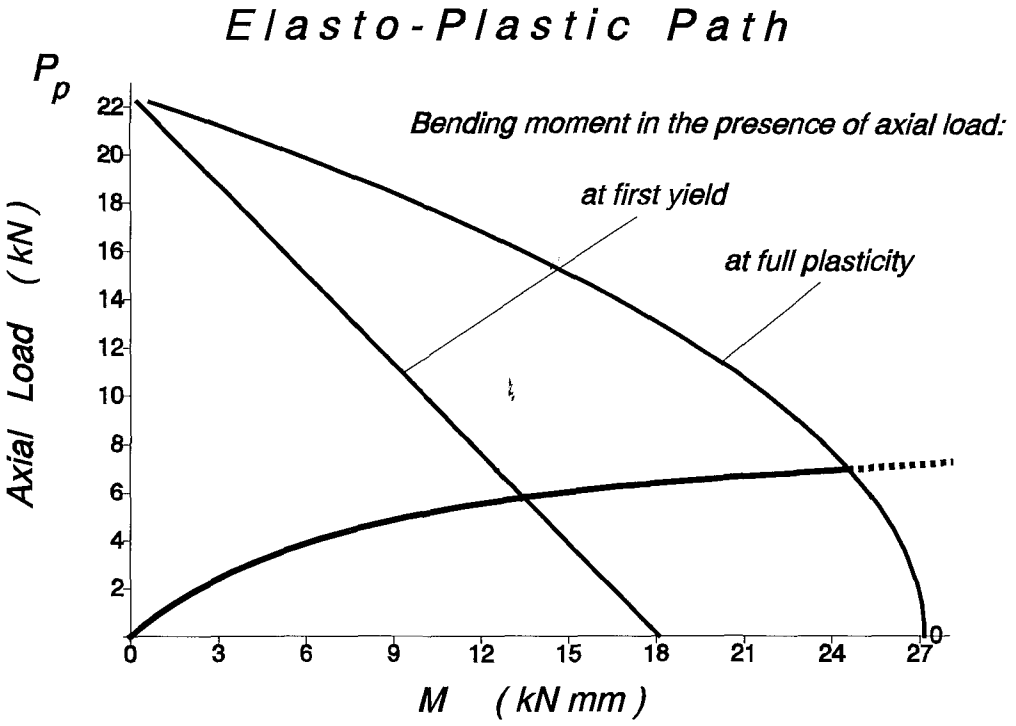

Figure 7-6

The experimental interpretation is finally completed with a brief summary of the theoretical results. This summary consists mainly of two parts. The first part comprises the necessary data given for this particular test. These data are initially the number of different property sets (members) along with the applied imperfections of both modes, experimentally found through Southwell plot. Then, for each member, shown are respectively its given geometry, i.e. length, thickness and breadth in mm, its calculated cross sectional properties, i.e. area in mm^2, second moment of area in mm^4, elastic and plastic section modulus in mm^3 and finally its given material property, i.e. yield stress in N/mm^2. The second part comprises the calculated results from the above data, starting from the three frame stiffnesses, i.e. rotational symmetric for the non-sway mode, rotational antisymmetric and translational for the sway mode, as discussed in Appendix B. Following is the Eigenvalue analysis as discussed in Appendix G, where, for each one of the demanded solutions (buckling modes), calculated and given are respectively:

1) the root kL of the determinant of the coefficient matrix of Eq. (3.26)

2) the modal critical load in kN and

3) the coefficients C_1, C_2, δ, and θ_A of the column matrix of Eq. (3.26) along with the mode-type (sway or non-sway).

Finally, for the given amount of imperfections, the load level to cause initiation of yielding and full plasticity are calculated and given along with the squash load.

SUMMARY OF THEORETICAL RESULTS

PROP_sets = 3, SWAY_imp = -1.30 mm, NON-SWAY_imp = 0.80 mm

MEMBER PROPERTIES

MEM	L	b	d	A	I	Zel	Zpl	σ_y N/mm^2
1	298.0	5.0	13.0	62.44	125.70	50.28	81.45	360
2	286.0	6.0	13.0	73.44	209.00	69.67	117.71	360
3	292.0	6.0	13.0	73.44	209.00	69.67	117.71	360

Rotational SYMMETRIC (Non-sway) Stiffness of frame : 1398.21 kN*mm/rad

Rotational ANTISYMMETRIC (Sway) Stiffness of frame : 1706.41 kN*mm/rad

Translational (Sway) Stiffness of frame : 27.93 N/mm

EIGENVALUES & EIGENVECTORS

Solut	kL	Pc	C1	C2	delta	theta_A	Mode-type
1	5.642	8.7871	1.00	-0.332	0.000	0.006	Non-Sway
2	5.736	9.0802	1.00	3.560	-24.004	-0.005	* Sway
3	8.866	21.6964	1.00	-0.287	-3.245	-0.013	* Sway
4	11.386	35.7838	1.00	-0.670	0.000	0.026	Non-Sway

First YIELD Load = 5.769 kN

First HINGE Load = 6.917 kN

SQUASH Load = 22.477 kN

7.2 Preliminary Experimental Results and Interpretation

Provided the experimental procedure has been carefully carried out without significant errors for each of the two buckling modes, sway and non-sway, two pieces of important information can be obtained from Southwell Plot:

1) The classical **critical load**, given as the gradient of the best-fit line that passes through the experimental points and

2) The **total equivalent imperfection**, which represents the sum of geometric and loading imperfections.

The fact that the plot-points lie on a straight line verifies experimentally the validity of theory. The slope of this line (critical load) is independent of any form of imperfections. It depends only on the geometry (length, cross section), material and boundary conditions of the column. The value of critical load can then be compared with the corresponding value obtained theoretically (computer program for Eigenvalue Problem).

The total equivalent imperfection is another vital experimentally determined parameter. It plays a controlling influence of the first yield P_{fy} and the first plastic hinge P_{fh} loads. The load to form the first plastic hinge load is generally close to the load necessary to convert the structure into a mechanism; a mechanism will usually require formation of more than one plastic hinges. The two theoretical loads, P_{fy}, P_{fh}, constitute a lower and a close upper bound solution for the ultimate load of the column, obtained experimentally.

Table 7_2 summarizes the main characteristics of the frames used for the preliminary programme of experiments, and includes

i) frame geometries (lengths and cross sectional dimensions of members)

ii) frame stiffnesses (rotational symmetric C_A for the non-sway mode, rotational antisymmetric C_A' and translational K_A for the sway mode)

iii) Squash load P_y for the central column's cross section.

Table 7_2 Main characteristics of preliminary experimental frames

Test No	Frame Geometry					Frame Stiffness			
	$L_1 = L_3$ mm	L_2 mm	b_1 mm	b_2 mm	b_3 mm	C_A $kN \cdot mm/rad$	C_A' $kN \cdot mm/rad$	K_A N/mm	P_y kN/mm^2
2M	298	286	5	6	6	1398.21	1706.41	27.93	22.48
3M	298	286	5	6	6	1398.21	1706.41	27.93	22.48
7M	310	286	5	6	6	1390.39	1692.42	25.12	22.48
13M1	310	286	5	6	6	1390.39	1692.42	25.12	22.48
13M2	310	286	5	6	6	1390.39	1692.42	25.12	22.48
16M1	298	286	5	6	6	1398.21	1706.41	27.93	22.48
21M	310	286	5	6	6	1402.34	1713.65	27.78	22.48
27JL	317	320	5	6	6	1204.45	1447.85	21.19	22.48
28JL	324	295	5	6	6	1328.85	1607.92	21.65	22.48
29JL	330	290	5	6	6	1354.48	1639.36	20.94	22.48
4AU	470	330	5	6	6	1105.79	1294.46	7.18	22.48
4AUa	470	330	5	6	6	1105.79	1294.46	7.18	22.48
19S	470	330	5	6	6	1105.79	1294.46	7.18	22.48
20S	470	330	5	6	6	1105.79	1294.46	7.18	22.48

Table 7_3 demonstrates the theoretical and experimental results obtained for this range of experiments.

Columns 2 and 3 contain the experimental values for the lowest sway and non-sway critical loads, obtained from interpretation of the Southwell Plot.

From the same plot the total equivalent imperfections for the above two

modes are presented in columns 4 and 5.

The respective theoretical values of the critical loads, calculated through the Eigenvalue problem software as discussed in the preceding Section, for the same frame geometry are shown in columns 6 and 7.

For the total equivalent imperfections found through the Southwell Plot, columns 7 and 8 provide the theoretical levels of the first yield and the first plastic hinge loads.

Column 10 shows the maximum applied axial load recorded from the tests, and finally, columns 11 and 12 list the ratios of the experimental to theoretical critical loads obtained for each of the modes.

The theoretical model of the limited frame, seemed to give a good agreement between the theoretically calculated elastic critical loads and those obtained experimentally. As can be concluded from columns 11 and 12, the observed discrepancy was less than $\pm 5\%$. In two only cases on the sway mode has this discrepancy found to be in excess of this value, at 12% and 13% respectively. This may be ascribed to the lack of verticality of the applied axial load, causing at every stage of the experiment a continuous development of a small horizontal force component, which in turn affects both the horizontal deflections of the column.

A comparison between the listed maximum applied axial load and the theoretical load levels to cause first yield and full plasticity shows that P_{max} was in some cases less than the first yield load, but in the main it was somewhere in between P_{fy} *and* P_{ph}. This is because the maximum axial load was not generally applied in a way to convert the structure into a collapse mechanism; it was increased until a level where the column was considered to present relatively larger deflections without seeming to show a significant increase in the axial load.

Although for most of the cases, it can be seen that a close agreement exists between experiments and theory, this experimental procedure was revised and

Table 7_3 Summary of Theoretical and Experimental Results

Test No	$P_{CS}(Exp.)$ kN (2)	$P_{CN}(Exp.)$ kN (3)	ξ_S mm (4)	ξ_N mm (5)	$P_{CS}(Th.)$ kN (6)	$P_{CN}(Th.)$ kN (7)	P_{fy} kN (8)	P_{fh} kN (9)	P_{max} kN (10)	$\frac{P_{CS}(Exp.)}{P_{CS}(Th.)}$ (11)	$\frac{P_{CN}(Exp.)}{P_{CN}(Th.)}$ (12)
2M	8.69	8.48	-1.10	-1.02	9.08	8.79	6.31	7.35	6.00	0.95	0.96
3M	8.17	8.71	-1.00	-1.02	9.08	8.79	6.45	7.46	6.00	0.90	0.99
7M	7.40	8.17	-0.36	-1.00	8.45	8.17	5.84	6.87	6.20	0.88	1.00
13M1	8.17	7.93	-1.00	-0.93	8.45	8.17	5.22	6.37	6.31	0.97	0.97
13M2	9.55	7.92	-0.40	-1.05	8.45	8.17	5.74	6.79	6.50	1.13	0.97
16M1	8.00	8.65	-1.30	-0.80	9.08	8.79	6.06	7.17	6.60	0.88	0.98
21M	8.35	8.04	-1.07	-0.50	9.06	8.18	5.55	6.17	5.70	0.90	0.98
27JL	7.53	7.80	-0.88	-0.60	7.54	7.63	6.35	6.94	6.20	1.00	1.02
28JL	7.65	7.50	-0.65	-0.50	7.66	7.48	6.26	6.83	6.00	1.00	1.00
29JL	7.36	7.21	-1.65	-0.85	7.50	7.26	5.04	5.92	5.95	0.98	0.99
4AU	3.49	3.65	-1.40	-1.05	3.67	3.67	3.25	3.43	3.00	0.95	0.99
4AUa	3.37	3.62	-1.45	-1.40	3.67	3.67	3.11	3.34	2.80	0.92	0.99
19S	3.54	3.64	-1.18	-1.00	3.67	3.67	3.20	3.40	3.27	0.96	0.99
20S	3.73	3.62	-0.65	-0.23	3.67	3.67	El. fail.	El. fail.	3.70	1.02	0.99

developed into a more consistent programme discussed in the next section.

7.3 Final Experimental Results and Interpretation

The experimental procedure, leading to results outlined in table 7_3, followed a new series of experiments, where, as discussed below, a range of different test results were obtained to cover a certain buckling behaviour of the central column.

For each frame geometry three different and independent experiments have been carried out, corresponding to the elastic, elastic-plastic and plastic collapse buckling behaviour of the central column. The collected data were readings which corresponded to both the loading and the **unloading** stage of the column.

In a way similar to that presented in section 7.1, table 7_4 lists the experimental data obtained from a typical test along with the necessary interpretations of results to allow the Southwell Plot for both modes. It is clear that the two additional columns of tabulated experimental data that have been added, are to provide the corresponding points for the unloading path of the load versus displacements diagram. The rest of the procedure, for developing the Southwell Plots for both modes, remains the same as that described in section 7.1.

The fact that three independent experiments were carried out for each frame geometry was dictated from the procedure itself, according to which:

1. a specific frame geometry is initially chosen after a large parametric study on numerical experiments undertaken with the developed software. Frame geometry was chosen to achieve selected ratios between the first two critical loads.

2. for selected frame geometry a notional loading imperfection was given to the central column and the theoretical values for the first yield and first hinge loads were obtained.

3. Prior to starting the **first experiment** concerning the elastic buckling behaviour, the maximum axial load, was chosen in advance to be well below the first yield load, allowing suitable increments of axial load to be selected.

4. Having more or less applied the above loading imperfections, (the column initially is considered to be geometrically perfect), deflection readings at the top and

middle are taken for increasing and decreasing loads.

5. These data are then developed as in section 7.1. Figs. 7-7, and 7-8 show the Southwell Plots for both modes while Fig. 7-9 depicts the deflections for both loading and unloading of the top and the middle cross section of the column against the applied axial load.

6. Having validated the theoretical values for the first critical loads obtained from the Southwell Plot, the values for the total equivalent imperfections obtained through Southwell Plot for both modes were then put in the program to give new values for the first yield and first hinge load; in most cases the 'actual' imperfections differed from the 'notional' imperfections applied for the same frame. A check that the maximum applied axial load was still less than the calculated first yield load, was a necessary step for this stage.

7. The next two graphs, shown in Figs. 7-10 and 7-11, corresponding to the buckling shape and the bending moment contribution at first yield for the sway and the non-sway modes along the column, were then obtained through the software for the same frame geometry and imperfections. This was followed by the elasto_plastic path graph, as discussed in section 7.1, shown in Fig. 7-12. Finally a brief summary of theoretical data and results, as those described in section 7.1, was provided by the program; these are shown on the next pages.

8. At the **second experiment** (elasto-plastic buckling) the same loading imperfections were applied and the same procedure followed, with the difference that the experiment was continued just beyond the calculated first yield load.

9. The same interpretation procedure as that of the first experiment is followed, except that the last points of both Southwell Plots correspond to elasto-plastic regime and are excluded.

10. The **third experiment** is usually carried out under larger imperfections developed as a result of earlier plastic deformations. This aims to show the reduction of the maximum load carrying capacity of the column. The procedure is the same as that followed for the second experiment.

The following pages outline the procedure for a typical frame geometry.

Table 7_4 Test: 25oc1
Elastic Buckling

Experimental Data					Southwell Plot			
Load P kN	Loading		Unloading		Sway Mode		Non-Sway Mode	
	Top reads	Mid reads	Top reads	Mid reads	$\frac{\delta_t}{100}$ mm	$\frac{\delta_t}{100P}$ mm/kN	$\frac{\delta_m-\delta_t/2}{100}$ mm	$\frac{\delta_m-\delta_t/2}{100P}$ mm/Kn
0	969	1156	988	1148.	0.000	0.000	0.000	0.000
0.2	973	1156.5	997	1149	0.040	0.200	0.025	0.125
0.4	977	1156.5	1001	1151.	0.080	0.200	0.045	0.113
0.6	981	1157	1007.5	1152	0.120	0.200	0.070	0.117
0.8	986	1158	1013	1152.	0.170	0.213	0.105	0.131
1	990.5	1158	1019	1153	0.215	0.215	0.128	0.128
1.2	996.5	1158	1025	1153	0.275	0.229	0.158	0.131
1.4	1002.5	1158.5	1031	1154	0.335	0.239	0.193	0.138
1.6	1009	1159.5	1038	1155	0.400	0.250	0.235	0.147
1.8	1016.5	1160.5	1045	1156	0.475	0.264	0.283	0.157
2	1024	1163	1052.5	1157	0.550	0.275	0.345	0.173
2.1	1028	1163.5	1056	1157.	0.590	0.281	0.370	0.176
2.2	1032	1164.5	1061	1158.	0.630	0.286	0.400	0.182
2.3	1036	1166	1066.5	1159.	0.670	0.291	0.435	0.189
2.4	1040	1167	1071	1160	0.710	0.296	0.465	0.194
2.5	1045	1168.5	1076	1161	0.760	0.304	0.505	0.202
2.6	1051	1171	1080	1163	0.820	0.315	0.560	0.215
2.7	1057.5	1172.5	1083	1165	0.885	0.328	0.608	0.225
2.8	1064	1174.5	1087	1166	0.950	0.339	0.660	0.236
2.9	1069.5	1176.5	1091.5	1168	1.005	0.347	0.708	0.244
3	1078	1178.5	1095.5	1171.	1.090	0.363	0.770	0.257
3.1	1083	1181.5	1097	1176	1.140	0.368	0.825	0.266
3.2	1090	1184.5	1098	1180	1.210	0.378	0.890	0.278
3.3	1098	1188	1098	1188	1.290	0.391	0.965	0.292

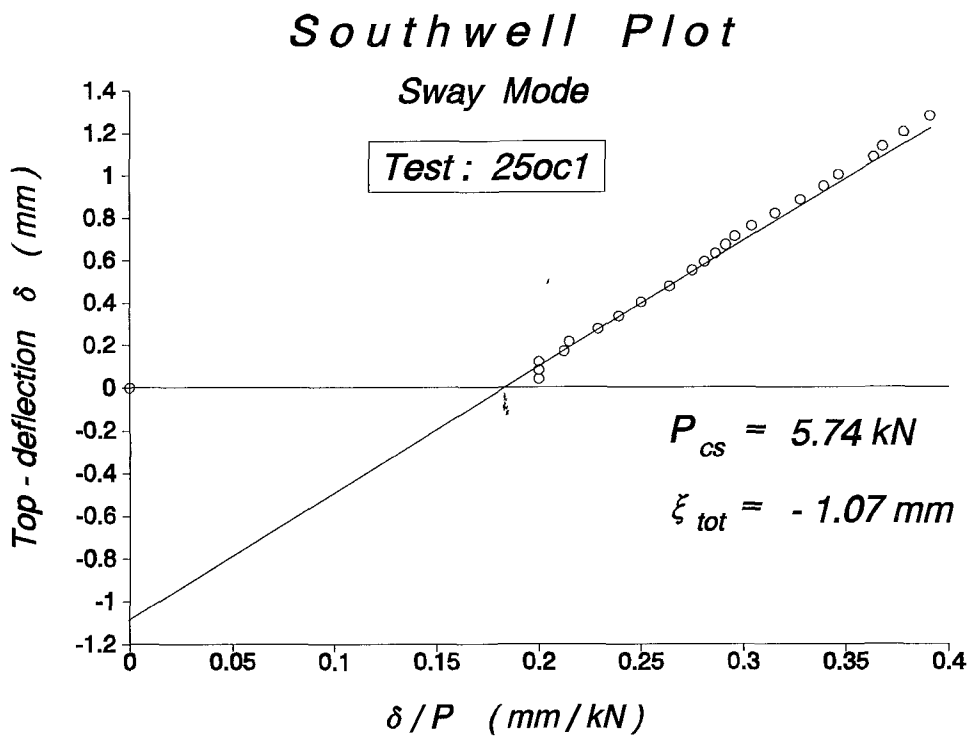

Figure 7-7

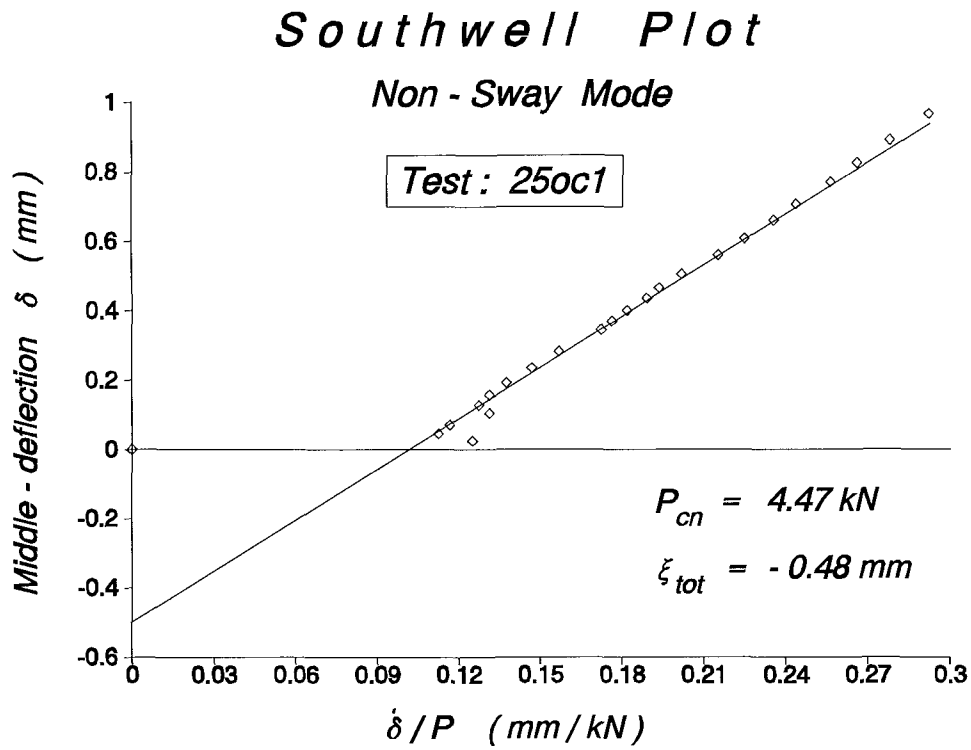

Figure 7-8

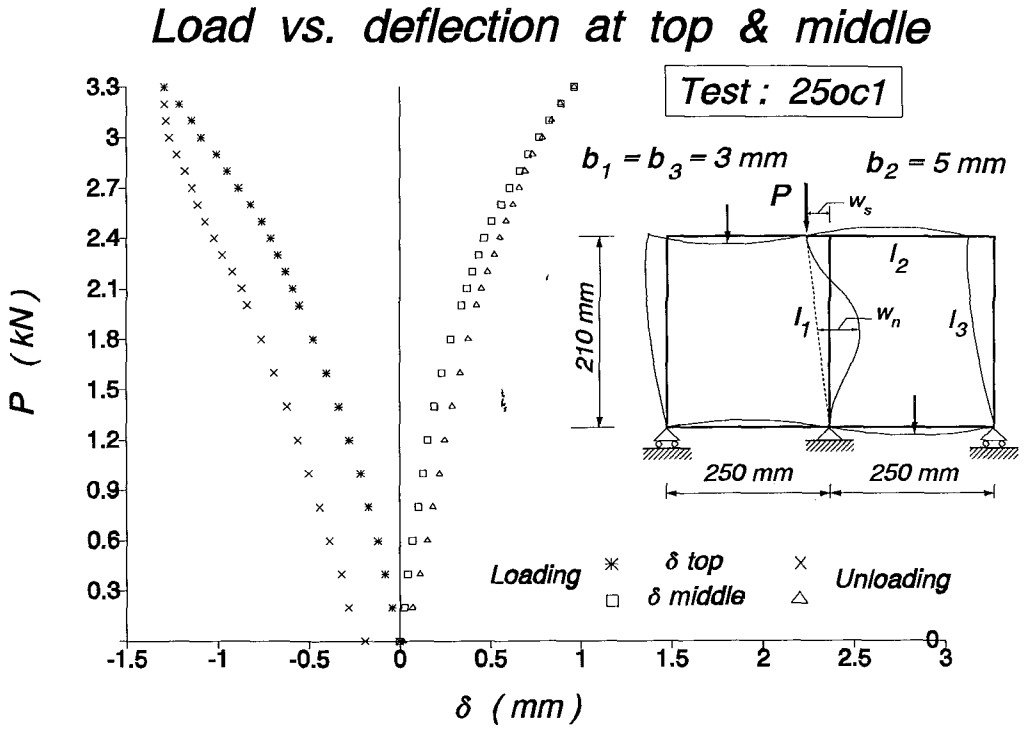

Figure 7-9

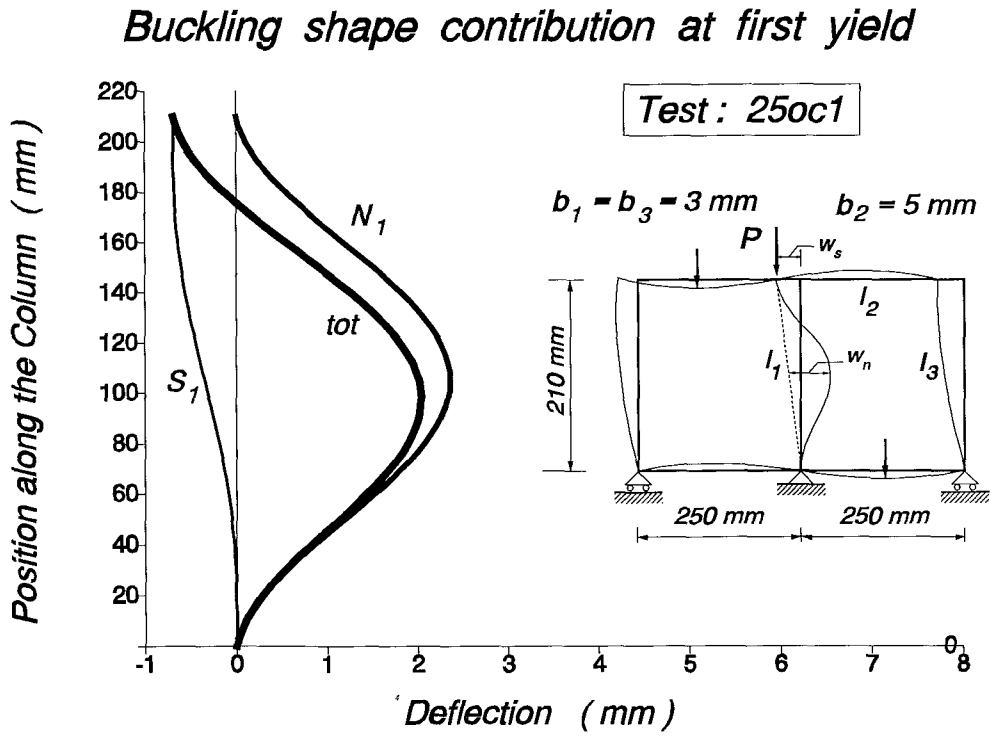

Figure 7-10

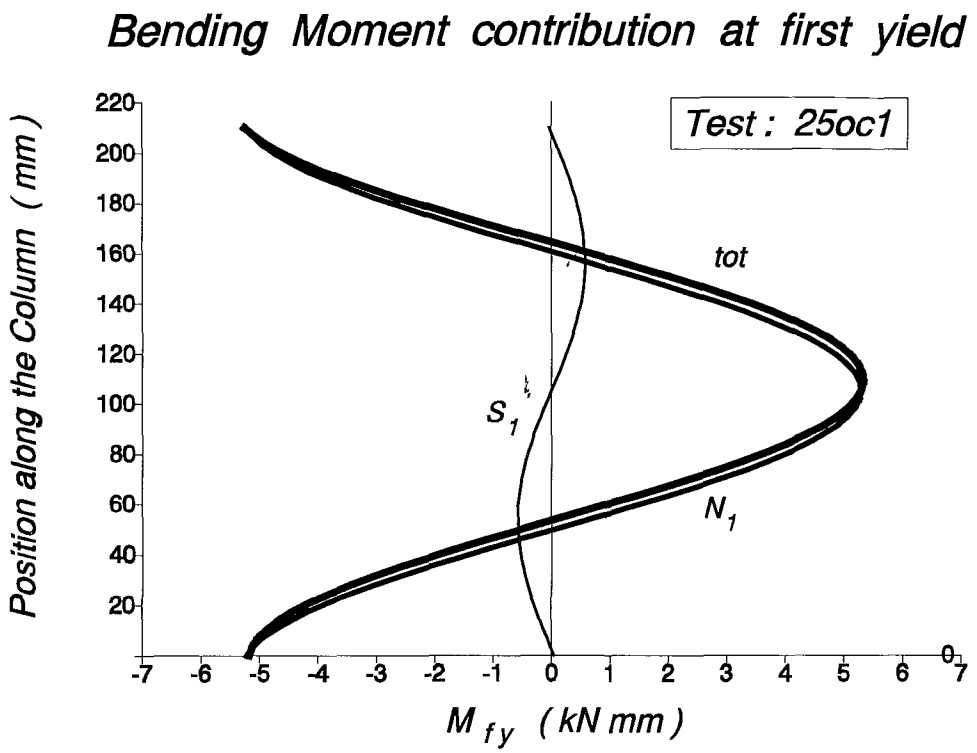

Figure 7-11

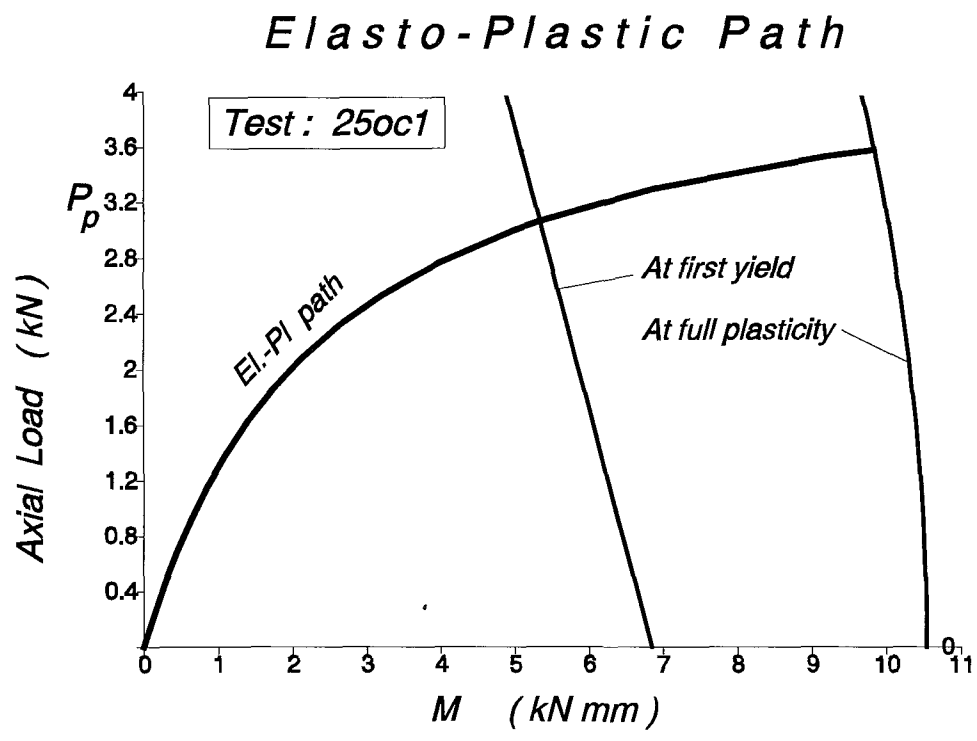

Figure 7-12

THEORETICAL DATA & RESULTS OF TEST **25oc1**

PROP_sets = 3, SWAY_imp = -1.07 mm, NON-SWAY_imp = -0.48 mm

MEMBER PROPERTIES

MEM	L	b	d	A	I	Zel	Zpl	Y.str
1	210.0	3.0	13.0	38.47	28.53	19.02	29.26	360
2	250.0	5.0	13.0	62.44	125.70	50.28	81.45	360
3	210.0	3.0	13.0	38.47	28.53	19.02	29.26	360

Rotational SYMMETRIC (Non-sway) Stiffness of frame : 920.69 kN*mm/rad

Rotational ANTISYMMETRIC (Sway) Stiffness of frame : 1112.57 kN*mm/rad

Translational (Sway) Stiffness of frame : 25.34 N/mm

EIGENVALUES & EIGENVECTORS

Solut	kL	Pc	C1	C2	delta	theta_A	Mode-Case
1	5.944	4.4573	1.00	-0.171	0.000	0.005	Non-Sway
2	6.423	5.2043	1.00	-14.263	88.629	-0.005	* Sway

First YIELD Load = 3.066 kN

First HINGE Load = 3.579 kN

SQUASH Load = 13.848 kN

Test: 25oc2
Elastic_Plastic Buckling

Experimental Data					Southwell Plot			
Load P kN	Loading		Unloading		Sway Mod		Non-Sway Mode	
	Top reads	Mid reads	Top reads	Mid reads	$\frac{\delta_t}{100}$ mm	$\frac{\delta_t}{100P}$ mm/kN	$\frac{\delta_m-\delta_t/2}{100}$ mm	$\frac{\delta_m-\delta_t/2}{100P}$ mm/kN
0	987	1148.5	1008	1195	0.000	0.000	0.000	0.000
0.2	988.5	1150	1019	1196	0.015	0.075	0.023	0.113
0.4	990	1151	1026	1200	0.030	0.075	0.040	0.100
0.6	991	1152	1033	1203	0.040	0.067	0.055	0.092
0.8	993	1152.5	1038	1207	0.060	0.075	0.070	0.088
1	995	1154	1044	1210	0.080	0.080	0.095	0.095
1.2	998.5	1155	1052	1215	0.115	0.096	0.123	0.102
1.4	1003.5	1156	1059	1219.	0.165	0.118	0.158	0.113
1.6	1009	1157.5	1068	1224.	0.220	0.138	0.200	0.125
1.8	1016	1159.5	1078	1231	0.290	0.161	0.255	0.142
2	1023	1162	1087	1238	0.360	0.180	0.315	0.158
2.2	1031.5	1164.5	1098	1247.	0.445	0.202	0.383	0.174
2.4	1040	1166	1109	1258	0.530	0.221	0.440	0.183
2.6	1050	1171	1122	1272	0.630	0.242	0.540	0.208
2.8	1063	1175	1139	1285	0.760	0.271	0.645	0.230
3	1074.5	1180.5	1155	132	0.875	0.292	0.758	0.253
3.2	1085.5	1187.5	1178	1323	0.985	0.308	0.883	0.276
3.4	1103	1193.5	1198.5	1350	1.160	0.341	1.030	0.303
3.5	1113.5	1197.5	1210	1368.	1.265	0.361	1.123	0.321
3.6	1123	1203	1220	1385	1.360	0.378	1.225	0.340
3.7	1135	1210	1231	1405.	1.480	0.400	1.355	0.366
3.8	1149.5	1218	1236	1428.	1.625	0.428	1.508	0.397
3.9	1164	1229.5			1.770	0.454	1.695	0.435
4	1182	1241.5			1.950	0.488	1.905	0.476
4.1	1195	1263			2.080	0.507	2.185	0.533
4.2	1214	1290			2.270	0.540	2.550	0.607
3.93	1233	1463			2.460	0.626	4.375	1.113

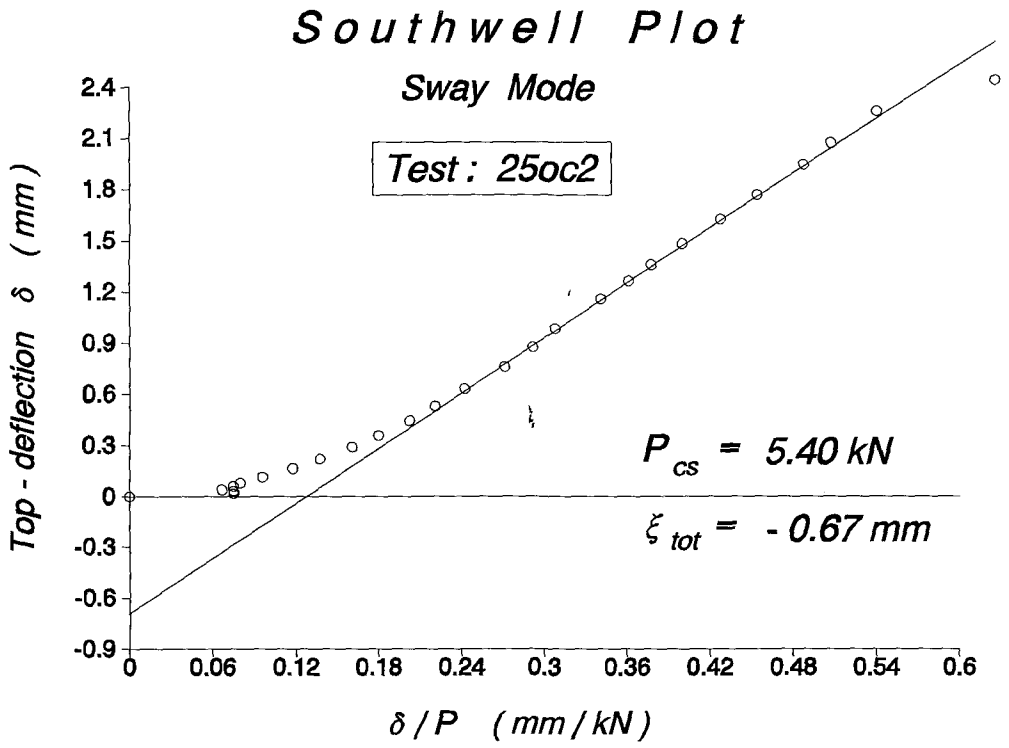
Southwell Plot
Sway Mode
Test : 25oc2
P_{cs} = 5.40 kN
ξ_{tot} = - 0.67 mm
Top - deflection δ (mm)
δ / P (mm / kN)
2.4
2.1
1.8
1.5
1.2
0.9
0.6
0.3
0
-0.3
-0.6
-0.9
0
0.06
0.12
0.18
0.24
0.3
0.36
0.42
0.48
0.54
0.6

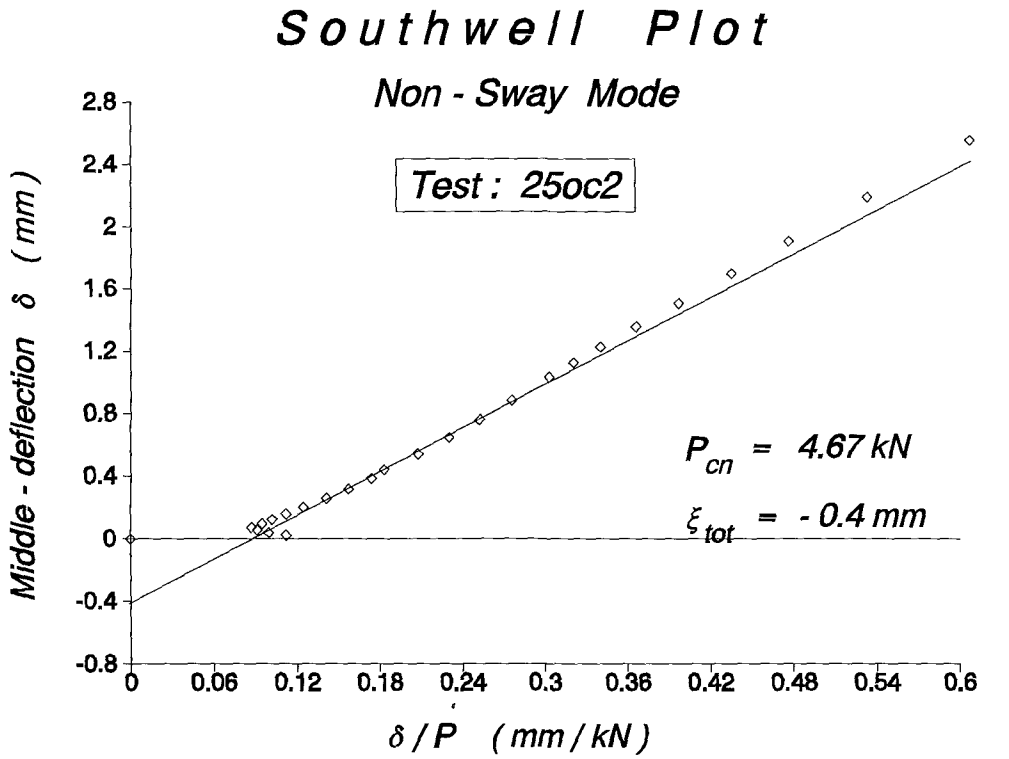
Southwell Plot
Non - Sway Mode
Test : 25oc2
P_{cn} = 4.67 kN
ξ_{tot} = - 0.4 mm
Middle - deflection δ (mm)
δ / P (mm / kN)
2.8
2.4
2
1.6
1.2
0.8
0.4
0
-0.4
-0.8
0
0.06
0.12
0.18
0.24
0.3
0.36
0.42
0.48
0.54
0.6

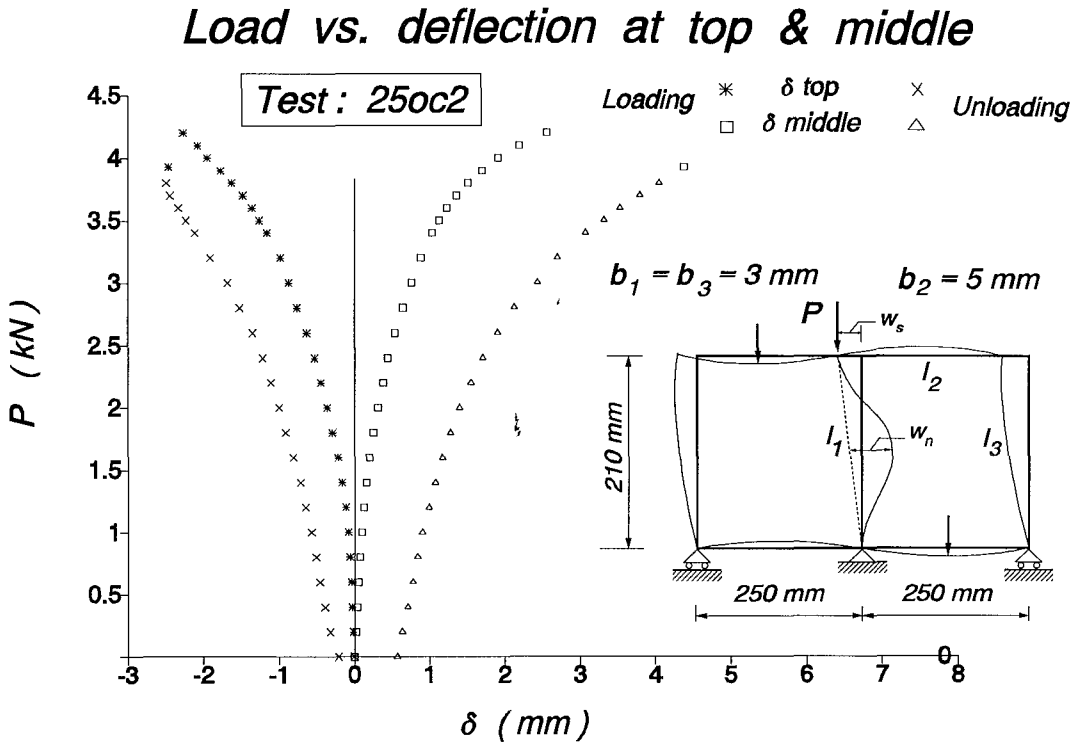
Load vs. deflection at top & middle
Test : 25oc2
Loading
δ top
δ middle
Unloading
P (kN)
δ (mm)
b1 = b3 = 3 mm
b2 = 5 mm
P
ws
l2
l1
wn
l3
210 mm
250 mm
250 mm

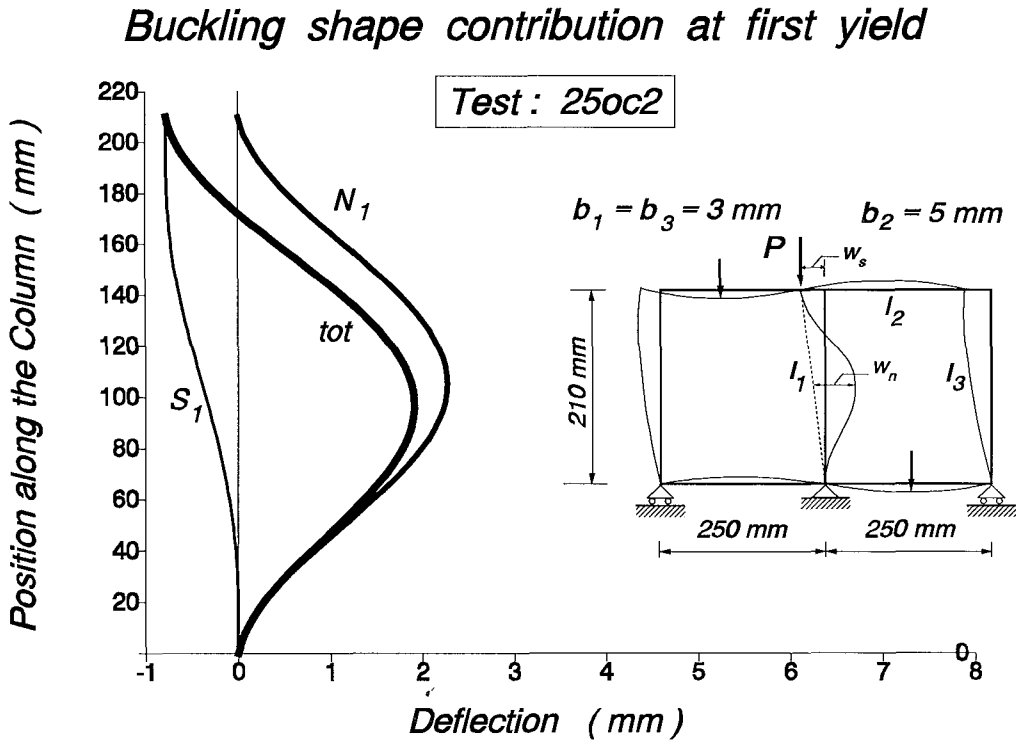
Buckling shape contribution at first yield
Test : 25oc2
Position along the Column (mm)
Deflection (mm)
N1
tot
S1
b1 = b3 = 3 mm
b2 = 5 mm
P
ws
l2
l1
wn
l3
210 mm
250 mm
250 mm

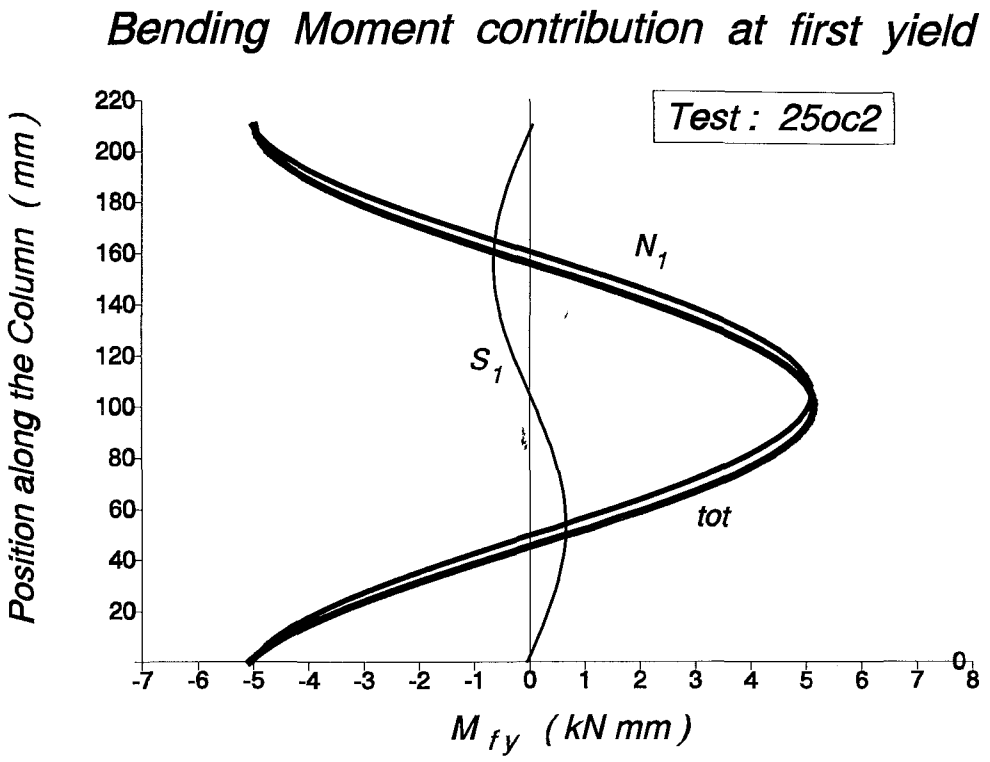
Bending Moment contribution at first yield
Test : 25oc2
Position along the Column (mm)
220
200
180
160
140
120
100
80
60
40
20
N_1
S_1
tot
-7 -6 -5 -4 -3 -2 -1 0 1 2 3 4 5 6 7 8
M_{fy} (kN mm)

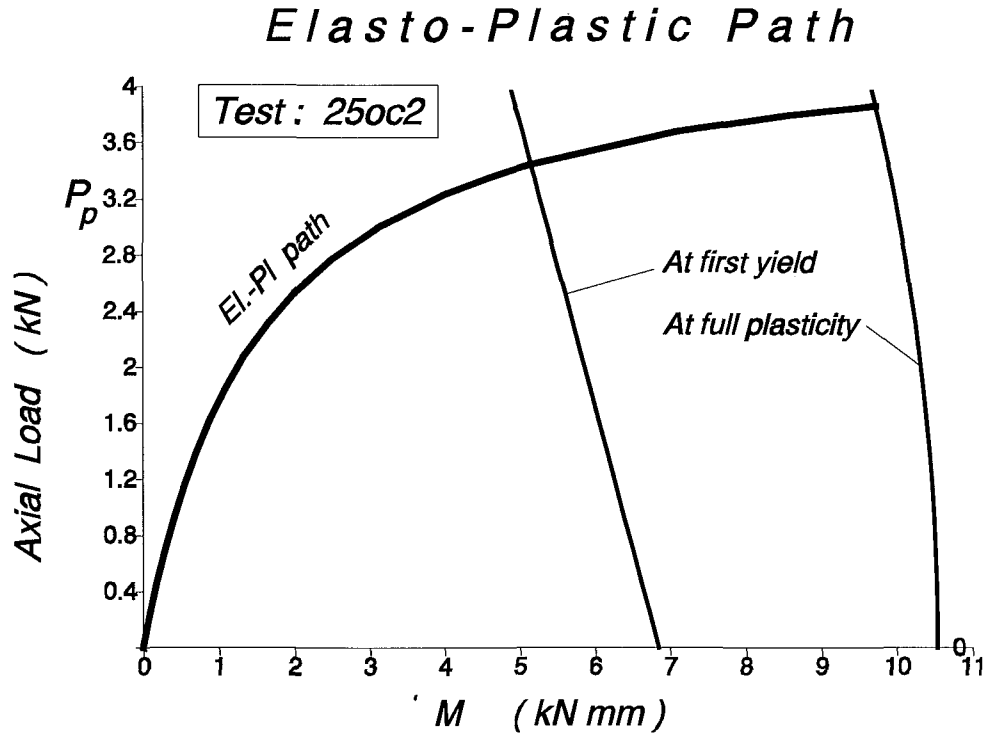
Elasto-Plastic Path
Test : 25oc2
Axial Load (kN)
P_p
4
3.6
3.2
2.8
2.4
2
1.6
1.2
0.8
0.4
El.-Pl path
At first yield
At full plasticity
0 1 2 3 4 5 6 7 8 9 10 11
M (kN mm)

THEORETICAL DATA & RESULTS OF TEST **25oc2**

PROP_sets = 3, SWAY_imp = -0.67 mm, NON-SWAY_imp = -0.40 mm

MEMBER PROPERTIES

MEM	L	b	d	A	I	Zel	Zpl	Y.str
1	210.0	3.0	13.0	38.47	28.53	19.02	29.26	360
2	250.0	5.0	13.0	62.44	125.70	50.28	81.45	360
3	210.0	3.0	13.0	38.47	28.53	19.02	29.26	360

Rotational SYMMETRIC (Non-sway) Stiffness of frame : 920.69 kN*mm/rad

Rotational ANTISYMMETRIC (Sway) Stiffness of frame : 1112.57 kN*mm/rad

Translational (Sway) Stiffness of frame : 25.34 N/mm

EIGENVALUES & EIGENVECTORS

Solut	kL	Pc	C1	C2	delta	theta_A	Mode-Case
1	5.944	4.4573	1.00	-0.171	0.000	0.005	Non-Sway
2	6.423	5.2043	1.00	-14.263	88.629	-0.005	* Sway

First YIELD Load = 3.442 kN

First HINGE Load = 3.857 kN

SQUASH Load = 13.848 kN

Test: 25oc3
Plastic Collapse Buckling

Experimental Data					Southwell Plot			
Load P kN	Loading		Unloading		Sway Mode		Non-Sway Mode	
	Top reads	Mid reads	Top reads	Mid reads	$\frac{\delta_t}{100}$ mm	$\frac{\delta_t}{100P}$ mm/kN	$\frac{\delta_m - \delta_t/2}{100}$ mm	$\frac{\delta_m - \delta_t/2}{100P}$ mm/kN
0	1007	1094.5	1050	1484	0.000	0.000	0.000	0.000
0.2	1009	1096.5	1064	1502	0.020	0.100	0.030	0.150
0.4	1010	1100	1072	1520	0.030	0.075	0.070	0.175
0.6	1012	1103	1080	1540	0.050	0.083	0.110	0.183
0.8	1014	1106.5	1088	1561	0.070	0.088	0.155	0.194
1	1017.5	1109	1096	1586	0.105	0.105	0.198	0.198
1.2	1022.5	1112	1103.5	1611	0.155	0.129	0.253	0.210
1.4	1028.5	1116	1112	1639	0.215	0.154	0.323	0.230
1.6	1035.5	1120.5	1123	1671	0.285	0.178	0.403	0.252
1.8	1043.5	1126	1135	1704	0.365	0.203	0.498	0.276
2	1052.2	1132.5	1149	1741	0.452	0.226	0.606	0.303
2.2	1062.5	1141	1163	1780	0.555	0.252	0.743	0.338
2.4	1072	1151.5	1179	1818	0.650	0.271	0.895	0.373
2.6	1084	1163			0.770	0.296	1.070	0.412
2.8	1098	1178.5			0.910	0.325	1.295	0.463
3	1113	1194			1.060	0.353	1.525	0.508
3.2	1128	1216			1.210	0.378	1.820	0.569
3.4	1148	1245			1.410	0.415	2.210	0.650
3.6	1173	1281			1.660	0.461	2.695	0.749
3.7	1186	1303			1.790	0.484	2.980	0.805
3.8	1200	1331			1.930	0.508	3.330	0.876
3.9	1209	1370			2.020	0.518	3.765	0.965
2.53	1288	1842			2.810	1.111	8.880	3.510

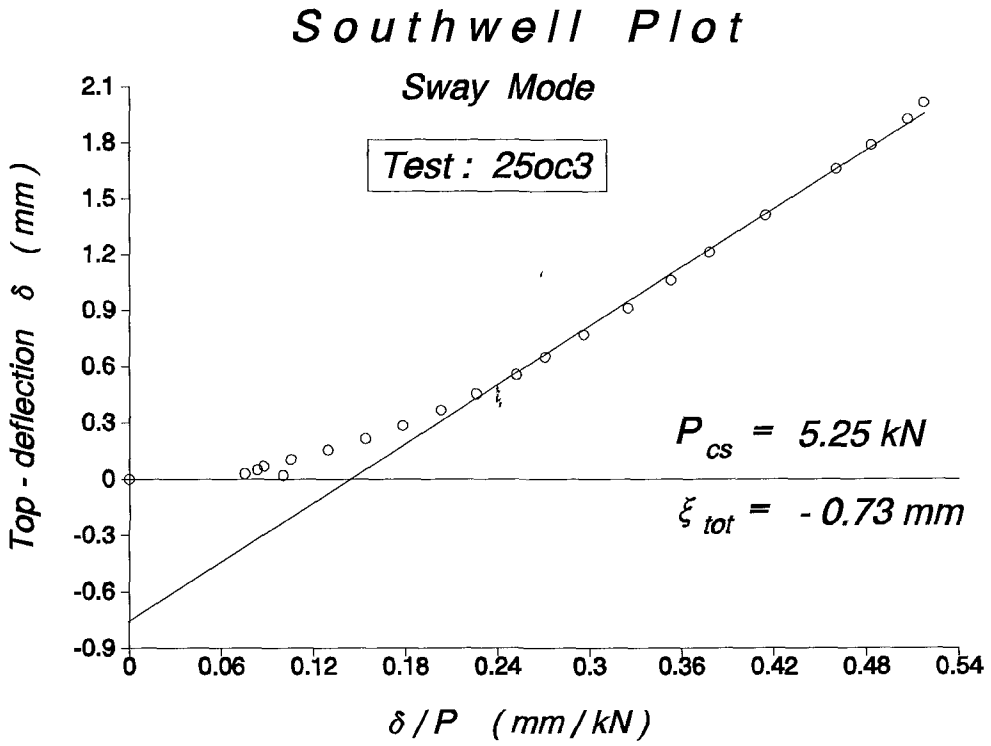
Southwell Plot
Sway Mode
Test : 25oc3
Top - deflection δ (mm)
2.1
1.8
1.5
1.2
0.9
0.6
0.3
0
-0.3
-0.6
-0.9
0
0.06
0.12
0.18
0.24
0.3
0.36
0.42
0.48
0.54
δ / P (mm / kN)
P cs = 5.25 kN
ξ tot = - 0.73 mm

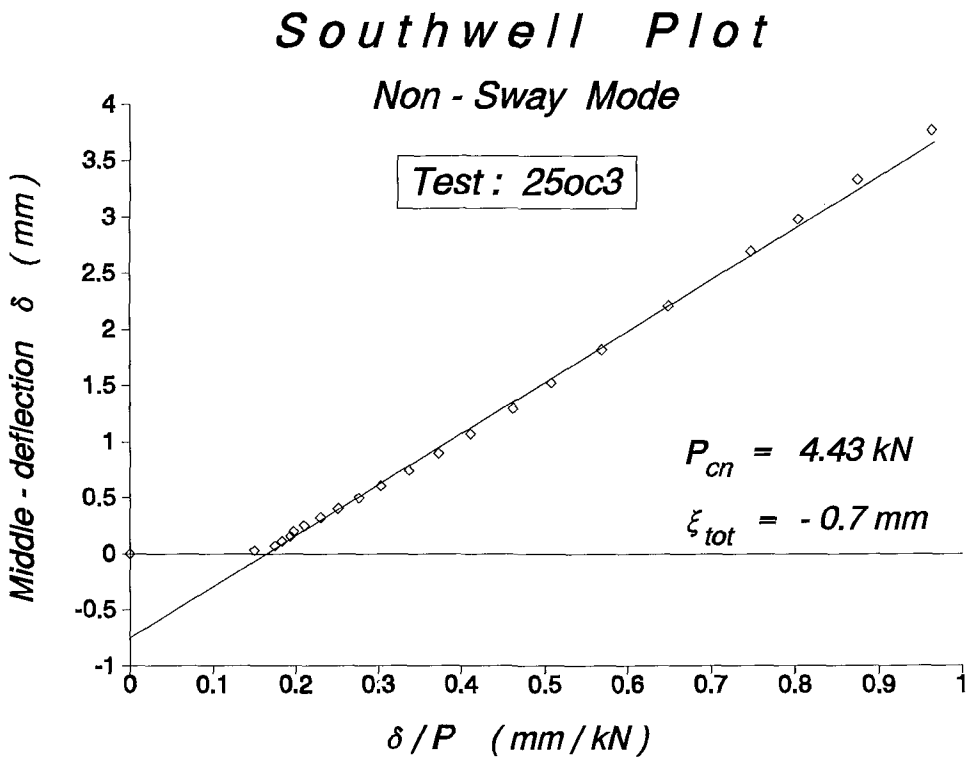
Southwell Plot
Non - Sway Mode
Test : 25oc3
Middle - deflection δ (mm)
4
3.5
3
2.5
2
1.5
1
0.5
0
-0.5
-1
0
0.1
0.2
0.3
0.4
0.5
0.6
0.7
0.8
0.9
1
δ / P (mm / kN)
P cn = 4.43 kN
ξ tot = - 0.7 mm

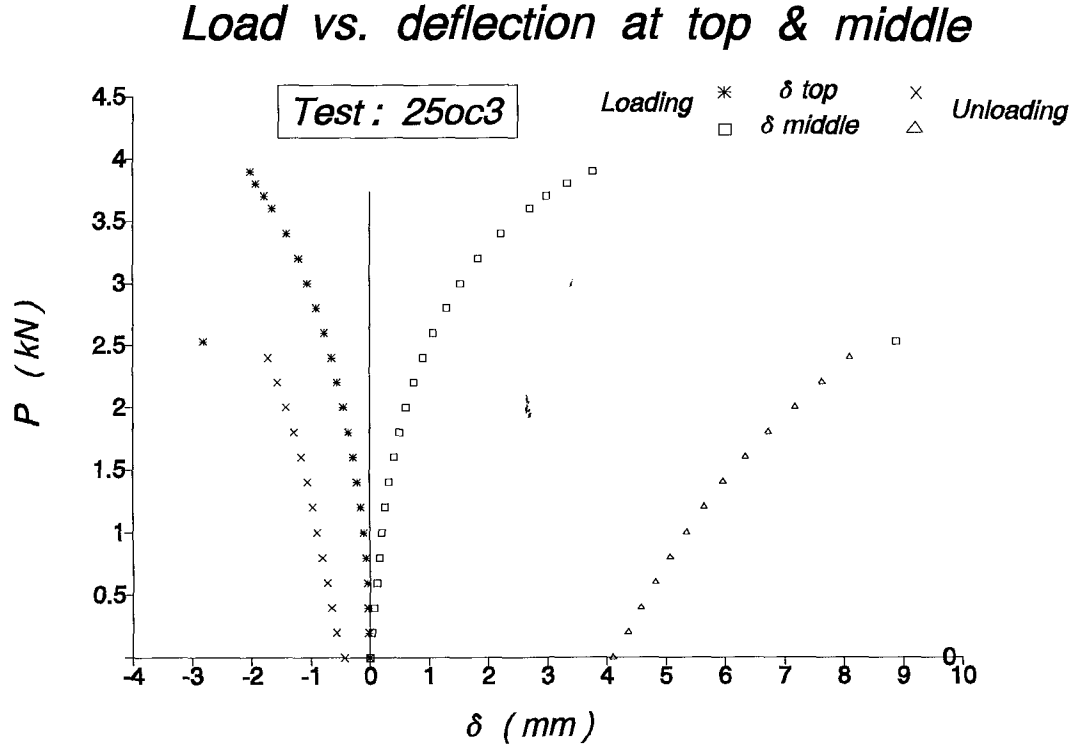
Load vs. deflection at top & middle
Test : 25oc3
Loading
δ top
δ middle
Unloading
P (kN)
δ (mm)

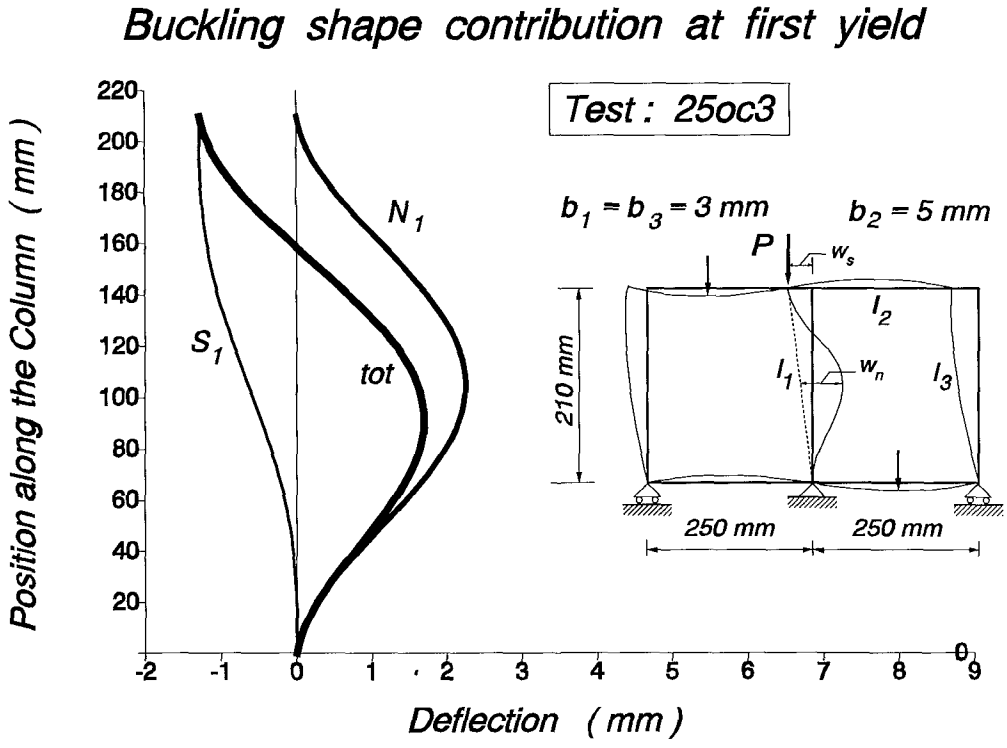
Buckling shape contribution at first yield
Test : 25oc3
$b_1 = b_3 = 3$ mm
$b_2 = 5$ mm
P
w_s
w_n
l_1
l_2
l_3
210 mm
250 mm
250 mm
N_1
S_1
tot
Position along the Column (mm)
Deflection (mm)

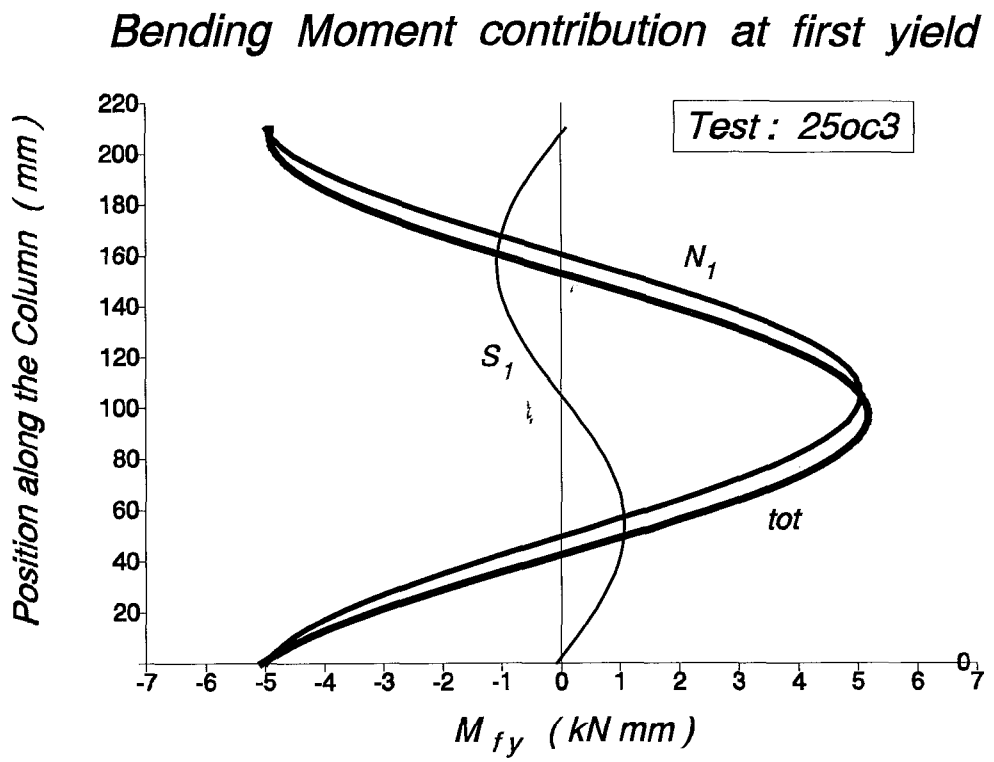
Bending Moment contribution at first yield
Test : 25oc3
Position along the Column (mm)
220
200
180
160
140
120
100
80
60
40
20
N_1
S_1
tot
-7 -6 -5 -4 -3 -2 -1 0 1 2 3 4 5 6 7
M_{fy} (kN mm)

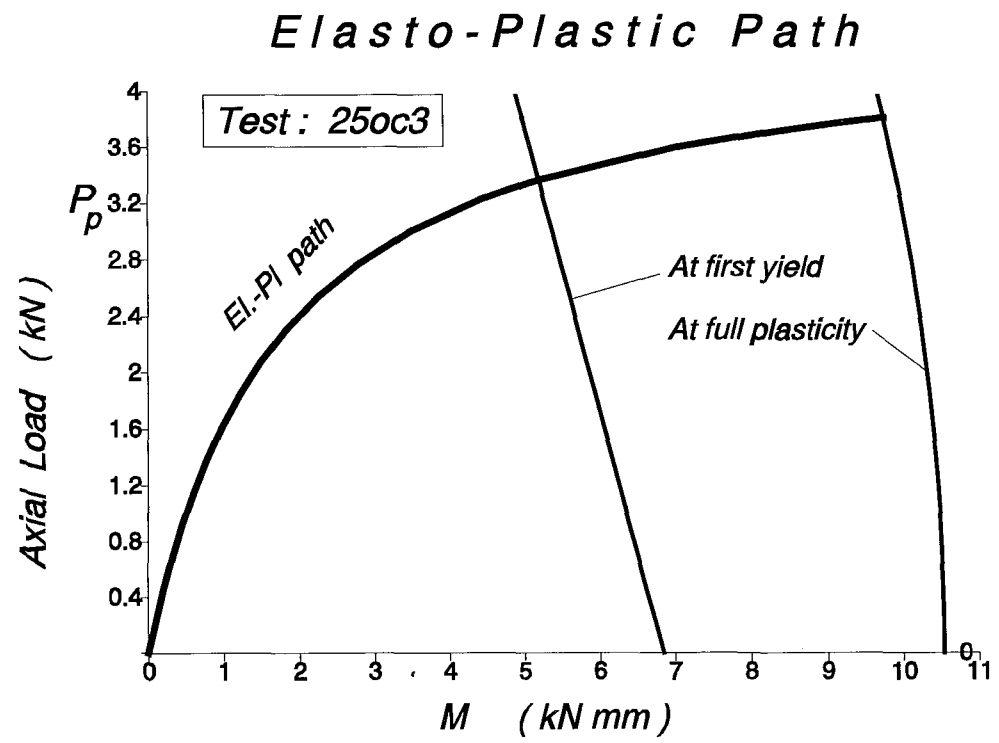
Elasto-Plastic Path
Test : 25oc3
Axial Load (kN)
P_p
4
3.6
3.2
2.8
2.4
2
1.6
1.2
0.8
0.4
El.-Pl path
At first yield
At full plasticity
0 1 2 3 4 5 6 7 8 9 10 11
M (kN mm)

THEORETICAL DATA & RESULTS OF TEST **25oc3**

PROP_sets = 3, SWAY_imp = -0.73 mm, NON-SWAY_imp = -0.70 mm

MEMBER PROPERTIES

MEM	L	b	d	A	I	Zel	Zpl	Y.str
1	210.0	3.0	13.0	38.47	28.53	19.02	29.26	360
2	250.0	5.0	13.0	62.44	125.70	50.28	81.45	360
3	210.0	3.0	13.0	38.47	28.53	19.02	29.26	360

Rotational SYMMETRIC (Non-sway) Stiffness of frame : 920.69 kN*mm/rad

Rotational ANTISYMMETRIC (Sway) Stiffness of frame : 1112.57 kN*mm/rad

Translational (Sway) Stiffness of frame : 25.34 N/mm

EIGENVALUES & EIGENVECTORS

Solut	kL	Pc	C1	C2	delta	theta_A	Mode-type
1	5.944	4.4573	1.00	-0.171	0.000	0.005	Non-Sway
2	6.423	5.2043	1.00	-14.263	88.629	-0.005	* Sway

First YIELD Load = 3.366 kN

First HINGE Load = 3.807 kN

SQUASH Load = 13.848 kN

7.4 Tabulated Comparisons between experiments and Theory

Following the procedure outlined in section 7.3 a programme of experiments has been undertaken to cover a parametric range which represents wide variations in the ratio of sway to the non-sway critical loads. This should allow thorough testing at the theoretical modelling developed for interactive elastic-plastic buckling. This range of test frames is described in the following pages. Table 7_5 indicates that test frames were in three major groups, which are classified according to the ratio of their sway to non-sway critical loads as discussed in section 6.2.

The first column shows the group-case, which, depending upon the ratio of P_{cS}/P_{cN} will determine whether buckling is sway dominated, strongly coupled or non-sway dominated.

The numbering used for this final programme of experiment is given in column 2.

Columns 3 to 7 describe the geometry of the frame by giving the length of the central (L_1) and side (L_3) columns, the length L_2 of the beams along with their corresponding thickness b_1, b_2, *and* b_3. The breadth for all members is 13 mm.

Columns 8 to 13 provide the theoretically derived results. Columns 8 and 9 list the lowest sway and non-sway critical loads, while the squash load is given in column 10. The ratio of the sway to non-sway critical load is in column 11. It may be noted that this ratio:

i) covers a range from 0.659 to 0.875 for the first group;

ii) is 1.00 for the second group frames; and

iii) covers a range from 1.1 to 1.6 for the third group frames.

Columns 12 and 13 provide an approximate first yield and first hinge loads, because they have been calculated on the assumption that a notional total sway imperfection is $\xi_1 = L_1/400\ mm$, while the respective non-sway is $\xi_2 = \xi_1 (P_{c1}/P_{c2})^{1/2}$.

The last column contains the name of each frame geometry in terms of the date (number followed by the first letter(s) of the month) of performance.

An experimental procedure outlined in the preceding section, for each of the frame geometries, gave results, which, for comparison reasons are summarised according to the expected behaviour in the subsequent tables.

For the sake of space, a detailed record of the experimental results listed in tables 7_6, 7_7 and 7_8 is presented in Appendix E. In this Appendix for each experiment a full list of the experimental data along with the Southwell Plot information are kept on the first page; on the second page the Southwell plots for both modes are depicted along with the corresponding information about the critical loads and the total equivalent imperfections, whilst the load vs displacement diagram with the inserted figure of frame geometry, along with the theoretically obtained data are presented on the third page.

A general observation which holds for every single experiment, independently of the central column's buckling behaviour, is the linearity of the Southwell Plot points at the elastic regime.

The fluctuation of the ratio of the experimental to the theoretical critical loads for both modes was between 0.9 and 1.1 although there were some odd cases where this ratio was beyond these limits, and only in the elasto-plastic behaviour of L_1=235 and L_2=400 frame geometry did the discrepancy reach 0.81 and 1.23.

The ultimate axial load level (buckling load) was for almost all cases of elasto-plastic or plastic collapse buckling behaviour greater than the theoretically predicted first hinge load. This justifies the fact that the second and probably the third plastic hinges have been formed shortly after the formation of the first hinge. In only two cases, the L_1/L_3=260/300 and L_1/L_3=235/370 frame geometries, was the buckling load, respectively, a little less and equal to the first yield load. This may be attributed to the interaction between the two buckling modes as a result of the large applied imperfections.

Table 7_5 List of Experiments within the parametric range

The theoretical results have been calculated for a notional $\xi_1 = L_1/400\ mm$, $\xi_2 = \xi_1(P_{c1}/P_{c2})^{1/2}\ mm$ and cross section's breadth 13 mm.

Case	No.	Frame Geometry					Theoretical Results						Date Numbering
		$L_1=L_3$ mm	L_2 mm	b_1 mm	b_2 mm	b_3 mm	P_{cS} kN	P_{cN} kN	P_p kN	P_{cS}/P_{cN}	P_{fy} kN	P_{fh} kN	
$\frac{P_{cS}}{P_{cN}} \le 1$	1	280	300	6	5	5	8.04	12.19	26.437	0.659	7.05	8.81	18oc*
	2	270	350	5	5	5	6.53	8.66	22.447	0.754	6.07	6.34	16oc
	3	330	300	5	6	5	6.24	7.14	"-"	0.875	5.61	6.00	12oc
$\frac{P_{cS}}{P_{cN}} \approx 1$	4	340	314	5	6	6	6.75	6.75	"-"	1.000	5.51	6.06	4oc
	5	260	300	5	6	6	11.13	11.13	"-"	"-"	8.30	9.58	23oc*
$\frac{P_{cS}}{P_{cN}} \ge 1$	6	210	250	3	5	3	5.20	4.46	13.848	1.170	3.60	3.97	25oc
	7	235	400	3	5	5	4.63	3.41	"-"	1.357	2.87	3.09	26oc
	8	235	370	3	5	5	4.89	3.45	"-"	1.416	2.89	3.13	6N

* Possible increase of imperfections.

Table 7_6 Comparisons on **Elastic** Buckling Experiments

Frame Geometry					**Experimental Results**				**Theoretical Results**				**Comparisons**	
$L_1=L_3$ mm	L_2 mm	b_1 mm	b_2 mm	b_3 mm	P_{cS} kN	P_{cN} kN	ξ_S mm	ξ_N mm	P_{cS} kN	P_{cN} kN	P_{fy} kN	P_{fh} kN	P_{cS}^{Ex}/P_{cS}^{Th}	P_{cN}^{Ex}/P_{cN}^{Th}
280	300	6	5	5	8.58	10.42	1.25	0.80	8.04	12.19	7.08	7.63	1.07	0.85
270	350	5	5	5	6.76	8.38	0.75	0.70	6.53	8.66	5.98	6.31	1.03	0.97
330	300	5	6	5	6.74	7.54	1.40	0.145	6.24	7.14	5.64	5.93	1.08	1.05
340	314	5	6	6	6.63	6.94	1.20	0.75	6.75	6.75	5.18	5.84	0.98	1.03
260	300	5	6	6	10.53	11.35	0.98	0.88	11.13	11.14	7.75	9.19	0.95	1.02
210	250	3	5	3	5.74	4.47	1.07	0.48	5.20	4.46	3.07	3.58	1.10	1.00
235	400	3	5	5	4.20	3.55	0.65	0.036	4.63	3.41	2.83	3.07	0.91	1.04
235	370	3	5	5	4.09	3.50	0.83	0.82	4.89	3.45	2.71	3.01	0.84	1.01

Table 7_7 Comparisons on **Elastic-Plastic** Buckling Experiments

Frame Geometry					**Experimental Results**					**Theoretical Results**				**Comparisons**		
$L_1=L_3$ mm	L_2 mm	b_1 mm	b_2 mm	b_3 mm	P_{cS} kN	P_{cN} kN	ξ_S mm	ξ_N mm	P_b kN	P_{cS} kN	P_{cN} kN	P_{fy} kN	P_{fh} kN	P_{cS}^{Ex}/P_{cS}^{Th}	P_{cN}^{Ex}/P_{cN}^{Th}	P_{fh}/P_b
280	300	6	5	5	8.58	11.47	1.05	1.05	8.20	8.03	12.19	7.09	7.67	1.07	0.94	0.94
270	350	5	5	5	6.92	8.42	0.75	0.70	6.70	6.53	8.66	5.98	6.31	1.06	0.97	0.94
330	300	5	6	5	7.03	7.54	1.35	0.12	6.5	6.24	7.14	5.66	5.94	1.12	1.05	0.91
340	314	5	6	6	7.44	7.32	1.60	0.86	6.02	6.75	6.75	4.84	5.60	1.10	1.08	0.93
260	300	5	6	6	11.17	11.33	1.05	0.75	8.70	11.13	11.13	7.95	9.34	1.00	1.02	1.07
210	250	3	5	3	5.40	4.67	0.67	0.40	4.20	5.20	4.46	3.44	3.86	1.04	1.05	0.92
235	400	3	5	5	4.20	3.76	0.80	0.05	3.80	3.41	4.63	2.83	3.07	1.23	0.81	0.81
235	370	3	5	5	4.13	3.49	0.85	0.85	3.00	4.89	3.45	2.70	3.00	0.84	1.01	1.00

Table 7_8 Comparisons on **Plastic Collapse** Buckling Experiments

Frame Geometry					**Experimental Results**					**Theoretical Results**				**Comparisons**		
$L_1=L_3$ mm	L_2 mm	b_1 mm	b_2 mm	b_3 mm	P_{cS} kN	P_{cN} kN	ξ_S mm	ξ_N mm	P_b kN	P_{cS} kN	P_{cN} kN	P_{fy} kN	P_{fh} kN	P_{cS}^{Ex}/P_{cS}^{Th}	P_{cN}^{Ex}/P_{cN}^{Th}	P_{fh}/P_b
280	300	6	5	5	9.32	13.54	2.20	1.80	8.00	8.04	12.19	6.15	7.20	1.16	1.11	0.90
270	350	5	5	5	6.90	8.49	2.25	1.80	5.80	6.53	8.66	4.80	5.71	1.05	0.98	0.98
330	300	5	6	5	6.33	7.59	1.50	0.275	6.30	6.24	7.14	5.58	5.90	1.13	1.06	0.94
340	314	5	6	6	7.10	7.13	1.50	1.10	5.95	6.75	6.75	4.90	5.65	1.05	1.05	0.95
260	300	5	6	6	12.20	10.53	0.72	0.90	8.60	11.13	11.13	7.43	8.95	1.09	0.95	1.04
210	250	3	5	3	5.25	4.43	0.73	0.70	3.90	5.20	4.46	3.37	3.81	1.01	0.99	0.97
235	400	3	5	5	4.05	3.86	1.00	0.30	3.50	4.63	3.41	2.60	2.91	0.87	1.13	0.83
235	370	3	5	5	4.07	3.47	1.35	2.05	2.50	4.89	3.45	2.38	2.77	0.83	1.00	1.10

7.5 Graphical Comparisons between Experiments and Theory

The tabulated presentation of comparisons between experimental and theoretical results for all the experiments outlined in the preceding Section is summarised in graphical form in Figs. 7-13 to 7-16.

Making use of the data presented in Table 7_2 along with that of Tables 7_7 and 7_8, four different graphs have been developed to demonstrate the observed deviations between the experimental and theoretical results. The comparisons have been made for:

a) the sway and non-sway critical loads, Fig. 7-13 and 7_14

b) the buckling load against the first yield and the buckling load against first hinge load, shown in Figs. 7-15 and 7-16.

In all graphs the axes represent axial loads, which, for simplicity reasons, have been non-dimensionalised with respect to the squash load P_y.

On the top right end of each graph a few values of the ratio P^{th}/P^{ex} have been used to draw the lines between which indicate the correlations of the experimental points.

A comparison on the sway critical loads (Fig. 7-13), shows that the scattering points have a greater spread than that of the non-sway critical loads (Fig. 7-14), where they seem to be more concentrated along the diagonal line ($P^{th}/P^{ex} = 1$).

Comparing the maximum applied load to the first yield and first hinge load it seems that the first yield scattering points (Fig. 7-15) are further away from the diagonal line than those of the first hinge (Fig. 7-16). This seems to be quite reasonable in the sense that the buckling loads have to be closer to the first hinge loads rather than the first yield loads.

Finally, through the graphs it can easily be established that in general, the majority of the deviations observed in all comparisons does not exceed 10%.

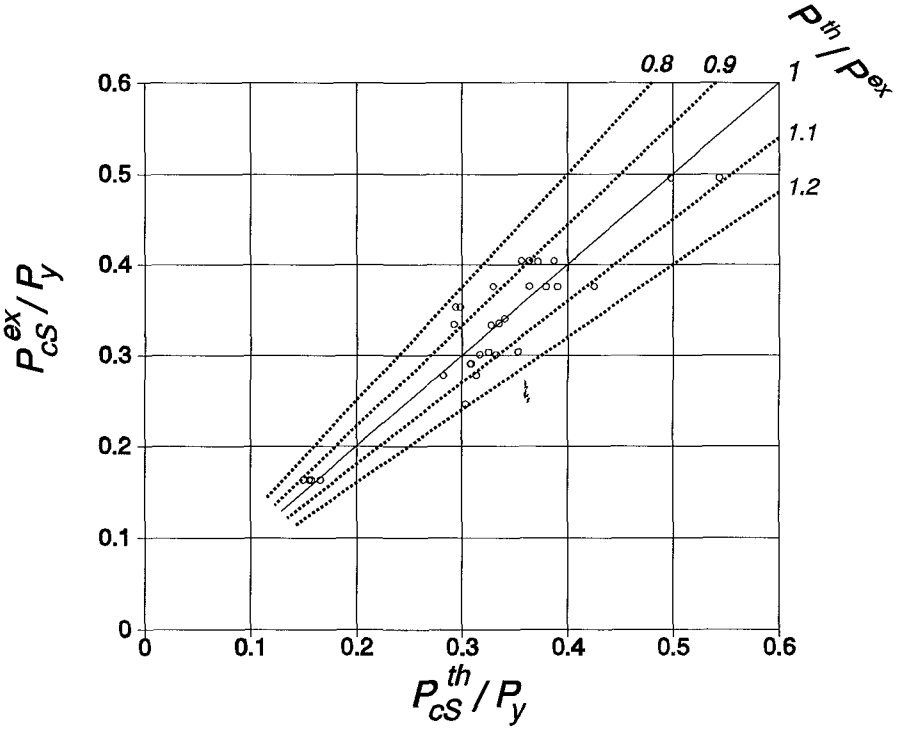

Figure 7-13

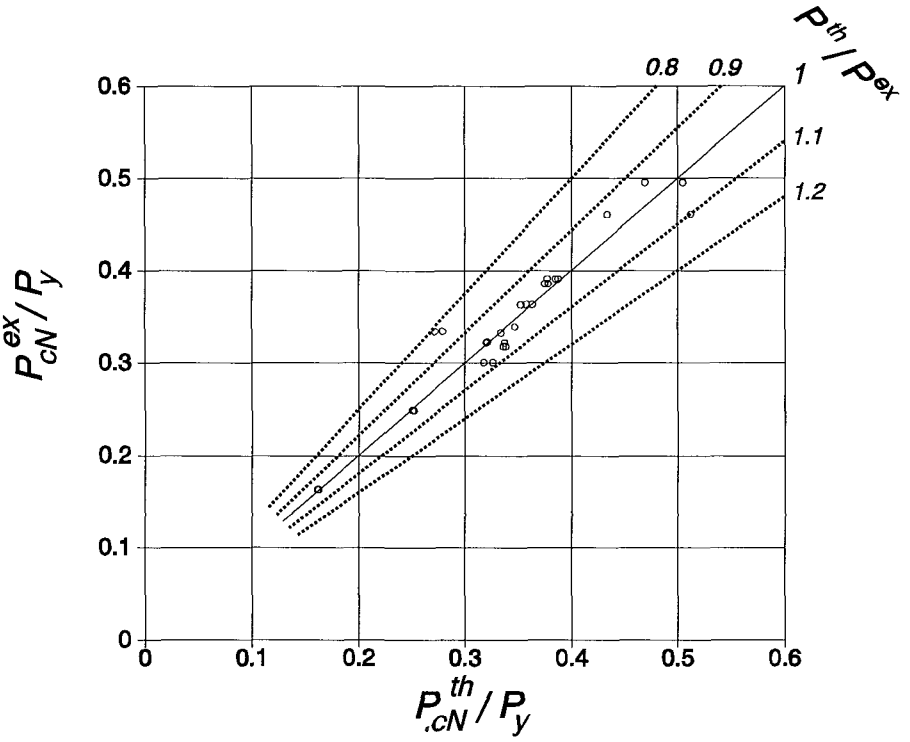

Figure 7-14

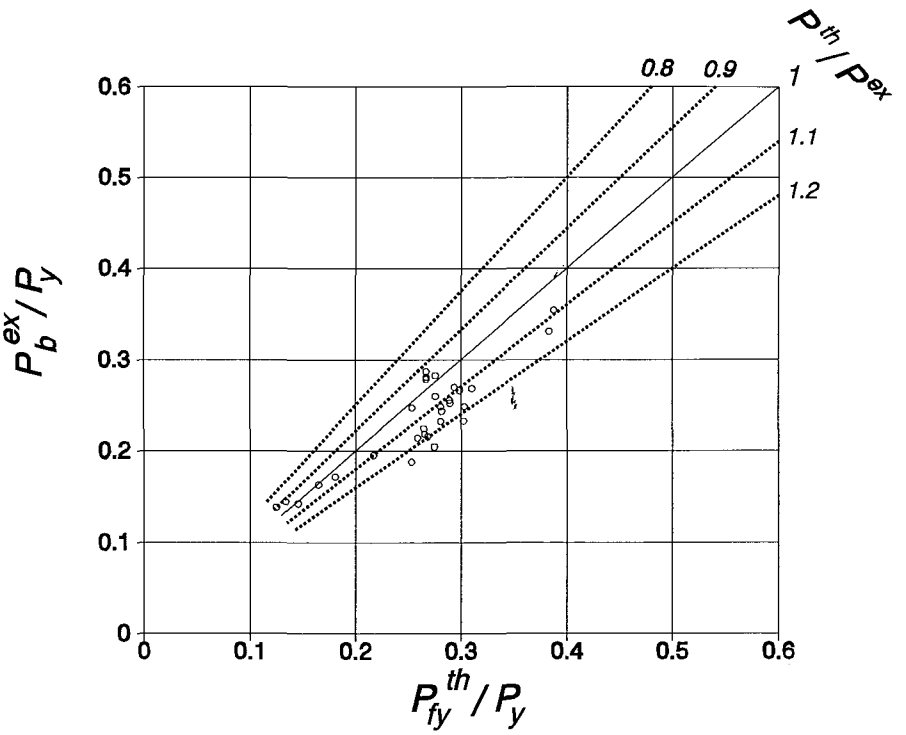

Figure 7-15

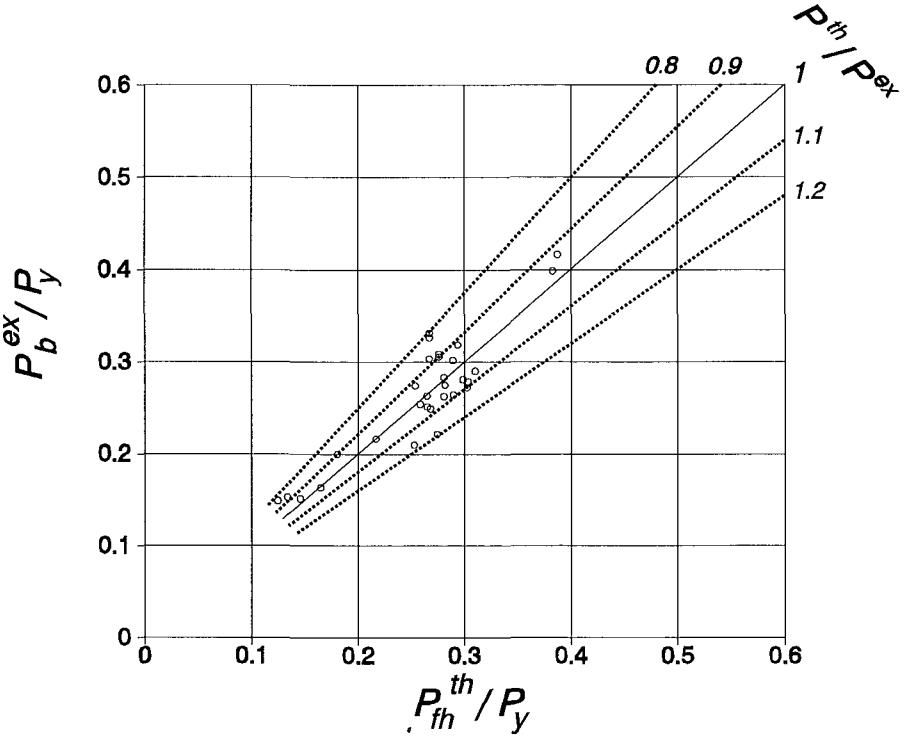

Figure 7-16

Chapter 8

Existing Design Methods and a New Simplified Design Procedure

8.1 Current Bases for Column Buckling

In design practice the theoretical bases of column design formulae, curves or charts are based today on one of the three following concepts:

(i) Bifurcation Approach According to this approach a perfectly straight column will start to bend only when the load reaches a certain upper limit. This upper limit would then represent the criterion for column strength, and would be based upon either the Euler elastic critical load or the Tangent modulus plastic strength load, depending respectively upon the range (elastic or inelastic) of the stress-strain curve.

(a) Elastic stability - Euler load

A centrally loaded, elastic, perfectly straight, pin-ended column of length L, moment of inertia I, and elastic modulus E, ceases to be stable at Euler load, P_E, given by the equation

$$P_E = \frac{\pi^2 EI}{L^2} \tag{8.1}$$

Introducing the slenderness ratio $\lambda = L/r$, where r is the radius of gyration of the cross section, the average stress corresponding to the Euler Load is

$$\sigma_E = \frac{\pi^2 E}{\lambda^2} \tag{8.2}$$

The slenderness ratio, $\lambda_y = \pi \sqrt{\frac{E}{\sigma_y}}$, represents the situation where the elastic critical stress is equal to the material yield stress, and provides a limit for determining the average stress σ at failure. This limiting stress is then

$$\sigma = \begin{cases} \sigma_y & \text{for } \lambda \le \lambda_y \\ \sigma_E & \text{for } \lambda > \lambda_y \end{cases} . \tag{8.3}$$

Reminded is the relationship $\frac{\lambda_y}{\lambda} = \left(\frac{\sigma_E}{\sigma_y}\right)^{1/2}$.

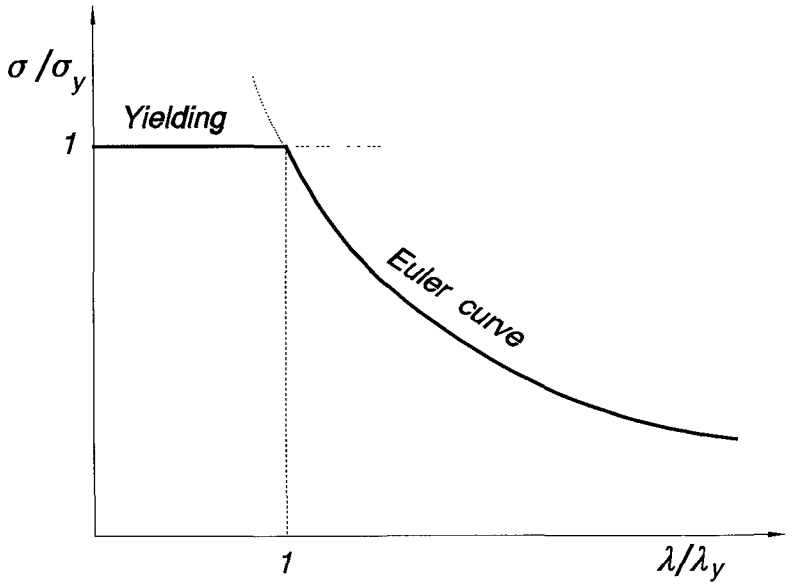

Figure 8-1

Eq. (8.3) is plotted in a non-dimensional way in Fig. 8-1 to show the range of elastic buckling as predicted by Euler.

(b) Inelastic stability - Tangent modulus load

According to the tangent modulus theory, a perfectly straight column, similar

to the former one of case (a), will start to bend either at the Euler load or Tangent modulus load, depending on whether the average stress is less or greater than the proportional limit σ_p. Indeed, after this limit, the relation between stress and strain is not linear and the Tangent modulus E_t, which is the slope of this curve, may replace the elastic modulus in Euler equation. Therefore, the Tangent modulus load, given by Eq. (A.2) in Appendix A, holds only for $\sigma \geq \sigma_p$.

The application of the tangent modulus theory is limited to those straight columns whose axes of symmetry coincide with the axes of symmetry of the residual stresses. However, due to random distribution of initial stresses, even a perfectly straight column will start to bent at an early stage of loading.

The lack of current design methods based upon σ_E and σ_y justifies the fact that even the Rankine formula,

$$\frac{1}{\sigma_b} = \frac{1}{\sigma_E} + \frac{1}{\sigma_y}$$

developed in section 2.6.3 and any of its empirically based extensions are not really rational.

(ii) Imperfection Approach This is the most rational treatment for the buckling problem. The strength of the column is determined by considering the interaction between elastic stability and material plasticity by geometrical imperfections. Under the assumption that the initial non-straight shape of the column has a sine form, the relation between the axial load, P, and final deflection, w, is given by

$$w = \frac{1}{1 - \frac{P}{P_E}} w^o \qquad \textbf{(8.4)}$$

This equation, shown in Fig. 8-2 by the curve ABC, represents the behaviour of a column with pure elastic material behaviour and an initial deflection w^o. Young[2], in

1807 was the first to establish the imperfection approach.

In practical situations the range of response for which the material remains elastic, is limited. Eventually the maximum stressed fibres will reach material yield, and an elastic plastic response will start in the column. The load deflection diagram for this regime is shown by the curve BDE with the peak point at D, corresponding to the maximum capacity of load, P_b, that the column can carry. Many parameters are involved in determining this load, making the whole procedure very complicated. As a lower bound to the maximum load, P_b, Ayrton and Perry chose the load corresponding with first yield, P_{fy}; this represents the maximum load that the column can carry while remaining elastic. They gave this load in a form equivalent to the formula

$$(P_E - P_{fy})(P_y - P_{fy}) = \rho P_{fy} P_E \qquad (8.5)$$

where $P_y = \sigma_y A$ is the squash load

$\rho = w^o / (Z/A)$ is the imperfection parameter

Z is the elastic section modulus.

If it is assumed that the column remains elastic until a fully formed plastic hinge occurs at a point G, it is normally the case that the corresponding load P_{fh}, is a close estimate of the buckling collapse load P_b. The first hinge load will usually represent an upper bound solution to the buckling load.

In order to calculate the first **plastic** hinge load P_{fh}, the full section plasticity curve FGH has to be determined. This curve is often approximated by assuming that the material is rigid-plastic. Under this assumption there will be no lateral deflection until the load reaches P_y, when, a plastic hinge forms somewhere in the column. This hinge causes a deformation on the column and consequently, through the axial load, a bending moment is generated; this in turn produces an extra deflection and thus an additional bending moment. This procedure results eventually in the reduction of the load carrying capacity of the column, the behaviour of which is shown in Fig. 8-2 by the curve FGH. The intersection of this curve with the elastic

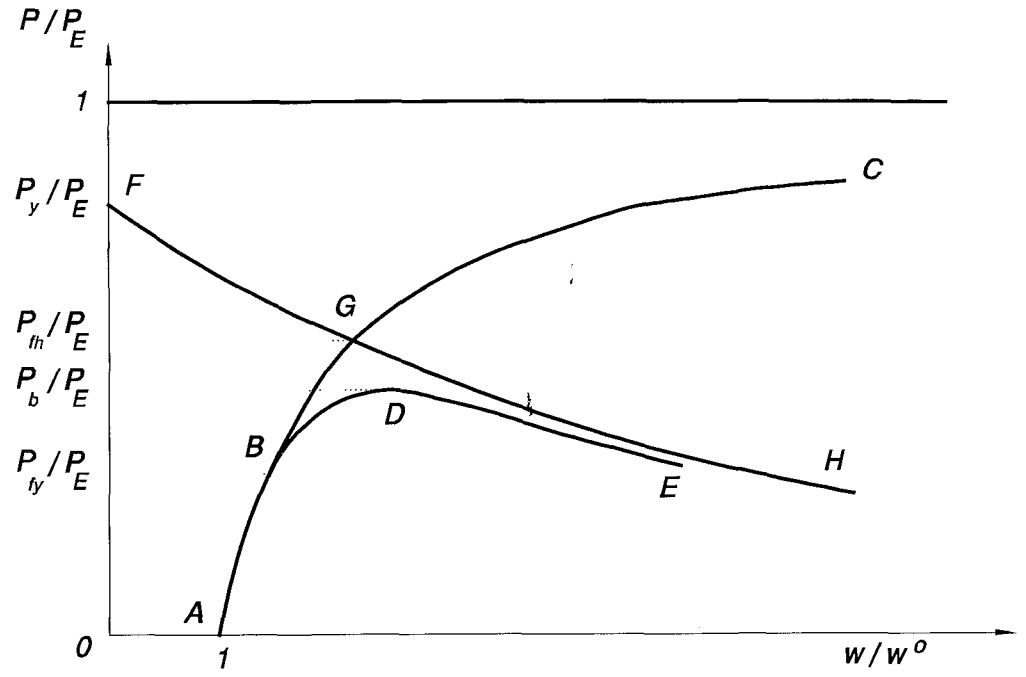

Figure 8-2

curve ABC corresponds to the first plastic hinge load, P_{fh}.

There is a number of currently important design codes, like BS 449, BS 5950, ECCS which make use of P_y without going into details or employing P_{fh}.

(iii) Empirical Approach Here the calculation of the maximum strength of axially loaded columns may be a complicated process including both physical and numerical experiments. The load-displacement curve of an imperfect column is traced, involving numerical integration or empirical simplification. The design formulae or curves obtained rely upon curve fitting to the numerical results. SSRC multiple column curves discussed in the next section would be classified under this approach.

A small number of currently significant design curves is discussed in the next section, where, each one of the curves will be located within one of the above three approach philosophies.

8.2 Column Design Curves in Codes of Practice

There are various column design curves used in design to predict the strength of a column. A number of these curves have been plotted as lines to provide lower bounds to the scatter band of test or numerical results. They are based theoretically on one of the approaches described in the preceding section. In this section emphasis will be placed on interaction formulae employed in a number of currently important design codes.

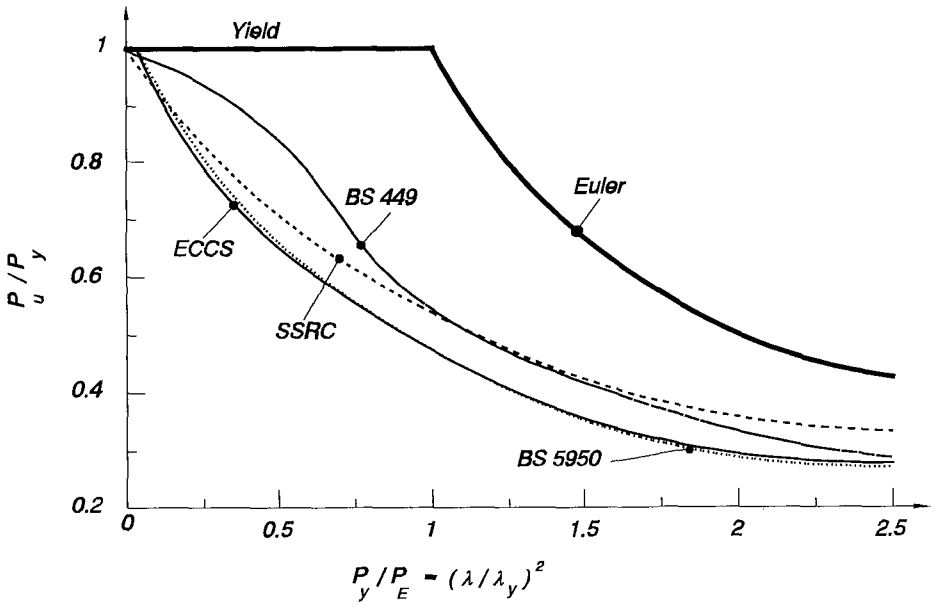

Figure 8-3

In Fig. 8-3 four of the more commonly adopted curves are plotted in a non-dimensional form of P_u/P_y versus P_y/P_E, where P_u is the ultimate compression capacity of an axially loaded column proposed by the design codes.

Some design codes adopt different curves for each class of cross sectional shape. Taking this into account, with the aim of a better comparison, all the column curves are plotted for an **I**-cross-section, buckling about its minor axis. Since some of the curves do not lend themselves to a dimensionless form, they have been plotted for a mild steel with a yield stress of 265 N/mm^2 and elastic modulus of 205 kN/mm^2.

The variation in the experimentally observed buckling loads which have been used to justify a particular design curve, is emphasized by the spread of the curves. The heavy line represents the Euler curve which has been cut off at a stress which corresponds to the yield point. The four curves are:

8.2.1 British Standard (BS 449) column curve

The BS 449[53] column curve is based on the imperfection approach, using the Ayrton-Perry formula

$$(P_E - P_{fy})(P_y - P_{fy}) = \rho P_{fy} P_E \qquad (8.6)$$

After calculating the imperfection parameter ρ, the load P_{fy} obtained by the formula, was equal to the lower bound of the scattered buckling loads obtained from experiments.

Robertson[54] suggested for ρ a value of $\rho = 0.3\left(\frac{L}{r}\right)10^{-2}$, which was used in British Code for many years. On the basis of Godfrey's[55] recommendation in 1962, the Standard adopted the modified value for imperfection parameter

$$\rho = 0.3\left(\frac{L}{r}\right)^2 10^{-4}.$$

Since 1969 the design curve in BS 449 has been based on this value of parameter; it is this curve that is plotted in Fig. 8-3.

8.2.2 British Standard (BS 5950) column curves

In the recent British Standard BS 5950[30] different column curves were adopted for different types of columns. These curves are again based on the imperfection approach using the same equation as BS 449. Dwight[56] proposed a

modified form of the Ayrton-Perry equation that matched the European curves very closely. So he attributed to ρ the value

$$\rho = 0.001\,\alpha\,(\lambda - \lambda_o) \geq 0 \tag{8.7}$$

where the value of α, (Robertson's constant), depending upon the shape of the cross section and the axis of buckling, has one of the four values

$$\alpha = \begin{cases} 2.0 \\ 3.5 \\ 5.5 \\ 8.0 \end{cases} \tag{8.8}$$

and λ_0 is the limiting slenderness and should be taken as

$$\lambda_o = 0.2\pi\sqrt{\frac{E}{\sigma_y}} = 0.2\,\lambda_y \tag{8.9}$$

In Fig. 8-3 a BS 5950 column curve has been plotted for the case of $\alpha = 0.0055$, which corresponds to the strength of a wide flange **I**-section column, buckling about its minor axis.

8.2.3 Structural stability Research Council (SSRC) multiple column curves

The SSRC multiple column curves were developed on the basis of results from a numerical approach. Bjorhovde[57] in 1972, using a computer model, generated by numerical techniques some 112 column curves for pin-ended members with realistic residual stress distributions and with a sinusoidal shape of initial deflection having a maximum amplitude $L/1000$. Each column curve was obtained by regression of a set of points which in turn were the peak points of the load-deflection curves of a column at different slenderness ratios.

He then classified these curves in three multiple column curves, each one of

which represented a specific category of columns and was approximated by a set of five equations related to a specific range of slenderness ratio.

Later in 1979, Rondal and Maquoi[58] showed that the SSRC equations could be represented quite accurately by the Ayrton-Perry formula, under the assumption that the imperfection parameter, ρ has the value

$$\rho = \begin{cases} \alpha(\bar{\lambda} - 0.15) & \bar{\lambda} \geq 0.15 \\ 0 & \bar{\lambda} < 0.15 \end{cases}, \tag{8.10}$$

where $\bar{\lambda}$ is a dimensionless slenderness ratio, with a value given by

$$\bar{\lambda} = \frac{1}{\pi}\left(\frac{L}{r}\right)\sqrt{\frac{\sigma_y}{E}} = \frac{\lambda}{\lambda_y} = \left(\frac{\sigma_y}{\sigma_E}\right)^{1/2} \tag{8.11}$$

and α is a numerical coefficient for each one of the three SSRC curves; values of α are given as

$$\alpha = \begin{cases} 0.103 & for \quad SSRC \quad curve \quad 1 \\ 0.293 & for \quad SSRC \quad curve \quad 2 \\ 0.622 & for \quad SSRC \quad curve \quad 3 \end{cases} \tag{8.12}$$

These values of α had been calculated in order to minimize the deviation between the Bjorhovde equations for the above three multiple column curves and the analytical expression coming from the Ayrton-Perry equation (8.6), where the imperfection parameter ρ is replaced by the values of equation (8.10). For $\alpha = 0.293$ the Rondal-Maquoi proposal is almost coinciding with the analytical expressions.

8.2.4 European (ECCS) column curves

ECCS column curves, like the SSRC multiple column curves, were obtained empirically. The European studies used theoretical data as a basis for computations

of column design curves which then were compared with test results. These design recommendations[28] employ three basic column curves, the use of which depends upon the shape of the cross section.

Originally they were published in tabular form without mathematical expressions. The validity of the curves is limited to those steel structures with a yield point up to 430 N/mm^2. For high strength steel an additional design curve was introduced. Another curve was also added for the design of heavy sections. In Fig. 8-3 only the last curve, applied to a wide flange **I**-shape about its weak axis, has been plotted.

8.3 Interaction Column Design in Codes of Practice

8.3.1 In BS 5950

For columns subjected to a combined action of bending moments and axial load, BS 5950 gives three interaction formulae to be used for a safe design. Each formula checks the capacity (local and overall) at the sections of maximum bending moment and axial load.

i) Local capacity check. The code assumes linear interaction between the applied axial load and the moments about two axes (major x and minor y), giving the relationship

$$\frac{P}{A\sigma_y} + \frac{M_x}{M_{cx}} + \frac{M_y}{M_{cy}} \leq 1 \qquad \textbf{(8.13)}$$

where: M_x, M_y are the applied moments about the major and minor axes at critical region and

M_{cx}, M_{cy} are the moment capacities about the major and minor axes when no axial load is present.

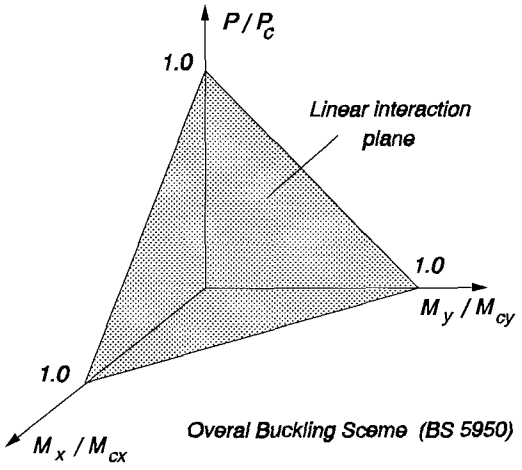

Figure 8-4

ii) Overall buckling check. For this check there are two approaches:

a) The simplified approach, requiring the satisfaction of equation

$$\frac{P}{A\sigma_y} + \frac{mM_x}{M_b} + \frac{mM_y}{\sigma_y Z_y} \leq 1 \qquad \textbf{(8.14)}$$

b) The more exact approach, with the following relation

$$\frac{mM_x}{M_{ax}} + \frac{mM_y}{M_{ay}} \leq 1 \qquad \textbf{(8.15)}$$

where: m is the equivalent uniform moment factor; m = 1 for end supports with equal moments, and, depending on the ratio of the smaller to the larger end moment, takes a minimum value of 0.43 (see Eq. 2.18).

M_b is the buckling resistance moment capacity with respect to the major axis ($=S_x p_b$)

S_x is the plastic modulus of the section about the major axis

p_b is the bending strength and is a function of slenderness ratio

Z_y is the elastic section modulus about the minor axis

M_{ax} is the maximum buckling moment about the major axis in the presence of axial load, taken to be the lesser of

$$M_{cx}\frac{\left(1-\frac{P}{P_{cx}}\right)}{\left(1+\frac{0.5P}{P_{cx}}\right)} \quad or \quad M_b\left(1-\frac{P}{P_{cy}}\right)$$

M_{ay} is the maximum buckling moment about the minor axis in the

presence of axial load taken as

$$M_{cy}\frac{\left(1-\frac{P}{P_{cy}}\right)}{\left(1+\frac{0.5P}{P_{cy}}\right)}$$

where: p_{cx}, p_{cy} are the compression resistances about the major and minor axes respectively which are usually identical.

The above interaction formulae refer to linear bending moments derived from linear analysis of the overall structure of which the column is a part. These linear moments include bending moments which are considered to be generated by eccentric loading. Nowhere in BS 5950 is made any reference in the non-linear bending moments of the column.

8.3.2 In SSRC

Following a similar approach, this code gives the formula

$$\frac{P}{P_y}+\frac{C_m M_o}{M_p(1-P/P_E)} \le 1 \qquad \textbf{(8.16)}$$

where P_y is the compression capacity of the axially loaded column obtained from the **SSRC** column design curves, M_o is a linear bending moment, M_p is the plastic moment capacity and

$$C_m = 0.6 + 0.4\beta \ge 0.4 \qquad \textbf{(8.17)}$$

is the equivalent uniform moment factor, in which β is the ratio of the smaller to the greater end moment similar to the parameter in **BS 5950**. The curves are empirically obtained assuming an initial deflection $0.001L$ at mid-height of the column.

8.3.3 In ECCS

A similar approach to that of BS 5950 led to the use of the equation

$$\frac{P}{P_y} + \frac{C_m M_o + Pe^*}{M_p(1 - P/P_E)} \leq 1 \qquad (8.18)$$

where e^* is a notional eccentricity which accounts for all imperfections and M_o is a linear bending moment.

The value of e^* can be obtained from the following equation

$$\frac{P}{P_y} + \frac{Pe^*}{M_p(1 - P/P_E)} \leq 1 \qquad (8.19)$$

where P is the axial compression capacity of the column obtained from appropriate **ECCS** column design curves. The value for C_m is the same as that given in ***SSRC***. The theoretical results were developed on the assumption that an initial deflection of $0.001L$ was always present at mid-height of the column.

8.4 Multi-storey Rigid Frame Design

In this section a design method is described for multi-storey multi-span steel frames. For these frames attention will be drawn on the method which is in use by BS 5950.

i. Elastic Design

For an elastic design the forces and moments in the members are determined from a **linear elastic analysis** of the entire frame or of suitable sub-frame.

After specifying some general conditions to be met, concerning

1. the loading (vertical, horizontal, notional horizontal)

2. the base stiffness and

3. the classification of a multi-storey frame (sway, non-sway),

the code refers to the necessary conditions for a modification up to 10% of the peak elastic moments in any member. It finishes with the general remark that **the capacity and the buckling resistance should be determined in accordance** with what was discussed in section **8.3.1.**

Specifically for the non-sway frames the code suggests that they should be analysed using ordinary **linear** elastic methods, whilst for the sway proposes:

a) an *extended simple design* using the effective length and

b) an *amplified sway method* where the moments due to horizontal loading should be amplified by the factor

$$\frac{\lambda_{cr}}{(\lambda_{cr}-1)}$$

where: $\lambda_{cr} = \dfrac{1}{200\phi_{s.max}}$ is the elastic critical load factor.

$\phi_{s\,max}$ is here the largest value of any storey with the sway index, $\phi_s = \dfrac{\delta_U - \delta_L}{h}$,

where : h is the storey hight

δ_U is the horizontal deflection on the top of the storey and

δ_L is the horizontal deflection on the bottom of the storey.

ii. Plastic Design

Provided the frame is braced against sidesway out of its own plane, the code specifies again the above general conditions to be met, plus:

1. the type of loading (static)

2. the grades of steel (yield plateau, $p_{ult}/p_y \geq 1.2$, elongation > 15%)

3. the geometrical properties (symmetry of cross section with respect to axis perpendicular to that of hinge rotation)

4. the restraints (location with respect to plastic hinges)

5. the stiffness at hinge locations and

6. the fabrication restrictions (holes et.c.).

Referring to the **buckling resistance**, the code:

a) for the non-sway frame members again goes back to section 8.3.1 and

b) for the sway members suggests either a full elastic-plastic analysis, or a simplified method to be used, where

(1) in the sway mode mechanism, the plastic hinges occur in all the beams and the base of each column, but no other plastic hinges form in the column

(2) the other lengths of the columns remain elastic

(3) for all combinations of loading there should be an equilibrium with the applied loads under which all members remain elastic

(4) the restrictions for the clad frames are satisfied and finally

(5) for unclad frames the following relationship should be used

(a) $\lambda_{cr} \geq 5.75$

(b) when $5.75 \leq \lambda_{cr} < 20$: $\lambda_p \geq \dfrac{0.95\,\lambda_{cr}}{(\lambda_{cr} - 1)}$

(c) when $\lambda_{cr} \geq 20$: $\lambda_p \geq 1$

where λ_p is the ratio by which the factored loads would have to be increased to cause plastic collapse of the actual frame.

In conclusion, while an extensive study has been made to cover every possible case in the design of frames, nowhere in the code is the non linear response generated by axial loading of an imperfect column of the frame addressed.

For buckling into a single mode (either sway or non-sway) the imperfection effects of the linear moments are only partially treated as shown in cases i and ii of section 8.3.1. Where two or more potential buckling modes occur at the same or similar load levels there is no attempt to look at the potentially serious interactions

that can occur.

8.5 Simplified Equation for Ultimate Load

Consider the general expression for bending moments in terms of modal imperfections, characteristic functions and linear moments given in Eq. (5.18). The maximum stress of the column, occurring at the extreme fibres on the concave side of the cross section that bears the maximum bending moment, in the case of having a contribution from the lowest two critical modes, namely, the sway mode associated with antisymmetric configuration and the non-sway associated with symmetric mode, is given by equation (5.21), as

$$\sigma_m = \frac{P}{A} + \frac{EI}{Z}\left[\frac{P}{P_{cs}-P}\xi_s\phi_s''(x) + \frac{P}{P_{cn}-P}\xi_n\phi_n''(x)\right] + \frac{m^p(x)}{Z} + \frac{m^n(x)}{Z} \qquad \textbf{(8.20)}$$

Assuming the column to have failed when $\sigma_m = \sigma_y$, in the absence of linear moments, a lower bound to the collapse load, P_b, is given by the solution of the equation

$$P_y = P_b + \frac{P_b P_{cs}}{P_{cs}-P_b}\cdot\rho_s\alpha + \frac{P_b P_{cn}}{P_{cn}-P_b}\cdot\rho_n\beta \qquad \textbf{(8.21)}$$

where : P_{cs}, P_{cn} are respectively the 1st and 2nd elastic critical loads,

ρ_s, ρ_n are the corresponding dimensionless imperfection parameters and

α, β are curvature parameters as described in section 5.7.

This equation expresses the buckling load of the column in the presence of sway and non-sway imperfections, in terms of the first two critical loads. In order to avoid having to relate this buckling strength to the four independent parameters involved (two imperfections and two critical loads), and to make the equation more

suitable for design, we need to make some further sensible simplifying assumptions.

The main assumption which can be made here is the fact that the first two critical loads can approach each other in such a degree that they can almost be considered as identical. This assumption is not far from logic, since, otherwise, due to the lack of interaction between the first two critical modes, the beam-column could be treated as presenting a single degree of freedom, which is not the purpose of the present research. This interaction, occurring for close values of the first two critical loads, becomes stronger as P_{cs} approaches P_{cn}; and since this research is not concerned about a weak interaction between the first two critical modes, it is not only logical but becomes an important simplifying assumption to consider an equalisation of the first two magnitudes of critical loads. If P_c is the common value of these loads, substituting P_{cs} and P_{cn} for P_c, the previous equation can take the non-dimensionalised form

$$1 = p + \frac{pp_c}{p_c - p}\left(\rho_s a + \rho_n \beta\right) \tag{8.22}$$

where: $p = \dfrac{P_b}{P_y}$ is the dimensionless buckling load characterising first material failure and

$p_c = \dfrac{P_c}{P_y}$ is the ratio of the compound critical load to the squash load, corresponding to a certain frame geometry of the beam-column.

For a certain value of p_c, calculated for a given topology of the beam-column frame geometry through either an eigenvalue analysis or a conventional method, Eq. (8.22) enables the failure surface envelop to be calculated and drawn in a non-dimensionalised form as a function of the sway and non-sway imperfections.

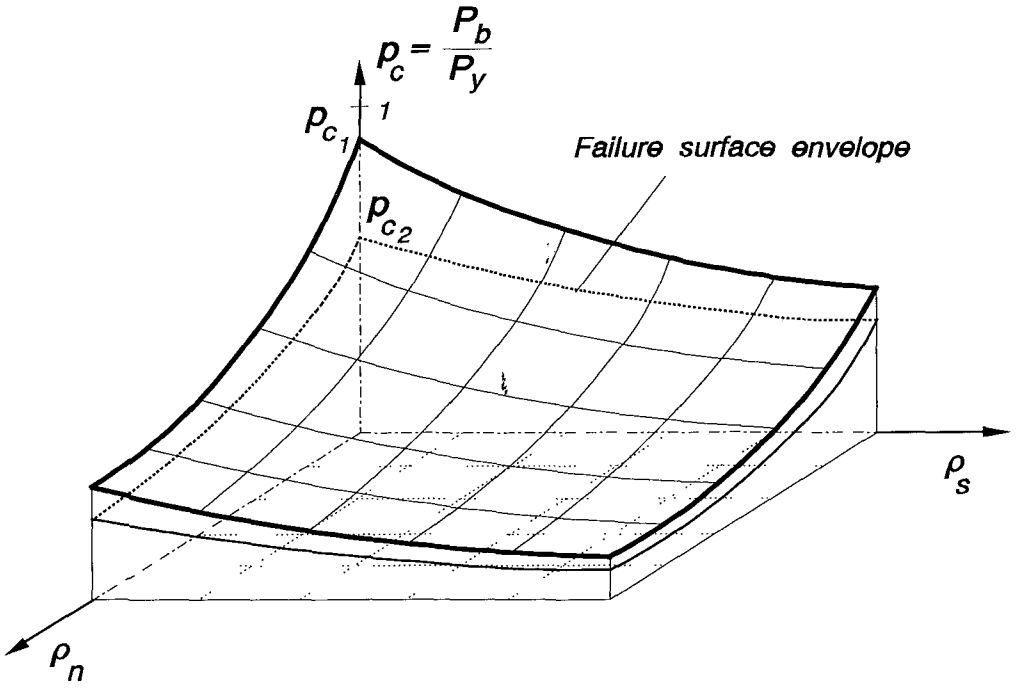

Figure 8-5

Fig. 8-5 shows two notional failure surface envelopes corresponding to values p_{c_1} and p_{c_2}.

A new subroutine was incorporated in the main computer program to calculate the value of x from Eq. (8.22), using the Newton-Raphson iteration technique. Depending on the difference between the first two critical loads, resulting from the geometric form of the frame, the results obtained from this equation for the first yield load were *as closer to excellent as the values of* $\boldsymbol{P}_{c_1}$ *and* $\boldsymbol{P}_{c_2}$ *were approaching each other*, being very useful for a simplified design procedure.

For this purpose a systematic series of numerical experiments has been carried out for different values of lengths and cross-section-sizes to identify different frame-geometries, where the first two critical loads were almost identical. These cases were then allocated according to their first critical load over the squash load

Table 8_1 FRAME GEOMETRIES

for which the first two critical loads are almost identical

Case	$L_1 = L_3$ mm	L_2 mm	b_1 mm	$b_2 = b_3$ mm	P_{cS}/P_{cN}	P_{cS} kN	P_{c_1}/P_y
1	470	330	5	6	1.000	3.673	0.163
2	240	400	3	4	1.002	2.921	0.211
3	280	350	4	5	1.001	5.073	0.278
4	340	314	5	6	1.001	6.753	0.300
5	330	314	5	6	0.999	7.118	0.317
6	250	340	4	5	0.998	6.263	0.343
7	170	200	3	3	0.999	5.512	0.398
8	230	330	4	5	1.001	7.361	0.403
9	170	350	3	4	0.995	5.614	0.405
10	220	325	4	5	1.001	8.019	0.439
11	160	200	3	3	0.999	6.146	0.444
12	260	300	5	6	0.999	11.129	0.495
13	150	330	3	4	0.998	7.183	0.519
14	200	314	4	5	1.004	9.647	0.526
15	170	300	4	5	0.999	13.050	0.715
16	210	286	5	6	1.000	16.619	0.739
17	150	286	4	5	1.001	16.650	0.911
18	110	286	3	4	0.997	13.197	0.953
19	125	150	5	4	0.980	39.10	1.740
20	68	90	3	3	0.994	43.04	3.100

ratio, P_{c_1}/P_y, where a wide range of random values was covered. Table 8_1 contains some basic details of these geometries along with their P_{c_1}/P_y ratios.

For design reasons, for every case of the above geometries, a chart like those of Fig. 8-8 onwards was produced, to relate the first yield capacity of the corresponding beam-column in the presence of both sway and non-sway imperfections. For this reason the main program was specially modified to organize the iterative technique dealing with imperfections, which eventually were given in a pure-number incremental procedure. According to this procedure, the beam-column imperfection parameter, expressed in Eq. (5.23) as $\rho = \frac{\xi A}{Z}$, was bound to values no greater than

$$\rho_{max} = \frac{1}{100} \cdot \frac{y_{max}}{r} \cdot \frac{L_1}{r} \quad , \tag{8.23}$$

since the total equivalent imperfection parameter ξ, for serviceability requirements, was taken as limited to less than $L_1/100$. The incremental value for ρ, coming from this equation, where y_{max} is the distance of the extreme fibre from the centre of bending of the cross section and r the radius of gyration, is

$$\delta\rho = \frac{1}{1000} \cdot \frac{y_{max}}{r} \cdot \frac{L_1}{r} \tag{8.24}$$

A chart presentation for the various values of P_{c_1}/P_y is given in the end of this section.

Taking into account the discussion in section 5.9, referring to the effect of the buckling mode interaction on the failure at different locations of the beam-column, two imperfection sensitivity failure surfaces have been schematically drawn in Fig. 8-6, corresponding to the ends and the middle of the column. This drawing

has been based on the fact that the sway imperfections do not actually affect failure at mid span; their effect is mainly limited at the ends of the column. The opposite applies with the non-sway imperfections, which influence the yielding failure mainly at the middle of the column.

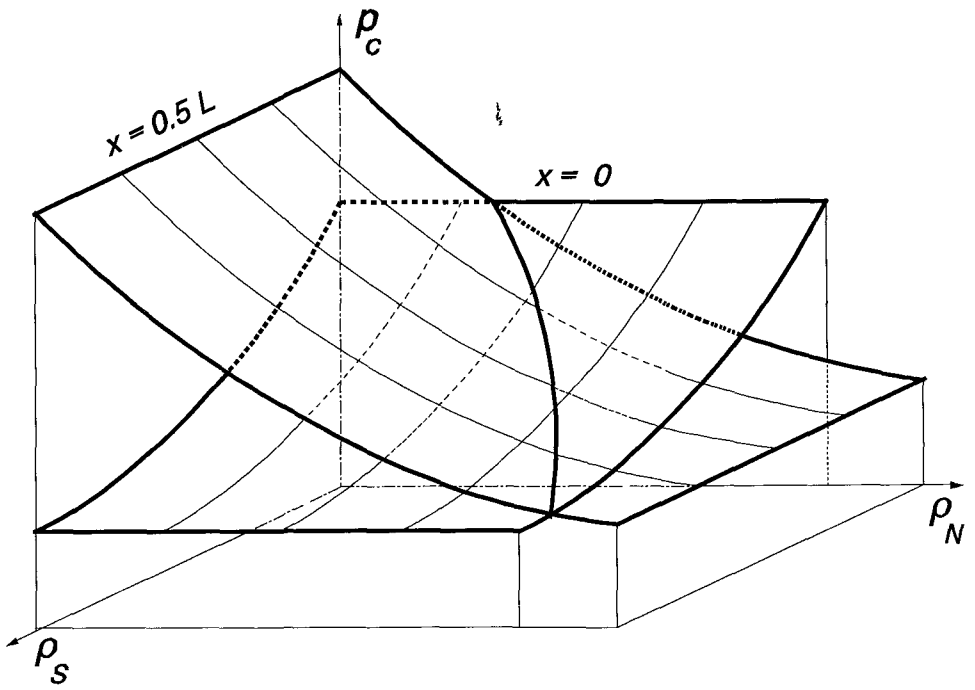

Figure 8-6

A simplified design interaction formula for a beam-column, having a fairly reasonable conservative nature could be

$$\frac{P_b}{P_f} = \frac{P_{bS}}{P_f} \times \frac{P_{bN}}{P_f} \tag{8.25}$$

where: P_b is the buckling load at first yield in the presence of both imperfections

P_f is the failure load corresponding to the lesser of the first critical load (instability failure), or the squash load (material failure)

P_{bS} and P_{bN} are respectively the buckling loads in the presence of only

sway or non-sway imperfections. These loads have to be calculated for the above *two different locations of failure* (ends, mid span).

For this reason the basic software for the eigenvalue problem was modified to provide both P_{bS} and P_{bN} in the cases when failure occurred either at the **ends** (regular for P_{bS}, hypothetical for P_{bN}), or in the **middle** of the column (hypothetical for P_{bS}, normal for P_{bN}), choosing each time the lesser of the two products.

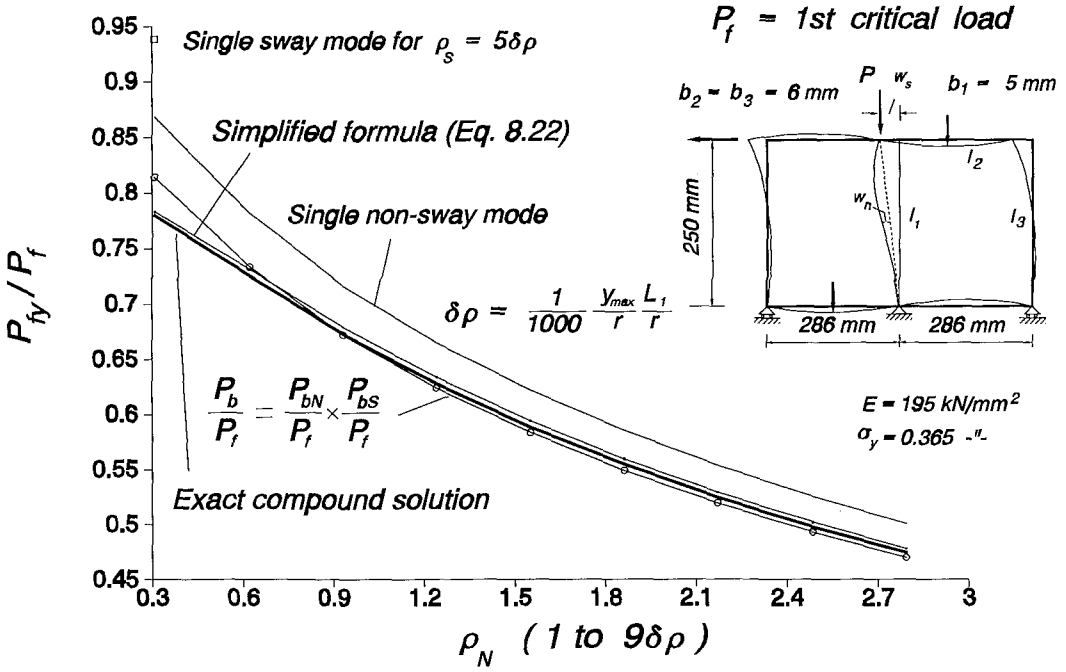

Figure 8-7

For reasons of comparison, Fig. 8-7 depicts the calculated buckling strength of a beam-column, presenting a certain level of sway imperfections and a range of non-sway imperfections for a certain frame-geometry (stiffness). The performed calculations comprised the single buckling mode strength (sway and non-sway) in the absence of non-sway and sway imperfections, the exact numerical method (computer program) and the simplified design formula of Eq. (8.25). In this figure it is clear that:

a) for a certain level of sway imperfections the single sway buckling strength keeps constant values for $\rho_N = 0$, whilst the single non-sway buckling strength decreases with an increase in ρ_N.

b) due to the close values between the first two critical loads, ($P_{cS}/P_{cN} = 0.98$), shown in the following list of eigenvalues and eigenvectors, the results coming from the simplified formula of Eq. (8.22) seem to be almost throughout identical with those obtained from the exact solution through the software.

c) the simplified formula of Eq. (8.25), which holds for *any* P_{cS}/P_{cN} ratio, provides results, that, keeping a smooth conservative character almost throughout, are close to those obtained theoretically. They have a non-conservative character only for small ρ_N.

M E M B E R P R O P E R T I E S

MEM	L	b	d	A	I	Zel	Zpl	Y.str
1	250.0	5.0	13.0	62.44	125.70	50.28	81.45	0.360
2	286.0	6.0	13.0	73.44	209.00	69.67	117.71	0.360
3	250.0	6.0	13.0	73.44	209.00	69.67	117.71	0.360

	Rot.Sym.Non-sway	Rot.Antisym.Sway	Transl.Sway
Stiffness of frame :	1436.42 kN*mm/rad	1769.23 kN*mm/rad	44.445 N/mm.

E I G E N V A L U E S & E I G E N V E C T O R S

Solut	kL	Pc	C1	C2	delta	theta_A	Mode-Case
1	5.558	12.1152	1.00	-0.379	0.000	0.008	Non-Sway
2	5.613	12.3556	1.00	2.871	-19.860	-0.007	* Sway

For this frame geometry the yield load is depicted in Fig. 8-8, through the exact solution, the simplified formula of Eq. (8.22) and the corresponding of Eq.

(8.25), where, two values of sway imperfections are combined with a range of non-sway imperfections.

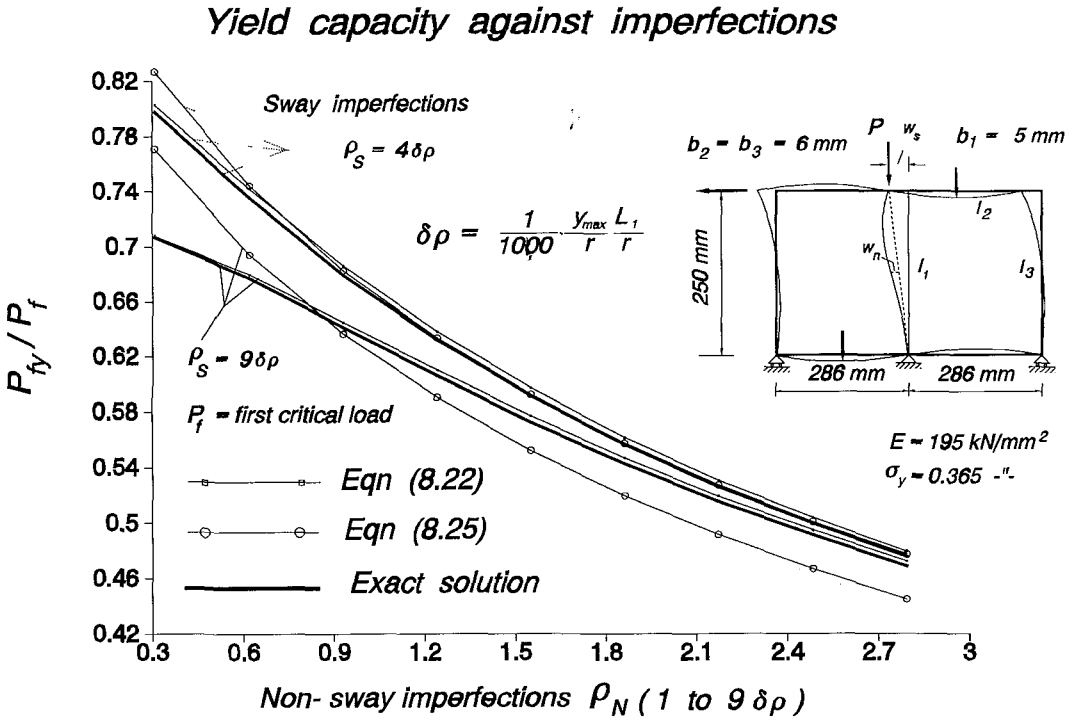

Figure 8-8

The yield capacity of frame geometries where the ratio P_{cS}/P_{cN} is different from unity is depicted in Figs. 8-9 and 8-10. Compared with the exact solution, formula of Eq. (8.22) keeps throughout a conservative character up to 5%, while Eq. (8.25) does not seem to exhibit the conservativeness that had for $P_{cS}/P_{cN}=1$.

In conclusion, depending on the P_{cS}/P_{cN} ratio, a use of Eq. (8.22) might give from accurate to, say, 10% conservative results whilst Eq. (8.25) may provide conservative to non-conservative results.

The problem, therefore, which a designer might face in predicting the first yield capacity for a given frame geometry, is mainly confined in the calculation of the first two critical loads, if a single buckling mode is considered in the frame. This procedure is briefly outlined in the next section according to BS 5950 codes.

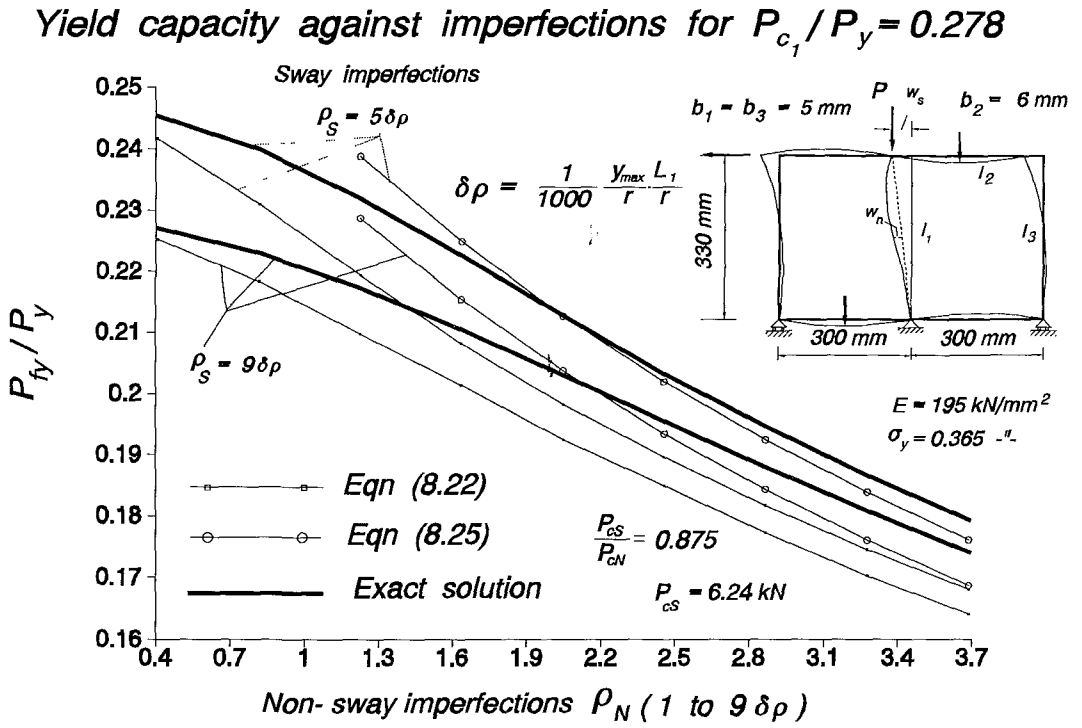

Figure 8-9

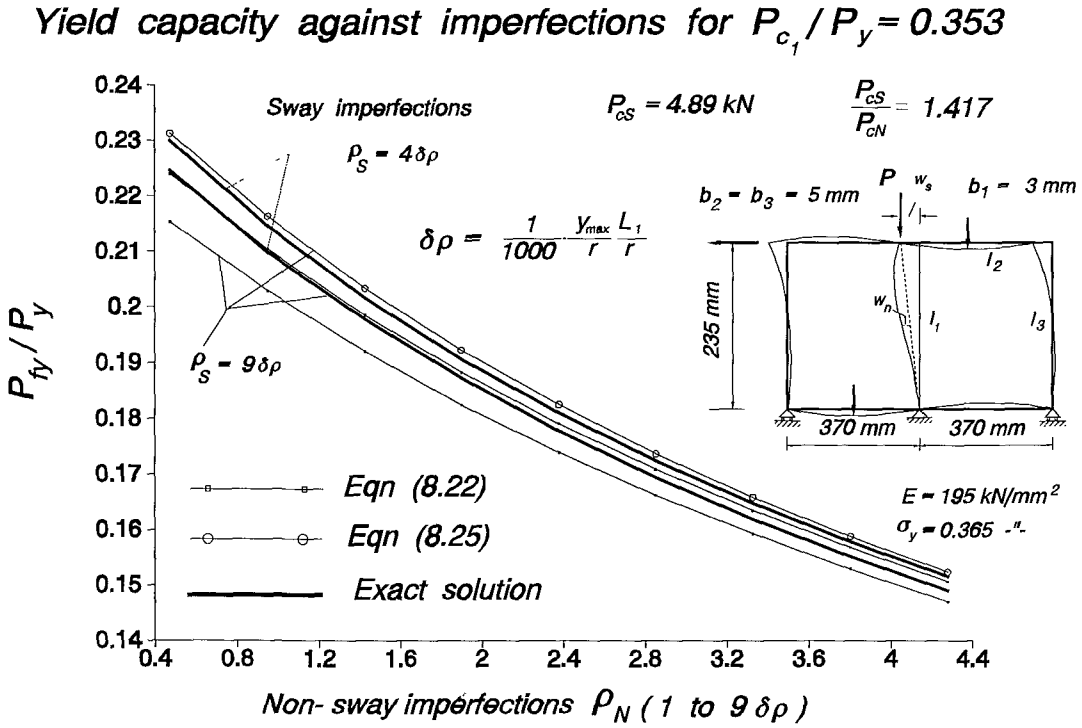

Figure 8-10

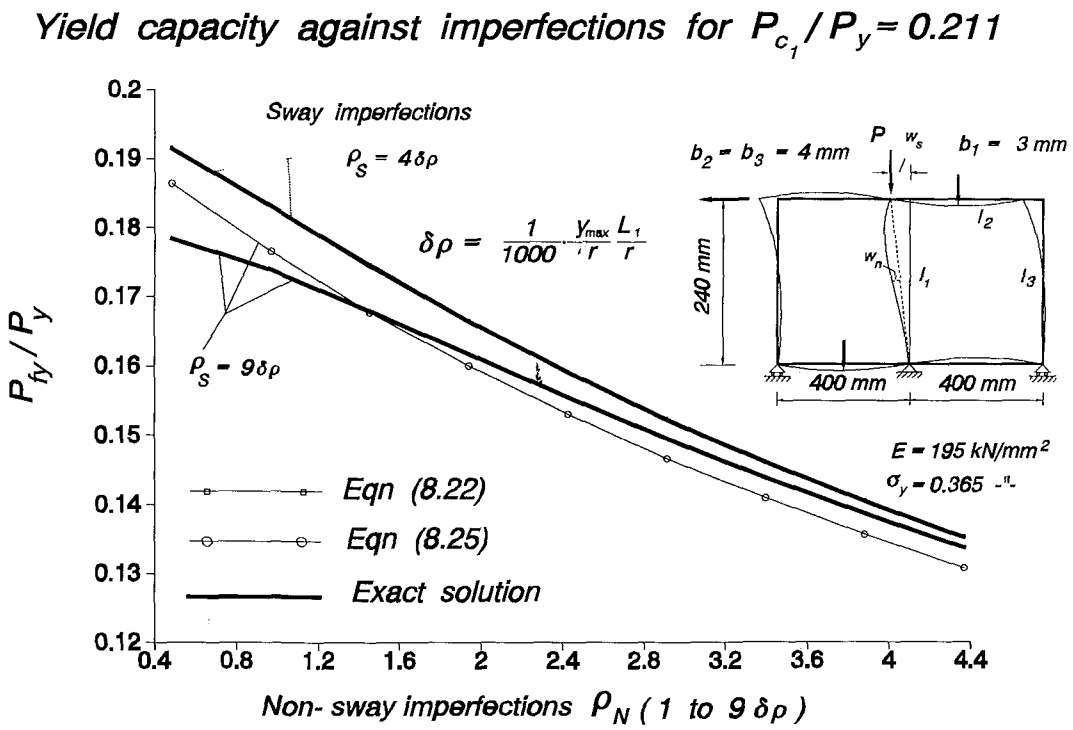

Figure 8-11

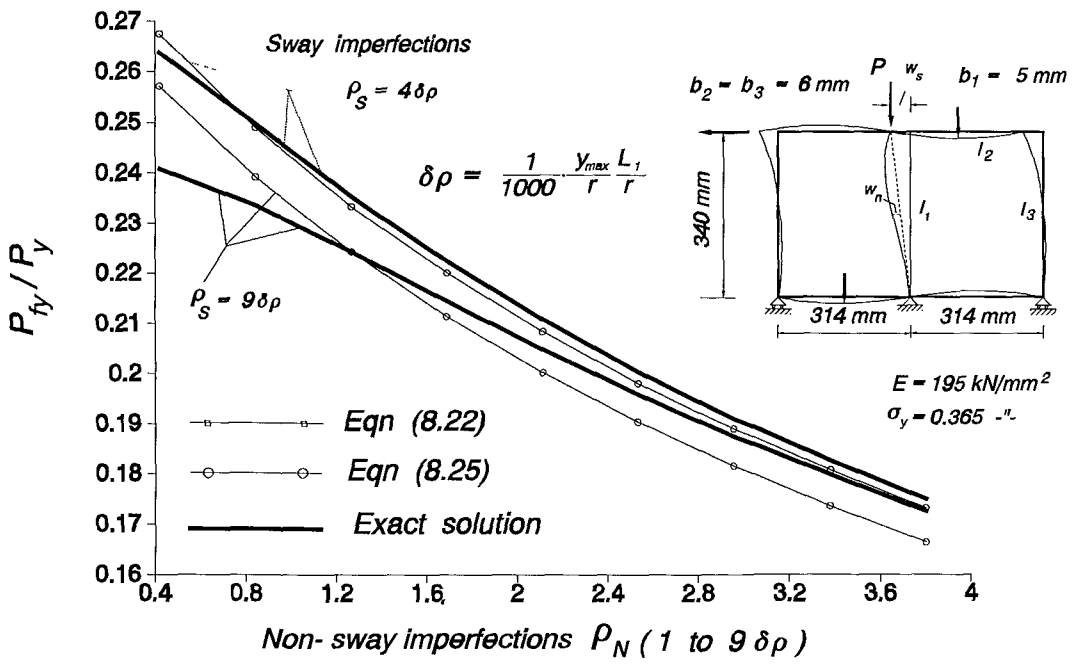

Figure 8-12

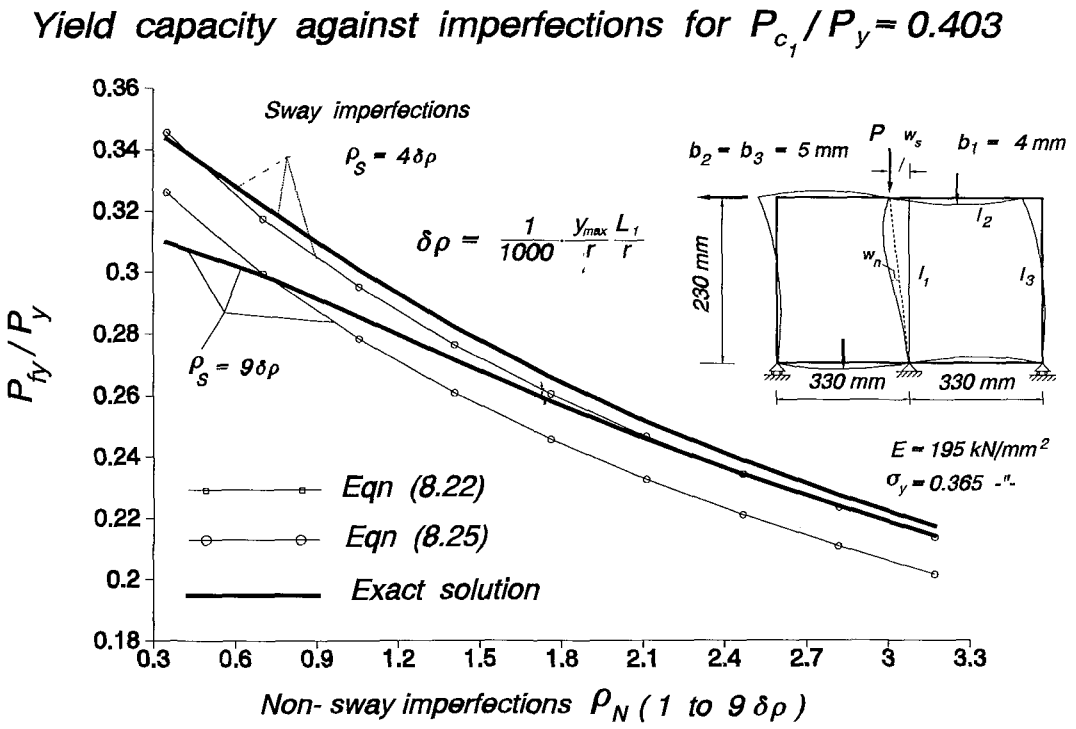

Figure 8-13

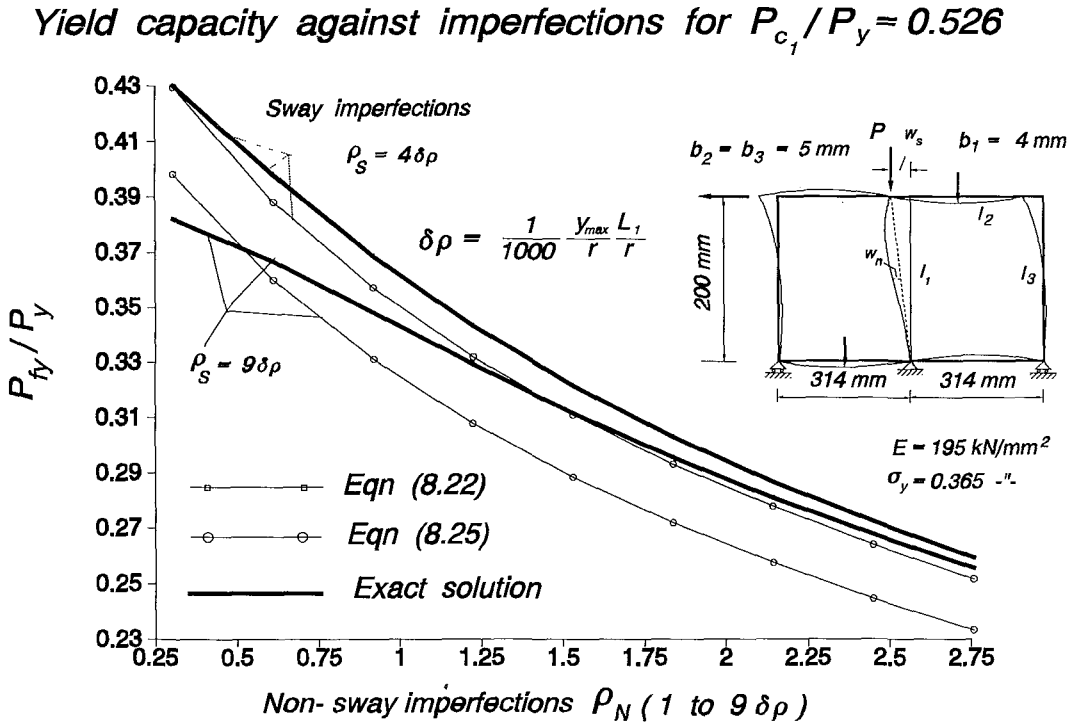

Figure 8-14

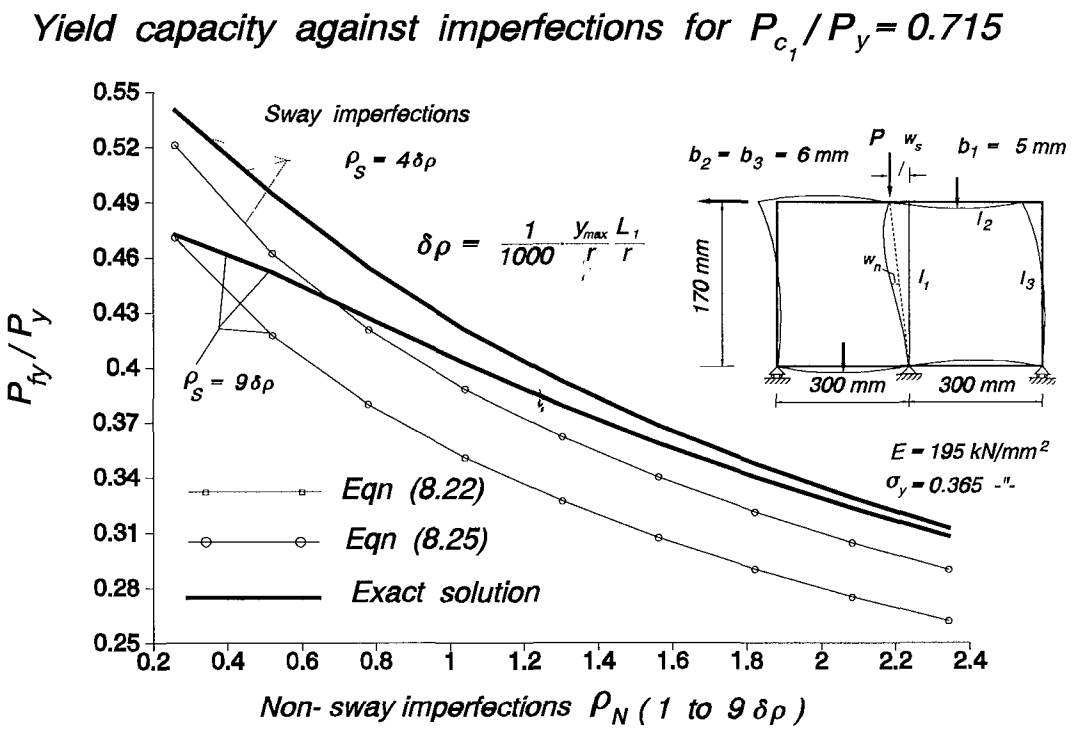

Figure 8-15

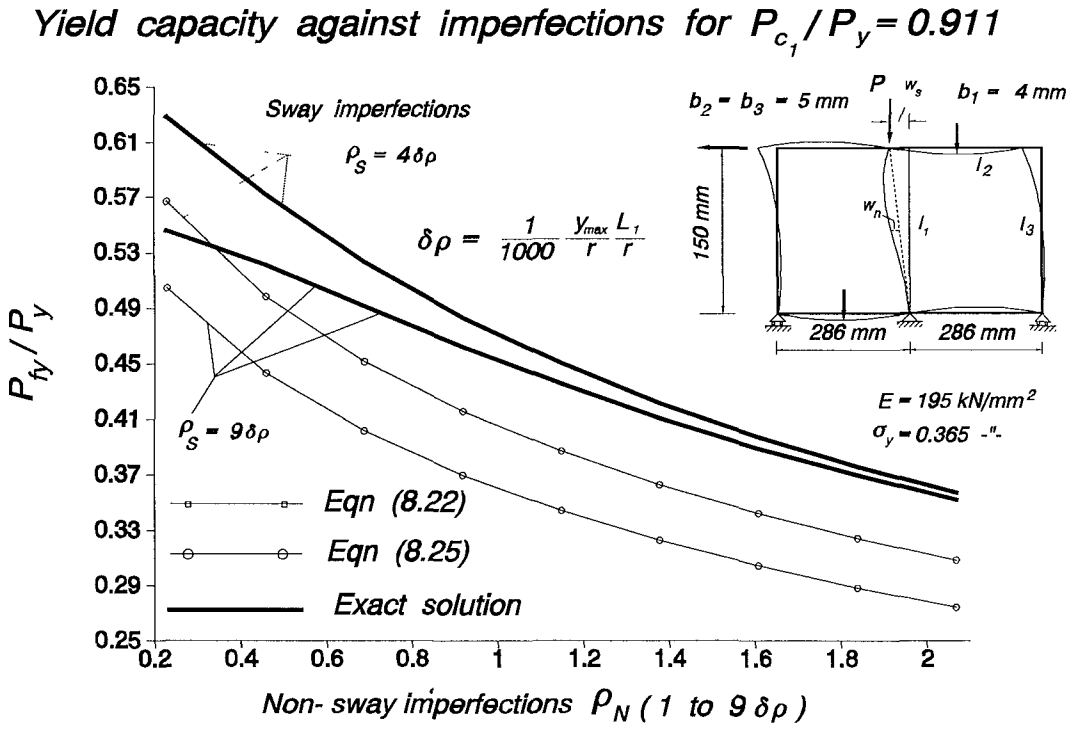

Figure 8-16

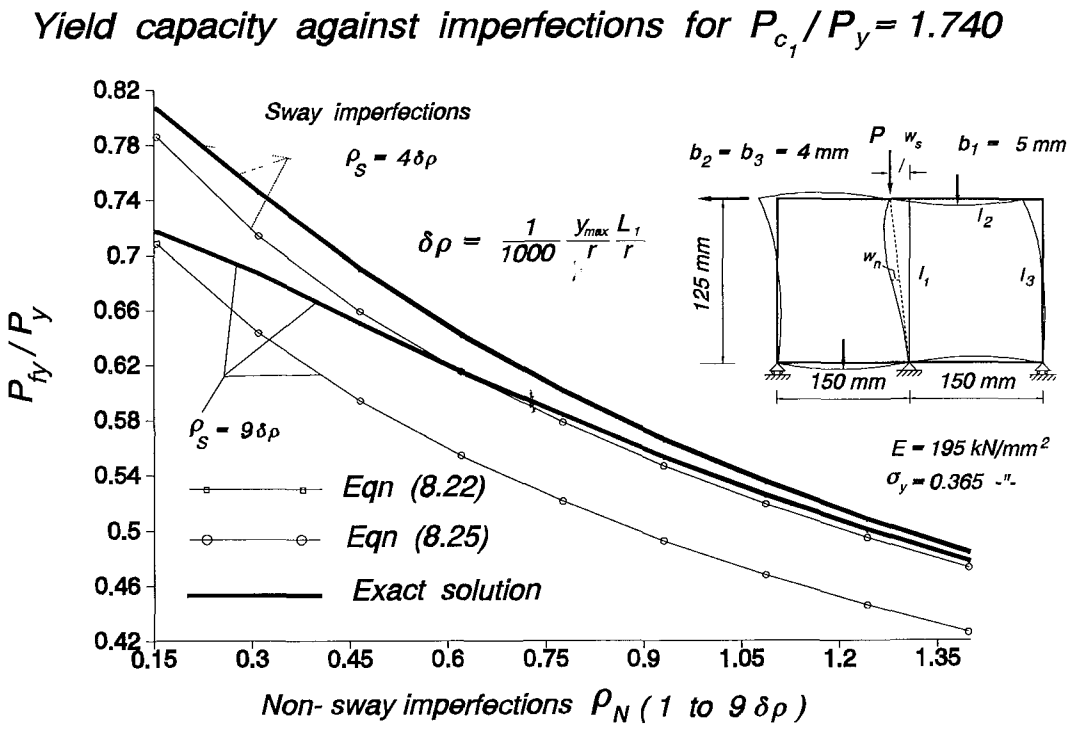

Figure 8-17

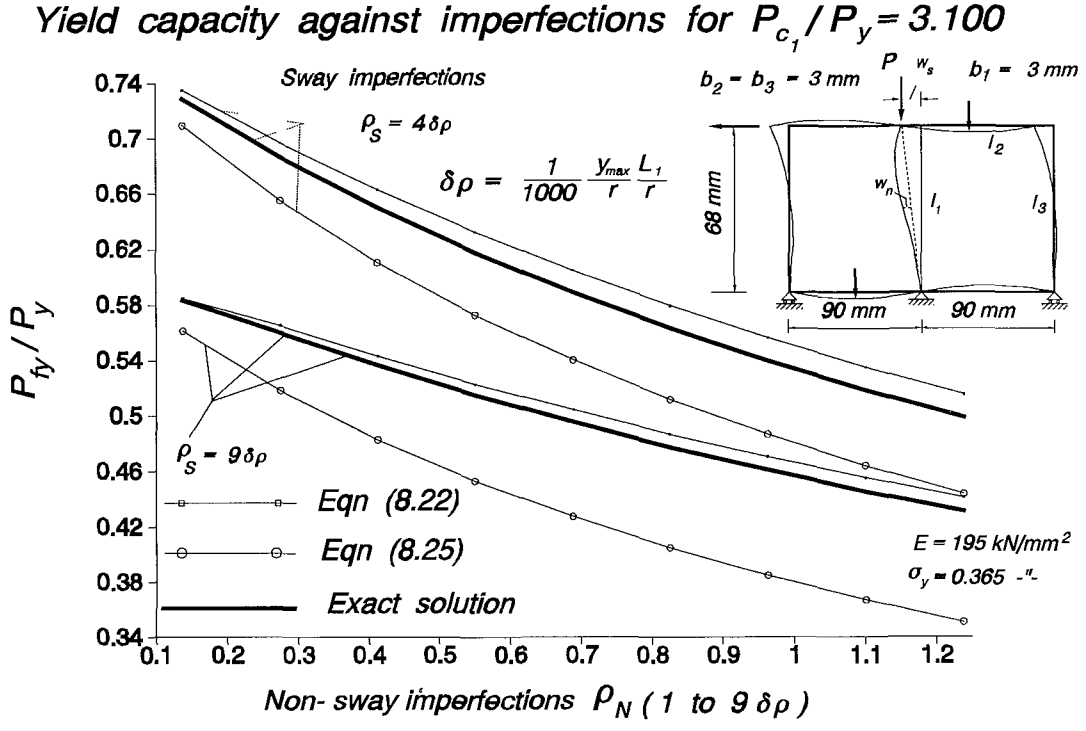

Figure 8-18

For each mode, an expression of α and β curvature parameters with respect to the effective length of the column, would of course lead to a calculation of a notional imperfection parameter, ρ^*, which in turn substitutes the content of the parenthesis of Eq. (8.22). This imperfection parameter, involving imperfections of both modes, would result in a single-mode-buckling-load-graph, like the one of Fig. 8-19, which may substitute every graph similar to those of Figs. 8-11 to 8-18.

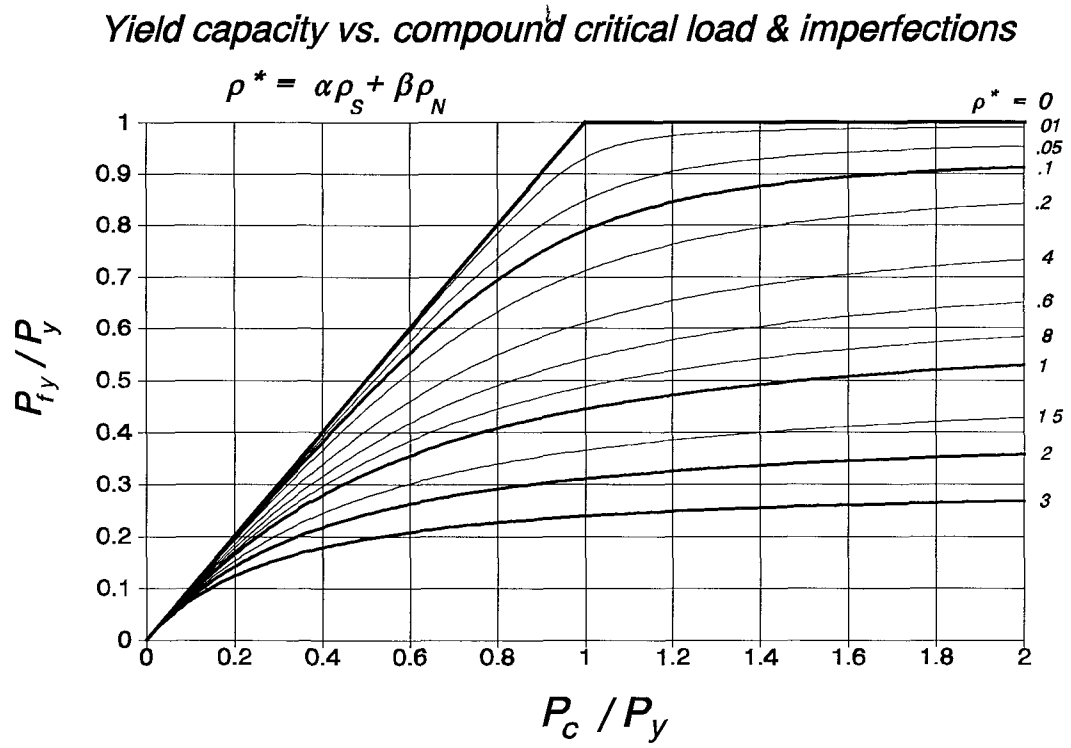

Figure 8-19

Through this procedure, which may well be the subject of a future paper, any combination of sway and/or non-sway imperfections would be replaced by ρ^*, thus reducing the number of independent variables by one. In the graph P_c/P_y is the ratio of the compound critical load to the squash load and P_{fy}/P_y is the dimensionless buckling load characterising first material failure.

8.6 Step by Step Calculation of the Yield Capacity on Beam-columns in a Simplified procedure

It was shown in the previous section, that the load, necessary to cause initiation of yielding in a beam-column which is considered as a part of a frame where sway is uninhibited, in the case of a strong interaction between the first two critical modes, is a function of the level of the first critical load. This load level actually takes into account the geometry of both the beam-column and its surrounding frame, i.e. the overall frame geometry.

For a simplified design procedure used in the office, if a run of the computer program, developed for this research is not feasible, the above buckling strength can be approximately obtained through the following simplified steps:

1) Through a linear analysis, calculate the loading imperfections for both modes, sway and non-sway, and add the most possibility of the geometric tolerances of the given symmetric frame geometry. A program like the one developed for this research could be used to calculate the loading imperfections at this stage.

2) Calculate the ratios of second moment of area to length, (I/L), which correspond to both the column (K_c) and its adjacent beams (K_b) stiffnesses.

3) Obtain the joint restraint coefficients K_1 and K_2 from the formula

$$K_1 = K_2 = \frac{2K_c}{2K_c+3K_b} \quad , \tag{8.26}$$

given in BS 5950.

4) Taking into account the horizontal stiffness of the frame, S_p, as theoretically calculated in Eq. (B.4) of the Appendix B, assess the relative stiffness, K_3, through the code formula

$$K_3 = \frac{h^2 S_p}{80E\sum K_c} \quad but \leq 2 \tag{8.27}$$

where : h is the height of beam-column

S_p is the horizontal force per unit deflection of the frame

E is the modulus of elasticity of steel and

$\sum K_c$ is the sum of the stiffness I/L of the columns in the frame.

The code determines the stiffness S_p using another simplified formula, where a wall panel is considered. Again, a program like the one developed for this research could be used to calculate the values K_1, K_2 and K_3.

5) The above value of K_3 will be used for interpolation between two of the three graphs found in the codes, i.e. in either Figs. 24 and 25 ($K_3 = 0, 1$), or 25 and 26 ($K_3 = 1, 2$). This procedure locates the effective length ratio K, through which, the first critical load of the beam-column is eventually obtained.

Although this value for P_c, compared to the accurate one obtained through the program, is about 10% to 15% conservative, it can give fairly comparable results for the yield strength of the beam-column.

6) Making use of the initially calculated imperfections, interpolate the P_c/P_y ratio, (equivalent to k-value of the preceding Section), between two adjacent charts relating the yield capacity of a beam-column with sway and/or non-sway imperfections, locating thus finally the first yield strength of the beam-column.

In the case where an interaction between the two modes takes place, the code suggests a rather complicated empirical procedure to calculate the design load of the beam-column, using the linear bending moments arising for a practical level of imperfections applied for each mode.

In order to highlight the difference in the results obtained through the procedure developed in this project and the corresponding of the codes, a strength-result-comparison is cited in Appendix H.

Chapter 9

Conclusions and Recommendations

9.1 General Discussion

The present work has been concentrated on the buckling behaviour of plane rigid jointed steel frames for which sidesway is unrestricted and the plane of bending is coincided with the plane of buckling. As a result of the detailed theoretical and experimental study this two-degree-of-freedom buckling response has been clearly elucidated. A simplified design procedure for the prediction of the first yield load carrying capacity of frame columns has been proposed, where the first two critical loads for the sway and non-sway buckling modes are close together.

Observations and conclusions derived in the course of this work are summarized in the following sub-sections.

9.2 Theoretical Field

As discussed in Chapter 2, the majority of the simplified approaches on the beam-columns' buckling behaviour rely upon procedures using empirical data, which are often lacking in crucial information on all the forms of imperfections (geometric or loading), usually present in all real structures. The design procedure therefore do not succeed in making explicit allowance for the effects of imperfections.

In the present work the non-linear elastic response has been related to the linear one for both degrees of freedom. A total equivalent imperfection parameter for each mode (degree of freedom) has been defined, accounting for the effects of both the geometric tolerances adopted and all the loading based imperfections. This then allows complete specification of the non-linear elastic response of the column.

In Chapter 4 a method to calculate the non-linear contributions of the total response is presented, although the contributions from the linear response associated with the first antisymmetric (sway) and symmetric (non-sway) modes, dominate the total non-linear response of the column. A simplified method to calculate these dominant contributions has been developed in Chapter 8. The results of this method, being dependant on the difference between the values of the first two critical loads, were in a very good agreement with those obtained from a complete non-linear elastic analysis for very small difference on the magnitudes of critical loads.

For design purposes the non-linear elastic response is used to define the loads at which plastic failure is initiated. The interaction between elastic stability and material failure has been taken into consideration by the use of the total equivalent imperfection parameter through the Ayrton-Perry method, which was extended to a two-degree-of-freedom formula involving two imperfections and two critical loads as parameters. The superiority of the Ayrton-Perry imperfection approach, providing rational explanations on every aspect of the column's buckling behaviour, is at the end of the analysis obvious.

Regarding the whole mechanism by which failure takes place, current design methodologies, even for single mode buckling, are not clear enough. They put a lot of emphasis on the slenderness of columns, suggesting a linear analysis, whilst they pay less attention to imperfections. Consequently the whole design procedure, leads generally to results which deviate from the actual magnitudes. This deviation, in the cases where the results have a conservative character, entails larger cross sections, consequently more material or less economy; on the contrary non-conservative results are lacking in safety.

9.3 Experimental Field

Past experimental work on a single buckling mode behaviour was to mainly establish the Ayrton-Perry formula based on an imperfection analysis; this work was

combined with an accurate measurement on every kind of imperfections.

Throughout this project an extended experimental programme has been implemented on columns within small sub-frames subject to sidesway. The overall frame geometry was varying, covering a range of different stiffnesses and loading imperfection parameters. For each test two Southwell Plots were drawn, one for each mode. The conclusions derived from this study may in brief be summarised as:

1) In most of Southwell plots, the points, corresponding to the obtained experimental data, were practically laying on a straight line. This validates the theory associated with both modes of Southwell plot.

2) The close agreement (90-110%) on the values of the first two critical loads, obtained through theory and experiments

a) establishes the theoretical developments on the Eigenvalue analysis along with the relative software, associated with the solutions

b) demonstrates the validity of the Southwell plot, making it a useful and powerful tool for a quick, real answer on a critical load

c) justifies and validates the extended form of the Ayrton-Perry formula, rendering it an important implement in the engineering design.

3) The close values between the failure load levels (either for first yield or for full plasticity) predicted by the extended Generalized Ayrton-Perry method, with those obtained experimentally provide an interrelating bond between lab and theory.

Such experimental conclusions, apart from any theoretical justifications, increase in general the confidence in theory.

9.4 General Conclusions

There are many parameters affecting the values of the first two critical loads in a beam column; in the main they can be represented in two forms:

1) the column geometry (length and cross section sizes) and

2) the geometry of the surrounding the column frame, where, different lengths and cross section sizes of the beams and side columns compose different stiffness of the frame, either as rotational (symmetric, antisymmetric) or as translational.

3) The presence of imperfections, even in very small quantities, is an inevitable event for the vast majority of beam-columns; from this point of view it causes a reduction on the axial load necessary to generate failure, either in the form of initiation of yielding or at full plasticity. This reduction, depending on the magnitude of each imperfection parameter, might be crucial, and, under a certain frame geometry where the first two critical loads are close to each other, may lead to an interaction between the first two buckling modes (sway and non-sway), which aggregates even more the whole situation.

4) The ratio of the load necessary to cause failure over the squash load, (P_{cl}/P_y or P_{fy}/P_y), for a nearly perfect column, has a certain value for each frame geometry. This value can be affected by imperfections of both modes. In a three dimensional graph, where the above ratio is related against the different combinations of imperfections, the resulting points can be represented by an imperfection sensitivity failure surface.

5) The location of first plasticity is mainly dependant on the relative magnitude of the sway and non-sway imperfections. A relatively larger sway imperfection tends to create first plasticity at or near the ends of the column, while a relatively larger non-sway imperfection, at or near the middle. The frame stiffness (symmetric - antisymmetric), might play a secondary role in the position of first plastic hinge. In any case, the location of first plasticity actually dictates the kind of failure (sway at/near the ends, non-sway at/near the middle).

Therefore the presence of imperfections has to always be seriously taken into account for any buckling strength estimation.

9.5 Recommendations

The present work has been focused on the buckling behaviour of plane rigid jointed steel-frames where there is a possibility of sidesway. The columns of such structures exhibit two degrees of freedom and the plane of bending is the same as that of buckling. It has been shown that the non-linearities arising from the contribution of the two first two critical modes, sway and non-sway, are the most dominant to the full non-linear response.

In a buckling condition where the beam column, presenting a biaxial buckling response, is a part of a rigid jointed steel frame having the possibility of sidesway in one direction, each column has to be considered as such having three-degrees-of-freedom; in this particular environment if the geometry and the boundary conditions of the frame permit a sway in both directions, then the column has to be considered as such having a four-degree-of-freedom behaviour. In this case the proposed two-degree-of-freedom Generalized Ayrton-Perry formula has to be further extended by modifying the total equivalent imperfection parameter.

This case, being potentially more important since it totally reflects the reality, might then be generalized to cover a multi-degree-of-freedom buckling phenomenon. In any case, for a more than two-degree-of-freedom buckling phenomenon, the boundary conditions arising from each degree-of-freedom have to be taken into account to form the governing differential equation. A research in this direction, apart from any theoretical difficulties arising from the complicated system of equations, might have a further experimental difficulty in building a proper test-rig which will accommodate the appropriate specimen and loading conditions.

Appendix A

Theoretical Aspects and First-stage experimental Graphs

A.1 Plastic Buckling

For intermediate or short columns, the assumption of fully elastic behaviour may not hold. Indeed, under the action of the applied axial load some fibres of the cross section - usually the extreme - will yield before the inception of buckling. Therefore, the only part of the cross section, able in resisting the additional applied force, will be its inner elastic core. Consequently, the Euler load will overestimate the strength of the column.

To account for the effect of inelasticity[55], two main theories were proposed: the *double modulus theory* and the *tangent modulus theory*.

The double modulus theory, was developed by Considère[6] in 1889, and is known as the **reduced modulus theory**. As a result of his experiments, Considère concluded that Euler's formula could hold to slender struts as long as the stresses at failure load of the member were less than the proportional limit σ_p of its material. When this stress is exceeded, in order to predict the strength of columns which buckle inelastically, he proposed the modulus of elasticity in Euler's equation to be substituted by a variable one. Under the assumption that the strut begins to bent only after the point of failure, he reasoned that if the proportional limit had been passed in direct compression, the stresses on the fibres of the concave side of the strut (up to the neutral axis of the cross-section), see Fig. A-1, would increase; so the tangent modulus, E_t, would govern the stress-strain behaviour of the fibres. However, the

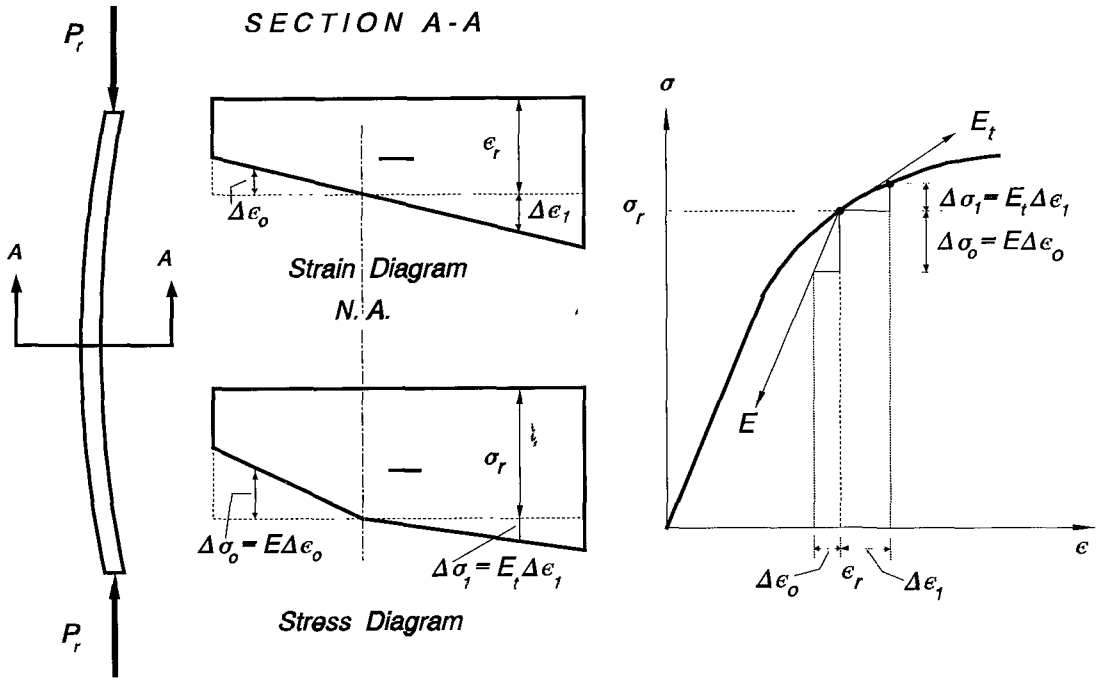

Figure A-1 Double (Reduced) modulus configuration

stresses on the convex side, conversely, would decrease proportionally to the strain; so the elastic modulus, E, would govern the stress-strain behaviour of these fibres. As a result, an effective (reduced) modulus, E_r, with a value somewhere between the above two, could be replaced in the Euler's equation. The critical load obtained on this concept is referred to as the reduced modulus load, given by

$$P_r = \frac{\pi^2 E_r I}{(KL)^2} = \frac{E_r}{E} P_E \qquad \textbf{(A.1)}$$

The reduced modulus is a function of the geometry of the cross section and the tangent modulus. Therefore, it depends on both the shape of the cross section and the material property. The load P_r is always lower than the Euler because the ratio E_r/E in Eq. A.1 is always less than unity. It should be noted that this load, P_r, can only be reached if the column is artificially held in a straight position when the *tangent modulus load* (which follows in discussion), has been exceeded. This is the reason why the reduced modulus load can never be reached even if the slightest

geometrical imperfection is present. No theory was presented to determine the value of E_r.

In the **tangent modulus theory**[7,8], Fig. A-2, the axial load is assumed to

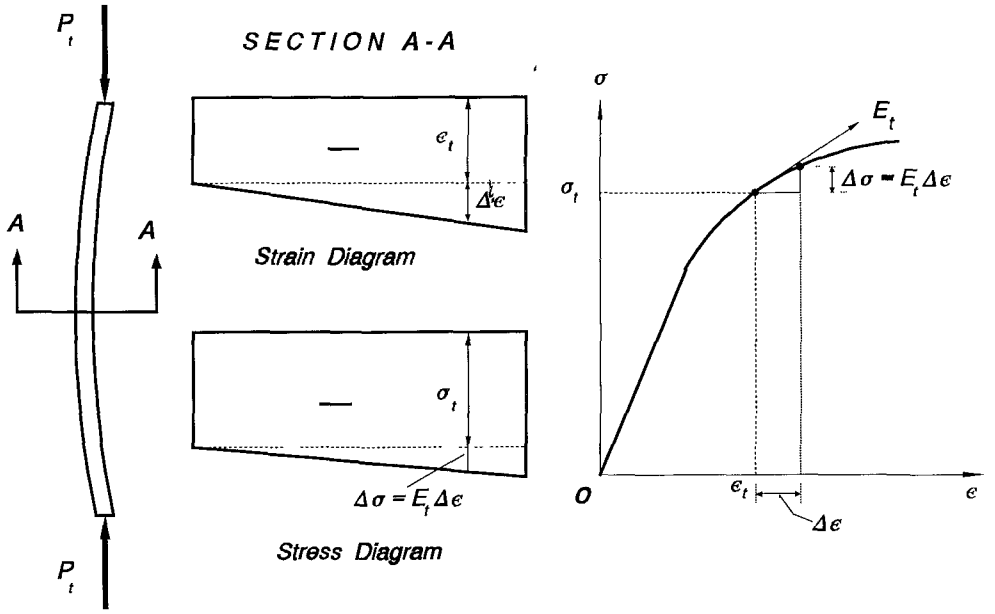

Figure A-2 Tangent modulus configuration

increase during buckling. The increment here is such, that, strain reversal, as in reduced modulus theory, is not occurring. Therefore, the tangent modulus, E_t, governs the stress-strain behaviour of the entire cross section. The critical load obtained, known as the tangent modulus load, is given by

$$P_t = \frac{\pi^2 E_t I}{(KL)^2} = \frac{E_t}{E} P_E \qquad \textbf{(A.2)}$$

The tangent modulus load, P_t, unlike the reduced modulus load, P_r, is independent of the geometry of the cross section, depending only on the material property. The non-linearity of an average stress-strain behaviour for a steel column is due to the presence of residual stresses, which are arise as a result of the manufacturing process. When a short column is carrying an axial force, the fibres that have already residual compressive stresses will yield first. Later will yield the

fibres that have tensile residual stresses. Consequently, yielding process on the cross section will take place gradually. The slope of the stress-strain curve after first

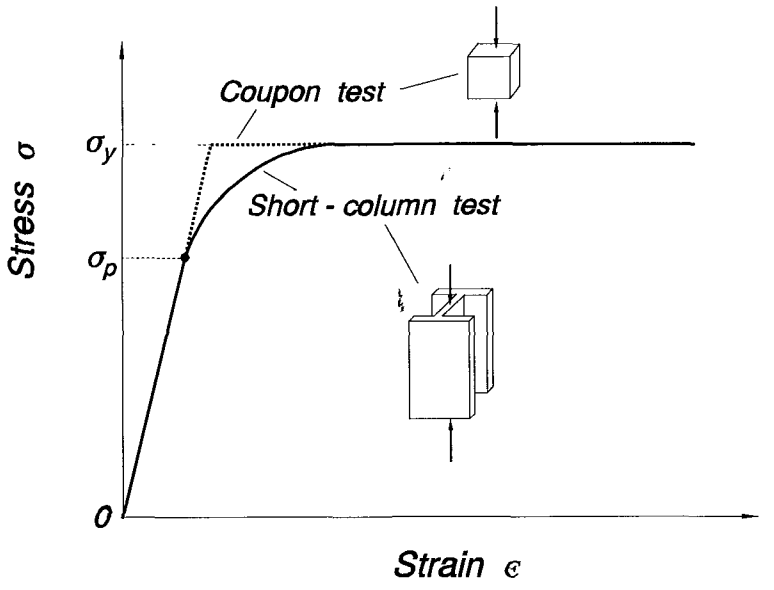

Figure A-3 Stress-strain curve for steel

yielding, Fig. A-3, is the tangent modulus E_t, of the member. Shown is also the stress-strain path of a specimen free of residual stresses, called *coupon*. This path is obviously an elastic-perfectly plastic behaviour.

The load P_t actually marks the point of bifurcation of a perfectly straight inelastic column. It is lower from both the Euler and the reduced modulus load, and, from this point of view, it represents the lowest load at which bifurcation of equilibrium can take place.

A.2 Experimental Figures and Graphs

All but the first three figures are some of the test results obtained from the frame shown in the following figure. Although the material, geometry and dimensions of the frame were kept constant, the loading conditions were varied, giving each time a different relation between deflections at both the top and the mid-hight of the central column against the corresponding load.

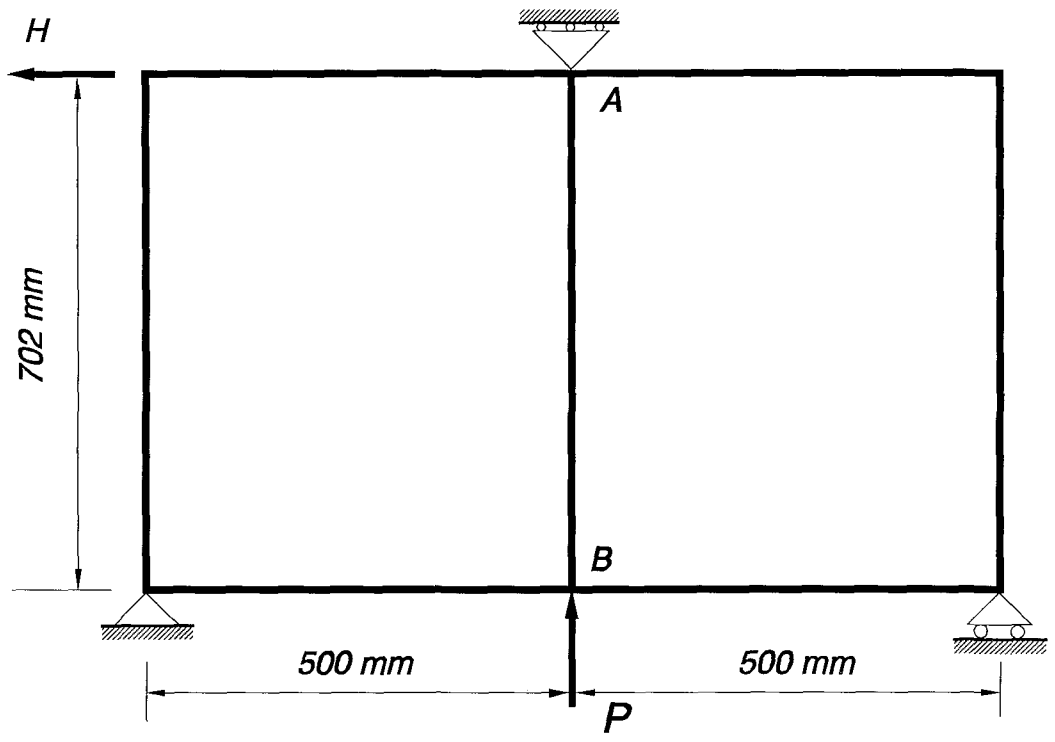

Fig. A.2.1 Geometry and loading pattern of the frame

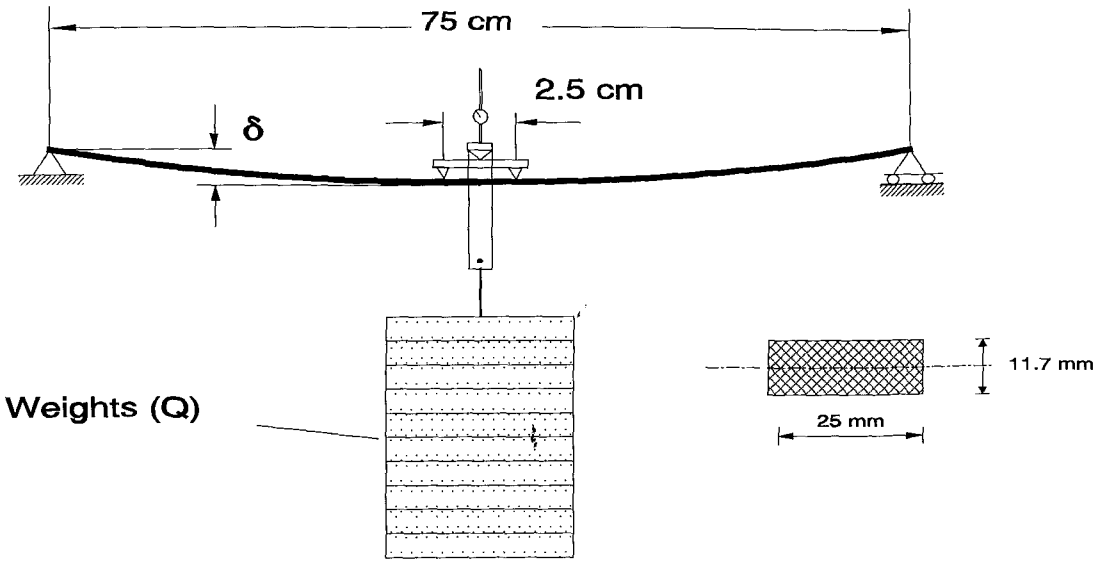

Bending test configuration

A.2.2

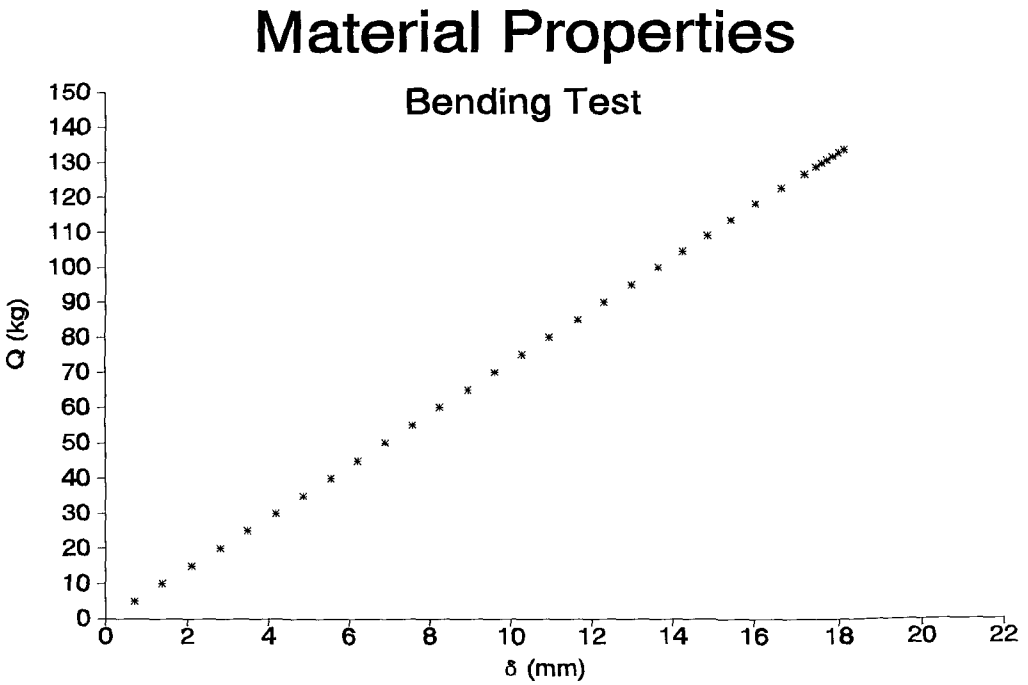

A.2.3

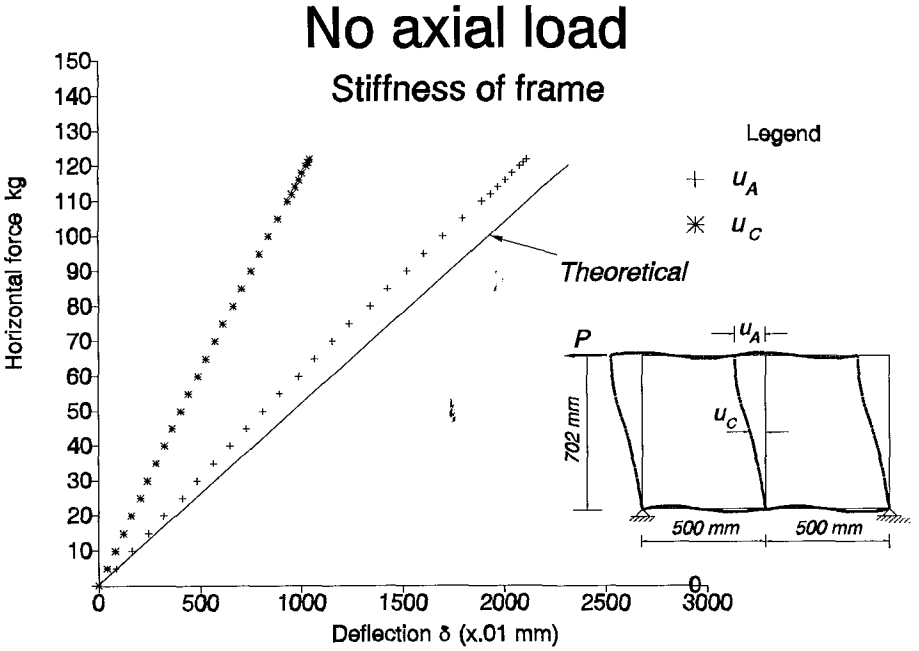
No axial load
Stiffness of frame
Horizontal force kg
150
140
130
120
110
100
90
80
70
60
50
40
30
20
10
0
0
500
1000
1500
2000
2500
3000
Deflection δ (x.01 mm)
Legend
u_A
u_C
Theoretical
P
u_A
u_C
702 mm
500 mm
500 mm

A.2.4

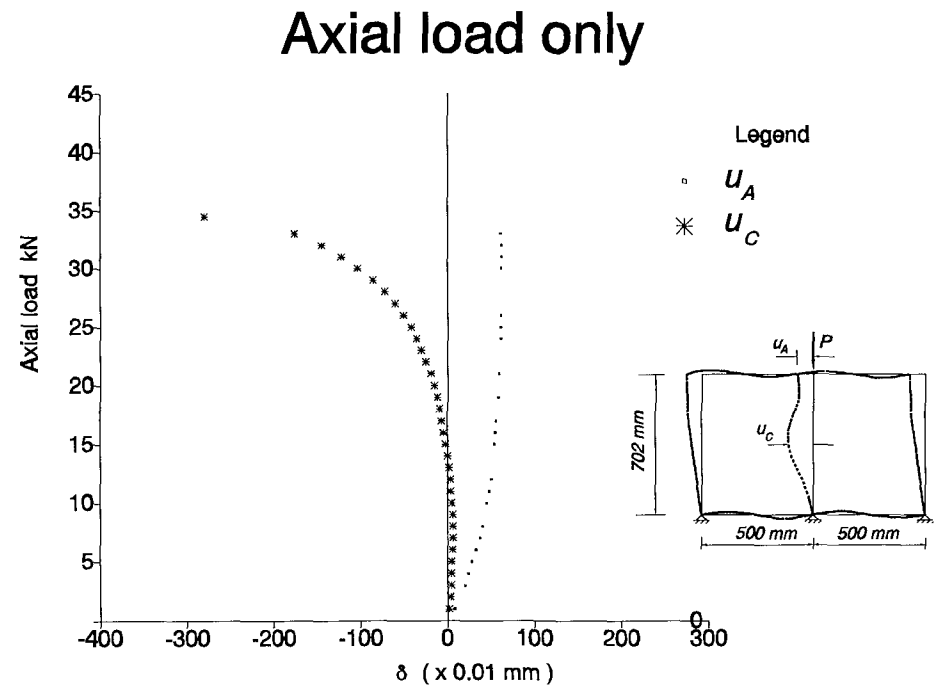
Axial load only
Axial load kN
45
40
35
30
25
20
15
10
5
0
-400
-300
-200
-100
0
100
200
300
δ (x 0.01 mm)
Legend
u_A
u_C
u_A
P
u_C
702 mm
500 mm
500 mm

A.2.5

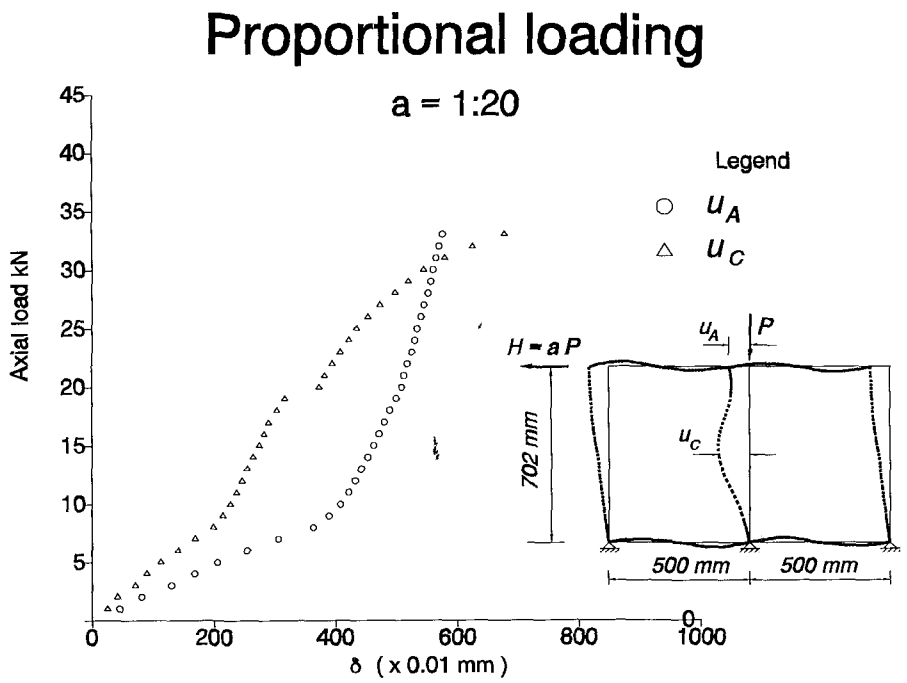
Proportional loading
a = 1:20
Legend
u_A
u_C
Axial load kN
δ (x 0.01 mm)
H = aP
P
u_A
u_C
702 mm
500 mm
500 mm

A.2.6

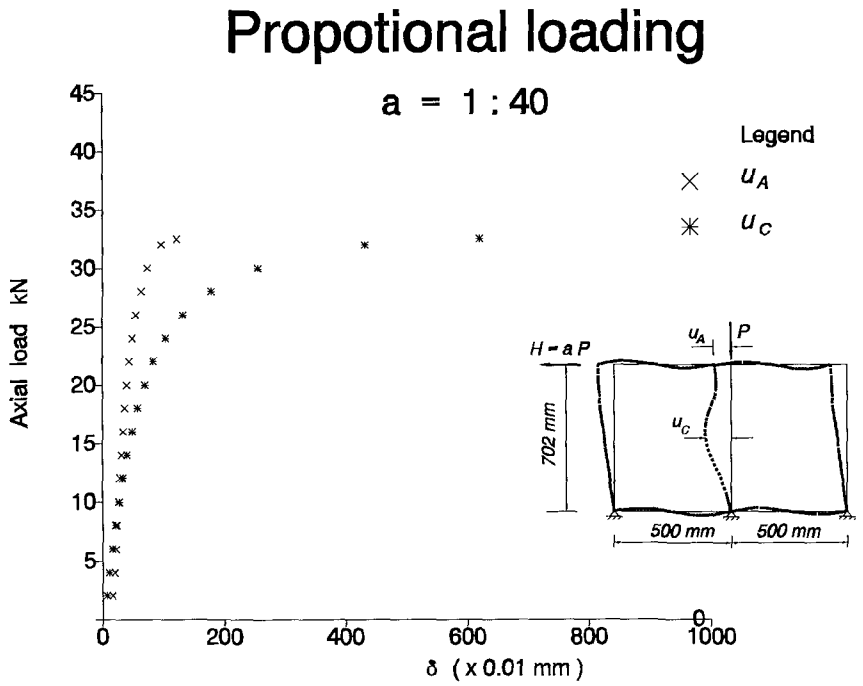
Propotional loading
a = 1 : 40
Legend
u_A
u_C
Axial load kN
δ (x 0.01 mm)
H = aP
P
u_A
u_C
702 mm
500 mm
500 mm

A.2.7

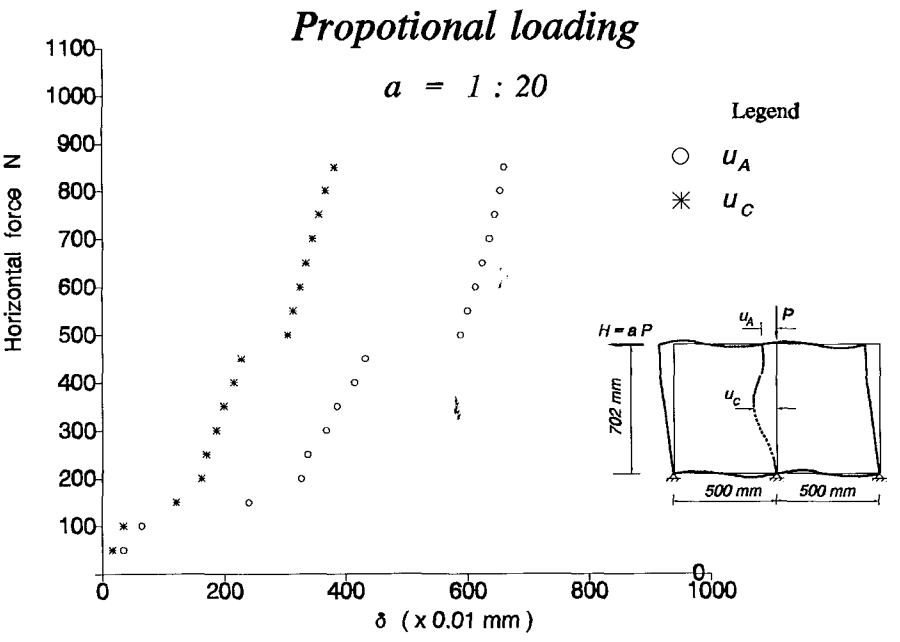
Propotional loading
a = 1 : 20
Legend
u_A
u_C
Horizontal force N
1100
1000
900
800
700
600
500
400
300
200
100
0
0
200
400
600
800
1000
δ (x 0.01 mm)
H = aP
P
u_A
u_C
702 mm
500 mm
500 mm

A.2.8

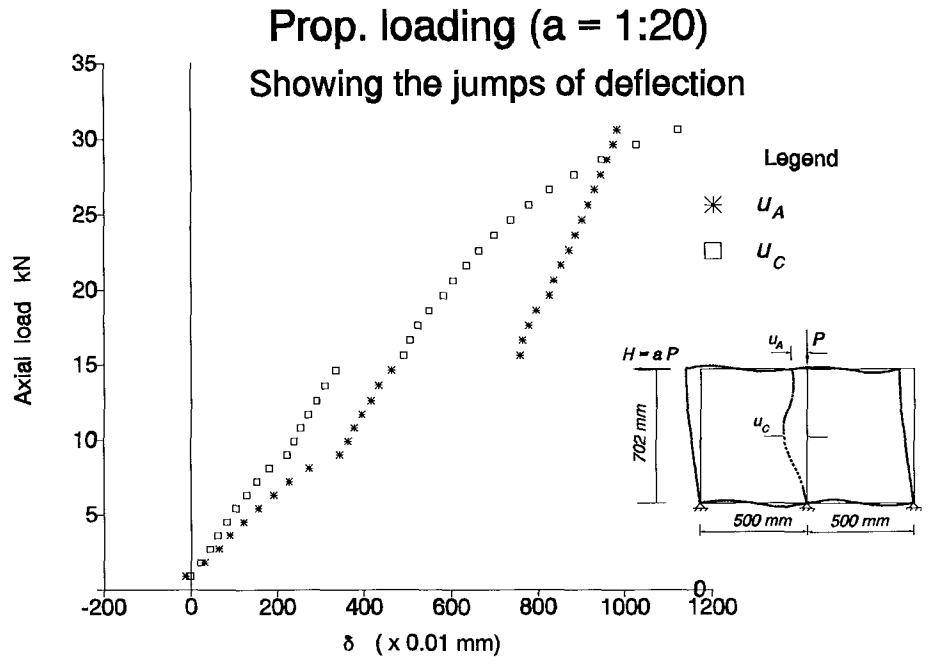
Prop. loading (a = 1:20)
Showing the jumps of deflection
Legend
u_A
u_C
Axial load kN
35
30
25
20
15
10
5
0
-200
0
200
400
600
800
1000
1200
δ (x 0.01 mm)
H = aP
P
u_A
u_C
702 mm
500 mm
500 mm

A.2.9

Appendix B

Theoretical Calculations of Frame-model

B.1 Calculation of Horizontal Displacement of the Frame due to Horizontal Load

Taking advantage of the symmetry of the structure with respect to the A-z axis, along with the asymmetric loading, and the fact that the points A, B and C are thus points of contraflexure, at which $M = 0$, we can make a cut at these points, considering the actual loading for the upper half, taking A, B and C as pin-supports.

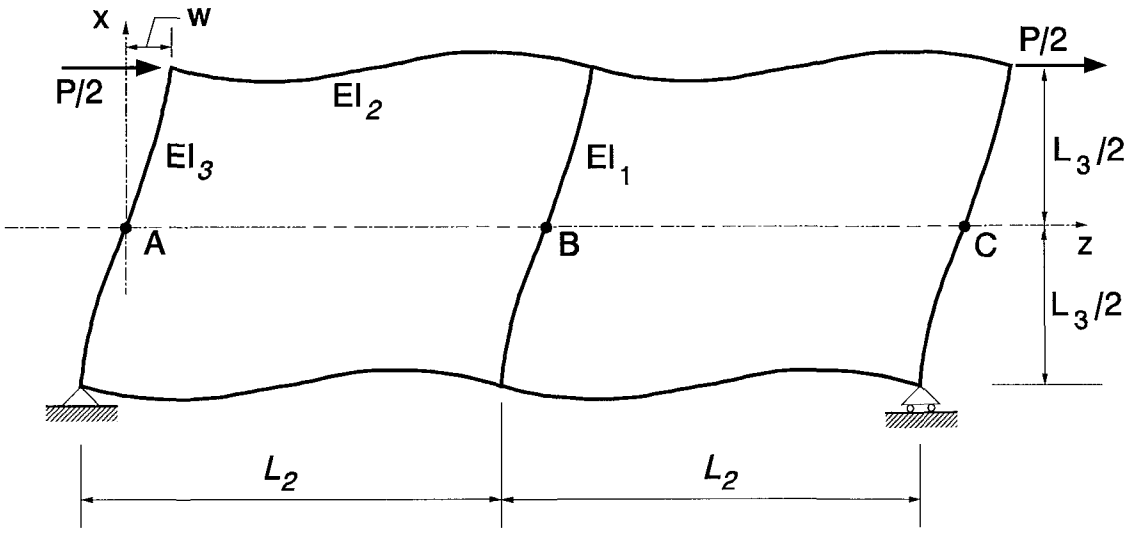

Figure B-1

Due to symmetry of structure and asymmetric loading the vertical reaction at B is zero, while the horizontal reactions at A and C are equal. The vertical

reactions at A and C, forming a couple, are each $\frac{PL}{2L_2}$.

Taking the horizontal reaction, H, at B, as redundant, the horizontal reactions at A and C are thus (P-H)/2.

The resultant diagram of real curvature, (χ), is shown in Fig. B-2. The sign is positive from the side where the inner extreme fibres are in tension.

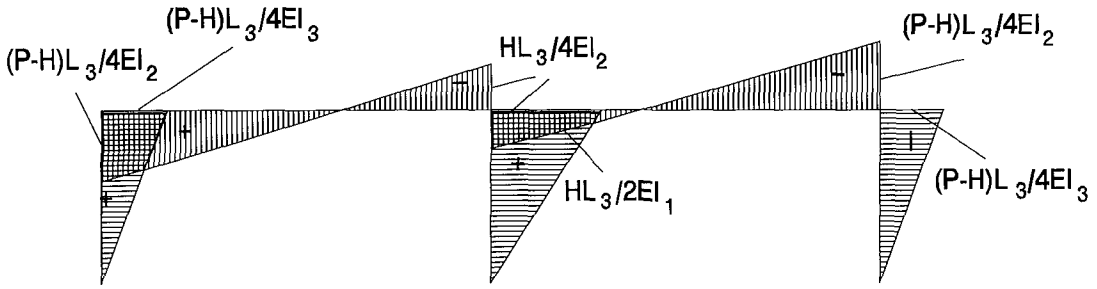

Figure B-2

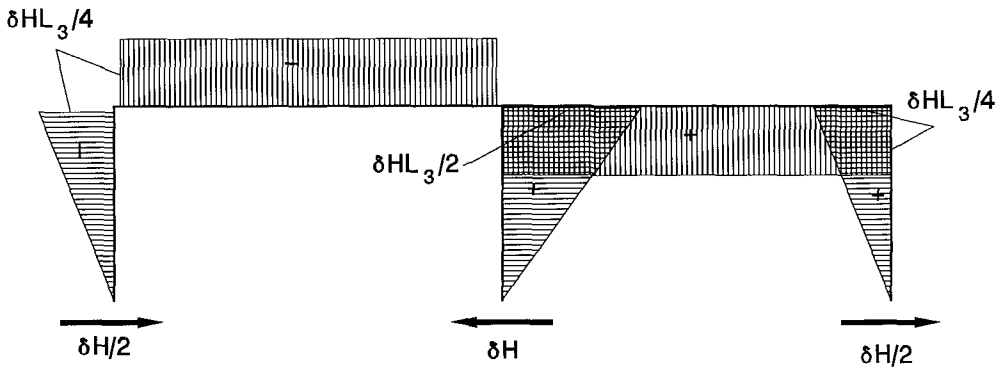

Figure B-3

Now, we can develop a virtual force system to find the redundant H. Indeed, if we put a virtual horizontal force δH at the support B of the structure, make the bending moment diagram which results from the statically admissible reactions at

A and C, Fig. B-3, and combine this diagram with the corresponding (χ) by taking the product integrals for each member, once the displacement at B is zero, we will have:

$$[\textit{Virtual ext. work} = \sum \textit{Virt. force} \times \textit{real displ.} = 0\ ] = [\sum \textit{Virt. internal work}]$$

or $$\sum \delta F_i \times u_i = 0 = \sum \int \chi \cdot \delta m \cdot ds$$

from which we obtain

$$-2\frac{1}{3}\frac{\delta HL_3}{4}\frac{(P-H)L_3}{4EI_3}\frac{L_3}{2}+\frac{1}{3}\frac{\delta HL_3}{2}\frac{HL_3}{2EI_1}\frac{L_3}{2}-\frac{1}{2}\frac{1}{EI_2}\left[\frac{(P-H)L_3}{4}+\left(-\frac{HL_3}{4}\right)\right]$$

$$\cdot\frac{\delta HL_3}{4}L_2+\frac{1}{2}\frac{1}{EI_2}\left[\frac{HL_3}{4}+\left(-\frac{(P-H)L_3}{4}\right)\right]\frac{\delta HL_3}{4}L_2 = 0$$

$$H = P\frac{L_3/2I_3+3L_2/2I_2}{L_3/2I_3+L_3/I_1+3L_2/I_2} \qquad \textbf{(B.1)}$$

For $I_1 = I_2 = I_3 = I$ and $L_2 = L_3$, it results

$$H = P\frac{1+3}{1+2+6} = \frac{4}{9}P\,. \qquad \textbf{(B.2)}$$

Following the same procedure, we develop a **virtual force system to find the horizontal displacement** u. If we put a virtual horizontal force $\delta P\left(=2\frac{\delta P}{2}\right)$ at the joints where the horizontal displacement w is to be calculated, make the bending moment diagram (δm_2), as shown in Fig. B-4, which results from the statically admissible reactions at A and C, (for convenience we take zero horizontal reaction at B), and combine this diagram with the corresponding one of real curvature, (χ), Fig. B-2, by taking the product integrals for each member we find similarly

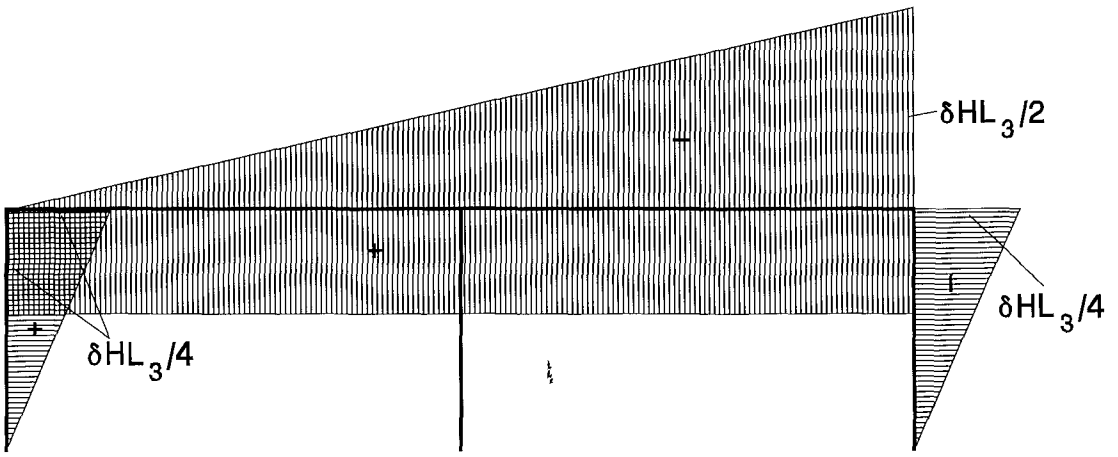

Figure B-4

$$u = \frac{(P-H)L_3^3}{48EI_3} + \frac{PL_2L_3^2}{24EI_2} - \frac{HL_2L_3^2}{16EI_2} . \qquad \textbf{(B.3)}$$

Eventually the horizontal displacement takes the form

$$u = \frac{PL_3^3}{96EI_1}\left[\frac{2(1-h)}{\xi_2} + \frac{4\bar{a}}{\xi_3} - \frac{6h\bar{a}}{\xi_3}\right], \qquad \textbf{(B.4)}$$

where $h = \frac{H}{P}$ $\xi_2 = \frac{I_2}{I_1}$ $\xi_3 = \frac{I_3}{I_1}$ $\bar{a} = \frac{L_2}{L_3}$.

For $\xi_2 = 1$, $\xi_3 = 1$, $\bar{a} = 1$ and $h = \frac{4}{9}$

one obtains $$u = \frac{11PL_3^3}{432EI_1} .$$

It is obvious that this displacement must be doubled if the real system (whole structure) is considered.

B.2 Calculation of stiffness coefficient at the top-middle of the frame

B.2.1 Rotational Stiffness

a) Non-sway mode (symmetric case)

Taking advantage of the symmetry of both the frame and loading with respect to horizontal axis, as shown in Fig. B-5, when the moment C_A produces the unity of rotation at A, there is no rotation at C.

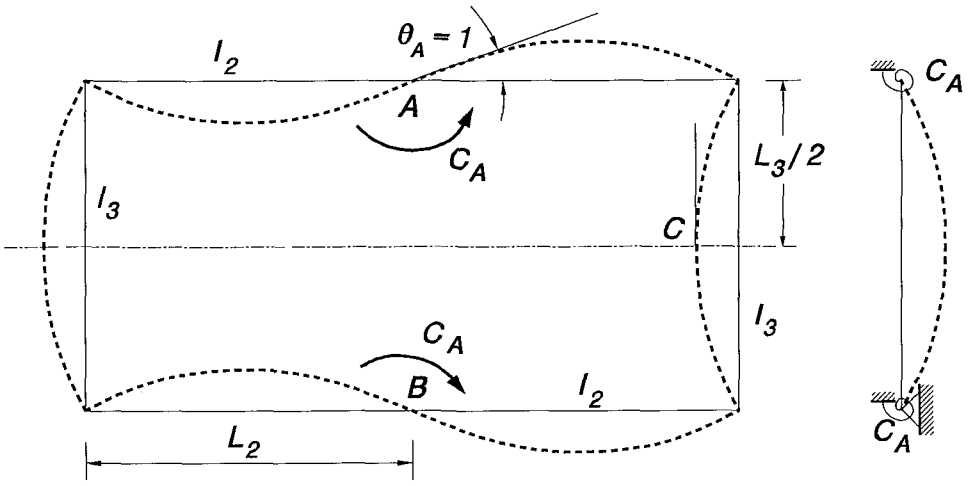

Figure B-5

The frame can be modeled as shown in Fig. B-6.

If M_c is the bending moment at C, this moment can be calculated through the virtual force method. The bending moment diagram of ABC, resulting in the real curvature (χ) diagram is drawn in Fig. B-7.

If we apply at A a virtual moment $\delta C_A/2$, make the bending moment diagram (δm), resulting from the statically admissible reaction at C, and combine this diagram with (χ) by taking the product integrals for each member, since there

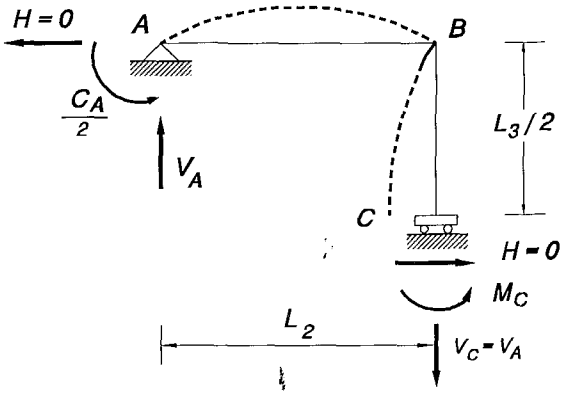

Figure B-6

is no virtual work associated with the moment at C (θ_C=0), we will have

$$\frac{\delta C_A}{2}\theta_A = \int \chi \cdot \delta m \cdot dx \tag{B.5}$$

For $\theta_A = 1$, we obtain

$$1 = \frac{1}{2}\cdot\frac{C_A}{2EI_2}\cdot L_2 - \frac{1}{2}\cdot\frac{M_C}{2EI_2}\cdot L_2 - \frac{M_C}{2EI_3}\cdot\frac{L_3}{2} \tag{B.6}$$

To find M_C we can similarly obtain another equation using the virtual force system, shown in Fig. B-8, where (δm) is the bending moment diagram resulting from the statically admissible reactions of frame ABC after the application of the virtual moment δM_C at C. Since all the external virtual forces have zero real displacement, there is no external virtual work. Hence

$$-\frac{1}{6}\cdot\delta M_C\cdot\frac{C_A}{2EI_2}\cdot L_2 + \frac{1}{3}\cdot\delta M_C\cdot\frac{M_C}{2EI_2}\cdot L_2 + \delta M_C\frac{M_C}{2EI_3}\cdot\frac{L_3}{2} = 0 \tag{B.7}$$

$$\frac{C_A}{12EI_2} = \frac{M_C}{6EI_2} + \frac{M_C}{4EI_3}\cdot\frac{L_3}{L_2} \tag{B.8}$$

from which

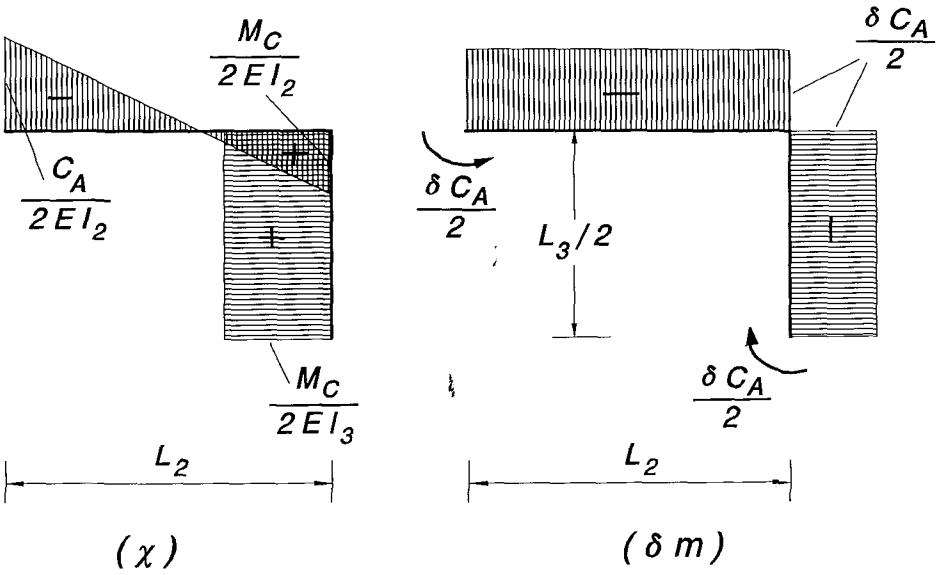

Figure B-7

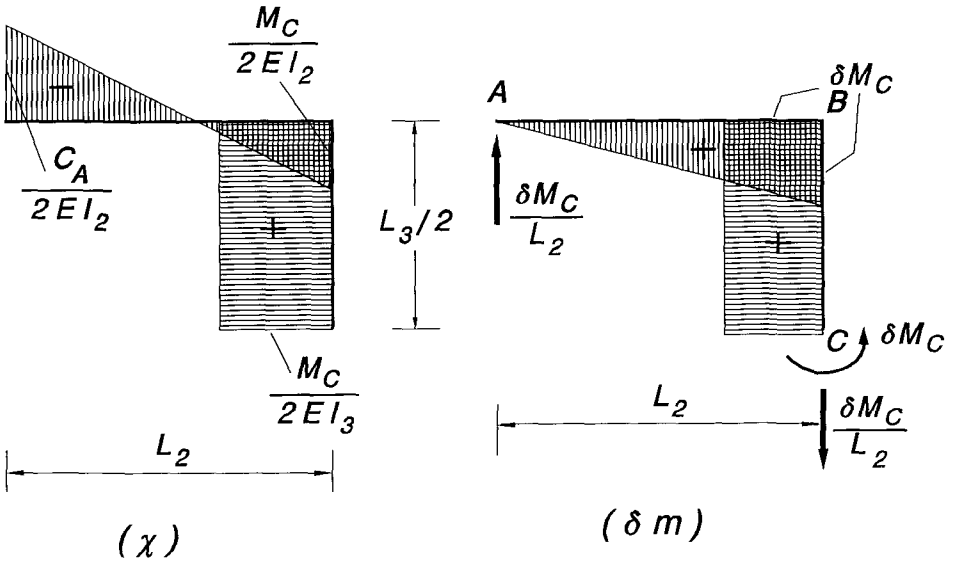

Figure B-8

$$M_C = C_A \cdot \frac{1}{2+3h} \tag{B.9}$$

where $$h = \frac{I_2 L_3}{I_3 L_2} \quad .$$

Substituting the value of M_C into B.6 we obtain the value of the stiffness coefficient C_A for a non-sway mode

$$C_A = 4\eta \cdot \frac{2+3h}{1+2h} \qquad \textbf{(B.10)}$$

where $$\eta = \frac{EI_2}{L_2} \quad .$$

b) Sway mode (antisymmetric case)

Similarly, taking antisymmetry of loading, putting the moment C_A' at A for a unity rotation, the original frame, shown in Fig. B-9, can be modeled as the frame

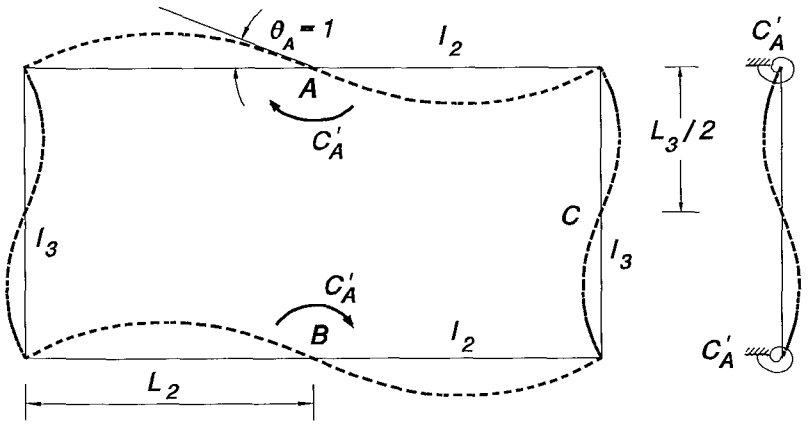

Figure B-9

shown in Fig. B-10, where the vertical reaction V_A can be expressed in terms of the unknown horizontal reaction H from the static equilibrium equation

$$\frac{C_A'}{2} = \frac{HL_3}{2} + V_A L_2 \qquad \textbf{(B.11)}$$

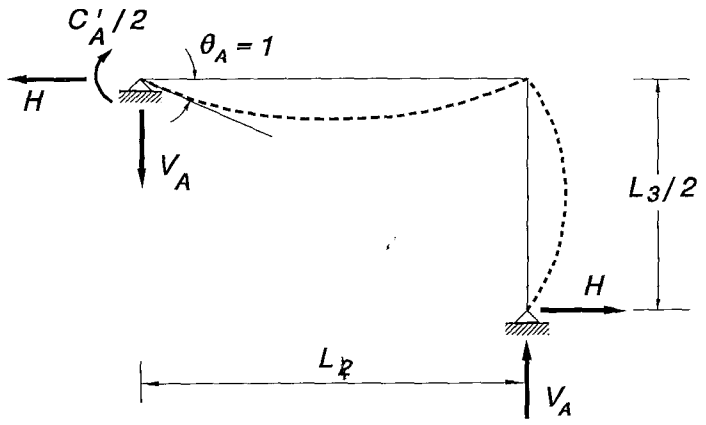

Figure B-10

For this model, if from bending moment diagram, we draw the real curvature diagram and use the virtual force system in Fig. B-11, the stiffness C_A' can be calculated in terms of the horizontal reaction H, which has been taken as redundant.

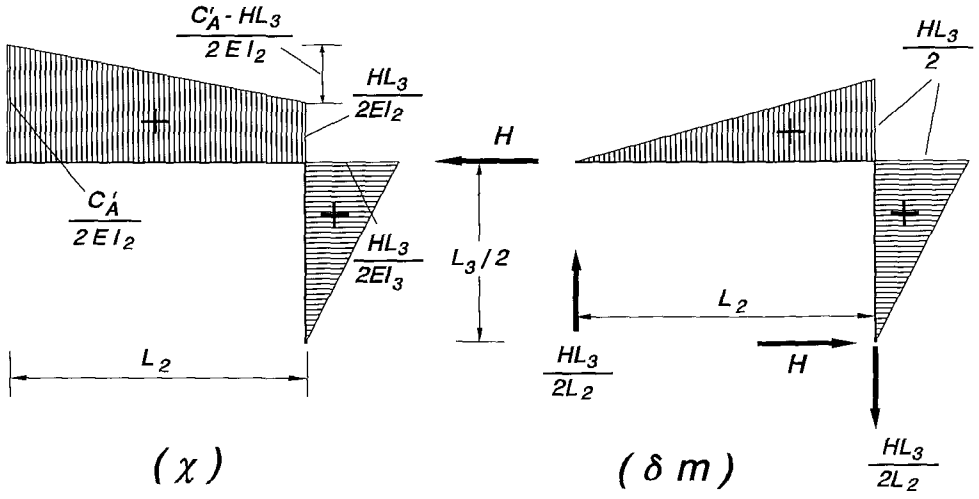

Figure B-11

Since there is no work of external forces, the equation obtained is

$$\frac{1}{2}\cdot\frac{HL_3}{2}\cdot\frac{C_A'}{2EI_2}\cdot L_2 - \frac{1}{3}\cdot\frac{HL_3}{2}\cdot\frac{C_A'-HL_3}{2EI_2}\cdot L_2 + \frac{1}{3}\cdot\frac{HL_3}{2}\cdot\frac{HL_3}{2EI_3}\cdot\frac{L_3}{2} = 0 \qquad \textbf{(B.12)}$$

which yields

$$H = -\frac{C_A'}{(2+h)L_3} . \tag{B.13}$$

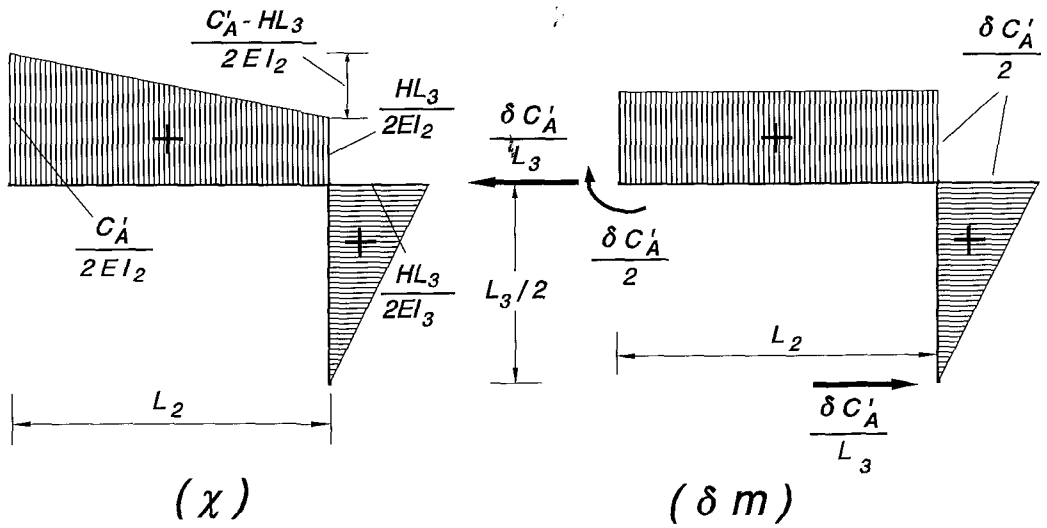

Figure B-12

Now, applying the virtual force system (δm) showing in Fig. B-12, one more equation between C_A' and H can be obtained, i.e.

$$\frac{\delta C_A'}{2} \cdot \theta_A = \int \chi \cdot \delta m \cdot dx , \tag{B.14}$$

from which, for $\theta_A = 1$, yields

$$\frac{\delta C_A'}{2} \cdot 1 = \frac{\delta C_A'}{2} \cdot \frac{C_A'}{2EI_2} \cdot L_2 - \frac{1}{2} \cdot \frac{\delta C_A'}{2} \cdot \frac{C_A' - HL_3}{2EI_2} \cdot L_2 + \frac{1}{3} \cdot \frac{\delta C_A'}{2} \cdot \frac{HL_3}{2EI_3} \cdot \frac{L_3}{2} \tag{B.15}$$

or

$$1 = \frac{C_A' L_2}{4EI_2} - \frac{(3L_2I_3 + L_3I_2)L_3}{12EI_3I_2} \cdot H . \tag{B.16}$$

Substituting the value of H from Eq. B.13 we obtain

$$C_A' = 12\eta \frac{2+h}{3+2h}, \tag{B.17}$$

where h and η have the same values as before.

B.2.2 Translational stiffness

Sway mode (the joint moves due to horizontal force without rotation)

If K_A is the horizontal force necessary to produce the unity of horizontal displacement without rotation of node A, the original frame, shown in Fig. B-13, can be modeled as shown in Fig. B-14.

The values of M_A', V_A' and K_A can be related by the equation of equilibrium

$$\frac{K_A}{2}\cdot\frac{L_3}{2} + M_A' = V_A' L_2 \tag{B.18}$$

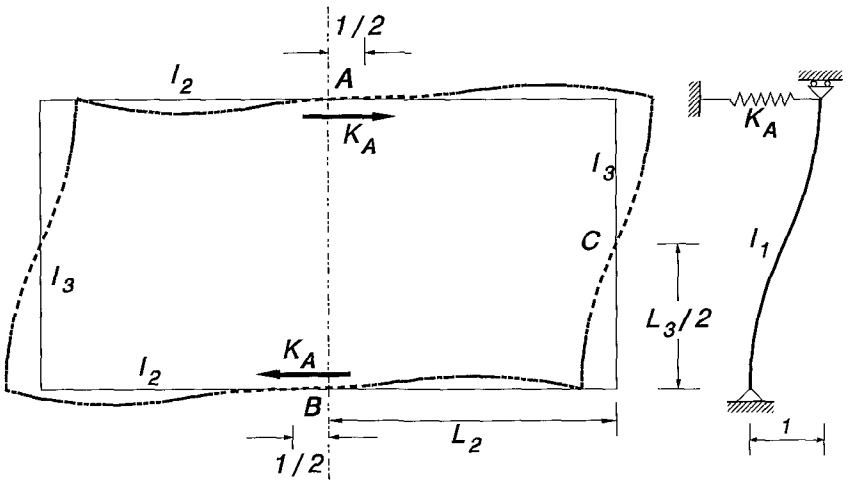

Figure B-13

Making the real curvature diagram (χ) and combining this with the bending moment

diagram (δm), resulting from the virtual force system shown in Fig. B-15, we take the virtual force equation

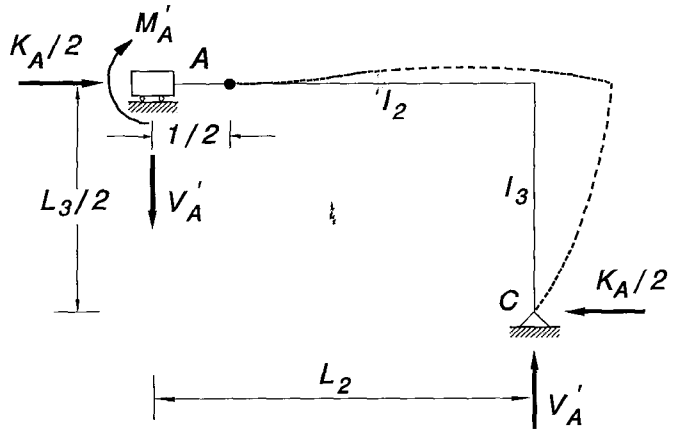

Figure B-14

$$0 = \frac{1}{3}\delta M_A' \frac{M_A'}{EI_2} L_2 - \frac{1}{6}\delta M_A' \frac{K_A L_3}{4EI_2} L_2 \tag{B.19}$$

$$M_A' = \frac{K_A L_3}{8} \tag{B.20}$$

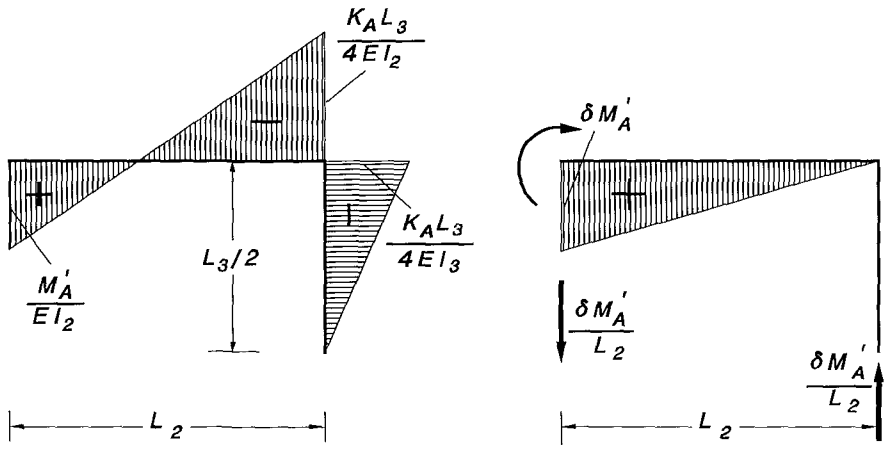

Figure B-15

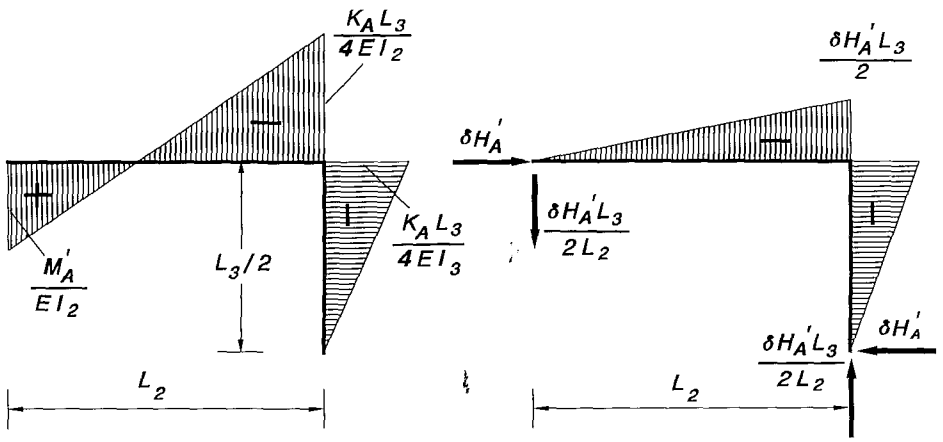

Figure B-16

If we now apply the virtual force system shown in Fig. B-16, the virtual work equation will give again

$$\delta H_A' \frac{1}{2} = -\frac{1}{6}\frac{\delta H_A' L_3}{2}\frac{M_A'}{EI_2}L_2 + \frac{1}{3}\frac{\delta H_A' L_3}{2}\frac{K_A L_3}{4EI_2}L_2 + \frac{1}{3}\frac{\delta H_A' L_3}{2}\frac{K_A L_3}{4EI_3}\frac{L_3}{2} \qquad \textbf{(B.21)}$$

or

$$1 = -\frac{M_A' L_3 L_2}{6EI_2} + \frac{K_A L_3^2 L_2}{12EI_2} + \frac{K_A L_3^3}{24EI_3} \qquad \textbf{(B.22)}$$

Substituting M_A' from B.20 into B.22 we obtain the value of K_A

$$K_A = 48\eta \frac{1}{3+2h}\cdot\frac{1}{L_3^2} \qquad \textbf{(B.23)}$$

where η and h keep the same values as before.

All the above theoretical calculations have been independently verified through the F.E. computer program, used initially for numerical experiments,

where an excellent agreement was observed.

B.3 Accurate calculation of stiffness coefficient at the top-middle of the real frame-model used for the experiments

The frame model used for the experiments, needed to have the possibility of using different members (beams or columns). For this purpose it had to be builded through different end-blocks which were specially constructed to keep a monolithic connection throughout its members. Even though these end-blocks had the minimum possible length, they resulted in a substantial increase of the total frame stiffness.

In the sections that follow a similar procedure to that developed in section B.2 shows only the main steps, which lead to an accurate calculation of the stiffness coefficient of the top-middle of the experimental frame-model. These calculations have come through an extended computational procedure made specially for this purpose.

B.3.1 Rotational Stiffness

a) Non-sway mode (symmetric case)

Referring to the modeled sub-frame of Fig. B-6, the following system of 2 equations in the x and y unknowns has been created by combining the real curvature diagram (χ_s) in Fig. B-17 with each one of the statically admissible virtual force systems (δm_{1s}), (δm_{2s}) shown in Fig. B-18. These diagrams have been made from the corresponding of Figs. B-7 and B-8, taking into account the geometry of the end-blocks as shown in detail in chapter 6. The combination has been made by taking the product integrals of the above diagrams in the same way as shown in section B.2.1.

In this system, are:

x : The rotational stiffness for the Non-sway (symmetric) modes of buckling in y kN*mm/rad;

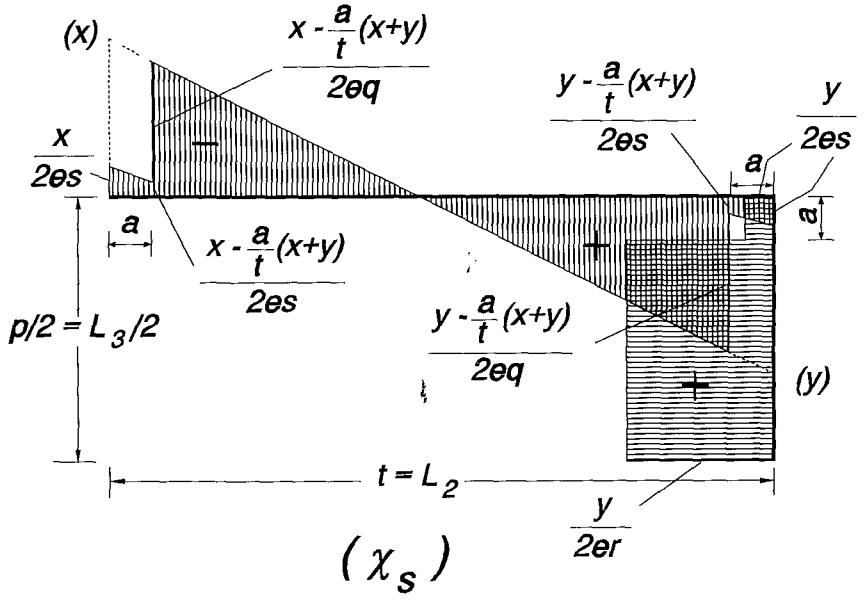

Figure B-17

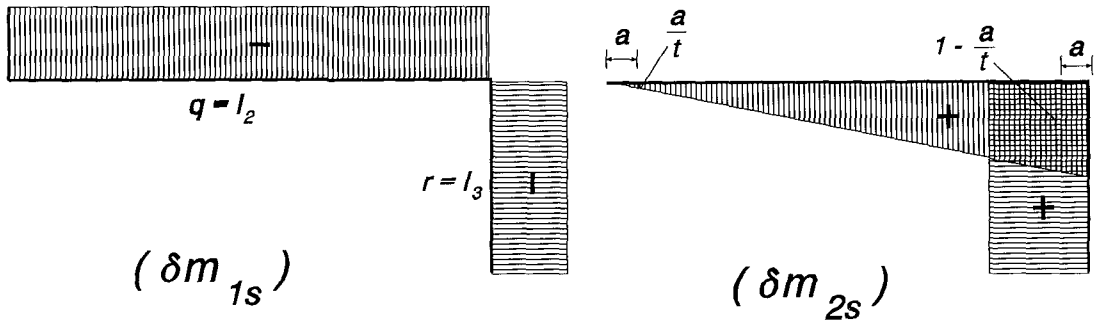

Figure B-18

: The bending moment at the right end of the beam (top end of side-column) in kN*mm;

e : The Young's modulus of elasticity in kN/mm^2;

q : The second moment of area of beam's free part (without end-blocks) in mm^4;

r : -"- -"- side column's -"- -"- -"-

t : The whole length of beam (including the end-blocks) in mm;

p : -"- side-column -"- -"-

The length of the end-blocks has been taken 30 mm, while the total second moment of area (end-block + beam) for this part of length only, 15x555 mm^4. This moment of area, tending to infinity, about corresponds to a 20 mm thickness of end-block. The equations of the system are:

(x-2*y)/(15*37*e)+(t-60)*(x-y)/(4*e*q)-(p-60)*y/(4*e*r)=1 **and**

-(3*x-60/t*(x+y))/(15*(7.4)*e*t)+(3*(2*y-30/t*(x+y))-30/t*(3*y-60/t*(x+y)))/(15*222*e)+(t-60)/(12*e*q)*(2*y-x-60/t*(x+y)*(1-30/t))+y/(15*37*e)+(p-60)*y/(4*e*r)=0

A computerised procedure of the above system gave the solution:

x=2220*e*q*(555*p*q*t^2+2*(2*q*(2*r*(t^2-15*t+300)-8325*t^2)+185*r*(t-60)*(t^~

2-30*t+900)))/(1110*p*q*(2*q*(t^2-30*t+600)+185*(t-60)*(t^2-30*t+900))+16*q^2*~

(2*r*(t^2-45*t+900)-8325*(t^2-30*t+600))+4440*q*(t-60)*(r*(t^2-60*t+1500)-2775~

*(t^2-30*t+900))+1.02675*10^5*r*(t-60)^4) **and**

y=11100*e*q*r*(24*q*(t-20)+37*(t-60)*(t^2+60*t-1800))/(1110*p*q*(2*q*(t^2-30~*t+600)+185*(t-60)*(t^2-30*t+900))+16*q^2*(2*r*(t^2-45*t+900)-8325*(t^2-30*t+~600))+4440*q*(t-60)*(r*(t^2-60*t+1500)-2775*(t^2-30*t+900))+1.02675*10^5*r*(t-60)^4)

which has been incorporated in the STIFFNESS subroutine of the FORTRAN program that solves the Eigenvalue Problem of the frame.

b) Sway mode (antisymmetric case)

Referring to the modeled sub-frame of Fig. B-10, the following system of 2 equations in the x and y unknowns has been created by combining the real curvature diagram (χ_a) in Fig. B-18 with each one of the statically admissible virtual force

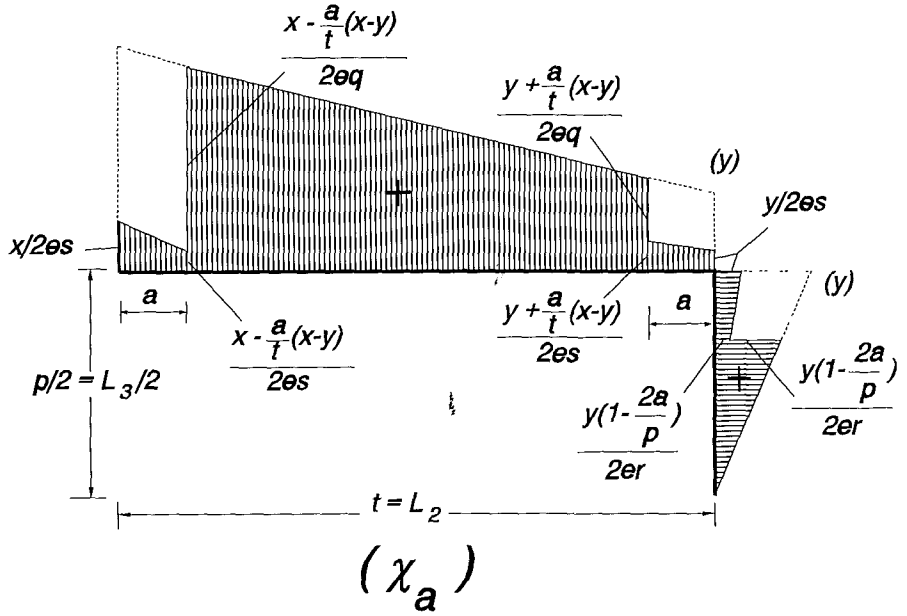

Figure B-19

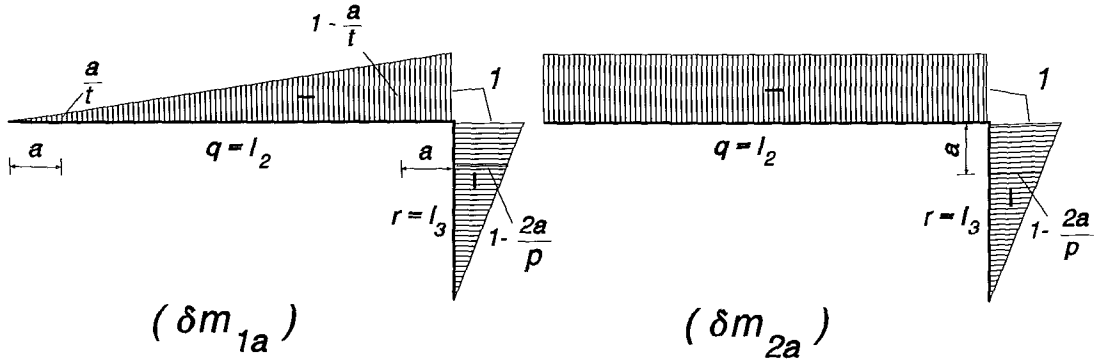

Figure B-20

systems (δm_{1a}), (δm_{2a}) shown in Fig. B-19. These diagrams have been made from the corresponding of Figs. B-11 and B-12, taking into account the geometry of the end-blocks as shown in detail in chapter 6. The combination has been made by taking the product integrals of the above diagrams in the same way as shown in section B.2.1.

In this system, are:

x : The rotational stiffness for the Sway (antisymmetric) modes of buckling in

kN*mm/rad;

y : The bending moment at the right end of the beam (top end of side-column) in kN*mm;

e : The Young's modulus of elasticity in kN/mm^2;

q : The second moment of area of the beam's free part (excluding end-blocks) in mm^4;

r : -"- -"- column's -"- -"- -"-

t : The whole length of beam (including the end-blocks) in mm;

p : -"- side-column -"- -"-

The length of the end-blocks has been taken 30 mm, while the total second moment of area (end-block + beam) for this part of length only, 15x555 mm^4. This moment of area, tending to infinity, about corresponds to a 20 mm thickness of end-block. The equations of the system are:

(3*x-60/t*(x-y*p))/(15*7.4*e*t)+(t-60)/(12*e*q)*((x-30/t*(x-y*p))*(30/t+1)+~

(y*p+30/t*(x-y*p))*(2-30/t))+((y*p+30/t*(x-y*p))*(3-60/t)+y*p*(9-30/t-360/p+72~

00/p^2))/(15*222*e)+y*p*(p-60)/(12*e*r)*(1-60/p)^2=0 **and**

(1/(15*37*e)+(t-60)/(4*e*q))*(x+y*p)+y*p*((3-180/p+3600/p^2)/(15*111*e)+(p-6

0)/(12*e*r)*(1-60/p)^2)=1

A computerised procedure of the above system gave the solution:

x=2220*e*q*(185*p^3*q*t^2+2*p^2*(2*q*(2*r*(t^2-15*t+300)-8325*t^2)+185*r

*(t-6~

0)*(t^2-30*t+900))-240*p*q*t^2*(r-8325)+4800*q*t^2*(r-8325))/(370*p^3*q*(2*

q*(~

t^2-30*t+600)+185*(t-60)*(t^2-30*t+900))+p^2*(16*q^2*(2*r*(t^2-45*t+900)-83

25*~

(t^2-30*t+600))+4440*q*(t-60)*(r*(t^2-60*t+1500)-2775*(t^2-30*t+900))+102675
*r~

*(t-60)^4)-480*p*q*(r-8325)*(2*q*(t^2-30*t+600)+185*(t-60)*(t^2-30*t+900))+960~

0*q*(r-8325)*(2*q*(t^2-30*t+600)+185*(t-60)*(t^2-30*t+900))) **and**

y=(-11100*e*p*q*r*(24*q*(t-20)+37*(t-60)*(t^2+60*t-1800))/(370*p^3*q*(2*q*(
t^2-30*t+600)+185*(t-60)*(t^2-30*t+900))+p^2*(16*q^2*(2*r*(t^2-45*t+900)-83
25*(t^2-30*t+600))+4440*q*(t-60)*(r*(t^2-60*t+1500)-2775*(t^2-30*t+900))+102
675*r*(t-60)^4)-480*p*q*(r-8325)*(2*q*(t^2-30*t+600)+185*(t-60)*(t^2-30*t+90
0))+9600*q*(r-8325)*(2*q*(t^2-30*t+600)+185*(t-60)*(t^2-30*t+900))))

which has been incorporated in the STIFFNESS subroutine of the FORTRAN program that solves the Eigenvalue Problem of the frame.

B.3.2 Translational stiffness

Sway mode (the joint moves horizontally without rotation)

Referring to the modeled sub-frame of Fig. B-14, the following system of 2 equations in the x and y unknowns has been created by combining the real curvature diagram (χ_t) of Fig. B-21 with each one of the statically admissible virtual force systems (δm_{1t}), (δm_{2t}) shown in Fig. B-22. These diagrams have been made from the corresponding of Figs. B-15 and B-16, taking into account the geometry of the end-blocks as shown in detail in chapter 6. The combination has been made by taking the product integrals of the above diagrams in the same way as shown in section B.2.2.

In this system, are:

y : The translational stiffness K_A for the Sway (antisymmetric) mode of buckling in kN/mm multiplied by *p/4e*;

x : The bending moment at the left end of the beam (top end of central-column) in kN*mm divided by *e*;

e : The Young's modulus of elasticity in kN/mm^2;

q : The second moment of area of the beams' free part (without blocks) in mm^4;

r : -"- -"- side column's -"- -"- -"-

t : The whole length of beam (including the end-blocks) in mm;

p : -"- side-column ; -"- -"-

The length of the end-blocks has been taken 30 mm, while the total second moment of area (end-block + beam) for this part of length only, 15x555 mm^4. This moment of area, tending to infinity, about corresponds to a 20 mm thickness of end-block. The equations of the system are:

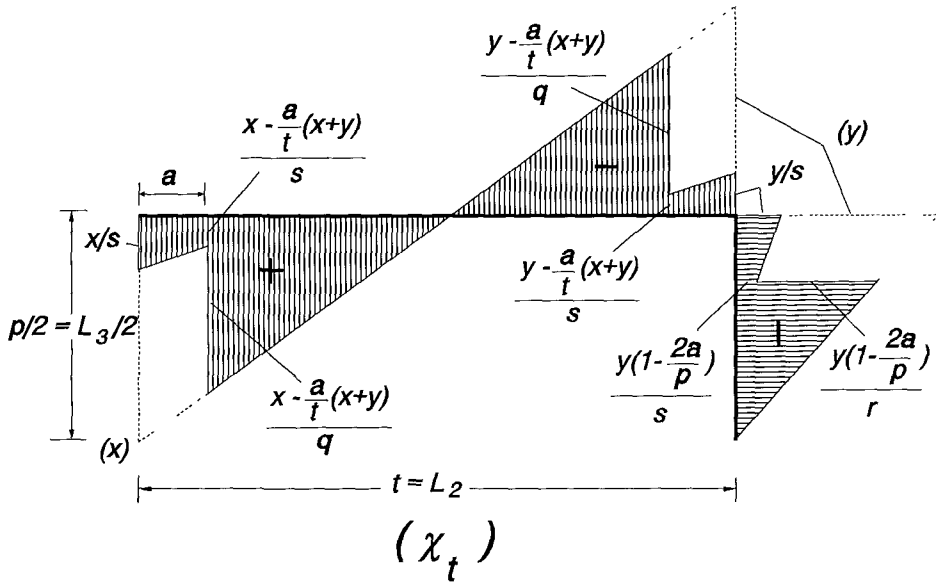

Figure B-21

(6*x-90/t*(2*x+y)+1800/t^2*(x+y))/(15*111)+(t-60)/(6*q)*(2*x-y-60/t*(x+y)*(1-30/t))-(3*y-60/t*(x+y))/(15*(3.7)*t)=0 **and**

-p*(3*x-60/t*(x+y))/(15*(7.4)*t)+p*(t-60)/(12*q*t)*(t*(2*y-x)-60*(x+y)*(1-30/t))+p/(15*222)*(3*y*(2-30/t)-30/t*(x+y)*(3-60/t))+p*y/(15*111)*(3-60/p*(3-60/p))+p*y*(p-60)/(12*r)*(1-60/p)^2=0.5

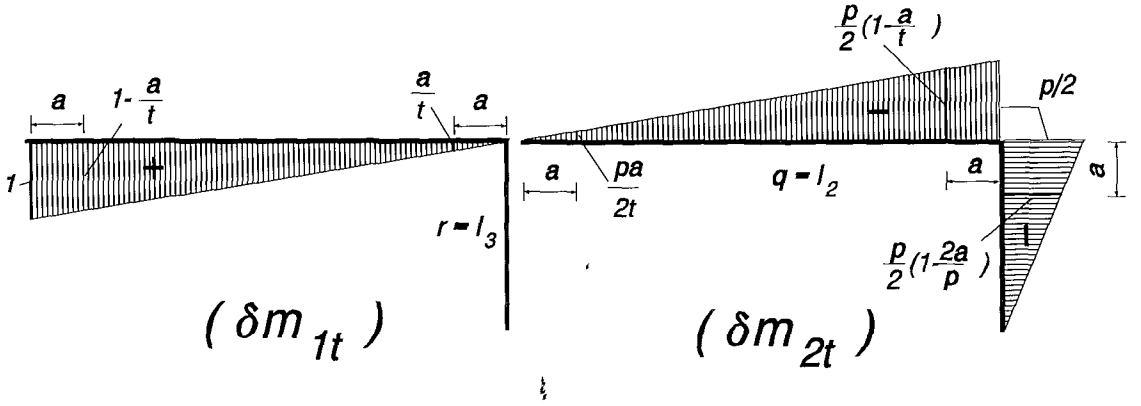

Figure B-22

A computerised procedure of the above system gave the solution:

x=5550*p*q*r*(24*q*(t-20)+37*(t-60)*(t^2+60*t-1800))/(370*p^3*q*(2*q*(t^2-30*~

t+600)+185*(t-60)*(t^2-30*t+900))+p^2*(16*q^2*(2*r*(t^2-45*t+900)-8325*(t^2-30~

*t+600))+4440*q*(t-60)*(r*(t^2-60*t+1500)-2775*(t^2-30*t+900))+1.02675*10^5*r*~

(t-60)^4)-480*p*q*(r-8325)*(2*q*(t^2-30*t+600)+185*(t-60)*(t^2-30*t+900))+9600~

q(r-8325)*(2*q*(t^2-30*t+600)+185*(t-60)*(t^2-30*t+900))) **and**

y=2220*p*q*r*(2*q*(t^2-30*t+600)+185*(t-60)*(t^2-30*t+900))/(370*p^3*q*(2*q*(t^2-30*t+600)+185*(t-60)*(t^2-30*t+900))+p^2*(16*q^2*(2*r*(t^2-45*t+900)-8325*(t^2-30*t+600))+4440*q*(t-60)*(r*(t^2-60*t+1500)-2775*(t^2-30*t+900))+1.02675*10^5*r*(t-60)^4)-480*p*q*(r-8325)*(2*q*(t^2-30*t+600)+185*(t-60)*(t^2-30*t+900))+9600*q*(r-8325)*(2*q*(t^2-30*t+600)+185*(t-60)*(t^2-30*t+900)))

which has been incorporated in the STIFFNESS subroutine of the FORTRAN program that solves the Eigenvalue Problem of the frame.

B.4 Example of Calculation of Maximum Deflection due to Sway Loading Imperfections for the Case where Both Ends are Fixed Rollers

B.4.1 Elastic Critical Load Analysis

Considering the column of the figure below, since there is not lateral load, the general differential equation is[4]

$$EIw^{iv} + Pw'' = 0 \tag{B.24}$$

or, substituting $k^2 = \frac{P}{EI}$,

$$w^{iv} + k^2 w'' = 0 . \tag{B.25}$$

The general solution of this equation is

$$w = A\sin kx + B\cos kx + Cx + D \tag{B.26}$$

The constants in this equation and the value of critical load are to be found from the end conditions of the column. At x=0, the deflection and the bending moment are zero due to symmetry. The first condition gives

$$B + D = 0 \tag{B.27}$$

while from the second condition

$$w'' = -k^2 A\sin kx - k^2 B\cos kx \tag{B.28}$$

yields $k^2 B = 0$ and therefore

$$B = D = 0 . \tag{B.29}$$

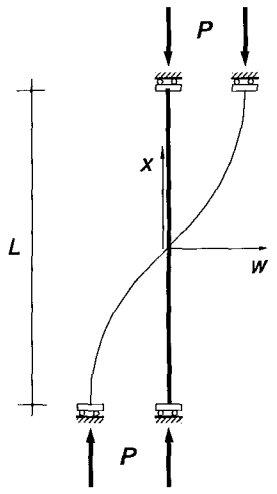

Figure B-23

Since the ends are fixed, at $x = \pm\frac{L}{2}$ is $w' = 0$;

i.e.

$$C = -kA\cos k\frac{L}{2} \tag{B.30}$$

Again at $x = \pm\frac{L}{2}$ the shear force is zero. Hence

$$w''' = -k^3 A\cos k\frac{L}{2} = 0 \tag{B.31}$$

The constant A has here the meaning of a maximum deflection. Since k is not zero $(P \neq 0)$, it remains

$$\cos k\frac{L}{2} = 0 \tag{B.32}$$

from which a zero value for C is obtained and

$$k\frac{L}{2} = \frac{(2i-1)\pi}{2} \qquad (i = 1,2,..) \tag{B.33}$$

$$k^2 = \frac{P_{ci}}{EI} = \frac{(2i-1)^2}{L^2} \qquad (i = 1,2,..) \tag{B.34}$$

So the critical load corresponding to the first mode of buckling (i=1) is

$$P_{c1} = \frac{\pi^2 EI}{L^2} \tag{B.35}$$

The deflection curve of the column can be expressed from the general solution for the found value of k, i.e.

$$w_i(x) = A\sin\frac{(2i-1)\pi}{L}x \qquad (i = 1,2,..) \tag{B.36}$$

B.4.2 Deflection due to Horizontal Loading

At the idealised model of the following picture, if we put at the top support an initial horizontal force, H, along with the corresponding -H at the bottom one, a moment HL/2 will appear at each end. The bending moment diagram along the height of the column is linear. The differential equation for the deflection curve is:

$$EI\frac{d^2w}{dx^2} = -M = -xH \ . \qquad \textbf{(B.37)}$$

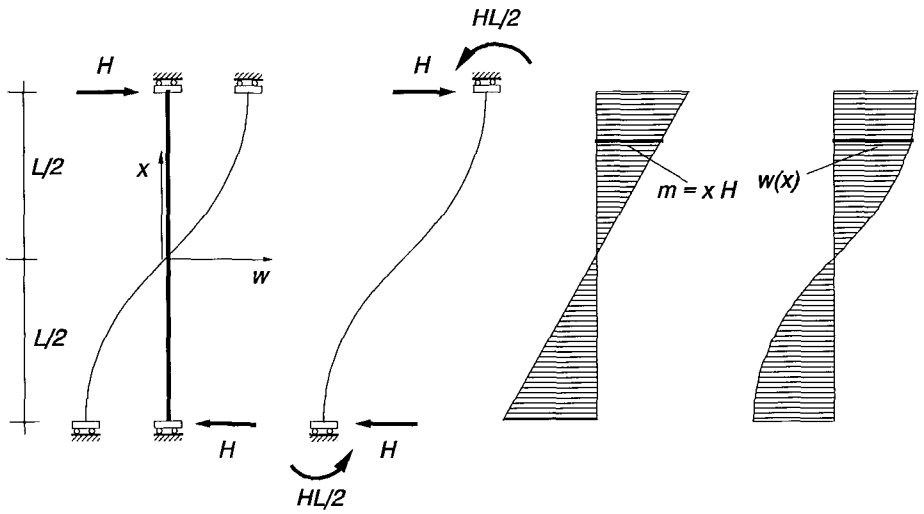

Figure B-24

After two integrations the deflection curve becomes

$$EIw = -H\frac{x^3}{6} + C_1x + C_2 \ . \qquad \textbf{(B.38)}$$

The boundary conditions, i.e. at x = 0 and $x = \pm\frac{L}{2}$ the corresponding deflection and slope are w = 0 and $w' = 0$, result in the constants C_1 and C_2 taking the values

$$C_2 = 0 \quad \textit{and} \quad C_1 = \frac{HL^2}{8EI} \qquad \textbf{(B.39)}$$

Therefore the equation that expresses the deflection curve is

$$w = \frac{H}{2EI}\left(\frac{L^2}{4}x - \frac{1}{3}x^3\right). \tag{B.40}$$

B.4.3 Theoretical Deflection through Amplitude Factors

According to amplitude factors of loading imperfections, as developed in Section 4.9, the expression for the i^{th} factor of loading imperfection is given from Eq. (4.54), i.e.

$$w_i^n = \frac{\sum_M \int_0^L EI\phi_i''(x)w^{n''}(x)dx}{\sum_M \int_0^L EI\phi_i''^2(x)dx}. \tag{B.41}$$

where

$$\phi_i(x) = \sin\frac{(2i-1)\pi}{L}x \tag{B.42}$$

is the characteristic function of the i^{th} critical mode and

$$w^l(x) = \frac{H}{2EI}\left(\frac{L^2}{4}x - \frac{x^3}{3}\right) \tag{B.43}$$

is the deflected shape of the column due to loading imperfections. The maximum deflection, occurring at the ends of the column, is

$$w^l_{\left(\frac{L}{2}\right)} = \frac{HL^3}{24EI}. \tag{B.44}$$

The second derivatives of Eqs. (B.42) and (B.43)

$$\phi_i'' = -\frac{(2i-1)^2\pi^2}{L^2}\sin\frac{(2i-1)\pi}{L}x$$
$$w^{l''} = -\frac{H}{EI}x \qquad \textbf{(B.45)}$$

reform Eq. (B.41) into

$$w_i^l = \frac{\int_{-L/2}^{L/2}\frac{HP_{ci}}{EI}x\sin\frac{(2i-1)\pi}{L}x\,dx}{\int_{-L/2}^{L/2}\frac{P_{ci}^2}{EI}\sin^2\frac{(2i-1)\pi}{L}x\,dx} = \frac{N}{D} \qquad \textbf{(B.46)}$$

Simplifying separately the numerator and denominator of Eq. (B.46) we obtain

Numerator: Since $\frac{HP_{ci}}{EI}$ is constant, we call the rest of numerator

$$\int_{-L/2}^{L/2}\{x\}\left\{\sin\frac{(2i-1)\pi}{L}x\,dx\right\} = A\ , \qquad \textbf{(B.47)}$$

which, using the known relation between two functions

$$\int v\,du = uv - \int u\,dv\ , \qquad \textbf{(B.48)}$$

becomes

$$A = \frac{-xL}{(2i-1)\pi}\cos\frac{(2i-1)\pi}{L}x\Big|_{-L/2}^{L/2} + \int_{-L/2}^{L/2}\frac{L}{(2i-1)\pi}\cos\frac{(2i-1)\pi}{L}x\,dx =$$

$$= \frac{-\frac{L^2}{2}}{(2i-1)\pi}\cos\frac{(2i-1)\pi L}{2L} - \frac{\frac{L^2}{2}}{(2i-1)\pi}\cos\frac{(2i-1)\pi\left(-\frac{L}{2}\right)}{L} +$$

$$+ \frac{L^2}{(2i-1)^2\pi^2}\sin\frac{(2i-1)\pi}{L}x\Big|_{-L/2}^{L/2} = \tag{B.49}$$

$$= \frac{L^2}{(2i-1)^2\pi^2}\sin\frac{(2i-1)\pi}{L}\left(\frac{L}{2}\right) - \frac{L^2}{(2i-1)^2\pi^2}\sin\frac{(2i-1)\pi}{L}\left(-\frac{L}{2}\right) =$$

$$= \frac{2L^2(-1)^{i+1}}{(2i-1)^2\pi^2} .$$

The numerator of Eq. (B.44) therefore becomes

$$N = \frac{HP_{ci}}{EI}\cdot\frac{2L^2(-1)^{i+1}}{(2i-1)^2\pi^2} . \tag{B.50}$$

Denominator: Similarly, since $\frac{P_{ci}^2}{EI}$ is constant and $\sin^2 a = \frac{1-\cos 2a}{2}$, we call

$$\int_{-L/2}^{L/2}\left(\frac{1}{2} - \frac{1}{2}\cos\frac{2(2i-1)\pi}{L}x\right)dx = B . \tag{B.51}$$

Hence

$$B = \frac{L}{2} - \frac{1}{2}\cdot\frac{L}{2(2i-1)\pi}\sin\frac{2(2i-1)\pi}{L}x\Big|_{-L/2}^{L/2} = \tag{B.52}$$

$$= \frac{L}{2} , .$$

and the denominator becomes

$$D = \frac{P_{ci}^2}{EI} \cdot \frac{L}{2} \quad . \tag{B.53}$$

Since $P_{ci} = \frac{(2i-1)^2\pi^2 EI}{L^2}$, Eq. (B.46) takes eventually the form

$$w_i^I = (-1)^{i+1} \times \frac{4L^3 H}{(2i-1)^4\pi^4 EI} \quad . \tag{B.54}$$

Taking only the contribution of the first critical mode, we find

$$w_1^I = \frac{4HL^3}{\pi^4 EI} = \frac{HL^3}{24.35\,EI} \quad , \tag{B.55}$$

which, in percentage of the total theoretical one, is

$$\frac{\frac{4HL^3}{\pi^4 EI}}{\frac{HL^3}{24EI}} \times 100 = \frac{96}{\pi^4} \times 100 = 98.55\,\% \tag{B.56}$$

Similarly the contribution of the second critical mode is

$$w_2^I = -\frac{1}{3^4} \times \frac{4HL^3}{\pi^4 EI} = -0.012\, w_1^I \, , \tag{B.57}$$

and therefore it can be negligible.

Appendix C

Part 1

Theoretical Background on Beam-columns

C.1.1 Introduction

It is known from the elementary theory of bending, that deflections and stresses in beams are directly proportional to the applied loads. This condition requires that the change in shape of the beam due to bending must not affect the action of the applied loads. The presence of only lateral loads, for example, on the beam in Fig. 1-1a, Q_1 and Q_2, cause small deflections δ_1 and δ_2 and slight changes in the vertical lines of action of the loads. This will only have an insignificant effect on the moments and shear forces. It is possible therefore, to make calculations for deflections, stresses, moments etc., on the basis of the initial configuration of the beam. If Hooke's law holds for the material, the deflections are proportional to the acting forces and the principle of superposition is valid; i.e. the final deformation is obtained by summation of the deformations produced by each individual force separately.

The analogous situation is entirely different when both axial and lateral loads act simultaneously on the beam (Fig. 1-1b). The bending moments, shear forces, stresses and deflections in the beam will not be proportional to the magnitude of the axial load. Their values will be dependent upon the magnitude of the deflections produced and furthermore, they will be sensitive to even slight eccentricities in the application of the axial load.

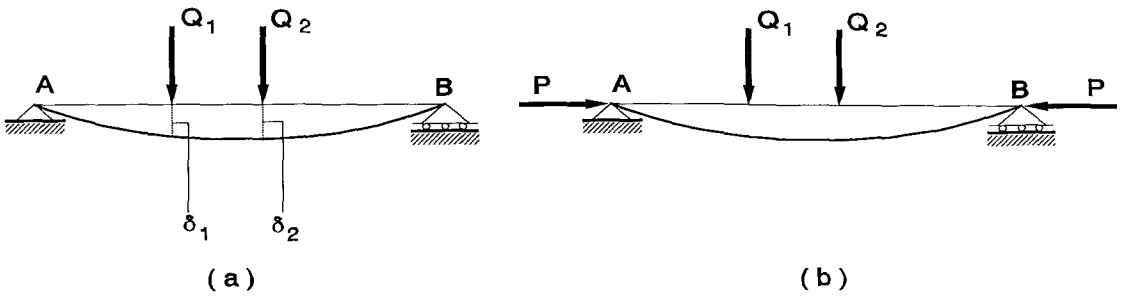

Fig. 1-1

Beams which support lateral loads while simultaneously subject to axial compression are known as *beam-columns*. In this Appendix beam-columns of symmetrical cross section with various conditions of support and loading will be analyzed[25].

C.1.2 Differential Equations for Beam-columns

Consider the beam in Fig. 1-2a which is subjected to an axial compressive force P along with a distributed lateral load of intensity $q(x)$ which varies with the distance x from the end of the beam. An element of length dx between two cross sections taken normal to the originally straight axis of the beam is shown in Fig. 1-2b. On this element the lateral load may be considered as having constant intensity q over the distance dx and is assumed to be positive when in the direction of the positive y axis, downwards. The shearing force V and the bending moment M acting on the sides of the element are assumed positive in the directions shown.

The relations among load, shearing force and bending moment are obtained from the equilibrium of the element in fig. 1-2b. Summing forces in the y direction we obtain

$$-V+qdx+(V+dV)=0$$

or

$$q = -\frac{dV}{dx} \tag{1-1}$$

Taking moments about point *n* and assuming the angle between the axis of the beam and the horizontal is small, we have

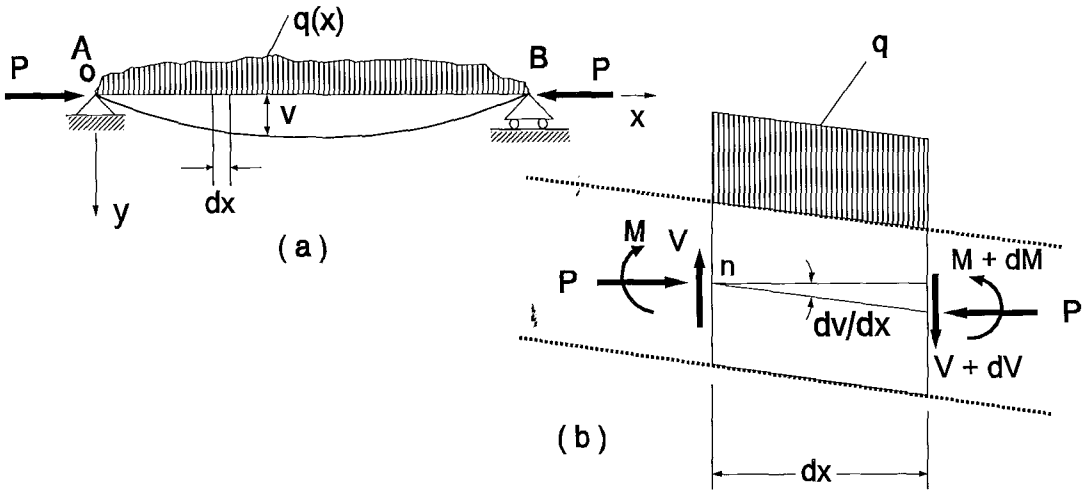

Fig. 1-2

$$M+q\,dx\frac{dx}{2}+(V+dV)\,dx-(M+dM)+P\frac{dv}{dx}dx=0\ .$$

If terms of second order are neglected, this equation gives

$$V=\frac{dM}{dx}-P\frac{dv}{dx}\ . \tag{1-2}$$

If the effects of shearing deformations and shortening of the beam axis are neglected, the expression for the curvature of the axis of the beam is

$$EI\frac{d^2v}{dx^2}=-M\ , \tag{1-3}$$

where *EI* is the flexural rigidity of the beam in the plane of bending, i.e. the *xy* plane which is assumed to be a plane of symmetry. Combining Eq. (1-3) with Eqs.(1-1) and (1-2) we can express the differential equation of the axis of the beam in the following alternative forms:

$$EI\frac{d^3v}{dx^3} + P\frac{dv}{dx} = -V \tag{1-4}$$

and

$$EI\frac{d^4v}{dx^4} + P\frac{d^2v}{dx^2} = q \ . \tag{1-5}$$

Equations (1-1) to (1-5) are the basic differential equations for bending of beam-columns. If there is no axial force P, these equations reduce to the usual equations for bending by lateral loads only.

C.1.3 Beam-column with a Concentrated Lateral Load

Consider in Fig. 1-3 a beam of length l on two simple supports carrying a single lateral load Q at distance c from the right end. If Q was acting alone, the bending moments could be found readily by statics. The axial force P in this case however, causes bending moments which cannot be found until the deflections are determined. The beam-column is thus statically indeterminate, and we have to solve first the differential equation for the deflection curve of the beam.

The bending moments for the left and right-hand portions of the beam in Fig. 1-3 are respectively

$$M = \frac{Qc}{l}x + Pv \qquad M = \frac{Q(l-c)}{l}(l-x) + Pv \ ,$$

and therefore, using Eq. (1-3), we obtain

$$EI\frac{d^2v}{dx^2} = -\frac{Qc}{l}x - Pv \tag{a}$$

$$EI\frac{d^2v}{dx^2} = -\frac{Q(l-c)(l-x)}{l} - Pv \ . \tag{b}$$

If we introduce the notation $k^2 = \frac{P}{EI}$, (1-6)

Eq. (a) becomes $\frac{d^2v}{dx^2} + k^2 v = -\frac{Qc}{EIl}x$.

The general solution of this equation is

$$v = A\cos kx + B\sin kx - \frac{Qc}{Pl}x \ . \tag{c}$$

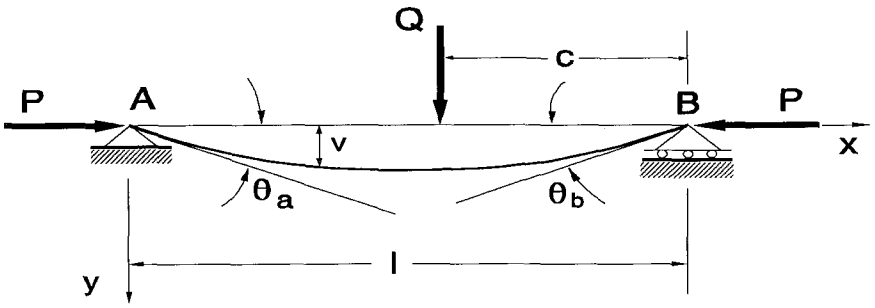

Fig. 1-3

In the same manner the general solution of Eq. (b) is

$$v = C\cos kx + D\sin kx - \frac{Q(l-c)(l-x)}{Pl} \ . \tag{d}$$

The constants of integration *A, B, C,* and *D* will be determined from the conditions at the ends of the beam as well as at the point of application of the load *Q*. Since the deflections at the ends of the bar are zero, we obtain

$$A = 0 \qquad C = -D\tan kl \ . \tag{e}$$

At the cross section where the load *Q* is applied, the two portions of the deflection curve, as given by Eqs. (c) and (d), have the same deflection and a common tangent. These conditions require respectively

$$B\sin k(l-c) - \frac{Qc}{Pl}(l-c) = D[\sin k(l-c) - \tan kl\cos k(l-c)] - \frac{Qc}{Pl}(l-c)$$

$$Bk\cos k(l-c) - \frac{Qc}{Pl} = Dk[\cos k(l-c) + \tan kl\sin k(l-c)] + \frac{Q(l-c)}{Pl} \quad ,$$

from which

$$B = \frac{Q\sin kc}{Pk\sin kl} \qquad D = -\frac{Q\sin k(l-c)}{Pk\tan kl} \quad . \tag{f}$$

Substituting the values of the constants from (e) and (f) into Eqs. (c) and (d), we obtain the following equations for the two portions of the deflection curve:

$$v = \frac{Q\sin kc}{Pk\sin kl}\sin kx - \frac{Qc}{Pl}x \qquad 0 \le x \le l-c \tag{1-7}$$

$$v = \frac{Q\sin k(l-c)}{Pk\sin kl}\sin k(l-x) - \frac{Q(l-c)(l-x)}{Pl} \qquad l-c \le x \le l \tag{1-8}$$

It is seen that Eq. (1-8) can be obtained from Eq.(1-7) by substituting l - c for c and l - x for x.

Differentiation of Eqs. (1-7) and (1-8) gives

$$\frac{dv}{dx} = \frac{Q\sin kc}{P\sin kl}\cos kx - \frac{Qc}{pl} \qquad 0 \le x \le l-c \tag{1-9}$$

$$\frac{dv}{dx} = -\frac{Q\sin k(l-c)}{P\sin kl}\cos k(l-x) + \frac{Q(l-c)}{Pl} \qquad l-c \le x \le l \tag{1-10}$$

$$\frac{d^2v}{dx^2} = -\frac{Qk\sin kc}{P\sin kl}\sin kx \qquad 0 \le x \le l-c \tag{1-11}$$

$$\frac{d^2v}{dx^2} = -\frac{Qk\sin k(l-c)}{P\sin kl}\sin k(l-x) \qquad l-c \le x \le l \quad . \tag{1-12}$$

If the load Q is applied at the centre of the beam, the deflection curve is symmetrical; thus we consider only the portion to the left of the load. The maximum deflection in this case, is obtained by substituting $x = c = l/2$ in Eq. (1-7), which gives

$$\delta = (v)_{x=l/2} = \frac{Q}{2Pk}\left(\tan\frac{kl}{2} - \frac{kl}{2}\right) . \tag{g}$$

Using the additional notation

$$u = \frac{kl}{2} = \frac{l}{2}\sqrt{\frac{P}{EI}} , \tag{1-13}$$

Eq. (g) can be simplified to

$$\delta = \frac{Ql^3}{48EI}\frac{3(\tan u - u)}{u^3} = \frac{Ql^3}{48EI}\chi(u) . \tag{1-14}$$

The first factor on the right -hand side of this equation is the deflection obtained if the lateral load Q acts alone. The second factor, $\chi(u)$, gives the influence of the axial force on the deflection δ.

When P is small, the quantity u is also small [Eq. (1-13)]. The factor $\chi(u)$ then approaches unity, as can be shown by using the series

$$\tan u = u + \frac{u^3}{3} + \frac{2u^5}{15} + \ldots$$

if we retain only the first two terms. It is also seen that $\chi(u)$ becomes infinite when u approaches $\pi/2$. When $u = \pi/2$, we find from Eq. (1-13)

$$P = \frac{\pi^2 EI}{l^2} . \tag{1-15}$$

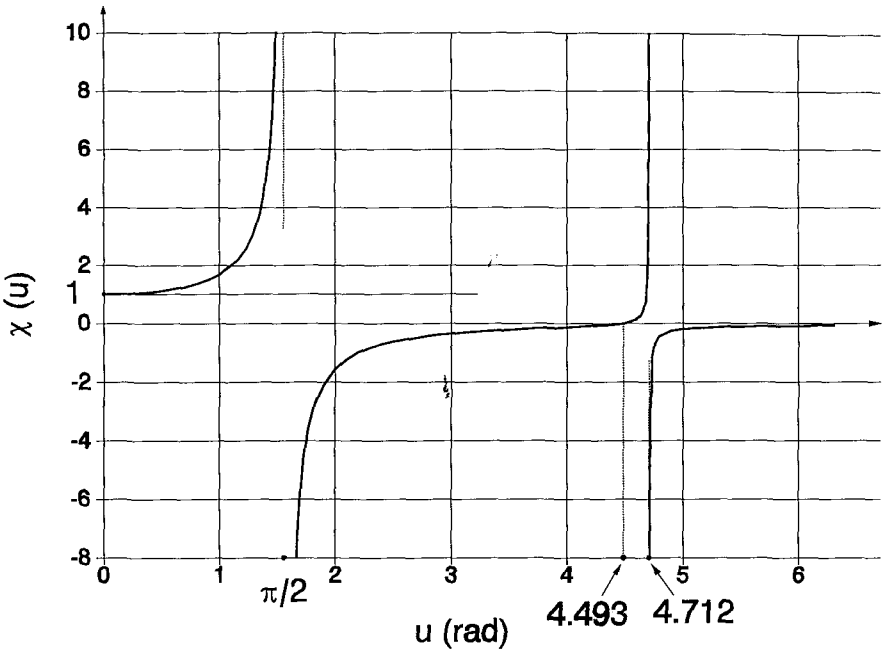

Fig. 1-c

Therefore, if the axial load approaches the limiting value given by Eq. (1-15), even the smallest lateral load will produce considerable lateral deflection. The limiting value of this compressive load is called the *critical load* and is denoted by P_{cr}. For the critical value of axial load, the quantity u from Eq. (1-13) takes the form:

$$u = \frac{\pi}{2}\sqrt{\frac{P}{P_{cr}}} \; . \tag{1-16}$$

Thus u depends only on the magnitude of the ratio P/P_{cr}.

The slope of the deflection curve at the end of the beam can be found from Eq. (1-9), if we substitute $x = 0$ and $c = l/2$

$$\left(\frac{dv}{dx}\right)_{x=0} = \frac{Q}{2P}\left(\frac{1}{\cos kl/2} - 1\right) = \frac{Ql^2}{16EI}\frac{2(1-\cos u)}{u^2\cos u} = \frac{Ql^2}{16EI}\lambda(u) \; . \tag{1-17}$$

Again, the first factor is the slope when the lateral load Q acts alone at the centre of the beam while the second factor is the effect of the axial load P.

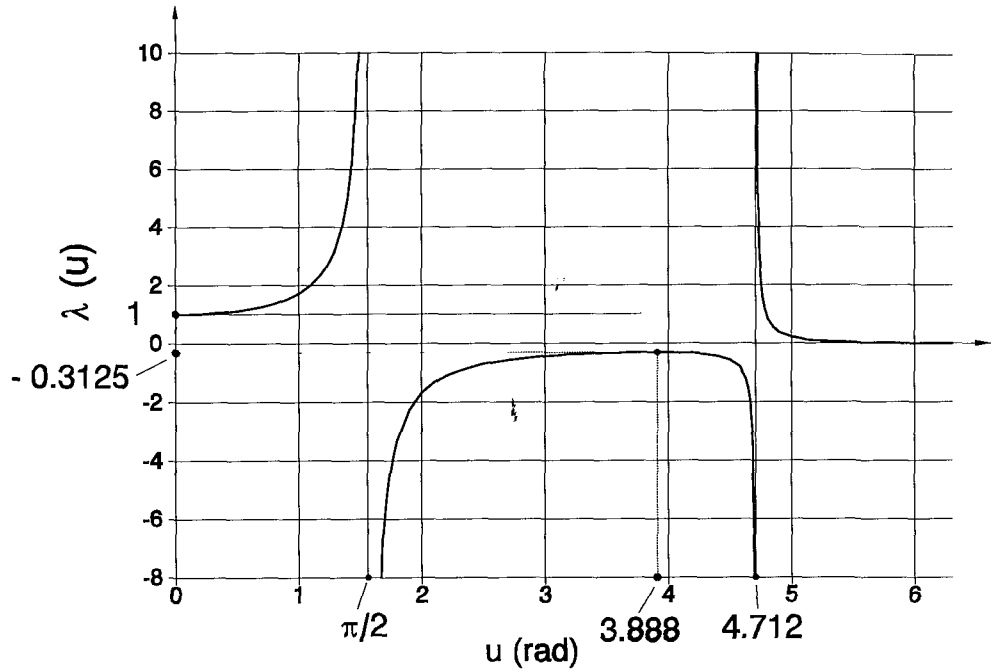

Fig. 1-d

The maximum bending moment can be obtained from Eq. (1-11)

$$M_{\max} = -EI\left(\frac{d^2v}{dx^2}\right)_{x=l/2} = \frac{QkEI}{2P}\tan\frac{kl}{2} = \frac{Ql}{4}\frac{\tan u}{u},$$

if we multiply the bending moment produced by the lateral load by the factor $(\tan u)/u$. The value of this factor, shown in Fig. 2-3, as well as the previous trigonometric factors $\lambda(u)$ and $\chi(u)$, approaches unity as the axial load becomes smaller and smaller and increases indefinitely when the quantity u approaches $\pi/2$, i.e. when the axial load approaches the critical value given by Eq. (1-15).

C.1.4 Beam-Column bending by Couples

Having the solution for a single concentrated lateral load Q (Fig. 1-3) we can now obtain the equation of the deflection curve for the case when a couple is applied at the end of the beam. This is feasible if we assume that the distance c in

Fig. 1-3 decreases to a finite very small value, and, at the same time, Q is increasing, so that the product Qc remains finite and equal to M_b, we obtain the couple M_b acting at the right end of the beam (Fig. 1-4). The deflection curve can then be derived from Eq. (1-7) if we substitute $\sin kc = kc$ and $Qc = M_b$

$$v = \frac{M_b}{P}\left(\frac{\sin kx}{\sin kl} - \frac{x}{l}\right) . \tag{1-18}$$

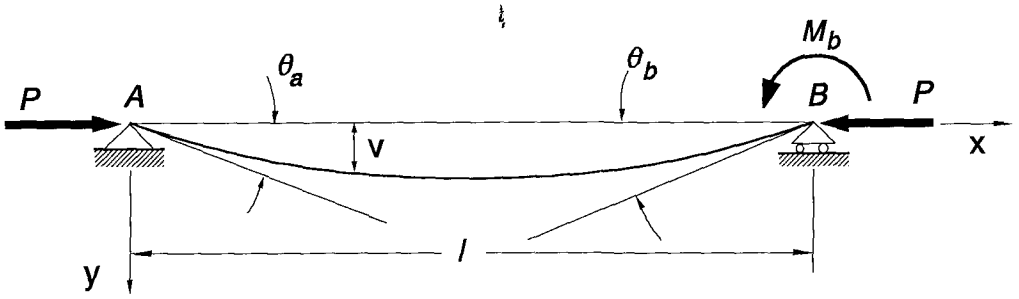

Fig. 1-4

The small angles of rotation θ_a and θ_b at the ends of the bar are considered as positive when the ends rotate in the direction of positive bending moment as shown in Fig. 1-4. Taking the derivative of Eq. (1-18), we obtain

$$\theta_a = \left(\frac{dv}{dx}\right)_{x=0} = \frac{M_b}{P}\left(\frac{k}{\sin kl} - \frac{1}{l}\right) = \frac{M_b l}{6EI}\frac{3}{u}\left(\frac{1}{\sin 2u} - \frac{1}{2u}\right) \tag{1-19}$$

$$\theta_b = -\left(\frac{dv}{dx}\right)_{x=l} = -\frac{M_b}{P}\left(\frac{k\cos kl}{\sin kl} - \frac{1}{l}\right) = \frac{M_b l}{3EI}\frac{3}{2u}\left(\frac{1}{2u} - \frac{1}{\tan 2u}\right) \tag{1-20}$$

It can be seen that the known expressions $M_b l/6EI$ and $M_b l/3EI$, which represent the angles produced by the couple M_b acting alone, are multiplied by trigonometric factors which express the influence of the axial load P on the angles of rotation at the ends of the beam. These factors

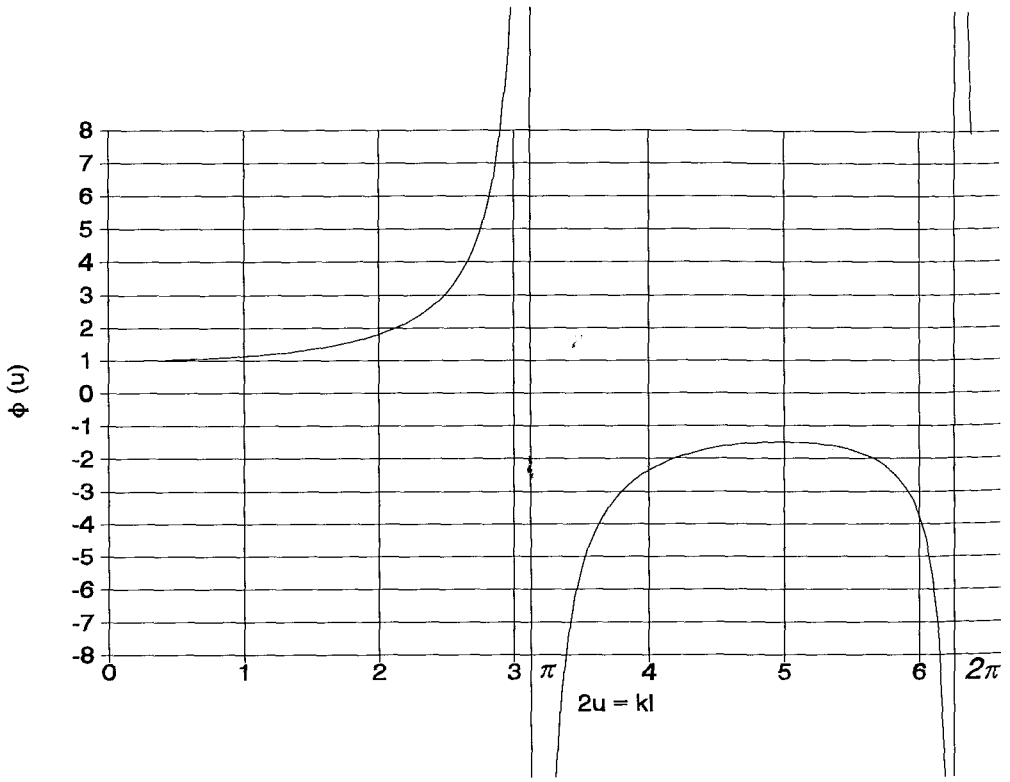

Fig. 1-a

$$\phi(u) = \frac{3}{u}\left(\frac{1}{\sin 2u} - \frac{1}{2u}\right) \tag{1-21}$$

$$\psi(u) = \frac{3}{2u}\left(\frac{1}{2u} - \frac{1}{\tan 2u}\right) \tag{1-22}$$

approach unity when u approaches zero and increase indefinitely as u approaches

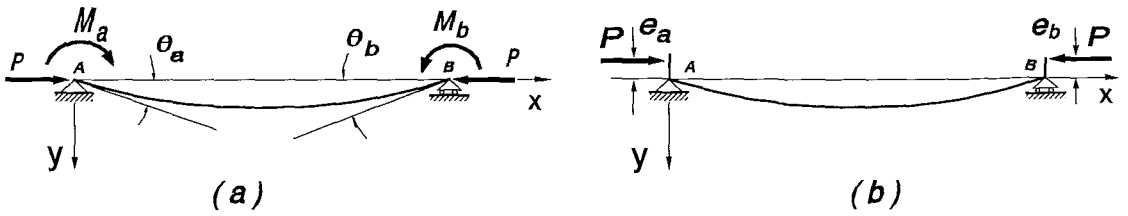

Fig. 1-5

$\pi/2$, as shown in Figs. 1-a and 1-b.

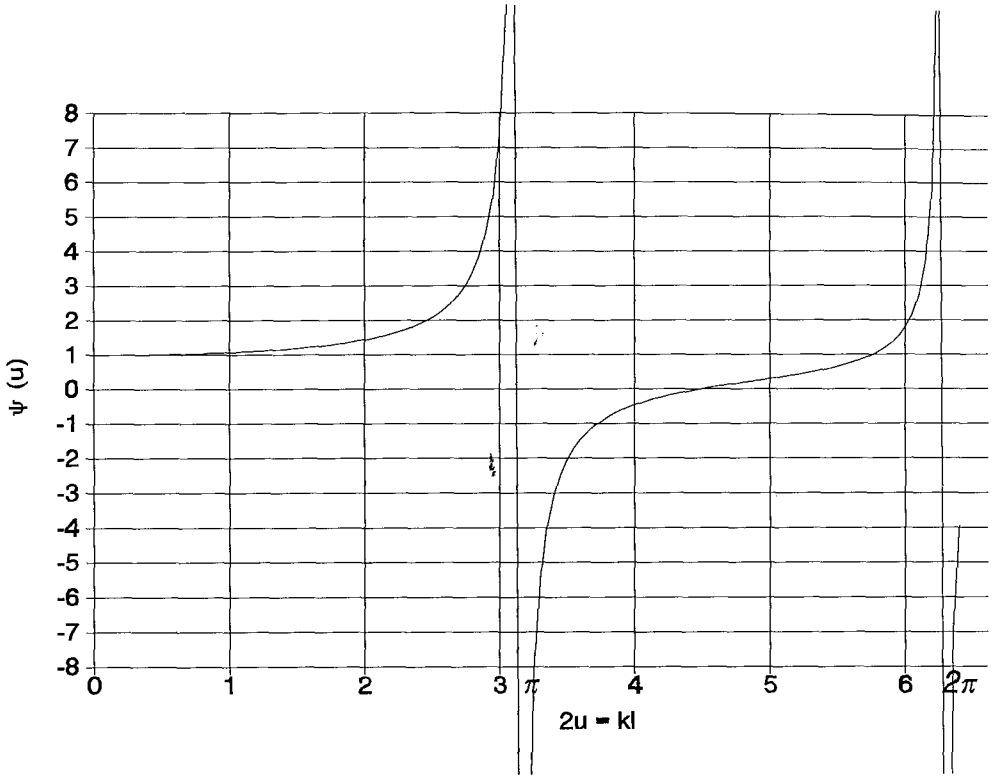

Fig. 1-b

Now if two couples M_a and M_b are applied at the ends A and B of the bar (Fig. 1-5a), the deflection curve can be obtained by superposition. Indeed, from Eq.(1-18) we can take the deflections produced by the couple M_b. Then by substituting M_a for M_b and $(l - x)$ for x in the same equation, we find the deflections produced by the couple M_a. Adding these results together, we can obtain the deflection curve for the case in Fig. 1-5a

$$v = \frac{M_b}{P}\left(\frac{\sin kx}{\sin kl} - \frac{x}{l}\right) + \frac{M_a}{P}\left[\frac{\sin k(l-x)}{\sin kl} - \frac{l-x}{l}\right]. \tag{1-23}$$

This type of loading may occur when two eccentrically applied compressive forces act as shown in Fig. 1-5b. Substituting $M_a = Pe_a$ and $M_b = Pe_b$ in Eq. (1-23), we obtain

$$v = e_b\left(\frac{\sin kx}{\sin kl} - \frac{x}{l}\right) + e_a\left[\frac{\sin k(l-x)}{\sin kl} - \frac{l-x}{l}\right]. \tag{1-24}$$

The angles θ_a and θ_b, giving the rotation at the ends of the bar, in Fig. 1-5a, are obtained from Eqs. (1-19) and (1-20). Then by superposition, we have

$$\theta_a = \frac{M_a l}{3EI}\psi(u) + \frac{M_b l}{6EI}\phi(u) \tag{1-25a}$$

$$\theta_b = \frac{M_b l}{3EI}\psi(u) + \frac{M_a l}{6EI}\phi(u) \tag{1-25b}$$

In the case of two equal couples $M_a = M_b = M_0$, we obtain from Eq. (1-23)

$$\begin{aligned} v &= \frac{M_0}{P\cos\left(\frac{kl}{2}\right)}\left[\cos\left(k\frac{l}{2} - kx\right) - \cos\frac{kl}{2}\right] \\ &= \frac{M_0 l^2}{8EI}\frac{2}{u^2\cos u}\left[\cos\left(u - \frac{2ux}{l}\right) - \cos u\right] \end{aligned} \tag{1-26}$$

The deflection at the centre of the beam can be found from this equation by substituting $x = l/2$

$$\delta = (v)_{x=l/2} = \frac{M_0 l^2}{8EI}\frac{2(1-\cos u)}{u^2\cos u} = \frac{M_0 l^2}{8EI}\lambda(u) \; . \tag{1-27}$$

We can find the angles at the ends by taking the derivative of Eq. (1-26) and substituting $x = 0$. The result is

$$\theta_a = \theta_b = \left(\frac{dv}{dx}\right)_{x=0} = \frac{M_0 l}{2EI}\frac{\tan u}{u} \; . \tag{1-28}$$

The maximum bending moment, occurring at the middle of the bar, is obtained from the second derivative of Eq. (1-26)

$$M_{max} = -EI\left(\frac{d^2v}{dx^2}\right)_{x=l/2} = M_0 \sec u \quad . \tag{1-29}$$

This equation can be used in a bar with eccentrically applied compressive forces (Fig. 1-5b), if both eccentricities are equal. When the axial load P is small in comparison with its critical value, the quantity u is small and sec u can be taken equal to unity, which means that the bending moment can be assumed constant along the length of the bar. As u approaches $\pi/2$ and P approaches P_{cr}, sec u increases indefinitely. At such values of P the slightest eccentricity of the applied load produces a considerable bending moment at the centre of the bar.

C.1.5 Beam-columns with Built-in Ends

Equations (1-7) and (1-8) show that for a given axial load on a beam-column the deflections are proportional to the lateral load Q. At the same time the relation between deflections and axial load is more complicated, since this load enters into the trigonometric functions containing k. The fact that deflections are linear functions of Q indicates that the *principle of superposition*, which is widely used when only lateral loads act on a beam, can also be applied in the case of combined action of lateral and axial loads, but in a somewhat modified form. One can see from Eqs. (1-7) and (1-8) that if we increase the lateral load Q by an amount Q_1, we can obtain the resultant deflection by superposing the deflections produced by the load Q_1 on the corresponding deflections produced by the load Q, provided the *same* axial load acts on the beam.

It can be shown that the method of superposition can be used when several lateral loads act on the compressed bar. The resultant deflections can be obtained by superposition of the deflections produced separately by each lateral load which acts in combination with the axial load.

On the basis of this statement we can write the equation of the deflection

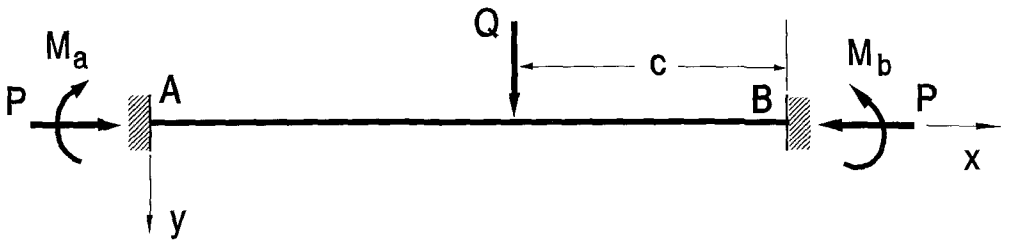

Fig. 1-6

curve of the bar for any number of lateral loads; we can also solve various statically indeterminate problems. Take, for instance, a lateral load Q acting on a beam-column with built-in ends in Fig. 1-6.

The statically indeterminate reactive moments at the ends are found from the conditions that the slopes at the ends are zero. Therefore, for each end of the beam, the rotation produced by the lateral load Q acting alone with hinged ends [found from one of the corresponding equations (1-9) or (1-10)], plus the rotation from the action of both moments [found from equations (1-19) or (1-20) respectively], must be zero. These conditions, for the beam shown in Fig. 1-6, can be expressed by the equations

$$\left.\begin{aligned} \theta_a &= \theta_{0a} + \frac{M_a l}{3EI}\psi(u) + \frac{M_b l}{6EI}\phi(u) = 0 \\ \theta_b &= \theta_{0b} + \frac{M_a l}{6EI}\phi(u) + \frac{M_b l}{3EI}\psi(u) = 0 \end{aligned}\right| , \qquad (1\text{-}30)$$

through which the end moments M_a and M_b can be obtained.

C.1.6 Beam-columns with Elastic Restraints

Considering a more general case of statically indeterminate problem, let us take the beam-column in Fig. 1-7. The beam is connected to vertical bars at A and B and is loaded laterally by the load Q and axially by the force P. If θ_a and θ_b are

respectively the angles of rotation at the ends A and B of the beam, there will be, as a result, couples M_a and M_b which we can express in the form

$$M_a = -\alpha\theta_a , \qquad M_b = -\beta\theta_b . \tag{1-31}$$

The moments and angles of rotation are positive in the directions shown in Fig. 1-7. The factors α and β are coefficients which define the degree of fixity at the ends of the beam and are called *coefficients of end restraint.* Numerically this coefficient is the reactive moment at that end when the rotation is equal to unity. The value of the coefficient may vary from zero (pinned end) to infinity (built-in end). If EI_a is the flexural rigidity of the vertical bar at A which bar is assumed to have hinged ends, the relation between the angle of rotation θ_a and the moment M_a is

$$\theta_a = -\frac{M_a b}{12EI_a}$$

and thus $$\alpha = \frac{12EI_a}{b} .$$

Considering the bending of the bar AB, the angles θ_a and θ_b can be determined from the equations

$$\left.\begin{aligned} \theta_a &= \theta_{0a} + \frac{M_a l}{3EI}\psi(u) + \frac{M_b l}{6EI}\phi(u) \\ \theta_b &= \theta_{0b} + \frac{M_a l}{6EI}\phi(u) + \frac{M_b l}{3EI}\psi(u) \end{aligned}\right| , \tag{1-32}$$

where again the angles θ_{0a} and θ_{0b} are calculated for hinged ends of the beam. Finally , combining the Eqs. (1-31) and (1-32) we obtain the following equations for the moments at the ends

$$\left.\begin{aligned} -\frac{M_a}{\alpha} &= \theta_{0a} + \frac{M_a l}{3EI}\psi(u) + \frac{M_b l}{6EI}\phi(u) \\ -\frac{M_b}{\beta} &= \theta_{0b} + \frac{M_b l}{3EI}\psi(u) + \frac{M_a l}{6EI}\phi(u) \end{aligned}\right| \qquad (1\text{-}33)$$

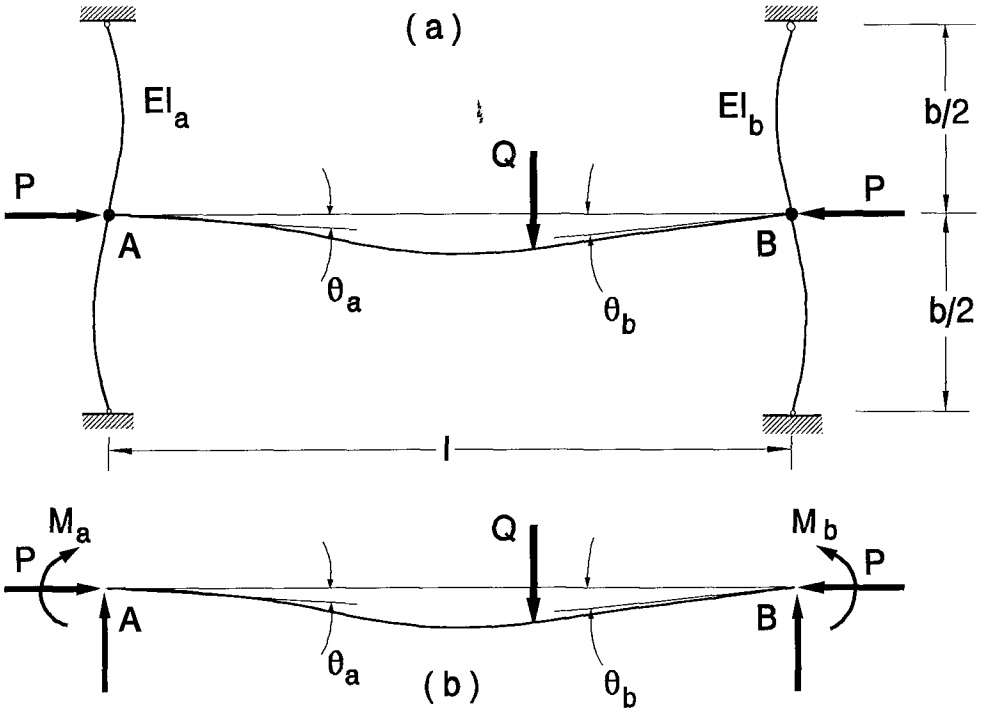

Fig. 1-7

Solving these equations for the moment M_a gives

$$M_\alpha = \frac{-\theta_{0a}\left[\frac{1}{\beta} + \frac{l}{3EI}\psi(u)\right] + \theta_{0b}\left[\frac{l}{6EI}\phi(u)\right]}{\left[\frac{1}{\alpha} + \frac{l}{3EI}\psi(u)\right]\left[\frac{1}{\beta} + \frac{l}{3EI}\psi(u)\right] - \left[\frac{l}{6EI}\phi(u)\right]^2} \qquad (1\text{-}34)$$

The solution for M_b is obtained similarly and has the same expression in the denominator.

Using equations (1-33), we can consider various conditions at the ends of the

beam-column. Taking, for instance, $\alpha = 0$ and $\beta = \infty$, we obtain the case where the left end of the beam is free to rotate while the right end is rigidly built-in. In this case $M_a = 0$ while the moment at the end B, from the second of Eqs. (1-33), is

$$M_b = -\frac{3EI\theta_{0b}}{l\psi(u)} \tag{1-34}$$

By taking $\alpha = \beta = \infty$, we have the case of a beam-column with built-in ends, and Eqs. (1-33) reduce to Eqs. (1-30).

Part 2

Elastic Buckling of Columns and Frames

C.2.1 Differential Equation for Determining Critical Loads

So far the critical load for an ideal column was found by beginning with the differential equation (1-3), which expresses its curvature in terms of the bending moment. An alternate method is to begin with Eq. (1-5)

$$EI\frac{d^4v}{dx^4} + P\frac{d^2v}{dx^2} = q \quad .$$

In determining critical loads of a bar, however, there is no lateral load; hence, the former equation has the form

$$EI\frac{d^4v}{dx^4} + P\frac{d^2v}{dx^2} = 0 \quad ,$$

or, introducing $k^2 = P/EI$, (a)

$$\frac{d^4v}{dx^4} + k^2\frac{d^2v}{dx^2} = 0 \quad . \tag{2-1}$$

The general solution of this equation is

$$v = A\sin kx + B\cos kx + Cx + D \quad . \tag{2-2}$$

The constants in this equation, as well as the value of the critical load, will be found from the end conditions of the bar. A few basic cases will now be considered.

1) Column with hinged ends. In this case the end conditions of the bar are zero deflection and bending moment at both ends; i.e.

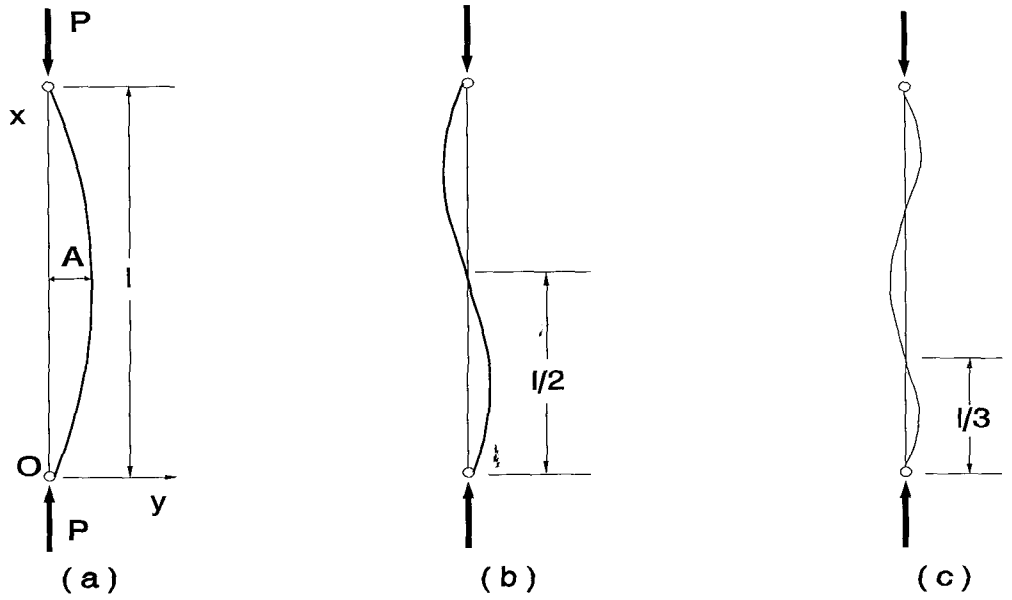

Fig. 2-1

$$v = \frac{d^2v}{dx^2} = 0 \qquad at\ x = 0 \quad and \quad x = l\ .$$

Applying these conditions to the general solution [Eq. (2-2)], results

$$B = C = D = 0\ , \qquad \sin kl = 0$$

and therefore $$kl = i\pi \qquad (i = 1,2,..)\ . \tag{b}$$

The values of critical loads are determined from Eq. (b) in combination with (a). For $i = 1$ the lowest critical load of equation (1-15) is obtained. Higher values of critical load are obtained for $i = 2, 3,..$ from the same equation. The shape of the deflection curve is expressed by the equation

$$v = A\sin kx = A\sin\frac{i\pi x}{l}\ , \tag{c}$$

where A is a constant which has an undetermined amplitude of the deflection. Fig. 2-1 shows the different buckled shapes for $i = 1, 2, 3$.

2) Column with one end fixed and the Other Pinned. For such bar, shown in Fig. (1-2), fixed at the base and pinned at the upper end, a reactive force is

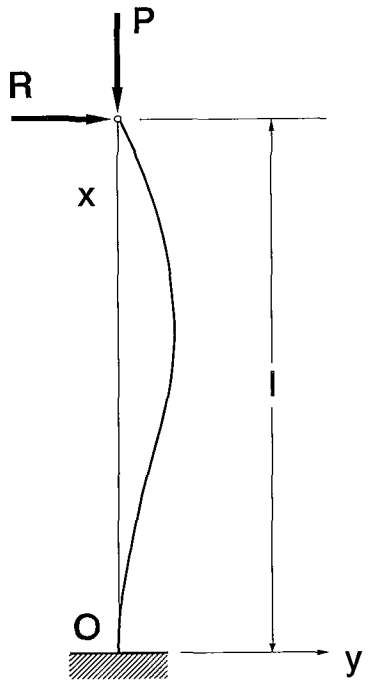

Fig. 2-2

developed when lateral buckling occurs. Its direction is determined by noting that it must oppose the reactive moment at the fixed end. The end conditions are

$$v = \frac{dv}{dx} = 0 \qquad at \quad x = 0$$

$$v = \frac{d^2v}{dx^2} = 0 \qquad at \quad x = l$$

Combining these conditions with the general solution (2-2), results the following system of equations for the constants:

$$\begin{aligned} B + D &= 0 \\ Ak + C &= 0 \\ Cl + D &= 0 \\ A\sin kl + B\cos kl &= 0 \end{aligned}$$

These equations will be satisfied if $A = B = C = D = 0$, where, from Eq. (2-2), the resultant deflection vanishes and we have the straight form of equilibrium. In order to have a buckled shape of equilibrium, we need a solution other than the trivial one. From the first three equations, solving for A in terms of B and substituting into the last one we obtain

$$-B\frac{\sin kl}{kl} + B\cos kl = 0 \ , \qquad \text{or} \qquad \tan kl = kl \ . \qquad (2\text{-}3)$$

This is a transcendental equation which can be solved graphically.

The curves in Fig. 2-3, showing *tan kl* as a function of *kl*, are asymptotic to the vertical lines $kl = \pi/2,\ 3\pi/2,..$ since for these values of *kl*, *tan kl* becomes

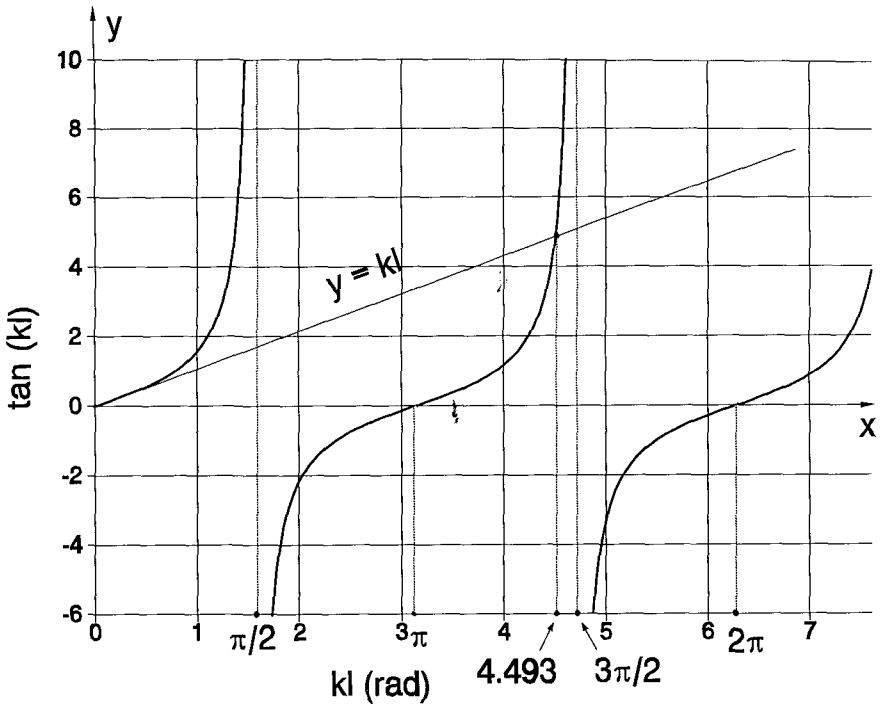

Fig. 2-3

infinite. The roots of Eq. (2-3) are thus the intersection points of the above curves with the line $y = kl$. The smallest root, corresponding to point A, is $kl = 4.493$ and the resulting critical load is

$$P_{cr} = \frac{20.19EI}{l^2} = \frac{\pi^2 EI}{(0.699l)^2} \tag{2-4}$$

This critical load is the same as for a pinned bar having a reduced length of $0.699l$.

3) Fixed end Column. In the case, that both ends of the bar are fixed, the end conditions are

$$v = \frac{dv}{dx} = 0 \qquad at\ x = 0 \quad and \quad x = l\ .$$

These conditions, combined with the general solution, give the following system of equations:

$$\begin{aligned} B + D &= 0 \\ Ak + C &= 0 \\ A\sin kl + B\cos kl + Cl + D &= 0 \\ Ak\cos kl - Bk\sin kl + C &= 0 \end{aligned} \tag{c}$$

In order to have the possibility of curved forms of equilibrium, i.e. non-trivial solution, the determinant of the coefficients of system (c) must be equal to zero. Thus

$$\begin{vmatrix} 0 & 1 & 0 & 1 \\ k & 0 & 1 & 0 \\ \sin kl & \cos kl & l & 1 \\ k\cos kl & -k\sin kl & 1 & 0 \end{vmatrix} = 0 ,$$

which furnishes the equation

$$2(\cos kl - 1) + kl\sin kl = 0 . \tag{d}$$

Substituting $\cos kl = 1 - 2\sin^2(kl/2)$ and $\sin kl = 2\sin(kl/2)\cos(kl/2)$ in (d) and rearranging, results in

$$\sin\frac{kl}{2}\left(\frac{kl}{2}\cos\frac{kl}{2} - \sin\frac{kl}{2}\right) = 0 . \tag{e}$$

One solution of this equation is obtained from

$$\sin\frac{kl}{2} = 0 \quad \text{or} \quad kl = 2i\pi \quad , \text{and therefore}$$

$$P_{cr} = \frac{4i^2\pi^2 EI}{l^2} . \tag{2-5}$$

Using Eqs. (c) and noting that $\sin kl = 0$ and $\cos kl = 1$ whenever $\sin(kl/2) = 0$, we find the following values for the constants:

$$A = C = 0 \quad \textit{and} \quad B = -D \ ,$$

which eventually give the equation of the deflection curve

$$v = B\left(\cos\frac{2i\pi x}{l} - 1\right) \ . \tag{2-6}$$

For $i = 1$, we obtain the lowest critical load $P_{cr} = \dfrac{4\pi^2 EI}{l^2}$, and the column has the symmetrical buckled shape in Fig. 2-4b.

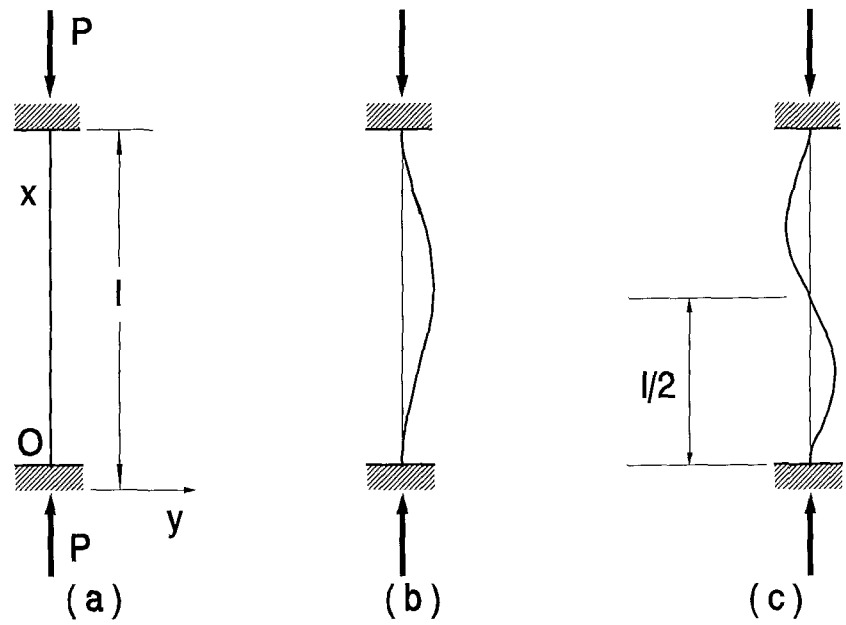

Fig. 2-4

A second solution of Eq. (e) is obtained if we set the term in parentheses equal to zero; the resulting equation is

$$\tan\frac{kl}{2} = \frac{kl}{2} \ ,$$

which, as in case (2), gives the lowest root $kl/2 = 4.493$, and therefore

$$P_{cr} = \frac{8.18\pi^2 EI}{l^2} \quad . \tag{2-7}$$

This critical load corresponds to the antisymmetric buckling shape, shown in Fig. 2-4c. However, this value has no practical interest once it is larger than the previous one of symmetrical pattern.

C.2.2 Critical loads obtained from Beam-column Theory

In many cases, instead of the differential equation of the deflection curve, the problem of calculating critical loads can be tackled by using results obtained from theory of beam-columns. In section 1.3 it was shown that for certain values of axial load P the deflections and bending moments tend to increase indefinitely. Those values of compressive force are evidently critical values.

As an example let us determine the critical loads for a bar with elastically restrained ends (Fig. 1-7). When the bar bears a lateral load, the moments at the ends are obtained from Eqs. (1-33)

$$\left.\begin{aligned} -\frac{M_a}{\alpha} &= \theta_{0a} + \frac{M_a l}{3EI}\psi(u) + \frac{M_b l}{6EI}\phi(u) \\ -\frac{M_b}{\beta} &= \theta_{0b} + \frac{M_b l}{3EI}\psi(u) + \frac{M_a l}{6EI}\phi(u) \end{aligned}\right| \tag{a}$$

where α, β are coefficients of end restraint [see Eq. (1-31)], θ_{0a} and θ_{0b} are the angles of rotation at the ends due to the lateral load only, while the functions $\phi(u)$ and $\psi(u)$ are given by Eqs. (1-21) and (1-22) respectively. The moments M_a and M_b acting at the ends of the bar are positive in the direction shown. The value of M_a, obtained from Eq. (1-34) is

$$M_a = \frac{-\theta_{0a}\left[\frac{1}{\beta} + \frac{l}{3EI}\psi(u)\right] + \theta_{0b}\left[\frac{l}{6EI}\phi(u)\right]}{\left[\frac{1}{\alpha} + \frac{l}{3EI}\psi(u)\right]\left[\frac{1}{\beta} + \frac{l}{3EI}\psi(u)\right] - \left[\frac{l}{6EI}\phi(u)\right]^2},$$

and therefore becomes infinitely large when the denominator is zero. Thus the equation for determining the critical condition is

$$\left[\frac{1}{\alpha} + \frac{l}{3EI}\psi(u)\right]\left[\frac{1}{\beta} + \frac{l}{3EI}\psi(u)\right] - \left[\frac{l}{6EI}\phi(u)\right]^2 = 0 . \qquad (2\text{-}8)$$

For particular values of α and β, this equation can be solved for u and the critical load calculated.

In the particular case of symmetry, shown in Fig. 2-5a, we have

$$\alpha = \beta , \quad \theta_{0a} = \theta_{0b} , \quad M_a = M_b$$

and therefore Eqs. (a) are replaced by the single equation

$$-\frac{M_a}{\alpha} = \theta_{0a} + \frac{M_a l}{3EI}\psi(u) + \frac{M_a l}{6EI}\phi(u) . \qquad (2\text{-}9)$$

If we solve this equation for M_a and set the denominator of the resulting expression equal to zero, we obtain the equation for the critical load

$$\frac{1}{\alpha} + \frac{l}{3EI}\psi(u) + \frac{l}{6EI}\phi(u) = 0 .$$

If now we substitute the expressions for $\psi(u)$ and $\phi(u)$ from Eqs. (1-21) and (1-22), noting that $\tan u = (1 - \cos 2u)/\sin 2u$, we can write this equation in the form

$$\frac{\tan u}{u} = -\frac{2EI}{\alpha l} . \qquad (2\text{-}10)$$

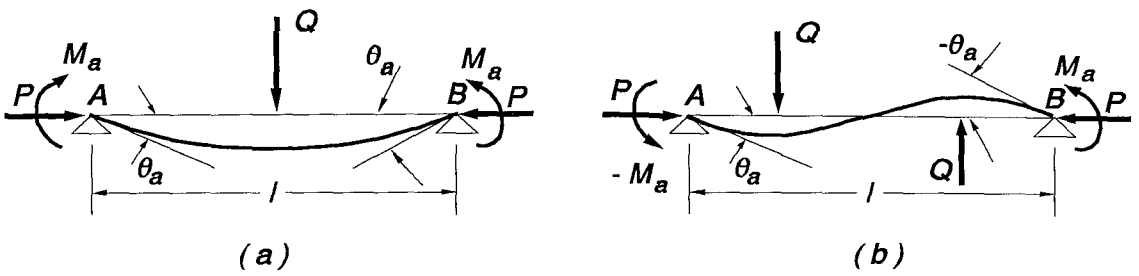

Fig. 2-5

In this equation u may vary between $\pi/2$ and π. The value $\pi/2$ corresponds to $\alpha = 0$, which means that the ends of the bar are free to rotate, and the critical load is given by Eq. (1-15) for the fundamental case. When the ends of the bar are fixed, α becomes infinite; then the value of u is π, and the critical load is $P_{cr} = 4\pi^2 EI/l^2$. For intermediate values of α Eq. (2-10) can be solved using the graph of function $(\tan x)/x$ in Fig.2-3.

For the case of antisymmetrical loading (Fig. 2-5b), we have

$$\alpha = \beta , \quad \theta_{0a} = -\theta_{0b} , \quad M_a = -M_b .$$

The critical load is then determined by the equation

$$\frac{1}{\alpha} + \frac{l}{3EI}\psi(u) - \frac{l}{6EI}\phi(u) = 0$$

or

$$\frac{3}{u}\left(\frac{1}{u} - \frac{1}{\tan u}\right) = -\frac{6EI}{\alpha l} \qquad (2\text{-}11)$$

The critical loads obtained from this equation correspond to antisymmetric buckling shapes. The equation can be solved for any value of α from the graph in Fig. 1-b (on page 10), which give the function $\psi(u)$, since the expression on the left-hand side is the function ψ but with u in place of $2u$.

For $\alpha = 0$ we have the case of pinned ends; then $u = \pi$ and the critical load is $P_{cr} = 4\pi^2 EI/l^2$, corresponding to the buckling pattern in Fig. 2-1b.

For $\alpha = \infty$ we have the case of fixed ends, $u = 4.493$, and the critical load is given by Eq. (2-7).

C.2.3 Buckling of Frames

The method described in the preceding section will be used now for considering the buckling of frames, once each member of a framework with rigid joints is in the same condition of a bar with elastically restrained ends. Consider as an example, the frame ABCD in Fig. 2-6, which is symmetrical horizontally and vertically. The columns AC and BD are compressed by axial loads P, while the whole frame is braced horizontally. The columns begin to buckle when the load P reaches its critical value. This buckling is accompanied by bending of the two horizontal bars AB and CD which exercise reactive moments at the ends of the vertical bars and tend to resist buckling. The moments at the ends are proportional to the angles of joints; the columns can thus considered as bars with elastically restraint ends.

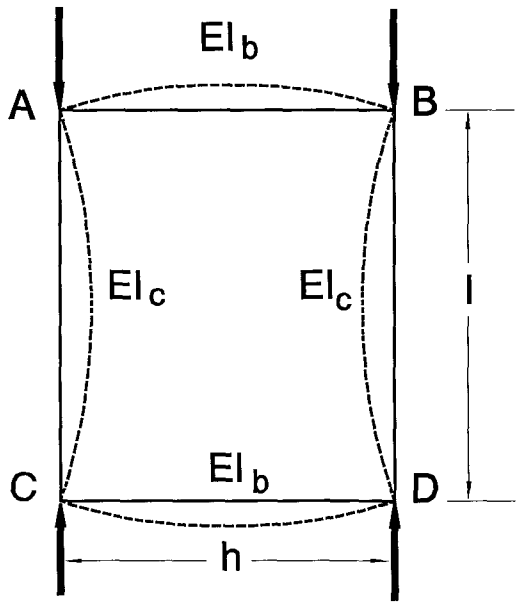

Fig. 2-6

The coefficient of restraint α at the ends of the columns will be found from a bending consideration of the horizontal bars having equal and symmetrical couples at the ends. If EI_b is the flexural rigidity of the horizontal bars, then

$$\alpha = \frac{2EI_b}{h} . \qquad \text{(a)}$$

Since the columns buckle in a **symmetrical pattern**, the critical load can be obtained from Eq. (2-10). Denoting by EI_c the flexural rigidity of the columns, this equation becomes

$$\frac{\tan u}{u} = -\frac{I_c}{I_b}\cdot\frac{h}{l} \qquad \text{(b)}$$

and the critical load can be obtained from this equation for each particular case.

If the frame consists of four identical bars, then $\frac{\tan u}{u} = -1$. The lowest root of this equation is $u = 2.029 = \frac{kl}{2}$, and the critical load is

$$P_{cr} = \frac{16.47 \cdot EI}{l^2}.$$

If the horizontal bars are absolutely rigid, then $I_b = \infty$, and the right-hand side of (b) becomes zero. Then $\tan u = 0$, $u = \pi$, and

$$P_{cr} = \frac{4\pi^2 EI}{l^2},$$

which is the case of column with fixed ends. Finally if $I_b = 0$ we obtain $u = \pi/2$ and $P_{cr} = \frac{\pi^2 EI}{l^2}$, as for a column with pinned ends.

In Fig. 2-7 is shown a buckled frame corresponding to **antisymmetric** buckling shape. In this case the critical load is found from Eq. (2-11) by substituting $\alpha = \frac{6EI_b}{h}$, which is the corresponding coefficient of the horizontal bars by antisymmetric couples at the ends. Then Eq. (2-11) becomes

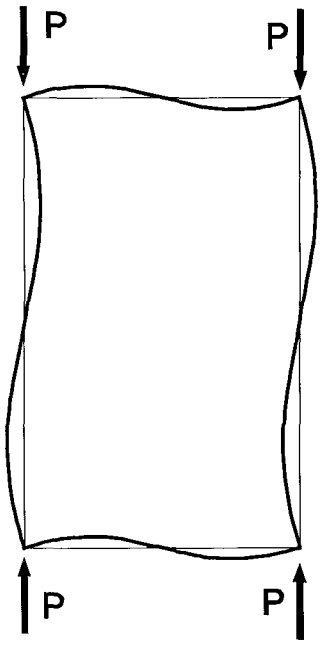

Fig. 2-7

$$\frac{3}{u}\left(\frac{1}{u}-\frac{1}{\tan u}\right) = -\frac{I_c}{I_b}\cdot\frac{h}{l} \quad . \qquad \text{(c)}$$

Critical loads for this buckling mode are larger than those for the symmetrical mode and hence are not usually so important.

Again, if the frame in Fig. 2-7 consists of four identical bars, Eq. (c) becomes $\frac{3}{u}\left(\frac{1}{u}-\frac{1}{tanlu}\right) = -1$. The lowest root of this equation is $u = 3.3805 = \frac{kl}{2}$, and hence

$$P_{cr} = \frac{45.71EI}{l^2} \quad .$$

If the horizontal bars are absolutely rigid, the right-hand side of equation (c) becomes zero. Therefore

$$\frac{1}{u}-\frac{1}{\tan u} = 0, \quad \tan u = u, \quad u = \frac{kl}{2} = 4.493$$

and

$$P_{cr} = \frac{80.75EI}{l^2} \quad .$$

Finally, the case of antisymmetric buckling for a column with pinned ends is obtained if $I_b = 0$. Then $\psi(u) = \infty$, $u = kl/2 = \pi$ (see Fig. 1-b), and

$$P_{cr} = \frac{4\pi^2 EI}{l^2} \quad .$$

If the flexural rigidities of the two horizontal bars of the frame in Fig. 2-6 are

not the same, the end conditions for the compressed column are no longer the same and the critical load will be obtained from Eq. (2-8).

C.2.4 Buckling of Frames with Sway

In the previous discussion it was assumed that the ends of the compressed columns do not displace laterally. The case we consider now in Fig. 2-8, is a frame, whose compressed vertical columns are free to move laterally at the top. If the frame has a vertical axis of symmetry, each vertical column can be considered separately as a compressed bar rotationally free at the lower end and elastically restrained at the upper end. If EI_b and EI_c are the flexural rigidities of the bar and columns respectively, taking a coordinate system of axes as shown in the figure, the differential equation of the deflection curve of the bar is

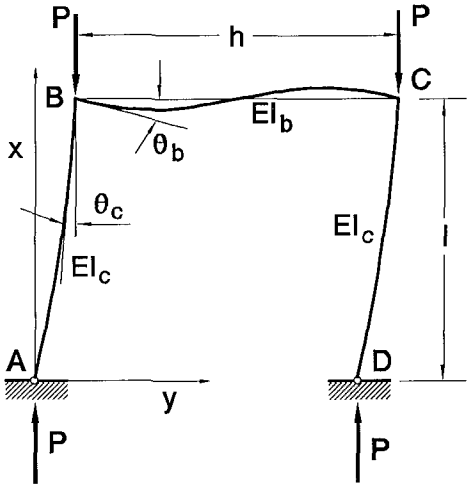

Fig. 2-8

$$EI_c \frac{d^2v}{dx^2} = -Pv \ .$$

By putting $k^2 = P/EI_c$, the solution of this equation, satisfying conditions at the lower end, is

$$v = A \sin kx. \qquad \text{(a)}$$

The angles θ_c and θ_b at the upper end must be equal. Since the horizontal bar is bent by two couples M, each equal to $P(y)_{x=l}$, the coefficient of restraint at the ends of

the bar is $\alpha = 6EI_b/h$. The condition at the upper end, $M = \alpha \cdot \theta$, where θ the angle of rotation at *B*, becomes therefore

$$\left.\frac{dv}{dx}\right|_{x=l} = \frac{h}{6EI_b} P(v)_{x=l}$$

or , combining with expression (a), $$k\cos kl = \frac{Ph\sin kl}{6EI_b} . \qquad (b)$$

In the general case, Eq. (b) can be expressed in the form

$$kl\tan(kl) = 6\frac{I_b}{I_c}\frac{l}{h} . \qquad (c)$$

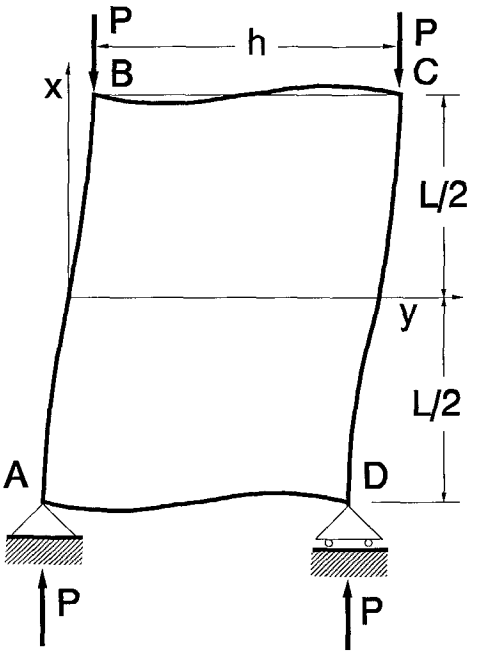

Fig. 2-9

The critical value of the load *P* can be found for any numerical value of the ratio $I_b l/I_c h$. If the horizontal bar is absolutely rigid, then $EI_b = \infty$, and we obtain

$$\tan kl = \infty \quad kl = \frac{\pi}{2} \quad P_{cr} = \frac{\pi^2 EI}{4l^2} .$$

If all three bars of the frame are identical, we obtain $kl\tan kl = 6$, from which, through the graph in Fig. 2-3, we obtain

$$kl = 1.35 \qquad P_{cr} = \frac{1.822EI}{l^2} .$$

In fig. 2-9 a frame similar to that in Fig. 2-6 but subjected to sway is

presented. It is symmetrical with respect to horizontal and vertical axes and its upper part presents exactly the same properties and response with the previous one. Therefore, keeping the same notation apart from the length $L = 2l$ of the columns, we can rewrite equation (c) as

$$k\left(\frac{L}{2}\right)\tan\left(k\frac{L}{2}\right) = 6\frac{I_b}{I_c}\frac{(L/2)}{h} = 3\frac{I_b}{I_c}\frac{L}{h} \qquad \text{(d)}$$

which express the general case of the above frame subject to sway, if both ends of the columns are elastically restrained. As before, if the horizontal bars are absolutely rigid, $EI_b = \infty$, and we obtain

$$\left(k\frac{L}{2}\right) = \frac{\pi}{2} \qquad P_{cr} = \frac{\pi^2 EI}{L^2}.$$

Assuming that all four bars of the frame are identical, we obtain

$$k\frac{L}{2}\tan\left(k\frac{L}{2}\right) = 3$$

from which, through the same graph, it results

$$k\frac{L}{2} = 1.193 \qquad P_{cr} = \frac{5.693EI}{L^2}.$$

Appendix D

Graphs of Parametric Study

The graphs given on the next pages are symbolically chosen to show various capabilities of the computer program listed in Appendix E. This program solves the Eigenvalue Problem for a beam-column considered as a part of a frame for which a sway-mode is possible.

Many of graphs are accompanied from the content of the corresponding files, where the results, in the form of coordinates or else, have been directly allocated through the program.

Attention has been paid so that some necessary information concerning the graph be attached to it.

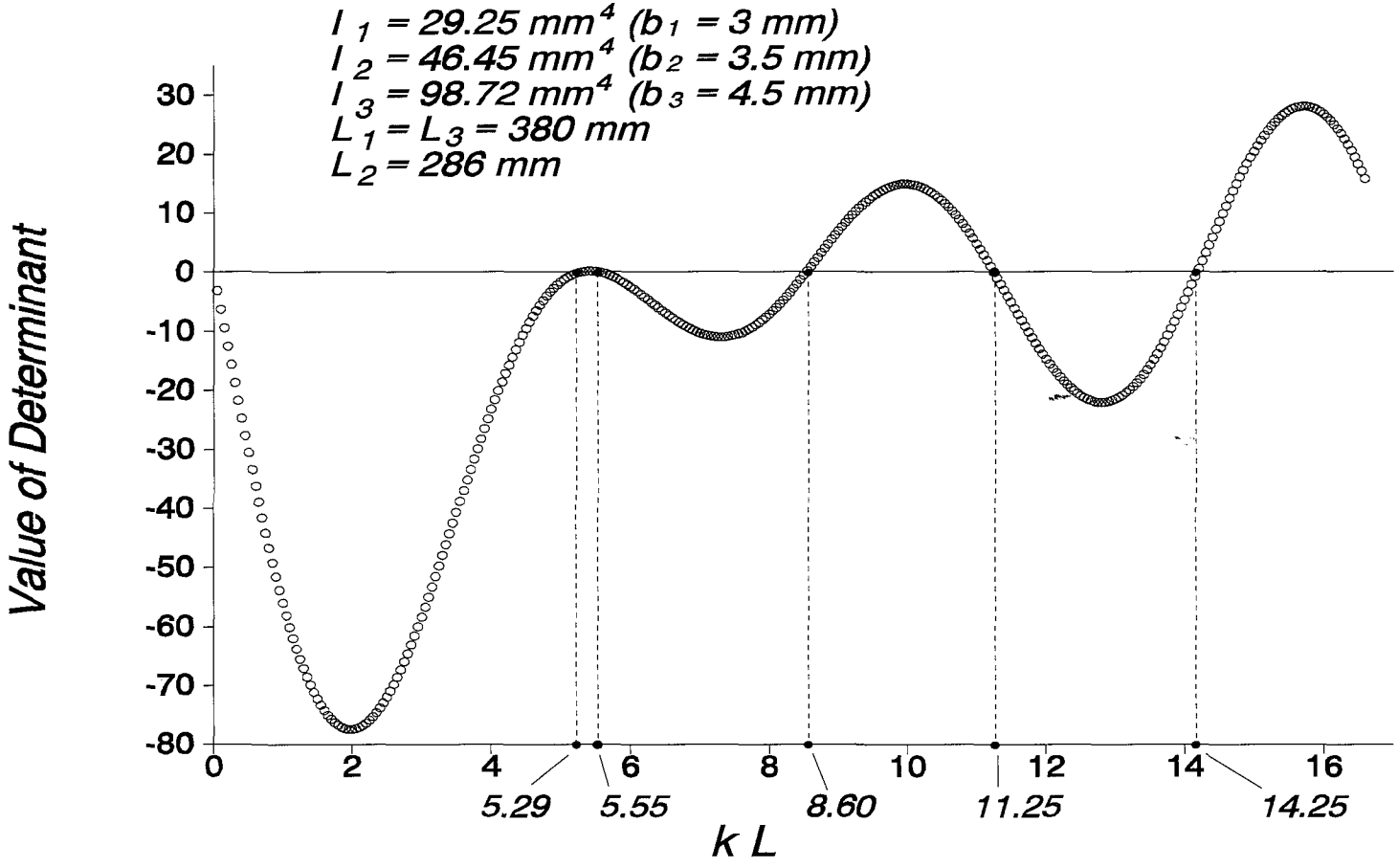
$I_1 = 29.25\ mm^4$ ($b_1 = 3\ mm$)
$I_2 = 46.45\ mm^4$ ($b_2 = 3.5\ mm$)
$I_3 = 98.72\ mm^4$ ($b_3 = 4.5\ mm$)
$L_1 = L_3 = 380\ mm$
$L_2 = 286\ mm$
Value of Determinant
30
20
10
0
-10
-20
-30
-40
-50
-60
-70
-80
0
2
4
6
8
10
12
14
16
5.29
5.55
8.60
11.25
14.25
k L

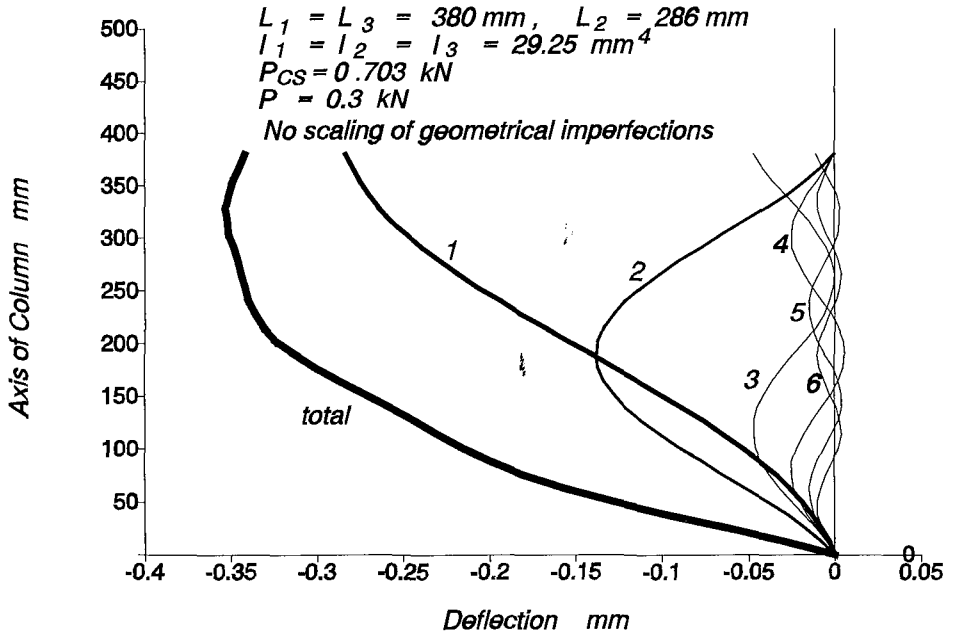

Fig. D-1 Higher mode Eigenvectors multiplied by $w_1^o P/(P_{ci}-P)$

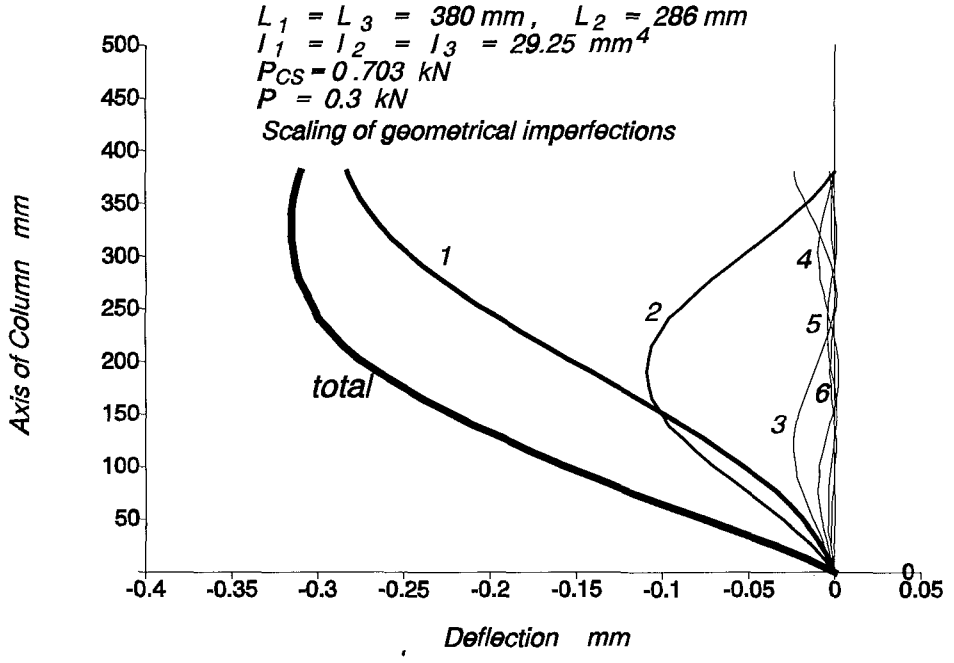

Fig. D-2 Higher mode Eigenvectors multiplied by $w_{i-1}{}^o P\ L_{ei} / (P_{ci} - P)L_{ei-1}$

X	Utotal	U1(X)	U2(X)	U3(X)	U4(X)	U5(X)	U6(X)
0.00	0.000	0.000	0.000	0.000	0.000	0.000	0.000
12.67	-0.016	-0.003	-0.006	-0.003	-0.002	-0.001	-0.001
25.33	-0.035	-0.008	-0.013	-0.006	-0.004	-0.002	-0.002
38.00	-0.056	-0.013	-0.022	-0.009	-0.006	-0.004	-0.002
50.67	-0.077	-0.019	-0.031	-0.013	-0.008	-0.004	-0.002
63.33	-0.099	-0.026	-0.041	-0.016	-0.009	-0.004	-0.002
76.00	-0.120	-0.034	-0.051	-0.019	-0.010	-0.004	-0.001
88.67	-0.139	-0.044	-0.061	-0.022	-0.009	-0.003	0.000
101.33	-0.158	-0.054	-0.071	-0.023	-0.009	-0.002	0.000
114.00	-0.176	-0.065	-0.080	-0.024	-0.007	-0.001	0.001
126.67	-0.192	-0.076	-0.088	-0.024	-0.005	0.000	0.001
139.33	-0.209	-0.088	-0.096	-0.023	-0.003	0.001	0.000
152.00	-0.224	-0.101	-0.101	-0.021	-0.001	0.001	-0.001
164.67	-0.239	-0.114	-0.106	-0.018	0.001	0.001	-0.002
177.33	-0.252	-0.128	-0.108	-0.015	0.002	0.000	-0.002
190.00	-0.265	-0.141	-0.109	-0.012	0.002	-0.002	-0.003
202.67	-0.276	-0.155	-0.108	-0.009	0.002	-0.003	-0.002
215.33	-0.285	-0.168	-0.106	-0.006	0.001	-0.004	-0.002
228.00	-0.292	-0.182	-0.101	-0.003	-0.001	-0.004	-0.001
240.67	-0.299	-0.194	-0.096	-0.001	-0.003	-0.004	0.000
253.33	-0.303	-0.207	-0.088	0.000	-0.005	-0.004	0.001
266.00	-0.307	-0.218	-0.080	0.000	-0.007	-0.003	0.001
278.67	-0.311	-0.229	-0.071	-0.001	-0.009	-0.002	0.000
291.33	-0.313	-0.239	-0.061	-0.002	-0.009	0.000	0.000
304.00	-0.314	-0.248	-0.051	-0.005	-0.010	0.001	-0.001
316.67	-0.315	-0.257	-0.041	-0.008	-0.009	0.001	-0.002
329.33	-0.315	-0.264	-0.031	-0.011	-0.008	0.001	-0.002
342.00	-0.315	-0.270	-0.022	-0.015	-0.006	0.000	-0.002
354.67	-0.314	-0.275	-0.013	-0.018	-0.004	-0.001	-0.002
367.33	-0.312	-0.279	-0.006	-0.022	-0.002	-0.002	-0.001
380.00	-0.310	-0.283	0.000	-0.024	0.000	-0.003	0.000

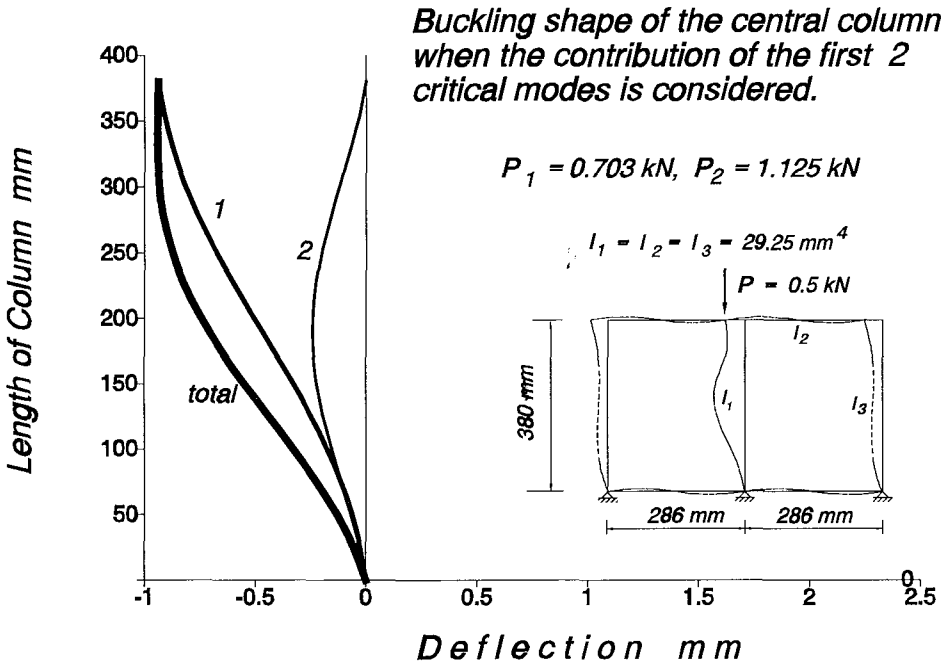
Buckling shape of the central column when the contribution of the first 2 critical modes is considered.
P 1 = 0.703 kN, P2 = 1.125 kN
I1 = I2 = I3 = 29.25 mm4
P = 0.5 kN
380 mm
286 mm
286 mm
Length of Column mm
Deflection mm
total
1
2

Fig. D-3

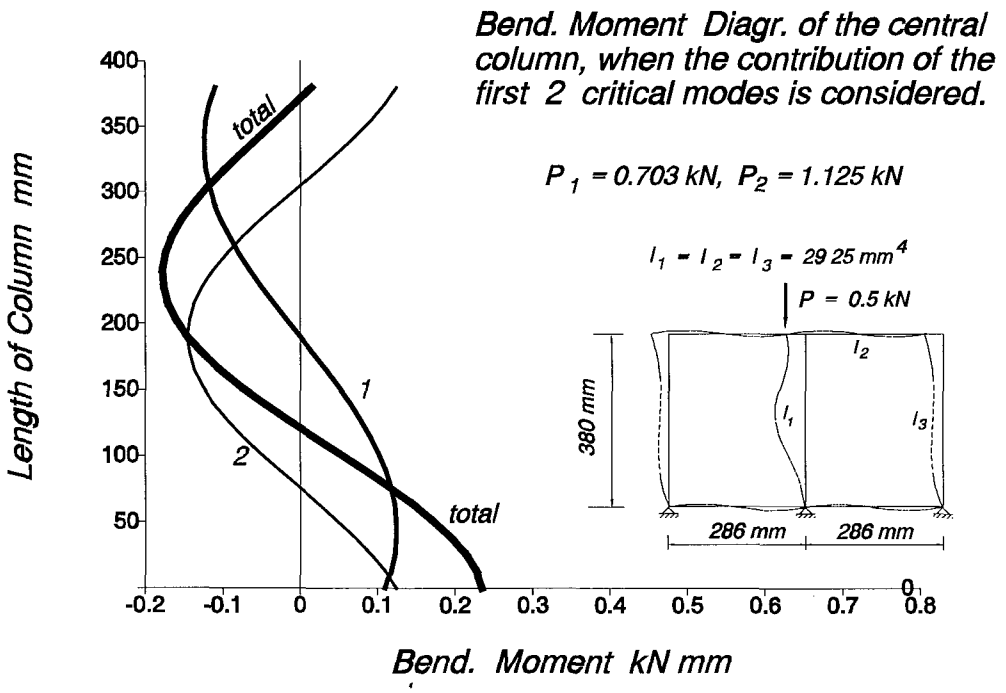
Bend. Moment Diagr. of the central column, when the contribution of the first 2 critical modes is considered.
P 1 = 0.703 kN, P2 = 1.125 kN
I1 = I2 = I3 = 29 25 mm4
P = 0.5 kN
380 mm
286 mm
286 mm
Length of Column mm
Bend. Moment kN mm
total
1
2

Fig. D-4

X	Mtotal	M1(X)	M2(X)
0.00	0.235	0.110	0.125
12.67	0.227	0.117	0.110
25.33	0.214	0.122	0.092
38.00	0.195	0.124	0.071
50.67	0.172	0.124	0.048
63.33	0.146	0.122	0.024
76.00	0.116	0.117	-0.001
88.67	0.084	0.111	-0.026
101.33	0.051	0.102	-0.051
114.00	0.018	0.091	-0.074
126.67	-0.015	0.079	-0.094
139.33	-0.047	0.065	-0.112
152.00	-0.077	0.050	-0.126
164.67	-0.103	0.034	-0.137
177.33	-0.126	0.017	-0.143
190.00	-0.146	0.000	-0.146
202.67	-0.160	-0.017	-0.143
215.33	-0.171	-0.034	-0.137
228.00	-0.176	-0.050	-0.126
240.67	-0.177	-0.065	-0.112
253.33	-0.173	-0.079	-0.094
266.00	-0.165	-0.091	-0.074
278.67	-0.153	-0.102	-0.051
291.33	-0.137	-0.111	-0.026
304.00	-0.119	-0.117	-0.001
316.67	-0.098	-0.122	0.024
329.33	-0.076	-0.124	0.048
342.00	-0.053	-0.124	0.071
354.67	-0.030	-0.122	0.092
367.33	-0.007	-0.117	0.110
380.00	0.015	-0.110	0.125

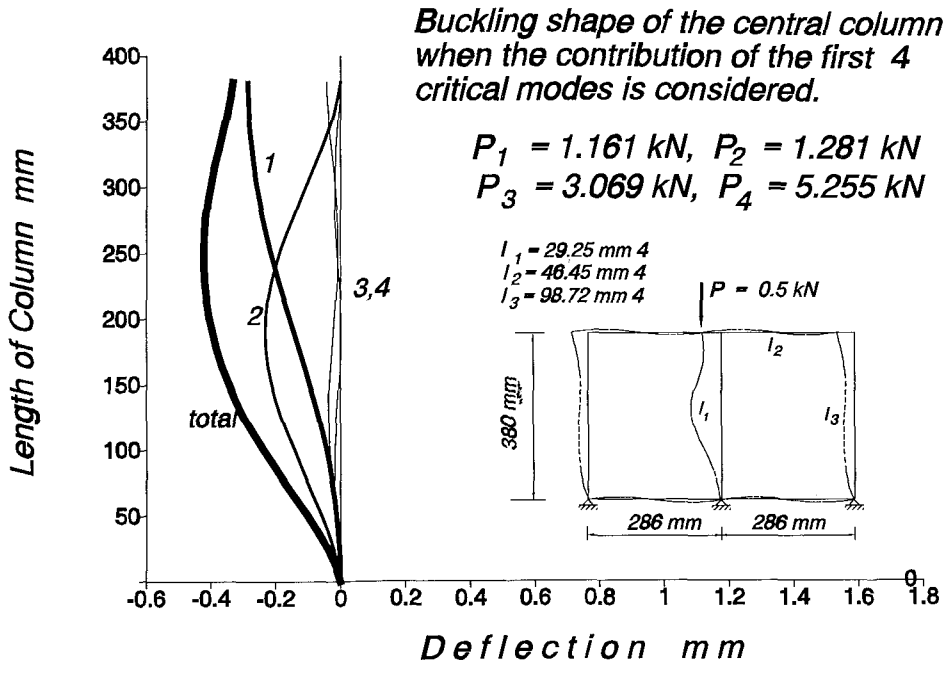
Buckling shape of the central column when the contribution of the first 4 critical modes is considered.
P1 = 1.161 kN, P2 = 1.281 kN
P3 = 3.069 kN, P4 = 5.255 kN
I1 = 29.25 mm 4
I2 = 46.45 mm 4
I3 = 98.72 mm 4
P = 0.5 kN
380 mm
286 mm
286 mm
Length of Column mm
Deflection mm
total
1
2
3,4

Fig. D-5

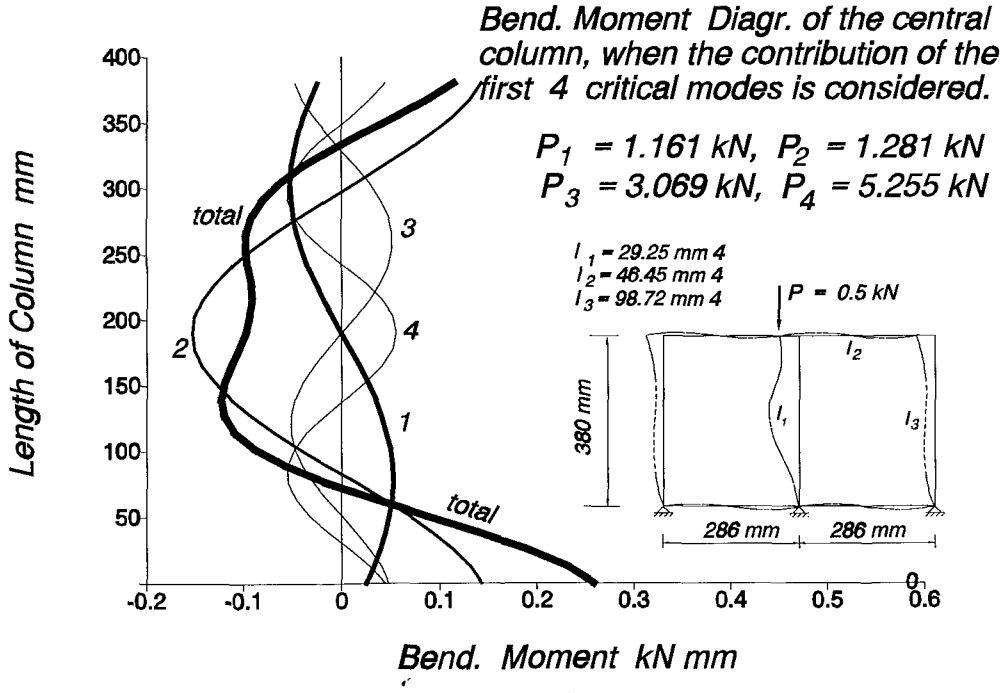
Bend. Moment Diagr. of the central column, when the contribution of the first 4 critical modes is considered.
P1 = 1.161 kN, P2 = 1.281 kN
P3 = 3.069 kN, P4 = 5.255 kN
I1 = 29.25 mm 4
I2 = 46.45 mm 4
I3 = 98.72 mm 4
P = 0.5 kN
380 mm
286 mm
286 mm
Length of Column mm
Bend. Moment kN mm
total
total
1
2
3
4

Fig. D-6

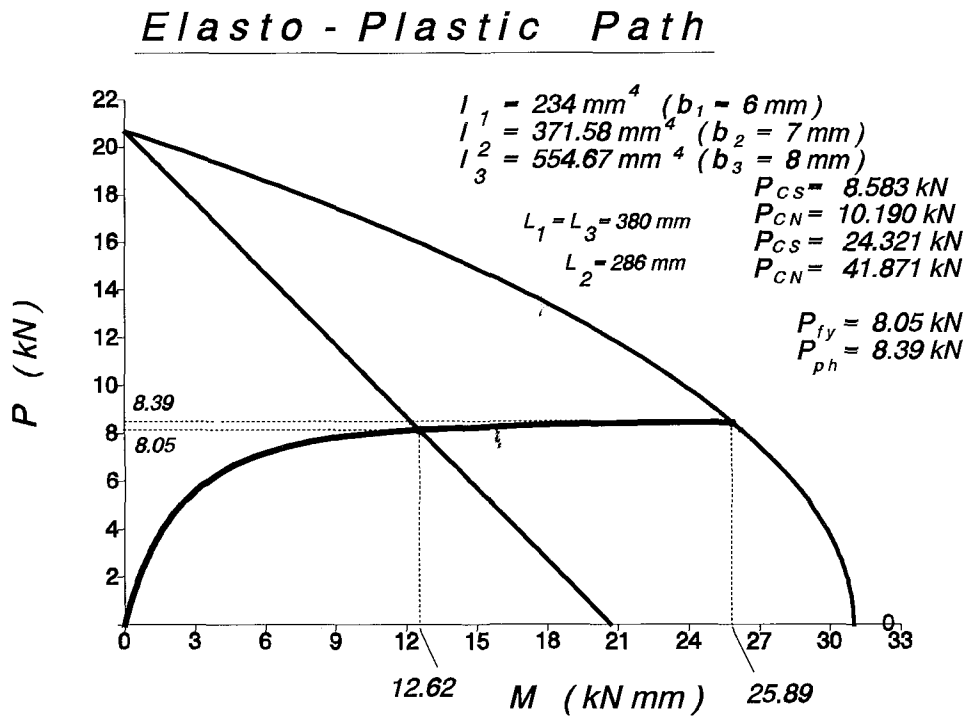
Elasto - Plastic Path
I 1 = 234 mm4 (b1 = 6 mm)
I 2 = 371.58 mm4 (b2 = 7 mm)
I 3 = 554.67 mm 4 (b3 = 8 mm)
L1 = L3 = 380 mm
L2 = 286 mm
Pcs = 8.583 kN
PCN = 10.190 kN
Pcs = 24.321 kN
PCN = 41.871 kN
Pfy = 8.05 kN
Pph = 8.39 kN
8.39
8.05
P (kN)
M (kN mm)
12.62
25.89

Fig. D-7

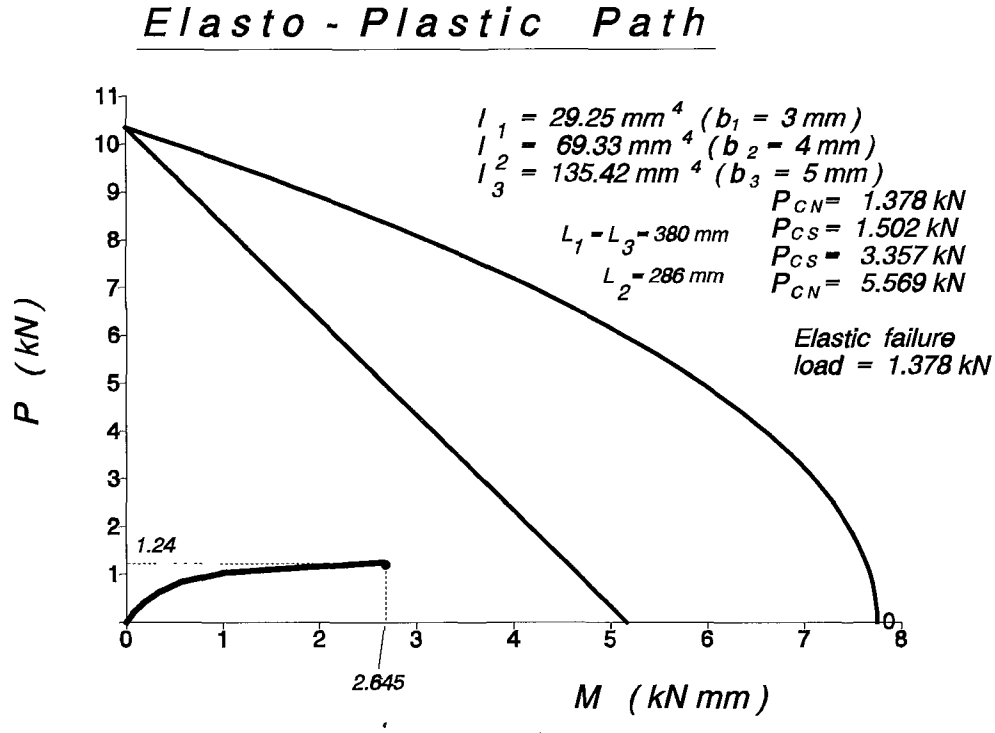
Elasto - Plastic Path
I 1 = 29.25 mm4 (b1 = 3 mm)
I 2 = 69.33 mm 4 (b2 = 4 mm)
I 3 = 135.42 mm 4 (b3 = 5 mm)
L1 = L3 = 380 mm
L2 = 286 mm
PCN = 1.378 kN
Pcs = 1.502 kN
Pcs = 3.357 kN
PCN = 5.569 kN
Elastic failure load = 1.378 kN
1.24
P (kN)
M (kN mm)
2.645

Fig. D-8

The following results are a typical output of the EV-Problem and correspond to the Fig. D-7.

NO. OF PROPERTY SETS = 3

MEM	L	b	d	A	I	Z	Y.str
1	380.00	6.00	13.00	78.00	234.00	78.00	0.265
2	286.00	7.00	13.00	91.00	371.58	106.17	0.265
3	380.00	8.00	13.00	104.00	554.67	138.67	0.265

EIGENVALUES & EIGENVECTORS

Solut	kL	Pc	C1	C2	delta	theta_A	Mode-Case
1	5.083	8.5825	1.00	1.461	-11.114	-0.004	* Sway
2	5.538	10.1897	1.00	-0.391	0.000	0.006	Non-Sway
3	8.556	24.3206	1.00	-0.464	-2.814	-0.013	* Sway
4	11.227	41.8712	1.00	-0.792	0.000	0.023	Non-Sway

First YIELD Load = 8.046 kN

First HINGE Load = 8.393 kN

SQUASH Load = 20.670 kN

The following results are an output of the Elasto-Plastic Analysis and correspond to the Fig. D-7.

P	Mfy	Mph	Non-lin.El.Mom.	Location X
0.000	20.670	31.005	0.000	0.000
0.413	20.257	30.993	0.153	0.000
0.827	19.843	30.955	0.315	0.000

1.240	19.430	30.893	0.488	0.000
1.654	19.016	30.807	0.674	0.000
2.067	18.603	30.695	0.875	0.000
2.480	18.190	30.559	1.092	0.000
2.894	17.776	30.397	1.327	0.000
3.307	17.363	30.211	1.586	0.000
3.721	16.949	30.000	1.871	0.000
4.134	16.536	29.765	2.189	0.000
4.547	16.123	29.504	2.546	0.000
4.961	15.709	29.219	2.953	0.000
5.374	15.296	28.909	3.424	0.000
5.788	14.882	28.574	3.978	0.000
6.201	14.469	28.215	4.646	0.000
6.614	14.056	27.830	5.479	0.000
7.028	13.642	27.421	6.567	0.000
7.441	13.229	26.987	8.097	0.000
7.855	12.815	26.528	10.592	0.000
7.958	12.712	26.409	11.541	0.000
8.010	12.660	26.349	12.142	7.600
8.035	12.635	26.319	12.477	7.600
8.042	12.628	26.312	12.565	7.600
8.045	12.625	26.308	12.610	7.600
8.046	12.624	26.307	12.621	7.600
8.046	12.624	26.307	12.623	7.600
8.046	12.624	26.307	12.624	7.600
8.253	12.417	26.062	17.082	15.200
8.356	12.314	25.938	22.461	30.400
8.382	12.288	25.906	24.711	30.400
8.389	12.281	25.899	25.363	30.400
8.392	12.278	25.895	25.712	38.000
8.393	12.277	25.894	25.804	38.000
8.393	12.277	25.893	25.850	38.000
8.393	12.277	25.893	25.873	38.000

8.393	12.277	25.893	25.885	38.000
8.393	12.277	25.893	25.891	38.000
8.393	12.277	25.893	25.892	38.000
8.393	12.277	25.893	25.893	38.000
8.807	11.863	25.377		
9.220	11.450	24.836		
9.634	11.036	24.270		
10.047	10.623	23.680		
10.460	10.210	23.065		
10.874	9.796	22.425		
11.287	9.383	21.760		
11.701	8.969	21.070		
12.114	8.556	20.356		
12.527	8.143	19.616		
12.941	7.729	18.852		
13.354	7.316	18.064		
13.768	6.902	17.250		
14.181	6.489	16.411		
14.594	6.076	15.548		
15.008	5.662	14.660		
15.421	5.249	13.747		
15.835	4.835	12.810		
16.248	4.422	11.847		
16.661	4.009	10.860		
17.075	3.595	9.848		
17.488	3.182	8.811		
17.902	2.768	7.749		
18.315	2.355	6.663		
18.728	1.942	5.551		
19.142	1.528	4.415		
19.555	1.115	3.254		
19.969	0.701	2.069		
20.382	0.288	0.858		

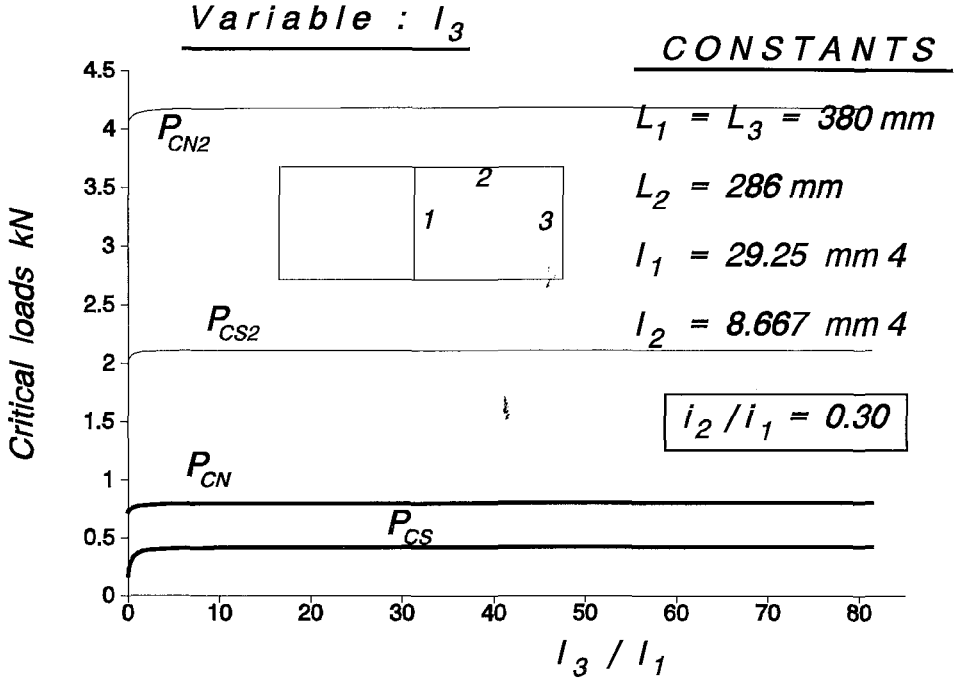

Fig. D-9

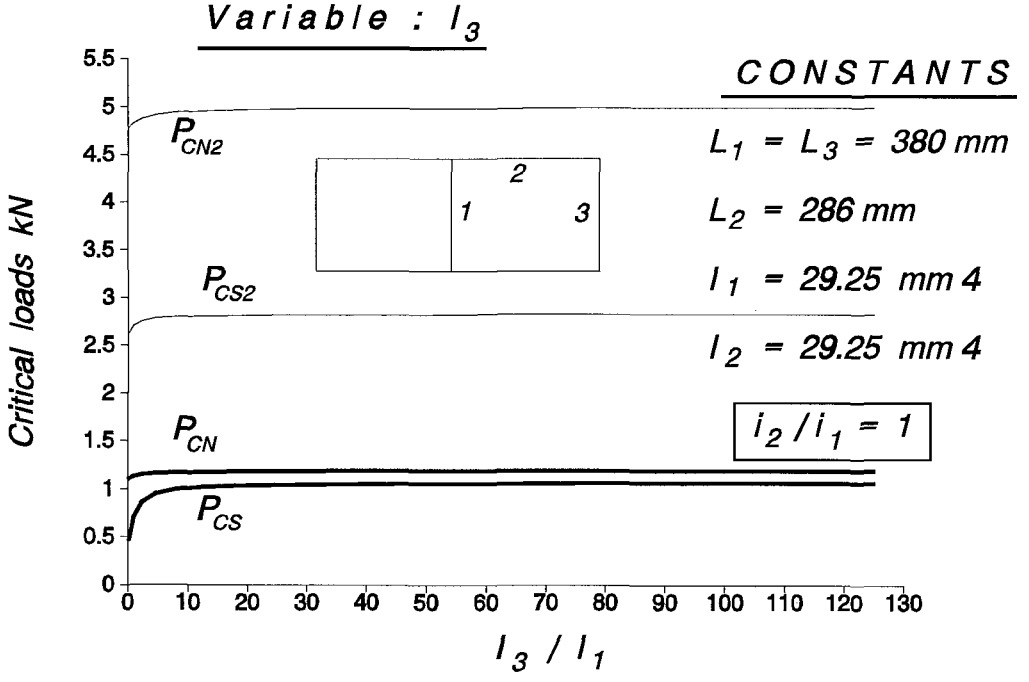

Fig. D-10

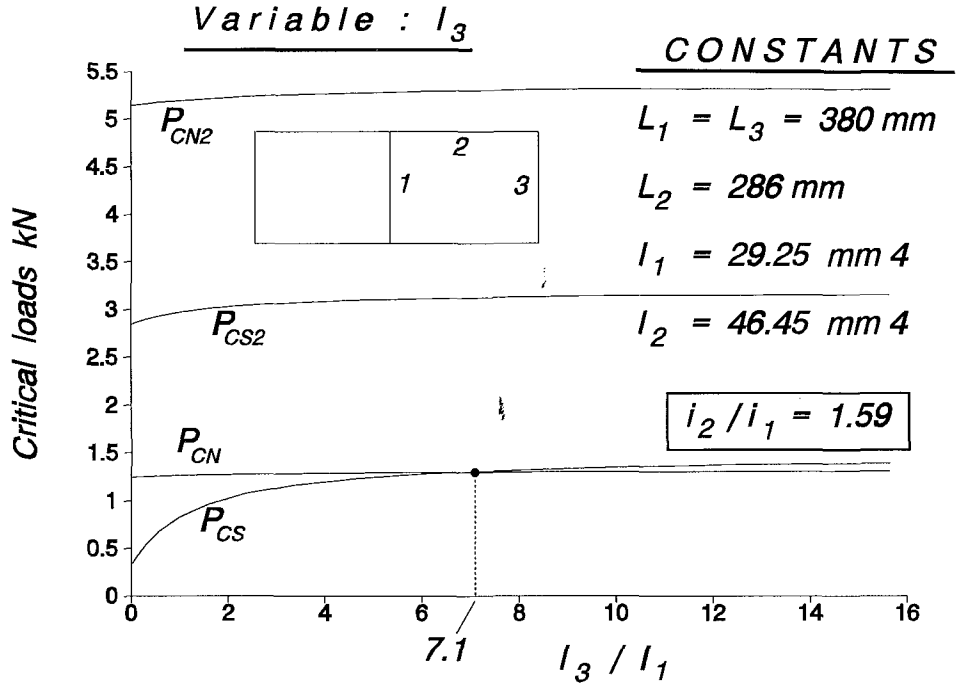

Fig. D-11

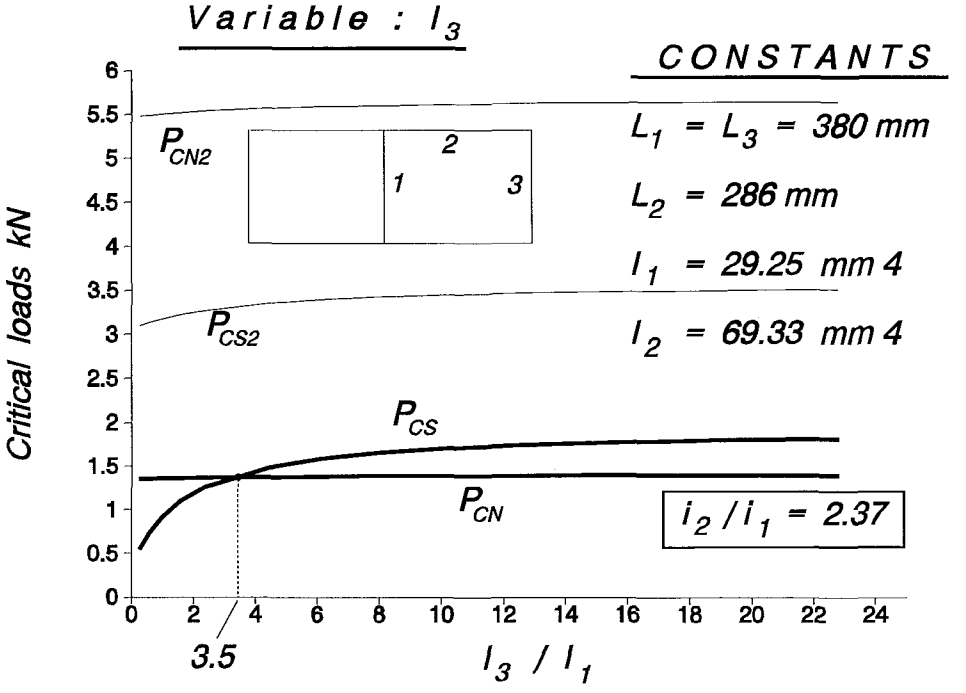

Fig. D-12

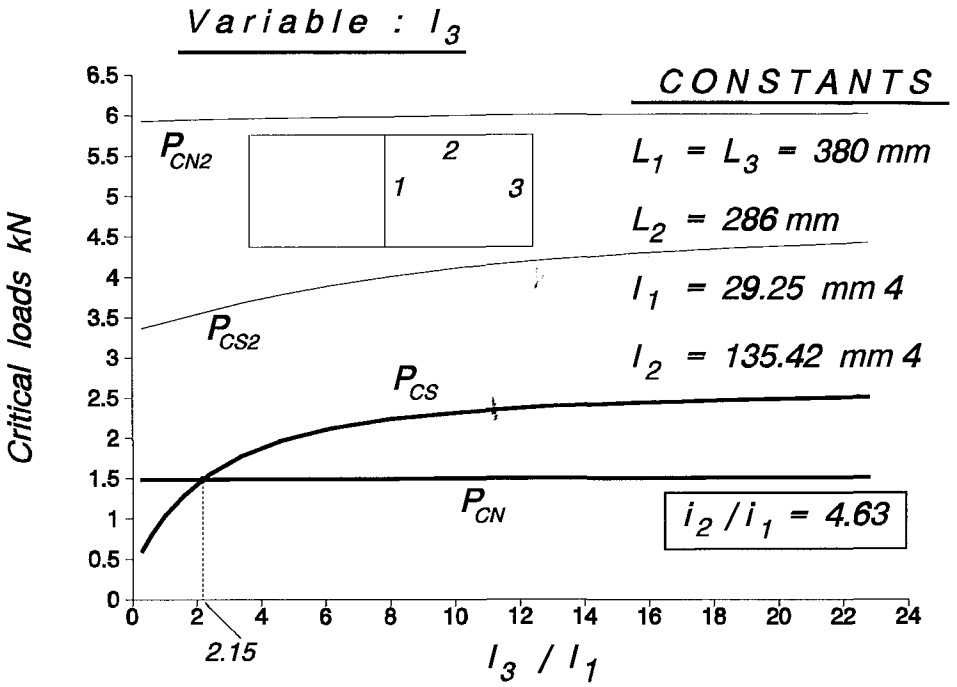

Fig. D-13

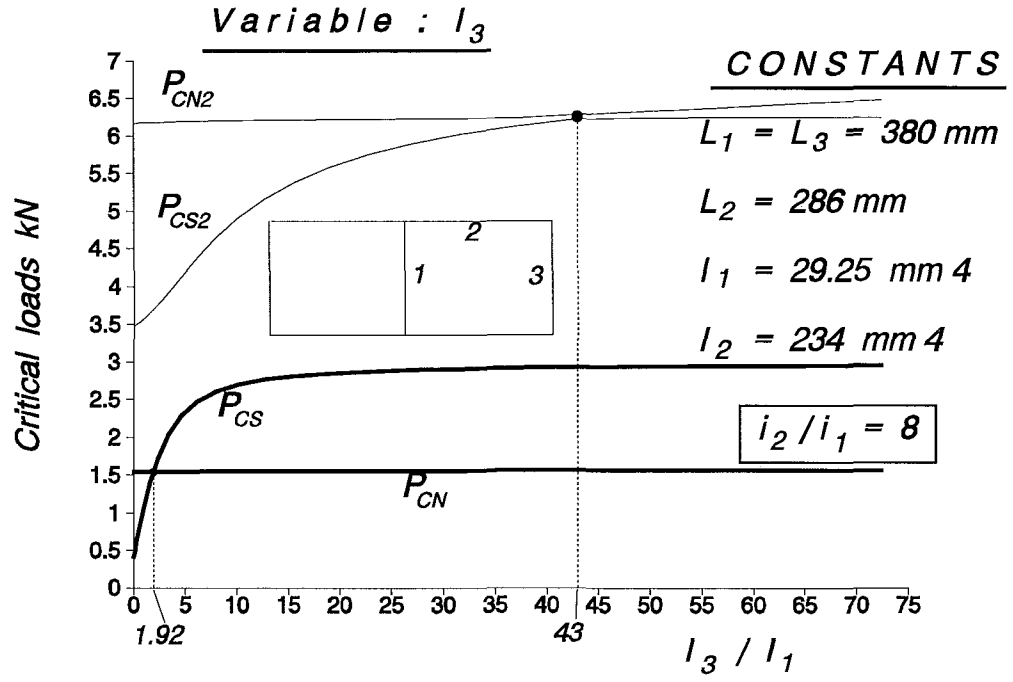

Fig. D-14

This file of results is a typical one

NO. OF PROPERTY SETS = 3

MEM	L	b	d	A	I	Z	Y.str
1	380.00	3.00	13.00	39.00	29.25	19.50	0.265
2	286.00	4.00	13.00	52.00	69.33	34.67	0.265
3	380.00	1.00	13.00	13.00	1.08	2.17	0.265

****

Run 1) EIGENVALUES & EIGENVECTORS (I2/I1 = 2.37)

Solut	kL	Pc	C1	C2	delta	theta_A	Mode-Case
1	2.976	0.3677	1.00	-0.083	-2.219	-0.001	* Sway
2	5.698	1.3484	1.00	-0.301	0.000	0.005	Non-Sway
3	8.581	3.0578	1.00	-0.449	-2.024	-0.010	* Sway
4	11.477	5.4693	1.00	-0.606	0.000	0.018	Non-Sway

Elastic FAILURE Load = 0.368 kN

****

*For the same set of data, but breadth of cross-section, b3 = 1.50 mm, are:

A3 = 19.50 mm2, I3 = 3.66 mm4, Z3 = 4.88 mm3, I3/I1 = 0.13

Run 2) EIGENVALUES & EIGENVECTORS (I2/I1 = 2.37)

Solut	kL	Pc	C1	C2	delta	theta_A	Mode-Case
1	3.253	0.4394	1.00	0.056	-2.731	-0.001	* Sway
2	5.701	1.3495	1.00	-0.300	0.000	0.004	Non-Sway
3	8.600	3.0712	1.00	-0.437	-2.080	-0.010	* Sway
4	11.480	5.4729	1.00	-0.604	0.000	0.018	Non-Sway

Elastic FAILURE Load = 0.439 kN

****

*For the same set of data, but breadth of cross-section, b3 = 2.00 mm, are:

A3 = 26.00 mm2, I3 = 8.67 mm4, Z3 = 8.67 mm3, I3/I1 = 0.30

Run 3) EIGENVALUES & EIGENVECTORS (I2/I1 = 2.37)

Solut	kL	Pc	C1	C2	delta	theta_A	Mode-Case
1	3.680	0.5624	1.00	0.276	-3.704	-0.002	* Sway
2	5.705	1.3515	1.00	-0.297	0.000	0.004	Non-Sway
3	8.634	3.0952	1.00	-0.418	-2.182	-0.010	* Sway
4	11.487	5.4794	1.00	-0.599	0.000	0.018	Non-Sway

Elastic FAILURE Load = 0.562 kN

****

*For the same set of data, but breadth of cross-section, b3 = 2.50 mm, are:

A3 = 32.50 mm2, I3 = 16.93 mm4, Z3 = 13.54 mm3, I3/I1 = 0.58

Run 4) EIGENVALUES & EIGENVECTORS (I2/I1 = 2.37)

Solut	kL	Pc	C1	C2	delta	theta_A	Mode-Case
1	4.187	0.7280	1.00	0.576	-5.278	-0.002	* Sway
2	5.711	1.3545	1.00	-0.294	0.000	0.004	Non-Sway
3	8.682	3.1298	1.00	-0.390	-2.338	-0.010	* Sway
4	11.498	5.4894	1.00	-0.592	0.000	0.018	Non-Sway

First YIELD Load = 0.720 kN

Elastic FAILURE Load = 0.728 kN

****

*For the same set of data, but breadth of cross-section, b3 = 3.00 mm, are:

A3 = 39.00 mm2, I3 = 29.25 mm4, Z3 = 19.50 mm3, I3/I1 = 1.00

Run 5) EIGENVALUES & EIGENVECTORS (I2/I1 = 2.37)

Solut	kL	Pc	C1	C2	delta	theta_A	Mode-Case
1	4.692	0.9141	1.00	0.980	-7.648	-0.003	* Sway
2	5.720	1.3585	1.00	-0.289	0.000	0.004	Non-Sway
3	8.741	3.1728	1.00	-0.356	-2.541	-0.010	* Sway
4	11.511	5.5026	1.00	-0.583	0.000	0.018	Non-Sway

Elastic FAILURE Load = 0.914 kN

****

*For the same set of data, but breadth of cross-section, b3 = 3.50 mm, are:

A3 = 45.50 mm2, I3 = 46.45 mm4, Z3 = 26.54 mm3, I3/I1 = 1.59

Run 6) EIGENVALUES & EIGENVECTORS (I2/I1 = 2.37)

Solut	kL	Pc	C1	C2	delta	theta_A	Mode-Case
1	5.139	1.0968	1.00	1.554	-11.207	-0.003	* Sway
2	5.730	1.3632	1.00	-0.284	0.000	0.004	Non-Sway
3	8.807	3.2206	1.00	-0.319	-2.777	-0.009	* Sway
4	11.528	5.5182	1.00	-0.572	0.000	0.017	Non-Sway

Elastic FAILURE Load = 1.097 kN

****

*For the same set of data, but breadth of cross-section, b3 = 4.00 mm, are:

A3 = 52.00 mm2, I3 = 69.33 mm4, Z3 = 34.67 mm3, I3/I1 = 2.37

Run 7) EIGENVALUES & EIGENVECTORS (I2/I1 = 2.37)

Solut	kL	Pc	C1	C2	delta	theta_A	Mode-Case
1	5.507	1.2593	1.00	2.445	-16.830	-0.004	* Sway
2	5.740	1.3682	1.00	-0.278	0.000	0.004	Non-Sway
3	8.873	3.2692	1.00	-0.283	-3.028	-0.009	* Sway
4	11.545	5.5352	1.00	-0.560	0.000	0.017	Non-Sway

Elastic FAILURE Load = 1.259 kN

****

This file of results is a summary of the previous one

I3/I1	Pcr 1	Pcr 2	Pcr 3	Pcr 4
0.04	0.368	1.348	3.058	5.469
0.13	0.439	1.350	3.071	5.473
0.30	0.562	1.352	3.095	5.479
0.58	0.728	1.355	3.130	5.489
1.00	0.914	1.358	3.173	5.503
1.59	1.097	1.363	3.221	5.518
2.37	1.259	1.368	3.269	5.535

Appendix E

Experimental Data and Results

In this appendix the experimental data and results are presented in a way that they might be used in the future as reference.

The way in which the results are presented is similar with that used in Chapter 7, where, three different groups of buckling behaviours, the elastic, the elasto-plastic and the plastic collapse were listed for each frame geometry.

Each experimental presentation consists, due to lack of space, of three only pages.

On the first page the date number and the group of experiment are standing as title, while the full experimental data along with the results of Southwell plots for both modes are tabulated.

The Southwell Plots are provided along with the critical loads and total equivalent imperfections for both modes on the second page. These two pages are similar to what in Chapter 7 is presented as a sample.

On the third page a load vs both displacements diagram is shown for both the loading and unloading stages. The theoretically obtained results for the imperfections that result from Southwell Plots are also presented on the same page for comparison reasons.

Test: 18oc1
Elastic Buckling

Experimental Data					Southwell Plot			
Load P kN	Loading		Unloading		Sway Mod		Non-Sway Mode	
	Top reads	Mid reads	Top reads	Mid reads	$\frac{\delta_t}{100}$ mm	$\frac{\delta_t}{100P}$ mm/kN	$\frac{\delta_m-\delta_t/2}{100}$ mm	$\frac{\delta_m-\delta_t/2}{100P}$ mm/kN
0	670	1360	670	1362	0.000	0.000	0.000	0.000
0.3	670.5	1360.5	676	1364	0.005	0.017	0.008	0.025
0.6	672.5	1360.5	682.5	1365	0.025	0.042	0.018	0.029
0.9	675.5	1360.5	692	1365	0.055	0.061	0.033	0.036
1.2	679	1362	700	1365.5	0.090	0.075	0.065	0.054
1.5	684	1363	710	1367	0.140	0.093	0.100	0.067
1.8	689	1363.5	718	1368	0.190	0.106	0.130	0.072
2.1	695	1365	728.5	1368	0.250	0.119	0.175	0.083
2.4	705.5	1364.5	740.5	1368.5	0.355	0.148	0.223	0.093
2.7	716.5	1363.5	7522	1368.5	0.465	0.172	0.268	0.099
3	726.5	1363	765	1368	0.565	0.188	0.313	0.104
3.3	739	1362.5	780	1367	0.690	0.209	0.370	0.112
3.6	752.5	1361.5	795	1365	0.825	0.229	0.428	0.119
3.8	764	1360	805	1364.5	0.940	0.247	0.470	0.124
4	775	1358	817.5	1362	1.050	0.263	0.505	0.126
4.2	787.5	1357.5	829	1360.5	1.175	0.280	0.563	0.134
4.4	799.5	1356	841	1359	1.295	0.294	0.608	0.138
4.6	814	1355	856	1356	1.440	0.313	0.670	0.146
4.8	830	1352.5	873	1352	1.600	0.333	0.725	0.151
5	844.5	1351	887	1347	1.745	0.349	0.783	0.157
5.2	863.5	1348	903	1344	1.935	0.372	0.848	0.163
5.4	879	1347	915.5	1340.5	2.090	0.387	0.915	0.169
5.6	897	1345.5	925	1340	2.270	0.405	0.990	0.177
5.8	921	1341	932	1340	2.510	0.433	1.065	0.184
6	945	1337	945	1337	2.750	0.458	1.145	0.191

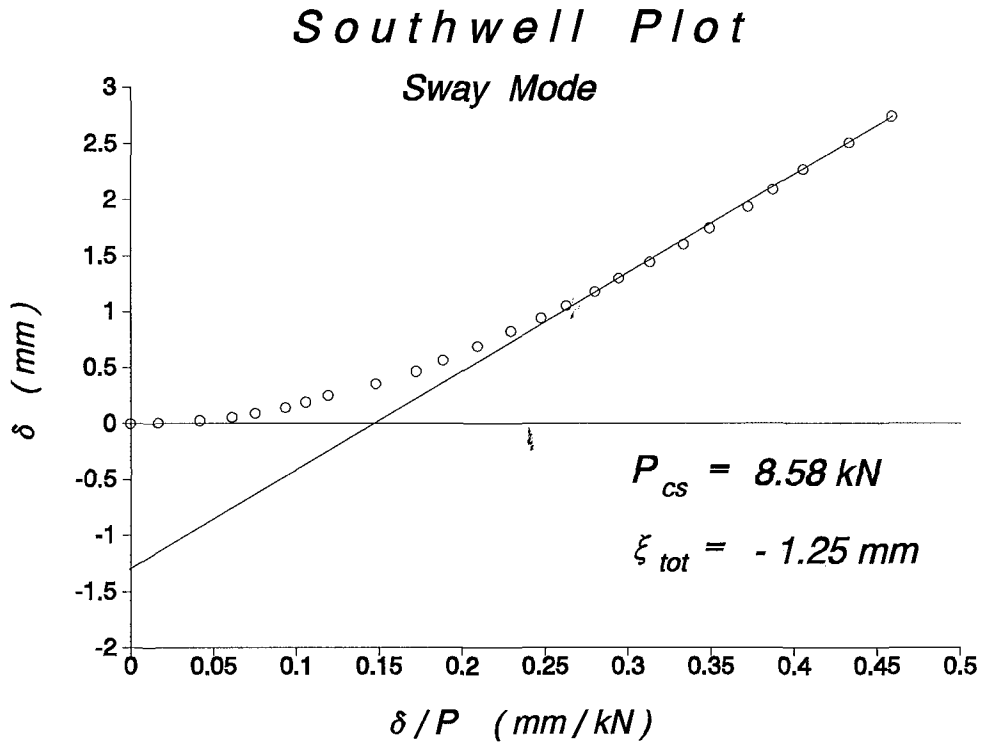
Southwell Plot
Sway Mode
δ (mm)
δ / P (mm / kN)
P cs = 8.58 kN
ξ tot = - 1.25 mm
3
2.5
2
1.5
1
0.5
0
-0.5
-1
-1.5
-2
0
0.05
0.1
0.15
0.2
0.25
0.3
0.35
0.4
0.45
0.5

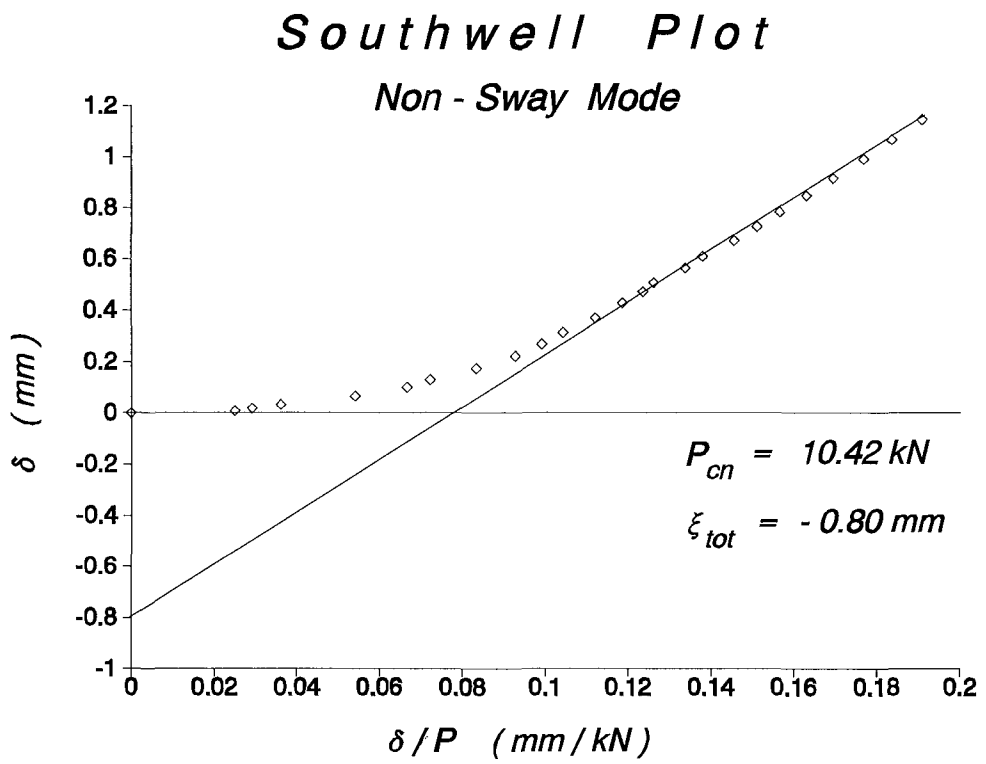
Southwell Plot
Non - Sway Mode
δ (mm)
δ / P (mm / kN)
P cn = 10.42 kN
ξ tot = - 0.80 mm
1.2
1
0.8
0.6
0.4
0.2
0
-0.2
-0.4
-0.6
-0.8
-1
0
0.02
0.04
0.06
0.08
0.1
0.12
0.14
0.16
0.18
0.2

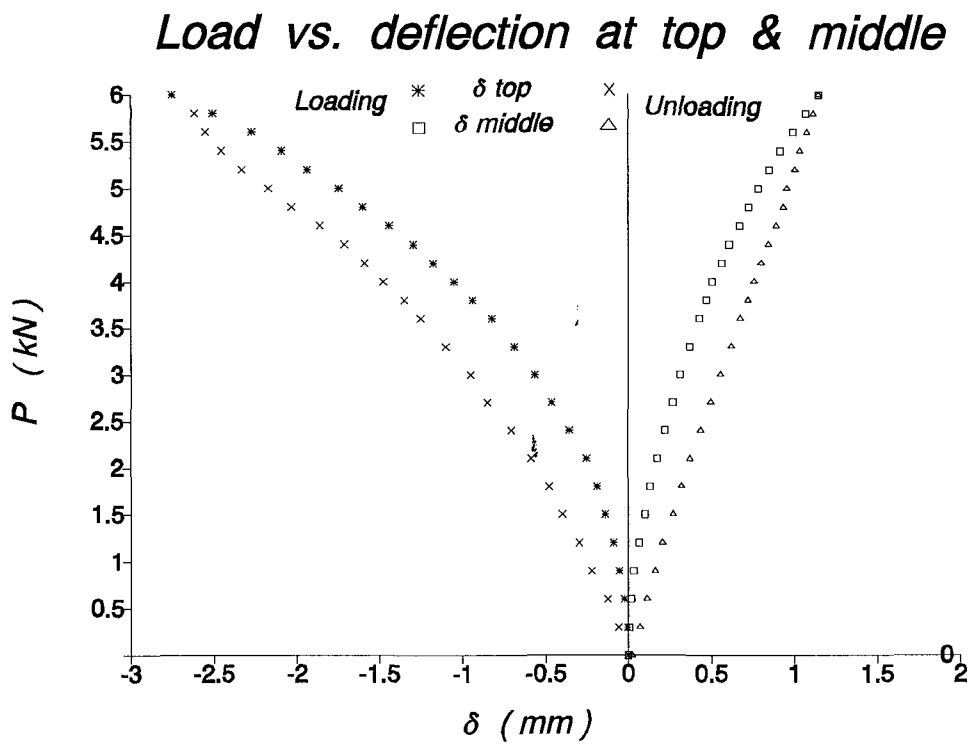

THEORETICAL DATA & RESULTS

PROP_sets = 3, SWAY_imp = 1.25 mm, NON-SWAY_imp = -0.80 mm

MEMBER PROPERTIES

MEM	L	b	d	A	I	Zel	Zpl	Y.str
1	280.0	6.0	13.0	73.44	209.00	69.67	117.71	0.360
2	300.0	5.0	13.0	62.44	125.70	50.28	81.45	0.360
3	280.0	5.0	13.0	62.44	125.70	50.28	81.45	0.360

Rotational SYMMETRIC (Non-sway) Stiffness of frame : 802.89 kN*mm/rad

Rotational ANTISYMMETRIC (Sway) Stiffness of frame : 980.22 kN*mm/rad

Translational (Sway) Stiffness of frame : 19.03 N/mm

EIGENVALUES & EIGENVECTORS

Solut	kL	Pc	C1	C2	delta	theta_A	Mode-Case
1	3.932	8.0359	1.00	0.417	-5.935	-0.008	* Sway
2	4.842	12.1892	1.00	-0.878	0.000	0.015	Non-Sway

First YIELD Load = 7.082 kN

First HINGE Load = 7.626 kN

SQUASH Load = 26.437 kN

Test: 16oc1
Elastic Buckling

Experimental Data					Southwell Plot			
	Loading		Unloading		Sway Mode		Non-Sway Mode	
Load P kN	Top reads	Mid reads	Top reads	Mid reads	$\frac{\delta_t}{100}$ mm	$\frac{\delta_t}{100P}$ mm/kN	$\frac{\delta_m-\delta_t/2}{100}$ mm	$\frac{\delta_m-\delta_t/2}{100P}$ mm/kN
0	953	1526	967	1522	0.000	0.000	0.000	0.000
0.3	955	1526	975	1520	0.020	0.067	0.010	0.033
0.6	960	1526	983.5	1519	0.070	0.117	0.035	0.058
0.9	964	1526	990	1519	0.110	0.122	0.055	0.061
1.2	969	1526	998	1518.5	0.160	0.133	0.080	0.067
1.5	973	1527	1005	1518	0.200	0.133	0.110	0.073
1.8	980	1527	1015	1518	0.270	0.150	0.145	0.081
2.1	988	1528	1024	1518	0.350	0.167	0.195	0.093
2.4	997	1528	1034	1518	0.440	0.183	0.240	0.100
2.7	1007	1529	1047	1518	0.540	0.200	0.300	0.111
3	1019	1530	1060	1516	0.660	0.220	0.370	0.123
3.2	1029	1530	1070	1517	0.760	0.238	0.420	0.131
3.4	1039	1530	1078	1517	0.860	0.253	0.470	0.138
3.6	1047	1530.5	1089	1516	0.940	0.261	0.515	0.143
3.8	1059.5	1530.5	1097.5	1517	1.065	0.280	0.578	0.152
4	1069	1531	1102.5	1520	1.160	0.290	0.630	0.158
4.1	1076	1531	1106.5	1521	1.230	0.300	0.665	0.162
4.2	1082	1531.5	1110	1522.5	1.290	0.307	0.700	0.167
4.3	1089	1531.5	1114	1524	1.360	0.316	0.735	0.171
4.4	1096	1531.5	1118	1525.5	1.430	0.325	0.770	0.175
4.5	1106	1531	1120	1526.5	1.530	0.340	0.815	0.181
4.6	1115	1530	1115	1530	1.620	0.352	0.850	0.185

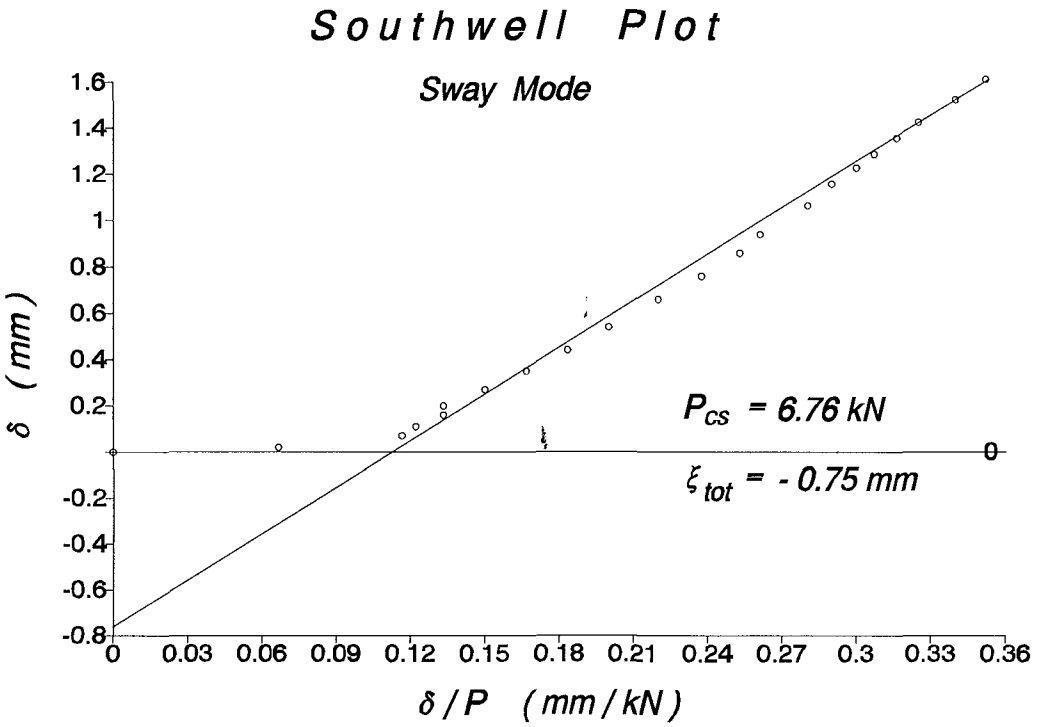
Southwell Plot
Sway Mode
1.6
1.4
1.2
1
0.8
0.6
0.4
0.2
0
-0.2
-0.4
-0.6
-0.8
δ (mm)
P_{cs} = 6.76 kN
ξ_{tot} = - 0.75 mm
0 0.03 0.06 0.09 0.12 0.15 0.18 0.21 0.24 0.27 0.3 0.33 0.36
δ / P (mm / kN)

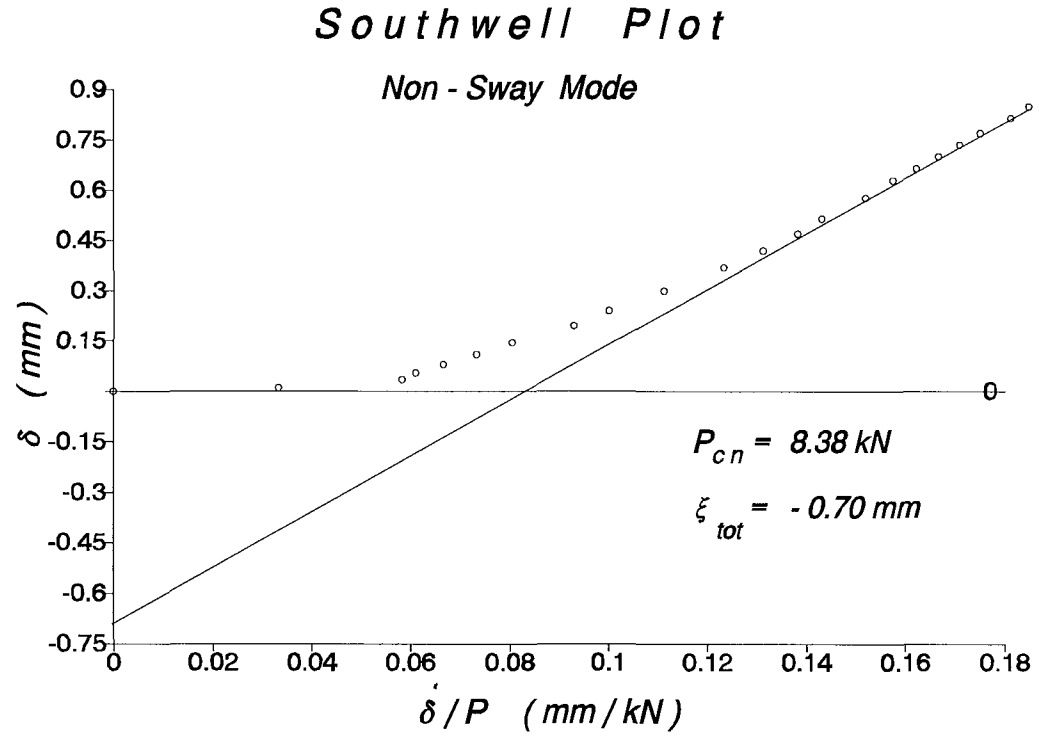
Southwell Plot
Non - Sway Mode
0.9
0.75
0.6
0.45
0.3
0.15
0
-0.15
-0.3
-0.45
-0.6
-0.75
δ (mm)
P_{cn} = 8.38 kN
ξ_{tot} = - 0.70 mm
0 0.02 0.04 0.06 0.08 0.1 0.12 0.14 0.16 0.18
δ / P (mm / kN)

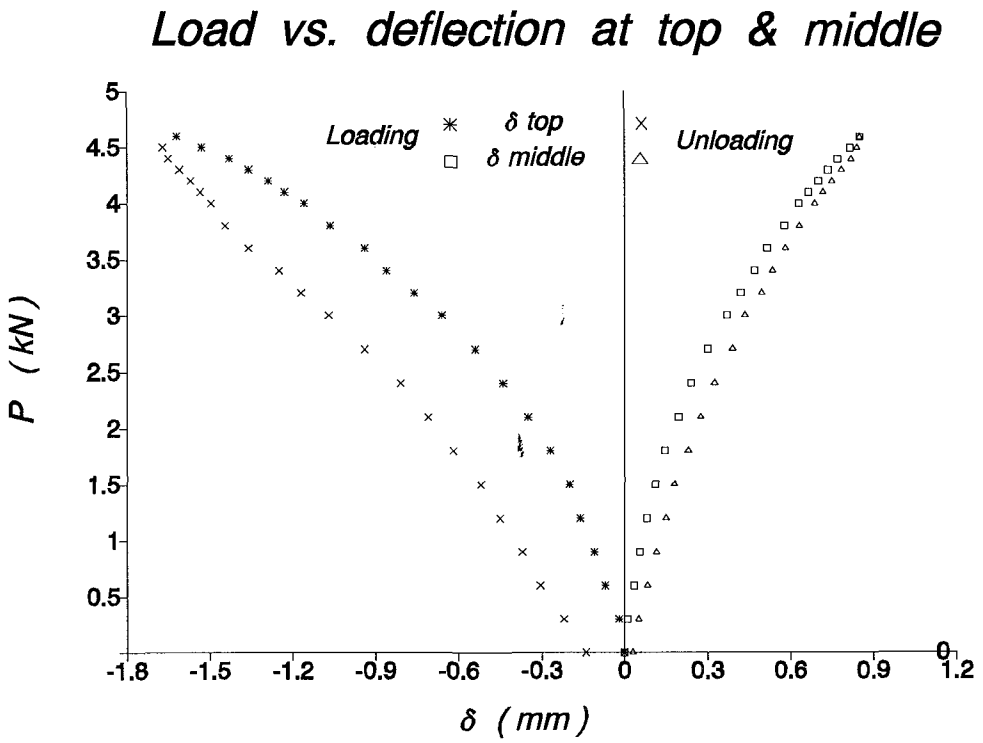

THEORETICAL DATA & RESULTS

PROP_sets = 3, SWAY_imp = 0.75 mm, NON-SWAY_imp = 0.70 mm

MEMBER PROPERTIES

MEM	L	b	d	A	I	Zel	Zpl	Y.str
1	270.0	5.0	13.0	62.44	125.70	50.28	81.45	0.360
2	350.0	5.0	13.0	62.44	125.70	50.28	81.45	0.360
3	270.0	5.0	13.0	62.44	125.70	50.28	81.45	0.360

Rotational SYMMETRIC (Non-sway) Stiffness of frame : 667.41 kN*mm/rad
Rotational ANTISYMMETRIC (Sway) Stiffness of frame : 799.47 kN*mm/rad
Translational (Sway) Stiffness of frame : 17.68 N/mm

EIGENVALUES & EIGENVECTORS

Solut	kL	Pc	C1	C2	delta	theta_A	Mode-Case
1	4.407	6.5299	1.00	0.733	-7.436	-0.008	* Sway
2	5.075	8.6594	1.00	-0.690	0.000	0.013	Non-Sway

First YIELD Load = 5.981 kN
First HINGE Load = 6.307 kN
SQUASH Load = 22.477 kN

Test: 12oc1
Elastic Buckling

Experimental Data					Southwell Plot			
	Loading		Unloading		Sway Mode		Non-Sway Mode	
Load P kN	Top reads	Mid reads	Top reads	Mid reads	$\frac{\delta_t}{100}$ mm	$\frac{\delta_t}{100P}$ mm/kN	$\frac{\delta_m-\delta_t/2}{100}$ mm	$\frac{\delta_m-\delta_t/2}{100P}$ mm/kN
0	671	1208	672	1209	0.000	0.000	0.000	0.000
0.2	673.2	1207	677.5	1208	0.022	0.110	0.001	0.005
0.4	681	1202.5	684	1204	0.100	0.250	0.005	0.013
0.6	685.5	1199.5	690	1200	0.145	0.242	0.013	0.021
0.8	690.5	1195	695.5	1197	0.195	0.244	0.033	0.041
1	695	1193	702	1194	0.240	0.240	0.030	0.030
1.2	701	1189	708.5	1189.5	0.300	0.250	0.040	0.033
1.4	707	1185.5	715	1185.5	0.360	0.257	0.045	0.032
1.6	714	1181.5	722.5	1181.5	0.430	0.269	0.050	0.031
1.8	722	1177	731	1176.5	0.510	0.283	0.055	0.031
2	731	1172	741	1171.5	0.600	0.300	0.060	0.030
2.2	741.5	1166	751	1166.5	0.705	0.320	0.068	0.031
2.4	752	1161	760	1162	0.810	0.338	0.065	0.027
2.6	762	1155	769	1156.5	0.910	0.350	0.075	0.029
2.8	772.3	1149.5	780	1150	1.013	0.362	0.079	0.028
3	785	1142	791	1144	1.140	0.380	0.090	0.030
3.1	791.5	1138.5	799	1138.5	1.205	0.389	0.093	0.030
3.2	797	1135.5	801.5	1133	1.260	0.394	0.095	0.030
3.3	805.5	1131	816	1129.5	1.345	0.408	0.098	0.030
3.4	812.5	1127	822.5	1124	1.415	0.416	0.103	0.030
3.5	818	1123.5	832	1118.5	1.470	0.420	0.110	0.031
3.6	825	1120	842.5	1112	1.540	0.428	0.110	0.031
3.7	831.5	1115.5	850	1107.5	1.605	0.434	0.123	0.033
3.8	839	1111.2	856	1103.5	1.680	0.442	0.128	0.034
3.9	850	1105	859.5	1101	1.790	0.459	0.135	0.035
4	861.5	1099	861.5	1099	1.905	0.476	0.138	0.034

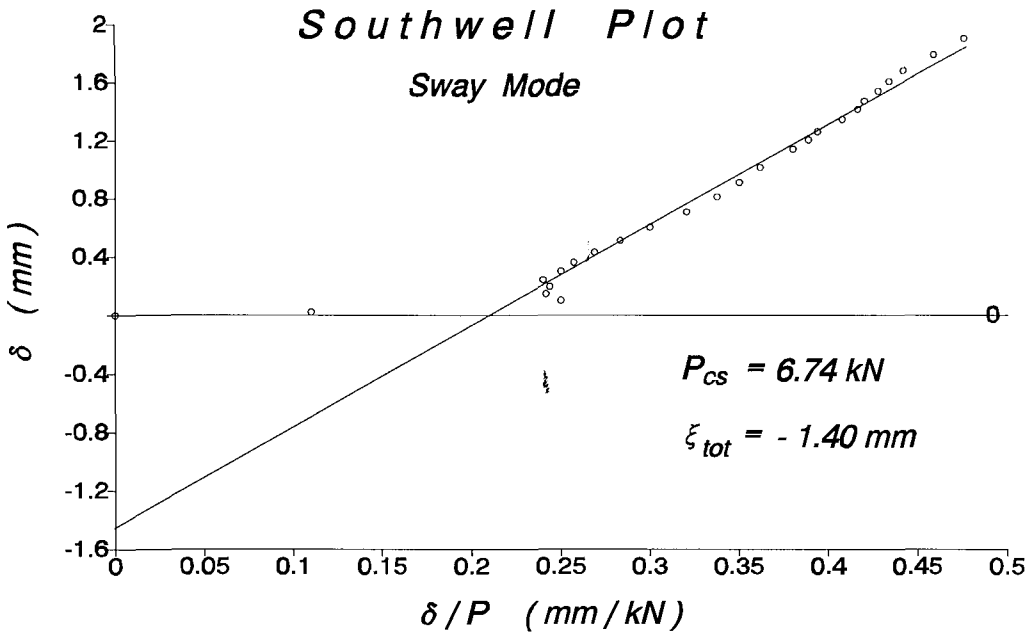
Southwell Plot
Sway Mode
δ (mm)
δ / P (mm / kN)
P_{cs} = 6.74 kN
ξ_{tot} = - 1.40 mm
2
1.6
1.2
0.8
0.4
0
-0.4
-0.8
-1.2
-1.6
0
0.05
0.1
0.15
0.2
0.25
0.3
0.35
0.4
0.45
0.5

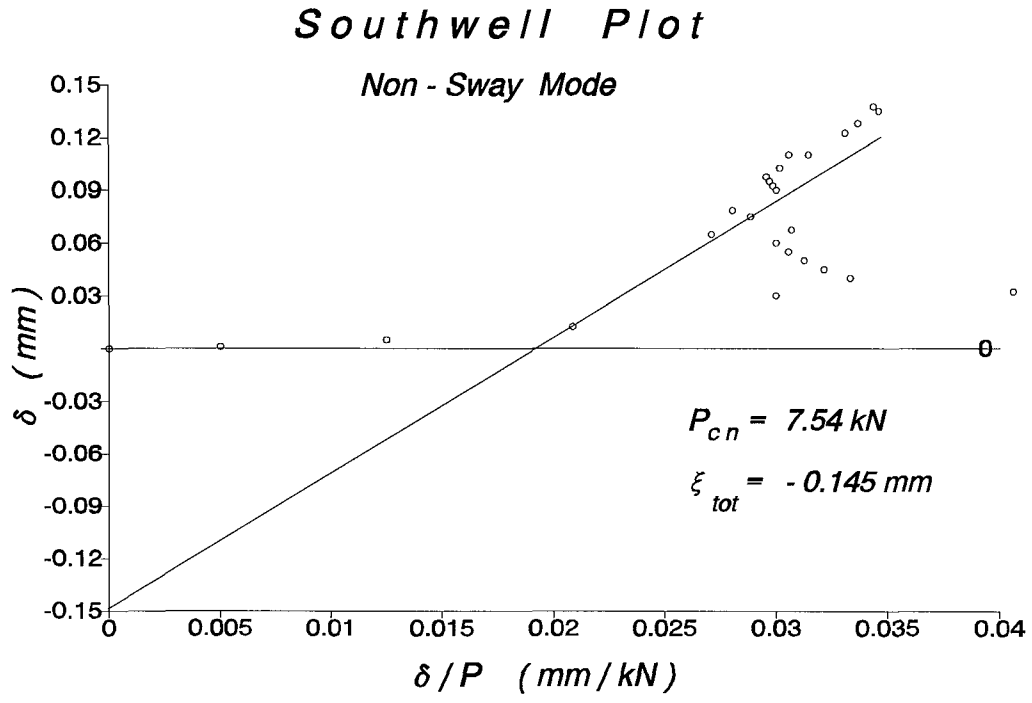
Southwell Plot
Non - Sway Mode
δ (mm)
δ / P (mm / kN)
P_{cn} = 7.54 kN
ξ_{tot} = - 0.145 mm
0.15
0.12
0.09
0.06
0.03
0
-0.03
-0.06
-0.09
-0.12
-0.15
0
0.005
0.01
0.015
0.02
0.025
0.03
0.035
0.04

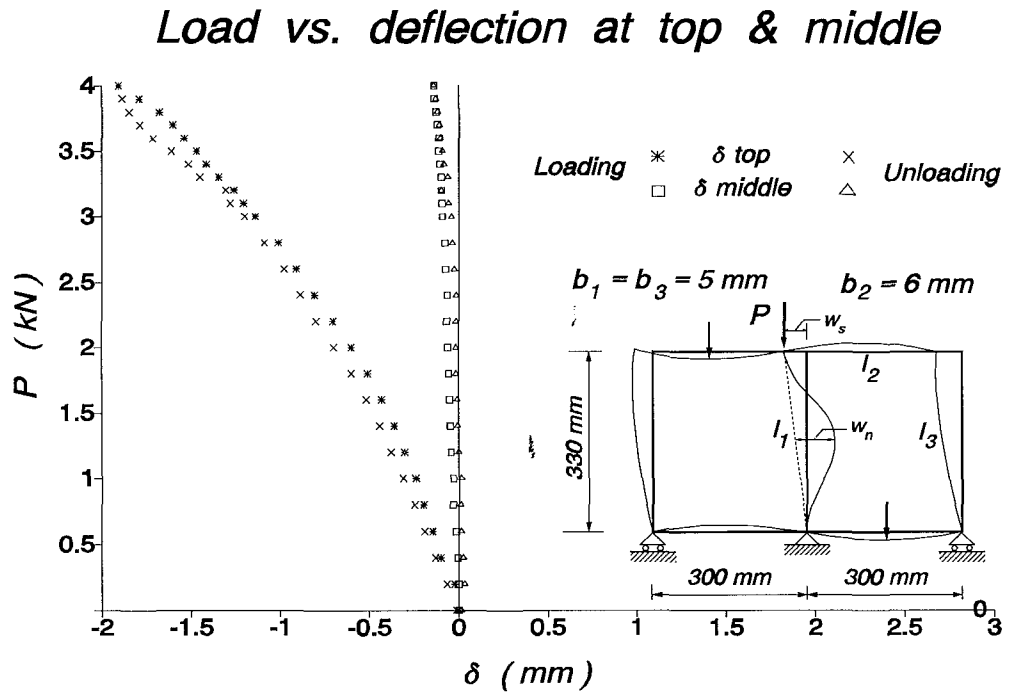

THEORETICAL DATA & RESULTS

PROP_sets = 3, SWAY_imp = 1.40 mm, NON-SWAY_imp = 0.14 mm

MEMBER PROPERTIES

MEM	L	b	d	A	I	Zel	Zpl	Y.str
1	330.0	5.0	13.0	62.44	125.70	50.28	81.45	0.360
2	300.0	6.0	13.0	73.44	209.00	69.67	117.71	0.360
3	330.0	5.0	13.0	62.44	125.70	50.28	81.45	0.360

Rotational SYMMETRIC (Non-sway) Stiffness of frame : 1234.98 kN*mm/rad
Rotational ANTISYMMETRIC (Sway) Stiffness of frame : 1468.91 kN*mm/rad
Translational (Sway) Stiffness of frame : 15.96 N/mm

EIGENVALUES & EIGENVECTORS

Solut	kL	Pc	C1	C2	delta	theta_A	Mode-Case
1	5.265	6.2396	1.00	1.792	-12.836	-0.004	* Sway
2	5.630	7.1350	1.00	-0.339	0.000	0.006	Non-Sway

First YIELD Load = 5.642 kN
First HINGE Load = 5.931 kN
SQUASH Load = 22.477 kN

Test: 4oc1
Elastic Bucling

Experimental Data					Southwell Plot			
Load P kN	Loading		Unloading		Sway Mode		Non-Sway Mode	
	Top reads	Mid reads	Top reads	Mid reads	$\frac{\delta_t}{100}$ mm	$\frac{\delta_t}{100P}$ mm/kN	$\frac{\delta_m-\delta_t/2}{100}$ mm	$\frac{\delta_m-\delta_t/2}{100P}$ mm/kN
0	1493	425	1483	441	0.000	0.000	0.000	0.000
0.2	1492	427.5	1480	446	0.010	0.050	0.020	0.100
0.4	1490	430	1476	451.5	0.030	0.075	0.035	0.088
0.6	1487	434	1472	456	0.060	0.100	0.060	0.100
0.8	1482.5	438.5	1469	460	0.105	0.131	0.083	0.103
1	1479	443	1465	466	0.140	0.140	0.110	0.110
1.2	1475	449	1459.5	471	0.180	0.150	0.150	0.125
1.4	1471	454	1454	477.5	0.220	0.157	0.180	0.129
1.6	1466	461	1448	484	0.270	0.169	0.225	0.141
1.8	1461	468	1442	490	0.320	0.178	0.270	0.150
2	1456	474	1439	495	0.370	0.185	0.305	0.153
2.2	1450	482	1430	505	0.430	0.195	0.355	0.161
2.4	1444	490	1423	513	0.490	0.204	0.405	0.169
2.6	1438	499	1417	521	0.550	0.212	0.465	0.179
2.8	1430	509	1409	529	0.630	0.225	0.525	0.188
3	1420	520	1401	540	0.730	0.243	0.585	0.195
3.2	1411	532.5	1394	548	0.820	0.256	0.665	0.208
3.4	1399	547	1388	558	0.940	0.276	0.750	0.221
3.6	1389	561	1378	573	1.040	0.289	0.840	0.233
3.8	1378	576	1369	583	1.150	0.303	0.935	0.246
4	1365	595	1365	595	1.280	0.320	1.060	0.265

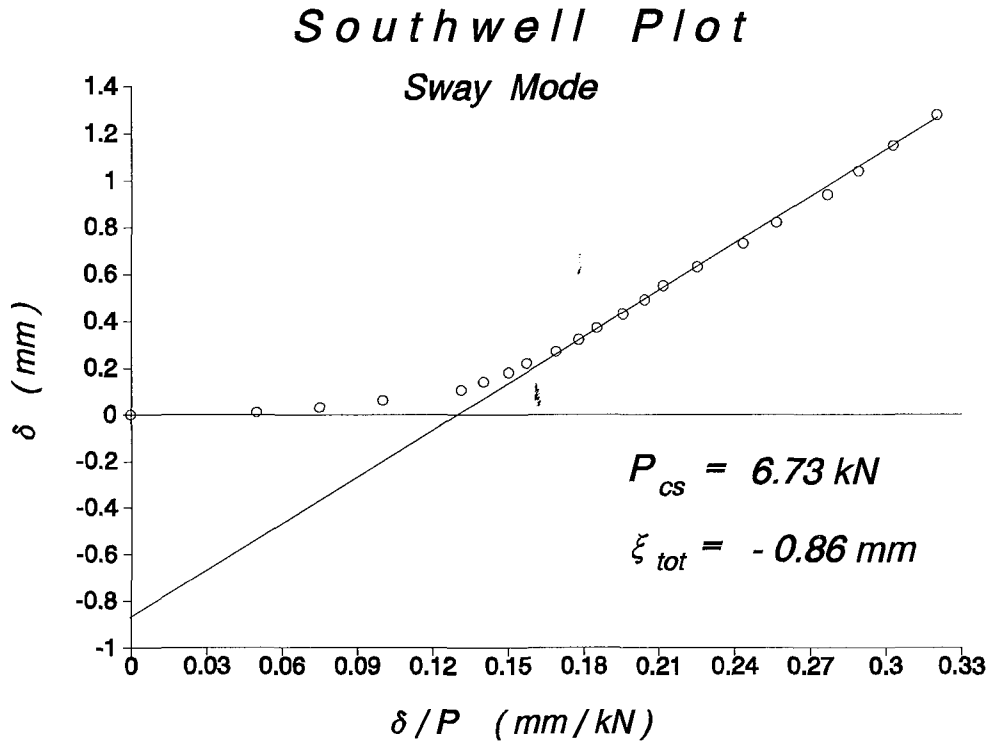
Southwell Plot
Sway Mode
δ (mm)
δ / P (mm / kN)
P cs = 6.73 kN
ξ tot = - 0.86 mm
1.4
1.2
1
0.8
0.6
0.4
0.2
0
-0.2
-0.4
-0.6
-0.8
-1
0
0.03
0.06
0.09
0.12
0.15
0.18
0.21
0.24
0.27
0.3
0.33

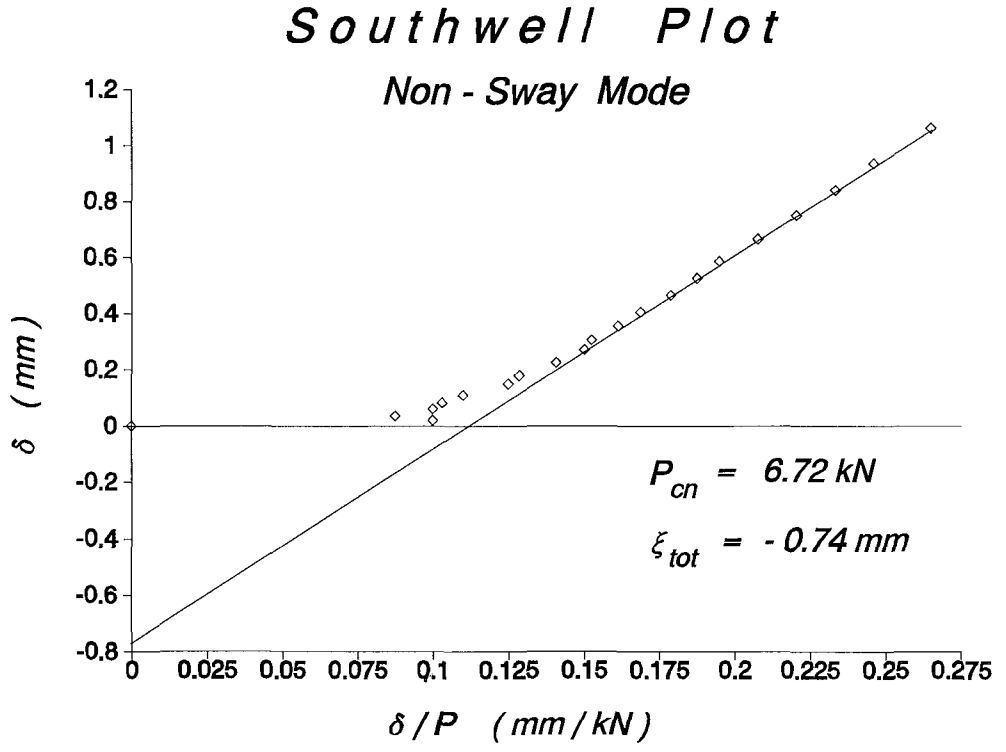
Southwell Plot
Non - Sway Mode
δ (mm)
δ / P (mm / kN)
P cn = 6.72 kN
ξ tot = - 0.74 mm
1.2
1
0.8
0.6
0.4
0.2
0
-0.2
-0.4
-0.6
-0.8
0
0.025
0.05
0.075
0.1
0.125
0.15
0.175
0.2
0.225
0.25
0.275

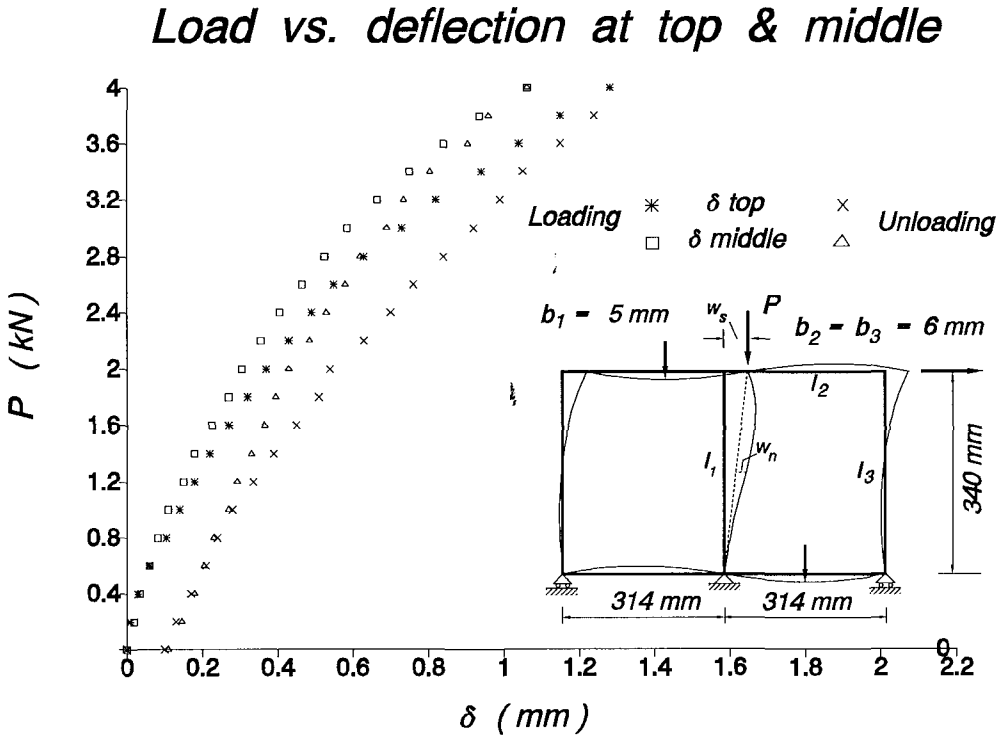

THEORETICAL DATA & RESULTS

PROP_sets = 3, SWAY_imp = 0.86 mm, NON-SWAY_imp = -0.74 mm

MEMBER PROPERTIES

MEM	L	b	d	A	I	Zel	Zpl	Y.str
1	340.0	5.0	13.0	62.44	125.70	50.28	81.45	0.360
2	314.0	6.0	13.0	73.44	209.00	69.67	117.71	0.360
3	340.0	6.0	13.0	73.44	209.00	69.67	117.71	0.360

	Rot.Sym.Non-sway	Rot.Antisym.Sway	Transl.Sway
Stiffness of frame :	1221.35 kN*mm/rad	1465.26 kN*mm/rad	17.933 N/mm.

EIGENVALUES & EIGENVECTORS

Solut	kL	Pc	C1	C2	delta	theta_A	Mode-Case
1	5.640	6.7459	1.00	-0.333	0.000	0.006	Non-Sway
2	5.643	6.7528	1.00	3.018	-20.600	-0.005	* Sway

First YIELD Load = 5.507 kN

First HINGE Load = 6.061 kN

SQUASH Load = 22.477 kN

Test: 23oc1
Elastic Buckling

Experimental Data					Southwell Plot			
Load P kN	Loading		Unloading		Sway Mode		Non-Sway Mode	
	Top reads	Mid reads	Top reads	Mid reads	$\frac{\delta_t}{100}$ mm	$\frac{\delta_t}{100P}$ mm/kN	$\frac{\delta_m-\delta_t/2}{100}$ mm	$\frac{\delta_m-\delta_t/2}{100P}$ mm/kN
0	681	1303	689	1304.5	0.000	0.000	0.000	0.000
0.3	682	1303	962	1308.5	0.010	0.033	0.005	0.017
0.6	683	1303	696	1309	0.020	0.033	0.010	0.017
0.9	685.5	1304	700	1309.5	0.045	0.050	0.033	0.036
1.2	688	1306	705	1310	0.070	0.058	0.065	0.054
1.5	690.5	1309	710	1311	0.095	0.063	0.108	0.072
1.8	694	1312	715	1312	0.130	0.072	0.155	0.086
2.1	697	1313	720	1313	0.160	0.076	0.180	0.086
2.4	701	1314	724	1314	0.200	0.083	0.210	0.088
2.7	704.5	1315.5	728	1315	0.235	0.087	0.243	0.090
3	710	1316	732	1317.5	0.290	0.097	0.275	0.092
3.3	718	1317	736	1318.5	0.370	0.112	0.325	0.098
3.6	727	1319	744	1320	0.460	0.128	0.390	0.108
3.9	736	1320.5	748	1322	0.550	0.141	0.450	0.115
4.2	744.5	1321	757	1322	0.635	0.151	0.498	0.118
4.4	750	1323	765	1322.5	0.690	0.157	0.545	0.124
4.6	757	1323	772.5	1323	0.760	0.165	0.580	0.126
4.8	765	1324	780	1323	0.840	0.175	0.630	0.131
5	772	1325	789	1323	0.910	0.182	0.675	0.135
5.2	779	1326.5	799	1323	0.980	0.188	0.725	0.139
5.4	789	1327	809	1323	1.080	0.200	0.780	0.144
5.6	795	1329	817.5	1324.5	1.140	0.204	0.830	0.148
5.8	805	1330	823	1325	1.240	0.214	0.890	0.153
6	814	1331	829	1328	1.330	0.222	0.945	0.158
6.2	824	1333	835	1330	1.430	0.231	1.015	0.164
6.4	833	1336	833	1336	1.520	0.238	1.090	0.170

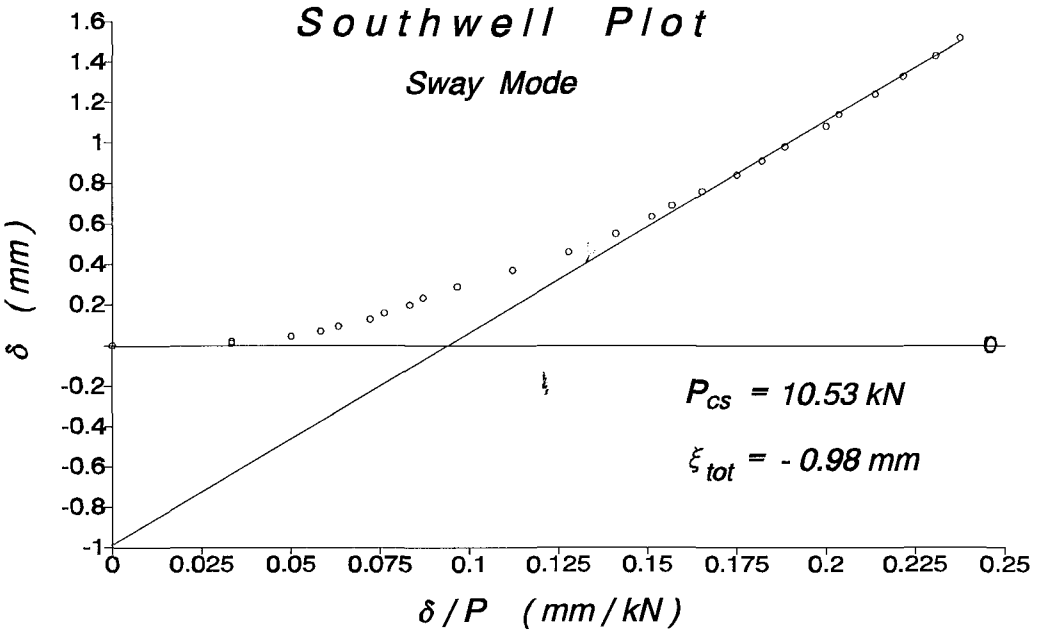
Southwell Plot
Sway Mode
δ (mm)
δ / P (mm / kN)
P_cs = 10.53 kN
ξ_tot = - 0.98 mm
1.6
1.4
1.2
1
0.8
0.6
0.4
0.2
0
-0.2
-0.4
-0.6
-0.8
-1
0
0.025
0.05
0.075
0.1
0.125
0.15
0.175
0.2
0.225
0.25

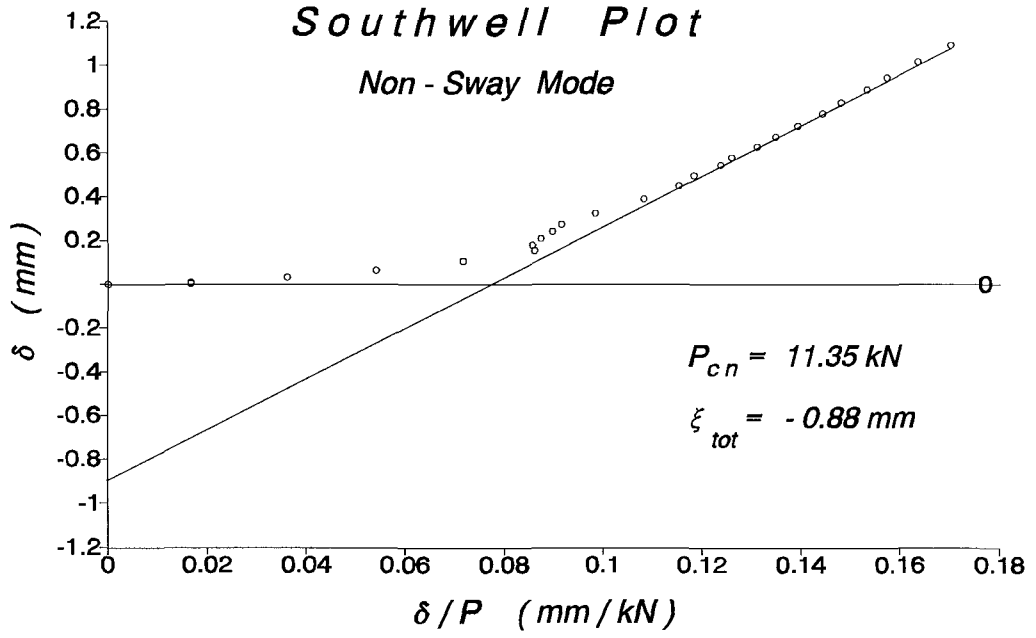
Southwell Plot
Non - Sway Mode
δ (mm)
δ / P (mm / kN)
P_cn = 11.35 kN
ξ_tot = - 0.88 mm
1.2
1
0.8
0.6
0.4
0.2
0
-0.2
-0.4
-0.6
-0.8
-1
-1.2
0
0.02
0.04
0.06
0.08
0.1
0.12
0.14
0.16
0.18

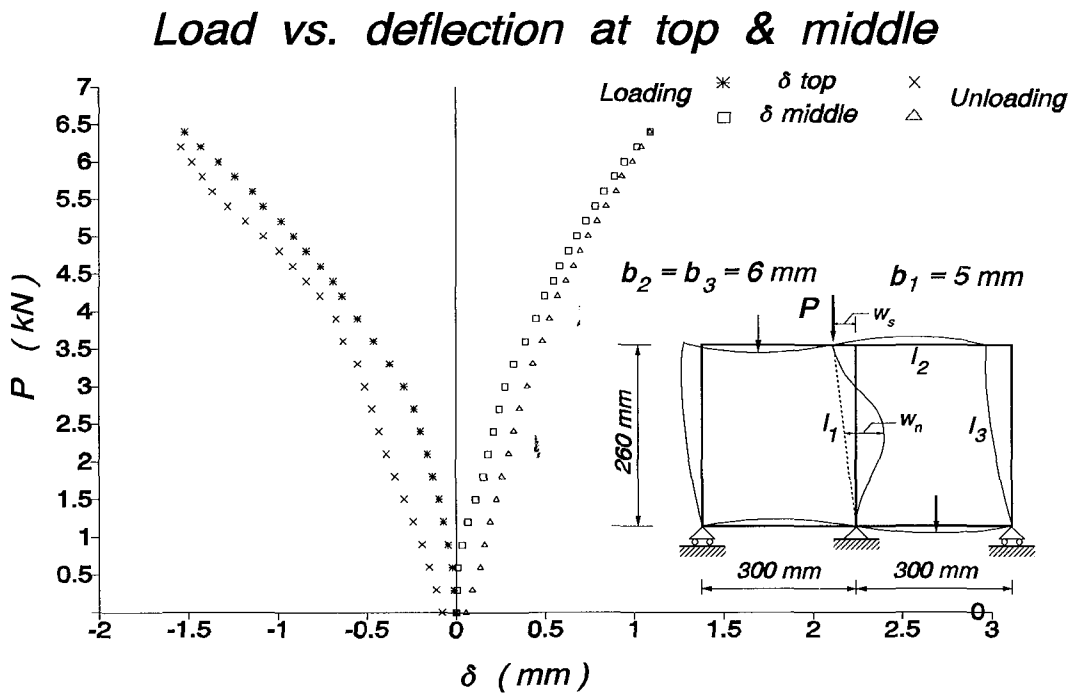

THEORETICAL DATA & RESULTS

PROP_sets = 3, SWAY_imp = 0.98 mm, NON-SWAY_imp = -0.85 mm

MEMBER PROPERTIES

MEM	L	b	d	A	I	Zel	Zpl	Y.str
1	260.0	5.0	13.0	62.44	125.70	50.28	81.45	0.360
2	300.0	6.0	13.0	73.44	209.00	69.67	117.71	0.360
3	260.0	6.0	13.0	73.44	209.00	69.67	117.71	0.360

Rotational SYMMETRIC (Non-sway) Stiffness of frame : 1343.77 kN*mm/rad
Rotational ANTISYMMETRIC (Sway) Stiffness of frame : 1641.35 kN*mm/rad
Translational (Sway) Stiffness of frame : 38.04 N/mm

EIGENVALUES & EIGENVECTORS

Solut	kL	Pc	C1	C2	delta	theta_A	Mode-Case
1	5.540	11.1290	1.00	2.566	-17.980	-0.007	* Sway
2	5.542	11.1352	1.00	-0.389	0.000	0.008	Non-Sway

First YIELD Load = 7.753 kN
First HINGE Load = 9.188 kN
SQUASH Load = 22.477 kN

Test: 25oc1
Elastic Buckling

Experimental Data					Southwell Plot			
Load P kN	Loading		Unloading		Sway Mode		Non-Sway Mode	
	Top reads	Mid reads	Top reads	Mid reads	$\frac{\delta_t}{100}$ mm	$\frac{\delta_t}{100P}$ mm/kN	$\frac{\delta_m-\delta_t/2}{100}$ mm	$\frac{\delta_m-\delta_t/2}{100P}$ mm/kN
0	969	1156	988	1148.5	0.000	0.000	0.000	0.000
0.2	973	1156.5	997	1149	0.040	0.200	0.025	0.125
0.4	977	1156.5	1001	1151.5	0.080	0.200	0.045	0.113
0.6	981	1157	1007.5	1152	0.120	0.200	0.070	0.117
0.8	986	1158	1013	1152.5	0.170	0.213	0.105	0.131
1	990.5	1158	1019	1153	0.215	0.215	0.128	0.128
1.2	996.5	1158	1025	1153	0.275	0.229	0.158	0.131
1.4	1002.5	1158.5	1031	1154	0.335	0.239	0.193	0.138
1.6	1009	1159.5	1038	1155	0.400	0.250	0.235	0.147
1.8	1016.5	1160.5	1045	1156	0.475	0.264	0.283	0.157
2	1024	1163	1052.5	1157	0.550	0.275	0.345	0.173
2.1	1028	1163.5	1056	1157.5	0.590	0.281	0.370	0.176
2.2	1032	1164.5	1061	1158.5	0.630	0.286	0.400	0.182
2.3	1036	1166	1066.5	1159.5	0.670	0.291	0.435	0.189
2.4	1040	1167	1071	1160	0.710	0.296	0.465	0.194
2.5	1045	1168.5	1076	1161	0.760	0.304	0.505	0.202
2.6	1051	1171	1080	1163	0.820	0.315	0.560	0.215
2.7	1057.5	1172.5	1083	1165	0.885	0.328	0.608	0.225
2.8	1064	1174.5	1087	1166	0.950	0.339	0.660	0.236
2.9	1069.5	1176.5	1091.5	1168	1.005	0.347	0.708	0.244
3	1078	1178.5	1095.5	1171.5	1.090	0.363	0.770	0.257
3.1	1083	1181.5	1097	1176	1.140	0.368	0.825	0.266
3.2	1090	1184.5	1098	1180	1.210	0.378	0.890	0.278
3.3	1098	1188	1098	1188	1.290	0.391	0.965	0.292

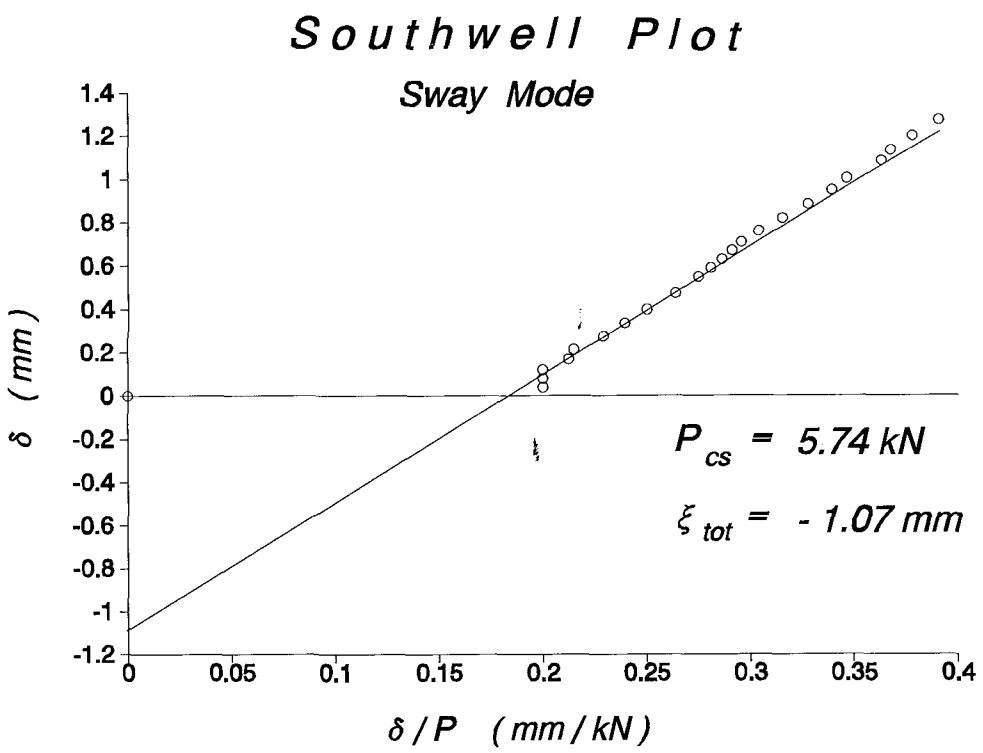
Southwell Plot
Sway Mode
δ (mm)
δ / P (mm / kN)
P cs = 5.74 kN
ξ tot = - 1.07 mm
1.4
1.2
1
0.8
0.6
0.4
0.2
0
-0.2
-0.4
-0.6
-0.8
-1
-1.2
0
0.05
0.1
0.15
0.2
0.25
0.3
0.35
0.4

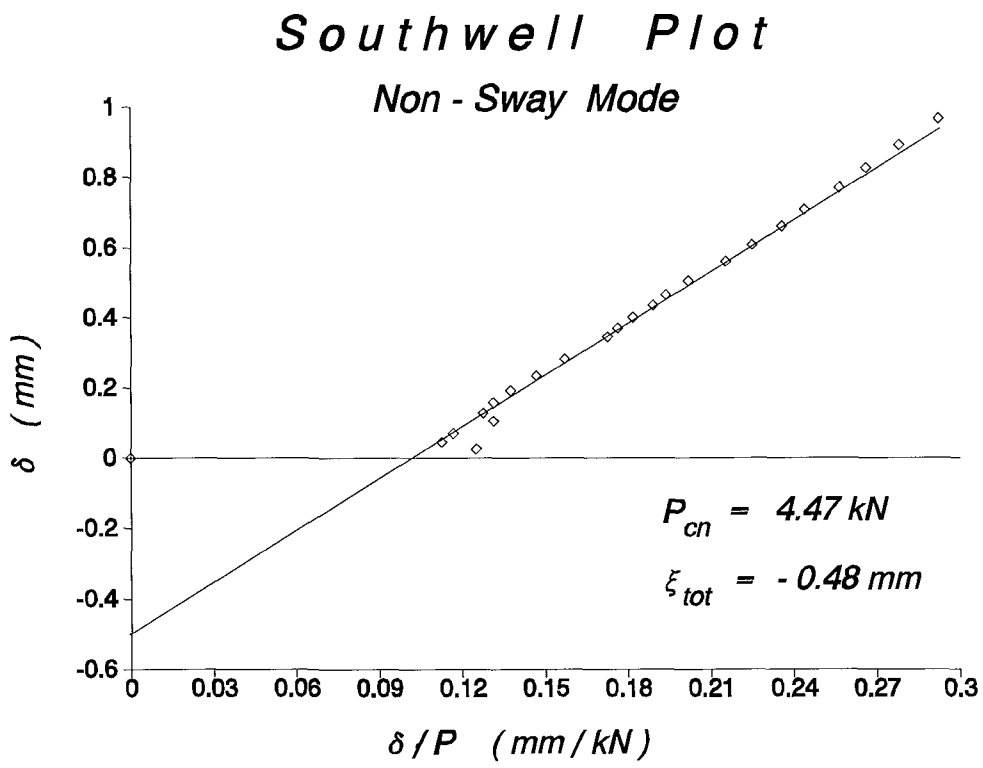
Southwell Plot
Non - Sway Mode
δ (mm)
δ / P (mm / kN)
P cn = 4.47 kN
ξ tot = - 0.48 mm
1
0.8
0.6
0.4
0.2
0
-0.2
-0.4
-0.6
0
0.03
0.06
0.09
0.12
0.15
0.18
0.21
0.24
0.27
0.3

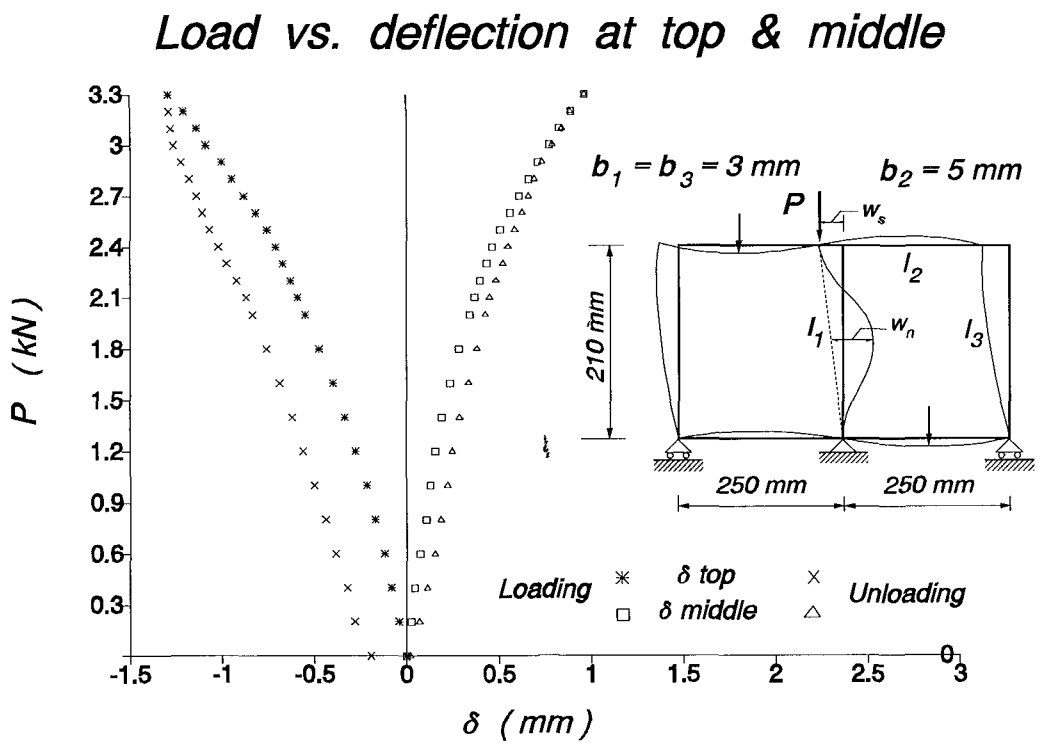

THEORETICAL DATA & RESULTS

PROP_sets = 3, SWAY_imp = -1.07 mm, NON-SWAY_imp = -0.48 mm

MEMBER PROPERTIES

MEM	L	b	d	A	I	Zel	Zpl	Y.str
1	210.0	3.0	13.0	38.47	28.53	19.02	29.26	0.360
2	250.0	5.0	13.0	62.44	125.70	50.28	81.45	0.360
3	210.0	3.0	13.0	38.47	28.53	19.02	29.26	0.360

Rotational SYMMETRIC (Non-sway) Stiffness of frame : 920.69 kN*mm/rad
Rotational ANTISYMMETRIC (Sway) Stiffness of frame : 1112.57 kN*mm/rad
Translational (Sway) Stiffness of frame : 25.34 N/mm

EIGENVALUES & EIGENVECTORS

Solut	kL	Pc	C1	C2	delta	theta_A	Mode-Case
1	5.944	4.4573	1.00	-0.171	0.000	0.005	Non-Sway
2	6.423	5.2043	1.00	-14.263	88.629	-0.005	* Sway

First YIELD Load = 3.066 kN
First HINGE Load = 3.579 kN
SQUASH Load = 13.848 kN

Test: 26oc1
Elastic Buckling

Experimental Data					Southwell Plot			
Load P kN	Loading		Unloading		Sway Mode		Non-Sway Mode	
	Top reads	Mid reads	Top reads	Mid reads	$\frac{\delta_t}{100}$ mm	$\frac{\delta_t}{100P}$ mm/kN	$\frac{\delta_m-\delta_t/2}{100}$ mm	$\frac{\delta_m-\delta_t/2}{100P}$ mm/kN
0	334	1063	353	1054	0.000	0.000	0.000	0.000
0.2	337	1062	361	1040	0.030	0.150	0.005	0.025
0.4	344	1060	369	1037.5	0.100	0.250	0.020	0.050
0.6	347	1056	377	1035	0.130	0.217	0.005	0.008
0.8	351	1051	385	1032	0.170	0.213	0.035	0.044
1	355.5	1048.5	393	1029	0.215	0.215	0.038	0.038
1.1	358.5	1047.5	399	1027	0.245	0.223	0.033	0.030
1.2	361	1046.5	404.5	1025	0.270	0.225	0.030	0.025
1.3	365	1046	409	1023	0.310	0.238	0.015	0.012
1.4	369	1044.5	415	1021	0.350	0.250	0.010	0.007
1.5	373	1043	421	1019	0.390	0.260	0.005	0.003
1.6	378	1041	426	1017	0.440	0.275	0.000	0.000
1.7	383	1039.5	434	1013.5	0.490	0.288	0.010	0.006
1.8	389	1037	441	1011	0.550	0.306	0.015	0.008
1.9	394	1035	446	1009.5	0.600	0.316	0.020	0.011
2	400	1033	455	1006	0.660	0.330	0.030	0.015
2.1	408	1031	462	1003	0.740	0.352	0.050	0.024
2.2	416	1028	471	998.5	0.820	0.373	0.060	0.027
2.3	424	1025	476.5	996.5	0.900	0.391	0.070	0.030
2.4	434	1021	483.5	993.5	1.000	0.417	0.080	0.033
2.5	447	1016	490	991	1.130	0.452	0.095	0.038
2.6	459	1009.5	495	989	1.250	0.481	0.090	0.035
2.7	472	1005	499	989.5	1.380	0.511	0.110	0.041
2.8	486	999	501	990	1.520	0.543	0.120	0.043
2.9	501.5	991.5	501.5	991.5	1.675	0.578	0.123	0.042

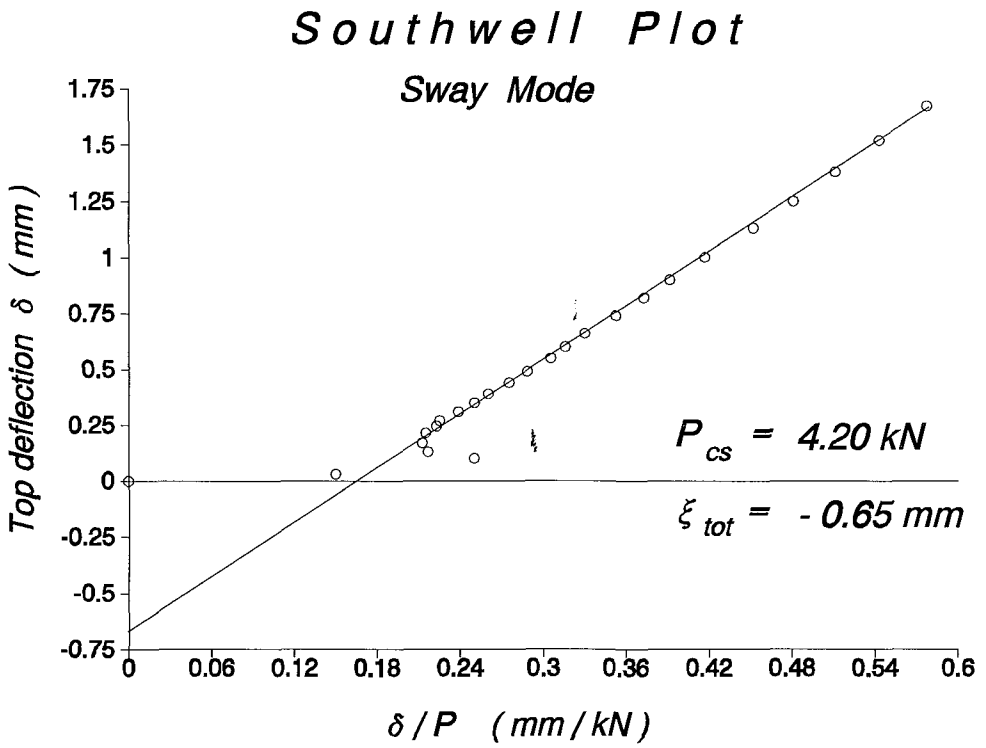
Southwell Plot
Sway Mode
Top deflection δ (mm)
1.75
1.5
1.25
1
0.75
0.5
0.25
0
-0.25
-0.5
-0.75
0
0.06
0.12
0.18
0.24
0.3
0.36
0.42
0.48
0.54
0.6
δ / P (mm / kN)
P cs = 4.20 kN
ξ tot = - 0.65 mm

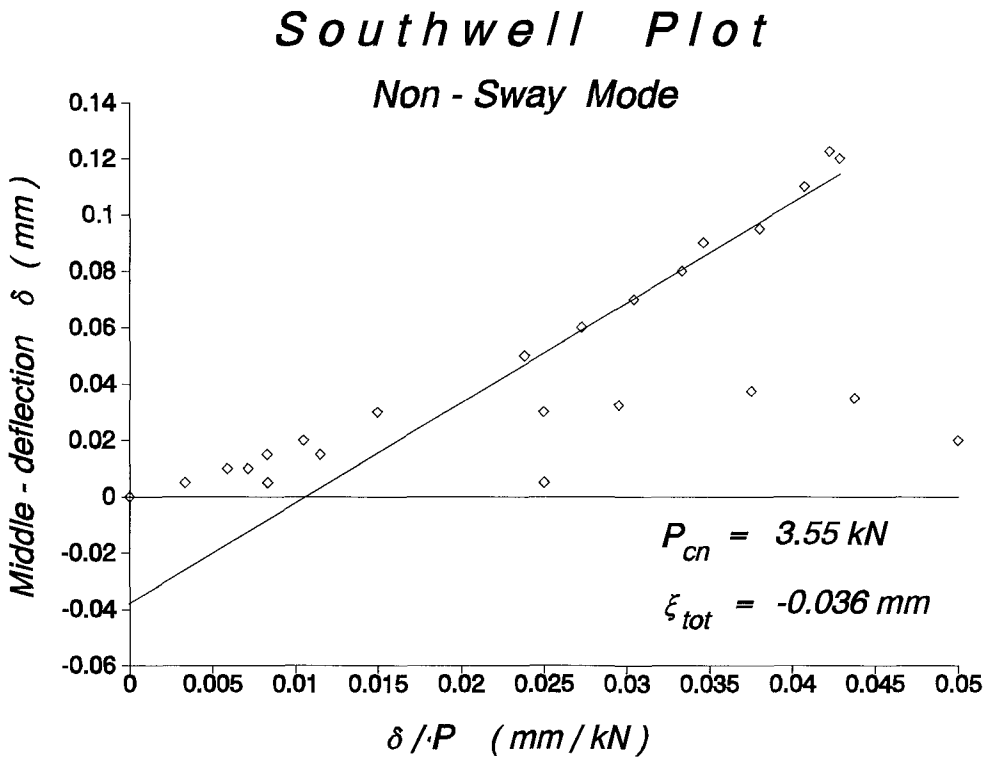
Southwell Plot
Non - Sway Mode
Middle - deflection δ (mm)
0.14
0.12
0.1
0.08
0.06
0.04
0.02
0
-0.02
-0.04
-0.06
0
0.005
0.01
0.015
0.02
0.025
0.03
0.035
0.04
0.045
0.05
δ / P (mm / kN)
P cn = 3.55 kN
ξ tot = -0.036 mm

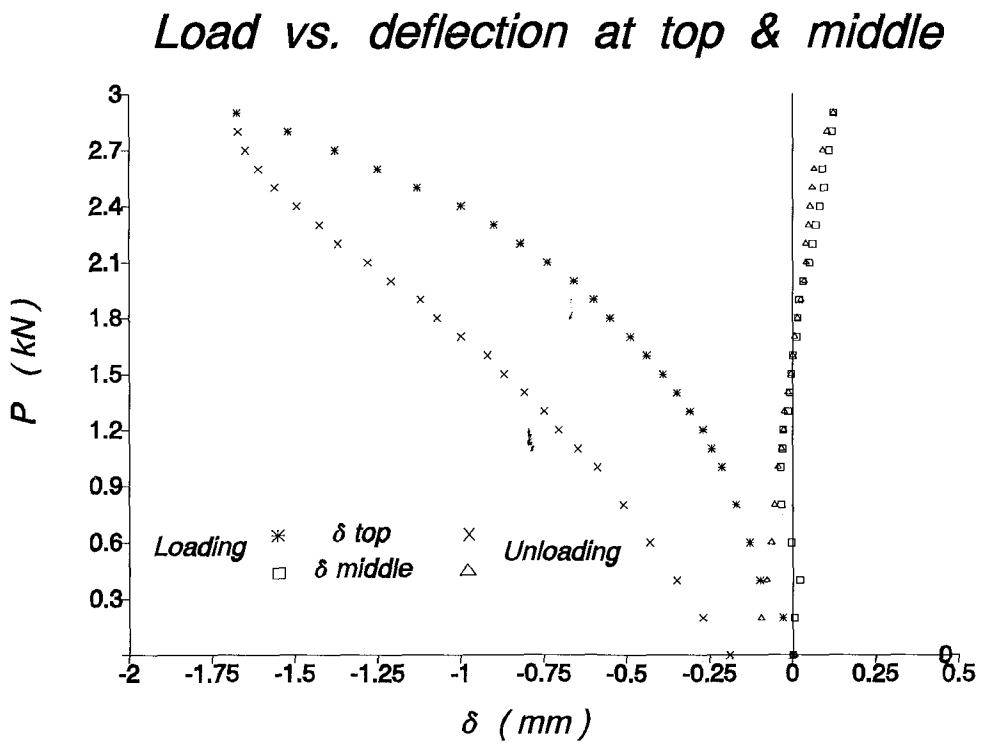

THEORETICAL DATA & RESULTS

PROP_sets = 3, SWAY_imp = -0.65 mm, NON-SWAY_imp = -0.04 mm

MEMBER PROPERTIES

MEM	L	b	d	A	I	Zel	Zpl	Y.str
1	235.0	3.0	13.0	38.47	28.53	19.02	29.26	0.360
2	400.0	5.0	13.0	62.44	125.70	50.28	81.45	0.360
3	235.0	5.0	13.0	62.44	125.70	50.28	81.45	0.360

Rotational SYMMETRIC (Non-sway) Stiffness of frame : 580.93 kN*mm/rad
Rotational ANTISYMMETRIC (Sway) Stiffness of frame : 682.39 kN*mm/rad
Translational (Sway) Stiffness of frame : 21.38 N/mm

EIGENVALUES & EIGENVECTORS

Solut	kL	Pc	C1	C2	delta	theta_A	Mode-Case
1	5.818	3.4092	1.00	-0.237	0.000	0.006	Non-Sway
2	6.777	4.6264	1.00	-3.967	23.289	-0.007	* Sway

First YIELD Load = 2.827 kN
First HINGE Load = 3.066 kN
SQUASH Load = 13.848 kN

Test: 6N1
Elastic Buckling

Experimental Data					Southwell Plot			
Load P kN	Loading		Unloading		Sway Mode		Non-Sway Mode	
	Top reads	Mid reads	Top reads	Mid reads	$\frac{\delta_t}{100}$ mm	$\frac{\delta_t}{100P}$ mm/kN	$\frac{\delta_m-\delta_t/2}{100}$ mm	$\frac{\delta_m-\delta_t/2}{100P}$ mm/kN
0	1377	1100	1374	1120	0.000	0.000	0.000	0.000
0.2	1376	1105	1369	1133	0.010	0.050	0.045	0.225
0.4	1372	1112.5	1365	1143	0.050	0.125	0.100	0.250
0.6	1367	1123	1360	1155	0.100	0.167	0.180	0.300
0.8	1361	1134	1353	1169	0.160	0.200	0.260	0.325
1	1355	1146	1345	1184	0.220	0.220	0.350	0.350
1.1	1350	1153	1341	1191	0.270	0.245	0.395	0.359
1.2	1346	1161	1337	1201	0.310	0.258	0.455	0.379
1.3	1341	1168	1332	1210	0.360	0.277	0.500	0.385
1.4	1336	1178	1327	1221	0.410	0.293	0.575	0 411
1.5	1330	1190	1322	1231	0.470	0.313	0.665	0.443
1.6	1325	1199	1316	1243	0.520	0.325	0.730	0.456
1.7	1319	1210	1310	1256	0.580	0.341	0.810	0.476
1.8	1311	1226	1303	1270	0.660	0.367	0.930	0.517
1.9	1304	1238	1295	1286	0.730	0.384	1.015	0.534
2	1296	1254	1287.5	1303	0.810	0.405	1.135	0.568
2.1	1287	1271	1277	1324	0.900	0.429	1.260	0.600
2.2	1278	1290	1267	1345	0.990	0.450	1.405	0.639
2.3	1267	1312	1256	1371	1.100	0.478	1.570	0.683
2.4	1255	1338	1246	1393	1.220	0.508	1.770	0.738
2.5	1242	1368	1232	1425	1.350	0.540	2.005	0.802
2.6	1226	1400	1212	1462	1.510	0.581	2.245	0.863
2.7	1209	1439	1189	1508	1.680	0.622	2.550	0.944
2.8	1189	1487	1168	1556	1.880	0.671	2.930	1.046
2.9	1167	1546	1143	1606	2.100	0.724	3.410	1.176
3	1131	1642	1131	1642	2.460	0.820	4.190	1.397

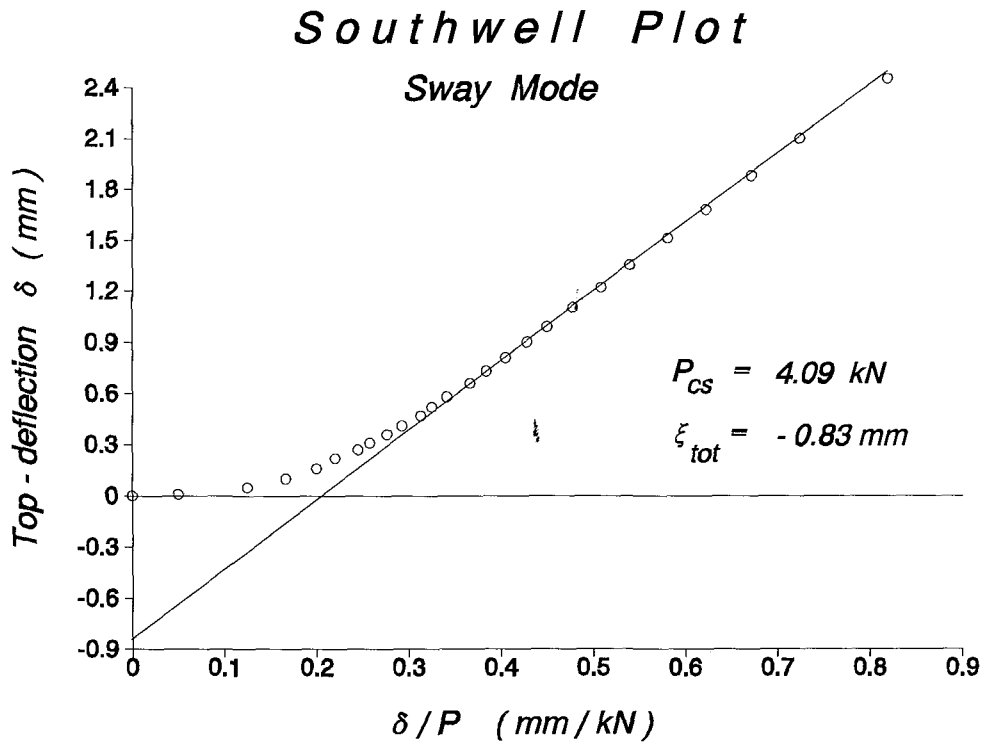
Southwell Plot
Sway Mode
Top - deflection δ (mm)
2.4
2.1
1.8
1.5
1.2
0.9
0.6
0.3
0
-0.3
-0.6
-0.9
0
0.1
0.2
0.3
0.4
0.5
0.6
0.7
0.8
0.9
δ / P (mm / kN)
P_{cs} = 4.09 kN
ξ_{tot} = - 0.83 mm

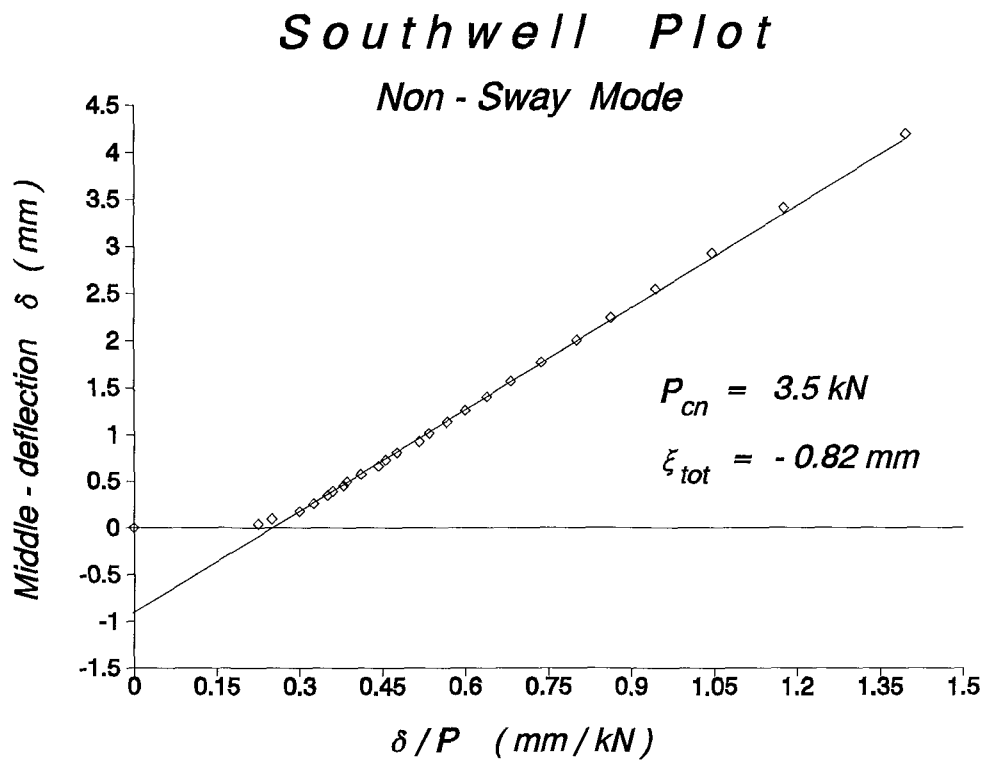
Southwell Plot
Non - Sway Mode
Middle - deflection δ (mm)
4.5
4
3.5
3
2.5
2
1.5
1
0.5
0
-0.5
-1
-1.5
0
0.15
0.3
0.45
0.6
0.75
0.9
1.05
1.2
1.35
1.5
δ / P (mm / kN)
P_{cn} = 3.5 kN
ξ_{tot} = - 0.82 mm

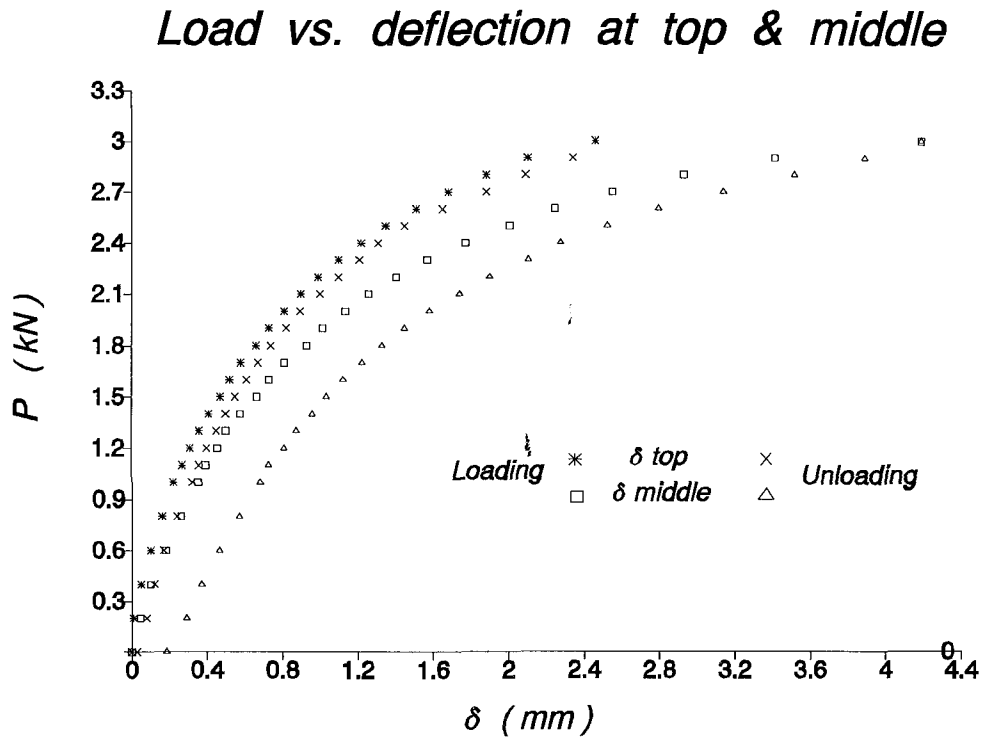

THEORETICAL DATA & RESULTS

PROP_sets = 3, SWAY_imp = -0.83 mm, NON-SWAY_imp = 0.82 mm

MEMBER PROPERTIES

MEM	L	b	d	A	I	Zel	Zpl	Y.str
1	235.0	3.0	13.0	38.47	28.53	19.02	29.26	0.360
2	370.0	5.0	13.0	62.44	125.70	50.28	81.45	0.360
3	235.0	5.0	13.0	62.44	125.70	50.28	81.45	0.360

Rotational SYMMETRIC (Non-sway) Stiffness of frame : 637.69 kN*mm/rad
Rotational ANTISYMMETRIC (Sway) Stiffness of frame : 757.60 kN*mm/rad
Translational (Sway) Stiffness of frame : 23.41 N/mm

EIGENVALUES & EIGENVECTORS

Solut	kL	Pc	C1	C2	delta	theta_A	Mode-Case
1	5.855	3.4533	1.00	-0.217	0.000	0.005	Non-Sway
2	6.968	4.8910	1.00	-2.805	16.026	-0.006	* Sway

First YIELD Load = 2.714 kN
First HINGE Load = 3.011 kN
SQUASH Load = 13.848 kN

Test: 18oc2
Elastic-Plastic Bucklilng

Experimental Data					Southwell Plot			
Load P kN	Loading		Unloading		Sway Mod		Non-Sway Mode	
	Top reads	Mid reads	Top reads	Mid reads	$\frac{\delta_t}{100}$ mm	$\frac{\delta_t}{100P}$ mm/kN	$\frac{\delta_m-\delta_t/2}{100}$ mm	$\frac{\delta_m-\delta_t/2}{100P}$ mm/kN
0	661	1264	679	1258.5	0.000	0.000	0.000	0.000
0.3	662	1264	687	1259.5	0.010	0.033	0.005	0.017
0.6	664.2	1264.5	697	1260	0.032	0.053	0.021	0.035
0.9	667.5	1265.5	704	1260	0.065	0.072	0.048	0.053
1.2	671	1266.2	713	1261	0.100	0.083	0.072	0.060
1.5	675	1267	723	1261	0.140	0.093	0.100	0.067
1.8	679	1268.5	730	1261	0.180	0.100	0.135	0.075
2.1	687	1269	740	1262	0.260	0.124	0.180	0.086
2.4	695.5	1268.5	752	1262	0.345	0.144	0.218	0.091
2.7	708.5	1268.5	765	1261.5	0.475	0.176	0.283	0.105
3	712.5	1268.5	779	1261	0.515	0.172	0.303	0.101
3.3	722.5	1269.5	796	1261	0.615	0.186	0.363	0.110
3.6	733	1269.5	812	1260	0.720	0.200	0.415	0.115
3.9	744.5	1270.5	828	1260	0.835	0.214	0.483	0.124
4.2	758	1271	850	1258	0.970	0.231	0.555	0.132
4.5	773	1271	871	1256	1.120	0.249	0.630	0.140
4.8	790.5	1271.5	894	1252	1.295	0.270	0.723	0.151
5	803	1272	915	1248	1.420	0.284	0.790	0.158
5.2	816	1272.5	921	1245	1.550	0.298	0.860	0.165
5.4	829.5	1273.5	962	1236	1.685	0.312	0.938	0.174
5.6	843.5	1274.5	988	1231	1.825	0.326	1.018	0.182
5.8	860	1275	1018	1222.5	1.990	0.343	1.105	0.191
6	877.5	1275	1051	1214	2.165	0.361	1.193	0.199
6.2	896	1274.5	1083	1206	2.350	0.379	1.280	0.206
6.4	918	1273	1125	1195	2.570	0.402	1.375	0.215
6.6	946	1268	1169	1181	2.850	0.432	1.465	0.222
6.8	977	1262.5	1215	1168	3.160	0.465	1.565	0.230
7	1014	1254.5	1264	1154	3.530	0.504	1.670	0.239
7.2	1056	1245	1307	1142	3.950	0.549	1.785	0.248
7.4	1099	1236	1341.5	1134	4.380	0.592	1.910	0.258
7.6	1156	1222	1371	1128	4.950	0.651	2.055	0.270
7.8	1210	1205	1383	1131	5.490	0.704	2.155	0.276
8	1285	1180	1385	1137	6.240	0.780	2.280	0.285
8.2	1375	1148	1375	1148	7.140	0.871	2.410	0.294

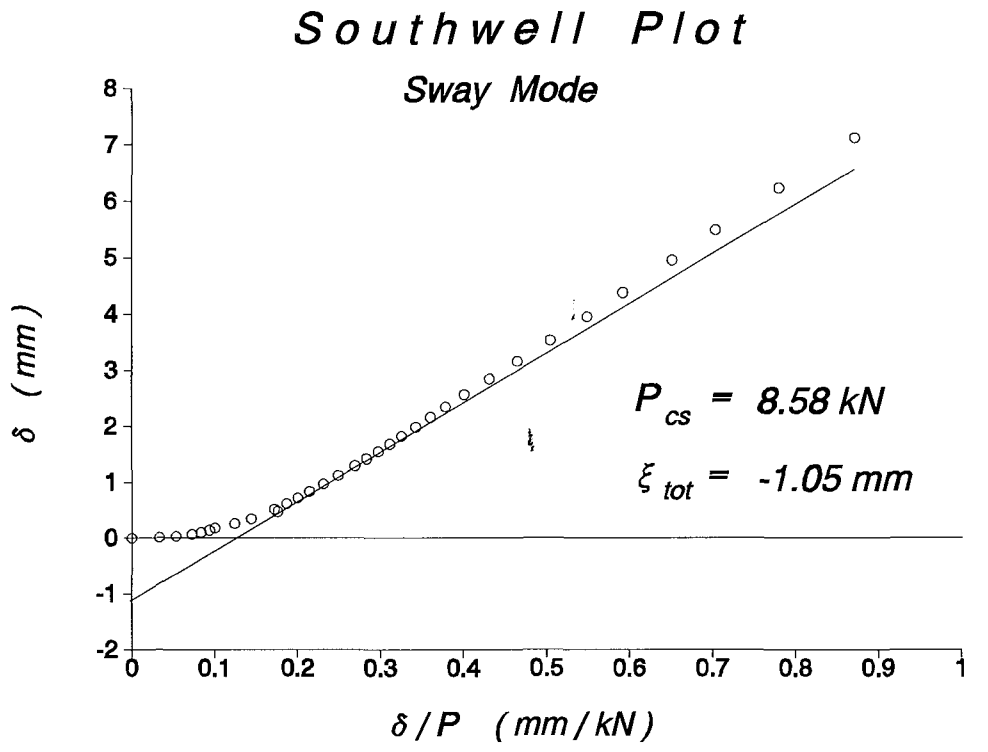
Southwell Plot
Sway Mode
δ (mm)
δ / P (mm / kN)
P cs = 8.58 kN
ξ tot = -1.05 mm
8
7
6
5
4
3
2
1
0
-1
-2
0
0.1
0.2
0.3
0.4
0.5
0.6
0.7
0.8
0.9
1

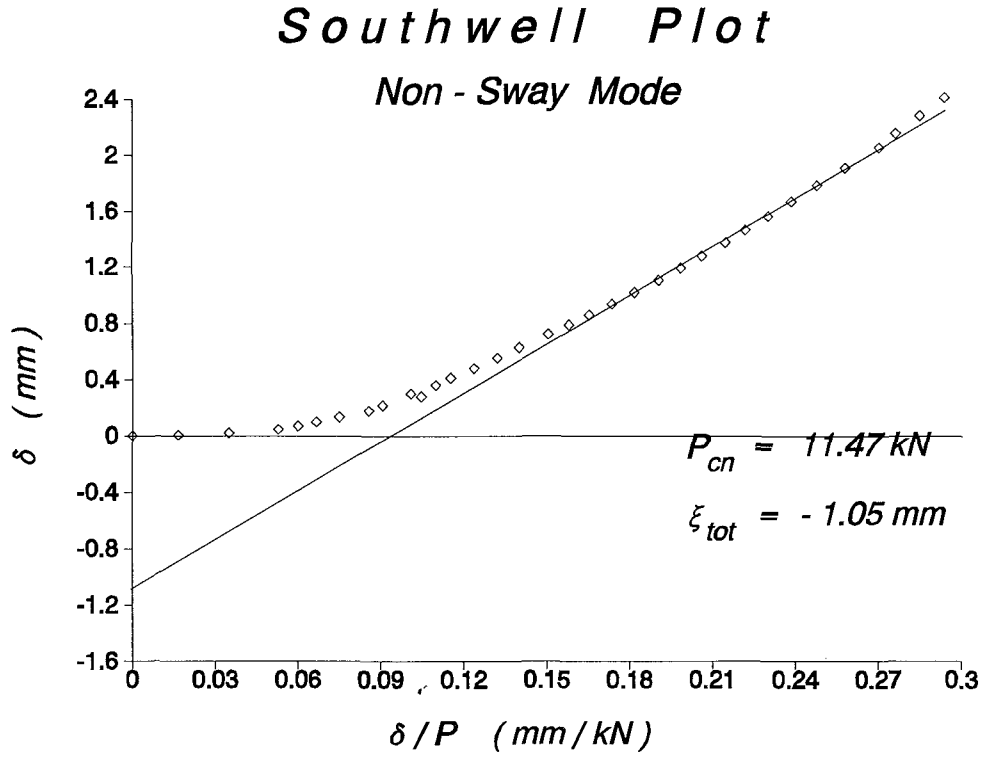
Southwell Plot
Non - Sway Mode
δ (mm)
δ / P (mm / kN)
P cn = 11.47 kN
ξ tot = - 1.05 mm
2.4
2
1.6
1.2
0.8
0.4
0
-0.4
-0.8
-1.2
-1.6
0
0.03
0.06
0.09
0.12
0.15
0.18
0.21
0.24
0.27
0.3

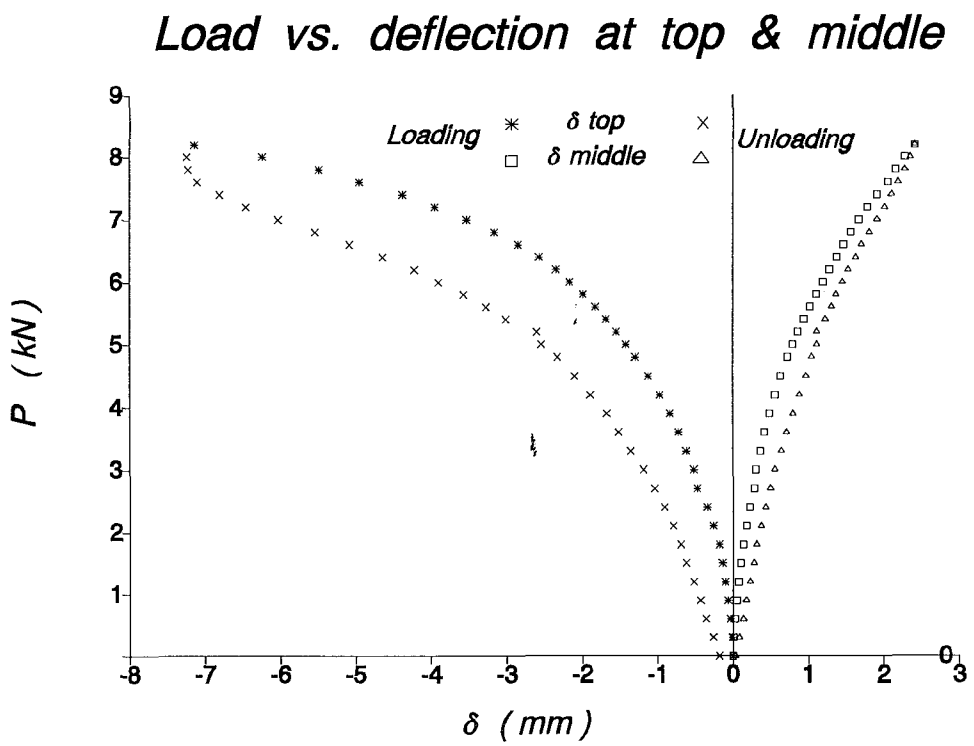

THEORETICAL DATA & RESULTS

PROP_sets = 3, SWAY_imp = 1.05 mm, NON-SWAY_imp = -1.05 mm

MEMBER PROPERTIES

MEM	L	b	d	A	I	Zel	Zpl	Y.str
1	280.0	6.0	13.0	73.44	209.00	69.67	117.71	0.360
2	300.0	5.0	13.0	62.44	125.70	50.28	81.45	0.360
3	280.0	5.0	13.0	62.44	125.70	50.28	81.45	0.360

Rotational SYMMETRIC (Non-sway) Stiffness of frame : 802.89 kN*mm/rad
Rotational ANTISYMMETRIC (Sway) Stiffness of frame : 980.22 kN*mm/rad
Translational (Sway) Stiffness of frame : 19.03 N/mm

EIGENVALUES & EIGENVECTORS

Solut	kL	Pc	C1	C2	delta	theta_A	Mode-Case
1	3.932	8.0359	1.00	0.417	-5.935	-0.008	* Sway
2	4.842	12.1892	1.00	-0.878	0.000	0.015	Non-Sway

First YIELD Load = 7.094 kN
First HINGE Load = 7.666 kN
SQUASH Load = 26.437 kN

Test: 16oc2
Elasto_Plastic Buckling

Experimental Data					Southwell Plot			
	Loading		Unloading		Sway Mode		Non-Sway Mode	
Load P kN	Top reads	Mid reads	Top reads	Mid reads	$\frac{\delta_t}{100}$ mm	$\frac{\delta_t}{100P}$ mm/kN	$\frac{\delta_m-\delta_t/2}{100}$ mm	$\frac{\delta_m-\delta_t/2}{100P}$ mm/kN
0	966.5	1522	1174	1550	0.000	0.000	0.000	0.000
0.3	967.5	1523.5	1192	1551	0.010	0.033	0.020	0.067
0.6	969	1524.5	1209	1551	0.025	0.042	0.038	0.063
0.9	972.5	1525	1228	1552	0.060	0.067	0.060	0.067
1.2	976.5	1525	1250	1553	0.100	0.083	0.080	0.067
1.5	981	1525	1270	1554	0.145	0.097	0.103	0.068
1.8	988	1526	1295	1554	0.215	0.119	0.148	0.082
2.1	994	1525.5	1326	1554	0.275	0.131	0.173	0.082
2.4	1002	1527.5	1358	1554	0.355	0.148	0.233	0.097
2.7	1012	1528	1392	1553	0.455	0.169	0.288	0.106
3	1024	1528	1433	1552.5	0.575	0.192	0.348	0.116
3.3	1037	1529	1480	1549.5	0.705	0.214	0.423	0.128
3.6	1050	1530	1543	1541	0.835	0.232	0.498	0.138
3.9	1063	1531.5	1611	1528	0.965	0.247	0.578	0.148
4.2	1083	1531	1692	1509	1.165	0.277	0.673	0.160
4.4	1098	1531.5	1757	1493	1.315	0.299	0.753	0.171
4.6	1115	1530.5	1828	1475	1.485	0.323	0.828	0.180
4.8	1137.5	1529.5	1922	1446	1.710	0.356	0.930	0.194
5	1156.5	1529	2022	1417	1.900	0.380	1.020	0.204
5.2	1180	1528.5	2099	1400	2.135	0.411	1.133	0.218
5.4	1213	1525	2192	1378	2.465	0.456	1.263	0.234
5.6	1252	1520	2290	1354	2.855	0.510	1.408	0.251
5.7	1281	1514	2349	1339	3.145	0.552	1.493	0.262
5.8	1315	1507	2379	1333	3.485	0.601	1.593	0.275
5.9	1347	1500	2397	1334	3.805	0.645	1.683	0.285
6	1383	1494						
6.1	1415	1488						
6.2	1460	1479						
6.3	1515	1467						
6.4	1567	1459						
6.5	1630	1444						
6.6	1717	1421						
6.7	1815	1391						
6.7	2145	1322						

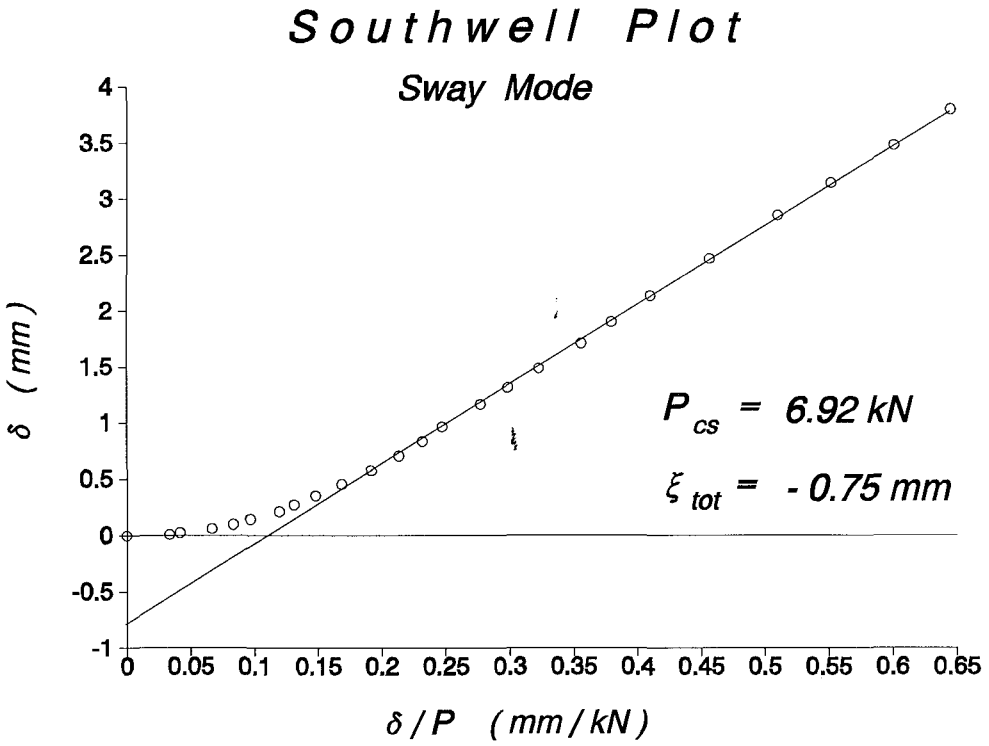
Southwell Plot
Sway Mode
δ (mm)
δ / P (mm / kN)
P cs = 6.92 kN
ξ tot = - 0.75 mm
4
3.5
3
2.5
2
1.5
1
0.5
0
-0.5
-1
0 0.05 0.1 0.15 0.2 0.25 0.3 0.35 0.4 0.45 0.5 0.55 0.6 0.65

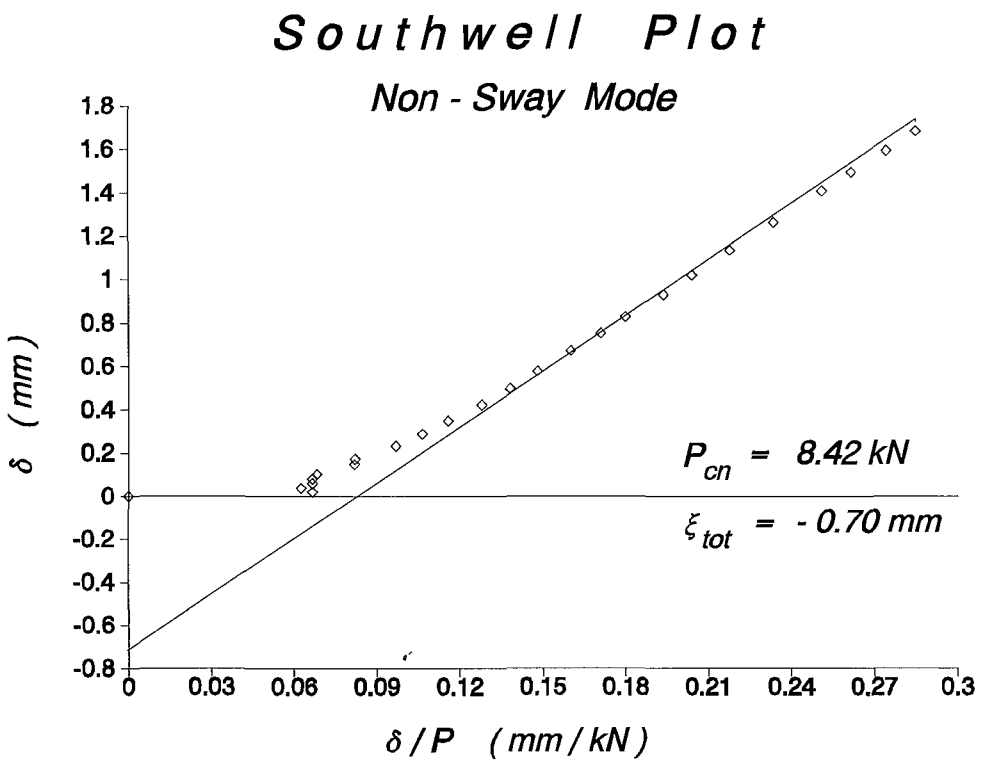
Southwell Plot
Non - Sway Mode
δ (mm)
δ / P (mm / kN)
P cn = 8.42 kN
ξ tot = - 0.70 mm
1.8
1.6
1.4
1.2
1
0.8
0.6
0.4
0.2
0
-0.2
-0.4
-0.6
-0.8
0 0.03 0.06 0.09 0.12 0.15 0.18 0.21 0.24 0.27 0.3

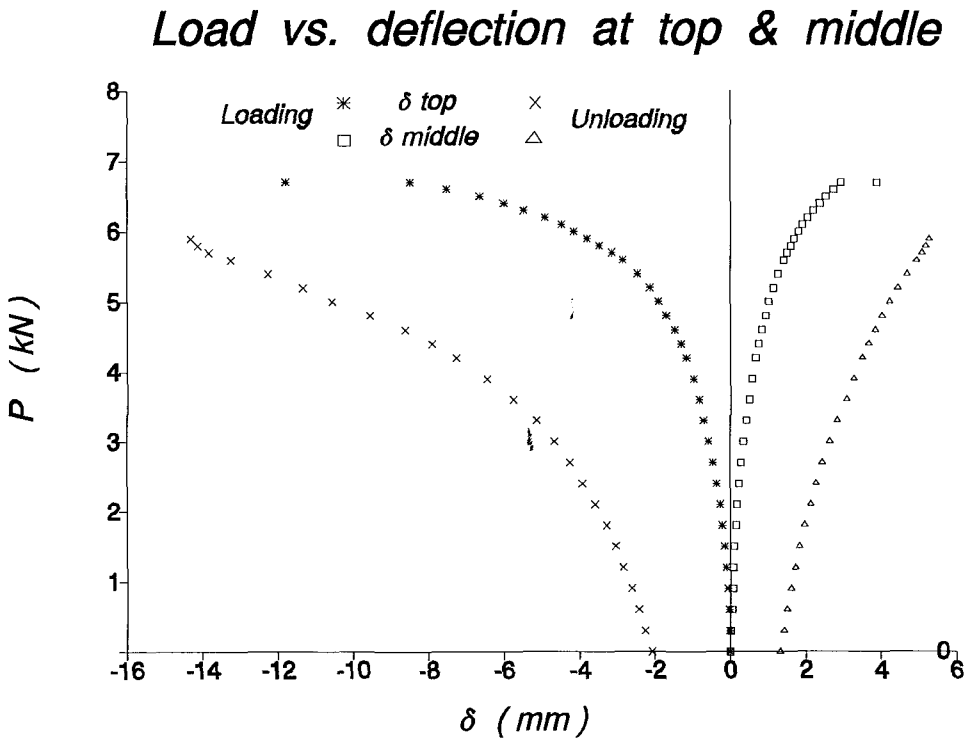

THEORETICAL DATA & RESULTS

PROP_sets = 3, SWAY_imp = 0.75 mm, NON-SWAY_imp = 0.70 mm

MEMBER PROPERTIES

MEM	L	b	d	A	I	Zel	Zpl	Y.str
1	270.0	5.0	13.0	62.44	125.70	50.28	81.45	0.360
2	350.0	5.0	13.0	62.44	125.70	50.28	81.45	0.360
3	270.0	5.0	13.0	62.44	125.70	50.28	81.45	0.360

Rotational SYMMETRIC (Non-sway) Stiffness of frame : 667.41 kN*mm/rad

Rotational ANTISYMMETRIC (Sway) Stiffness of frame : 799.47 kN*mm/rad

Translational (Sway) Stiffness of frame : 17.68 N/mm

EIGENVALUES & EIGENVECTORS

Solut	kL	Pc	C1	C2	delta	theta_A	Mode-Case
1	4.407	6.5299	1.00	0.733	-7.436	-0.008	* Sway
2	5.075	8.6594	1.00	-0.690	0.000	0.013	Non-Sway

First YIELD Load = 5.981 kN

First HINGE Load = 6.307 kN

SQUASH Load = 22.477 kN

Test: 12oc2
Elastic-Plastic Buckling

Experimental Data					Southwell Plot			
Load P kN	Loading		Unloading		Sway Mode		Non-Sway Mode	
	Top reads	Mid reads	Top reads	Mid reads	$\frac{\delta_t}{100}$ mm	$\frac{\delta_t}{100P}$ mm/kN	$\frac{\delta_m-\delta_t/2}{100}$ mm	$\frac{\delta_m-\delta_t/2}{100P}$ mm/kN
0	674	1204	726	1170	0.000	0.000	0.000	0.000
0.3	680	1201	733	1168	0.060	0.200	0.000	0.000
0.6	686	1197.5	741	1165	0.120	0.200	0.005	0.008
0.9	692.5	1193	751	1158	0.185	0.206	0.018	0.019
1.2	700.5	1188	761	1151	0.265	0.221	0.028	0.023
1.5	709	1182.5	773	1144	0.350	0.233	0.040	0.027
1.8	720	1176.5	787	1135	0.460	0.256	0.045	0.025
2.1	733.5	1169.5	802.5	1126	0.595	0.283	0.048	0.023
2.4	745	1163	816	1117	0.710	0.296	0.055	0.023
2.7	760	1154	834	1106	0.860	0.319	0.070	0.026
3	777	1145	855	1093	1.030	0.343	0.075	0.025
3.3	792	1136.5	886	1075	1.180	0.358	0.085	0.026
3.6	814	1124	916	1057	1.400	0.389	0.100	0.028
3.8	831	1114.5	944	1040	1.570	0.413	0.110	0.029
4	845	1106	979	1019	1.710	0.428	0.125	0.031
4.2	864	1095	1014	1000	1.900	0.452	0.140	0.033
4.4	886.5	1082	1065	970	2.125	0.483	0.158	0.036
4.6	913	1067	1101	949	2.390	0.520	0.175	0.038
4.8	933	1054	1146	913	2.590	0.540	0.205	0.043
5	975.5	1029.5	1241	870	3.015	0.603	0.238	0.048
5.2	998	1015	1325	823	3.240	0.623	0.270	0.052
5.3	1033	995	1385	790	3.590	0.677	0.295	0.056
5.4	1086	968	1455	751	4.120	0.763	0.300	0.056
5.5	1142	940	1533	709	4.680	0.851	0.300	0.055
5.6	1167	925	1611	666.5	4.930	0.880	0.325	0.058
5.7	1210	898	1709	611	5.360	0.940	0.380	0.067
5.8	1258	871	1805	556	5.840	1.007	0.410	0.071
5.9	1299	850	1866.5	418	6.250	1.059	0.415	0.070
6	1378	805	1898	492	7.040	1.173	0.470	0.078
6.1	1483	746	1927	467	8.090	1.326	0.535	0.088
6.2	1515	727						
6.3	1596	677	1976	410				
6.4	1731	596						
6.5	1813	530						

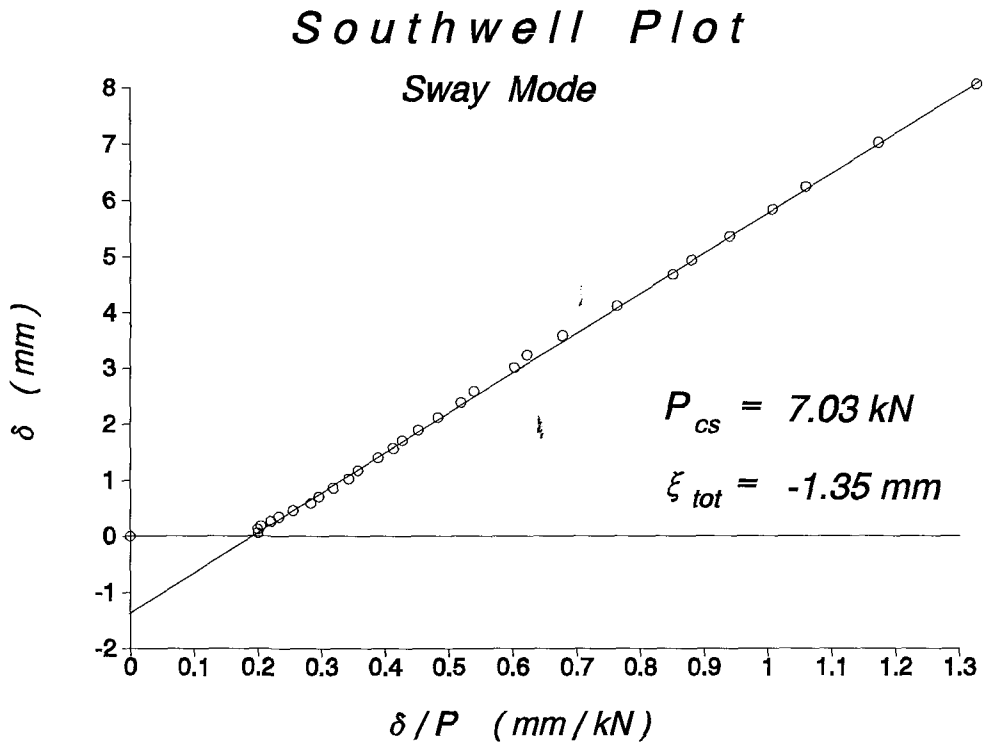
Southwell Plot
Sway Mode
δ (mm)
δ / P (mm / kN)
P cs = 7.03 kN
ξ tot = -1.35 mm
8
7
6
5
4
3
2
1
0
-1
-2
0
0.1
0.2
0.3
0.4
0.5
0.6
0.7
0.8
0.9
1
1.1
1.2
1.3

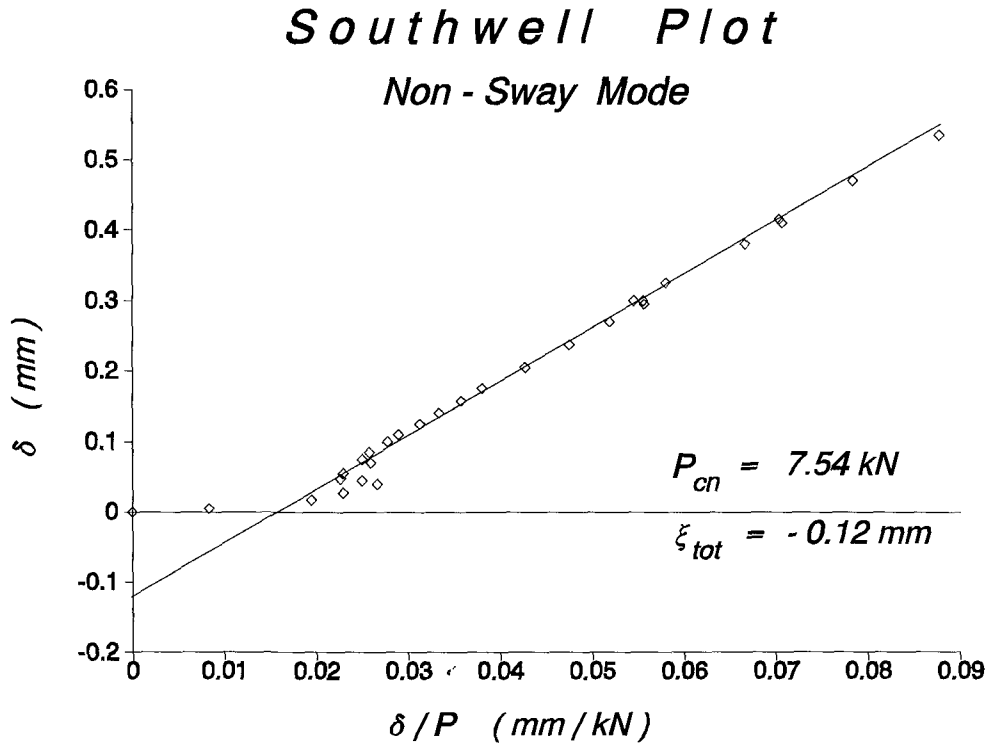
Southwell Plot
Non - Sway Mode
δ (mm)
δ / P (mm / kN)
P cn = 7.54 kN
ξ tot = - 0.12 mm
0.6
0.5
0.4
0.3
0.2
0.1
0
-0.1
-0.2
0
0.01
0.02
0.03
0.04
0.05
0.06
0.07
0.08
0.09

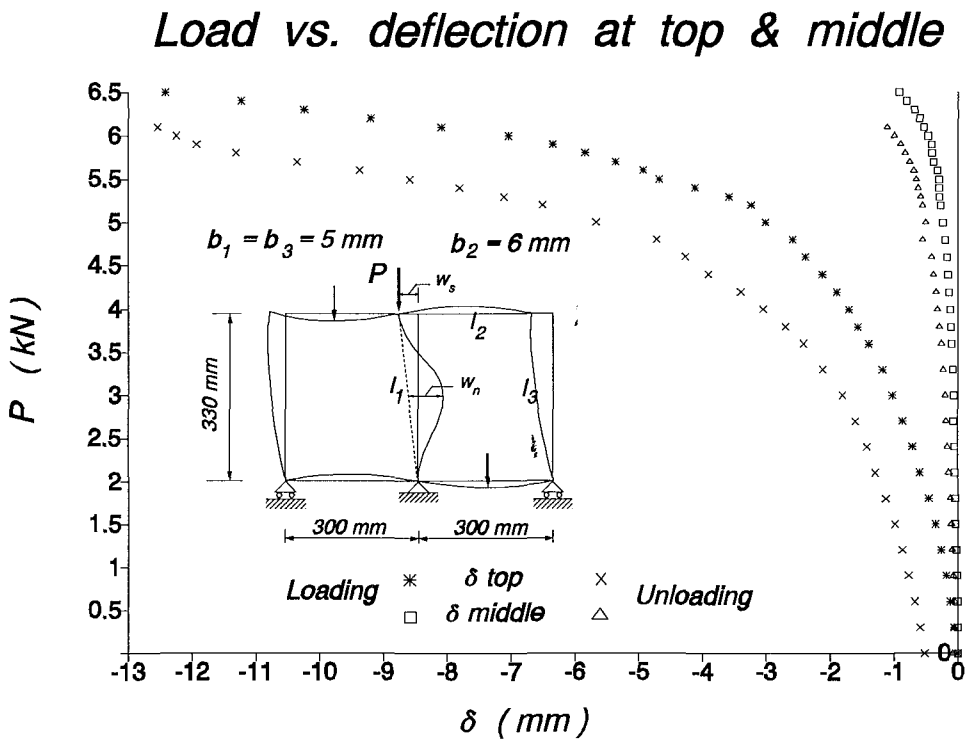

THEORETICAL DATA & RESULTS

PROP_sets = 3, SWAY_imp = 1.35 mm, NON-SWAY_imp = 0.12 mm

MEMBER PROPERTIES

MEM	L	b	d	A	I	Zel	Zpl	Y.str
1	330.0	5.0	13.0	62.44	125.70	50.28	81.45	0.360
2	300.0	6.0	13.0	73.44	209.00	69.67	117.71	0.360
3	330.0	5.0	13.0	62.44	125.70	50.28	81.45	0.360

Rotational SYMMETRIC (Non-sway) Stiffness of frame : 1234.98 kN*mm/rad
Rotational ANTISYMMETRIC (Sway) Stiffness of frame : 1468.91 kN*mm/rad
Translational (Sway) Stiffness of frame : 15.96 N/mm

EIGENVALUES & EIGENVECTORS

Solut	kL	Pc	C1	C2	delta	theta_A	Mode-Case
1	5.265	6.2396	1.00	1.792	-12.836	-0.004	* Sway
2	5.630	7.1350	1.00	-0.339	0.000	0.006	Non-Sway

First YIELD Load = 5.664 kN
First HINGE Load = 5.943 kN
SQUASH Load = 22.477 kN

Test: 4oc2
Plastic Bucling

Experimental Data					Southwell Plot			
Load P kN	Loading		Unloading		Sway Mode		Non-Sway Mode	
	Top reads	Mid reads	Top reads	Mid reads	$\frac{\delta_t}{100}$ mm	$\frac{\delta_t}{100P}$ mm/kN	$\frac{\delta_m-\delta_t/2}{100}$ mm	$\frac{\delta_m-\delta_t/2}{100P}$ mm/kN
0	1482	368	1439	427	0.000	0.000	0.000	0.000
0.3	1480.5	372.5	1428	439	0.015	0.050	0.038	0.125
0.6	1476	378.5	1417	451	0.060	0.100	0.075	0.125
0.9	1467	388	1404	465	0.150	0.167	0.125	0.139
1.2	1458.5	396	1389	481	0.235	0.196	0.163	0.135
1.5	1449	405	1374	495	0.330	0.220	0.205	0.137
1.8	1438	416	1356	514	0.440	0.244	0.260	0.144
2.1	1426	429	1339	532	0.560	0.267	0.330	0.157
2.4	1412.5	442	1318	553	0.695	0.290	0.393	0.164
2.7	1396	459	1295	578	0.860	0.319	0.480	0.178
3	1377	478	1271	605	1.050	0.350	0.575	0.192
3.3	1356	499	1245	635	1.260	0.382	0.680	0.206
3.6	1331	523	1214	668	1.510	0.419	0.795	0.221
3.8	1309	545	1193	691	1.730	0.455	0.905	0.238
4	1292	562	1168	718	1.900	0.475	0.990	0.248
4.2	1271.5	584.5	1131	756	2.105	0.501	1.113	0.265
4.4	1252.5	610	1098	789	2.295	0.522	1.273	0.289
4.6	1222	636.5	1063	828	2.600	0.565	1.385	0.301
4.8	1193	670	1026	868	2.890	0.602	1.575	0.328
5	1160.5	705	980	923	3.215	0.643	1.763	0.353
5.2	1121	746	931	982	3.610	0.694	1.975	0.380
5.4	1075	796	883	1040	4.070	0.754	2.245	0.416
5.6	1018	858	827	1114	4.640	0.829	2.580	0.461
5.8	950	934	755	1210	5.320	0.917	3.000	0.517
6	868	1029	730	1260	6.140	1.023	3.540	0.590
6.02	730	1260	730	1260	7.520	1.249	5.160	0.857

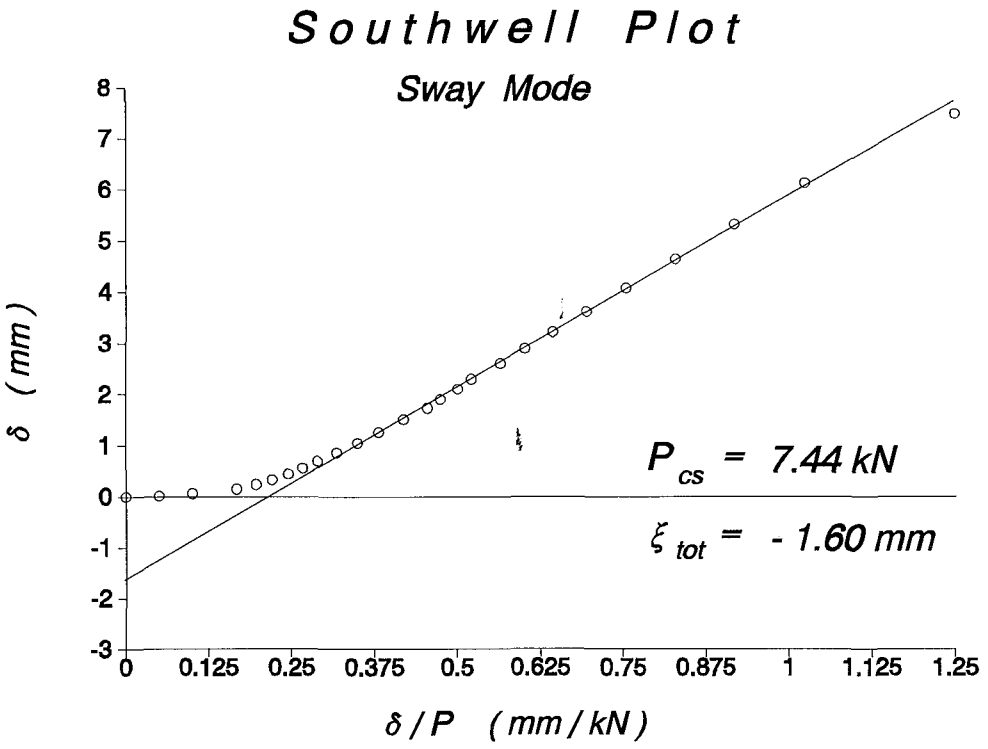
Southwell Plot
Sway Mode
δ (mm)
δ / P (mm / kN)
P cs = 7.44 kN
ξ tot = - 1.60 mm
8
7
6
5
4
3
2
1
0
-1
-2
-3
0
0.125
0.25
0.375
0.5
0.625
0.75
0.875
1
1.125
1.25

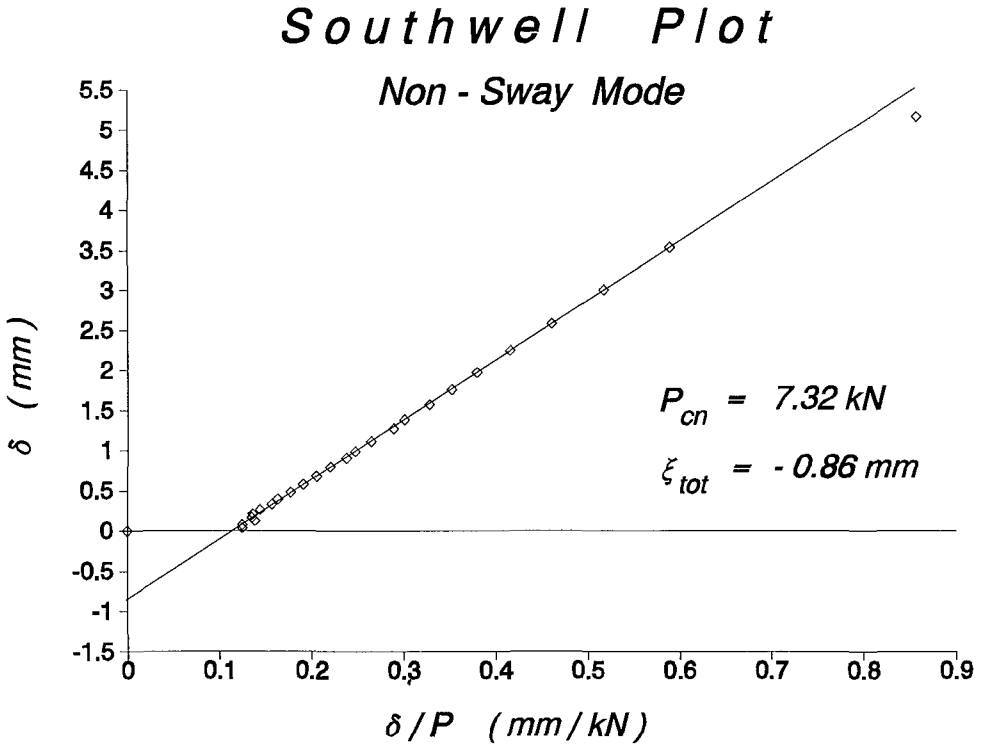
Southwell Plot
Non - Sway Mode
δ (mm)
δ / P (mm / kN)
P cn = 7.32 kN
ξ tot = - 0.86 mm
5.5
5
4.5
4
3.5
3
2.5
2
1.5
1
0.5
0
-0.5
-1
-1.5
0
0.1
0.2
0.3
0.4
0.5
0.6
0.7
0.8
0.9

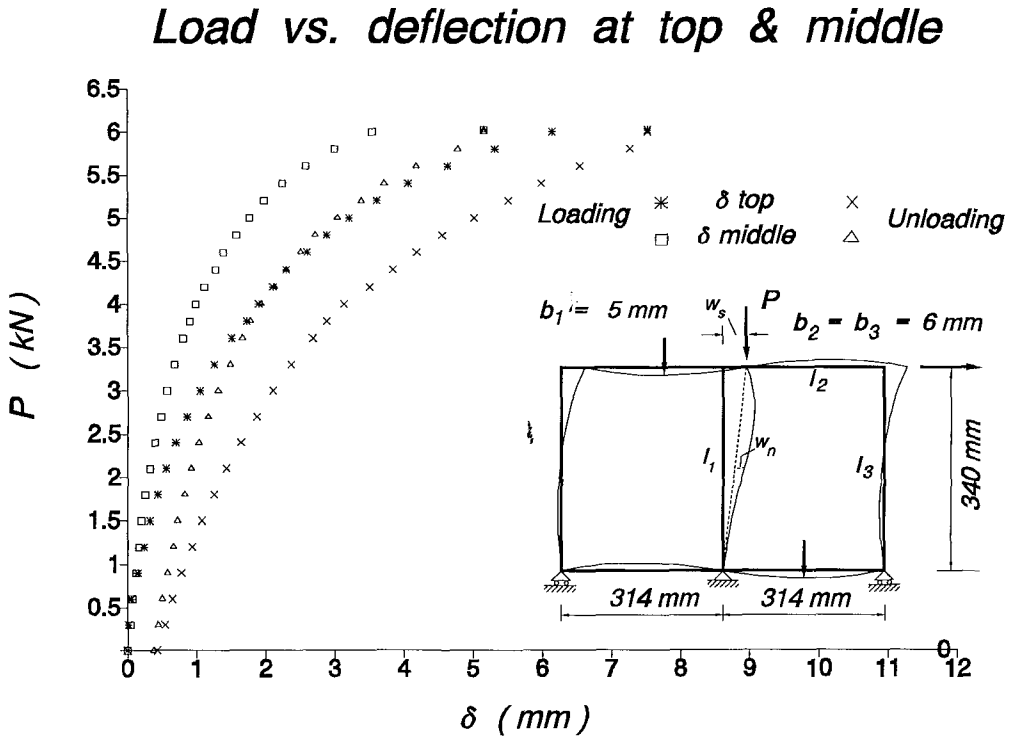

THEORETICAL DATA & RESULTS

PROP_sets = 3, SWAY_imp = -1.60 mm, NON-SWAY_imp = -0.90 mm

MEMBER PROPERTIES

MEM	L	b	d	A	I	Zel	Zpl	Y.str
1	340.0	5.0	13.0	62.44	125.70	50.28	81.45	0.360
2	314.0	6.0	13.0	73.44	209.00	69.67	117.71	0.360
3	340.0	6.0	13.0	73.44	209.00	69.67	117.71	0.360

	Rot.Sym.Non-sway	Rot.Antisym.Sway	Transl.Sway
Stiffness of frame :	1221.35 kN*mm/rad	1465.26 kN*mm/rad	17.933 N/mm.

EIGENVALUES & EIGENVECTORS

Solut	kL	Pc	C1	C2	delta	theta_A	Mode-Case
1	5.640	6.7459	1.00	-0.333	0.000	0.006	Non-Sway
2	5.643	6.7528	1.00	3.018	-20.600	-0.005	* Sway

First YIELD Load = 4.835 kN

First HINGE Load = 5.602 kN

SQUASH Load = 22.477 kN

Test: 23oc2
Elasto_Plastic Buckling

Experimental Data					Southwell Plot			
Load P kN	Loading		Unloading		Sway Mode		Non-Sway Mode	
	Top reads	Mid reads	Top reads	Mid reads	$\frac{\delta_t}{100}$ mm	$\frac{\delta_t}{100P}$ mm/kN	$\frac{\delta_m-\delta_t/2}{100}$ mm	$\frac{\delta_m-\delta_t/2}{100P}$ mm/kN
0	690	1300	697	1307	0.000	0.000	0.000	0.000
0.3	691	1300	701	1310	0.010	0.033	0.005	0.017
0.6	692	1300	705	1310.5	0.020	0.033	0.010	0.017
0.9	693.5	1300.5	710	1311	0.035	0.039	0.023	0.025
1.2	695	1302.5	716	1311	0.050	0.042	0.050	0.042
1.5	697	1304	721	1311.5	0.070	0.047	0.075	0.050
1.8	700	1305.5	729	1311.5	0.100	0.056	0.105	0.058
2.1	703	1306	739	1311.5	0.130	0.062	0.125	0.060
2.4	707	1308	745	1312	0.170	0.071	0.165	0.069
2.7	713	1309	751	1313.5	0.230	0.085	0.205	0.076
3	719	1310.5	758	1314	0.290	0.097	0.250	0.083
3.3	725	1311.5	767	1315	0.350	0.106	0.290	0.088
3.6	731	1313	777	1315.5	0.410	0.114	0.335	0.093
3.9	738.5	1315	788	1316	0.485	0.124	0.393	0.101
4.2	746	1317	801	1316	0.560	0.133	0.450	0.107
4.5	755	1319	813	1317.5	0.650	0.144	0.515	0.114
4.8	766	1320.5	825	1318	0.760	0.158	0.585	0.122
5.1	775	1323	837	1320	0.850	0.167	0.655	0.128
5.4	786	1325	854	1321	0.960	0.178	0.730	0.135
5.7	799	1327	870	1322	1.090	0.191	0.815	0.143
6	811	1330	892	1323	1.210	0.202	0.905	0.151
6.2	820	1332	908	1324	1.300	0.210	0.970	0.156
6.4	831	1334	923	1325	1.410	0.220	1.045	0.163
6.6	843	1336	936	1328	1.530	0.232	1.125	0.170
6.8	854	1339	944	1334	1.640	0.241	1.210	0.178
7	865	1342	958	1340	1.750	0.250	1.295	0.185
7.2	876	1347	965	1347	1.860	0.258	1.400	0.194
7.4	888	1353	976	1352	1.980	0.268	1.520	0.205
7.6	899	1360	984	1361	2.090	0.275	1.645	0.216
7.9	923	1327	997.5	1373	2.330	0.295	1.435	0.182
8.1	929	1385	1005	1381	2.390	0.295	2.045	0.252
8.2	937	1390	1009	1388	2.470	0.301	2.135	0.260
8.3	945	1395	1013	1390	2.550	0.307	2.225	0.268
8.4	953	1400	1015	1395	2.630	0.313	2.315	0.276
8.5	961	1405	1017	1401	2.710	0.319	2.405	0.283
8.6	970	1414	1016	1406	2.800	0.326	2.540	0.295
8.7	978	1422	1005	1419	2.880	0.331	2.660	0.306

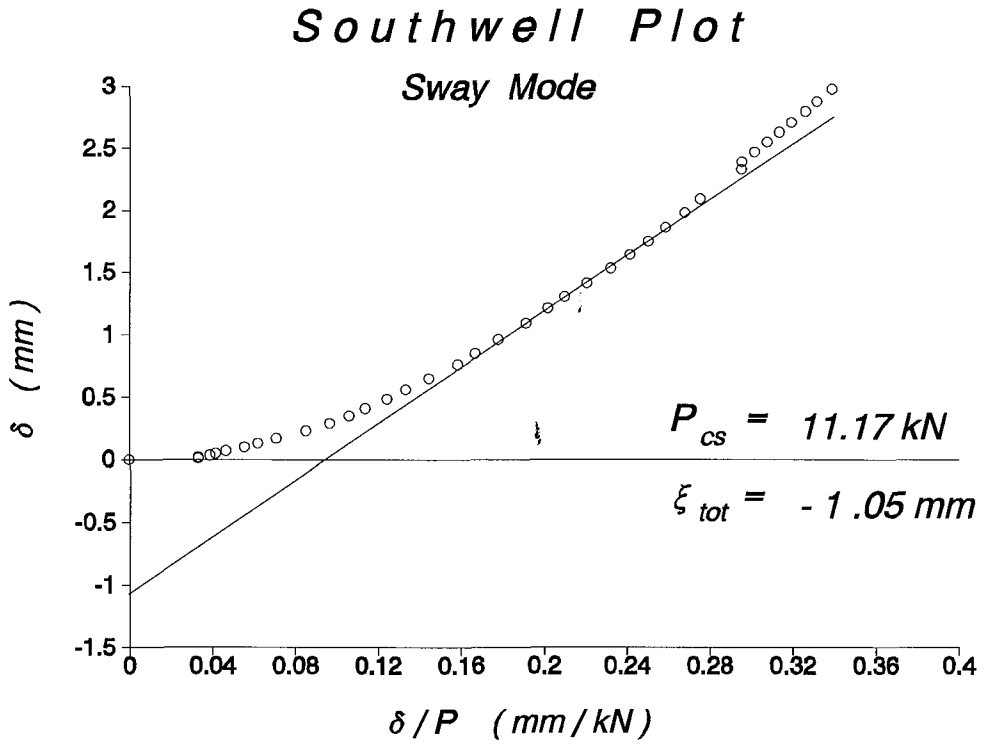
Southwell Plot
Sway Mode
δ (mm)
δ / P (mm / kN)
P cs = 11.17 kN
ξ tot = - 1 .05 mm
3
2.5
2
1.5
1
0.5
0
-0.5
-1
-1.5
0
0.04
0.08
0.12
0.16
0.2
0.24
0.28
0.32
0.36
0.4

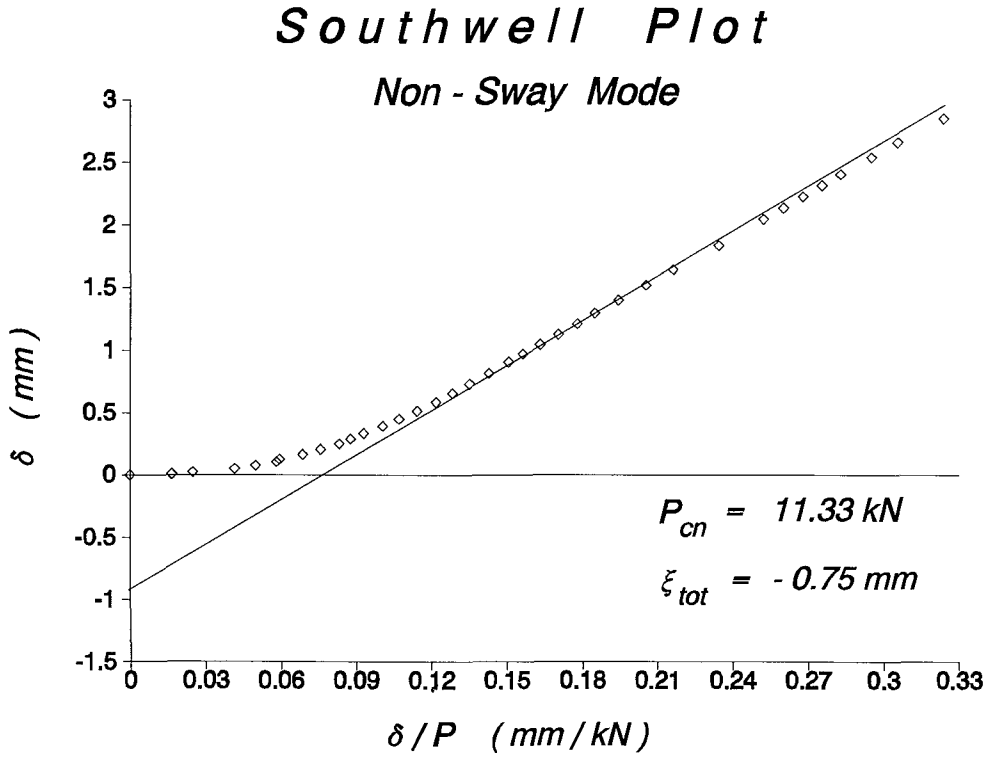
Southwell Plot
Non - Sway Mode
δ (mm)
δ / P (mm / kN)
P cn = 11.33 kN
ξ tot = - 0.75 mm
3
2.5
2
1.5
1
0.5
0
-0.5
-1
-1.5
0
0.03
0.06
0.09
0.12
0.15
0.18
0.21
0.24
0.27
0.3
0.33

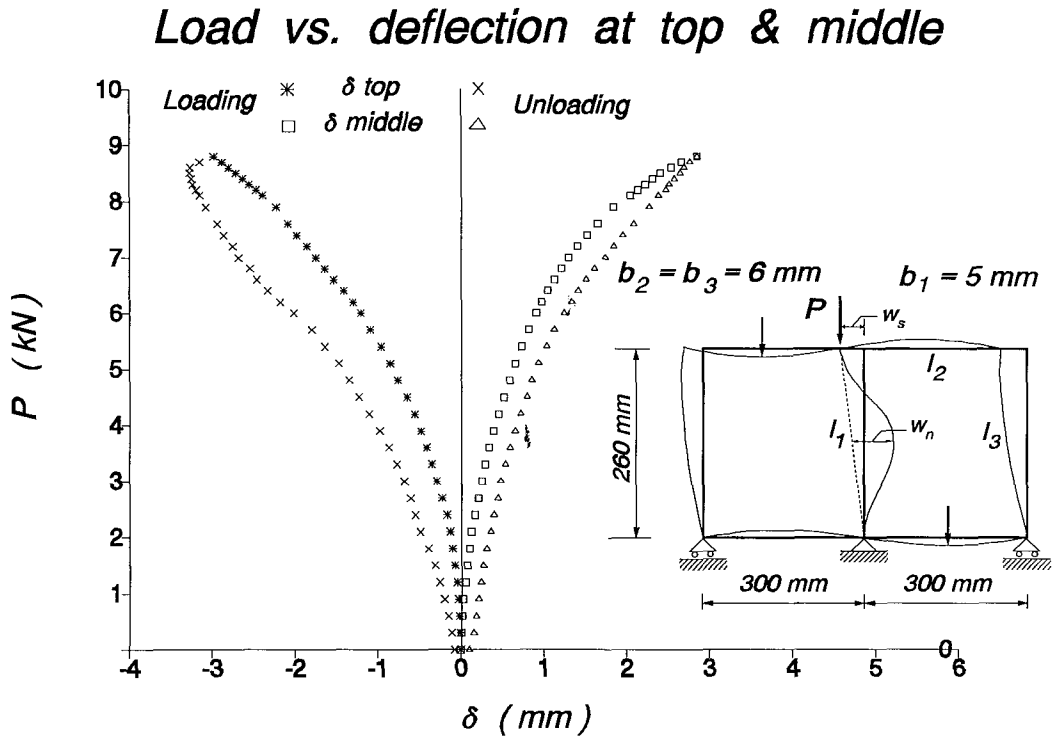

THEORETICAL DATA & RESULTS

PROP_sets = 3, SWAY_imp = 1.05 mm, NON-SWAY_imp = -0.75 mm

MEMBER PROPERTIES

MEM	L	b	d	A	I	Zel	Zpl	Y.str
1	260.0	5.0	13.0	62.44	125.70	50.28	81.45	0.360
2	300.0	6.0	13.0	73.44	209.00	69.67	117.71	0.360
3	260.0	6.0	13.0	73.44	209.00	69.67	117.71	0.360

Rotational SYMMETRIC (Non-sway) Stiffness of frame : 1343.77 kN*mm/rad
Rotational ANTISYMMETRIC (Sway) Stiffness of frame : 1641.35 kN*mm/rad
Translational (Sway) Stiffness of frame : 38.04 N/mm

EIGENVALUES & EIGENVECTORS

Solut	kL	Pc	C1	C2	delta	theta_A	Mode-Case
1	5.540	11.1290	1.00	2.566	-17.980	-0.007	* Sway
2	5.542	11.1352	1.00	-0.389	0.000	0.008	Non-Sway

First YIELD Load = 7.953 kN
First HINGE Load = 9.335 kN
SQUASH Load = 22.477 kN

Test: 25oc2
Elastic_Plastic Buckling

Experimental Data					Southwell Plot			
	Loading		Unloading		Sway Mode		Non-Sway Mode	
Load P kN	Top reads	Mid reads	Top reads	Mid reads	$\frac{\delta_t}{100}$ mm	$\frac{\delta_t}{100P}$ mm/kN	$\frac{\delta_m-\delta_t/2}{100}$ mm	$\frac{\delta_m-\delta_t/2}{100P}$ mm/kN
0	987	1148.5	1008	1195	0.000	0.000	0.000	0.000
0.2	988.5	1150	1019	1196	0.015	0.075	0.023	0.113
0.4	990	1151	1026	1200	0.030	0.075	0.040	0.100
0.6	991	1152	1033	1203	0.040	0.067	0.055	0.092
0.8	993	1152.5	1038	1207	0.060	0.075	0.070	0.088
1	995	1154	1044	1210	0.080	0.080	0.095	0.095
1.2	998.5	1155	1052	1215	0.115	0.096	0.123	0.102
1.4	1003.5	1156	1059	1219.5	0.165	0.118	0.158	0.113
1.6	1009	1157.5	1068	1224.5	0.220	0.138	0.200	0.125
1.8	1016	1159.5	1078	1231	0.290	0.161	0.255	0.142
2	1023	1162	1087	1238	0.360	0.180	0.315	0.158
2.2	1031.5	1164.5	1098	1247.5	0.445	0.202	0.383	0.174
2.4	1040	1166	1109	1258	0.530	0.221	0.440	0.183
2.6	1050	1171	1122	1272	0.630	0.242	0.540	0.208
2.8	1063	1175	1139	1285	0.760	0.271	0.645	0.230
3	1074.5	1180.5	1155	132	0.875	0.292	0.758	0.253
3.2	1085.5	1187.5	1178	1323	0.985	0.308	0.883	0.276
3.4	1103	1193.5	1198.5	1350	1.160	0.341	1.030	0.303
3.5	1113.5	1197.5	1210	1368.5	1.265	0.361	1.123	0.321
3.6	1123	1203	1220	1385	1.360	0.378	1.225	0.340
3.7	1135	1210	1231	1405.5	1.480	0.400	1.355	0.366
3.8	1149.5	1218	1236	1428.5	1.625	0.428	1.508	0.397
3.9	1164	1229.5			1.770	0.454	1.695	0.435
4	1182	1241.5			1.950	0.488	1.905	0.476
4.1	1195	1263			2.080	0.507	2.185	0.533
4.2	1214	1290			2.270	0.540	2.550	0.607
3.93	1233	1463			2.460	0.626	4.375	1.113

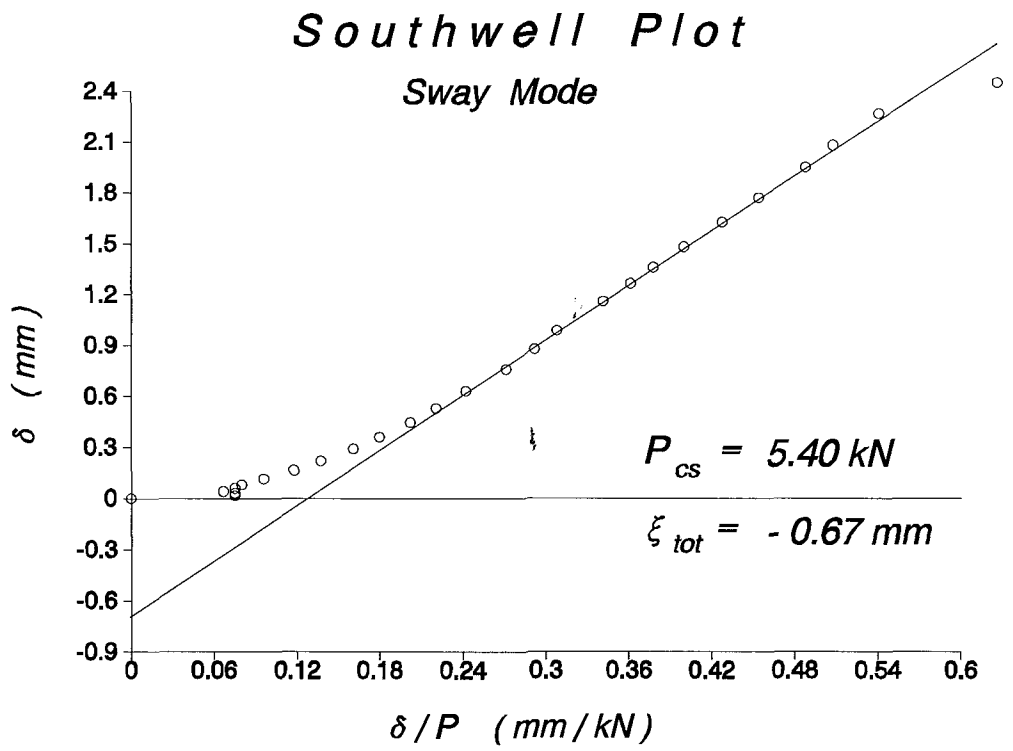
Southwell Plot
Sway Mode
2.4
2.1
1.8
1.5
1.2
0.9
0.6
0.3
0
-0.3
-0.6
-0.9
δ (mm)
0
0.06
0.12
0.18
0.24
0.3
0.36
0.42
0.48
0.54
0.6
δ / P (mm / kN)
P cs = 5.40 kN
ξ tot = - 0.67 mm

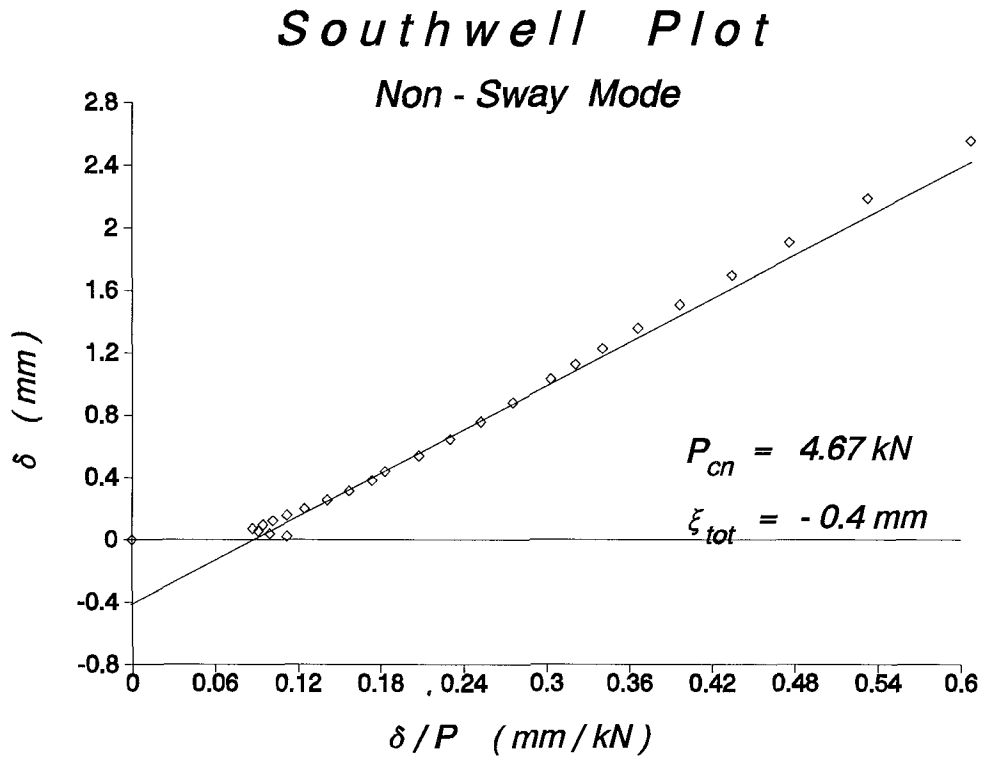
Southwell Plot
Non - Sway Mode
2.8
2.4
2
1.6
1.2
0.8
0.4
0
-0.4
-0.8
δ (mm)
0
0.06
0.12
0.18
0.24
0.3
0.36
0.42
0.48
0.54
0.6
δ / P (mm / kN)
P cn = 4.67 kN
ξ tot = - 0.4 mm

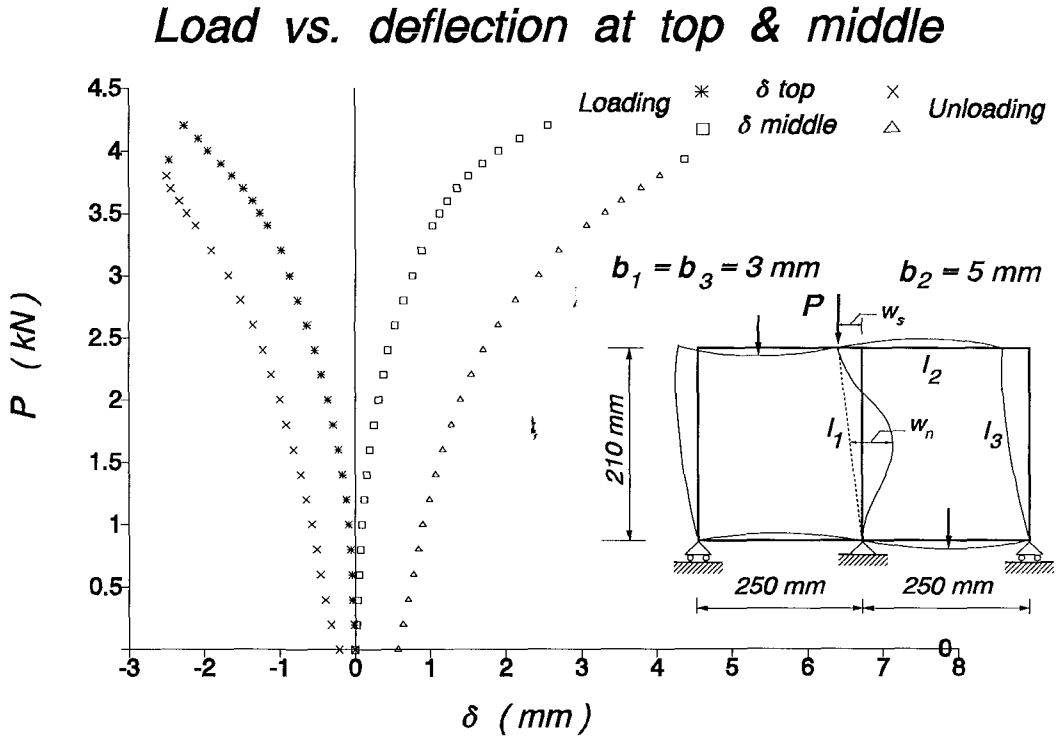

THEORETICAL DATA & RESULTS

PROP_sets = 3, SWAY_imp = -0.67 mm, NON-SWAY_imp = -0.40 mm

MEMBER PROPERTIES

MEM	L	b	d	A	I	Zel	Zpl	Y.str
1	210.0	3.0	13.0	38.47	28.53	19.02	29.26	0.360
2	250.0	5.0	13.0	62.44	125.70	50.28	81.45	0.360
3	210.0	3.0	13.0	38.47	28.53	19.02	29.26	0.360

Rotational SYMMETRIC (Non-sway) Stiffness of frame : 920.69 kN*mm/rad
Rotational ANTISYMMETRIC (Sway) Stiffness of frame : 1112.57 kN*mm/rad
Translational (Sway) Stiffness of frame : 25.34 N/mm

EIGENVALUES & EIGENVECTORS

Solut	kL	Pc	C1	C2	delta	theta_A	Mode-Case
1	5.944	4.4573	1.00	-0.171	0.000	0.005	Non-Sway
2	6.423	5.2043	1.00	-14.263	88.629	-0.005	* Sway

First YIELD Load = 3.442 kN
First HINGE Load = 3.857 kN
SQUASH Load = 13.848 kN

Test: 26oc2
Elastic_Plastic Buckling

Experimental Data					Southwell Plot			
Load P kN	Loading		Unloading		Sway Mode		Non-Sway Mode	
	Top reads	Mid reads	Top reads	Mid reads	$\frac{\delta_t}{100}$ mm	$\frac{\delta_t}{100P}$ mm/kN	$\frac{\delta_m-\delta_t/2}{100}$ mm	$\frac{\delta_m-\delta_t/2}{100P}$ mm/kN
0	337	1062.5	396	1005	0.000	0.000	0.000	0.000
0.2	344	1061.5	406	990	0.070	0.350	0.025	0.125
0.4	348	1061	418	982	0.110	0.275	0.040	0.100
0.6	354	1052.5	430	974	0.170	0.283	0.015	0.025
0.8	356.5	1050	442	967	0.195	0.244	0.028	0.034
1	361.5	1048.5	463	958	0.245	0.245	0.018	0.018
1.2	368	1046	472	947.5	0.310	0.258	0.010	0.008
1.4	376	1043	491	935	0.390	0.279	0.000	0.000
1.6	385	1040	512	921	0.480	0.300	0.015	0.009
1.8	395.5	1036	536	906	0.585	0.325	0.028	0.015
2	409	1032	563	887	0.720	0.360	0.055	0.028
2.1	418	1029	578	876	0.810	0.386	0.070	0.033
2.2	426	1026	599	862	0.890	0.405	0.080	0.036
2.3	435	1022	618	847	0.980	0.426	0.085	0.037
2.4	445	1019	645	828	1.080	0.450	0.105	0.044
2.5	456	1015	668	811	1.190	0.476	0.120	0.048
2.6	468	1010	697	789	1.310	0.504	0.130	0.050
2.7	481	1004	734	761	1.440	0.533	0.135	0.050
2.8	495	997.5	772	730	1.580	0.564	0.140	0.050
2.9	511	991	820	695	1.740	0.600	0.155	0.053
3	533	981	880	647	1.960	0.653	0.165	0.055
3.1	558	970	952	589	2.210	0.713	0.180	0.058
3.2	585	955	1028	522	2.480	0.775	0.165	0.052
3.3	617	938	1096	455	2.800	0.848	0.155	0.047
3.4	656	914	1179	372	3.190	0.938	0.110	0.032
3.5	710	879			3.730	1.066	0.030	0.009
3.6	780	827			4.430	1.231	0.140	0.039
3.7	891	735			5.540	1.497	0.505	0.136
3.8	1085	548			7.480	1.968	1.405	0.370
3.56	1276	241			9.390	2.638	3.520	0.989

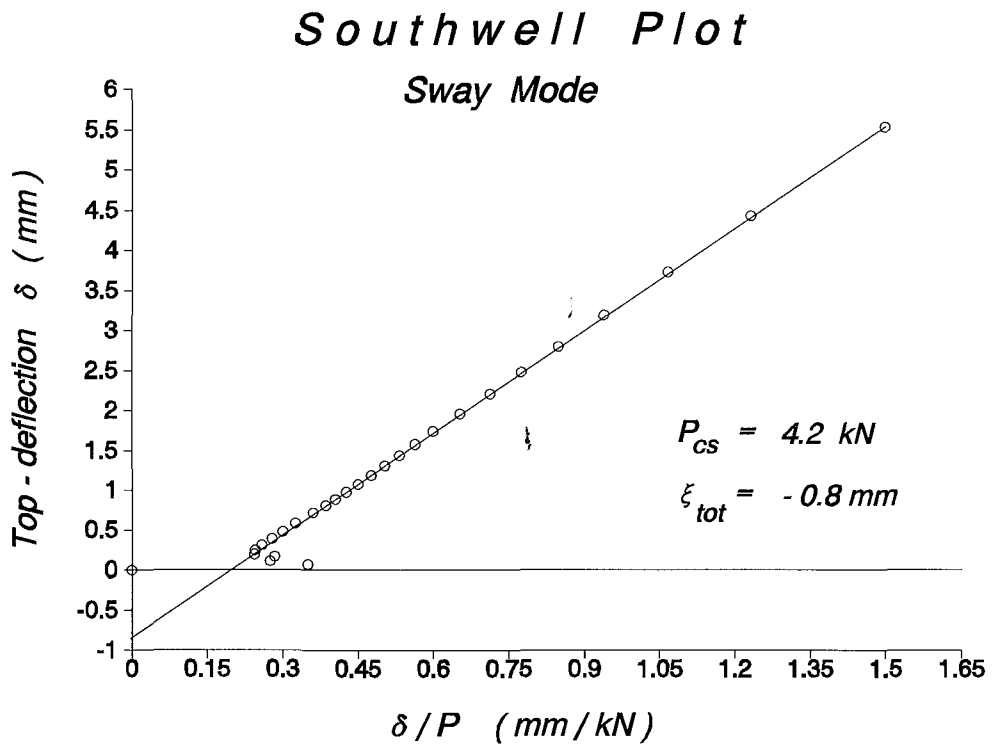
Southwell Plot
Sway Mode
Top - deflection δ (mm)
6
5.5
5
4.5
4
3.5
3
2.5
2
1.5
1
0.5
0
-0.5
-1
0
0.15
0.3
0.45
0.6
0.75
0.9
1.05
1.2
1.35
1.5
1.65
δ / P (mm / kN)
P_{cs} = 4.2 kN
ξ_{tot} = - 0.8 mm

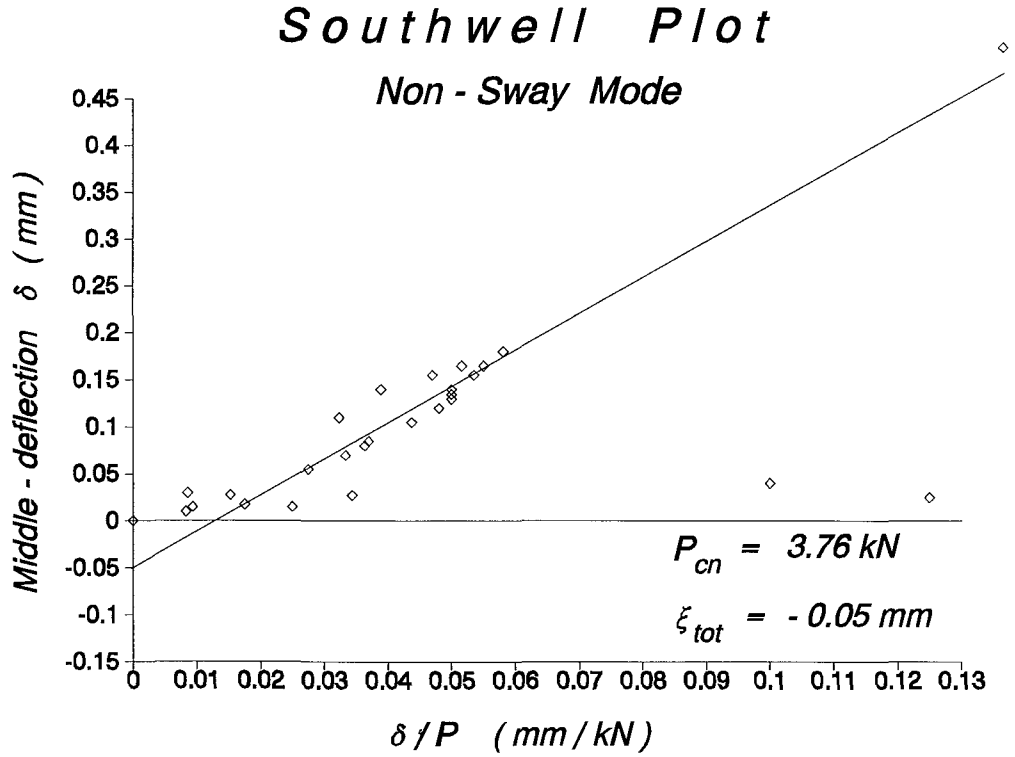
Southwell Plot
Non - Sway Mode
Middle - deflection δ (mm)
0.45
0.4
0.35
0.3
0.25
0.2
0.15
0.1
0.05
0
-0.05
-0.1
-0.15
0
0.01
0.02
0.03
0.04
0.05
0.06
0.07
0.08
0.09
0.1
0.11
0.12
0.13
δ / P (mm / kN)
P_{cn} = 3.76 kN
ξ_{tot} = - 0.05 mm

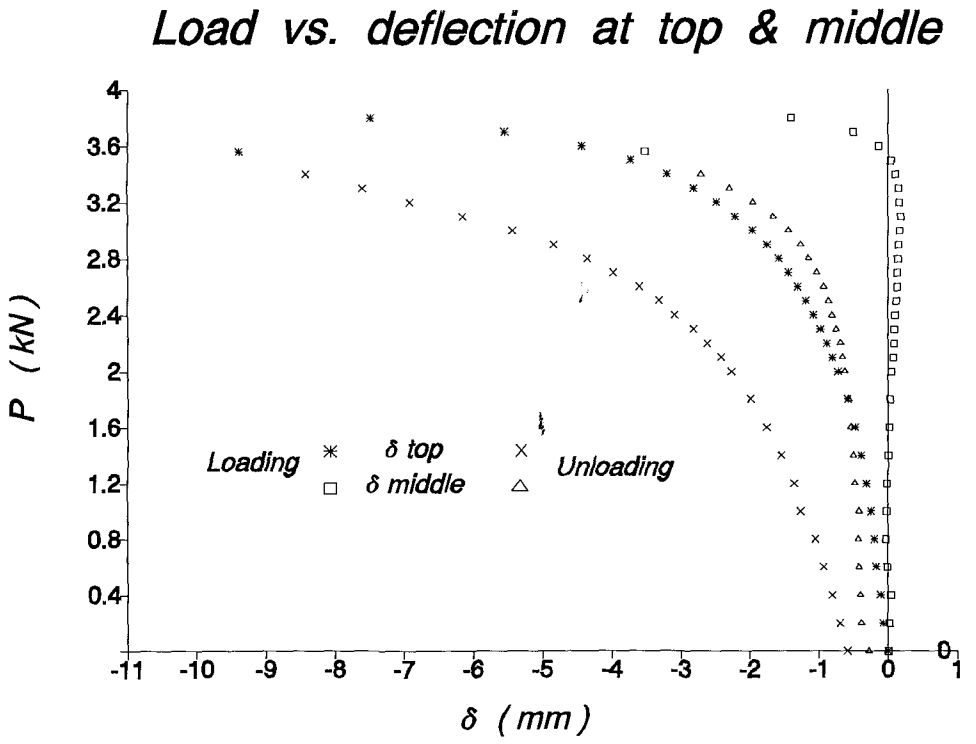

THEORETICAL DATA & RESULTS

PROP_sets = 3, SWAY_imp = -0.65 mm, NON-SWAY_imp = -0.04 mm

MEMBER PROPERTIES

MEM	L	b	d	A	I	Zel	Zpl	Y.str
1	235.0	3.0	13.0	38.47	28.53	19.02	29.26	0.360
2	400.0	5.0	13.0	62.44	125.70	50.28	81.45	0.360
3	235.0	5.0	13.0	62.44	125.70	50.28	81.45	0.360

Rotational SYMMETRIC (Non-sway) Stiffness of frame : 580.93 kN*mm/rad
Rotational ANTISYMMETRIC (Sway) Stiffness of frame : 682.39 kN*mm/rad
Translational (Sway) Stiffness of frame : 21.38 N/mm

EIGENVALUES & EIGENVECTORS

Solut	kL	Pc	C1	C2	delta	theta_A	Mode-Case
1	5.818	3.4092	1.00	-0.237	0.000	0.006	Non-Sway
2	6.777	4.6264	1.00	-3.967	23.289	-0.007	* Sway

First YIELD Load = 2.827 kN
First HINGE Load = 3.066 kN
SQUASH Load = 13.848 kN

Test: 6N2
Elastic - Plastic Buckling

Experimental Data					Southwell Plot			
Load P kN	Loading		Unloading		Sway Mode		Non-Sway Mode	
	Top reads	Mid reads	Top reads	Mid reads	$\frac{\delta_t}{100}$ mm	$\frac{\delta_t}{100P}$ mm/kN	$\frac{\delta_m-\delta_t/2}{100}$ mm	$\frac{\delta_m-\delta_t/2}{100P}$ mm/kN
0	1373	1121	1311	1305	0.000	0.000	0.000	0.000
0.2	1372	1126	1305	1327	0.010	0.050	0.045	0.225
0.4	1368.5	1134	1298	1345	0.045	0.113	0.108	0.269
0.6	1363	1143	1287	1377	0.100	0.167	0.170	0.283
0.8	1359	1152	1275	1407	0.140	0.175	0.240	0.300
1	1351.5	1165	1262	1442	0.215	0.215	0.333	0.333
1.2	1344	1180	1249	1480	0.290	0.242	0.445	0.371
1.4	1334	1197	1233	1523	0.390	0.279	0.565	0.404
1.5	1328	1208	1225	1549	0.450	0.300	0.645	0.430
1.6	1322	1218	1214	1580	0.510	0.319	0.715	0.447
1.7	1314	1231	1205	1610	0.590	0.347	0.805	0.474
1.8	1307	1244	1195	1641	0.660	0.367	0.900	0.500
1.9	1299	1259	1183	1677	0.740	0.389	1.010	0.532
2	1290	1273	1171	1715	0.830	0.415	1.105	0.553
2.1	1280	1290	1158	1759	0.930	0.443	1.225	0.583
2.2	1269	1309.5	1136	1709	1.040	0.473	1.365	0.620
2.3	1256	1332	1114	1858	1.170	0.509	1.525	0.663
2.4	1242	1360	1095	1948	1.310	0.546	1.735	0.723
2.5	1226	1390			1.470	0.588	1.955	0.782
2.6	1209	1425			1.640	0.631	2.220	0.854
2.7	1192	1464			1.810	0.670	2.525	0.935
2.8	1171	1516			2.020	0.721	2.940	1.050
2.9	1147	1578			2.260	0.779	3.440	1.186
3	1113	1675			2.600	0.867	4.240	1.413
2.5	1084	1945			2.890	1.156	6.795	2.718

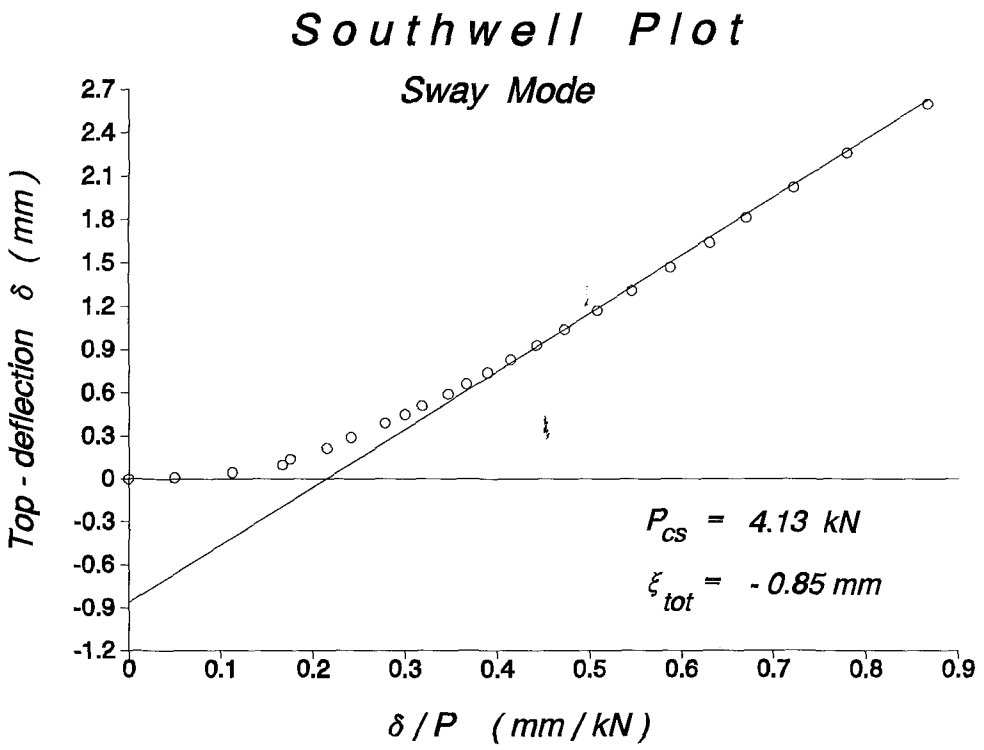
Southwell Plot
Sway Mode
Top - deflection δ (mm)
2.7
2.4
2.1
1.8
1.5
1.2
0.9
0.6
0.3
0
-0.3
-0.6
-0.9
-1.2
0
0.1
0.2
0.3
0.4
0.5
0.6
0.7
0.8
0.9
δ / P (mm / kN)
P_{cs} = 4.13 kN
ξ_{tot} = - 0.85 mm

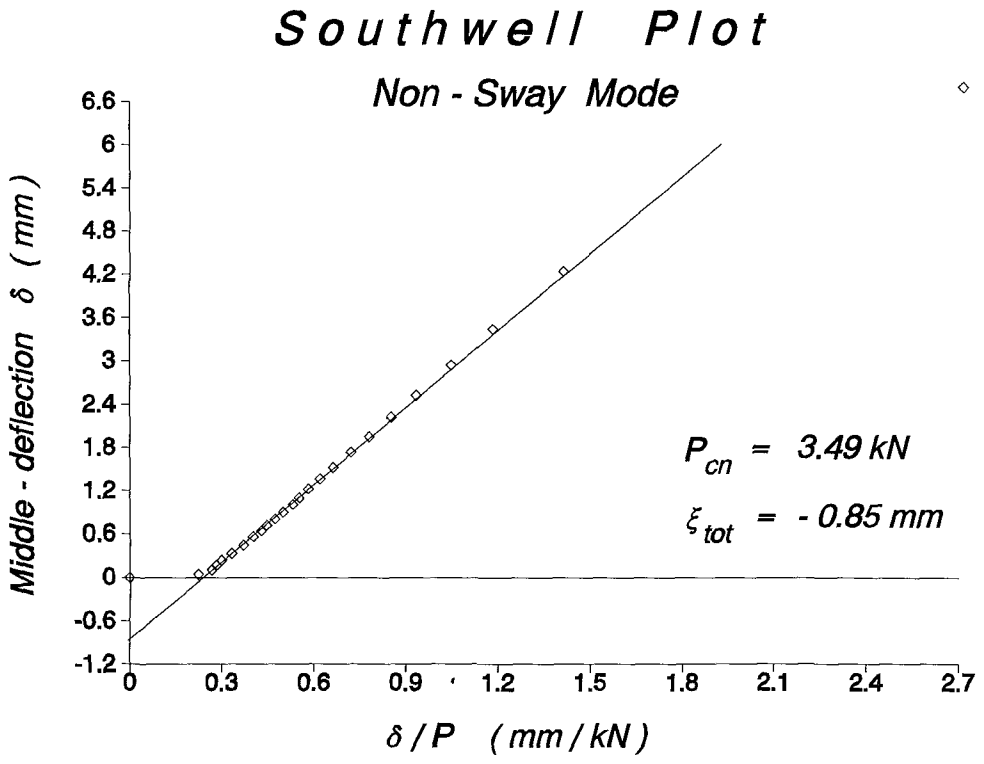
Southwell Plot
Non - Sway Mode
Middle - deflection δ (mm)
6.6
6
5.4
4.8
4.2
3.6
3
2.4
1.8
1.2
0.6
0
-0.6
-1.2
0
0.3
0.6
0.9
1.2
1.5
1.8
2.1
2.4
2.7
δ / P (mm / kN)
P_{cn} = 3.49 kN
ξ_{tot} = - 0.85 mm

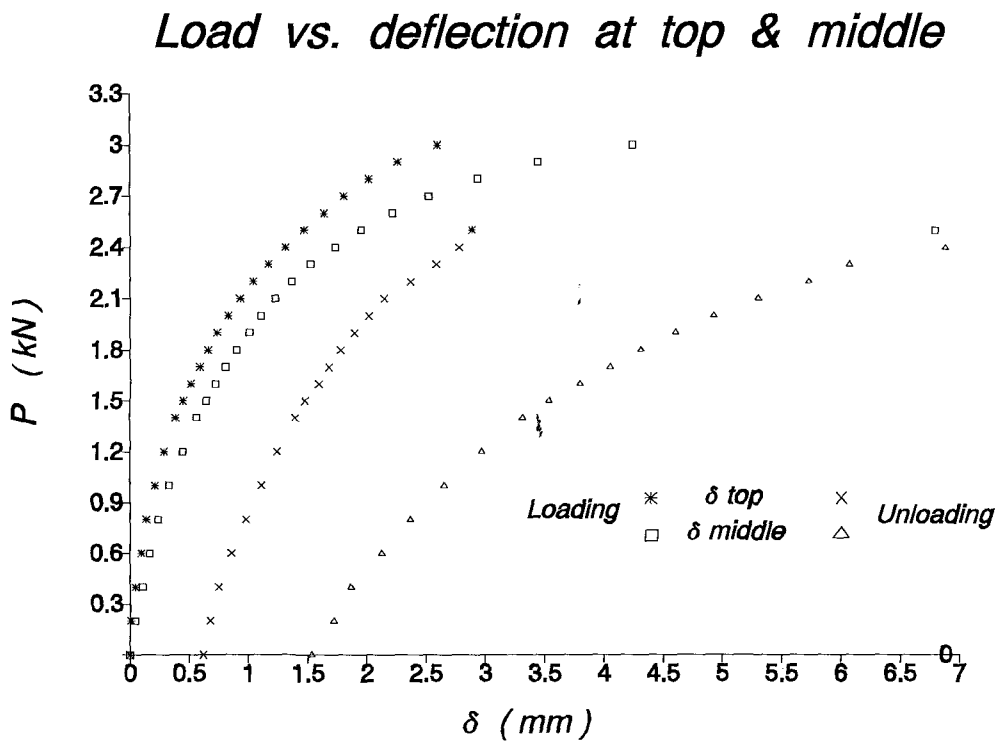

THEORETICAL DATA & RESULTS

PROP_sets = 3, SWAY_imp = -0.85 mm, NON-SWAY_imp = 0.85 mm

MEMBER PROPERTIES

MEM	L	b	d	A	I	Zel	Zpl	Y.str
1	235.0	3.0	13.0	38.47	28.53	19.02	29.26	0.360
2	370.0	5.0	13.0	62.44	125.70	50.28	81.45	0.360
3	235.0	5.0	13.0	62.44	125.70	50.28	81.45	0.360

Rotational SYMMETRIC (Non-sway) Stiffness of frame : 637.69 kN*mm/rad
Rotational ANTISYMMETRIC (Sway) Stiffness of frame : 757.60 kN*mm/rad
Translational (Sway) Stiffness of frame : 23.41 N/mm

EIGENVALUES & EIGENVECTORS

Solut	kL	Pc	C1	C2	delta	theta_A	Mode-Case
1	5.855	3.4533	1.00	-0.217	0.000	0.005	Non-Sway
2	6.968	4.8910	1.00	-2.805	16.026	-0.006	* Sway

First YIELD Load = 2.700 kN
First HINGE Load = 3.001 kN
SQUASH Load = 13.848 kN

Test: 18oc3
Plastic Collapse Buckling

Experimental Data					Southwell Plot			
Load P kN	Loading		Unloading		Sway Mod		Non-Sway Mode	
	Top reads	Mid reads	Top reads	Mid reads	$\frac{\delta_t}{100}$ mm	$\frac{\delta_t}{100P}$ mm/kN	$\frac{\delta_m-\delta_t/2}{100}$ mm	$\frac{\delta_m-\delta_t/2}{100P}$ mm/kN
0	414	1287	587	1249	0.000	0.000	0.000	0.000
0.3	421	1286	603	1248	0.070	0.233	0.025	0.083
0.6	431	1285	616	1245	0.170	0.283	0.065	0.108
0.9	437	1285	634	1243	0.230	0.256	0.095	0.106
1.2	446.5	1284.5	653	1239	0.325	0.271	0.138	0.115
1.5	457	1283.5	672	1235	0.430	0.287	0.180	0.120
1.8	467	1283.5	694	1230	0.530	0.294	0.230	0.128
2.1	478	1283	717	1225	0.640	0.305	0.280	0.133
2.4	491	1283	743	1219	0.770	0.321	0.345	0.144
2.7	503	1283	770	1212	0.890	0.330	0.405	0.150
3	517	1283	800	1205	1.030	0.343	0.475	0.158
3.3	533.5	1283	833	1197	1.195	0.362	0.558	0.169
3.6	550.5	1283	867	1188	1.365	0.379	0.643	0.178
3.9	570	1282	905	1178	1.560	0.400	0.730	0.187
4.2	589	1281	944	1166	1.750	0.417	0.815	0.194
4.5	612	1280	997	1150	1.980	0.440	0.920	0.204
4.8	637.5	1278	1052	1134	2.235	0.466	1.028	0.214
5	657	1275	1090	1121	2.430	0.486	1.095	0.219
5.2	676	1271	1137	1106	2.620	0.504	1.150	0.221
5.4	699	1266	1187	1089	2.850	0.528	1.215	0.225
5.6	724	1260	1260	1060	3.100	0.554	1.280	0.229
5.8	752	1253	1310	1047	3.380	0.583	1.350	0.233
6	784.5	1243.5	1390	1013	3.705	0.618	1.418	0.236
6.2	818	1234	1460	987	4.040	0.652	1.490	0.240
6.4	857	1224	1528	962	4.430	0.692	1.585	0.248
6.6	898	1212	1587	942	4.840	0.733	1.670	0.253
6.8	943	1199	1642	921	5.290	0.778	1.765	0.260
7	994	1182	1720	894	5.800	0.829	1.850	0.264
7.2	1052	1164	1790	867	6.380	0.886	1.960	0.272
7.4	1122	1141	1866	839	7.080	0.957	2.080	0.281
7.6	1204	1110	1925	816	7.900	1.039	2.180	0.287
7.8	1307	1072						
8	1473	1008						
7.95	1985	799						

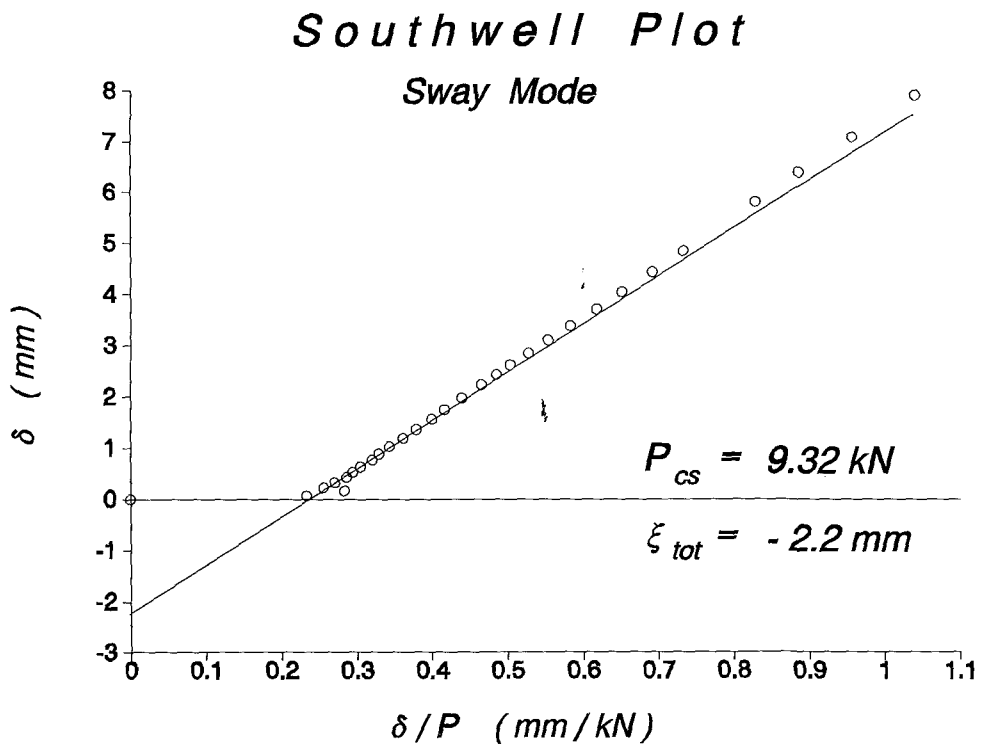
Southwell Plot
Sway Mode
δ (mm)
8
7
6
5
4
3
2
1
0
-1
-2
-3
0
0.1
0.2
0.3
0.4
0.5
0.6
0.7
0.8
0.9
1
1.1
δ / P (mm / kN)
P cs = 9.32 kN
ξ tot = - 2.2 mm

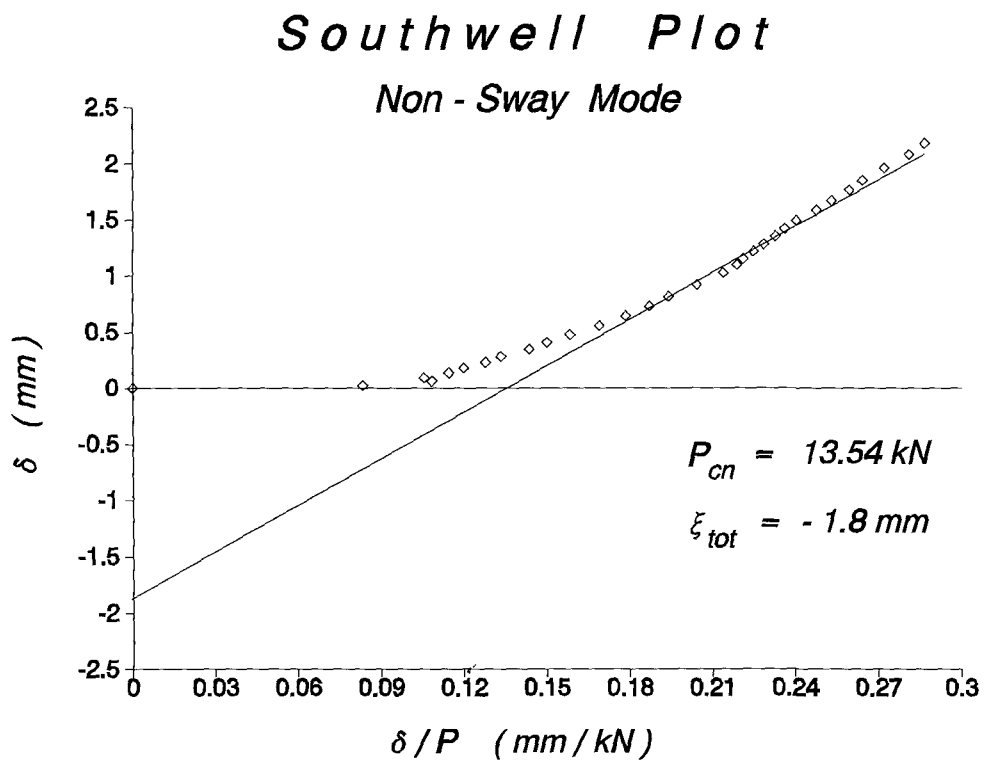
Southwell Plot
Non - Sway Mode
δ (mm)
2.5
2
1.5
1
0.5
0
-0.5
-1
-1.5
-2
-2.5
0
0.03
0.06
0.09
0.12
0.15
0.18
0.21
0.24
0.27
0.3
δ / P (mm / kN)
P cn = 13.54 kN
ξ tot = - 1.8 mm

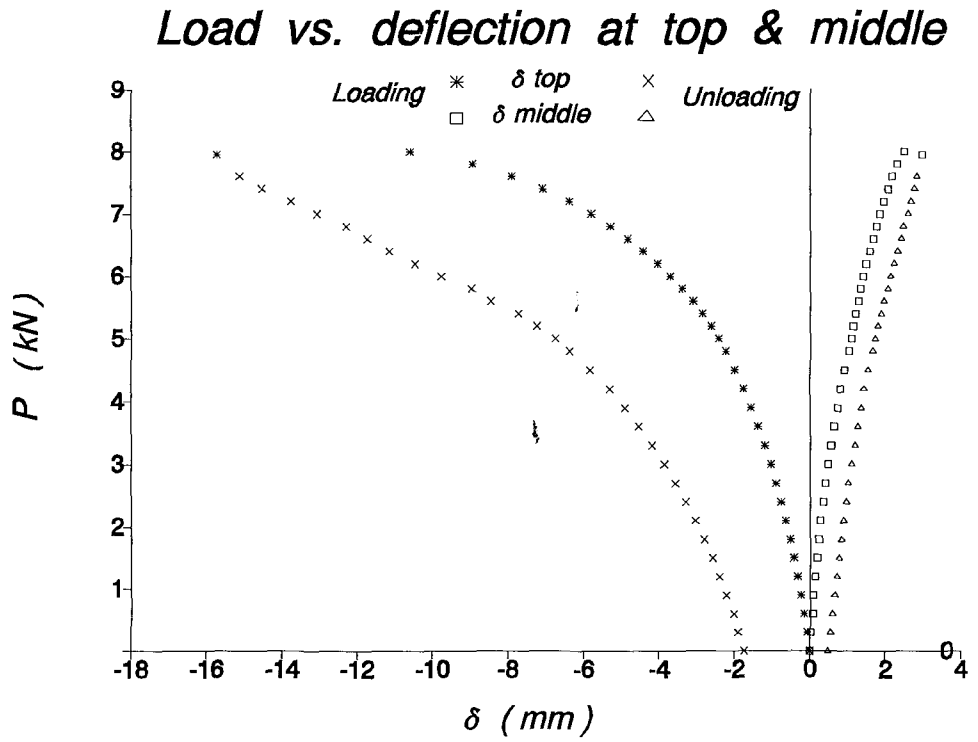

THEORETICAL DATA & RESULTS

PROP_sets = 3, SWAY_imp = 2.20 mm, NON-SWAY_imp = -1.80 mm

MEMBER PROPERTIES

MEM	L	b	d	A	I	Zel	Zpl	Y.str
1	280.0	6.0	13.0	73.44	209.00	69.67	117.71	0.360
2	300.0	5.0	13.0	62.44	125.70	50.28	81.45	0.360
3	280.0	5.0	13.0	62.44	125.70	50.28	81.45	0.360

Rotational SYMMETRIC (Non-sway) Stiffness of frame : 802.89 kN*mm/rad
Rotational ANTISYMMETRIC (Sway) Stiffness of frame : 980.22 kN*mm/rad
Translational (Sway) Stiffness of frame : 19.03 N/mm

EIGENVALUES & EIGENVECTORS

Solut	kL	Pc	C1	C2	delta	theta_A	Mode-Case
1	3.932	8.0359	1.00	0.417	-5.935	-0.008	* Sway
2	4.842	12.1892	1.00	-0.878	0.000	0.015	Non-Sway

First YIELD Load = 6.145 kN
First HINGE Load = 7.200 kN
SQUASH Load = 26.437 kN

Test: 16oc3
Plastic Collapse Buckling

Experimental Data					Southwell Plot			
Load P kN	Loading		Unloading		Sway Mode		Non-Sway Mode	
	Top reads	Mid reads	Top reads	Mid reads	$\frac{\delta_t}{100}$ mm	$\frac{\delta_t}{100P}$ mm/kN	$\frac{\delta_m-\delta_t/2}{100}$ mm	$\frac{\delta_m-\delta_t/2}{100P}$ mm/kN
0	1173	1550	1288	1586	0.000	0.000	0.000	0.000
0.3	1177	1551.5	1314	1586	0.040	0.133	0.035	0.117
0.6	1184	1554.5	1343	1587	0.110	0.183	0.100	0.167
0.9	1197	1557.5	1371	1587	0.240	0.267	0.195	0.217
1.2	1212.5	1557.5	1402	1587	0.395	0.329	0.273	0.227
1.5	1231	1558	1439	1586	0.580	0.387	0.370	0.247
1.8	1252	1559	1479	1583	0.790	0.439	0.485	0.269
2.1	1274	1561	1526	1576	1.010	0.481	0.615	0.293
2.4	1300	1562	1581	1566	1.270	0.529	0.755	0.315
2.7	1326	1563	1641	1555	1.530	0.567	0.895	0.331
3	1358	1565	1707	1543	1.850	0.617	1.075	0.358
3.3	1393	1566	1785	1527	2.200	0.667	1.260	0.382
3.6	1433	1567.5	1868	1510	2.600	0.722	1.475	0.410
3.8	1470	1567.5	1923	1499	2.970	0.782	1.660	0.437
4	1503	1567	1984	1487	3.300	0.825	1.820	0.455
4.2	1544	1559.5	2051	1475	3.710	0.883	1.950	0.464
4.4	1595	1549	2135	1458	4.220	0.959	2.100	0.477
4.6	1650	1537	2206	1442	4.770	1.037	2.255	0.490
4.8	1710	1523	2286	1425	5.370	1.119	2.415	0.503
5	1784	1505	2286	1405	6.110	1.222	2.605	0.521
5.2	1871	1482	2462	1390	6.980	1.342	2.810	0.540
5.4	1977	1453						
5.6	2109	1415						
5.8	2220	1391						
5.4	2500	1386						

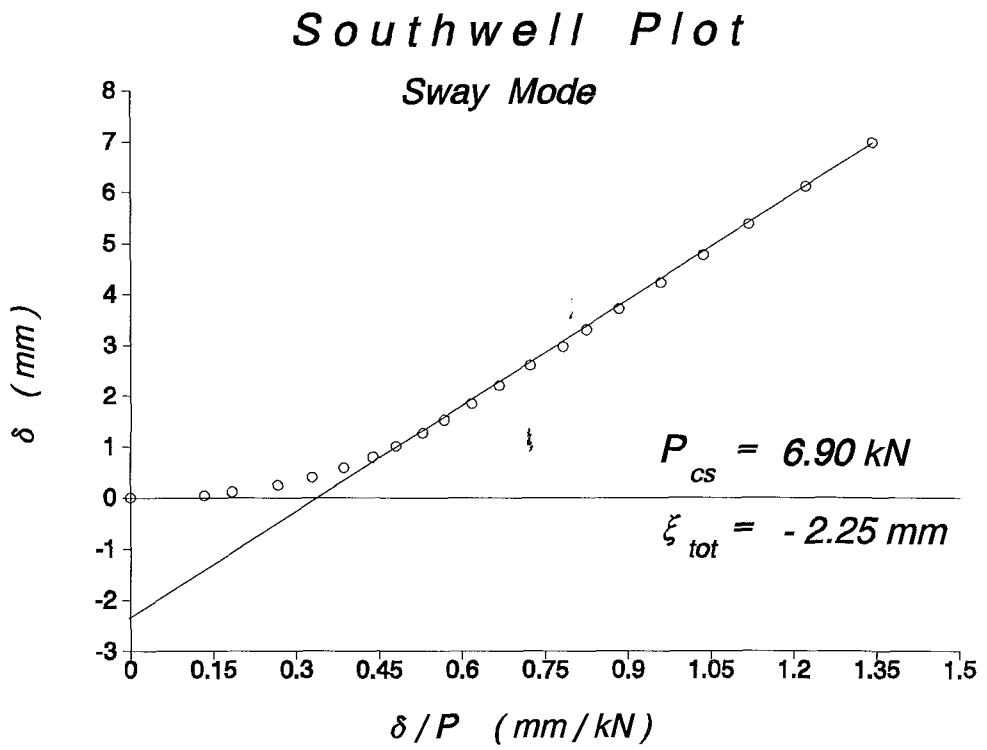
Southwell Plot
Sway Mode
δ (mm)
8
7
6
5
4
3
2
1
0
-1
-2
-3
0
0.15
0.3
0.45
0.6
0.75
0.9
1.05
1.2
1.35
1.5
δ / P (mm / kN)
P cs = 6.90 kN
ξ tot = - 2.25 mm

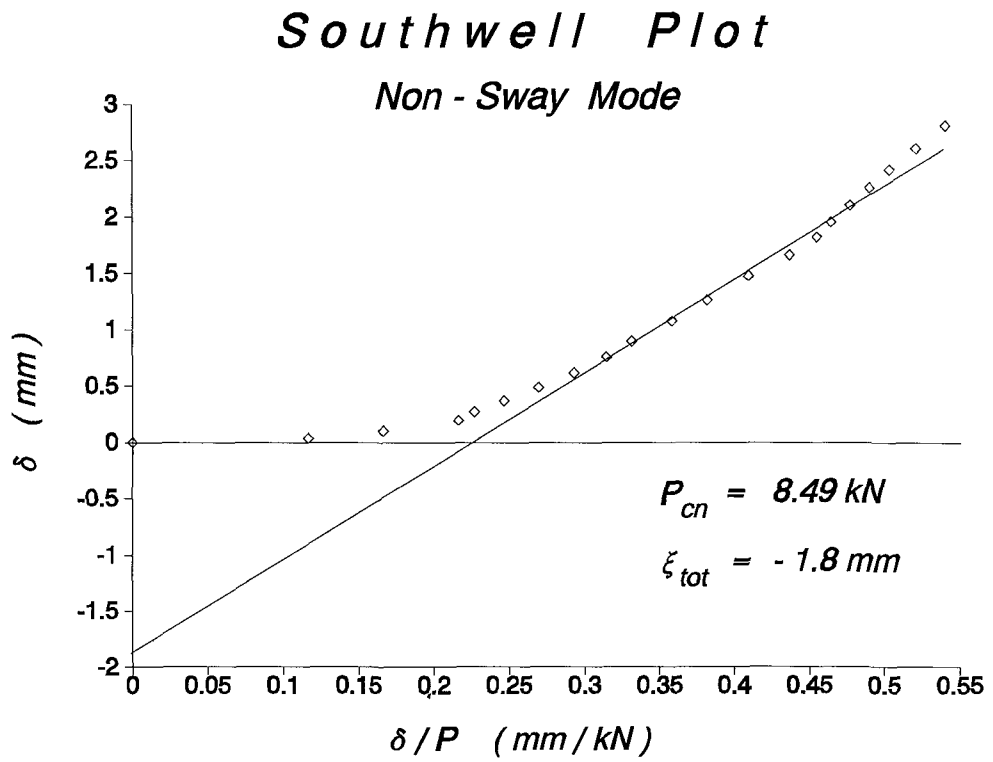
Southwell Plot
Non - Sway Mode
δ (mm)
3
2.5
2
1.5
1
0.5
0
-0.5
-1
-1.5
-2
0
0.05
0.1
0.15
0.2
0.25
0.3
0.35
0.4
0.45
0.5
0.55
δ / P (mm / kN)
P cn = 8.49 kN
ξ tot = - 1.8 mm

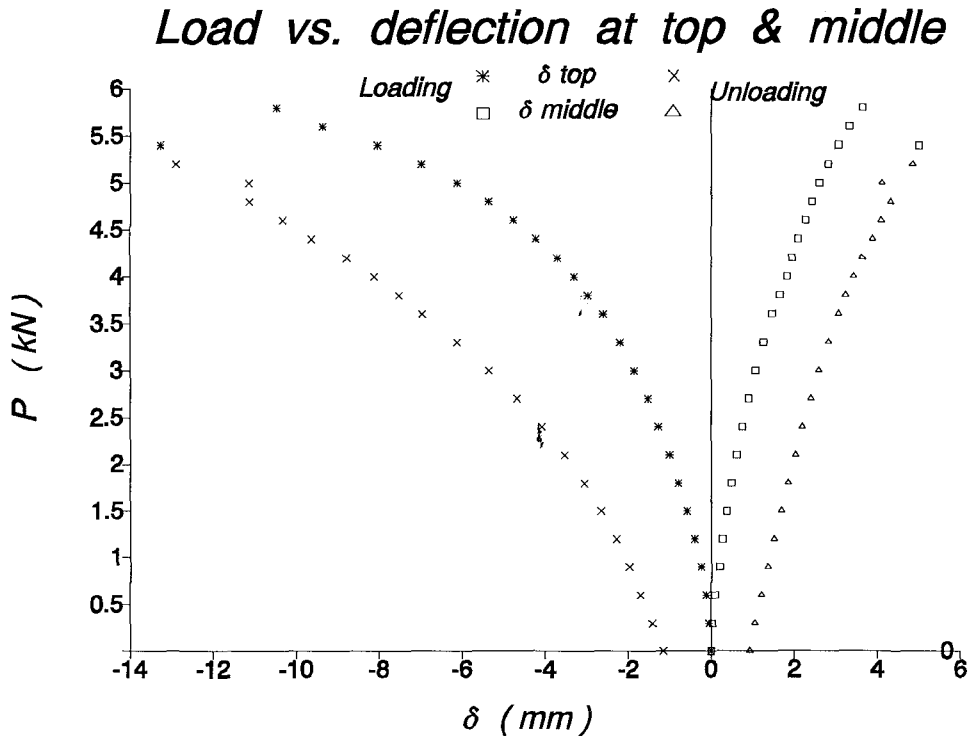

THEORETICAL DATA & RESULTS

PROP_sets = 3, SWAY_imp = 2.25 mm, NON-SWAY_imp = 1.80 mm

MEMBER PROPERTIES

MEM	L	b	d	A	I	Zel	Zpl	Y.str
1	270.0	5.0	13.0	62.44	125.70	50.28	81.45	0.360
2	350.0	5.0	13.0	62.44	125.70	50.28	81.45	0.360
3	270.0	5.0	13.0	62.44	125.70	50.28	81.45	0.360

Rotational SYMMETRIC (Non-sway) Stiffness of frame : 667.41 kN*mm/rad

Rotational ANTISYMMETRIC (Sway) Stiffness of frame : 799.47 kN*mm/rad

Translational (Sway) Stiffness of frame : 17.68 N/mm

EIGENVALUES & EIGENVECTORS

Solut	kL	Pc	C1	C2	delta	theta_A	Mode-Case
1	4.407	6.5299	1.00	0.733	-7.436	-0.008	* Sway
2	5.075	8.6594	1.00	-0.690	0.000	0.013	Non-Sway

First YIELD Load = 4.800 kN

First HINGE Load = 5.712 kN

SQUASH Load = 22.477 kN

Test: 12oc3
Plastic Collapse

Experimental Data					Southwell Plot			
Load P kN	Loading		Unloading		Sway Mode		Non-Sway Mode	
	Top reads	Mid reads	Top reads	Mid reads	$\frac{\delta_t}{100}$ mm	$\frac{\delta_t}{100P}$ mm/kN	$\frac{\delta_m-\delta_t/2}{100}$ mm	$\frac{\delta_m-\delta_t/2}{100P}$ mm/kN
0	726	1170.5	900	1007	0.000	0.000	0.000	0.000
0.3	733	1165	916	997	0.070	0.233	0.020	0.067
0.6	741	1159	936	982	0.150	0.250	0.040	0.067
0.9	750	1152.5	962	964	0.240	0.267	0.060	0.067
1.2	760	1145.5	990	943	0.340	0.283	0.080	0.067
1.5	774	1137.5	1018	922	0.480	0.320	0.090	0.060
1.8	789	1129	1052	898	0.630	0.350	0.100	0.056
2.1	803	1120	1091	869	0.770	0.367	0.120	0.057
2.4	818	1110	1131	841	0.920	0.383	0.145	0.060
2.7	838.5	1098.5	1180	807.5	1.125	0.417	0.158	0.058
3	859	1086	1246	758	1.330	0.443	0.180	0.060
3.3	879.5	1073	1323	705	1.535	0.465	0.208	0.063
3.6	907	1056	1412	646	1.810	0.503	0.240	0.067
3.9	939	1036	1525	571	2.130	0.546	0.280	0.072
4.2	965	1018	1672	476	2.390	0.569	0.330	0.079
4.5	1015	988	1852	360	2.890	0.642	0.380	0.084
4.8	1058	960	2076	215	3.320	0.692	0.445	0.093
5	1122	923	2186	131	3.960	0.792	0.495	0.099
5.2	1195	881	2257	63	4.690	0.902	0.550	0.106
5.4	1262	840						
5.6	1343	790						
5.8	1443	729						
6	1579	649						
6.1	1703	575						
6.2	1820	504						
6.3	2015	386						
5.95	2222	183						
5.38	2303	6						

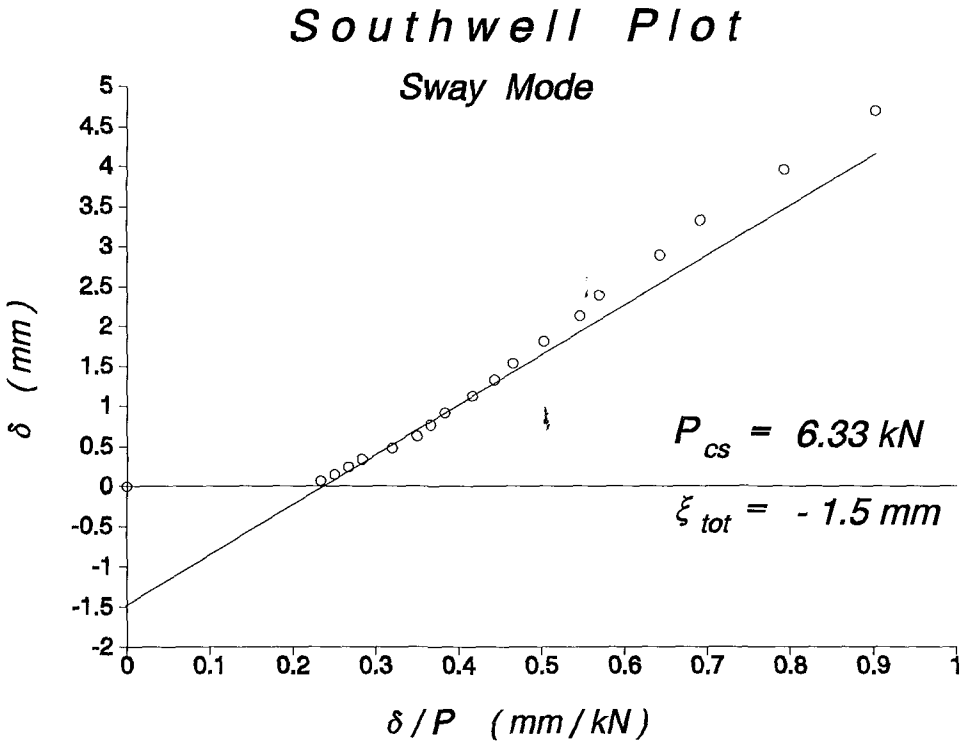
Southwell Plot
Sway Mode
δ (mm)
δ / P (mm / kN)
P cs = 6.33 kN
ξ tot = - 1.5 mm
5
4.5
4
3.5
3
2.5
2
1.5
1
0.5
0
-0.5
-1
-1.5
-2
0
0.1
0.2
0.3
0.4
0.5
0.6
0.7
0.8
0.9
1

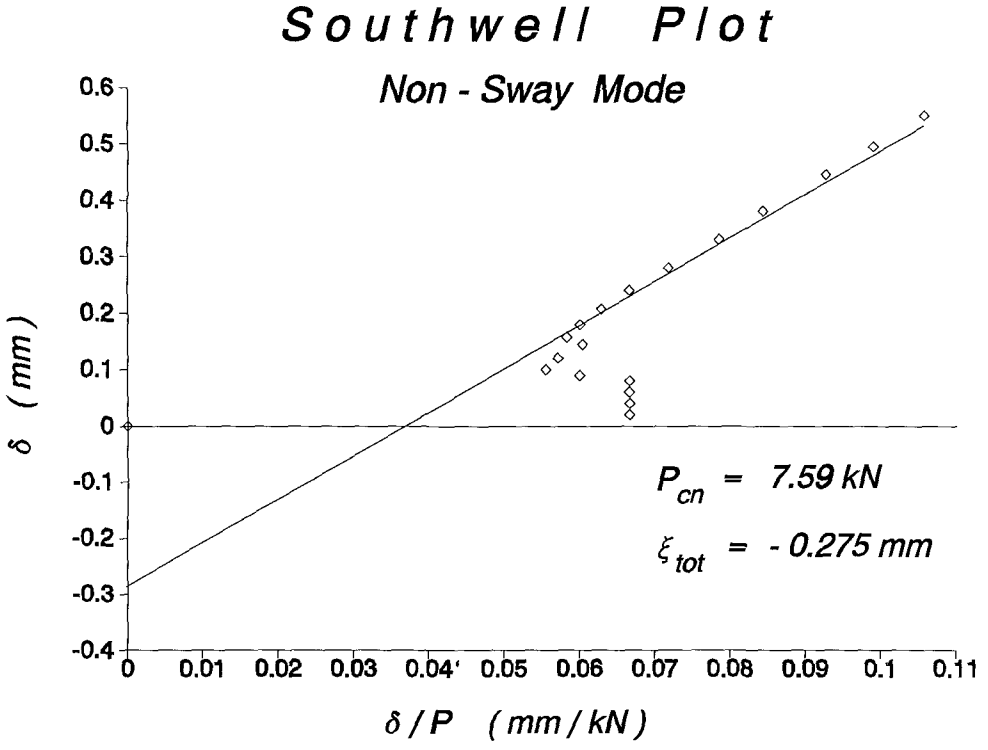
Southwell Plot
Non - Sway Mode
δ (mm)
δ / P (mm / kN)
P cn = 7.59 kN
ξ tot = - 0.275 mm
0.6
0.5
0.4
0.3
0.2
0.1
0
-0.1
-0.2
-0.3
-0.4
0
0.01
0.02
0.03
0.04
0.05
0.06
0.07
0.08
0.09
0.1
0.11

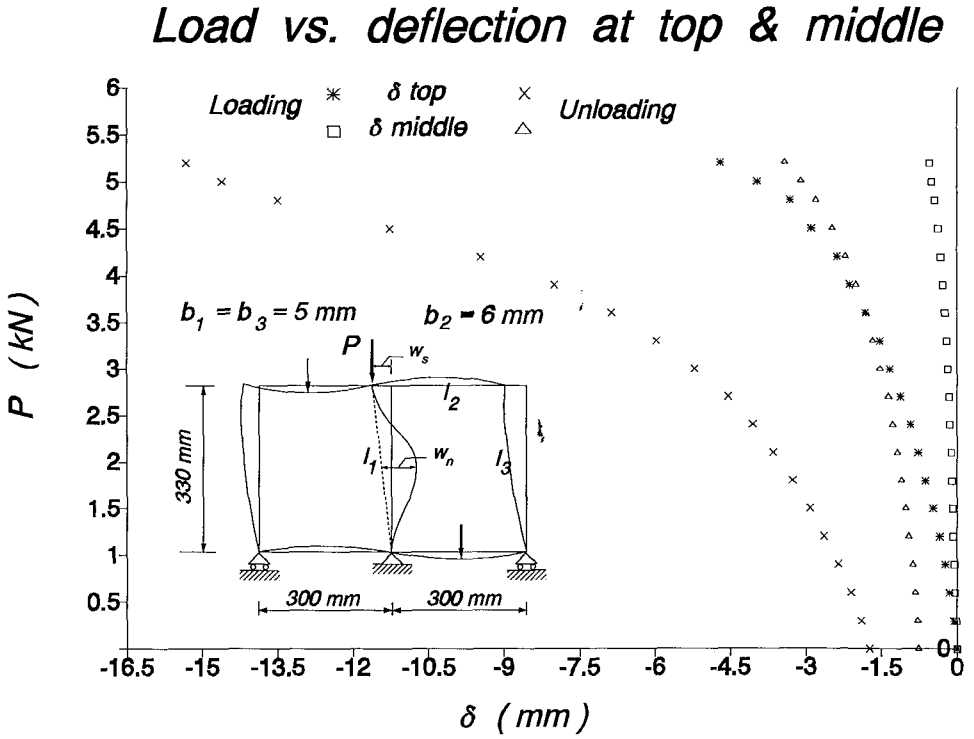

THEORETICAL DATA & RESULTS

PROP_sets = 3, SWAY_imp = 1.50 mm, NON-SWAY_imp = 0.28 mm

MEMBER PROPERTIES

MEM	L	b	d	A	I	Zel	Zpl	Y.str
1	330.0	5.0	13.0	62.44	125.70	50.28	81.45	0.360
2	300.0	6.0	13.0	73.44	209.00	69.67	117.71	0.360
3	330.0	5.0	13.0	62.44	125.70	50.28	81.45	0.360

Rotational SYMMETRIC (Non-sway) Stiffness of frame : 1234.98 kN*mm/rad
Rotational ANTISYMMETRIC (Sway) Stiffness of frame : 1468.91 kN*mm/rad
Translational (Sway) Stiffness of frame : 15.96 N/mm

EIGENVALUES & EIGENVECTORS

Solut	kL	Pc	C1	C2	delta	theta_A	Mode-Case
1	5.265	6.2396	1.00	1.792	-12.836	-0.004	* Sway
2	5.630	7.1350	1.00	-0.339	0.000	0.006	Non-Sway

First YIELD Load = 5.580 kN
First HINGE Load = 5.904 kN
SQUASH Load = 22.477 kN

Test: 4oc3
Plastic Collapse Buckling

Experimental Data					Southwell Plot			
	Loading		Unloading		Sway Mode		Non-Sway Mode	
Load P kN	Top reads	Mid reads	Top reads	Mid reads	$\frac{\delta_t}{100}$ mm	$\frac{\delta_t}{100P}$ mm/kN	$\frac{\delta_m-\delta_t/2}{100}$ mm	$\frac{\delta_m-\delta_t/2}{100P}$ mm/kN
0	1440	426	1244	842	0.000	0.000	0.000	0.000
0.3	1438	431	1227	874	0.020	0.067	0.040	0.133
0.6	1434	438	1203	913	0.060	0.100	0.090	0.150
0.9	1427	447	1178	955	0.130	0.144	0.145	0.161
1.2	1417	459	1152	998	0.230	0.192	0.215	0.179
1.5	1407	471	1130	1035	0.330	0.220	0.285	0.190
1.8	1397	487	1094	1088	0.430	0.239	0.395	0.219
2.1	1385	499	1057.5	1145	0.550	0.262	0.455	0.217
2.4	1372	515	1020	1204	0.680	0.283	0.550	0.229
2.7	1356	535	981	1267	0.840	0.311	0.670	0.248
3	1335	560	930	1344	1.050	0.350	0.815	0.272
3.3	1311	587	880	1423	1.290	0.391	0.965	0.292
3.6	1282	618	823	1515	1.580	0.439	1.130	0.314
3.9	1248	658	757	1621	1.920	0.492	1.360	0.349
4.2	1210	700	693	1731	2.300	0.548	1.590	0.379
4.4	1180	730	645	1805	2.600	0.591	1.740	0.395
4.6	1146	772	645	1805	2.940	0.639	1.990	0.433
4.8	1101	818	645	1805	3.390	0.706	2.225	0.464
5	1043	877	645	1805	3.970	0.794	2.525	0.505
5.2	997	930	645	1805	4.430	0.852	2.825	0.543
5.4	938	998	645	1805	5.020	0.930	3.210	0.594
5.6	850	1091	645	1805	5.900	1.054	3.700	0.661
5.8	760	1200	645	1805	6.800	1.172	4.340	0.748
5.95	650	1310	645	1805	7.900	1.328	4.890	0.822
5.2	640	1600	645	1805	8.000	1.538	7.740	1.488
4.4	645	1805	645	1805	7.950	1.807	9.815	2.231

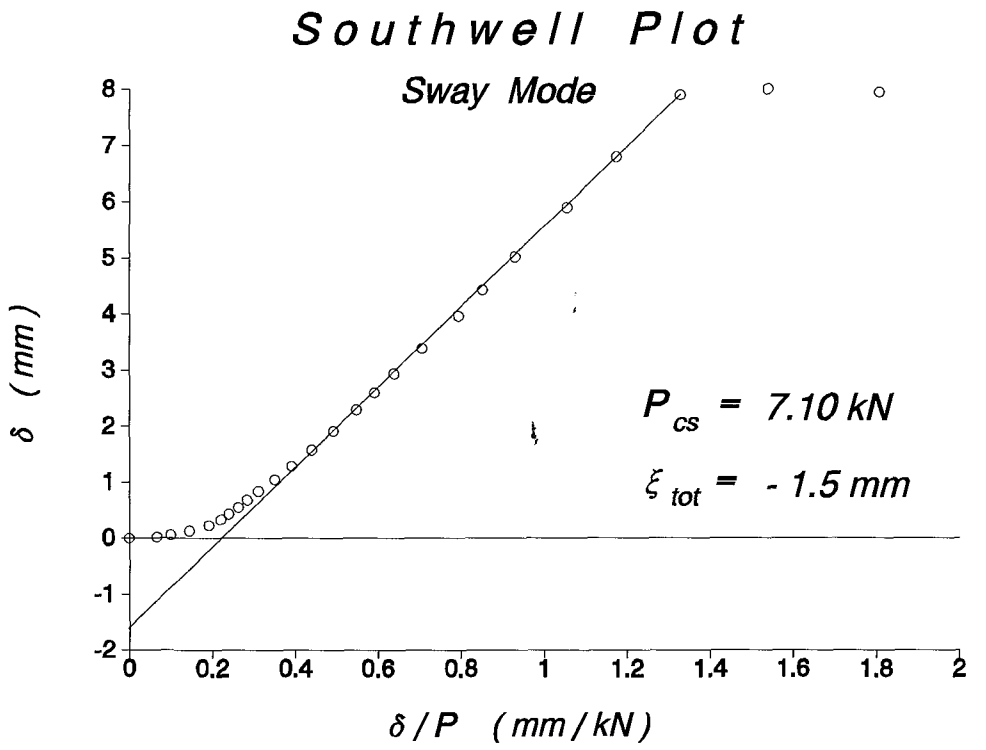
Southwell Plot
Sway Mode
δ (mm)
δ / P (mm / kN)
P cs = 7.10 kN
ξ tot = - 1.5 mm
8
7
6
5
4
3
2
1
0
-1
-2
0
0.2
0.4
0.6
0.8
1
1.2
1.4
1.6
1.8
2

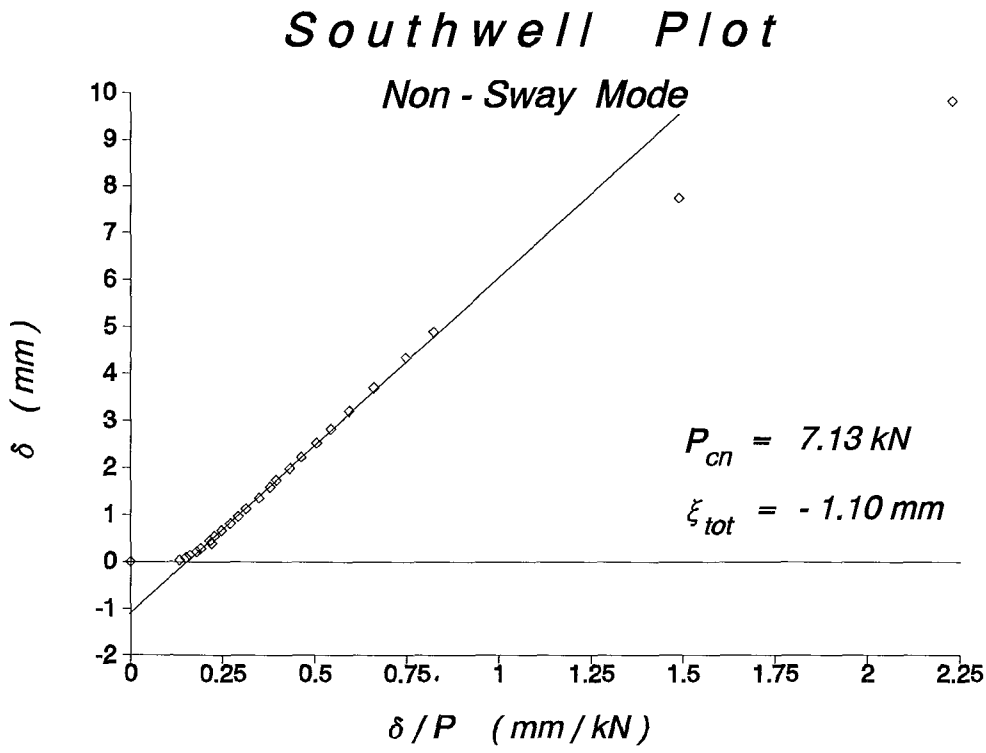
Southwell Plot
Non - Sway Mode
δ (mm)
δ / P (mm / kN)
P cn = 7.13 kN
ξ tot = - 1.10 mm
10
9
8
7
6
5
4
3
2
1
0
-1
-2
0
0.25
0.5
0.75
1
1.25
1.5
1.75
2
2.25

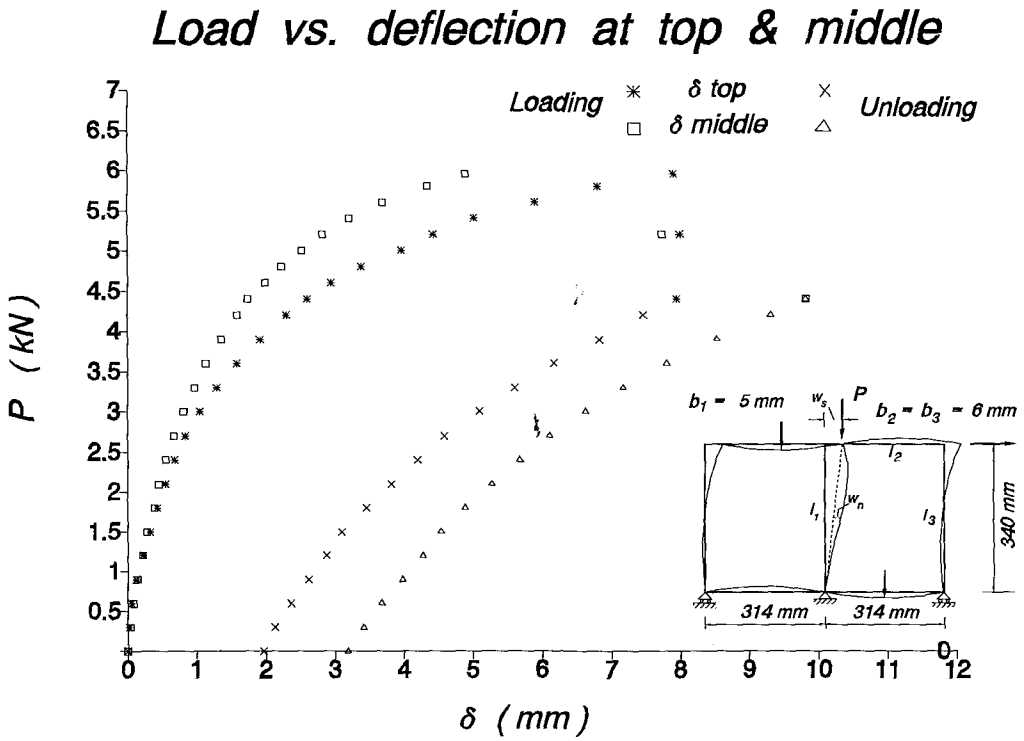

THEORETICAL DATA & RESULTS

PROP_sets = 3, SWAY_imp = -1.50 mm, NON-SWAY_imp = -1.10 mm

MEMBER PROPERTIES

MEM	L	b	d	A	I	Zel	Zpl	Y.str
1	340.0	5.0	13.0	62.44	125.70	50.28	81.45	0.360
2	314.0	6.0	13.0	73.44	209.00	69.67	117.71	0.360
3	340.0	6.0	13.0	73.44	209.00	69.67	117.71	0.360

	Rot.Sym.Non-sway	Rot.Antisym.Sway	Transl.Sway
Stiffness of frame :	1221.35 kN*mm/rad	1465.26 kN*mm/rad	17.933 N/mm.

EIGENVALUES & EIGENVECTORS

Solut	kL	Pc	C1	C2	delta	theta_A	Mode-Case
1	5.640	6.7459	1.00	-0.333	0.000	0.006	Non-Sway
2	5.643	6.7528	1.00	3.018	-20.600	-0.005	* Sway

First YIELD Load = 4.904 kN

First HINGE Load = 5.652 kN

SQUASH Load = 22.477 kN

Test: 230c3
Plastic Collapse Buckling

Experimental Data					Southwell Plot			
Load P kN	Loading		Unloading		Sway Mode		Non-Sway Mode	
	Top reads	Mid reads	Top reads	Mid reads	$\frac{\delta_t}{100}$ mm	$\frac{\delta_t}{100P}$ mm/kN	$\frac{\delta_m-\delta_t/2}{100}$ mm	$\frac{\delta_m-\delta_t/2}{100P}$ mm/kN
0	692	1321	772	2200	0.000	0.000	0.000	0.000
0.3	693	1322	780	2230	0.010	0.033	0.015	0.050
0.6	694.5	1324	788	2259	0.025	0.042	0.043	0.071
0.9	696	1325	796	2288	0.040	0.044	0.060	0.067
1.2	698	1327	804	2319	0.060	0.050	0.090	0.075
1.5	700	1330	812	2347	0.080	0.053	0.130	0.087
1.8	704	1334	822	2378	0.120	0.067	0.190	0.106
2.1	706.5	1335	832.5	2410	0.145	0.069	0.213	0.101
2.4	710	1338	843	2443	0.180	0.075	0.260	0.108
2.7	712	1341	852	2480	0.200	0.074	0.300	0.111
3	715	1346	859	2514	0.230	0.077	0.365	0.122
3.3	718	1349	867	2552	0.260	0.079	0.410	0.124
3.6	721	1354	872	2599	0.290	0.081	0.475	0.132
3.9	724	1359			0.320	0.082	0.540	0.138
4.2	730	1364			0.380	0.090	0.620	0.148
4.5	734	1369			0.420	0.093	0.690	0.153
4.8	736.5	1376			0.445	0.093	0.773	0.161
5.1	739.5	1382			0.475	0.093	0.848	0.166
5.4	743	1389			0.510	0.094	0.935	0.173
5.7	747.5	1396			0.555	0.097	1.028	0.180
6	751.5	1404.5			0.595	0.099	1.133	0.189
6.3	756	1412.5			0.640	0.102	1.235	0.196
6.6	762	1424			0.700	0.106	1.380	0.209
6.8	766	1435			0.740	0.109	1.510	0.222
7	776	1443			0.840	0.120	1.640	0.234
7.2	775	1455			0.830	0.115	1.755	0.244
7.4	778	1468			0.860	0.116	1.900	0.257
7.6	782	1481			0.900	0.118	2.050	0.270
7.8	788	1493			0.960	0.123	2.200	0.282
8	790	1510			0.980	0.123	2.380	0.298
8.2	791	1529			0.990	0.121	2.575	0.314
8.4	794	1547			1.020	0.121	2.770	0.330
8.6	797	1567			1.050	0.122	2.985	0.347
3.65	870	2599			1.780	0.488	13.670	3.745

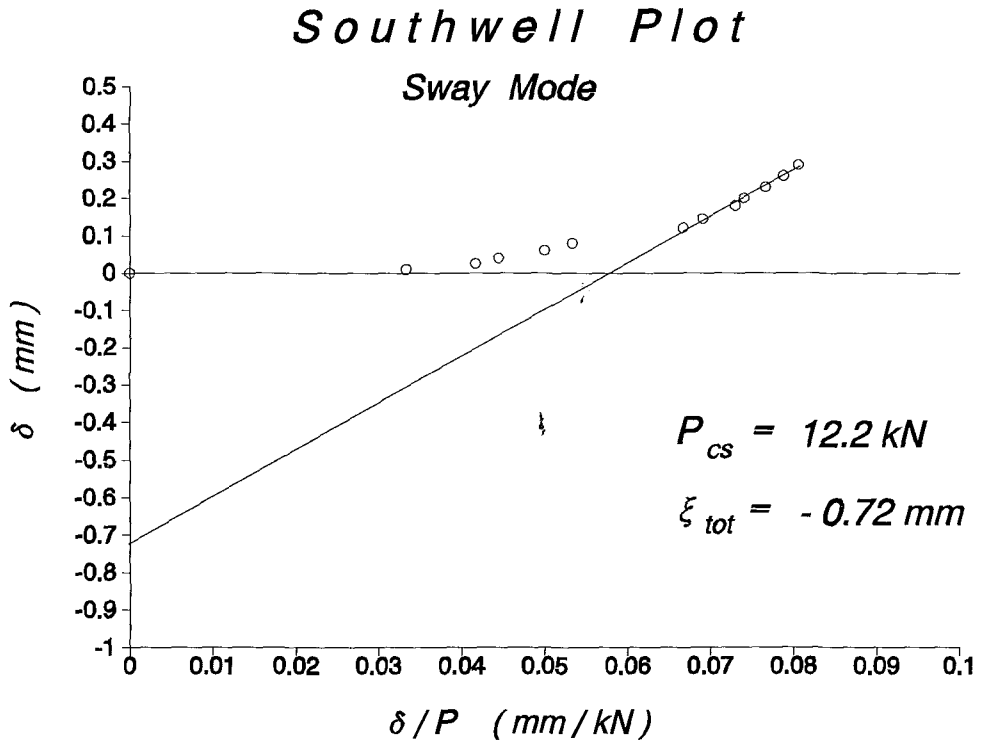
Southwell Plot
Sway Mode
δ (mm)
δ / P (mm / kN)
P cs = 12.2 kN
ξ tot = - 0.72 mm
0.5
0.4
0.3
0.2
0.1
0
-0.1
-0.2
-0.3
-0.4
-0.5
-0.6
-0.7
-0.8
-0.9
-1
0
0.01
0.02
0.03
0.04
0.05
0.06
0.07
0.08
0.09
0.1

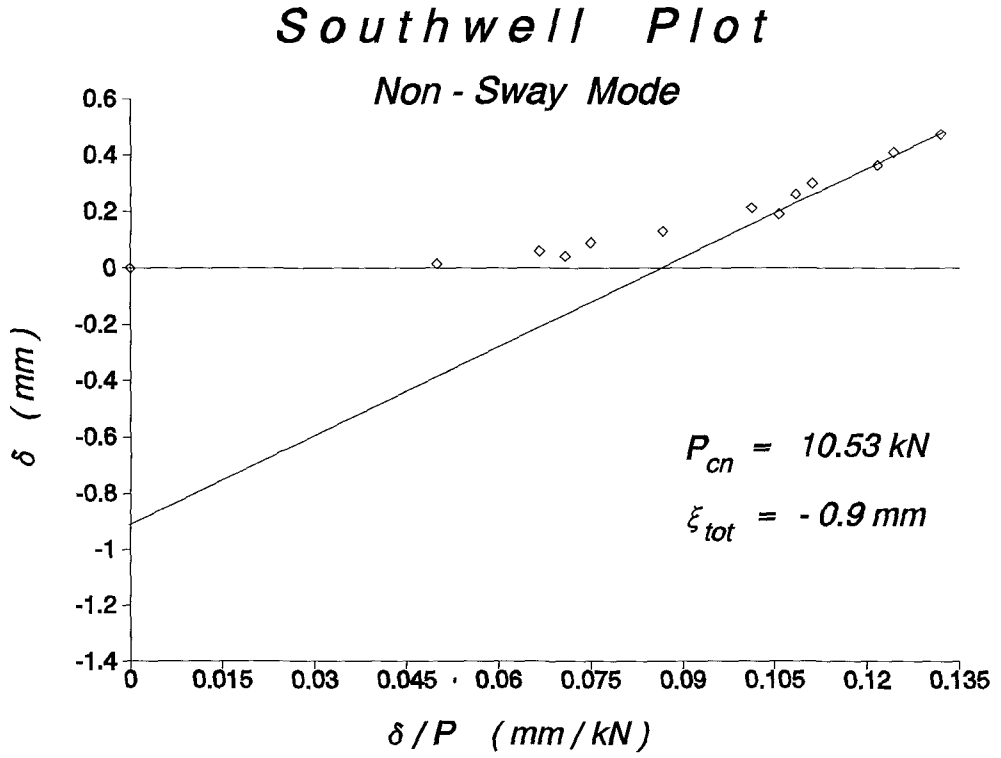
Southwell Plot
Non - Sway Mode
δ (mm)
δ / P (mm / kN)
P cn = 10.53 kN
ξ tot = - 0.9 mm
0.6
0.4
0.2
0
-0.2
-0.4
-0.6
-0.8
-1
-1.2
-1.4
0
0.015
0.03
0.045
0.06
0.075
0.09
0.105
0.12
0.135

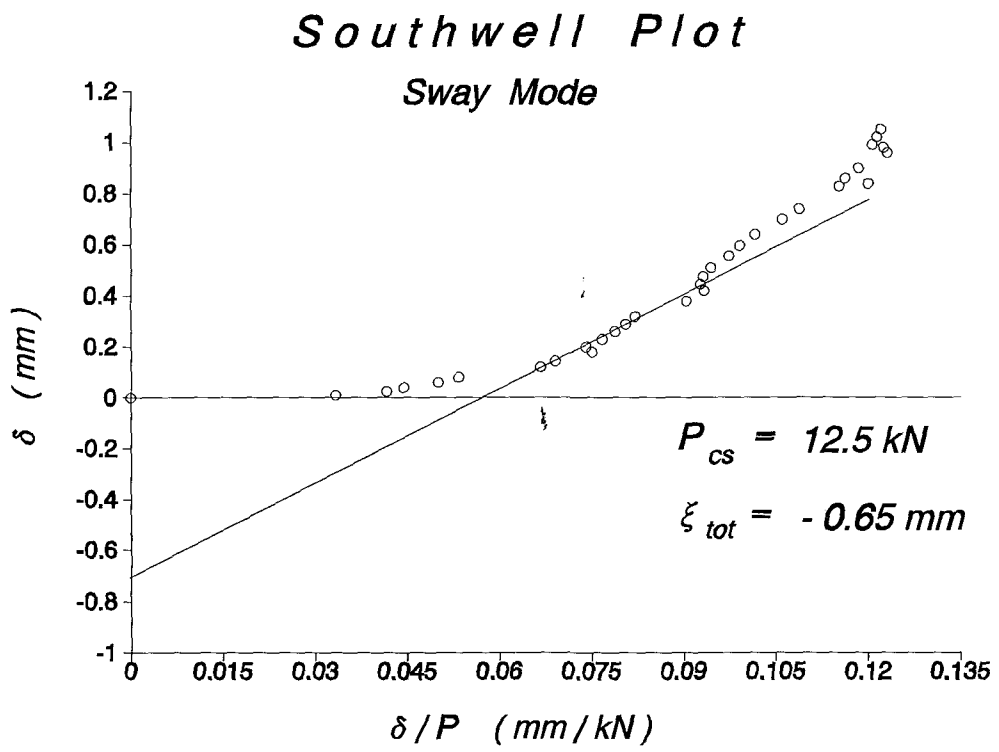
Southwell Plot
Sway Mode
δ (mm)
δ / P (mm / kN)
P cs = 12.5 kN
ξ tot = - 0.65 mm
1.2
1
0.8
0.6
0.4
0.2
0
-0.2
-0.4
-0.6
-0.8
-1
0
0.015
0.03
0.045
0.06
0.075
0.09
0.105
0.12
0.135

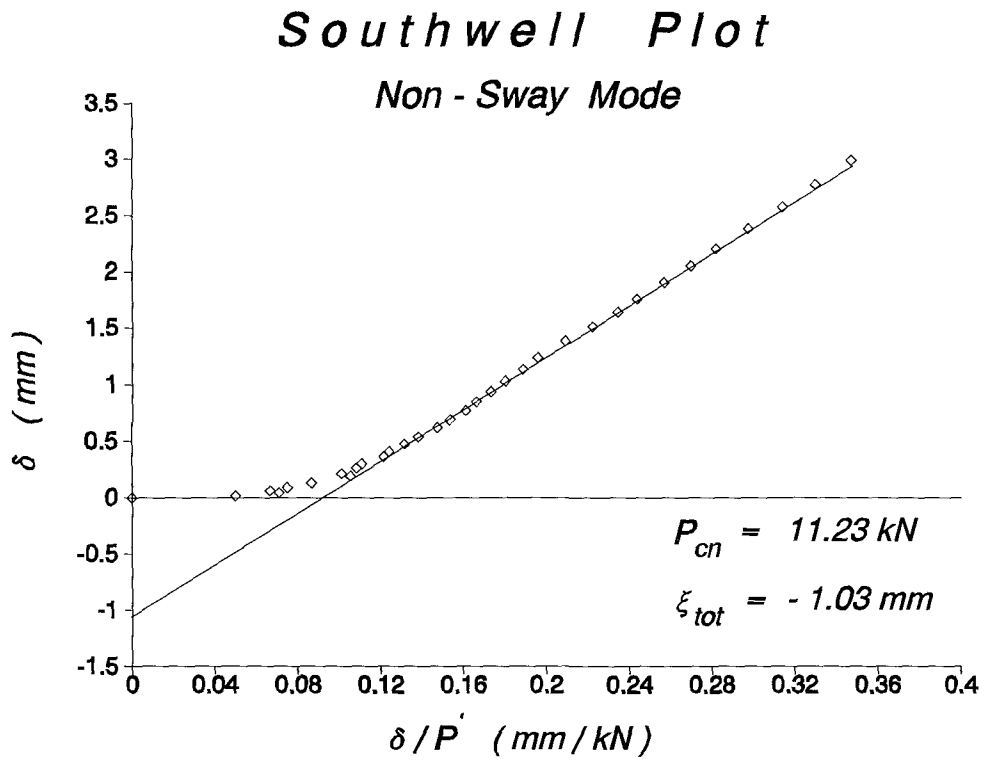
Southwell Plot
Non - Sway Mode
δ (mm)
δ / P' (mm / kN)
P cn = 11.23 kN
ξ tot = - 1.03 mm
3.5
3
2.5
2
1.5
1
0.5
0
-0.5
-1
-1.5
0
0.04
0.08
0.12
0.16
0.2
0.24
0.28
0.32
0.36
0.4

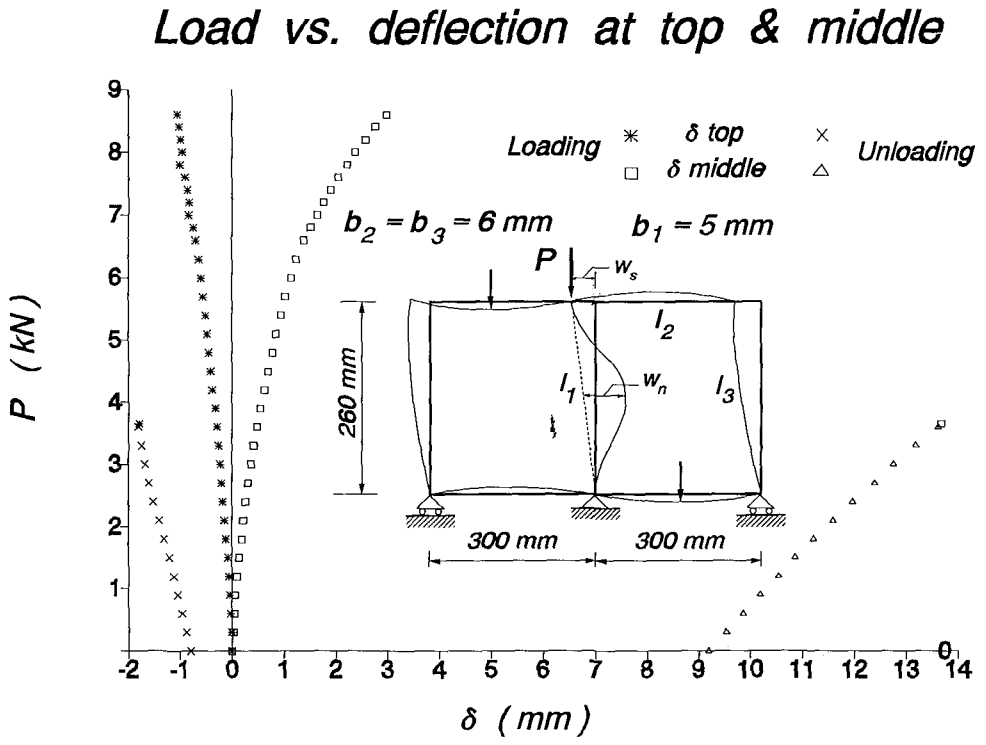

THEORETICAL DATA & RESULTS

PROP_sets = 3, SWAY_imp = 0.65 mm, NON-SWAY_imp = -1.03 mm

MEMBER PROPERTIES

MEM	L	b	d	A	I	Zel	Zpl	Y.str
1	260.0	5.0	13.0	62.44	125.70	50.28	81.45	0.360
2	300.0	6.0	13.0	73.44	209.00	69.67	117.71	0.360
3	260.0	6.0	13.0	73.44	209.00	69.67	117.71	0.360

Rotational SYMMETRIC (Non-sway) Stiffness of frame : 1343.77 kN*mm/rad
Rotational ANTISYMMETRIC (Sway) Stiffness of frame : 1641.35 kN*mm/rad
Translational (Sway) Stiffness of frame : 38.04 N/mm

EIGENVALUES & EIGENVECTORS

Solut	kL	Pc	C1	C2	delta	theta_A	Mode-Case
1	5.540	11.1290	1.00	2.566	-17.980	-0.007	* Sway
2	5.542	11.1352	1.00	-0.389	0.000	0.008	Non-Sway

First YIELD Load = 7.431 kN
First HINGE Load = 8.946 kN
SQUASH Load = 22.477 kN

Test: 25oc3
Plastic Collapse Buckling

Experimental Data					Southwell Plot			
Load P kN	Loading		Unloading		Sway Mode		Non-Sway Mode	
	Top reads	Mid reads	Top reads	Mid reads	$\frac{\delta_t}{100}$ mm	$\frac{\delta_t}{100P}$ mm/kN	$\frac{\delta_m-\delta_t/2}{100}$ mm	$\frac{\delta_m-\delta_t/2}{100P}$ mm/kN
0	1007	1094.5	1050	1484	0.000	0.000	0.000	0.000
0.2	1009	1096.5	1064	1502	0.020	0.100	0.030	0.150
0.4	1010	1100	1072	1520	0.030	0.075	0.070	0.175
0.6	1012	1103	1080	1540	0.050	0.083	0.110	0.183
0.8	1014	1106.5	1088	1561	0.070	0.088	0.155	0.194
1	1017.5	1109	1096	1586	0.105	0.105	0.198	0.198
1.2	1022.5	1112	1103.5	1611	0.155	0.129	0.253	0.210
1.4	1028.5	1116	1112	1639	0.215	0.154	0.323	0.230
1.6	1035.5	1120.5	1123	1671	0.285	0.178	0.403	0.252
1.8	1043.5	1126	1135	1704	0.365	0.203	0.498	0.276
2	1052.2	1132.5	1149	1741	0.452	0.226	0.606	0.303
2.2	1062.5	1141	1163	1780	0.555	0.252	0.743	0.338
2.4	1072	1151.5	1179	1818	0.650	0.271	0.895	0.373
2.6	1084	1163			0.770	0.296	1.070	0.412
2.8	1098	1178.5			0.910	0.325	1.295	0.463
3	1113	1194			1.060	0.353	1.525	0.508
3.2	1128	1216			1.210	0.378	1.820	0.569
3.4	1148	1245			1.410	0.415	2.210	0.650
3.6	1173	1281			1.660	0.461	2.695	0.749
3.7	1186	1303			1.790	0.484	2.980	0.805
3.8	1200	1331			1.930	0.508	3.330	0.876
3.9	1209	1370			2.020	0.518	3.765	0.965
2.53	1288	1842			2.810	1.111	8.880	3.510

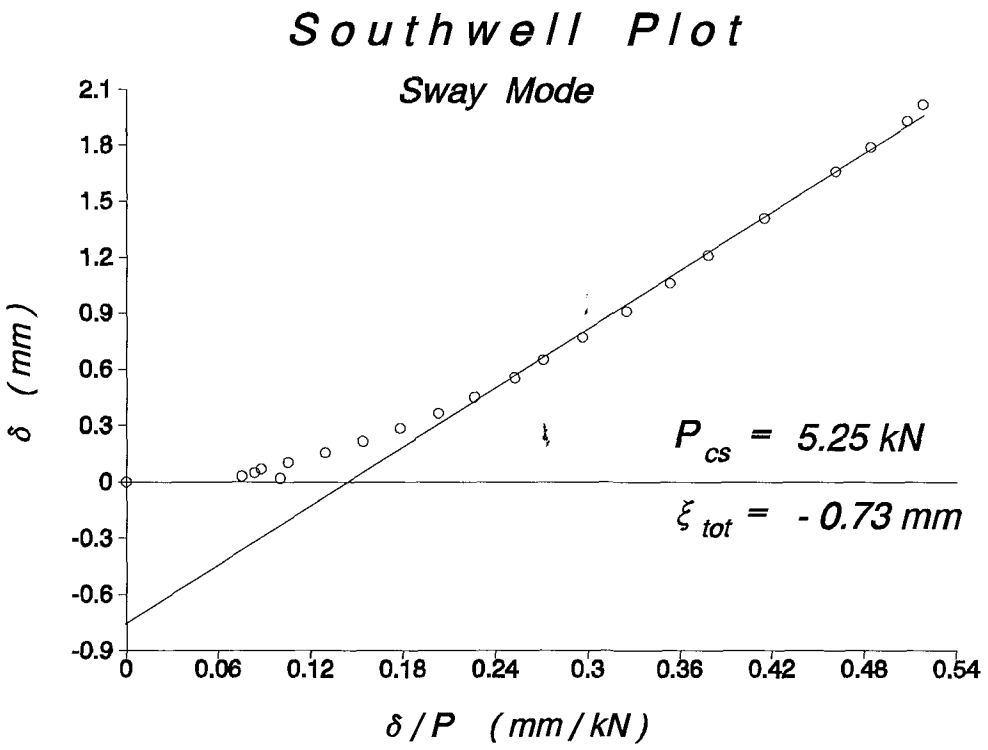
Southwell Plot
Sway Mode
2.1
1.8
1.5
1.2
0.9
0.6
0.3
0
-0.3
-0.6
-0.9
δ (mm)
P cs = 5.25 kN
ξ tot = - 0.73 mm
0
0.06
0.12
0.18
0.24
0.3
0.36
0.42
0.48
0.54
δ / P (mm / kN)

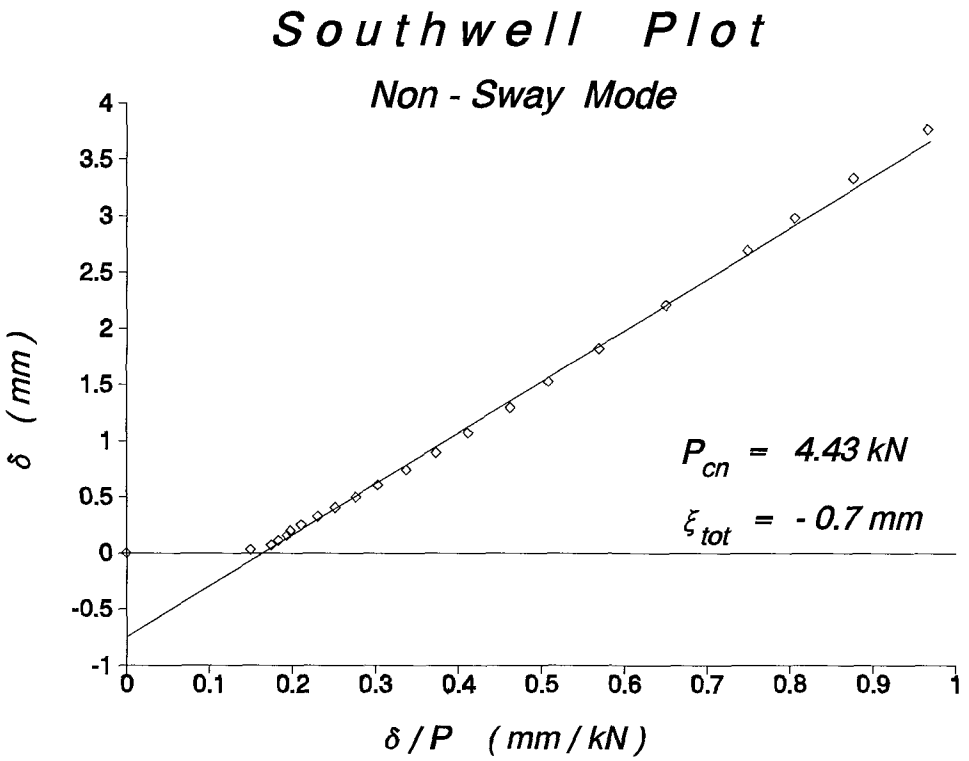
Southwell Plot
Non - Sway Mode
4
3.5
3
2.5
2
1.5
1
0.5
0
-0.5
-1
δ (mm)
P cn = 4.43 kN
ξ tot = - 0.7 mm
0
0.1
0.2
0.3
0.4
0.5
0.6
0.7
0.8
0.9
1
δ / P (mm / kN)

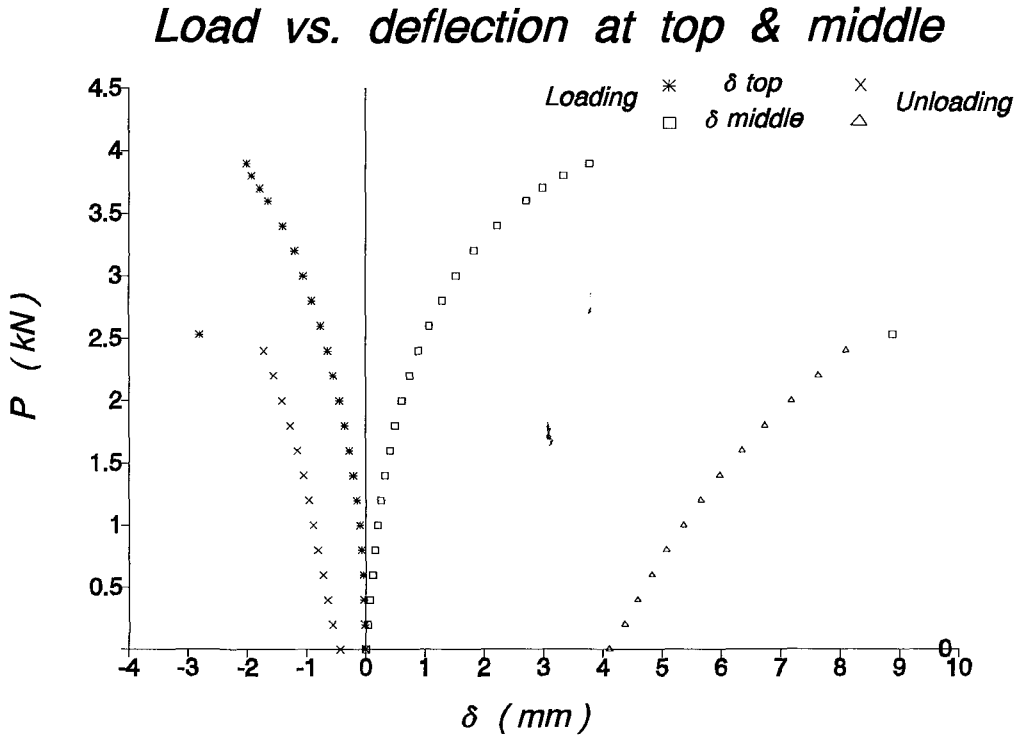

THEORETICAL DATA & RESULTS

PROP_sets = 3, SWAY_imp = -0.73 mm, NON-SWAY_imp = -0.70 mm

MEMBER PROPERTIES

MEM	L	b	d	A	I	Zel	Zpl	Y.str
1	210.0	3.0	13.0	38.47	28.53	19.02	29.26	0.360
2	250.0	5.0	13.0	62.44	125.70	50.28	81.45	0.360
3	210.0	3.0	13.0	38.47	28.53	19.02	29.26	0.360

Rotational SYMMETRIC (Non-sway) Stiffness of frame : 920.69 kN*mm/rad

Rotational ANTISYMMETRIC (Sway) Stiffness of frame : 1112.57 kN*mm/rad

Translational (Sway) Stiffness of frame : 25.34 N/mm

EIGENVALUES & EIGENVECTORS

Solut	kL	Pc	C1	C2	delta	theta_A	Mode-Case
1	5.944	4.4573	1.00	-0.171	0.000	0.005	Non-Sway
2	6.423	5.2043	1.00	-14.263	88.629	-0.005	* Sway

First YIELD Load = 3.366 kN

First HINGE Load = 3.807 kN

SQUASH Load = 13.848 kN

Test: 26oc3
Plastic Collapse Buckling

Experimental Data					Southwell Plot			
	Loading		Unloading		Sway Mode		Non-Sway Mode	
Load P kN	Top reads	Mid reads	Top reads	Mid reads	$\frac{\delta_t}{100}$ mm	$\frac{\delta_t}{100P}$ mm/kN	$\frac{\delta_m-\delta_t/2}{100}$ mm	$\frac{\delta_m-\delta_t/2}{100P}$ mm/kN
0	396	1006	465	877	0.000	0.000	0.000	0.000
0.2	397.5	1007	478	847	0.015	0.075	0.018	0.088
0.4	401.5	1006	495	830	0.055	0.138	0.028	0.069
0.6	409	1008.5	515	810	0.130	0.217	0.090	0.150
0.8	415	986	534	790	0.190	0.238	0.105	0.131
1	422	980	558	767	0.260	0.260	0.130	0.130
1.2	431	973	583	743	0.350	0.292	0.155	0.129
1.4	442	965	612	710	0.460	0.329	0.180	0.129
1.6	455	955	646	673	0.590	0.369	0.215	0.134
1.8	472	943	686	630	0.760	0.422	0.250	0.139
2	492.5	928	740	574	0.965	0.483	0.298	0.149
2.2	517.5	910	800	510	1.215	0.552	0.353	0.160
2.4	550	886	876	431	1.540	0.642	0.430	0.179
2.6	591	855	968	329	1.950	0.750	0.535	0.206
2.7	619	835	1020	273	2.230	0.826	0.595	0.220
2.8	646	811	1085	199	2.500	0.893	0.700	0.250
2.9	679	785	1152	121	2.830	0.976	0.795	0.274
3	713	756			3.170	1.057	0.915	0.305
3.1	761.5	714			3.655	1.179	1.093	0.352
3.2	820	663			4.240	1.325	1.310	0.409
3.3	891	600			4.950	1.500	1.585	0.480
3.4	983	508			5.870	1.726	2.045	0.601
3.5	1120	377			7.240	2.069	2.670	0.763
3.07	1240	30			8.440	2.749	5.540	1.805

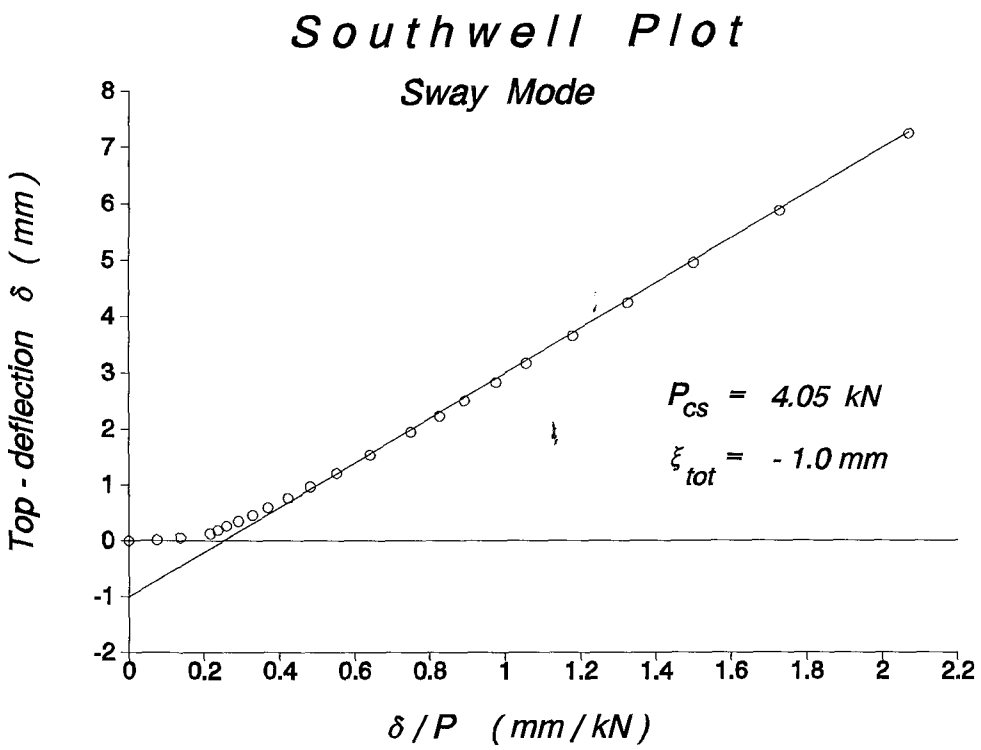
Southwell Plot
Sway Mode
Top - deflection δ (mm)
8
7
6
5
4
3
2
1
0
-1
-2
0
0.2
0.4
0.6
0.8
1
1.2
1.4
1.6
1.8
2
2.2
δ / P (mm / kN)
P_{cs} = 4.05 kN
ξ_{tot} = - 1.0 mm

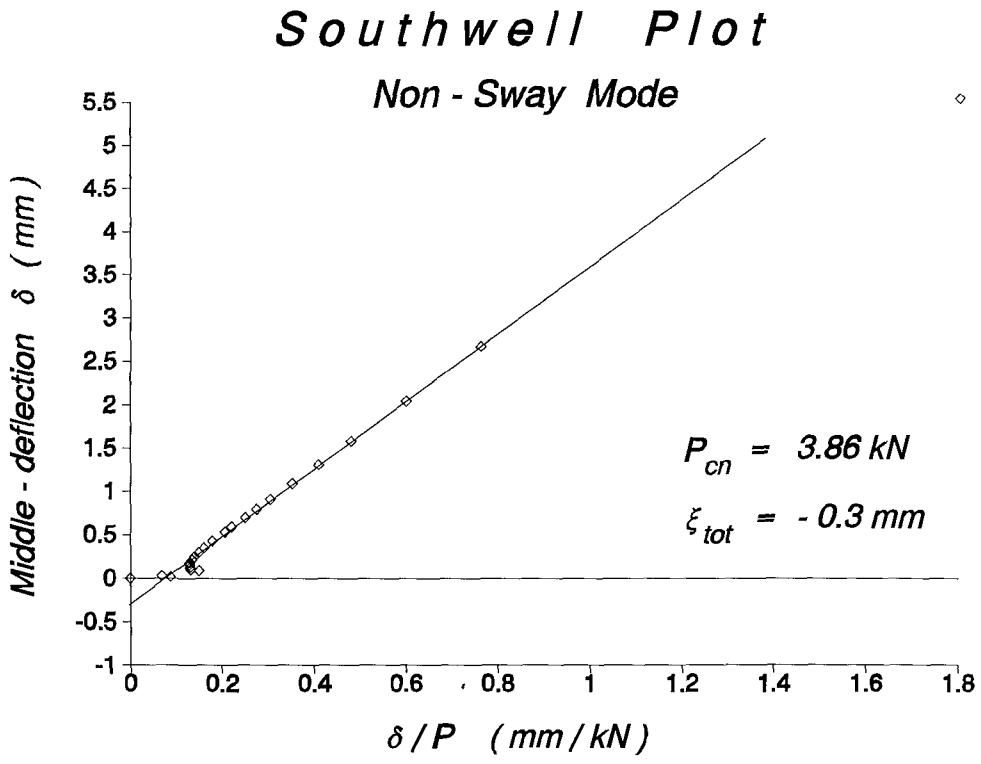
Southwell Plot
Non - Sway Mode
Middle - deflection δ (mm)
5.5
5
4.5
4
3.5
3
2.5
2
1.5
1
0.5
0
-0.5
-1
0
0.2
0.4
0.6
0.8
1
1.2
1.4
1.6
1.8
δ / P (mm / kN)
P_{cn} = 3.86 kN
ξ_{tot} = - 0.3 mm

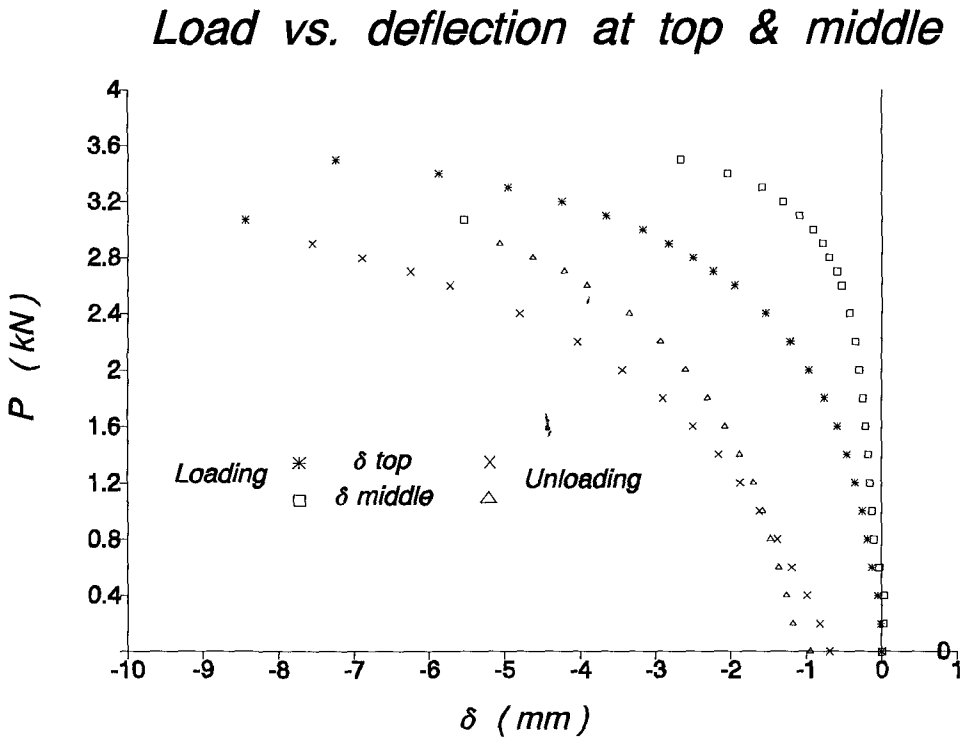

THEORETICAL DATA & RESULTS

PROP_sets = 3, SWAY_imp = -1.00 mm, NON-SWAY_imp = -0.30 mm

MEMBER PROPERTIES

MEM	L	b	d	A	I	Zel	Zpl	Y.str
1	235.0	3.0	13.0	38.47	28.53	19.02	29.26	0.360
2	400.0	5.0	13.0	62.44	125.70	50.28	81.45	0.360
3	235.0	5.0	13.0	62.44	125.70	50.28	81.45	0.360

Rotational SYMMETRIC (Non-sway) Stiffness of frame : 580.93 kN*mm/rad
Rotational ANTISYMMETRIC (Sway) Stiffness of frame : 682.39 kN*mm/rad
Translational (Sway) Stiffness of frame : 21.38 N/mm

EIGENVALUES & EIGENVECTORS

Solut	kL	Pc	C1	C2	delta	theta_A	Mode-Case
1	5.818	3.4092	1.00	-0.237	0.000	0.006	Non-Sway
2	6.777	4.6264	1.00	-3.967'	23.289	-0.007	* Sway

First YIELD Load = 2.600 kN
First HINGE Load = 2.910 kN
SQUASH Load = 13.848 kN

Test: 6N3
Plastic Collapse Buckling

Experimental Data					Southwell Plot			
Load P kN	Loading		Unloading		Sway Mode		Non-Sway Mode	
	Top reads	Mid reads	Top reads	Mid reads	$\frac{\delta_t}{100}$ mm	$\frac{\delta_t}{100P}$ mm/kN	$\frac{\delta_m - \delta_t/2}{100}$ mm	$\frac{\delta_m - \delta_t/2}{100P}$ mm/kN
0	1313	1318	1276	1445	0.000	0.000	0.000	0.000
0.2	1309	1331	1267.5	1474.5	0.040	0.200	0.110	0.550
0.4	1305	1348	1258	1506	0.080	0.200	0.260	0.650
0.6	1297	1369	1247	1540	0.160	0.267	0.430	0.717
0.8	1288	1391	1234	1580	0.250	0.313	0.605	0.756
1	1277	1418	1220	1624	0.360	0.360	0.820	0.820
1.1	1269	1435	1212	1647	0.440	0.400	0.950	0.864
1.2	1261	1453	1204	1675	0.520	0.433	1.090	0.908
1.3	1252.5	1472	1196	1704	0.605	0.465	1.238	0.952
1.4	1243	1492	1186	1737	0.700	0.500	1.390	0.993
1.5	1235	1511	1176	1771	0.780	0.520	1.540	1.027
1.6	1224	1534	1167	1805	0.890	0.556	1.715	1.072
1.7	1213	1560	1154	1846	1.000	0.588	1.920	1.129
1.8	1201	1589	1139	1886	1.120	0.622	2.150	1.194
1.9	1189	1624	1120	1928	1.240	0.653	2.440	1.284
2	1178	1658	1103	1974	1.350	0.675	2.725	1.363
2.1	1163	1712	1088	2021	1.500	0.714	3.190	1.519
2.2	1148	1746			1.650	0.750	3.455	1.570
2.3	1129	1800			1.840	0.800	3.900	1.696
2.4	1108	1869			2.050	0.854	4.485	1.869
2.5	1083	1956			2.300	0.920	5.230	2.092
2.2	1072	2067			2.410	1.095	6.285	2.857

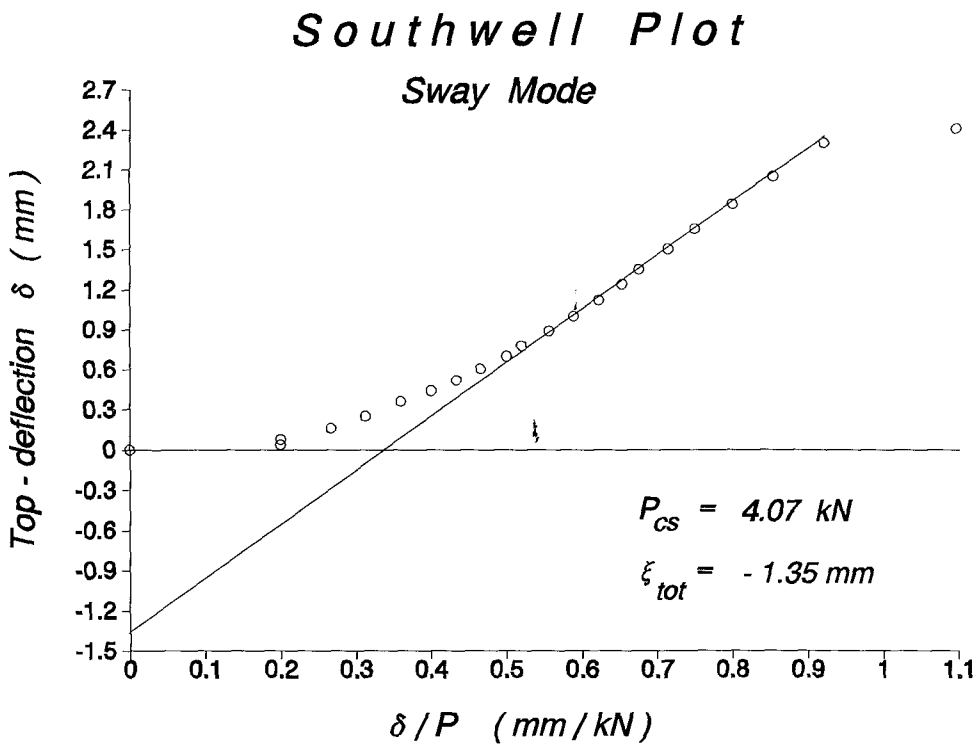
Southwell Plot
Sway Mode
Top - deflection δ (mm)
2.7
2.4
2.1
1.8
1.5
1.2
0.9
0.6
0.3
0
-0.3
-0.6
-0.9
-1.2
-1.5
0
0.1
0.2
0.3
0.4
0.5
0.6
0.7
0.8
0.9
1
1.1
δ / P (mm / kN)
P_{cs} = 4.07 kN
ξ_{tot} = - 1.35 mm

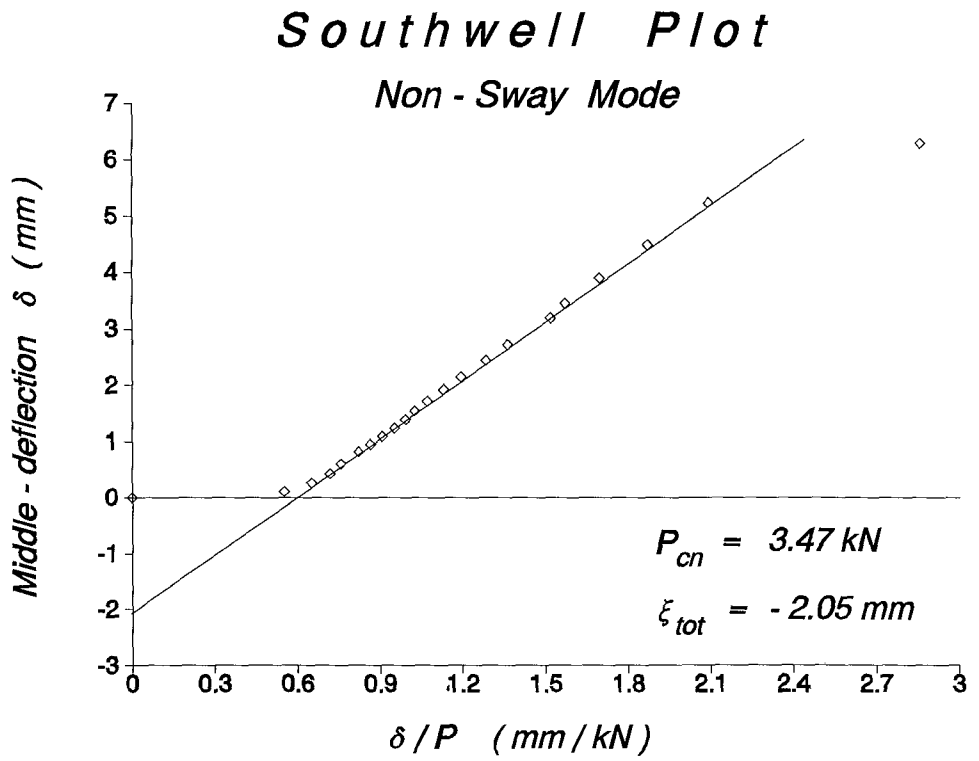
Southwell Plot
Non - Sway Mode
Middle - deflection δ (mm)
7
6
5
4
3
2
1
0
-1
-2
-3
0
0.3
0.6
0.9
1.2
1.5
1.8
2.1
2.4
2.7
3
δ / P (mm / kN)
P_{cn} = 3.47 kN
ξ_{tot} = - 2.05 mm

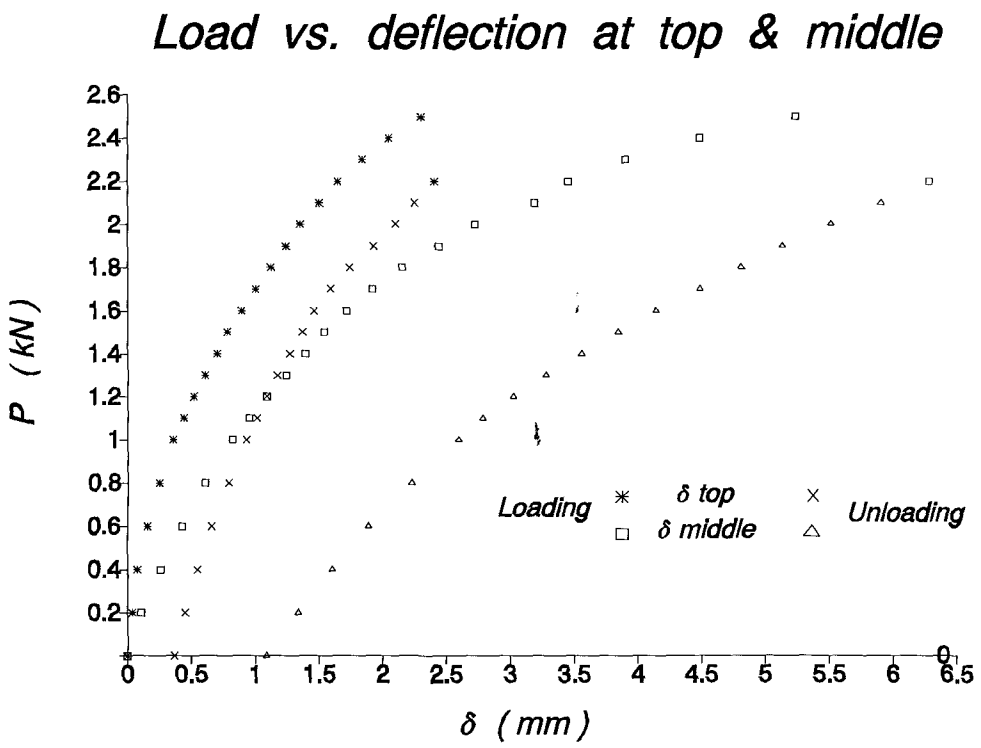

THEORETICAL DATA & RESULTS

PROP_sets = 3, SWAY_imp = -1.35 mm, NON-SWAY_imp = 2.05 mm

MEMBER PROPERTIES

MEM	L	b	d	A	I	Zel	Zpl	Y.str
1	235.0	3.0	13.0	38.47	28.53	19.02	29.26	0.360
2	370.0	5.0	13.0	62.44	125.70	50.28	81.45	0.360
3	235.0	5.0	13.0	62.44	125.70	50.28	81.45	0.360

Rotational SYMMETRIC (Non-sway) Stiffness of frame : 637.69 kN*mm/rad
Rotational ANTISYMMETRIC (Sway) Stiffness of frame : 757.60 kN*mm/rad
Translational (Sway) Stiffness of frame : 23.41 N/mm

EIGENVALUES & EIGENVECTORS

Solut	kL	Pc	C1	C2	delta	theta_A	Mode-Case
1	5.855	3.4533	1.00	-0.217	0.000	0.005	Non-Sway
2	6.968	4.8910	1.00	-2.805	16.026	-0.006	* Sway

First YIELD Load = 2.377 kN
First HINGE Load = 2.768 kN
SQUASH Load = 13.848 kN

Appendix F

Photos

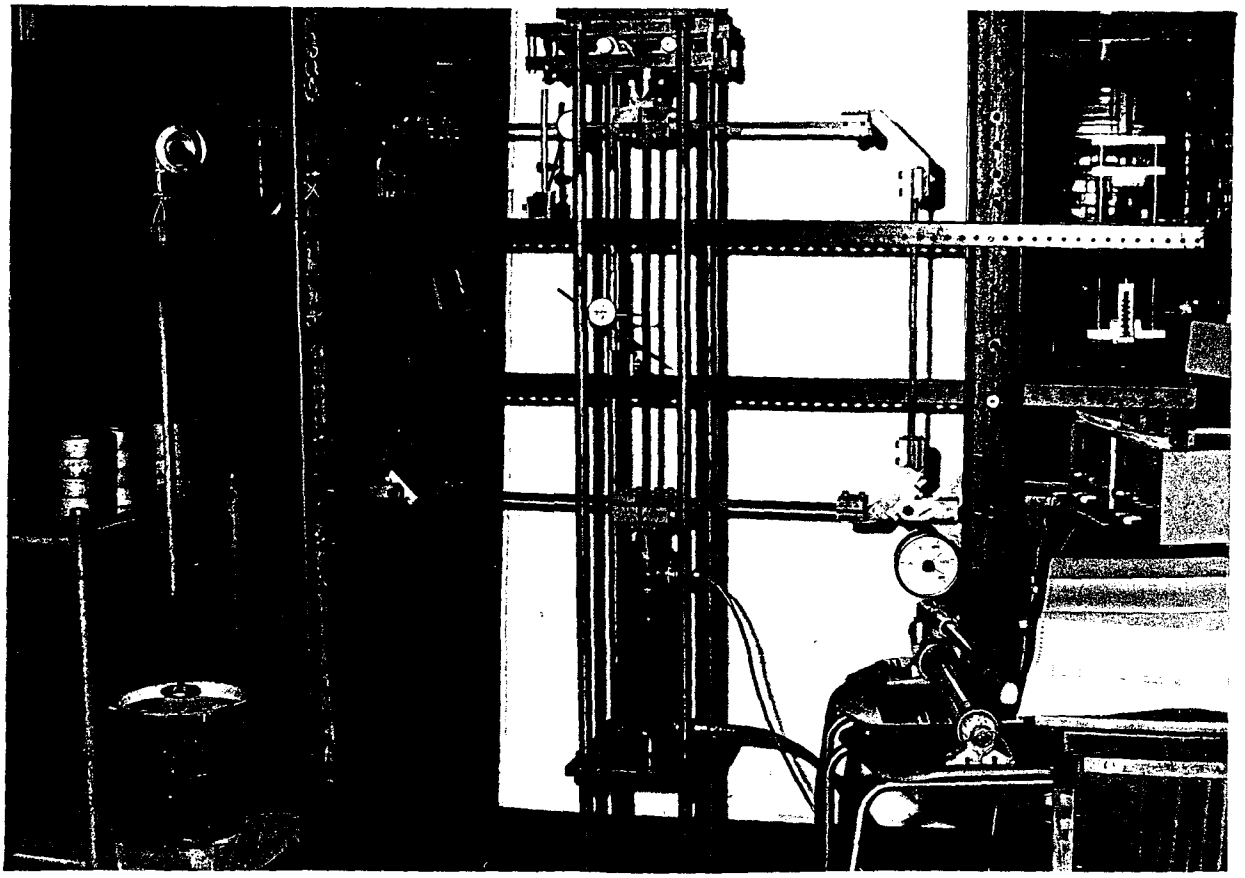

Photo 1. Rig layout before testing

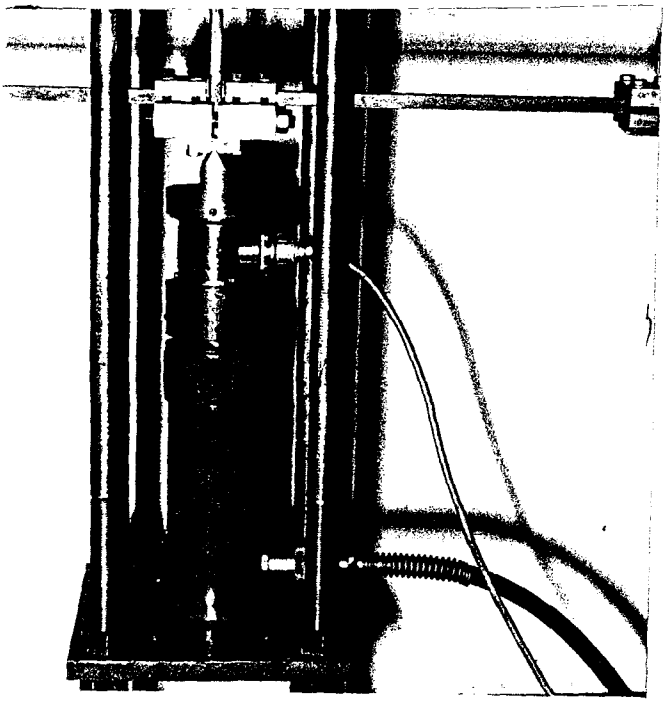

Photo 2.

Mid-block, Load-cell, Jack

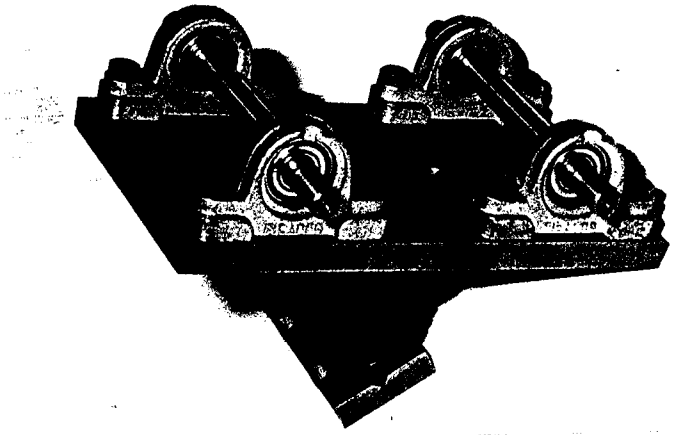

Photo 3. Trolley (initial form)

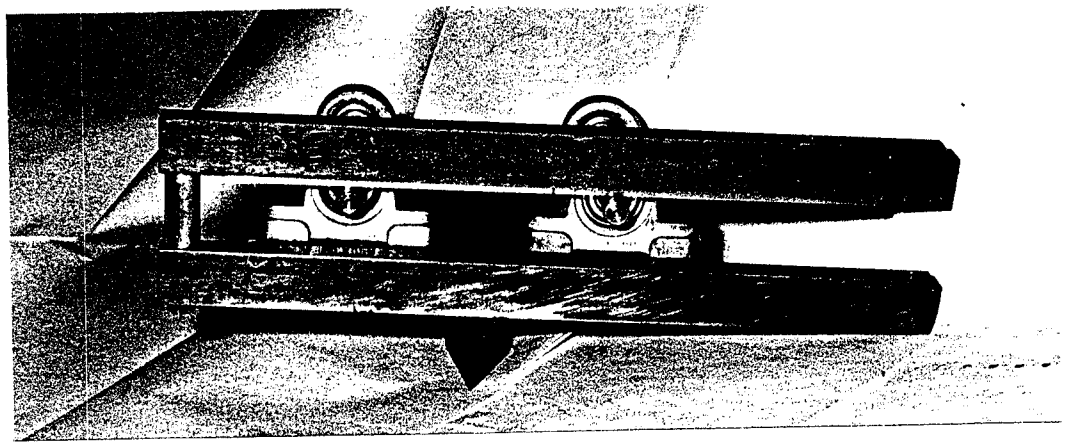

Photo 4. Horizontal rolling on the bars

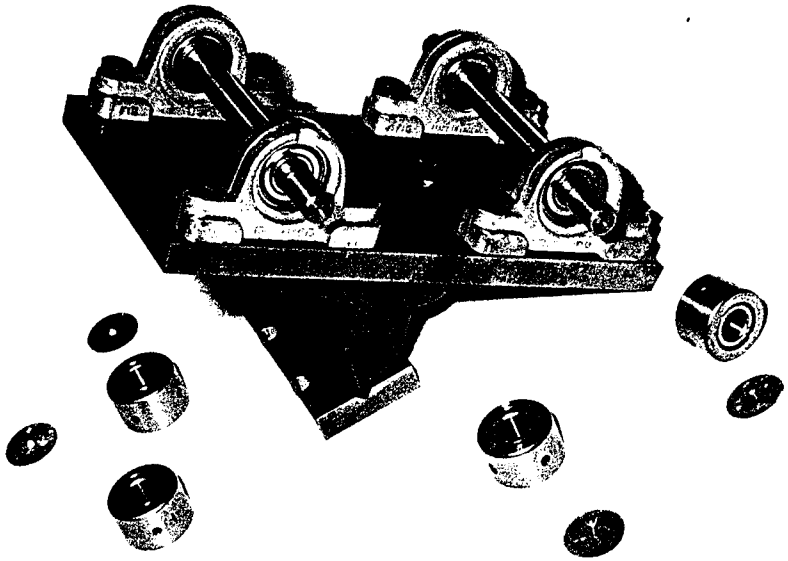

Photo 5. Four wide ball-bearings were added...

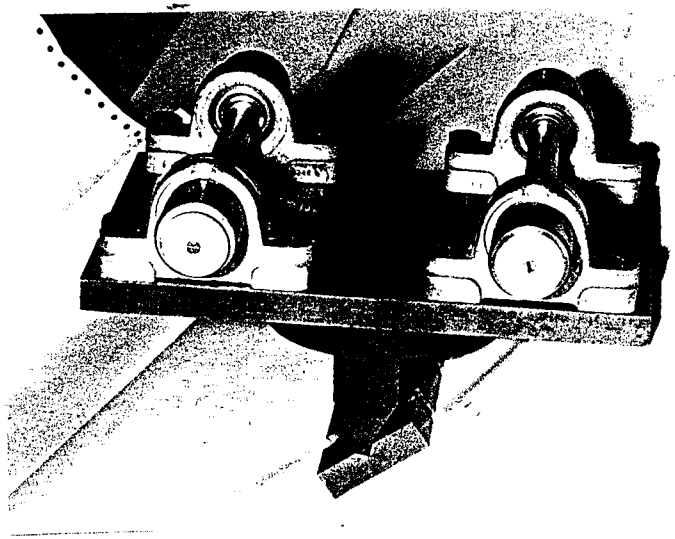

Photo 6. to give the improved form

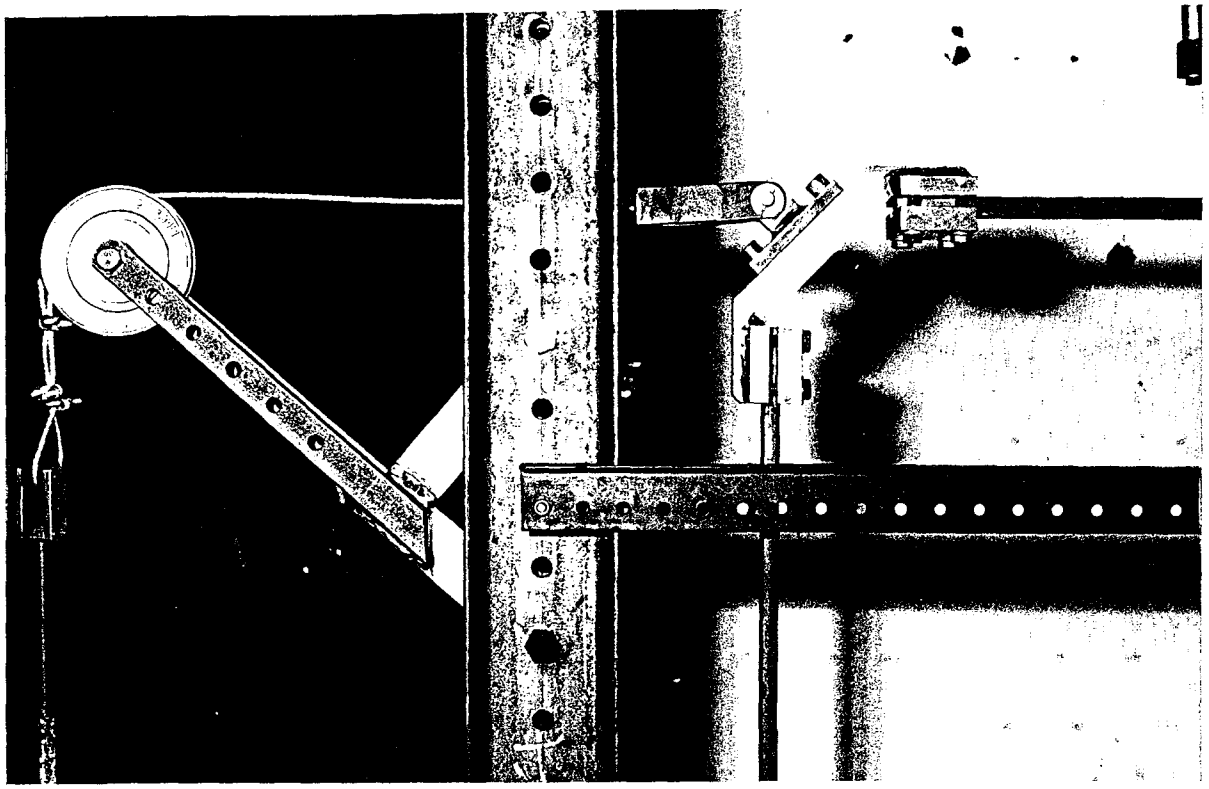

Photo 7. Detail of pulley mechanism and end-block

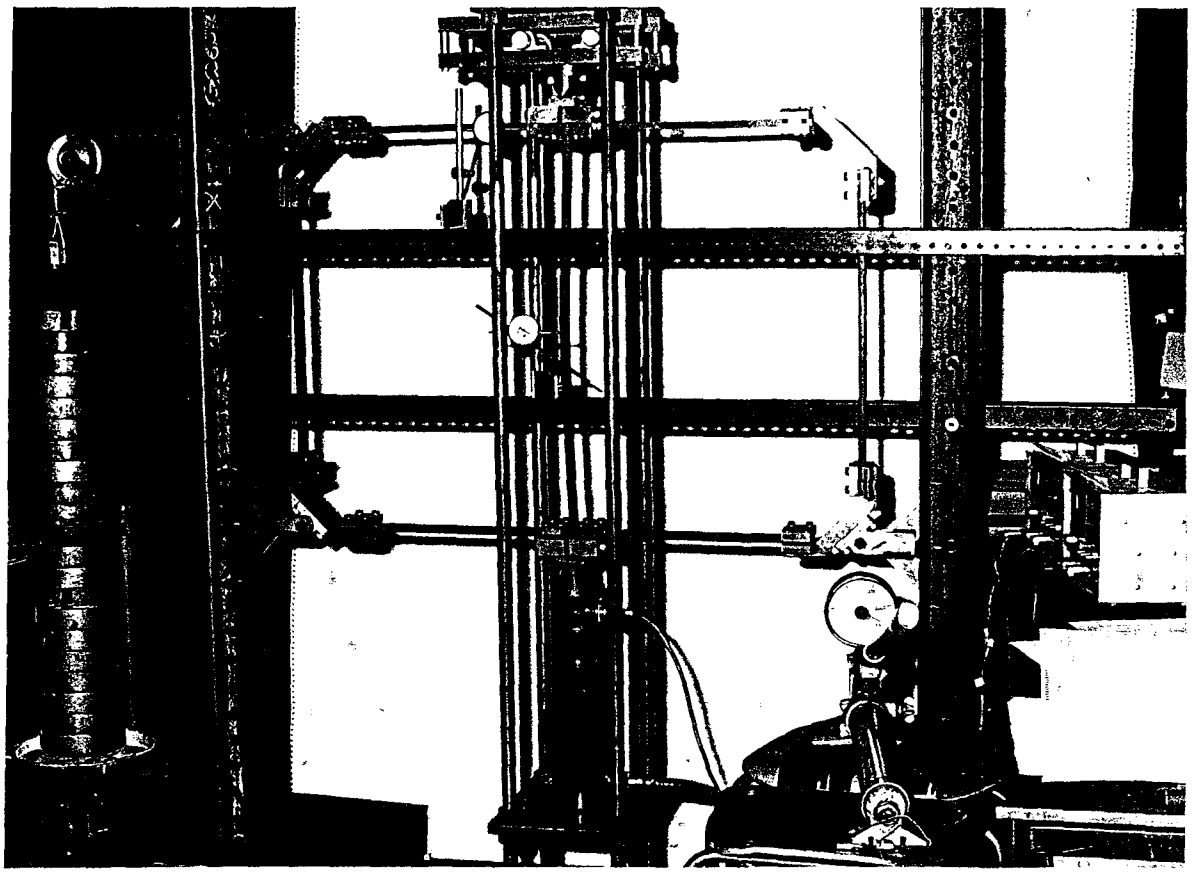

Photo 8. A typical case of proportional loading

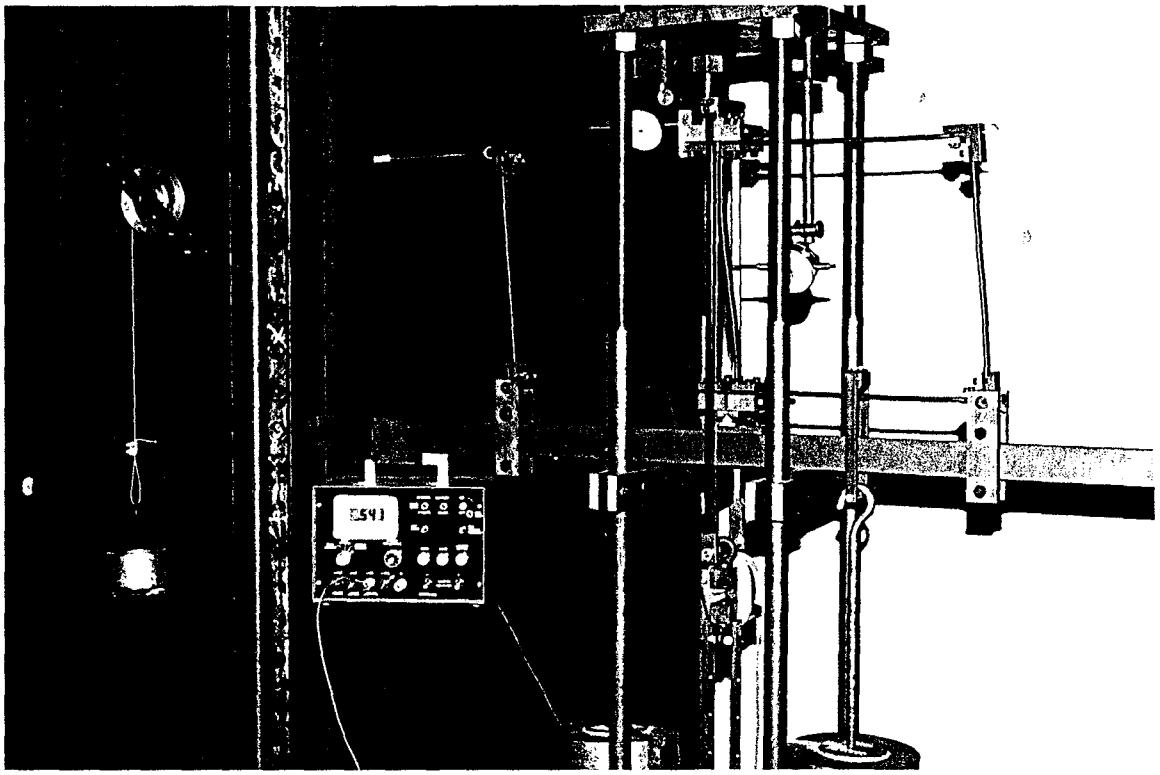

Photo 9. The new frame. Load-cell, bridge and weights for imperfections

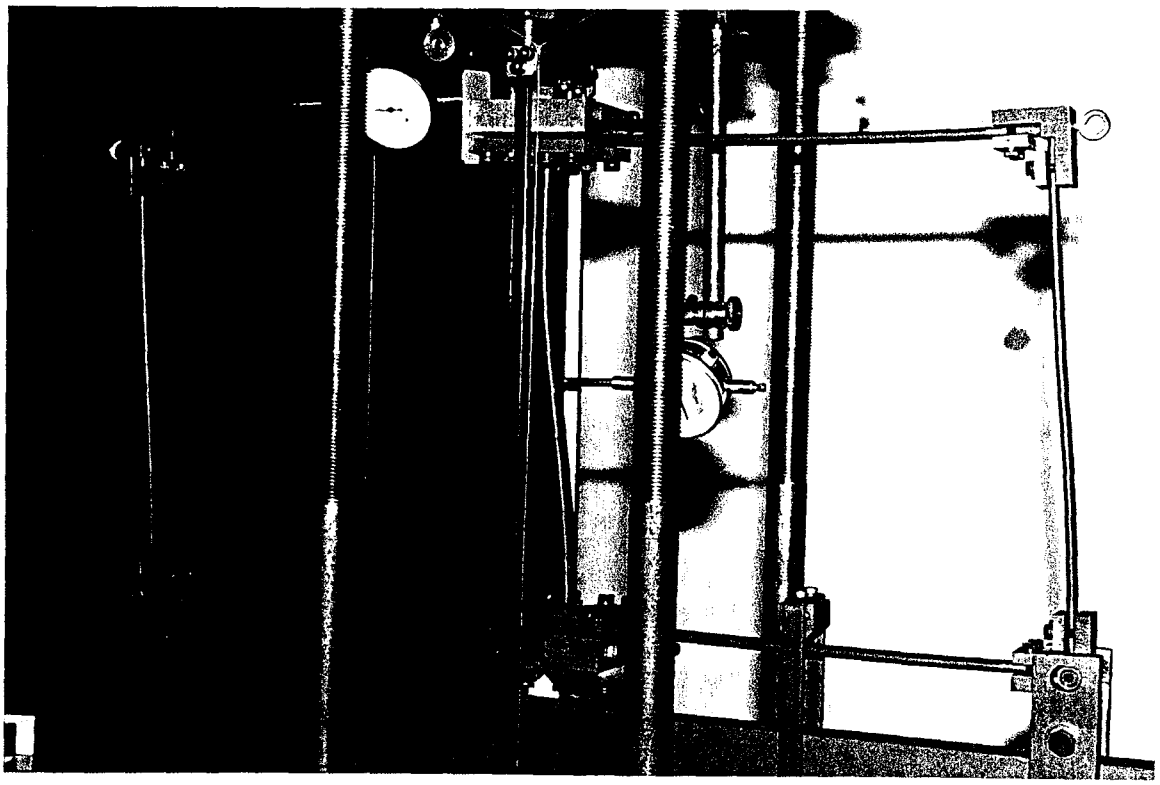

Photo 10. Details of the new frame. End-blocks, supports

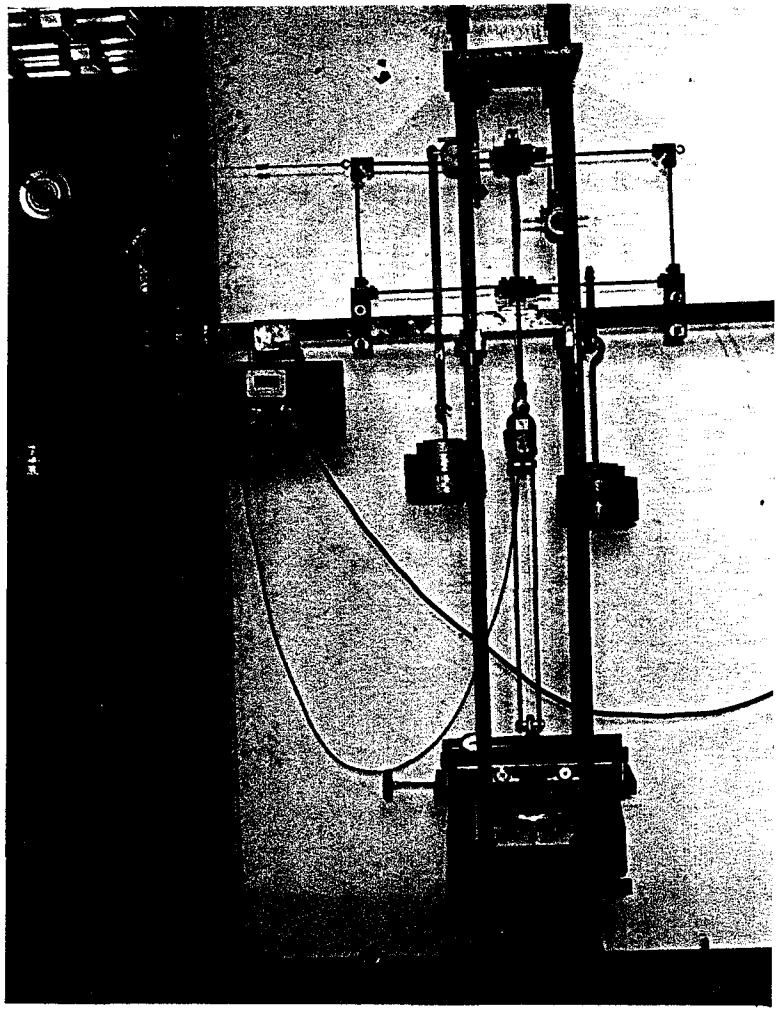

Photo 11. Overall view of the test rig

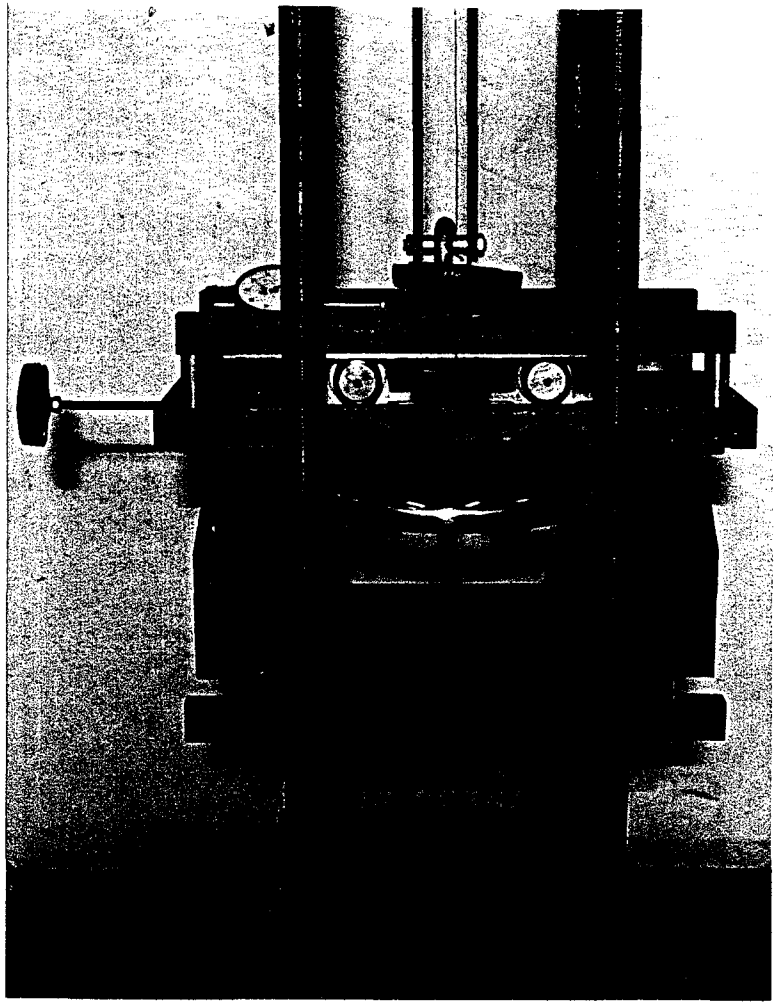

Photo 12. Detail of the trolley mechanism

Appendix G

G.1 Components of the computer program

Defining the computational problem in its substance, the main task of the program was to find the general solution of Eq. (3.23) coming from the governing differential equation of the deflected shape of the column. This means, taking the boundary conditions into account, to solve the eigenvalue problem, expressed by the matrix equation (3.26).

The roots of the non-dimensional determinant of Eq. (3.28) was therefore the first task, so that the critical loads for all modes could be calculated. The program, facing a more general problem, calculates a determinant with 10 rows, by using the Gauss elimination, until the determinant is reduced to one having three only rows.

Then, asking for the number of eigenvalues required, the program sets up the determinant and calculates it for both symmetric and antisymmetric stiffness of the ends of the column, by assigning to kL a zero value.

If the result is not zero, an initial increment of the value of kL is given until the determinant becomes zero or changes its sign, when, an opposite (negative) half increment is given. This iteration is repeated until the value of the determinant is less than the given accuracy (10^{-7}).

The value of kL is then printed as the first root of the determinant and a new increment, equal to the initial is given.

This procedure stops only when the required number of solutions for both stiffnesses is obtained.

Then, taking into account the boundary condition for delta, the program keeps only the solutions that give zero delta for symmetric stiffness and non-zero

for antisymmetric ones.

The flow chart below shows the above computational procedure, the solutions of which give the eigenvalues, i.e. the critical loads.

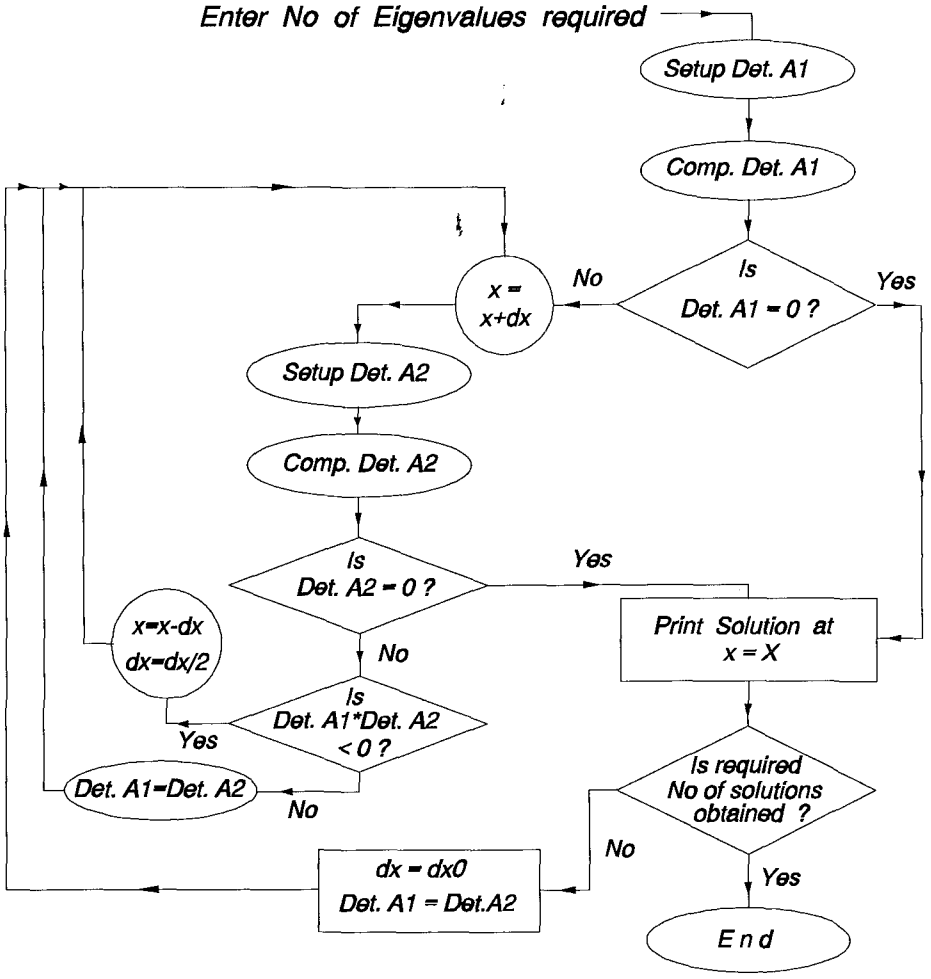

Figure G.1

The second task was the calculation of the Eigenvectors. Using the matrix equation (3.26) the program sets the value of 1 to the first unknown C_1 and calculates the other three by solving the system of three linearly independent equations of the matrix. Then, from the general solution of Eq. (3.23), and for the particular values of the already found unknowns, the characteristic equation is generated. This equation is indefinite as to amplitude but definite as to shape.

For each eigenvalue, the characteristic equation gives the corresponding

shape of the critical mode (Eigenvector). For each Eigenvector, the computer calculates the deflection at 100 different points at equal distance, and, after having found the maximum deflection, divides all the deflections by this value v_{max}, normalizing thus the critical mode shape. Then the normalized mode shape is multiplied by the modal amplitude factor to give the corresponding deflection due to the axial load. This amplitude factor for the 1st critical mode has been taken as

$$w_1 = \frac{L}{1000}, \text{ while for the i}^{th} \text{ mode (i = 2,3,..)}, \; w_i = w_{i-1}\frac{L_{e_i}}{L_{e_{i-1}}} = w_{i-1}\left(\frac{P_{c_{i-1}}}{P_{c_i}}\right)^{1/2}$$

As a next step, the program, asks for the current axial load, enabling thus for the drawing of the deflection and bending moment diagram of the column. This facility was eventually isolated from the main program.

The last and most important step, however, was the calculation of the ultimate (buckling) load, P_c, of the column, when all the demanded critical modes are contributing. On this step, P_c is considered either as a bound solution (upper for plastic hinge formation, lower for initiation of yielding), or as the first critical load (frame or member instability). The algorithm through which this step is realised is the following:

a) Initially a zero axial load, P, is given. This load, which is increased at each step by small increments, dP, is then compared with the first critical load, P_{cl} and the squash load, P_y.

b) If $P < P_{cl}$ and $P < P_y$, then the following c, d and e steps are executed, otherwise the first critical load or the squash load are respectively announced as failure load.

c) The contribution that each one of the demanded critical modes has,

i) in the deflection of the column (buckling shape)

ii) in the moment due to first yield, M_{fy} and plastic hinge, M_{ph} and

iii) in the elastic non-linear bending moment, M_{nl}, is calculated.

d) M_{nl} is compared with M_{fy}. If $M_{nl} < M_{fy}$, then the values of P, M_{nl}, M_{fy}

and M_{ph} are recorded in a file and a new increment of load is added to the previous value. This procedure is repeated until either $M_{nl} = M_{fy}$, or $M_{nl} > M_{fy}$, when a negative half increment, -dP/2 is added, so that the load level for initiation of yielding should be exactly located, when after it is announced.

e) Provided that $P < P_{cr}$, the load-level for plastic hinge formation is similarly located and announced, when further calculations stop.

In conclusion the program is able to give the following results:

1) The demanded number of Eigenvalues and Eigenvectors.

2) In the region of the above Eigenvalues, the different values that $\Delta(kL)$ takes. $\Delta(kL)$ is here the determinant of the coefficients of the equations which describe the boundary conditions of the ends of the column.

3) For each critical mode, the corresponding mode-case (Sway or Non-sway), along with the unknown values of:

a) the translation at the top end of the column

b) the rotation at top end and

c) the coefficient C_2

in terms of the coefficient C_1, which has been taken as unit.

4) As an alternative, for a certain load level, the buckling shape and the bending moment diagram of the column, along with the contribution of each demanded critical mode to both shape and diagram.

5) The buckling shape and the moment diagram when first yield is initiating.

6) The buckling shape and the moment diagram when plastic hinge is formatting.

7) The non-linear elasto-plastic path from which the ultimate loading capacity of the column is obtained.

8) The load level, P_b, at which failure occurs, along with the location of the cross section and the corresponding maximum bending moment.

A full listing of this program is given below.

G.2 Listing of Program

```
C*************************************************************
*C*                        PROGRAM EIGENVALUE ANALYSIS
C*************************************************************
*C:: Changes of E, in lines 453, 470 & 571::::::
C                      M A I N   P R O G R A M
C .....According to the PARAMETER please make a CHANGE in
lines: .........
*..97-101, ... 161-162, ...172-175, ... 405, 408, 412, .....
       PROGRAM Buckling with S_NS_imp
      IMPLICIT DOUBLE PRECISION (A-H,P-Z)
      DIMENSION  PL(3),  PA(3),PI(3),PZ(3),PY(3),VM(50),  CMODE
(50,4)
                            D   I   M   E   N   S   I   O   N
PP(50),PK(50),BUFFER(50),BUFFER2(50),PB(3),PD(3)
      DIMENSION CRB(2),CRT(2),CT(2),IMODE(50),SA(3,2), XXI(50),
PLZ(3)
      LOGICAL SFLAG
      CHARACTER MODECASE(2)*10
      CHARACTER*6 FNAME1 , FNAME2
      PARAMETER (N=4)
      open (9,file='er')
      OPEN (13,FILE='RES')
      OPEN (15,FILE='EP')
      open (23,'BL')
      open (31,file='P_C')
      MODECASE(1) = '  * Sway'
      MODECASE(2) = '  Non-Sway'
*NIT is a number showing the current iteration, starting from
1.....
      NIT = 1
C*******************************
C**          INPUT OF DATA
```

```
C*******************************
*::KNIT is the demanded number of iterations.......
*::VINCR is the given increase of parameter, at each
iteration.....
      READ *, M , KNIT, XSWAY, XNONS, VINCR, VINCR2
      WRITE (*,89) M,XSWAY,XNONS
      write (9,231) 'T H E O R E;T I C A L    D A T A    &
R E S U L T S'
      write (9,98)
      write (9,*)
231   format(13x,a)
      WRITE (13,89) M,XSWAY,XNONS
      WRITE (9,99) M,XSWAY,XNONS
      write (*,432)
*      write (9,433)
      write (13,432)
      write (9,*)
99    FORMAT (3X,'PROP_sets = ',I2,',    SWAY_imp = ',f5.2,'
mm,    NON-SWAY_imp = ',f5.2,' mm')
89    FORMAT (6X,'PROP_sets = ',I2,',    SWAY_imp = ',f5.2,'
mm,    NON-SWAY_imp = ',f5.2,' mm')
98    format (12x,77("-"))
433   format (2x,100("-"))
432   format (5x,68("-"))
      WRITE (*,101)   ' M E M B E R   P R O P E R T I E S'
      WRITE (*,101)   '==================================='
      WRITE (13,101)   ' M E M B E R   P R O P E R T I E S'
      WRITE (13,101)   '==================================='
      WRITE (9,117)   ' M E M B E R   P R O P E R T I E S'
      WRITE (9,117)   '============================='
101   FORMAT (20X,A)
117   format (28x,a)
      WRITE   (*,1021)   'MEM',   'L',   'b',   'd',   'A',
'I','Zel','Zpl','Y.str'
      WRITE   (13,102)   'MEM',   'L',   'b',   'd',   'A',
'I','Zel','Zpl','Y.str'
      WRITE   (9,118)   'MEM',   'L',   'b',   'd',   'A',
```

```
'I','Zel','Zpl','Y.str'
118   FORMAT (0X,A,4X,A,7X,A,8X,A,8X,A,10X,A,10X,A,7x,a,6X,A)
102   FORMAT (1X,A,5X,A,7X,A,8X,A,8X,A,8X,A,8X,A,7x,a,5X,A)
1021  FORMAT (2X,A,5X,A,7X,A,8X,A,8X,A,8X,A,8X,A,7x,a,5X,A)

      WRITE (*,105)
      WRITE (13,105)
      WRITE (9,125)
125   format (0x,93("-"))
      DO 10,I=1,M
C      READ *, PL(I) ,PA(I) , PI(I),PZ(I),PY(I)
      READ *, PL(I), PB(I), PD(I), PY(I)
c=======================================================
c In case the ccross section is RECTANGULAR ignore the
following calculations
c until the first following 3 stars(*), which have to be
activated.
c ------ Details of circular segment of radius 4.3 mm -------

c ANG is half of circular sector's angle in RADS, GAP is the
thick of segment,
c and VER is chord's distance from centre.
      VER=SQRT(4.3**2-(PB(I)/2)**2)
      GAP=4.3-VER
      ANG=ACOS(VER/4.3)
c PARTA is the area of two segments attached to the RESTA
rectangular area.
      PARTA=2*(4.3**2)*(ANG-SIN(ANG)*COS(ANG))
      RESTA=(PD(I)-2*GAP)*PB(I)
      PA(I)=PARTA+RESTA
c PARTI is the moment of inertia of both segments, RESTI the
rect. mom of in.
PARTI=.2666*(4.3**4)*(ANG**5)*(1-.4762*(ANG**2)+.1111*(ANG**4))
      RESTI=(PD(I)-2*GAP)*(PB(I)**3)/12
      PI(I)=PARTI+RESTI
c PZ(I) is the section's modulus, coming from moment of
inertia.          PZ(I)=PI(I)/(PB(I)/2.)
```

```
* PLZ(I) is the plastic section modulus
      PLZ(I)=1.5*PB(I)*PARTA/4+(PD(I)-2*GAP)*PB(I)**2/4
=============================================================*
      PA(I)=PB(I)*PD(I)
*       PI(I)=PD(I)*(PB(I)**3)/12
*       PZ(I)=PD(I)*(PB(I)**2)/6
      WRITE  (*,1031)  I,PL(I),PB(I),PD(I),PA(I),PI(I),PZ(I),
PLZ(I),PY(I)
      WRITE  (13,103)  I,PL(I),PB(I),PD(I),PA(I),PI(I),PZ(I),
PLZ(I),PY(I)
      WRITE   (9,123)  I,PL(I),PB(I),PD(I),PA(I),PI(I),PZ(I),
PLZ(I),PY(I)
103    FORMAT (1X,I2,2X,F7.2,1X,F7.2,2x,f7.2,1X,F8.2,2X,f8.2,
1X,f8.2,2x,f8.2,3X,F6.3)
123    FORMAT (2X,I2,3X,F6.1,1X,F6.1,3x,f6.1,1X,F8.2,2X,f8.2,
1X,f8.2,2x,f8.2,4X,F6.3)
1031   FORMAT (2X,I2,2X,F7.2,1X,F7.2,2x,f7.2,1X,F8.2,2X,f8.2,
1X,f8.2,2x,f8.2,3X,F6.3)
10     CONTINUE
      READ *, X0 , DX0 , ACC , MAXI
      READ *, NS , NDX,IGRAPH,ISCALE
*********************          Changing   the   parameter
***************       write (23,181) 'W_s-n', 'P_fy','P_ph'
      write (23,83)
83     format (2x,32("-"))
81     format (3X,A,7X,A,4(6X,A))
181    format (4X,A,6X,A,8x,a)
      write (31,82)
82     format (52("-"))
      CALL STIFFNESS(SA,CRB,CRT,CT,PI,PL)
      WRITE (*,)
      write (13,)
      write (9,)
      write    (9,775)'Rot.Sym.Non-sway','Rot.Antisym.Sway',
'Transl.Sway'
      write    (13,765)'Rot.Sym.Non-sway','Rot.Antisym.Sway',
'Transl.Sway'
```

```
      write    (*,765)'Rot.Sym.Non-sway','Rot.Antisym.Sway',
'Transl.Sway'
775   format(28x,a,5x,a,4x,a)
765   format(25x,a,4x,a,3x,a)
      write (9,774)
      write (13,764)
      write (*,764)
774   format (27x,73("-"))
764   format (24x,52("-"))
      write   (9,766)'Stiffness   of   frame   :',   SA(1,2),'
kN*mm/rad',
     $SA(1,1),' kN*mm/rad',SA(3,1)*1000,' N/mm.'
      write(13,766)'Stiffness   of   frame   :',   SA(1,2),'
kN*mm/rad',
     $SA(1,1),' kN*mm/rad',SA(3,1)*1000,' N/mm.'
766   format (2x,a,f9.2,a,f10.2,a,1x,f8.3,a)
      write   (*,766)'Stiffness   of   frame   :',   SA(1,2),'
kN*mm/rad',
     $SA(1,1),' kN*mm/rad',SA(3,1)*1000,' N/mm.'
      write (13,763)
      write (9,763)
763   format( )
      print
798   format (4x,a,5x,a,2(3x,a))
797   format (1x,51("-"))
796   format (2x,f6.2,4x,f8.2,6x,f8.2,6x,f8.3)
C*********************************
C**   END OF INPUT
C*********************************
C**   SOLVE EIGENVALUE PROBLEM
C*********************************
      CALL EIGENPROBLEM (X0,DX0,NS,MAXI,PL,PI,PP,PK,CMODE,
     1      IMODE,SA,CRB,CRT,CT,ACC,SFLAG)
C************************
C**   OUTPUT RESULTS
C************************
      write (*,34)'E I G E N V A L U E S   &   E I G E N V E C
```

```
T O R S'
      write (9,37)'E I G E N V A L U E S  &  E I G E N V E C
T O R S'
37    FORMAT(18X,A)
      write (13,34)'E I G E N V A L U E S  &  E I G E N V E
C T O R S'
34    FORMAT(14X,A)
      WRITE(*,35)
35    FORMAT (13X,53("="))
      WRITE (13,35)
      WRITE (9,38)
38    FORMAT (17X,45("="))
      WRITE    (13,229)'Solut','kL','Pc','C1','C2','delta',
'theta_A', 'Mode-Case'
      WRITE    (9,239)'Solut','kL','Pc','C1','C2','delta',
'theta_A','Mode-Case'
239   FORMAT (A5,5X,A2,2(8X,A2),8X,A2,7X,A5,4X,A7,4X,A9)
      WRITE       (*,226)'Solut','kL','Pc','C1','C2','delta',
'theta_A','Mode-Case'
226   FORMAT (2X,A5,5X,A2,2(8X,A2),7X,A2,7X,A5,4X,A7,3X,A9)
229   FORMAT (A5,5X,A2,2(8X,A2),7X,A2,7X,A5,4X,A7,4X,A9)
      WRITE (*,105)
      WRITE(13,105)
      write (9,125)
      DO 13,NSCOUNT=1,NS
      WRITE (*,227) NSCOUNT, PK(NSCOUNT) ,PP(NSCOUNT) ,
     1 (CMODE(NSCOUNT,L),L=1,N) ,MODECASE(IMODE(NSCOUNT))
      WRITE (13,228) NSCOUNT, PK(NSCOUNT) ,PP(NSCOUNT) ,
     1 (CMODE(NSCOUNT,L),L=1,N) ,MODECASE(IMODE(NSCOUNT))
      WRITE (9,238) NSCOUNT, PK(NSCOUNT) ,PP(NSCOUNT) ,
     1 (CMODE(NSCOUNT,L),L=1,N) ,MODECASE(IMODE(NSCOUNT))
13    CONTINUE
227   FORMAT (3X,I2,2X,F8.3,2X,F9.4,2X,F7.2,3(2X,F8.3),2X,A10)
228   FORMAT (1X,I2,2X,F8.3,2X,F9.4,2X,F7.2,3(2X,F8.3),3X,A10)
238   FORMAT (2X,I2,2X,F8.3,1X,F9.4,2X,F7.2,3(2X,F8.3),3X,A10)
      BOX=XSWAY-VINCR
      BOX2=XNONS-VINCR2
```

```
947    XSWAY=BOX+VINCR
       XNONS=BOX2+VINCR2
       IF (NIT .NE. 1) THEN
       write (*,)
       WRITE (*,92)
       write (*,)
       write (13,)
       WRITE (13,92)
       write (13,)
92     FORMAT (80("*"))
       WRITE (13,91)   'Run ',NIT,')   For SWAY_imp   W_s =
',XSWAY,',  and
      +NON-SWAY_imp  W_n = ',XNONS,' mm, are:'
       WRITE   (*,91)   'Run ',NIT,')   For SWAY_imp   W_s =
',XSWAY,',  and
      +NON-SWAY_imp  W_n = ',XNONS,' mm, are:'
91     FORMAT (3x,A,i2,2(A,F5.2),A)
77     FORMAT (4X,A,F7.2,A,4X,A,F8.2,A,4X,A,F7.2,A,4X,A,F6.2)
78     FORMAT (2X,A,F7.2,A,4X,A,F8.2,A,4X,A,F7.2,A,4X,A,F6.2)
       END IF
*-------------------------------------------------------------
-* NDX is the denominator of F-Yield Load, defining the
increment of axial
* load, which is put by the program at each stage of
Elasto_Plastic Path.
*-------------------------------------------------------------
-105   FORMAT ( 79("-"))
111    FORMAT (1X,22("="))
113    FORMAT (26X,22("="))
121    FORMAT (27X,A,I2,A,F5.2)
778    format (6X,A,10X,A,3(8X,A))
779    format (2X,35("-"))
C*************************************************************
*C**   CALCULATES MODESHAPES AND BENDING MOMENTS IF REQUIRED
C*************************************************************
       IF (IGRAPH .EQ.-1) STOP
       IF (.NOT.SFLAG) THEN
```

```
      WRITE (*,204)
      STOP
      END IF
204   FORMAT (' ',26X,'NO SOLUTIONS FOUND')
      X1=0
      X2=0
      XMAX=0
C*****************************************************
C*    NORMALIZE MODE SHAPES & LOCATE MAXIMUM MOMENTS
C*****************************************************
      P=PP(1)
* XSWAY,XNONS are imperfections for the sway and non sway
mode......
*       IF ((XSWAY .EQ. 0.0 ) .AND. (XNONS .EQ. 0.0)) THEN
*       XXI(1)=PL(1)/1000
*       XXI(2)=XXI(1)*SQRT(PP(1)/PP(2))
*       ELSE
      XXI(1)=XSWAY
      XXI(2)=XNONS
*       END IF
      IF (ISCALE .EQ. -1) THEN
      DO 206, I=3,NS,2
      XXI(I)=XXI(I-2)
206   CONTINUE
      DO 207,I=4,NS,2
      XXI(I)=XXI(I-2)
207   CONTINUE
      ELSE
      DO 208, I=3,NS,2
      XXI(I)=XXI(I-2)*SQRT(PP(I-2)/PP(I))
208   CONTINUE
      DO 209,I=4,NS,2
      XXI(I)=XXI(I-2)*SQRT(PP(I-2)/PP(I))
209   CONTINUE
      END IF
      CALL NORMALIZE (NS,NDX,SA,IMODE,CMODE,VM,
     1     PP,PI,PL)
```

```
C*************************************************************
C*    CALCULATE BUCKLING LOAD (FIRST YIELD & COLLAPSE)
C*************************************************************
C*    FIRST YIELD CALCULATIONS
       WRITE (15,306) 'P' , 'Mfy','Mph' , 'Non-lin.El.Mom.',
'Location X'
      WRITE (15,105)
306   FORMAT (6X,A,14X,A,13X,A,7X,A,3X,A)
*-------------------------------------------------------------
*  Variable NDX of next line defines the increment of P in
maximazation.
*-------------------------------------------------------------
      DXX=PY(1)*PA(1)/NDX
      DP=DXX
      PFY=0
      PFH=0
      P=-DP
1200  P=P+DP
      IF (P .GT.PP(1)) THEN
      WRITE  (*,1221) 'Elastic FAILURE Load  = ',PP(1) ,'kN'
      WRITE (13,1221) 'Elastic FAILURE Load  = ',PP(1), 'kN'
       WRITE (9,1121) 'Elastic FAILURE Load  = ',PP(1), 'kN'
        GOTO 1340
      END IF
      SM1=SMFY(P,PA(1),PZ(1),PY(1))
      SM2=SMP(P,PA(1),PZ(1),PY(1))
      SMOM=0
      DO 1210 , I=1,NS
      SMOM=SMOM+ALPHA(I,PP(I),PI(1),XMAX,CMODE,VM(I))
     1 *P*PP(I)*XXI(I)/(PP(I)-P)
1210  CONTINUE
      CALL MAXIMIZE (P,NS,NDX,CMODE,VM,
     1     PP,PI,PL,XXI,X1,X2,XMAX,SMOM)
      SMOM = ABS(SMOM)
1211    FORMAT  (7X,'P  =  ',F6.3,1X,'kN  ,          M_max  =
',F7.3,1X,'kN*mm ,
     +    X = ',F7.3,1X,'mm .')
```

```
      IF (ABS(SMOM-SM1) .LE.ACC) GOTO 1220
      IF (SMOM .GT.SM1) THEN
      P=P-DP
      DP=DP/2
      GOTO 1200
      ELSE
      WRITE(15,1201) P,SM1,SM2,SMOM,XMAX
      GOTO 1200
      END IF
1220  PFY=P
      WRITE (*,1221)  '    First YIELD Load  = ',PFY, 'kN'
      WRITE (13,1221) '    First YIELD Load  = ',PFY, 'kN'
      WRITE (9,1121) '    First YIELD Load  = ',PFY, 'kN'
      WRITE (15,1201) P,SM1,SM2,SMOM,XMAX
1221  FORMAT (/,19X,A23,F8.3,2X,A2)
1121  FORMAT (/,27X,A23,F8.3,2X,A2)
C*    PLASTIC HINGE FORMATION
      DP=DXX
1300  P=P+DP
      IF (P .GT.PP(1)) THEN
      WRITE (*,1221)  'Elastic FAILURE Load  = ',PP(1) ,'kN'
      WRITE (13,1221) 'Elastic FAILURE Load  = ',PP(1) ,'kN'
       WRITE (9,1121) 'Elastic FAILURE Load  = ',PP(1) ,'kN'
        GOTO 1340
      END IF
      SM1=SMFY(P,PA(1),PZ(1),PY(1))
      SM2=SMP(P,PA(1),PZ(1),PY(1))
      SMOM=0
      CALL MAXIMIZE (P,NS,NDX,CMODE,VM,
     1     PP,PI,PL,XXI,X1,X2,XMAX,SMOM)
      SMOM=ABS(SMOM)
      IF (ABS(SMOM-SM2) .LE.ACC) GOTO 1320
      IF (SMOM .GT.SM2) THEN
      P=P-DP
      DP=DP/2
      GOTO 1300
      ELSE
```

```
      WRITE(15,1201) P,SM1,SM2,SMOM,XMAX
      GOTO 1300
      END IF
1320  PFH=P
      WRITE (13,1221) '    First HINGE Load  = ',PFH, 'kN'
      WRITE (*,1221)  '    First HINGE Load  = ',PFH, 'kN'
      WRITE (9,1121) '    First HINGE Load  = ',PFH, 'kN'
      WRITE (15,1201) P,SM1,SM2,SMOM,XMAX
      WRITE  (*,1221)    '                    SQUASH  Load    =
',PY(1)*PA(1),'kN'
      WRITE  (13,1221)  '                    SQUASH  Load    =
',PY(1)*PA(1),'kN'
      WRITE (9,1121) '       SQUASH Load  = ',PY(1)*PA(1),'kN'
1201  FORMAT (1X,F8.3,4(F16.3))
1202  FORMAT (1X,F8.3,2(F16.3))
C-----------------------------------------
C*    REMAINDER OF PLASTIC AND ELASTIC SURFACE
      DP=DXX
1340  P=P+DP
      IF (P.GE. PY(1)*PA(1)+.001) GOTO 1350
      SM1=SMFY(P,PA(1),PZ(1),PY(1))
      SM2=SMP(P,PA(1),PZ(1),PY(1))
      WRITE(15,1202) P,SM1,SM2
      GOTO 1340
C---------------------------------
C*    END OF ELASTO-PLASTIC ANALYSIS
C*********************************************************
C*    PREPARE GRAPHICS FILE FOR MODE SHAPES AND B.MOMENTS
C*********************************************************
1350  CONTINUE
      DO 1600 , JJ=1,2
      DX=PL(1)/NDX
      IF (JJ.EQ.1) THEN
      P=PFY
      FNAME1 = 'FYS'
      FNAME2 = 'FYM'
      ELSE
```

```
      P=PFH
      FNAME1= 'PHS'
      FNAME2 ='PHM'
      END IF
      OPEN (12 ,FILE=FNAME1)
      OPEN (14,FILE=FNAME2)
      IF (JJ.EQ.1) THEN
      WRITE    (12,901)'X','Utotal','Ufy_1','Ufy_2','Ufy_3',
'Ufy_4','Ufy_5'
      WRITE (12,109)
      WRITE    (14,901)'X','Mtotal','Mfy_1','Mfy_2','Mfy_3',
'Mfy_4','Mfy_5'
      WRITE (14,109)
 901  FORMAT (2(6X,A), 6(5X,A))
 109  FORMAT (78("-"))
      ELSE
      WRITE    (12,901)'X','Utotal','Uph_1','Uph_2','Uph_3',
'Uph_4','Uph_5'
      WRITE    (14,901)'X','Mtotal','Mph_1','Mph_2','Mph_3',
'Mph_4','Mph_5'
      WRITE (12,109)
      WRITE (14,109)
      END IF
      X=-DX
      DO 920,J=1,NDX+1
      X=X+DX
      SUM =0
      SMOM=0
      DO 910,I=1,NS
      BUFFER(I)=   P*XXI(I)/(PP(I)-P)*U(I,PP(I),X,CMODE,SA(3,
IMODE(I)),SA(2,IMODE(I)), PL(1),PI(1))/VM(I)
*:::BUFFER(I) is the array of normalized buckling shape.......
      SUM=SUM+ BUFFER(I)
*:::BUFFER2(I) is the array of Non-linear Bend. Mom. for each
mode....
      BUFFER2(I)=ALPHA(I,PP(I),PI(1),X,CMODE,VM(I))
     1 *P*PP(I)*XXI(I)/(PP(I)-P)
```

```
      SMOM=SMOM+BUFFER2(I)
910   CONTINUE
      IF (SMOM .GE. SMAXBP) THEN
      X1=X
      SMAXBP=SMOM
      END IF
      IF (SMOM .LE. SMAXBN) THEN
      X2=X
      SMAXBN=SMOM
      END IF
      if (jj.eq.2) goto 929
929   continue
      WRITE (12,902) X, SUM, (BUFFER(I) ,I=1,NS)
      WRITE (14,903) X, SMOM, (BUFFER2(I) ,I=1,NS)
920   CONTINUE
902   FORMAT (1X,F8.2, 10(2X,F8.3))
903   FORMAT (1X,F8.2, 10(2X,F8.3))
      CLOSE (12)
      CLOSE (14)
1600  CONTINUE
777   FORMAT (1X,F8.2,4(1X,F12.3))
      IF (PFY .NE. 0) THEN
      IF (PFH .NE. 0) THEN
      WRITE (23,443) XNONS,PFY,PFH
443   FORMAT (2X,F6.2,2(5X,F7.3))
      ELSE
      WRITE (23,443) XNONS,PFY
      END IF
      END IF
      BOX=XSWAY
      BOX2=XNONS
      NIT=NIT+1
      IF (NIT .LE. KNIT) THEN
      GOTO 947
      END IF
      STOP
      END
```

```
C*     END OF PROGRAM
C**************************************
C*     SUBROUTINE EIGENPROBLEM
C*     SOLVES THE EIGENVALUE PROBLEM
C**************************************
       SUBROUTINE EIGENPROBLEM (X0,DX0,NS,MAXI,PL,PI,PP
      *,PK,CMODE,IMODE,SA,CRB,CRT,CT,ACC,SFLAG)
       IMPLICIT DOUBLE PRECISION (A-H,P-Z)
       DIMENSION A (10,10) ,PL(3), PI(3)
       DIMENSION  CMODE(50,4) ,PP(50) ,PK(50)
       DIMENSION CRB(2),CRT(2),CT(2),IMODE(50),SA(3,2)
       LOGICAL SFLAG
       PARAMETER (N=4)
       X=X0
       SFLAG = .FALSE.
       JF=0
C***   STIFFNESS CALCULATIONS
       CALL STIFFNESS(SA,CRB,CRT,CT,PI,PL)
       X=X0
       DO 236,NSCOUNT =1,INT((NS+1)/2)
C*     FIND ANTISYMMETRIC SOLUTIONS
       IMODE(NSCOUNT)=1
8          CALLFINDS(N,A,X,DX0,CRB(1),CRT(1),CT(1),PL(1),CMODE
(NSCOUNT,1)1,CMODE(NSCOUNT,2),CMODE(NSCOUNT,3),CMODE(NSCOUNT,
4),ACC,MAXI,JF)
       IF (JF.EQ.-1) THEN
       PRINT  ,  'MAX.  ITERATIONS  EEXCEEDED  ..INCREASE  MAXI
,INCREMENT '
       STOP
       ELSE
       SFLAG = .TRUE.
       END IF
       IF (ABS(CMODE(NSCOUNT,3)) .LE.1D-5) GOTO 8
       PK(NSCOUNT)=X
       PP(NSCOUNT)= 195.*(PI(1))*X**2/(PL(1))**2
       IMODE(NSCOUNT)=1
236    CONTINUE
```

```
      X=X0
      DO 215,NSCOUNT =INT((NS+1)/2)+1,NS+1
7          CALLFINDS(N,A,X,DX0,CRB(2),CRT(2),CT(2),PL(1),CMODE
(NSCOUNT,1)1,CMODE(NSCOUNT,2),CMODE(NSCOUNT,3),CMODE(NSCOUNT,
4), ACC,MAXI,JF)
      IF (JF.EQ.-1) THEN
      PRINT , 'MAX. ITERATIONS EEXCEEDED ..INCREASE MAXI
,INCREMENT '
      STOP
      ELSE
      SFLAG = .TRUE.
      END IF
      IF (ABS(CMODE(NSCOUNT,3)) .GE.1D-5) GOTO 7
      PK(NSCOUNT)=X
      PP(NSCOUNT)= 195.*(PI(1))*X**2/(PL(1))**2
      IMODE(NSCOUNT)=2
*      WRITE (*,227) PK(NSCOUNT) ,PP(NSCOUNT) ,
*     1 (CMODE(NSCOUNT,L),L=1,N) ,IMODE(NSCOUNT)
215   CONTINUE
C*****      ..SORTING BEGINS HERE ....
      DO 12, I=NS,1,-1
      DO 12, J=1,I
      IF (PP(J) .GT. PP(J+1)) THEN
      CALL SWAP (PP(J),PP(J+1))
      CALL SWAP (PK(J),PK(J+1))
      CALL SWAP (CMODE(J,1),CMODE(J+1,1))
      CALL SWAP (CMODE(J,2),CMODE(J+1,2))
      CALL SWAP (CMODE(J,3),CMODE(J+1,3))
      CALL SWAPI (IMODE(J),IMODE(J+1))
      CALL SWAP (CMODE(J,4),CMODE(J+1,4))
      END IF
12    CONTINUE
C-----------------------
C*    SORTING ENDS HERE
      RETURN
      END
C**************************************************
```

```
C**    SUBROUTINE WHICH NORMALIZES THE MODE-SHAPES
C*************************************************
       SUBROUTINE NORMALIZE (NS,NDX,SA,IMODE,CMODE,VM,
      +      PP,PI,PL)
       IMPLICIT DOUBLE PRECISION (A-H,P-Z)
       DIMENSION PL(3),PI(3),VM(50),CMODE(50,4)
       DIMENSION  PP(50) ,IMODE(50),SA(3,2)
       DX=PL(1)/NDX
       DO 900,I=1,NS
       VM(I)=0
       X=-DX
       DO 900,J=1,NDX+1
       X=X+DX
       IF (VM(I) .LE. ABS(U(I,PP(I),X,CMODE,SA(3,IMODE(I)),
      1 SA(2,IMODE(I)),PL(1),PI(1)))) THEN
       VM(I)    =    ABS(U(I,PP(I),X,CMODE,SA(3,IMODE(I)),SA(2,
IMODE(I)),PL(1),PI(1)))
       END IF
900    CONTINUE
       RETURN
       END
C--------------------------
C::: NORMALIZATION ENDS HERE
C*************************************************
C :::   SEARCH FOR MAX. MOMENTS AND POSITIONS
C*************************************************
       SUBROUTINE MAXIMIZE (P,NS,NDX,CMODE,VM,
      1      PP,PI,PL,XXI,X1,X2,XMAX,SMAX)
       IMPLICIT DOUBLE PRECISION (A-H,P-Z)
       DIMENSION PL(3),PI(3),VM(50),CMODE(50,4)
       DIMENSION  PP(50) ,BUFFER2(50),XXI(50)
       DX=PL(1)/NDX
       SMAXBP=0
       SMAXBN=0
       X1=0.
       X2=0.
       X=-DX
```

```
      DO 620,J=1,NDX+1
      X=X+DX
      SMOM=0
      DO 610,I=1,NS
605   CONTINUE
      BUFFER2(I)=ALPHA(I,PP(I),PI(1),X,CMODE,VM(I))
     1 *P*PP(I)*XXI(I)/(PP(I)-P)  ;
      SMOM=SMOM+BUFFER2(I)
610   CONTINUE
      IF (SMOM .GE. SMAXBP) THEN
      X1=X
      SMAXBP=SMOM
      ELSE IF (SMOM .LE. SMAXBN) THEN
      X2=X
      SMAXBN=SMOM
      ELSE
      END IF
620   CONTINUE
      IF (ABS(SMAXBP) .GT. ABS(SMAXBN)) THEN
      XMAX=X1
      SMAX = SMAXBP
      ELSE
      XMAX=X2
      SMAX = SMAXBN
      END IF
      RETURN
      END
C*************************************************************
*C:: SUBROUTINE STIFNESS: CALCULATES THE STIFFNESSES OF THE
FRAME FOR ANY MODE
C*************************************************************
*       SUBROUTINE STIFFNESS (SA,CRB,CRT,CT,PI,PL)
      IMPLICIT DOUBLE PRECISION (A-H,P-Z)
      DIMENSION SA(3,2),CRB(2),CRT(2),CT(2),PI(3),PL(3)
      E=195.
      e=E
      q=PI(2)
```

```
      r=PI(3)
      t=PL(2)
      p=PL(3)
*.........x = Ca for symmetric case.............
x=2220*e*q*(555*p*q*t**2+2*(2*q*(2*r*(t**2-15*t+300)-8325*t**
2)+185*r*(t-60)*(t**2-30*t+900)))/(1110*p*q*(2*q*(t**2-30*t+6
00)+185*(t-60)*(t**2-30*t+900))+16*q**2*(2*r*(t**2-45*t+900)-
8325*(t**2-30*t+600))+4440*q*(t-60)*(r*(t**2-60*t+1500)-2775*
(t**2-30*t+900))+1.02675*10**5*r*(t-60)**4)
      EE= (E*PI(2))/(PL(2)-60)
      H= PI(2)*(PL(1)-60)/(PI(3)*(PL(2)-60))
      SA(1,2)=x
      SA(2,2)=SA(1,2)
*.....................y = Ca'.................
y=2220*e*q*(185*p**3*q*t**2+2*p**2*(2*q*(2*r*(t**2-15*t+300)-
8325*t**2)+185*r*(t-60)*(t**2-30*t+900))-240*p*q*t**2*(r-8325
)+4800*q*t**2*(r-8325))/(370*p**3*q*(2*q*(t**2-30*t+600)+185*
(t-60)*(t**2-30*t+900))+p**2*(16*q**2*(2*r*(t**2-45*t+900)-83
25*(t**2-30*t+600))+4440*q*(t-60)*(r*(t**2-60*t+1500)-2775*(t
**2-30*t+900))+102675*r*(t-60)**4)-480*p*q*(r-8325)*(2*q*(t**
2-30*t+600)+185*(t-60)*(t**2-30*t+900))+9600*q*(r-8325)*(2*q*
(t**2-30*t+600)+185*(t-60)*(t**2-30*t+900)))
      SA(3,2)=48*EE/((3+2*H)*(PL(1)-60)**2)
      CT(2)= SA(3,2)*(PL(1))**3/(E*PI(1))
      CRB(2)=SA(1,2)*PL(1)/(E*PI(1))
      CRT(2)=CRB(2)
*      SA(1,1)=12*EE*(2+H)/(3+2*H)
      SA(1,1)=y
      SA(2,1)=SA(1,1)
*.............. z = Ka*L3/4E ..............
z=2220*p*q*r*(2*q*(t**2-30*t+600)+185*(t-60)*(t**2-30*t+900))
/(370*p**3*q*(2*q*(t**2-30*t+600)+185*(t-60)*(t**2-30*t+900))
+p**2*(16*q**2*(2*r*(t**2-45*t+900)-8325*(t**2-30*t+600))+444
0*q*(t-60)*(r*(t**2-60*t+1500)-2775*(t**2-30*t+900))+1.02675*
10**5*r*(t-60)**4)-480*p*q*(r-8325)*(2*q*(t**2-30*t+600)+185*
(t-60)*(t**2-30*t+900))+9600*q*(r-8325)*(2*q*(t**2-30*t+600)+
185*(t-60)*(t**2-30*t+900)))
```

```
      SA(3,1)=4*E*z/PL(1)
*      SA(3,1)=48*EE/((3+2*H)*(PL(1)-60)**2)
      CT(1)=SA(3,1)*PL(1)**3/(E*PI(1))
      CRB(1)=SA(1,1)*PL(1)/(E*PI(1))
      CRT(1)=CRB(1)
C*    END OF STIFFNESS CALCULATIONS
      RETURN
      END
C*************************************************************
*C::  SUBROUTINE FIND SOLUTION:: OBTAINS A ZERO OF THE
DETERMINANT
C*************************************************************
*      SUBROUTINE FINDS (N,A,X,DX0,CR1,CR2,CT,PL,C1,C2,C3
     +,C4,ACC,MAXI,IFLAG)
      IMPLICIT DOUBLE PRECISION (A-H,P-Z)
      DIMENSION A(10,10),V(10),B(10)
      XPAST=X
      ICOUNT =0
      DX=DX0
      X=X+DX
      CALL SETUP (A,CR1,CR2,CT,PL,X)
      CALL DET01(A,N,DET0)
      DET1 = DET0
      IF (ABS(DET1) .LE. ACC) GOTO 30
20    X = X+DX
      ICOUNT = ICOUNT+1
      IF (ICOUNT .GT. MAXI ) THEN
      IFLAG=-1
      RETURN
      END IF
      CALL SETUP (A,CR1,CR2,CT,PL,X)
      CALL DET01 (A,N,DET2)
151   FORMAT (' ' ,4X,F12.5,10X,F12.5)
      IF (ABS(DET2) .LE. ACC) GOTO 30
      IF (DET2*DET1 .LT.0) THEN
            X =X -DX
            DX =DX/2
```

```
            GOTO 20
      ELSE
            DET1=DET2
            GOTO 20
      END IF
C*************************
C::: A SOLUTION IS FOUND
C*************************
30    IF (ABS(XPAST-X) .LT. .0001) THEN
      DET1=DET2
      DX=DX0
      GOTO 20
      ELSE
      XPAST =X
      END IF
      DO 220 , L=1,N
      B(L)=0
220   CONTINUE
      CALL EGVC (A,B,N,V,JFLAG)
      C1=V(1)
      C2=V(2)
      C3=V(3)
      C4=V(4)
      IFLAG=0
      RETURN
      END
C--------------------------
C:: END OF SUBROUTINE FINDS
C************************************************
C:: SUBROUTINE EGVC FOR EIGNVECTORS' CALCULATIONS
C************************************************
C:: CALCULATES THE EIGNVECTORS FOR A SYSTEM OF N SIMULTANUOUS
EQUATIONS
C:: THE PROGRAM IS VALID WHEN THE RANK OF OF THE COEFFICIENT
C:: MATRIX IS EQUAL TO N-1
      SUBROUTINE EGVC (A,B,N,X,JFLAG)
      IMPLICIT DOUBLE PRECISION (A-H,P-Z)
```

```
      DIMENSION A(10,10) , B(10) ,X(10), TM(10,10)
      LOGICAL SINGULAR

      JFLAG = 1
      SINGULAR = .TRUE.
      MN=N
      DO 15, I=1,N
      IF ( ABS (B(I)) .GT. 1E-5 ) THEN
      SINGULAR =.FALSE.
      END IF
15    CONTINUE
      IF (SINGULAR) GOTO 55
      IFLAG = 0
      CALL SOLVE (A,MN,B,X,IFLAG)
      IF (IFLAG .EQ. 1) THEN
      PRINT , 'SYSTEM IS NON SINGULAR '
      PRINT ,
      WRITE (*,121) 'SOLUTION :'
      WRITE (*,121) '----------'
      PRINT ,
      JFLAG = -1
       RETURN
      ELSE IF (IFLAG .EQ.-1) THEN
      PRINT , 'SYSTEM IS UNSUITABLE FOR THIS PROGRAM '
       PRINT , 'PLEASE CHECK RESULTS INDEPENDENTLY'
      JFLAG = -2
      END IF
C:: SYSTEM IS SINGULAR
55    IEQ = 0
60    IEQ = IEQ+1
      IF (IEQ .GT.N) THEN
      PRINT ,'SYSTEM HAS MORE THAN ONE DEGREE OF FREEDOM'
      JFLAG=-3
      RETURN
      END IF
      IR=0
      DO 110 ,I=1,N-1
```

```
70      IR=IR+1
        IF (IR .EQ. IEQ ) GOTO 70
        JR=0
        DO 100, J=1,N-1
80      JR =JR+1
        IF (JR .EQ. IEQ ) GOTO 80
        TM(I,J) = A(IR,JR)
100     CONTINUE
        B(I)= -A(IR,IEQ)
110     CONTINUE
        CALL SOLVE (TM,MN-1,B,X,IFLAG)
        IF (IFLAG .EQ. -1) GOTO 60
        DO 120, J=N,IEQ+1,-1
        X(J)=X(J-1)
120     CONTINUE
        X(IEQ)=1
121     FORMAT (' ',26X,A12)
         RETURN
        END
C*****************************
C::: SUBROUTINE SOLVE
C*****************************
C:: THIS SUBROUTINE SOLVES (N) SIMULTANUOUS LINEAR EQUATIONS
C:: A IS THE COEFFICIENT MATRIX ,N IS THE NO. OF EQUATIONS
C:: X IS A VECTOR WHICH ON EXIT STORES THE SOLUTIONS
C:: B IS THE MATRIX (N X 1) HOLDING THE R.H.S. OF THE EQUATIONS
C:: IFLAG IS AN INDICATOR .
C:: ON EXIT ,IFLAG = -1 INDICATES A SINGULAR SYSTEM OF
EQUAITIONS
C*************************************************************
        SUBROUTINE SOLVE (A,N,B,X,IFLAG)
C*************************************************************
        IMPLICIT DOUBLE PRECISION (A-H,P-Z)
        DIMENSION A(10,10) , B(10) ,ST (10,10) ,X(10)
        DO 810 ,I=1,N
        DO 810, J=1,N
        ST(I,J) = A(I,J)
```

```
810    CONTINUE
       IFLAG=0
       CALL DET01 (A,N,DET0)
       IF (ABS(DET0) .LE. .0001) THEN
       IFLAG = -1
       RETURN
       ELSE
       IFLAG = 1
       END IF
       DO 8100, J=1,N
       DO 830,I=1,N
       A(I,J) = B(I)
830    CONTINUE
       CALL DET01 (A,N,X(J))
       DO 840 , I=1,N
       A(I,J) = ST(I,J)
840     CONTINUE
8100    CONTINUE
C*     SOLUTION COMPLETED
       DO 850, J=1,N
       X(J) =X(J)/DET0
*      WRITE (*,51) J , X(J)
51     FORMAT (' ',20X,'X(',I2,') =',2X,F10.3)
850     CONTINUE
       RETURN
       END
C**************************************************************
C:: SUBROUTINE DET01 (A,N,DET)
C**************************************************************
C:: THIS SUBROUTINE CALCULATES THE VALUE OF A DETERMINANT A, OF

C:: ORDER N. THE VALUE OF THE DETERMINANT WILL BE STORED IN THE

C:: DOUBLE PRECISION VARIABLE "DET". ON EXIT, THE DETERMINANT
A C:: WILL BE STORED TO ITS ORIGINAL CONTENT.
C**************************************************************
       SUBROUTINE DET01 (A,N,DET)
```

```
      IMPLICIT DOUBLE PRECISION (A-H,P-Z)
      DIMENSION A(10,10) , B(10,10) ,T(10,10)
      DET =1.
C      IG =1
      DO 250, I=1,N
      DO 250, J=1,N
      B(I,J) = A(I,J)
250   CONTINUE
C:: IG IS AN INTEGER USED TO HOLD THE SIGN OF THE DETERMINAT
C:: THE FIRST TASK IS TO REDUCE THE DETERMINANT TO  3 X 3 SIZE
      IF (N.EQ.3) GOTO 400
      IF( N .EQ. 2) GOTO 500
      DO 380, K=1,N-3
      IG =1
      IF (ABS(A(K,K)) .LE. .0001) THEN
      ICOUNT = K
270   ICOUNT = ICOUNT + 1
                  IF (ICOUNT .EQ. (N+1)) THEN
                  DET = 0
                  GOTO 700
C:: IN THE ACTUAL SUBROUTINE, STOP WILL BE PRECEEDED BY A
RETURN
                ELSE
                  END IF
        IF (ABS(A(K,ICOUNT)) .GE. .0001) THEN
            DO 280 , IC=K,N
            CALL SWAP (A(IC,K),A(IC,ICOUNT))
280         CONTINUE
            IG = -IG
            ELSE
            GOTO 270
            END IF
      END IF
      DET = A(K,K)*DET
C*************************************
C     END OF PHASE ONE OF THE PROGRAM
C*************************************
```

```
      DO 370 , J=K+1,N
            FACTOR = A(K,J)/A(K,K)
            DO 360 ,I=K,N
            A(I,J)=A(I,J) - FACTOR * A(I,K)
360         CONTINUE
370   CONTINUE
380   CONTINUE
C**********************************
C:: DETERMINANT IS REDUCED TO 3 X3
C**********************************
400   CONTINUE
      ICI=0
      DO 320, I=N-2,N
      ICI=ICI+1
      ICJ = 0
      DO 320 ,J=N-2,N
      ICJ=ICJ+1
      T(ICI,ICJ) =A(I,J)
320   CONTINUE
301   FORMAT ( 3(F10.4),2X)
      P = T(1,1)*T(2,2)*T(3,3)+T(1,2)*T(2,3)*T(3,1)+
     1 T(1,3)*T(2,1)*T(3,2)
      Q = T(3,1)*T(2,2)*T(1,3)+T(3,2)*T(2,3)*T(1,1)+
     1 T(3,3)*T(2,1)*T(1,2)
      DET = DET*IG*(P-Q)
      GOTO 700
************************
C:: DETERMINANT IS 2 X 2
************************
500   CONTINUE
      DET = A(1,1)*A(2,2)-A(1,2)*A(2,1)
*     WRITE (*,501) DET
501   FORMAT ('0',/,/,26X,'DETERMINANT = ',F12.4)
      GOTO 700
700   DO 750,I=1,N
      DO 750,J=1,N
      A(I,J) = B(I,J)
```

```
750   CONTINUE
      RETURN
      END
*************************************************
C**   SUBROUTINE SWAP (INTERCHANGE TWO VALUES)
*************************************************
      SUBROUTINE SWAP (X,Y)
      DOUBLE PRECISION X,Y,Z
      Z=X
      X=Y
      Y=Z
      RETURN
      END
C*****************************************************
C::  SUBROUTINE SWAPI(X,Y): SWAP INTEGER VALUES
C*****************************************************
      SUBROUTINE SWAPI (X,Y)
      INTEGER X,Y,Z
      Z=X
      X=Y
      Y=Z
      RETURN
      END
*************************************************
C:: SUBROUTINE SETUP: SETS UP THE DETERMINANT
*************************************************
      SUBROUTINE SETUP (A,CR1,CR2,CT,PL,X)
      IMPLICIT DOUBLE PRECISION (A-H,P-Z)
      DIMENSION A(10,10)
      IF (ABS(X).LE. .0001) THEN
      RETURN
      END IF
      A(1,1)=1
      A(1,2)=0
      A(1,3)=1-CT/X**2
      A(1,4)=-CR2/X**2*PL
      A(2,1)=COS(X)
```

```
      A(2,2)=SIN(X)
      A(2,3)=0
      A(2,4)=-CR2*PL/X**2
      A(3,1)=0
      A(3,2)=X
      A(3,3)=CT/X**2 -X**2/CR1 +CT/CR1
      A(3,4)=CR2*PL/CR1
      A(4,1)=-X*SIN(X)
      A(4,2)=X*COS(X)
      A(4,3)=CT/X**2
      A(4,4)=-1*PL
      RETURN
      END
C*********************************
C::: THE CHARACTERISTIC FUNCION
C*********************************
      FUNCTION U (MODE,P,X,C,CCK,CC2,PL,PI)
      IMPLICIT DOUBLE PRECISION (A-H,P-Z)
      DIMENSION C(50,4)
      SK = SQRT (P/(PI*195.) )
      VV = C(MODE ,1)*COS (SK*X) + C(MODE,2)*SIN(SK*X)
      VV =VV + CCK*C(MODE,3)/P*X
      VV = VV+C(MODE,3)*(1-CCK*PL/P)
      U=VV  - CC2*C(MODE,4)/P
      RETURN
      END
C***************************
C:: FUNCTION MOMENT
C***************************
      FUNCTION ALPHA (MODE,P,PI,X,C,SMAX)
      IMPLICIT DOUBLE PRECISION (A-H,P-Z)
      DIMENSION C(50,4)
      SK=SQRT(P/(195.*PI))
      ALPHA= 1/SMAX *(C(MODE,1)*COS(SK*X)
     1 +C(MODE,2)*SIN(SK*X))
      RETURN
      END
```

```
C-----------------------------------------------
C*     END OF FUNCTIONS
C***********************************************
C*     FUNCTION SMFY (P,A,Z,PY)
C*     CALCULATES MOMENT CAPACITY IN THE PRESENCE
C*     OF AXIAL LOAD (FIRST YIELD)
C***********************************************
       FUNCTION SMFY (P,A,Z,PY)
       IMPLICIT DOUBLE PRECISION (A-H,P-Z)
       SMFY =(PY-P/A)*Z
       RETURN
       END
C*************************************************************
C*     FUNCTION SMP (P,A,Z,PY)
C:: PLASTIC MOMENT CAPACITY IN THE PRESENCE of AXIAL LOAD
C*************************************************************
       FUNCTION SMP (P,A,Z,PY)
       IMPLICIT DOUBLE PRECISION (A-H,P-Z)
       SMP= 1.5*PY*Z*(1-P**2/((PY*A)**2))
       RETURN
       END
```

Appendix H

Further Considerations of Existing Design Practice

H.1 Introductory Remarks

In designing multi-stored frames the normal design process encourages a situation in which all components are at the design load detailed so as to produce a simultaneity of collapse; or more commonly so as to present consistent factors of safety against collapse. Where a given member has the possibility of more than one buckling mode, this procedure would correspond to that in which the resistance to buckling in the various modes are equalised. For example, in a column exhibiting the possibility of buckling about the major, x, and minor, y, axes, it would be normal to choose a cross section for which the buckling resistances about the two

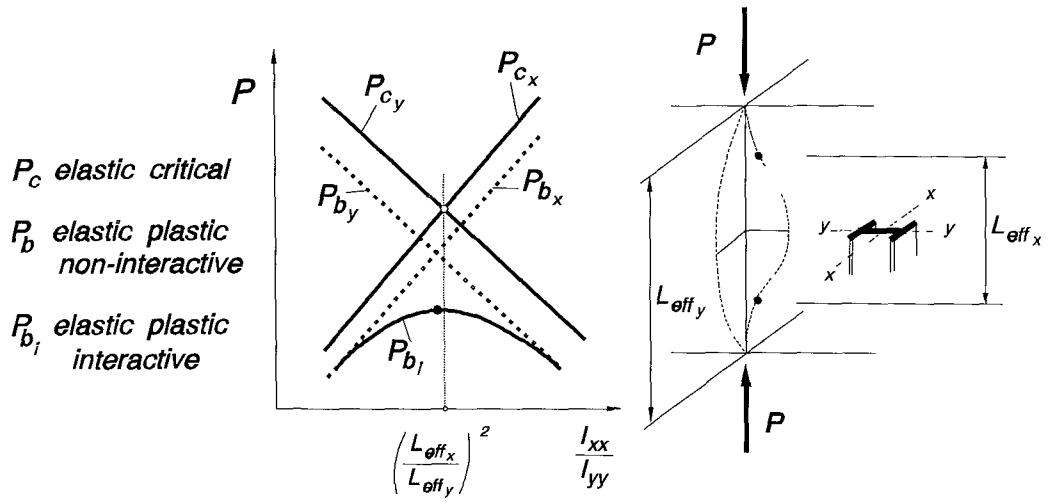

Figure H-1

axes are as near as possible equal to each other. Too high a stiffness about the major axis $\left[I_{xx}/I_{yy} > \left(l_{eff_x}/l_{eff_y}\right)^2\right]$ will mean collapse is precipitated by buckling about the

minor axis. Clearly, in this situation a redistribution of material on the cross-section to increase the stiffness about the minor axis, and consequently decrease the stiffness about the major axis, will allow an increased load carrying capacity. And similar reasoning would apply to the situation were major axis buckling precipitates collapse $\left[I_{xx}/I_{yy} < \left(l_{eff_x}/l_{eff_y}\right)^2\right]$. Clearly, the maximum load carrying capacity would occur when the buckling capacities are equalised about the two axes. This is discussed in Fig. H-1 and was alluded to in Fig. 5-7. More commonly, this optimisation would be framed as a minimisation of the material required for a given design load capacity.

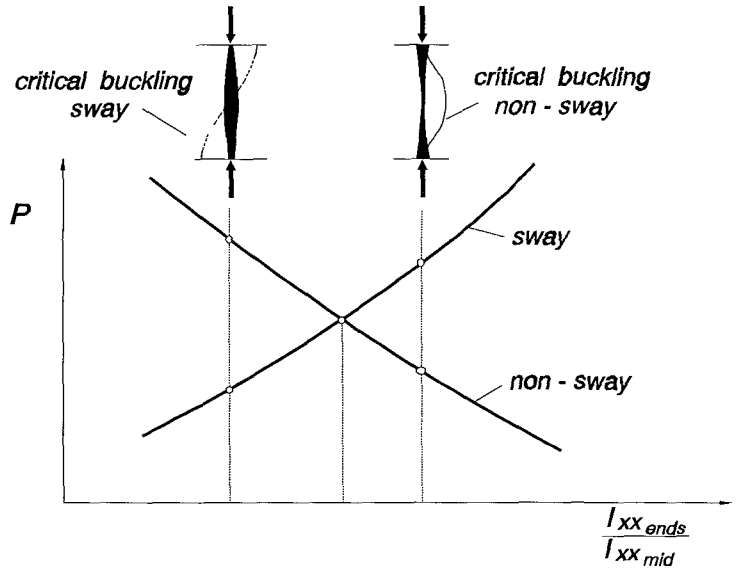

Figure H-2

A similar situation arises when a given column has in the same plane the potential for buckling into a sway mode and a non-sway mode. In this case we could think of the optimisation in terms of the distribution of material and stiffness along the axis of the column. A column with high stiffness and strength at its ends will offer high resistance to sway but low resistance to non-sway buckling. An improvement in load carrying capacity would result if material is moved towards the middle of the column. However, if too much redistribution of material was introduced it would be the sway mode, depending as it does on the weakened ends of the column, which precipitates collapse. An optimum design, and the one that our

usual design process would encourage, would be that for which the two resistances were equalised. These arguments are as true for a purely elastic buckling as they would be when elastic-plastic interactions are considered. And yet, our design practice is remarkable in its lack of clear advise on how to handle the inevitably greater interactions occurring when a simultaneous, 'optimum', buckling condition is achieved. It is this paucity of explicit design guidance that provided the motivation for the present thesis dealing with interactive elastic plastic buckling of sway and non-sway modes in columns, and an earlier study examining the related situation in biaxially buckling columns[59].

To highlight the inadequacy of existing design practice, the following presents comparisons of the theory developed in this thesis with the predictions arising from BS 5950.

H.2 Selection of frame geometry

Because it is likely to involve the most significant effects from modal interactions, a frame geometry is chosen for which the first two critical loads are close to each other. This will enable results from the simplified procedure of Eq. (8.22) to be also compared. Fig. H-3 shows the chosen geometry; this corresponds to that used for the experiment **4oc** (see Table 7_5).

The theoretical and experimental results for experiment 4oc are in Appendix E. For convenience the most important results **for experiment** 4oc are as outlined follows:

a) Theoretical results

The first two critical loads were $P_{cS} = P_{cN} = 6.75\ kN$.

For the total imperfections found experimentally through the Southwell Plot and shown below, the theoretically predicted failure loads were respectively:

- for the first yield initiation $P_{fy} = 5.51\ kN$, whilst

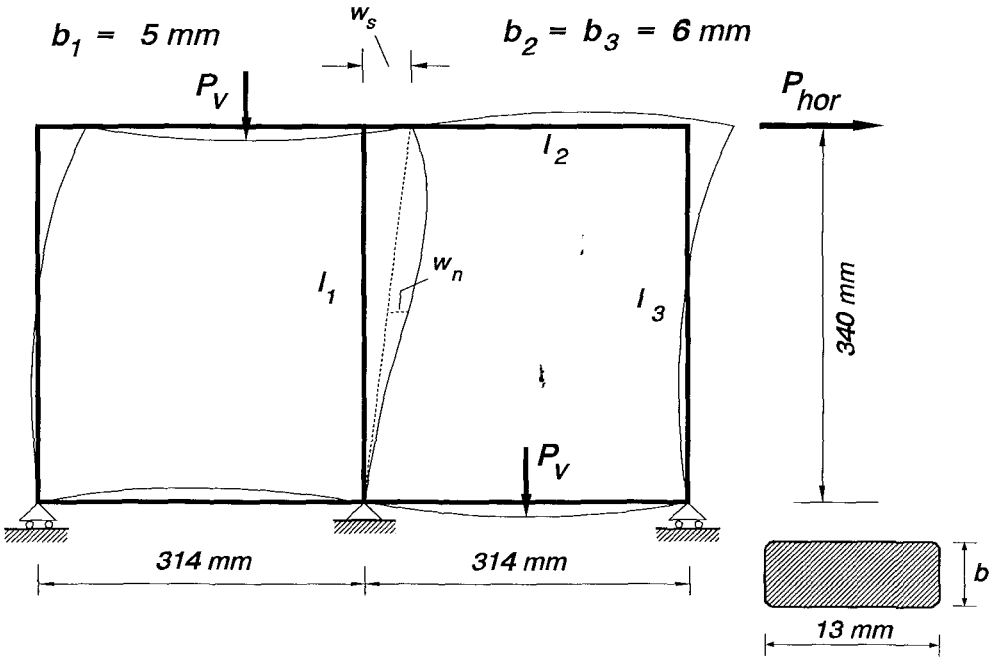

Figure H-3

- for the full plasticity (first hinge) P_{fh} = 6.06 kN.

The squash load was estimated to be P_p = 22.477 kN.

b) Experimental results

From the Southwell Plot the sway critical load was found to be P_{cS} = 6.73 kN, and the non-sway critical load P_{cN} = 6.72 kN.

The sway imperfection was found to be ξ_S = 0.86 mm, and the non-sway imperfection ξ_N = 0.74 mm. With these imperfections a maximum load of 6.4 kN was later recorded for this frame geometry.

H.3 Linear Analysis

To allow the procedure outlined in BS 5950[30] to be followed, two bending

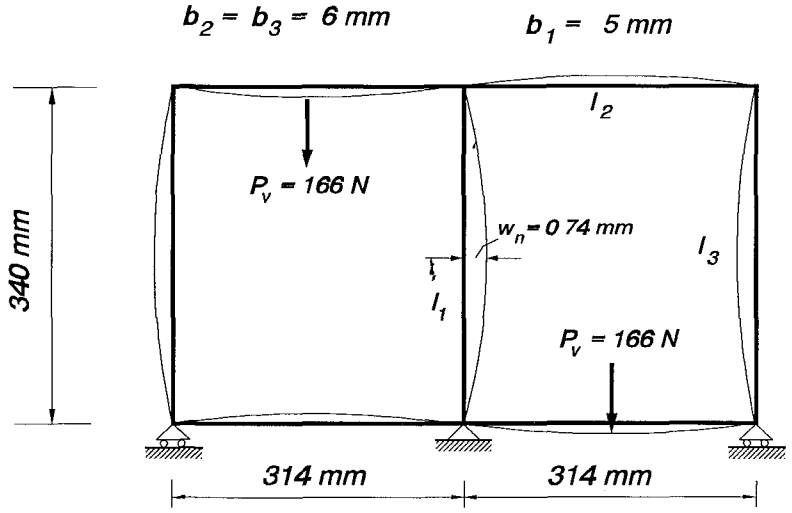

Figure H-4

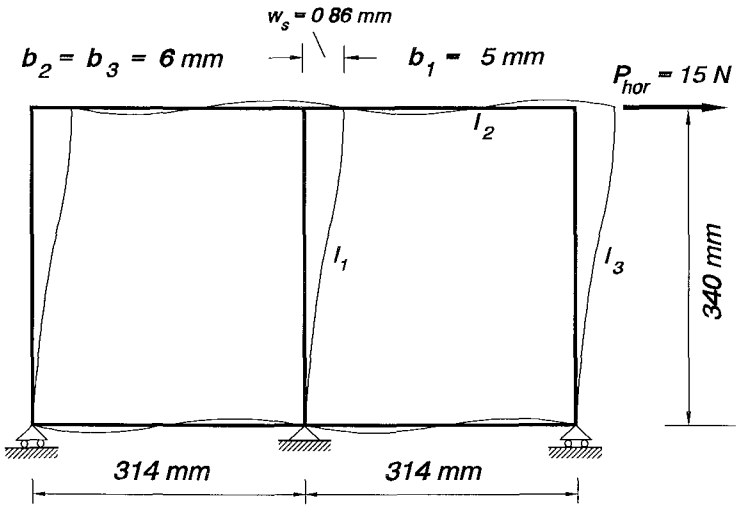

Figure H-5

moment diagrams of the frame have been drawn for the following loading cases:

a) **vertical loading**, on the top left and bottom right beam (at middle), shown in Fig. H-4 are the loads used in the experiment. These loads produce the column

deformation symmetric about its mid horizontal axis and are responsible for the non-sway imperfections on the central column.

b) **horizontal loading**, on the top right end of the frame, shown in Fig. H-5, necessary to cause antisymmetric deformation (symmetry about the column's mid point), responsible for the sway imperfections on the column.

In both cases the load levels were specially chosen to provide the total imperfections obtained separately for each mode through the Southwell Plot, which in turn were later used for the theoretical predictions of P_{fy} *and* P_{fh}.

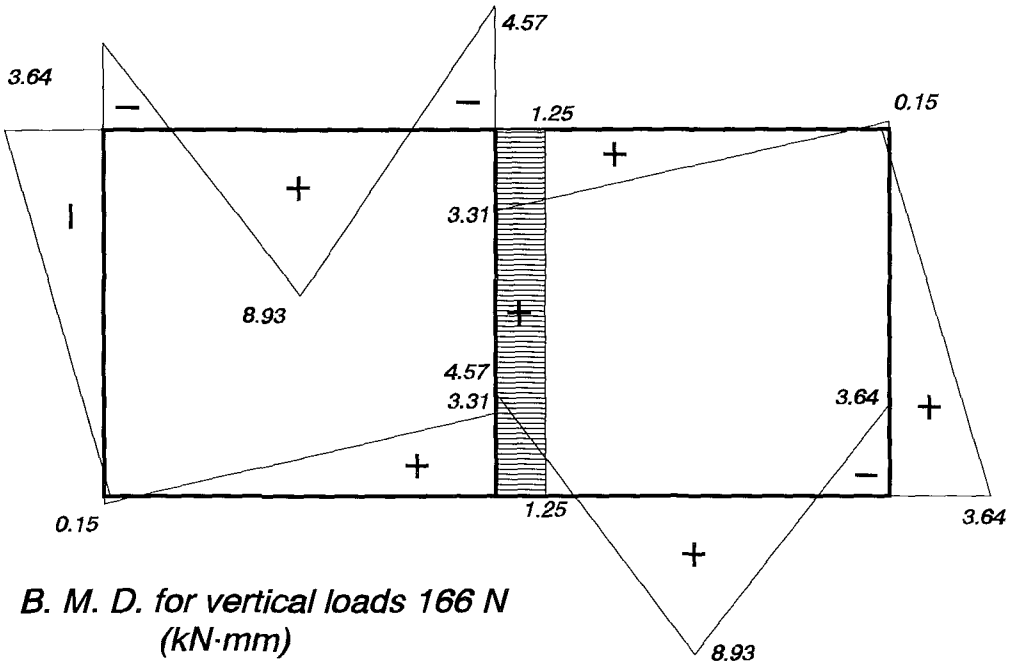

Figure H-6

Figs. H-6 and H-7 show the B.M.D. of the whole frame resulting from linear analyses, where the moments corresponding to the central column are shown shaded.

H.4 BS 5950[30] Procedure

Following a consultation with a member of the Ove Arup & Partners company, specialised on the way BS 5950 treats the buckling behaviour of beam-columns, it was confirmed that BS 5950 provides two different empirical approaches

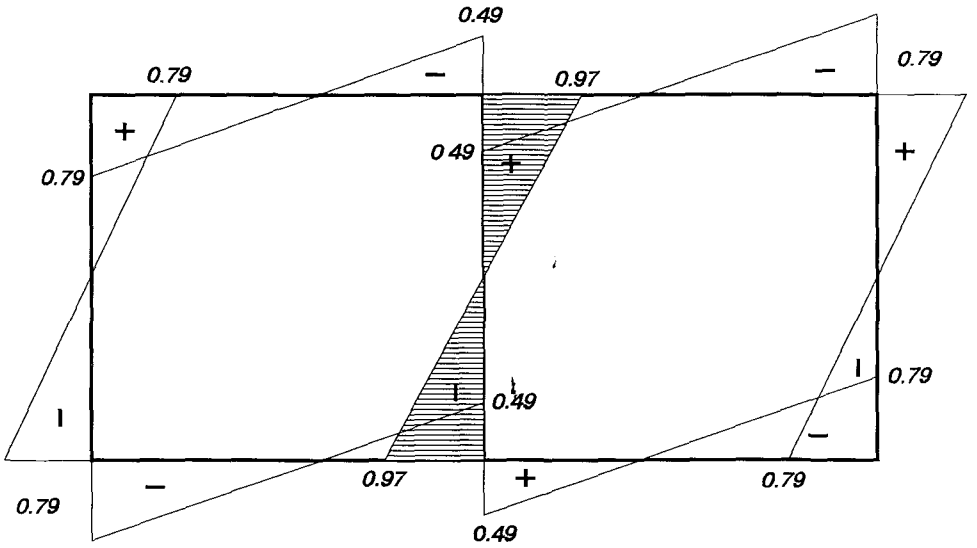

B. M. D. (kN·mm) for horizontal load 15 N

Figure H-7

for calculating the buckling strength resistance. In these approaches:

a) the effect of imperfections (sway and non-sway) are explicitly taken into account by considering the linear bending moments at the ends of the column and

b) the beam-column is treated as a strut, where the effect of imperfections have been implicitly taken into account (limited frame method).

Approach (a)

An approximate method for calculating the elastic critical loads for multi-storey plane frames, presented by Horne[38] in 1975, provides the background for a practical method for calculating sway effects in BS 5950. By introducing notional horizontal forces at each floor, equal to 0.5 % of the factored applied vertical load, allows calculation of the sway index, ϕ_s, (Ref[30], Appendix F, Eq. F.2.4), as

$$\phi_s = \frac{\delta_U - \delta_L}{h} \qquad \textbf{(H.1)}$$

where: h is the storey height

δ_U is the horizontal deflection of the top of the storey

δ_L is the horizontal deflection on the bottom of the storey.

Then the elastic critical load factor, λ_{cr}, (Eq. F.2.3 of Ref[30]), is defined as

$$\lambda_{cr} = \frac{1}{200\phi_s} \qquad \textbf{(H.2)}$$

through which the amplification factor, η, for the moments due to horizontal (sway) loading (see section 5.6.3 Ref[30]) may be calculated from

$$\eta = \frac{\lambda_{cr}}{\lambda_{cr} - 1} \qquad \textbf{(H.3)}$$

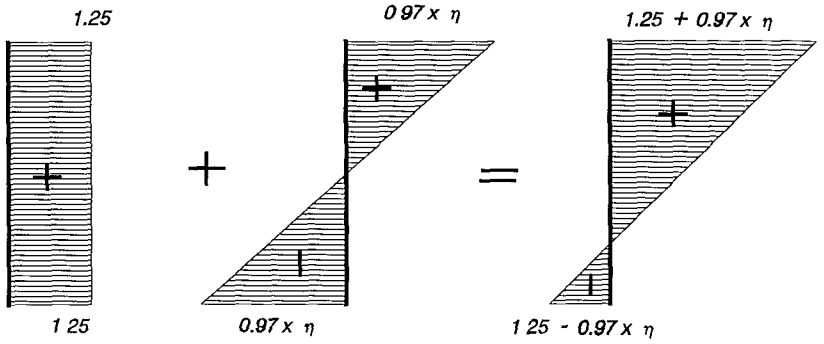

Figure H-8

The amplified maximum combined linear bending moment can therefore be obtained, as shown in Fig. H-8. Using Table 18 of Ref[30] the value of β, representing the ratio of the smaller to the larger end moment, can then be obtained, through which, the equivalent uniform moment factor, m, from the same Table is derived.

The simplified approach (section 4.8.3.3.1 Ref[30]), provides a design load governed by the equation

$$\frac{F}{P_c} = 1 - \frac{mM_x}{M_p}, \tag{H.4}$$

whilst the more exact approach (section 4.8.3.3.2 Ref[30]), upon rearrangement gives

$$\frac{F}{P_c} = \frac{1 - \dfrac{mM_x}{M_{cx}}}{1 + \dfrac{0.5mM_x}{M_{cx}}}, \tag{H.5}$$

where: F is the design load

P_c is the compressive strength force given from the table 27c

m is the equivalent uniform moment factor

M_x is the amplified maximum combined linear bending moment

M_{cx} is the moment capacity in the absence of axial load (=M_p)

The design load is evidently dictated by the satisfaction of equation (H.5), providing the smaller values for F.

The plastic moment capacity for the given column geometry is

$$M_p = Z_p \cdot \sigma_y = 81.45 \cdot 0.36 = 29.32 \ kN \cdot mm \tag{H.6}$$

and, for $L_e = 1.0L$ (section 5.6.3 Ref[30]), giving slenderness ratio

$$\lambda = \frac{340}{\sqrt{125.7/62.44}} = 239, \tag{H.7}$$

the compressive strength is, according to Table 27b, given by

$$P_c = 0.032 \times 62.44 = 2.0 \ kN \tag{H.8}$$

Therefore, application of Equation (H.5) will give for F a design load which has to be **the same** as that initially assumed in calculating the notional horizontal loading.

It is clear that this approach requires the design load to be obtained through an iterative calculation procedure. For this reason a program has been written in fortran to provide the design load. The program initially calculates the compressive strength (which otherwise was provided by Table 27b). Then it assumes a random factored vertical load, and, following the procedure outlined before, calculates the design load, which is then compared to the factored vertical load initially obtained; if it is not the same, the program, takes the revised value of the design load as a factored and repeats the process until the design load is equal to the factored.

A run of the above program gave the following output

BS 5950 Part 1: 1990

For slenderness = 239, the compr. strength is 0.032 kN/mm2

RESULTS OBTAINED FROM BS 5950 THROUGH ITERATIVE PROCEDURE

Loop	ϕ_s	λ_{cr}	η	Mmax	Mmin	β	m	D_strs	D_load
1	0.0008	5.9302	1.203	2.417	0.083	0.034	0.581	0.0302	1.886
2	0.0016	3.1443	1.466	2.672	-0.172	-.065	0.549	0.0301	1.880
3	0.0016	3.1545	1.464	2.670	-0.170	-.064	0.549	0.0301	1.880
4	0.0016	3.1545	1.464	2.670	-0.170	-.064	0.549	0.0301	1.880

The design Load according to the codes is **1.880 kN.**

Approach (b)

Following the procedure outlined in the limited frame method of Ref[30], the frame horizontal stiffness, S_p, obtained through the linear analysis (Section H.3), is

$$S_p = \frac{15}{0.86} = 17.44 \ N/mm \qquad \textbf{(H.9)}$$

The sum of the stiffnesses I/L of the columns of the frame, $\sum K_c$, is

$$\sum K_c = (2\times 209+125{,}7)/340 = 1.60\ mm^3 \qquad \textbf{(H.10)}$$

Therefore the relative stiffness, k_3, of the effective bracing, (Ref[30], E.3.2) is

$$k_3 = \frac{h^2 S_p}{80E\sum K_c} = \frac{340^2\times 17.44}{80\times 195000\times 1.6} = 0.081 \qquad \textbf{(H.11)}$$

Since the relative stiffness is less than 2, the frame has to be considered as a sway one, where the beams are bent in double curvature, and the relevant beam stiffnesses, K_b, should be taken as $1.5\times I/L$ (Ref[30], E.4.1). These stiffnesses for the beams are $K_b = 1.5\times 209/314 = 1.0$, and for the column $K_c = 125.7/340 = 0.37$.

The joint restraint coefficients, k_1 *and* k_2, from (Ref[30], E.2.1), are

$$k_1 = k_2 = \frac{K_c}{K_c+\sum K_b} = \frac{0.37}{0.37+2\cdot 1.0} = 0.16 \qquad \textbf{(H.12)}$$

Since the value of these coefficients is between zero and 1, the effective length ratio, L_E/L must be derived through interpolation between the graphs of Figs. 24 and 25 of Ref[30]. Following this interpolation, the effective length ratio is $L_E/L = 1.09$, providing thus an effective length $L_E = 1.09\times 340 = 371\ mm$.

The slenderness ratio, λ, for the column is consequently

$$\lambda = \frac{L_E}{r_y} = \frac{371}{\sqrt{125.7/62.44}} = 261\ , \qquad \textbf{(H.13)}$$

which, upon use of the Table 27b of Ref[30] for yield stress 360 N/mm^2, provides a compressive strength for this column $p_c = 28\ MPa$.

The design load for this column is therefore

$$P_c = 0.028 \times 62.44 = 1.75\ kN \qquad \textbf{(H.14)}$$

It would appear that for this model frame the design limit for axial load coming from both approaches of BS 5950, of 1.892 or 1.75 kN has an additional safety factor of 2.9 or 3.15 compared with the lower bound theoretical prediction, and 3.37 or 3.65 compared with the experimental buckling load. This suggests an extreme level of conservatism.

H.5 Further Comparisons

For a wide range of different frame geometries and loading conditions, P_{fy} has been shown to be a good lower bound estimate of the experimental collapse loads. In these comparisons, which have been made in the second experimental series (Tables 7_7 and 7_8), three different and independent experiments (elastic, elastic-plastic and collapse) were undertaken for each frame geometry (covering the cases of P_{cS}/P_{cN} being less, equal or greater than unity). It was found that in most of the cases P_{fy} was a close lower bound of the experimental collapse load.

Following the procedure outlined in section H.4 as to how the code treats the buckling strength of beam-columns under conditions of combined sway and non-sway, a second program has been written in Fortran to provide the design load in the cases where the horizontal loading, P_{hor}, (necessary for the sway imperfections) is kept constant, while the vertical loading, P_v, is gradually increased; then a third similar program was written for the case when P_v is kept constant while P_{hor} is increased. The results of these parametric studies, depicted in Figs. H-9 and H-10, show clearly that the code is excessively conservative. In particular Fig H-9 shows the vertical buckling load obtained experimentally for the level of imperfections addressed in Section H.2, and compares this with the first yield and first hinge loads obtained theoretically for the same level of sway imperfections but different levels of vertical loadings (non-sway imperfections). In the same Figure the design loads

obtained through Ref[30] are depicted for both approaches.

Fig. H-10 shows the same comparisons except that the level of vertical loading (non-sway imperfections) is kept constant and the buckling strengths are compared for different levels of sway imperfections.

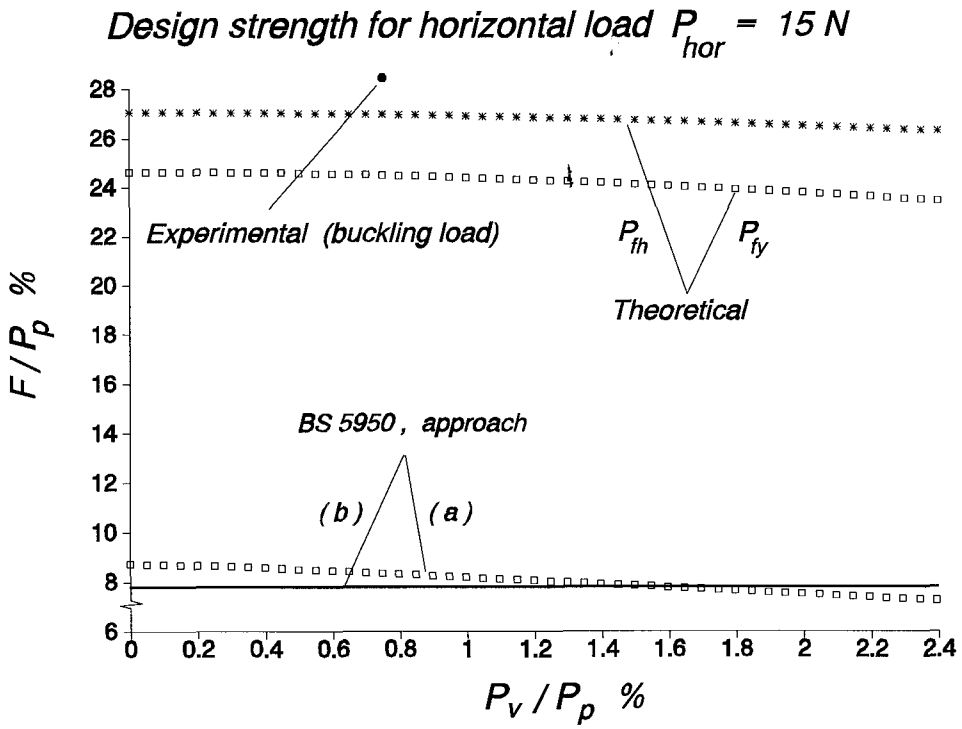

Figure H-9

H.6 Comments and Discussion

The results found from BS 5950 to represent the design loads for the central column of the experimental frame, seem to be unrelated to those obtained from the first yield loads, predicted by the developed theory. Where experimental loads are available, BS 5950 results in failure loads that compare poorly with those observed experimentally. This might be partially attributed to the nature of the idealised frame, in particular to the end blocks, used in the tests to hold the beams and columns together. This results in increased total stiffness of the frame, and hence increased column failure loads. However, the major cause for the discrepancies

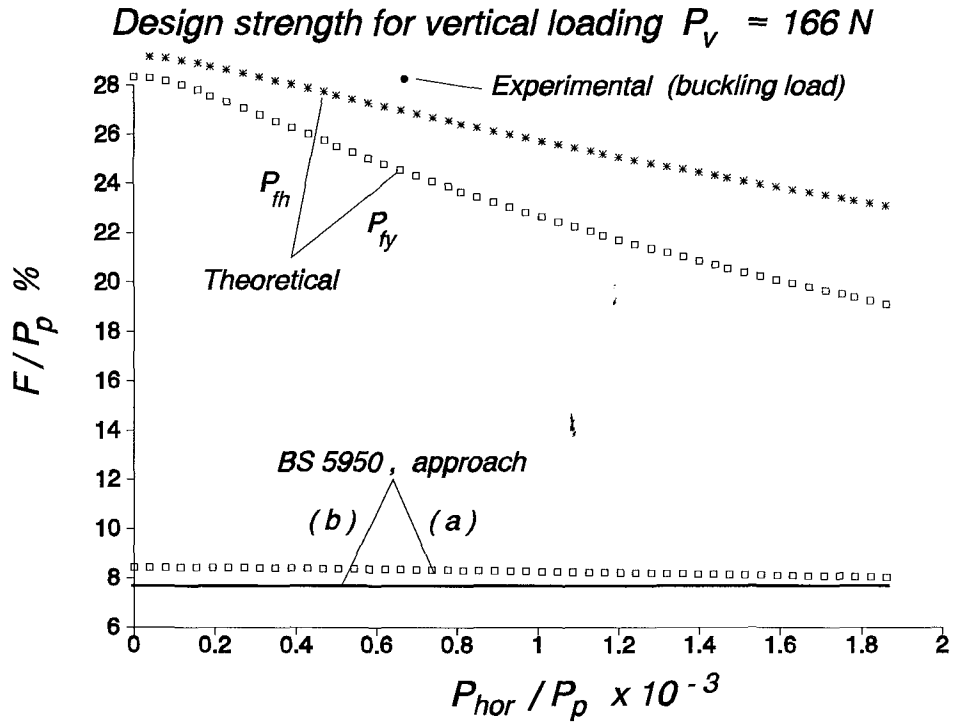

Figure H-10

seems to lie the basically inadequate procedure in the BS 5950 for taking account of combined sway and non-sway modes in rigid jointed frames. Although the present examples have been chosen so as to highlight the inadequacies it would appear that there exist deficiencies in the treatment of sway frames. These deficiencies may be attributed to an inadequate consideration (overly conservative in character) of the effects of the non-linearities arising from each mode and more specifically for the interaction developed between these modes. It would seem that a more rational treatment of sway buckling and its interaction with non-sway buckling, will require moment amplification factors that more truly reflect the levels of the critical loads and the amplitudes of the imperfections in both the sway and the non-sway buckling modes.

From the above discussion it has been observed that the code procedure does not appear to reflect the behaviour in the experimental observations linked with this project. In this respect the code provisions do not conform to the usual approach in choosing code curves to provide lower bounds to experimental scatter.

References

1. Van Musschenbroek, P., "Introductio ad Cohaerentiam Corporum Firmorum" Lugduni, 1729.

2. Young, T., "A course of lectures on natural philosophy and the mechanical arts" London, 1807, Vol. **1**, pp. 135-156 & Vol. **2**, pp. 46-49.

3. Lamarle, A. H. E., "Mémoire sur la flexion du bois", *Annales des Travaux Publiques de Belgique*, Part 1, Vol. **3**, 1845, pp. 1-64, and Part 2, Vol. **4**, 1846, pp. 1-36.

4. Ayrton, W. E., and Perry, J., "On struts", *The Engineer*, London, 1866, pp. 464-513.

5. Hodkinson, E., a) "Experimental researches on the strength of pilars of cast iron and other materials" *Roy. Soc.*, London, 1840.
   b) "Experimental researches on the strength of pilars of cast iron and other materials" *Roy. Soc.*, London,1857.
   c) "Experimental researches on the strength and other properties of cast iron" London, 1860.

6. Considère, A., "Resistance des pièces comprimées" *Congrès International des procédés de Construction*, Paris, Sept. 9-14, 1889, Proceedings published by Librairie Polytechnique, Paris, Vol. **3**, 1891, p. 371.

7. Engesser, F., "Ueber die Knickfestigkeit gerader Stäbe" *Zeitschrift für Architectur und Ingenieurwesen,* Vol. **35**, no. 4, 1889, pp. 455-462.

8. Engesser, F., "Knickfragen", *Schweizerishe Bauzeitung*, Vol. **25**, no. **13**, March 30, 1895, pp. 88-90.

9. Jasinski, F., "Noch ein wort zu den 'Knickfragen'" *Schweizerishe Bauzeitung*, Vol. **25**, no. **25**, June 22, 1895, pp. 172-175.

10. Engesser, F., "Ueber Knickfragen", *Schweizerishe Bauzeitung*, Vol. **26**, no. **4**, July 27, 1895, pp. 24-26.

11. von Karman, T., "Die Knickfestigkeit gerader Stäbe", *Physikalische Zeitschrift*, Vol. **9**, no. **4**, 1908, pp. 136-140.

12. Von Karman, T., "Untersuchungen über Knickfestigkeit", *Mitteilungen über Forschungsarbeiten auf dem Gebiete des Ingenieurwesens, Verien Deutscher Ingenieure,* Berlin, Heft **81**, 1910.

13. Southwell, R. V., "The strength of struts", *Engineering*, Vol. **94**, August 23, 1912, pp. 249-250.

14. Shanley, F. R., "The column paradox", *Journal of the Aeronautical Sciences*, Vol. **13**, no. **12**, December 1946, p. 678.

15. Shanley, F. R., "Inelastic column theory", *Journal of the Aeronautical Sciences*, Vol. **14**, no. **5**, May 1947, pp. 261-267.

16. Young, D. H. "Rational Design of Steel Columns" *Transactions*, ASCE, Vol. **101**, 1936, p. 422.

17. Timoshenko, S. P. and Gere, J. M., "Theory of elastic stability" 2nd Ed., McGraw-Hill, New York, 1961.

18. Austin, W. J., "Strength and design of metal beam-columns" *Journal of the structural division,* ASCE, Vol. **87**, No. **ST4**, April 1961.

19. Chwalla, E., a) "Die stabilität zentrisch und exzentrisch gedrückter Stäbe aus Baustahl" *Sitzungsberichte der Akademie der Wissenschaften in Wien*, Abt. IIa, 1928, p. 469.

b) "Über die experimentelle Untersuchung des Tragverhaltens gedrückter Stäbe aus Baustahl" *Der Stahlbau*, Vol. **7**, 1934, p. 10.

20. Jezek, K., "Die tragfähigkeit axial gedrückter und auf Biegung beanspruchter Stahlstäbe" *Der Stahlbau*, Vol. **9**, 1936, p. 12.

21. Horne, M., R., "The Elastic-Plastic Theory of Compression Members" *Journal of the Mechanics and Physics of Solids*, Vol. **4**, 1956, p. 104.

22. Galambos, T. V., and Ketter, R., "Columns under combined bending and thrust" *Journal of the Engineering Mechanics division*, ASCE, Vol. **85**, No. **EM2**, April 1959, pp. 1-30.

23. Chen, W. F. and Santathandaporn, S., "Curvature and the solution of eccentrically loaded columns" *Journal of the Engineering Mechanics division,* ASCE, Vol. **95**, No. **EM1**,1969, pp. 21-40.

24. Chen, W. F. and Atsuta, T., "Column curvature method for analysis of beam-columns" *The structural Engineer,* Vol. **50**, No. **6**, June 1972, pp. 233-240.

25. Timoshenko, S. P. and Gere, J. M., "Theory of elastic stability" 2nd Ed., McGraw-Hill, New York, 1961.

26. Campus, F. and Massonnet, C., "Recherches sur le flambement de colones en acier A37, á profil en double Té, solicitées obliquement" *Comptes Rendus de Recherches,* IRSIA, 1956.

27. Ballio, G. and Campanini, G., "Equivalent Bending Moments for Beam-Columns" *Journal of Constructional Steel Research*, Vol. **1**, No. **3**, 1981, pp. 13-23.

28. European Convention for Constructional Steelwork, "European recommendations for Steel construction" *The Construction Press,* London, March, 1978.

29. Nethercot, D. A. and Taylor, J. C., "Design approaches for steel beam-columns" *Final Report of Second International Colloquium on Stability of Steel Structures*, ECCS-IABSE-SSRC-CRC, Liege, April 1977, pp. 199-201.

30. British Standard 5950, "Structural use of steelwork in building" Part 1, *British Standard Institution*, 1990.

31. Chen, W. F. and Atsuta, T., "Theory of Beam-Columns" Vol. **1**, In-plane behaviour and design, McGraw-Hill, 1976.

32. Chen, W.F. and Lui, E. M., "Stability design of steel frames" CRC Press, 1991, U.S.A.

33. Kanchanalai, T. and Lu, L. W., "Analysis and design of Framed Columns under minor axis bending" *Engineering Journal*, AISC, Vol. **16**, No. **2**, Second quarter, 1979, pp. 29-41.

34. Massonet, C. E., "Forty Years Research on Beam-column in Steel" *Solid Mechanics Archives,* Vol. **1**, No. **2**, 1976, pp. 27-157.

35. Johnston, B. G., "Guide to stability Design Criteria for Metal Structures" SSRC, 3rd ed., New York, John Wiley & sons, 1976, pp. 410-454.

36. Horne, M. R. "An historical review on the interaction of plasticity and structural stability in the theory and its application to design" *R. H. Wood Memorial Conference*, Modern developments in frame and slab structures, November 1988, pp. 1-27.

37. Wood, R. H., "Effective lengths of columns in multi-storey buildings" *The Structural Engineer*, Part 1, Vol. **52**, No. **7**, July 1974, pp. 235-244, Part 2, Vol. **52**, No. **8**, August 1974, pp. 295-302, Part 3, Vol. **52**, No. **9**, September 1974, pp. 341-346.

38. Horne, M. R. "An approximate method for calculating the elastic critical loads of multi-storey plane frames" *The Structural Engineer*, Vol. **53**, No. **6**, June 1975, pp. 242-248.

39. Load & Resistance Factor Design, "Manual of steel construction" First edition, AISC, 1986.

40. Rankine, W. J. M., "Useful rules and tables", London, 1866.

41. Merchant, W., "The failure Load of Rigid Jointed Frameworks as Influenced by Stability" *The structural Engineer*, Vol. **32**, July 1954, pp. 185-190.

42. Horne, M. R., Elastic-plastic failure loads of plane frames" *Proc. Roy. Soc.*, **274**, A, No. **1358**, November 1963, pp. 343-364.

43. a. Bijlaard, P. P., "Some contributions to the theory of elastic and plastic stability" *Publ. IABSE*, Vol. **8,** 1947.

b. McGuire, W., "Steel structures" Prentice-Hall, INC./ Englewood Cliffs, N.J., 1968, p. 439.

c. Iyengar, N. G. R., "Structural stability of columns and plates" 1st ed., Ellis Horwood Limited, England, 1988, p. 123.

44. Gurfinkel, G. and Robinson, A. R., "Buckling of elastically restraint columns" Journal of Struct. Division, Proc. of the ASCE, Vol. 91, No ST6, Dec. 1965, pp.159-183.

45. Bleich, F., "Buckling strength of metal structures" New York, McGraw-Hill Company, Inc., 1952.

46. Ariaratnam, S. T., "the Southwell method for predicting critical loads of elastic structures" *Quart. Journal Mech. and Appl. Maths.*, Vol. **14** part 2, 1961, pp. 137-153.

47. Horne, M. R., "The effect of finite deformations in the elastic stability of plane frames" *Proc. Roy. Soc.*, **266**, A, 1962, pp. 47-67.

48. Chen, W. F., "Further studies of inelastic beam-column problem" *Journal of the structural division*, ASCE, Vol. **97,** No. **ST2,** 1971, pp. 529-544.

49. Nethercot, D. A., "Members with axial load and moments" SCI/I.STRUC.E Course, Design to BS 5950 Part 1, University College London, June 1987.

50. Salmon, E., H., "Columns" *Oxford Technical Publication*, 1921

51. Walker, A.C., Croll, J.G.A. and Wilson, E., "Experimental models to illustrate the non-linear behaviour of elastic structures" *Bulletin Mechanical Engineering Education*, Vol. **10**, 1971, pp 247-259.

52. Hosseini Hashemi, B., 'A consistent approach to the buckling design analysis of rigid jointed frames' Ph.D. thesis, UCL, October 1992.

53. British Standard 449, "Specification for the use of Structural Steel In Building" *British Standard Institution*, 1969.

54. Robertson, A., "the strength of struts" *Selected Engineering paper*, no. **28**, I.C.E., 1925.

55. Godfrey, B., "The Allowable Stresses in Axially-Loaded Steel Struts" *The Structural Engineer*, Vol. **40**, no. **3**, March 1962, pp. 97-112.

56. Dwight, J.B. Adaptation of Perry formula to represent the new European steel column-curves. *Steel Construction*, AISC, 9(1), 1975.

57. Bjorhovde, R., "Deterministic and probabilistic approaches to the strength of steel columns" *Ph.D. Dissertation*, Dept. of Civil Engineering, Lehigh University, Bethlehem, Pennsylvania, USA, 1972.

58. Rondal, J. and Maquoi, R., "Single Equation for SSRC Column-Strength Curves" Technical Notes, *Journal of Structural division*, ASCE, Vol. **105**, no. **ST1**, Jan 1979, pp. 247-250.

59. Abdel Gadir, R. and Imbrahim, E.I. "Biaxial Buckling of Columns", UCL, Final Year Project, May 1994.

References

1. Van Musschenbroek, P., "Introductio ad Cohaerentiam Corporum Firmorum" Lugduni, 1729.

2. Young, T., "A course of lectures on natural philosophy and the mechanical arts" London, 1807, Vol. **1**, pp. 135-156 & Vol. **2**, pp. 46-49.

3. Lamarle, A. H. E., "Mémoire sur la flexion du bois", *Annales des Travaux Publiques de Belgique*, Part 1, Vol. **3**, 1845, pp. 1-64, and Part 2, Vol. **4**, 1846, pp. 1-36.

4. Ayrton, W. E., and Perry, J., "On struts", *The Engineer*, London, 1866, pp. 464-513.

5. Hodkinson, E., a) "Experimental researches on the strength of pilars of cast iron and other materials" *Roy. Soc.*, London, 1840.
   b) "Experimental researches on the strength of pilars of cast iron and other materials" *Roy. Soc.*, London,1857.
   c) "Experimental researches on the strength and other properties of cast iron" London, 1860.

6. Considère, A., "Resistance des pièces comprimées" *Congrès International des procédés de Construction*, Paris, Sept. 9-14, 1889, Proceedings published by Librairie Polytechnique, Paris, Vol. **3**, 1891, p. 371.

7. Engesser, F., "Ueber die Knickfestigkeit gerader Stäbe" *Zeitschrift für Architectur und Ingenieurwesen,* Vol. **35**, no. 4, 1889, pp. 455-462.

8. Engesser, F., "Knickfragen", *Schweizerishe Bauzeitung*, Vol. **25**, no. **13**, March 30, 1895, pp. 88-90.

9. Jasinski, F., "Noch ein wort zu den 'Knickfragen'" *Schweizerishe Bauzeitung*, Vol. **25**, no. **25**, June 22, 1895, pp. 172-175.

10. Engesser, F., "Ueber Knickfragen", *Schweizerishe Bauzeitung*, Vol. **26**, no. **4**, July 27, 1895, pp. 24-26.

11. von Karman, T., "Die Knickfestigkeit gerader Stäbe", *Physikalische Zeitschrift*, Vol. **9**, no. **4**, 1908, pp. 136-140.

12. Von Karman, T., "Untersuchungen über Knickfestigkeit", *Mitteilungen über Forschungsarbeiten auf dem Gebiete des Ingenieurwesens, Verien Deutscher Ingenieure,* Berlin, Heft **81**, 1910.

13. Southwell, R. V., "The strength of struts", *Engineering*, Vol. **94**, August 23, 1912, pp. 249-250.

14. Shanley, F. R., "The column paradox", *Journal of the Aeronautical Sciences*, Vol. **13**, no. **12**, December 1946, p. 678.

15. Shanley, F. R., "Inelastic column theory", *Journal of the Aeronautical Sciences*, Vol. **14**, no. **5**, May 1947, pp. 261-267.

16. Young, D. H. "Rational Design of Steel Columns" *Transactions*, ASCE, Vol. **101**, 1936, p. 422.

17. Timoshenko, S. P. and Gere, J. M., "Theory of elastic stability" 2nd Ed., McGraw-Hill, New York, 1961.

18. Austin, W. J., "Strength and design of metal beam-columns" *Journal of the structural division,* ASCE, Vol. **87**, No. **ST4**, April 1961.

19. Chwalla, E., a) "Die stabilität zentrisch und exzentrisch gedrückter Stäbe aus Baustahl" *Sitzungsberichte der Akademie der Wissenschaften in Wien*, Abt. IIa, 1928, p. 469.

b) "Über die experimentelle Untersuchung des Tragverhaltens gedrückter Stäbe aus Baustahl" *Der Stahlbau*, Vol. **7**, 1934, p. 10.

20. Jezek, K., "Die tragfähigkeit axial gedrückter und auf Biegung beanspruchter Stahlstäbe" *Der Stahlbau*, Vol. **9**, 1936, p. 12.

21. Horne, M., R., "The Elastic-Plastic Theory of Compression Members" *Journal of the Mechanics and Physics of Solids*, Vol. **4**, 1956, p. 104.

22. Galambos, T. V., and Ketter, R., "Columns under combined bending and thrust" *Journal of the Engineering Mechanics division*, ASCE, Vol. **85**, No. **EM2**, April 1959, pp. 1-30.

23. Chen, W. F. and Santathandaporn, S., "Curvature and the solution of eccentrically loaded columns" *Journal of the Engineering Mechanics division,* ASCE, Vol. **95**, No. **EM1**,1969, pp. 21-40.

24. Chen, W. F. and Atsuta, T., "Column curvature method for analysis of beam-columns" *The structural Engineer,* Vol. **50**, No. **6**, June 1972, pp. 233-240.

25. Timoshenko, S. P. and Gere, J. M., "Theory of elastic stability" 2nd Ed., McGraw-Hill, New York, 1961.

26. Campus, F. and Massonnet, C., "Recherches sur le flambement de colones en acier A37, á profil en double Té, solicitées obliquement" *Comptes Rendus de Recherches,* IRSIA, 1956.

27. Ballio, G. and Campanini, G., "Equivalent Bending Moments for Beam-Columns" *Journal of Constructional Steel Research*, Vol. **1**, No. **3**, 1981, pp. 13-23.

28. European Convention for Constructional Steelwork, "European recommendations for Steel construction" *The Construction Press,* London, March, 1978.

29. Nethercot, D. A. and Taylor, J. C., "Design approaches for steel beam-columns" *Final Report of Second International Colloquium on Stability of Steel Structures*, ECCS-IABSE-SSRC-CRC, Liege, April 1977, pp. 199-201.

30. British Standard 5950, "Structural use of steelwork in building" Part 1, *British Standard Institution*, 1990.

31. Chen, W. F. and Atsuta, T., "Theory of Beam-Columns" Vol. **1**, In-plane behaviour and design, McGraw-Hill, 1976.

32. Chen, W.F. and Lui, E. M., "Stability design of steel frames" CRC Press, 1991, U.S.A.

33. Kanchanalai, T. and Lu, L. W., "Analysis and design of Framed Columns under minor axis bending" *Engineering Journal*, AISC, Vol. **16**, No. **2**, Second quarter, 1979, pp. 29-41.

34. Massonet, C. E., "Forty Years Research on Beam-column in Steel" *Solid Mechanics Archives,* Vol. **1**, No. **2**, 1976, pp. 27-157.

35. Johnston, B. G., "Guide to stability Design Criteria for Metal Structures" SSRC, 3rd ed., New York, John Wiley & sons, 1976, pp. 410-454.

36. Horne, M. R. "An historical review on the interaction of plasticity and structural stability in the theory and its application to design" *R. H. Wood Memorial Conference*, Modern developments in frame and slab structures, November 1988, pp. 1-27.

37. Wood, R. H., "Effective lengths of columns in multi-storey buildings" *The Structural Engineer*, Part 1, Vol. **52**, No. **7**, July 1974, pp. 235-244, Part 2, Vol. **52**, No. **8**, August 1974, pp. 295-302, Part 3, Vol. **52**, No. **9**, September 1974, pp. 341-346.

38. Horne, M. R. "An approximate method for calculating the elastic critical loads of multi-storey plane frames" *The Structural Engineer*, Vol. **53**, No. **6**, June 1975, pp. 242-248.

39. Load & Resistance Factor Design, "Manual of steel construction" First edition, AISC, 1986.

40. Rankine, W. J. M., "Useful rules and tables", London, 1866.

41. Merchant, W., "The failure Load of Rigid Jointed Frameworks as Influenced by Stability" *The structural Engineer*, Vol. **32**, July 1954, pp. 185-190.

42. Horne, M. R., Elastic-plastic failure loads of plane frames" *Proc. Roy. Soc.*, **274**, A, No. **1358**, November 1963, pp. 343-364.

43. a. Bijlaard, P. P., "Some contributions to the theory of elastic and plastic stability" *Publ. IABSE*, Vol. **8,** 1947.

b. McGuire, W., "Steel structures" Prentice-Hall, INC./ Englewood Cliffs, N.J., 1968, p. 439.

c. Iyengar, N. G. R., "Structural stability of columns and plates" 1st ed., Ellis Horwood Limited, England, 1988, p. 123.

44. Gurfinkel, G. and Robinson, A. R., "Buckling of elastically restraint columns" Journal of Struct. Division, Proc. of the ASCE, Vol. 91, No ST6, Dec. 1965, pp.159-183.

45. Bleich, F., "Buckling strength of metal structures" New York, McGraw-Hill Company, Inc., 1952.

46. Ariaratnam, S. T., "the Southwell method for predicting critical loads of elastic structures" *Quart. Journal Mech. and Appl. Maths.*, Vol. **14** part 2, 1961, pp. 137-153.

47. Horne, M. R., "The effect of finite deformations in the elastic stability of plane frames" *Proc. Roy. Soc.*, **266**, A, 1962, pp. 47-67.

48. Chen, W. F., "Further studies of inelastic beam-column problem" *Journal of the structural division*, ASCE, Vol. **97,** No. **ST2,** 1971, pp. 529-544.

49. Nethercot, D. A., "Members with axial load and moments" SCI/I.STRUC.E Course, Design to BS 5950 Part 1, University College London, June 1987.

50. Salmon, E., H., "Columns" *Oxford Technical Publication*, 1921

51. Walker, A.C., Croll, J.G.A. and Wilson, E., "Experimental models to illustrate the non-linear behaviour of elastic structures" *Bulletin Mechanical Engineering Education*, Vol. **10**, 1971, pp 247-259.

52. Hosseini Hashemi, B., 'A consistent approach to the buckling design analysis of rigid jointed frames' Ph.D. thesis, UCL, October 1992.

53. British Standard 449, "Specification for the use of Structural Steel In Building" *British Standard Institution*, 1969.

54. Robertson, A., "the strength of struts" *Selected Engineering paper*, no. **28**, I.C.E., 1925.

55. Godfrey, B., "The Allowable Stresses in Axially-Loaded Steel Struts" *The Structural Engineer*, Vol. **40**, no. **3**, March 1962, pp. 97-112.

56. Dwight, J.B. Adaptation of Perry formula to represent the new European steel column-curves. *Steel Construction*, AISC, 9(1), 1975.

57. Bjorhovde, R., "Deterministic and probabilistic approaches to the strength of steel columns" *Ph.D. Dissertation*, Dept. of Civil Engineering, Lehigh University, Bethlehem, Pennsylvania, USA, 1972.

58. Rondal, J. and Maquoi, R., "Single Equation for SSRC Column-Strength Curves" Technical Notes, *Journal of Structural division*, ASCE, Vol. **105**, no. **ST1**, Jan 1979, pp. 247-250.

59. Abdel Gadir, R. and Imbrahim, E.I. "Biaxial Buckling of Columns", UCL, Final Year Project, May 1994.